



**HAL**  
open science

# Mouvements moléculaires et sélectivité réactionnelle en chimie constitutionnelle dynamique des imines

Petr Kovaricek

► **To cite this version:**

Petr Kovaricek. Mouvements moléculaires et sélectivité réactionnelle en chimie constitutionnelle dynamique des imines. Other. Université de Strasbourg, 2014. English. NNT : 2014STRAF014 . tel-01059611

**HAL Id: tel-01059611**

**<https://theses.hal.science/tel-01059611v1>**

Submitted on 1 Sep 2014

**HAL** is a multi-disciplinary open access archive for the deposit and dissemination of scientific research documents, whether they are published or not. The documents may come from teaching and research institutions in France or abroad, or from public or private research centers.

L'archive ouverte pluridisciplinaire **HAL**, est destinée au dépôt et à la diffusion de documents scientifiques de niveau recherche, publiés ou non, émanant des établissements d'enseignement et de recherche français ou étrangers, des laboratoires publics ou privés.

**ÉCOLE DOCTORALE DES SCIENCES CHIMIQUES**  
**INSTITUT DE SCIENCE ET D'INGÉNIERIE SUPRAMOLÉCULAIRE**  
**UMR 7006**

# THÈSE

présentée par :

**Petr KOVAŘÍČEK**

soutenue le : **23 juin 2014**

pour obtenir le grade de : **Docteur de l'université de Strasbourg**

Discipline/ Spécialité : CHIMIE

## **MOTIONAL, REACTIONAL AND CONSTITUTIONAL DYNAMICS OF IMINES**

**THESE dirigée par :**

**M. LEHN, Jean-Marie**

Professeur Emérite, Université de Strasbourg

**RAPPORTEURS :**

**M. SCHMITTEL, Michael**

Professeur, Université de Siegen

**M. BARBOIU, Mihai**

Directeur de recherche CNRS, Université Montpellier II

**PRESIDENT DE JURY :**

**M. SAMORÍ, Paolo**

Professeur, Université de Strasbourg





# TABLE OF CONTENTS

<b>Table of Contents</b> .....	<b>3</b>
<b>Acknowledgements</b> .....	<b>5</b>
<b>Abstract</b> .....	<b>6</b>
<b>Abbreviations</b> .....	<b>8</b>
<b>Resumé</b> .....	<b>10</b>
<b>1. Molecular dynamics</b> .....	<b>23</b>
1.1. Types of molecular dynamics .....	23
1.1.1. Covalent constitutional dynamics .....	24
1.1.2. Configurational dynamics .....	24
1.1.3. Motional dynamics .....	25
1.1.4. Reaction dynamics .....	25
1.1.5. Other types of molecular dynamicity .....	26
1.2. Reversible chemical reactions .....	27
1.3. General aspects of the imine bond .....	30
1.3.1. Imine formation and imine exchange .....	31
1.3.2. Imines in coordination chemistry .....	34
1.3.3. Vitamin B6: biological imine-amine carrier .....	36
<b>2. The imine bond – A versatile chemical linkage</b> .....	<b>38</b>
2.1. Concept .....	38
2.2. Structural properties influencing imine formation .....	39
2.2.1. Electronic structure of Schiff bases through nitrogen NMR .....	44
2.2.2. Kinetic parameters of imine formation .....	47
2.2.3. Imines of aminoacids and metal catalysis .....	51
2.3. Imine exchange .....	56
2.4. Summary of Chapter 2 .....	61
<b>3. Molecular walking via dynamic imine bond</b> .....	<b>62</b>
3.1. Introduction: Molecular walking .....	62
3.1.1. Biological molecular walkers .....	62
3.1.2. Artificial molecular walkers .....	64
3.1.3. Concept .....	69
3.2. Imine bond-based small molecule walkers .....	69
3.2.1. Aldehydes with aliphatic $\alpha,\omega$ -diamines .....	70
3.2.2. Aldehydes with ethyleneimine oligomers .....	82
3.3. Directional walking .....	95
3.3.1. Lactone formation – trapping of iminium on secondary nitrogens .....	95
3.3.2. Desymmetrisation of the walking track .....	99
3.3.3. Directional small-molecule walking .....	103
3.4. Summary of Chapter 3 .....	106
<b>4. Dynamic reaction selectivity</b> .....	<b>107</b>
4.1. Introduction .....	107
4.2. Representation of dynamic reaction networks .....	107

4.2.1.	Quantification of selection for a two-component libraries .....	109
4.2.2.	Simplexity: selection in dynamic reaction networks .....	110
4.3.	Constitutional selection in aldehyde-amine libraries.....	111
4.3.1.	Selection in the 2+2 aldehyde-amine libraries .....	111
4.3.2.	Extended complexity in 3x3 aldehyde-amine library.....	120
4.3.3.	Multivalency and simplexity .....	121
4.4.	Applications – dynamic selective protection .....	124
4.4.1.	Selective mono-acylation of diamines .....	125
4.4.2.	Sequential selective bis-acylation of diamines .....	126
4.4.1.	Inverted selectivity of acylations .....	127
4.5.	Summary of Chapter 4.....	128
<b>5.</b>	<b>Dynamic imine bond at the solid-liquid interface .....</b>	<b>130</b>
5.1.	Introduction.....	130
5.2.	Dynamic imine bonds on surfaces.....	131
5.2.1.	Design of imine system for the HOPG surface.....	131
5.2.2.	On-surface generation of bis-imines .....	133
5.2.3.	Kinetics of bis-imine formation in solution.....	135
5.2.4.	Surface assisted transimination.....	139
5.2.5.	Kinetics and equilibria of transimination by NMR .....	141
5.2.6.	Reverse in situ bis-transimination .....	143
5.2.7.	On surface selection in dynamic imine library.....	144
5.3.	Summary of Chapter 5.....	146
<b>6.</b>	<b>Conclusions &amp; Perspectives .....</b>	<b>148</b>
<b>7.</b>	<b>Experimental part .....</b>	<b>150</b>
7.1.	Instrumentation .....	150
7.2.	Syntheses.....	151
7.2.1.	Imines .....	151
7.2.2.	Compounds for walking .....	154
7.2.3.	Experiments using dynamic protecting groups.....	157
7.2.4.	Compounds for the STM experiments.....	160
7.3.	Example of <sup>14</sup> N-NMR .....	161
7.4.	Kinetics experiments .....	164
7.4.1.	Mathematic models for kinetic data.....	164
7.4.2.	Results of kinetics experiments .....	167
7.5.	NMR experiments of imine-based molecular motion.....	185
7.5.1.	NMR experiments of linear imine motion .....	185
7.5.2.	Example of EXSY experiment .....	196
7.5.3.	Kinetic experiments of walking.....	199
7.5.4.	NMR experiments of circular motion .....	202
7.5.5.	NMR spectra for directional walking .....	208
7.6.	Dynamic reaction selectivity .....	213
7.6.1.	Selection matrices.....	213
7.7.	NMR comparison for STM results .....	217
<b>Bibliography.....</b>	<b>.....</b>	<b>220</b>

# ACKNOWLEDGEMENTS

I would like to thank to Prof. Jean-Marie Lehn for accepting my candidacy and giving me the opportunity to do my PhD in Strasbourg. It was a fantastic experience and a tremendous lesson. I would like in particular to thank for his inspiring guidance of my work, virulent enthusiasm, for being the personality he is and for teaching me a lecture above all that humanity is what defines the character.

Největší poděkování patří mojí ženě, Káče, která při mně stála po celou dobu a podporovala mě i za cenu vlastních obětí. Srdce by mi puklo, má drahá, kdyby ses měla kdy znovu trápit. Miluji tě můj brouku, a nikdy nezapomenu, Čmelák.

Ze srdce bych chtěl poděkovat také mojí rodině, mami, tati, ségra. Bez vaší podpory a především důvěry bych nikdy nevylezl zpod máminy sukně. Těžko by se hledal někdo šťastnější než já, páč já mám vás a vy máte mě, jsme rodina.

I would like to thank to Dr. Jean-Louis Schmitt, Jacline Claudon and Prof. Jack Harrowfield who were essential for my existence in the lab. Not a single page of this manuscript would exist without their help and their energy they gracefully invested in me. I wish I can find a way to pay you back.

Among all the friends I have, some left a particular mark and they deserve a particular word. Gaël, nundebibb, you're one of a kind, stay that way, because I appreciate every aspect of you. Andrea and Corinna, you can't imagine how much I miss you two. Gareth and Ylenia, you're the most kind and most honourable people I've ever met.

The special time I've had in Strasbourg would not have been possible without you my friends: Olly, Jenny and Elodie, I wish you as a family only happiness, Rafel and Cristina, my beloved refugees from Mediterranean to "sunny" England, Giorgi, caro mio, Pierre, a personality unlike any other, Serena and Redmond, my faithful crew of Monday beers, Claudio, an artist by soul and by heart, Ema, who visited my hometown maybe more often than me, Jan, a dokonce ti i odpustim, že jsi socan ☺

It was the lab members who were with me every day, taught me in practical skills and suffered from my temper. I would like to thank you for your patience with me: Ghislaine, je te souhaite tout le Bonheur du monde et un mariage superbe, Lars, send my regards to the penguins down there, Lutz, despite my envy I wish you just happiness and luck with your twin sons, Anne, a person of unique positivism and endless good mood, Tum, the icon of the Land of Smile, Nadine, amazing colleague and fantastic friend, Manuel, who warmly embraced me in the lab, Nema Hafezi, Nabarun Roy, Bama Bag, Mihail Stadler, Quin Yiang, for being wonderful colleagues,

I would in particular like to thank the people who helped me in proof-reading the manuscript, Ghislaine Vantomme, Dr. Gaëlle Bealle and Dr. Gaël Scheaffer for the French Résumé, Dr. Pierre Morieux, Dr. Alastair McEwen, Dr. Nema Hafezi, Dr. Oliver Fenwick and Prof. Jack Harrowfield for the English Chapters, and Dr. Jean-Louis Schmitt for the Experimental part.

Thank you!

## ABSTRACT

This thesis in seven chapters describes the dynamic covalent chemistry of imines on the interplay between motional, reactional and constitutional dynamic of molecules.

The introductory chapter defines the terms used throughout the thesis, such as different types of molecular dynamics. It gives an outline of the phenomena discussed in the thesis in different fields and discusses the concept of reversibility with particular attention to the imine bond. It also briefly reviews some general properties and applications based on the imine linkage.

Second chapter describes the initial screening of available aldehydes. Dynamic covalent chemistry based functional systems employing the reversible imine bond require three basic features: 1) fast rate of formation of the imine bond, 2) conversion to imine as high as possible, 3) fast rate of exchange of the components. This leads to important question "What are the best reagents to form imines?" First, thermodynamic parameters were examined, i.e. the conversion of the aldehyde to its corresponding imine was determined, addressing the need for high conversion in DCC systems. Small library of 19 aromatic aldehyde derivatives was chosen, containing several different substituents on several (hetero)aromatic rings. This library was titrated with amine and the relative conversion to imines was followed by NMR. This screening gave two hits: pyridine-2-carboxaldehyde (expected due to electron-withdrawing character of the pyridine ring) and salicylaldehyde (unexpected because of electron donating properties of the hydroxyl group). This was explained due to presence of a strong intramolecular OH...N hydrogen bond. The kinetic parameters are relevant to the need of fast rate of formation and fast rate of response to applied stimuli. Therefore the kinetics of imine formation and imine exchange were determined for the identified aldehyde hits and a few other derivatives for comparison, in various media. The Hammett plot for different salicylaldehyde derivatives substituted in position 5 (*meta* to carbonyl function, *para* to the OH group) was constructed.

Third chapter describes an interesting behaviour observed in the case of salicylaldehyde reacted with ethylenediamine. Fast intramolecular imine exchange reaction through a cyclic intermediate leads to methylene signal broadening. This process can be observed for many different aldehydes as it was revealed by the Dynamic NMR (DNMR) techniques (variable temperature NMR, line-shape fitting analysis, EXSY), but the composition of the mixture varies: while salicylaldehyde gives only imines, pyridine-2-carboxaldehyde gives mixture of its imine and cyclic amination with ratio dependent on diamine length and pH. Thus the DNMR of pyridine-2-carboxaldehyde reacted with ethylenediamine clearly proves the mechanism of the intramolecular exchange via the formation of a cyclic amination intermediate. For salicylaldehyde, the exchange process can be described as end-to-end displacement. Temperature profiling followed by line-shape fitting analysis allowed evaluation of the activation parameters of this process from the Eyring equation. The rate of the exchange depends on the substitution on the aromatic ring and also the diamine length plays an important role due to the formation of a cyclic intermediate. The phenomenon of the end-to-end displacement was extended from simple  $\alpha,\omega$ -diamines to linear ethyleneimine oligomers, like diethylenetriamine and triethylenetetraamine. Like in the previous case, salicylaldehyde reacted with polyamines gives only the imine, which is convenient for the analysis. Using EXSY, the rate of the end-to-end exchange can be determined; since this rate is independent of concentration and mixing ratio, the displacement process is intramolecular. For longer ethyleneimine oligomers, the rate of the intramolecular

exchange falls below the rate of the intermolecular one and cannot be determined. The displacement proceeds through reversible formation of cyclic aminal intermediates with secondary nitrogen atoms on the track. The intramolecular exchange was also studied on branched and cyclic ethyleneimine oligomers. The displacement process can be seen as small molecule walking along a polyamine track, a synthetic analogy to the biological walkers like the kinesin motor. In this perspective the challenging goal of directional small-molecule walker was studied. Among several possibilities, the pH driven displacement was chosen to explore, profiting from the ability of the 2-carboxybenzaldehyde to close a lactone ring on a secondary nitrogen atom. To achieve directional walking, the track must be oriented, i.e. one end must be different than the other. For this purpose, hydroxylamine terminated polyamines were synthesized and used to prove the concept of directional walking.

Chapter four develops the selectivity of aldehydes in formation of different condensation products with amines into an area of dynamic reaction selectivity. The selectivity of different aldehyde derivative in reaction with different amines represents a selection algorithm, or a self-sorting mechanism, driven by the complexity of the reaction mixture. Initially, a theoretical approach for quantification of the selection efficiency was developed using an algebraic representation of DCC libraries and demonstrated on the examples of selection in the literature. This approach was then extended to the complexity driven selection and demonstrated on the example of three different aldehydes reacted with three different amines. If all three aldehydes and amines are mixed together, only three matching-pair products are formed. However, high selectivity is achieved only if all reagents are present. If one or more of them are missing the selectivity is decreased, lost or even in some cases inverted. Full deconvolution of this example of complexity driven selection consisting of mixing all combinations of reagents was performed and discussed. This feature of complexity-driven selection was called simplexity. Finally, the dynamic reaction selectivity of aldehydes and amines was applied to the sequential selective derivatization of polyamines using aldehydes as protecting groups. The selective formation of imine, aminal or lactone derivatives allows to address specific nitrogen sites and to attach different acyl or alkyl residues. This was demonstrated on selective sequential on pot attachment of different acyl residues on a diamine.

Chapter five is devoted to the study of the dynamic nature of the imine bond at the solid-liquid interface using STM and was elaborated in cooperation with Dr. Artur Ciesielski, Dr. Mohamed El Garah and Sébastien Haar. Initially, a series of bis-imines formed by condensation of three  $\alpha,\omega$ -diamines with two equivalents of 4-hexadecyloxybenzaldehyde were prepared. These bis-imines form similar lamellar structures on the HOPG surface differing only in the distance between the aromatic rings. In the next step, these structures were formed by *in situ* condensation on the surface. In all cases, very fast full surface coverage by desired molecules was achieved. In cross-check experiments the same reactions were performed in NMR tube without the graphite and followed. It was found that the rate of the reaction at the surface is accelerated by approximately four orders of magnitude. In the following experiments the layer of one bis-imine was mixed with a competing diamine. The layer undergoes easy and fast reconstitution to give uniquely structures containing the longest  $\alpha,\omega$ -diamines chain available in the solution. Like in the case of layer formation, the exchange reactions were cross-checked by NMR and, in addition to significant rate acceleration, surface-induced amplification of bis-imine species with the longest spacer was observed.

Chapter six gives general conclusions and summarizes the partial conclusions following each chapter. Chapter seven consists of experimental part, providing crucial experimental data, processing details and synthetic procedures as well as characterization of the synthesized products.

# ABBREVIATIONS

A	4-hexadecyloxybenzaldehyde
Å	Angström, $10^{-10}$ m
A <sub>1</sub> B <sub>2</sub>	N-(4-hexadecyloxybenzylidene)-1,2-diaminoethane
A <sub>1</sub> B <sub>6</sub>	N-(4-hexadecyloxybenzylidene)-1,6-diaminohexane
A <sub>1</sub> B <sub>12</sub>	N-(4-hexadecyloxybenzylidene)-1,12-diaminododecane
A <sub>2</sub> B <sub>2</sub>	N,N'-bis(4-hexadecyloxybenzylidene)-1,2-diaminoethane
A <sub>2</sub> B <sub>6</sub>	N,N'-bis(4-hexadecyloxybenzylidene)-1,6-diaminohexane
A <sub>2</sub> B <sub>12</sub>	N,N'-bis(4-hexadecyloxybenzylidene)-1,12-diaminododecane
AcOH	acetic acid
B <sub>2</sub>	ethylenediamine, 1,2-diaminoethane
B <sub>6</sub>	hexamethylenediamine, 1,6-diaminohexane
B <sub>12</sub>	1,12-diaminododecane
BENZAL	benzaldehyde
Boc	<i>t</i> -butyloxycarbonyl
bp	boiling point
br s	in NMR, broad signal
C <sub>2</sub> DA <sup>1</sup>	ethylenediamine, 1,2-diaminoethane
C <sub>3</sub> DA	propylenediamine, 1,3-diaminopropane
C <sub>4</sub> DA	putrescine, 1,4-diaminobutane
C <sub>5</sub> DA	cadaverine, 1,5-diaminopentane
C <sub>8</sub> DA	1,8-diaminooctane
calc.	calculated
CAXAL	2-carboxybenzaldehyde
Cbz	benzyloxycarbonyl
CDC	constitutional dynamic chemistry
cyclen	1,4,7,10-tetraazacyclododecane
d	in NMR, doublet
DBU	1,8-diazabicyclo[5.4.0]undec-7-ene
DCC	dynamic covalent chemistry
DCL	dynamic combinatorial library
DCM	dichloromethane
DMF	<i>N,N</i> -dimethylformamide
DMSO	dimethylsulfoxide
dd	in NMR, doublet of doublets
dt	in NMR, doublet of triplets
E	electrophile
EA	elemental analysis
ED	electron-donating
EWG	electron-withdrawing group
EXSY	NMR exchange spectroscopy

<sup>1</sup> The abbreviation C<sub>2</sub>DA is a duplicate of the B<sub>2</sub>. This duplicity was created to keep consistent with nomenclature chosen in two different publication manuscripts, and here reported in two separate chapters.

FRET	Förster resonance energy transfer
hexacyclen	1,4,7,10,13,16-hexaazacyclooctadecane
HOPG	highly ordered pyrrolytic graphite
IPA	<i>iso</i> -pentylamine
kDa	kiloDalton, $10^3$ g mol <sup>-1</sup>
m	in NMR, multiplet
Me <sub>2</sub> EDA	<i>N,N'</i> -dimethyl-1,2-diaminoethane
Me <sub>2</sub> PDA	<i>N,N'</i> -dimethyl-1,3-diaminopropane
MePDA	<i>N</i> -methyl-1,3-diaminopropane
MeSO <sub>3</sub> H	methanesulfonic acid
mL	millilitre, $10^{-3}$ litre
mM	millimolar, $10^{-3}$ mol L <sup>-1</sup>
MMFF	Merck molecular force field
ms	millisecond, $10^{-3}$ second
μL	microliter, $10^{-6}$ litre
μm	micrometre, $10^{-6}$ metre
nm	nanometre, $10^{-9}$ m
NMR	nuclear magnetic resonance
Nu	nucleophile
P5P	pyridoxal-5-phosphate
pA	picoAmper, $10^{-12}$ Amper
pN	picoNewton, $10^{-12}$ Newton
PIP	piperidine
PYRAL	pyridine-2-carboxaldehyde
RT	room temperature
s	in NMR, singlet
SALAL	salicylaldehyde
t	in NMR, triplet
tacn	1,4,7-triazacyclononane
<i>t</i> -BuOK	potassium <i>tert</i> -butoxide
TFA	2,2,2-trifluoroacetic acid
TfOH	triflic acid, trifluoromethanesulfonic acid
tren	tris-(2-aminoethyl)amine
TsCl	<i>p</i> -toluenesulfonyl chloride
TsOH	<i>p</i> -toluenesulfonic acid
UHV	ultra-high vacuum
UV	ultra-violet
UV-VIS	ultra-violet-visible
VT-NMR	variable temperature NMR



## RESUME

Ce travail de thèse se divise en sept chapitres et décrit la chimie covalente dynamique des imines, à l'interface entre mouvement moléculaire, sélectivité réactionnelle et dynamique constitutionnelle des molécules.

Les systèmes fonctionnels basés sur la Chimie Covalente Dynamique (CCD) utilisant une liaison imine réversible doivent présenter trois caractéristiques : 1) la formation rapide de la liaison imine, 2) une conversion vers la formation de l'imine élevée, 3) un échange rapide entre les composants. Les deux premières caractéristiques sont nécessaires à la construction rapide du système dynamique tout en obtenant un rendement élevé. Le troisième point permet d'obtenir une réponse rapide aux stimuli appliqués. Regroupées, ces trois propriétés engendrent un contrôle thermodynamique efficace du système. Ces critères nous amènent à la problématique suivante : "Quels sont les meilleurs réactifs permettant de synthétiser des imines ?" La nucléophilie des amines a été largement étudiée et cette propriété est aujourd'hui bien décrite dans la plupart des manuels de chimie. En revanche, les données portant sur l'électrophilie des aldéhydes sont rares. Les amines sont également plus présentes dans la nature que les aldéhydes. Pour cette raison, l'utilisation de la chimie dynamique des imines dans les biosystèmes offre la possibilité de travailler seulement sur le composé aldéhydique, lequel peut être modifié et dérivatisé.

Le premier chapitre de ce travail de thèse introduit et définit les termes utilisés dans ce manuscrit, tels que les différents types de dynamiques moléculaires (dynamique constitutionnelle présentée en Figure 1, mouvement moléculaire en Figure 2 et sélectivité réactionnelle en Figure 3). Il apporte également un aperçu des phénomènes observés au cours de cette thèse dans les différents domaines abordés.

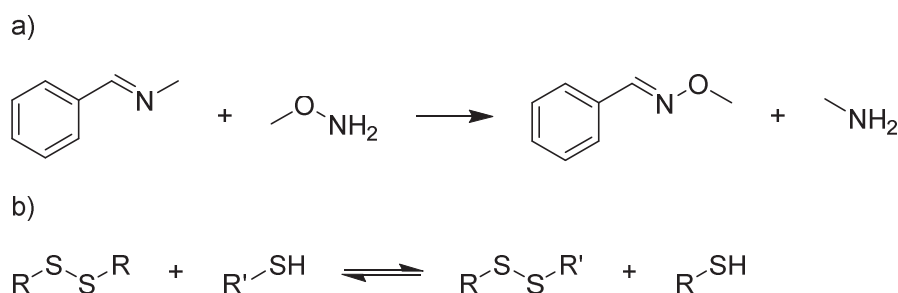


Figure 1. Deux exemples de dynamique constitutionnelle : a) réaction d'une imine avec la méthoxyamine pour obtenir une oxime et l'amine libérée ; b) échange dynamique d'un disulfure avec un thiol menant à un nouveau disulfure. La dynamique constitutionnelle covalente est décrite comme un processus d'échange d'une partie de la molécule. Ceci s'effectue par dissociation d'une liaison covalente et reformation de celle-ci avec un autre composant.

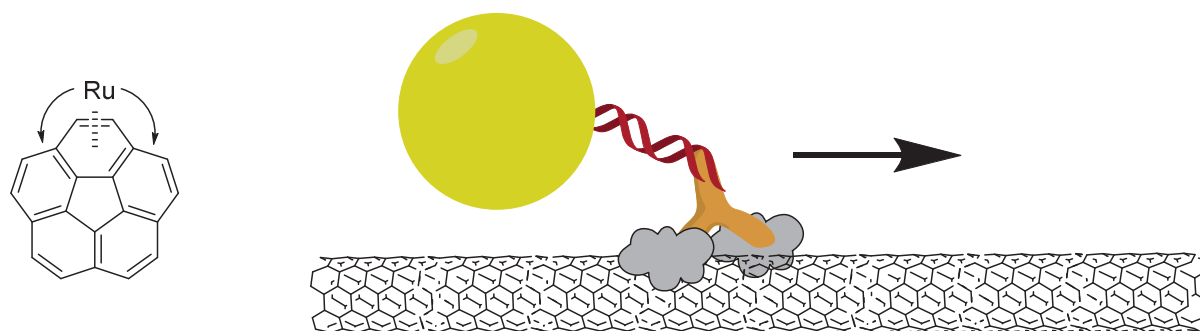


Figure 2. (Gauche) Exemple de mouvement moléculaire non-directionnel entre une molécule de corannuléne et un atome de ruthénium. L'atome de ruthénium peut se déplacer facilement parmi les cycles aromatiques conjugués menant à un système fluxionnaire. (Droite) Déplacement monodirectionnel permettant le transport d'un cargo, ici démontré par le mouvement d'une molécule de kinésine sur un microtubule cellulaire.

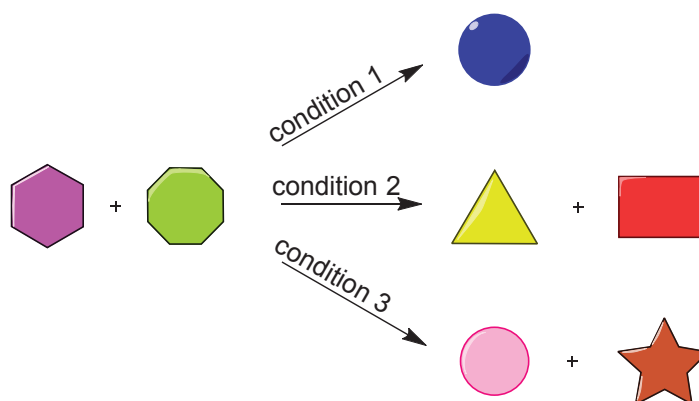


Figure 3. Représentation de dynamiques réactionnelles : un mélange de réactifs mène à des produits différents en fonction des conditions utilisées pendant la réaction. Si les liaisons formées sont réversibles, les produits peuvent se redistribuer pour s'adapter aux changements des conditions. Cette adaptation aux conditions est rendue possible grâce à un réseau de réactions connectant tous les composants.

Le second chapitre décrit les premières études menées sur le panel des aldéhydes disponibles. Dans un premier temps, les paramètres thermodynamiques sont examinés, et plus particulièrement la transformation des aldéhydes en imines correspondantes, abordant ainsi l'importance du taux de conversion dans la CCD. Un petit ensemble composé de 19 aldéhydes aromatiques a été choisi pour ce travail. Ce groupe, qui contient des cycles hétéroaromatiques greffés par différents substituants, a été divisé en 5 sous-groupes (chaque sous-groupe contient le benzaldéhyde, étudié de manière approfondie et utilisé comme référence) pour faciliter l'analyse. Chaque sous-groupe a été titré par une amine et la conversion relative en imine a été suivie par RMN.

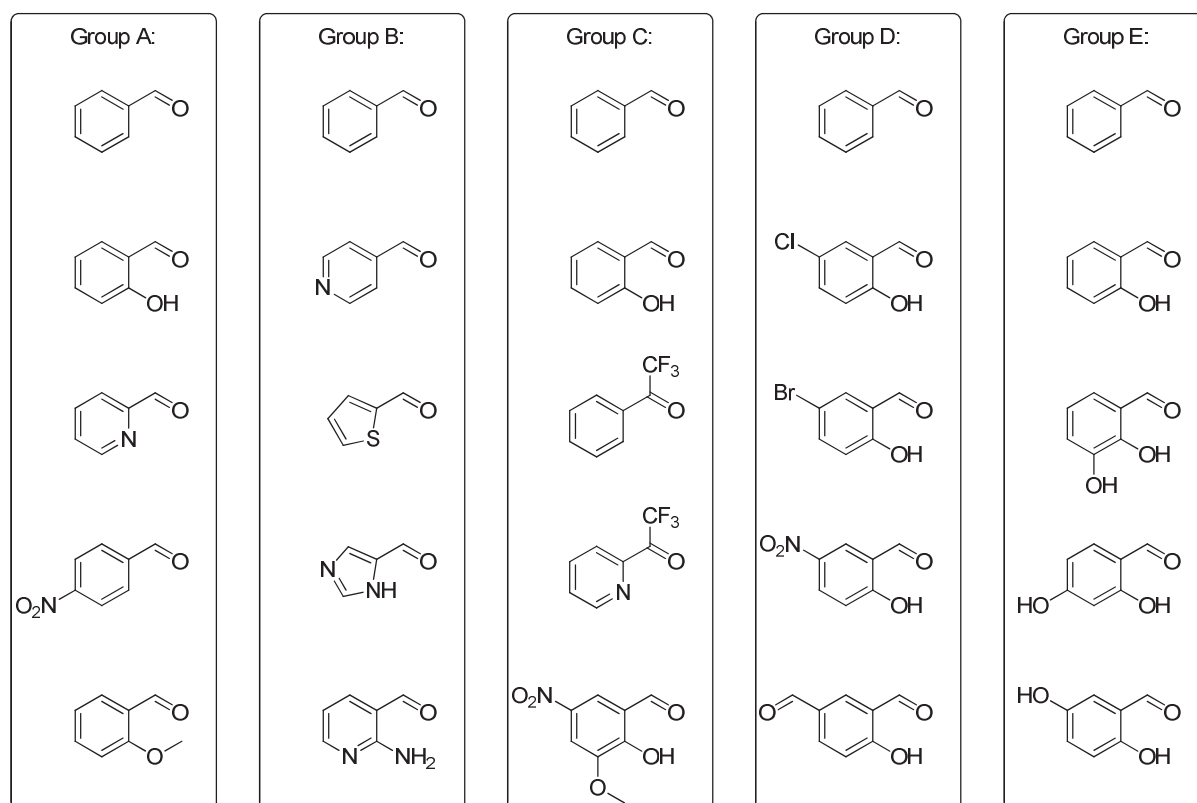


Figure 4. Bibliothèques des aldéhydes étudiés, divisées en quatre groupes. Différents aldéhydes aromatiques présentant différents substituants ont été étudiés pour découvrir les deux aldéhydes les plus attractifs en CCD : le salicylaldéhyde et le pyridine-2-carboxaldéhyde.

A l'issue de cette étude, deux molécules ont été sélectionnées : le pyridine-2-carboxaldéhyde (résultat attendu, en raison du caractère électroattracteur du cycle pyridine) et le salicylaldéhyde (résultat surprenant si l'on considère le caractère électrodonneur du groupe hydroxyle). Les salicylaldimines forment de fortes liaisons hydrogènes intramoléculaires OH...N, mises en évidence par les mesures de RMN (décalage du proton du groupement OH de 10,5 à 14 ppm), les mesures en UV-VIS (bande d'absorption à 406 nm) et par les expériences de cinétiques (voir plus bas). Ces liaisons intramoléculaires sont également décrites dans la littérature.

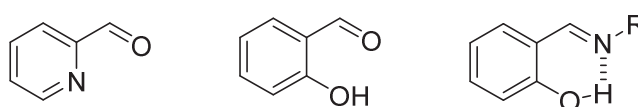
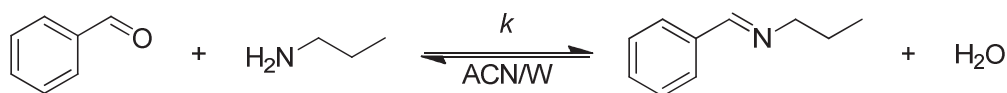


Figure 5. Les deux aldéhydes les plus intéressants en CCD sont le salicylaldéhyde (au milieu) et le pyridine-2-carboxaldéhyde (à gauche). La présence d'une liaison hydrogène favorise la formation des imines à partir de salicylaldéhyde (à droite). C'est aussi grâce à cette liaison hydrogène que les imines de salicylaldéhyde sont plus stables et l'échange de la partie amine est plus lent par rapport aux autres aldéhydes étudiés.

L'étude des paramètres cinétiques est cruciale pour l'obtention de vitesses de formation et de réponse aux stimuli élevées. Pour cette raison, les cinétiques de formation et d'échange des imines ont été déterminées pour les aldéhydes sélectionnés ainsi que pour d'autres aldéhydes à titre de comparaison, dans différents milieux. Nous avons découvert que la liaison hydrogène intramoléculaire de la salicylaldimine induit l'augmentation de la vitesse de formation de l'imine, mais diminue sa vitesse d'échange. En particulier, la constante de vitesse de formation de l'imine dans le chloroforme à partir du salicylaldéhyde est dix fois plus grande qu'à partir du benzaldéhyde. De manière surprenante, ceci montre que le groupement OH induit une accélération de la réaction, même par rapport au groupement *p*-nitro étudié dans la bibliothèque. Dans un mélange eau-acétonitrile (3:7 v/v), la cinétique de formation de l'imine à partir du salicylaldéhyde n'est plus que

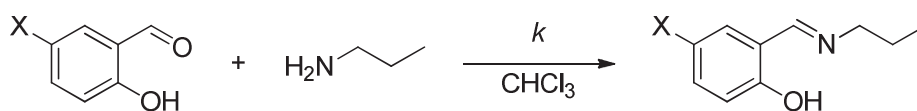
16 % plus élevée qu'à partir du benzaldéhyde. Cependant, la conversion est maintenue à 77 % pour le salicylaldéhyde alors qu'elle est de 20 % pour le benzaldéhyde. Le ralentissement de la réaction d'échange de l'imine due à la liaison hydrogène intramoléculaire se manifeste à la fois dans le chloroforme ainsi qu'en milieu aqueux. Dans le chloroforme, la constante de vitesse diminue d'un facteur 3. Dans un mélange eau-acétonitrile, seule la constante de vitesse de formation de la salicylaldimine peut être mesurée. En effet, elle se révèle trop rapide pour être évaluée dans le cas de la benzaldimine.



Aldéhyde	Paramètre	Valeur
benzaldéhyde	$\chi = (K)$	70.8 % (2.42)
	$k =$	$(24.29 \pm 0.22) \cdot 10^{-3} \text{ L mol}^{-1} \text{ s}^{-1}$
<i>p</i> -nitrobenzaldéhyde	$\chi = (K)$	91.2 % (10.36)
	$k =$	$(27.92 \pm 0.08) \cdot 10^{-3} \text{ L mol}^{-1} \text{ s}^{-1}$
salicylaldéhyde	$\chi = (K)$	93.4 % (14.15)
	$k =$	$(18.47 \pm 0.96) \cdot 10^{-2} \text{ L mol}^{-1} \text{ s}^{-1}$
pyridine-2-carboxaldéhyde	$\chi = (K)$	84.2 % (5.33)
	$k =$	$(29.22 \pm 0.48) \cdot 10^{-2} \text{ L mol}^{-1} \text{ s}^{-1}$
pyridine-4-carboxaldéhyde	$\chi = (K)$	89.0 % (8.09)
	$k =$	$(67.56 \pm 0.51) \cdot 10^{-3} \text{ L mol}^{-1} \text{ s}^{-1}$

Figure 6. Constantes de vitesse de formation d'une imine par réaction d'un aldéhyde avec la propylamine dans un mélange acétonitrile-eau (7:3 v/v) ; le pH étant fixé à 8,73 en utilisant un tampon de triéthanolamine (valeur de pH non-corrigé pour l'effet isotopique de deutérium). Deux paramètres importants sont donnés : la conversion ( $\chi$ , aussi présentée comme la constante d'équilibre  $K$ ) et la constant de vitesse ( $k$ ).

La courbe de Hammett a été tracée pour différents dérivés de la salicylaldéhyde substitués en position 5 (en *meta* de la fonction carbonyle et en *para* du groupement OH). Le tracé de la courbe est en accord avec la constante  $\sigma_p$ , montrant ainsi l'importance du groupe OH dans la cinétique des réactions de la salicylaldimine.



X =	$k = [\text{L mol}^{-1} \text{ s}^{-1}]$
H	$(3.83 \pm 0.06) \cdot 10^{-2}$
CHO	$(7.55 \pm 0.02) \cdot 10^{-1}$
Cl	$(5.76 \pm 0.01) \cdot 10^{-2}$
Br	$(6.67 \pm 0.02) \cdot 10^{-2}$
OH	$(1.56 \pm 0.04) \cdot 10^{-2}$
NO <sub>2</sub>	$4.48 \pm 0.01$

Figure 7. Constantes de vitesse de la réaction du salicylaldéhyde présentant différents substituants avec la propylamine. Les substituants riches en électrons diminuent la vitesse de la réaction, et à l'inverse les substituants électroattracteurs augmentent cette même vitesse.

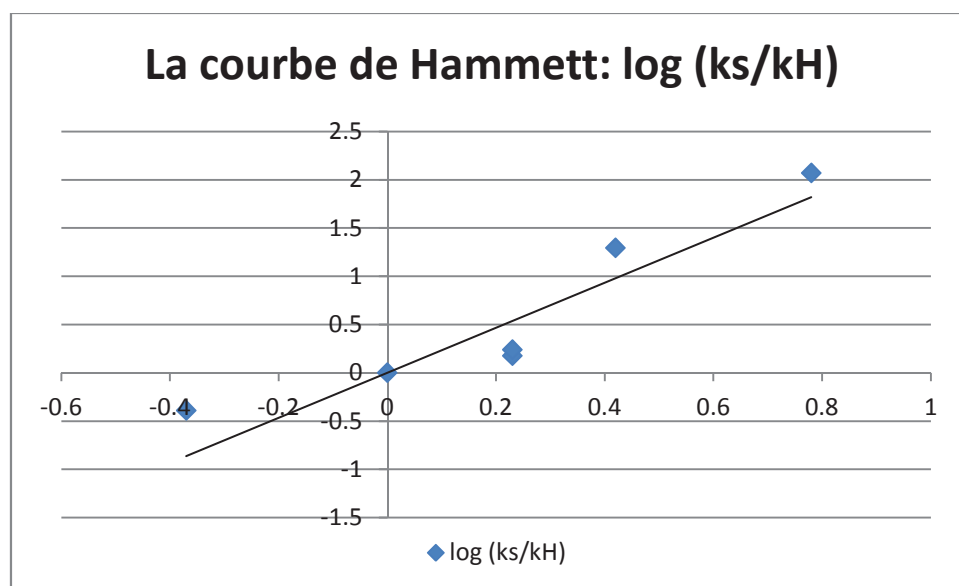


Figure 8. Courbe de Hammett qui explique le rôle des substituants greffés sur la molécule de salicylaldéhyde. Une corrélation a été observée uniquement avec les constantes  $\sigma_p$  et non pas avec les constantes  $\sigma_m$ . Ceci indique que l'effet électro-donneur ou attracteur se propage par conjugaison au groupe hydroxyle et que cet effet est plus important que l'effet du groupe carbonyle. Cette expérience prouve le rôle crucial de groupe hydroxyle sur la réactivité du salicylaldéhyde.

Le troisième chapitre résume l'état de l'art concernant les petites molécules motrices synthétiques ainsi que les machines moléculaires en général. Le travail décrit le comportement intéressant de la réaction entre le salicylaldéhyde et l'éthylènediamine. La réaction d'échange intramoléculaire de l'imine via la formation l'intermédiaire aminal est rapide et conduit ainsi à un élargissement des signaux méthylène en RMN. Ce phénomène a été observé pour de nombreux aldéhydes et mis en évidence par des techniques de RMN Dynamique (DRMN, RMN à température variable, l'analyse d'ajustement au modèle théorique, EXSY). Cependant, la composition du mélange varie : alors que le salicylaldéhyde ne donne que l'imine, la pyridine-2-carboxaldéhyde conduit à un mélange d'imine et d'aminal cyclique dont le rapport dépend de la longueur de la diamine et du pH. Ainsi, la DRMN de la réaction entre le pyridine-2-carboxaldéhyde et l'éthylènediamine prouve que le mécanisme d'échange intramoléculaire se fait via la formation d'un intermédiaire de type aminal cyclique. Dans le cas de le salicylaldéhyde, le processus d'échange peut être décrit selon un déplacement d'un bout à l'autre.

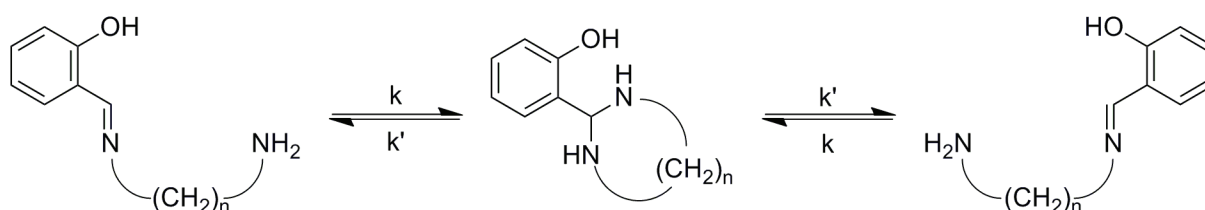


Figure 9. Mouvement intramoléculaire découvert dans la réaction du salicylaldéhyde avec l'éthylènediamine et d'autres diamines aliphatiques. Le groupe salicyl se déplace sur deux atomes d'azote formant ainsi une structure cyclique d'aminal intermédiaire. Le déplacement est non-directionnel car la diamine est totalement symétrique.

La vitesse de l'échange est indépendante du ratio du mélange ainsi que de la concentration, ce qui prouve sa nature intramoléculaire. Elle est également indépendante du pH dans la gamme 9-12. Le profil de température de 15°C à 75°C confirmé par un ajustement sur le modèle théorique permet l'évaluation des paramètres d'activation du processus à partir de l'équation de Eyring (pour le salicylaldehyde  $\Delta H^\ddagger = 38.8 \pm 0.5 \text{ kJ mol}^{-1}$ ,  $\Delta S^\ddagger = 66.0 \pm 1.5 \text{ J mol}^{-1} \text{ K}^{-1}$ ).

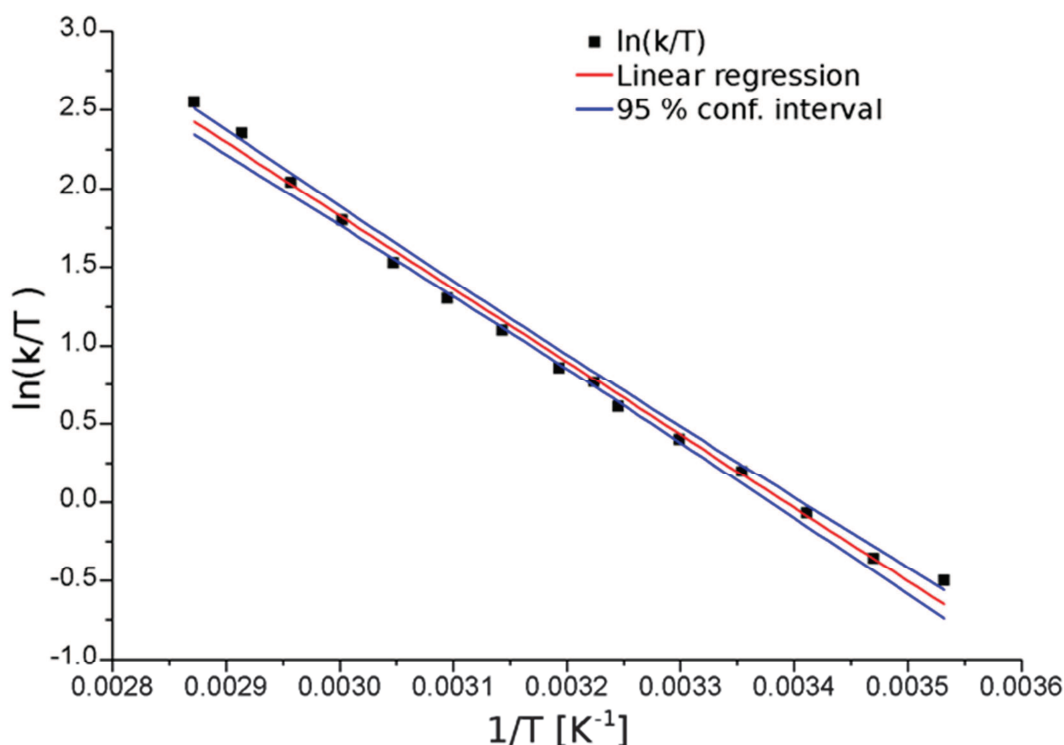


Figure 10. Régression linéaire de l'équation d'Eyring pour la vitesse de déplacement intramoléculaire dans la réaction du salicylaldéhyde avec l'éthylenediamine dans un mélange acétonitrile-eau (7:3 v/v). Les résultats et les paramètres de régression sont indiqués, notamment les valeurs expérimentales (points noirs), la régression (ligne rouge) et les intervalles de confiance dans un niveau  $\alpha=0.05$  (ligne bleue). Le coefficient de détermination  $R^2$  est de 0.9935.

La vitesse de l'échange dépend de la substitution du cycle aromatique et le ratio entre les vitesses d'échange de deux aldéhydes dérivés peut être inversée par la température. Par exemple, le 5-hydroxysalicylaldéhyde a une vitesse d'échange plus grande que le dérivé 4-hydroxy jusqu'à 30°C. Au-delà, la vitesse d'échange du 4-hydroxy est plus grande. La longueur de la diamine joue également un rôle important en raison de la formation du cycle intermédiaire et donc la vitesse d'échange d'un bout à l'autre diminue de 360 Hz pour l'éthylenediamine, à 190 Hz pour la propylènediamine et à 10 Hz pour la putrescine. Pour les diamines présentant une distance plus longue entre les groupes amino, la vitesse d'échange intermoléculaire est supérieure au procédé intramoléculaire. Ainsi, seul le procédé intermoléculaire est observé.

$H_2N-(CH_2)_n-NH_2$	n =	2	3	4	5
Salicylaldéhyde	intra	365	187	10	- <sup>[b]</sup>
	inter	- <sup>[a]</sup>	0.22	- <sup>[a]</sup>	0.32
Pyridine-2-carboxaldéhyde	intra	0.17	0.5	1.4	0.60
	Ouverture d'aminal $r'$	0.44	1	- <sup>[c]</sup>	- <sup>[c]</sup>
	Reformation d'aminal $r$	1.35	74	- <sup>[c]</sup>	- <sup>[c]</sup>

Tableau 1. La vitesse de déplacement intramoléculaire pour les deux aldéhydes les plus intéressants a été étudiée pour différentes diamines en fonction de la distance entre les atomes d'azotes. La vitesse de ce processus diminue avec cette distance entre les atomes d'azotes. Dans le cas du salicylaldéhyde, le processus d'échange intermoléculaire a été aussi observé et dans certains cas, la vitesse de ce processus a été déterminée (note a : processus observé mais n'ayant pas pu être quantifié). Dans le cas de la cadaverine, le processus de déplacement intramoléculaire ne peut pas être observé car le processus d'échange intermoléculaire est plus rapide masquant donc les processus plus lents (note b). Dans le cas du pyridine-2-carboxaldéhyde, le produit majoritaire de la réaction est l'aminal. Cependant, cet aminal est présent dans un équilibre dynamique avec la fonction imine et donc la vitesse de déplacement intramoléculaire a pu être déterminée par une expérience EXSY. La vitesse de déplacement est cependant calculée à partir de la vitesse d'ouverture de cycle aminal et la vitesse de reformation de ce cycle. Dans le cas des diamines plus longues, comme la putrescine et la cadaverine, cet aminal cyclique n'est pas observé (les cycles comportant sept ou huit atomes se formant moins facilement), ainsi les processus de déplacement ont pu être déterminés directement (note c).

Le phénomène de déplacement d'un bout à l'autre a été étendu des  $\alpha,\omega$ -diamines simples aux oligomères éthylèneimine, comme la diéthylènetriamine et la triéthylènetetramine. Comme dans le cas précédent, la réaction entre le salicylaldéhyde et le polyamine conduit seulement à une imine, ce qui se révèle pratique pour l'analyse. En utilisant l'EXSY, la vitesse d'échange d'un bout à l'autre peut être déterminée. Puisque la vitesse est indépendante de la concentration et du ratio entre réactifs, le processus de déplacement est intramoléculaire. Pour des oligomères éthylèneimine plus longs, la vitesse de l'échange intramoléculaire devient inférieure à la vitesse de l'échange intermoléculaire et ne peut donc pas être mesurée. Le déplacement se déroule par la formation réversible des intermédiaires cycliques avec les azotes secondaires sur le chemin polyamine. Lorsque ces atomes d'azote sont remplacés par des groupes méthylènes, des atomes d'oxygène ou des azotes tertiaires, l'échange devient dépendant de la concentration et donc intermoléculaire.

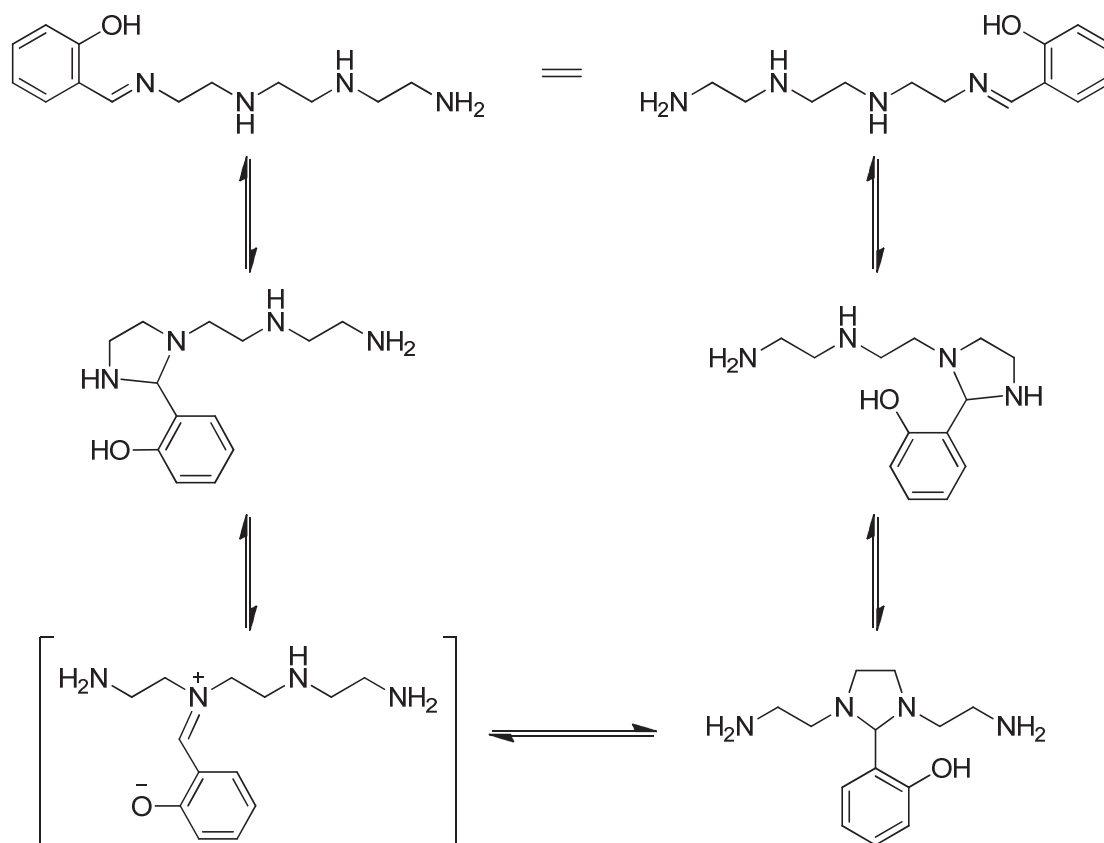


Figure 11. Processus de déplacement intramoléculaire décrit pour les diamines et pouvant aussi être appliqué sur les chaînes polyamines. Le salicylaldéhyde réagit avec le groupe amino terminal pour former une imine. Cette imine se transforme en un aminal intermédiaire qui se déplace sur les atomes d'azote présents dans la chaîne, formant un iminium avec les amines secondaires.

De plus, afin de démontrer que le procédé s'effectue en une seule étape, la triéthylènetetramine a été mise à réagir avec 3 équivalents de salicylaldéhyde pour donner une structure bis-imine-aminale. Cette molécule a ensuite été traitée avec 1 équivalent de méthoxyamine pour conduire à l'élimination d'un résidu salicylidène terminal donnant une mono-imine-aminale. Le dérivé aminal du salicylaldéhyde formé avec les deux atomes d'azote secondaires au centre de la voie se réarrange pour donner une structure bis-imine thermodynamiquement favorisée. Enfin, l'intermédiaire iminium formé pendant l'échange entre aminals peut être capturé sous forme de 2-carboxybenzaldéhyde, qui est capable de former des lactones relativement stables. Ainsi, toutes les étapes élémentaires de déplacements ont été identifiées et démontrées. L'échange intramoléculaire a également été étudié sur des oligomères éthylèneimine branchés (tris(2-aminoéthyl)amine, *tren*) ou cycliques (*cyclen*, *cyclam*, *hexacyclen*).

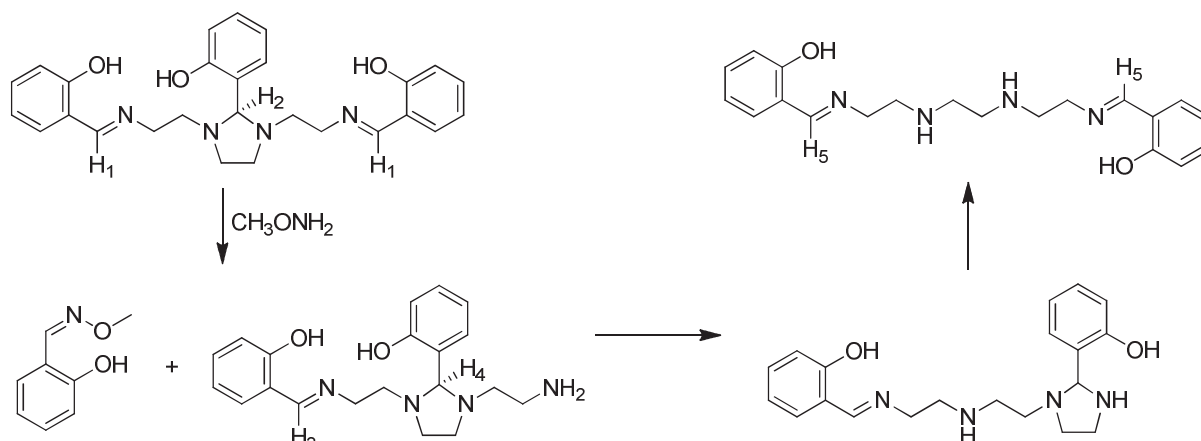


Figure 12. Démonstration de la capacité du salicylaldéhyde à effectuer un déplacement : ceci a été prouvé en utilisant un composé formé par la réaction de la triéthylène tétramine avec trois équivalents de salicylaldéhyde. Le produit de cette réaction comporte deux fonctionnes imines aux extrémités de la chaîne et un aminal au milieu. Lors de l'ajout d'une amine plus nucléophile, comme la méthoxyamine, une des fonctions imines est détruite, libérant l'amine primaire. Le salicylaldéhyde préférant la forme imine à la forme aminal, il se déplace du milieu vers l'extrémité de la chaîne. Les atomes d'hydrogène nommés H1-H5 présentent des signaux bien séparés en RMN, permettant donc l'observation de la cinétique de ces déplacements.

Les processus de déplacement mentionnés ci-dessus peuvent être vus comme de petites molécules aldéhydiques marchant le long d'un chemin polyamine. Par analogie, on pourrait les comparer aux molécules biologiques motrices, comme les kinésines, protéines capables de se déplacer le long des microtubules. Dans cette perspective, il serait très intéressant d'utiliser les machines synthétiques pour pouvoir changer les déplacements aléatoires, purement Browniens, en déplacements dirigés et mimer les molécules biologiques motrices. Dans notre cas, les déplacements contrôlés par le pH ont été choisis, profitant de la propriété du 2-carboxybenzaldéhyde de fermer les cycles lactone à 5 atomes sur l'atome d'azote secondaire.

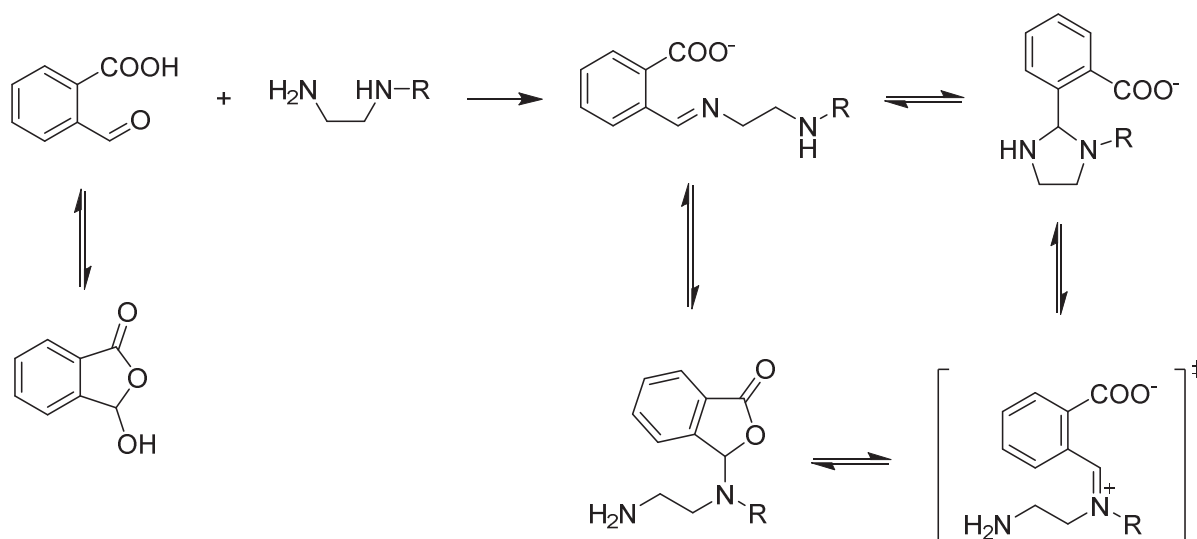


Figure 13. Un autre composé, le 2-carboxybenzaldéhyde, a été étudié pour la stabilisation de structures intermédiaires du déplacement sur les atomes d'azote secondaires. La présence d'un groupe carboxyle à proximité du groupe carbonyle permet la formation d'une lactone. Ce processus a été démontré par RMN. Ceci a inspiré l'exploration vers un système de déplacement intramoléculaire directionnel utilisant les chaînes polyamine non-symétrique, comportant une fonction amine primaire sur une extrémité et une fonction amine secondaire sur l'autre. La formation de lactone a été démontrée comme étant contrôlable par le pH : les valeurs de pH les plus élevées favorisent la formation de l'imine alors qu'un pH neutre voire un peu acide mène à la formation de lactones.



Pour obtenir un déplacement directionnel, le chemin doit être orienté, c'est-à-dire que l'extrémité d'un chemin doit être différente de l'autre. Pour cette raison, des polyamines linéaires possédant un groupe benzyle sur l'atome d'azote terminal ont été synthétisées. Dans le cas de la *N*-benzyléthylènediamine, le carboxybenzaldéhyde réagit en conditions basiques (pH > 10) pour donner l'imine. Diminuer le pH en dessous de 7 conduit aux déplacements intramoléculaires de résidus aldéhydiques sur l'azote secondaire et donc à la fermeture du cycle lactone, alors que le groupe amine primaire est protoné. Si l'on augmente à nouveau le pH jusqu'à 10, on induit l'ouverture réversible du cycle lactone et la migration de l'aldéhyde jusqu'à l'azote terminal pour former à nouveau l'imine. L'ouverture de la lactone se produit en milieu basique, tout comme l'hydrolyse d'un ester. Cependant, l'utilisation de polyamines plus longues (comme la *N*-benzyl-diéthylènetriamine ou la *N*-benzyl-triéthylènetetramine) a dans ce cas échoué en raison des petites différences de nucléophilie et de basicité entre les atomes d'azote. Pour remédier à ce problème, des dérivés hydroxylamines ont été synthétisés. L'hydroxylamine est un nucléophile très fort qui forme des oximes très stables en présence de composés carbonylés et l'échange requiert des conditions difficiles. Cependant, le dérivé *N,O*-disubstitué de l'hydroxylamine ne peut pas former d'oxime et sa basicité est faible comparée aux amines, bien qu'il soit toujours capable de former une structure lactone avec le 2-carboxybenzaldéhyde.

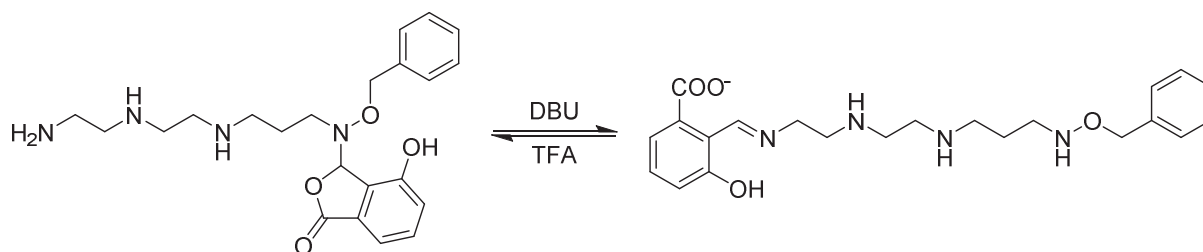


Figure 14. Schéma d'un système présentant un déplacement directionnel développé pendant ces travaux de thèse. Un aldéhyde présentant à la fois la fonction salicylaldéhyde et la fonction 2-carboxy-benzaléhyde peut réagir avec une chaîne polyamine terminée par une hydroxylamine. L'aldéhyde formé peut migrer entre la fonction lactone basée sur l'hydroxylamine terminale et la fonction imine de l'amine primaire par ajout d'acide ou de base. Le déplacement est donc directionnel et réversible. Il a été possible d'effectuer jusqu'à trois cycles d'addition d'acide et de base sans observer de perturbation en RMN.

Le chapitre 4 développe la sélectivité des aldéhydes précédemment mentionnée avec les amines pour la formation de différents produits de condensation dans le nouveau domaine de la sélectivité dynamique réactionnelle. La bibliothèque CCD présente l'avantage unique de générer des quantités importantes de produits variés sans avoir besoin de synthétiser les différentes molécules grâce à la réversibilité des connections entre les différents blocs. Cette incroyable complexité générée in situ peut être réduite en appliquant un stimulus qui permet de trier les espèces pour n'en garder que quelques-unes, comme cela a été démontré pour les imines triées par exemple grâce à la distillation. Dans ce cas, la bibliothèque d'imines se redistribue pour amplifier la formation de l'imine avec la température de distillation la plus basse dans toutes les combinaisons possibles, alors que les toutes les autres combinaisons des mêmes réactifs sont diminuées. Ainsi, la distillation ne donne que quelques imines, triées par température de distillation croissante. D'un autre côté, la sélectivité de différents aldéhydes réagissant avec différentes amines représente un algorithme de sélection dirigé par la complexité du mélange réactionnel.

Initialement, l'approche théorique pour quantifier l'efficacité de la sélection a été développée en utilisant la représentation algébrique de la bibliothèque CCD et démontré sur des exemples de sélection dans la littérature.

	$X_1$	$X_2$	...	$X_z$		$X_1$	$X_2$	...	$X_z$	
$Y_1$	$1/z$	$1/z$	...	$1/z$	sélection	$Y_1$	1	0	...	0
$Y_2$	$1/z$	$1/z$	...	$1/z$		$Y_2$	0	1	...	0
...	...	...	...	...		...	...	...	1	...
$Y_z$	$1/z$	$1/z$	...	$1/z$		$Y_z$	0	0	...	1

Figure 15. Proposition de représentation d'un phénomène de sélection dans une bibliothèque combinatoire dynamique. Une série de composants  $X$  est représentée par des colonnes, leurs partenaires réactionnels  $B$  étant listés dans les lignes. Ceci crée une matrice de produits possibles. Les éléments de cette matrice représentent les fractions molaires de ces différents produits. L'application d'une sélection mène à une redistribution, les produits sélectionnés étant amplifiés et à l'inverse la concentration de ceux ne l'étant pas diminuée. Un système de quantification de la force de sélection est proposé, basé sur cette représentation algébrique.

Cette approche a par la suite été étendue à la sélection conduite par la complexité et démontré sur un exemple de trois différents aldéhydes (salicylaldéhyde, pyridine-2-carboxaldéhyde et 2-carboxybenzaldéhyde) réagissant avec trois amines différentes (*iso*-pentylamine,  $N,N'$ -diméthylpropylènediamine et pipéridine). Le salicylaldéhyde avec l'*iso*-pentylamine forment une paire complémentaire pour la formation d'imine. Le pyridine-2-carboxaldéhyde et la  $N,N'$ -diméthylpropylènediamine forment une autre paire complémentaire pour la formation d'aminal et le 2-carboxybenzaldéhyde avec la pipéridine forment une paire pour la formation de lactone. Si les trois aldéhydes et les trois imines sont mélangés ensemble, seulement trois produits sont formés, les paires complémentaires citées précédemment.

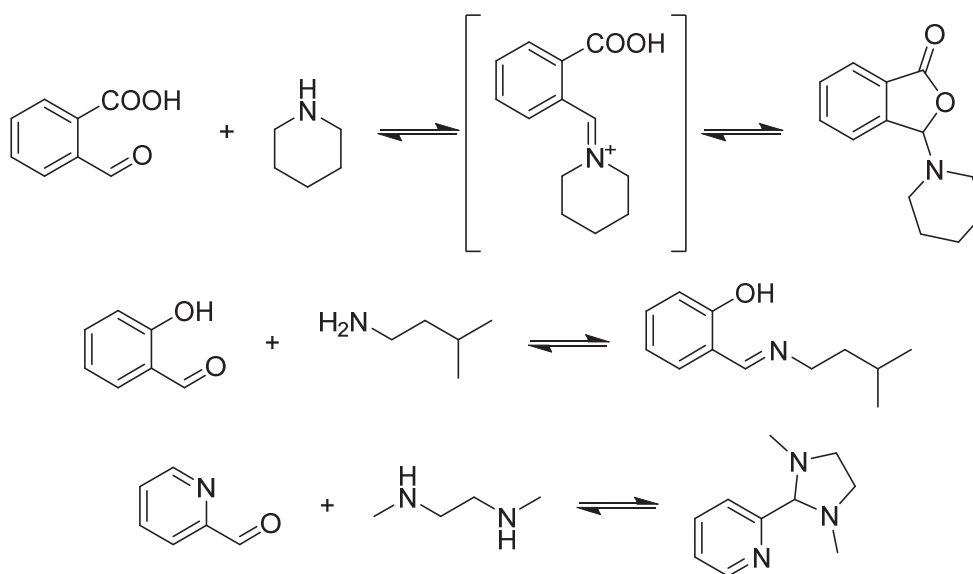


Figure 16. Un phénomène d'auto-sélection dans une bibliothèque combinatoire dynamique basé sur la complexité des composants réactionnels a été nommé « simplicity ». Ce processus a été démontré sur une série de bibliothèques dynamiques composées de 2-carboxybenzaldéhyde, de salicylaldéhyde et de pyridine-2-carboxaldéhyde. Ces composés réagissent chacun préférentiellement avec une amine différente (pipéridine, *iso*-pentylamine et  $N,N'$ -diméthyléthylènediamine, respectivement) pour former la lactone, l'imine et l'aminal correspondant.

Cependant, une grande sélectivité est obtenue seulement si tous les réactifs sont présents. Si un ou plus de ces réactifs est manquant, la sélectivité est diminuée, perdue voire dans certains cas inversée. Comme dans le cas du 2-carboxybenzaldéhyde : s'il est mélangé avec à la fois la pipéridine et l'*iso*-pentylamine, le produit majoritaire de la réaction est l'imine avec l'*iso*-pentylamine. Mais quand le salicylaldéhyde est ajouté, le mélange se redistribue pour donner seulement le salicylaldimine et la lactone du carboxybenzaldéhyde avec la pipéridine. L'analyse complète de cet exemple de sélection conduite par la complexité consistant à mélanger toutes les combinaisons de réactifs a été réalisée et discutée. Ce processus de sélection conduite par la complexité a été appelée simplicity.

	Salicylaldehyde	Pyridine-2-carboxaldehyde	2-Carboxybenzylaldehyde
<i>i</i> -Pentylamine	0.88	0.12	0
<i>N,N'</i> -dimethylpropylenediamine	0.12	0.88	0
Piperidine	0	0	1

Tableau 2 Le phénomène de « simplicity » a été démontré sur une bibliothèque composée de 3 amines et de 3 aldéhydes. Les espèces amplifiées se retrouvent sur la diagonale de la matrice 3\*3. L'importance de la complexité pour une meilleure sélection est démontrée par déconvolution de la matrice. Ceci s'effectue en examinant toutes les combinaisons possibles des composants et en déterminant leurs conversions relatives. Bien sûr, l'augmentation de la taille de la matrice mène à une augmentation exponentielle du nombre d'expériences de déconvolution à effectuer.

Pour finir, la sélectivité dynamique de la réaction entre aldéhydes et amines a été appliquée sur la dérivation séquentielle sélective de polyamines en utilisant les aldéhydes comme groupement protecteur. La formation sélective d'imines, d'aminals ou de lactones permet de cibler spécifiquement des atomes d'azote et d'y attacher différents résidus acyles ou alkyles. Ceci a été démontré sur des séquences sélectives d'attachement de différents résidus aminoacides sur les atomes d'azote de la chaîne spermidine en « one pot », mais la méthode est généralement applicable sur une grande variété de polyamines et fournit un accès facile à une large famille de composés.

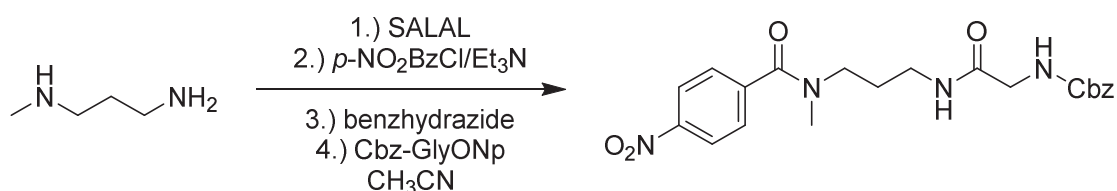


Figure 17. Bis-acylation sélective, séquentielle et « one pot » de la *N*-méthyl-1,3-diaminopropane par réaction initiale avec le chlorure de *p*-nitrobenzoyl puis avec un ester activé de glycine *N*-protégée. La formation de l'imine du salicylaldehyde rends cette séquence sélective. Cette sélectivité peut être inversée par l'usage de la pyridine-2-carboxaldehyde qui forme l'aminal. La déprotection a été effectuée sous conditions douces par échange d'imine. De plus, les produits mono-acétylés sont facilement accessibles par cette procédure et dans de meilleurs rendements que dans la littérature.

Le Chapitre 5 s'intéresse à l'étude de la nature dynamique de la liaison imine à l'interface solide-liquide par microscopie à effet tunnel. En premier lieu, des séries de bis-imines formées par condensation de trois  $\alpha,\omega$ -diamines (diamine-ethane, -hexane et -dodecane) avec deux équivalents de 4-hexadécyloxybenzaldehyde. Ces trois différentes bis-imines forment des structures lamellaires similaires entre elles, très organisées sur des surfaces de graphite HOPG dans le phényloctane, différant seulement par la distance entre les cœurs aromatiques. De manière intéressante, les chaînes alkyl latérales ne s'interpénètrent pas et des structures à couches multiples peuvent être observées pour des concentrations élevées en substrat.

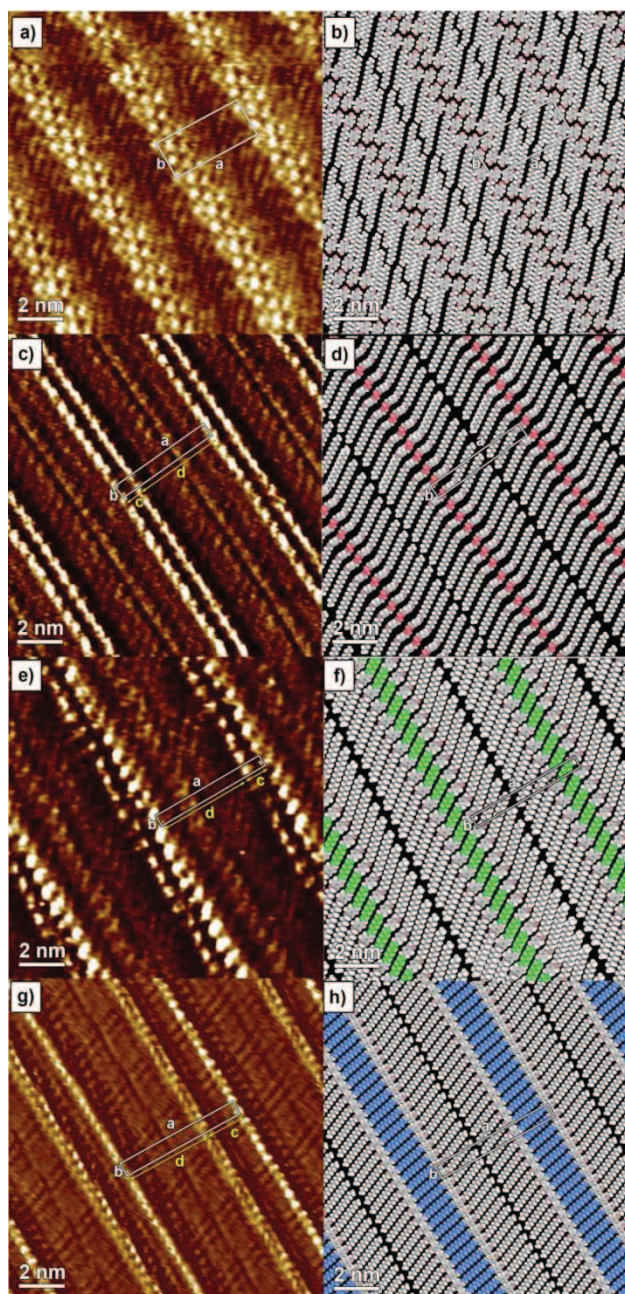


Figure 18. Images STM d'auto-assemblages en 2 dimensions. Monocouches de a) 4-hexadecyloxybenzaldéhyde, c) bis-imine de l'aldéhyde formée avec l'éthylènediamine, e) bis-imine formée avec le 1,6-diaminohexane et g) bis-imine formée avec le 1,12-diaminododécane à l'interface liquide-graphite, à partir d'une solution dans le 1-phényloctane. Les assemblages des molécules sont représentés dans les parties b), d), f), et h). Dans un souci de clarté, les espaceurs bis-imines (c'est-à-dire les chaînes aliphatiques entre les imines) ont été mis en valeur dans des couleurs différentes.

Dans l'étape suivante, ces structures ont été formées in situ par condensation sur la surface HOPG. Dans tous les cas, un recouvrement total et rapide de la surface par les molécules a été obtenu. Dans les expériences de contrôle, la même expérience a été suivie par  $^1\text{H}$ -RMN sans la présence de la surface de graphite. Nous avons observé que la vitesse de la réaction à la surface est multipliée par 10000, ce qui représente une augmentation de la vitesse de réaction jamais observée et due à l'effet de la surface.

Dans les expériences suivantes, les couches préformées de bis-imines ont été mises en présence d'une diamine compétitive. Comme l'énergie d'adsorption augmente avec un nombre croissant de groupes méthylène hydrophobes, la couche est soumise à une reconstitution facile et



rapide pour donner uniquement des structures ordonnées contenant la plus longue chaîne  $\alpha,\omega$ -diamine disponible dans la solution. En d'autres mots, la monocouche de bis-imine formée à partir du diaminoéthane réagit immédiatement avec la diaminohexane pour former une monocouche très organisée, identique à celle formée à partir de la bis-imine préparée ex situ. De la même manière, la monocouche contenant l'espaceur diaminohexane réagit avec la diaminododécane pour donner la monocouche contenant seulement l'espaceur diaminododécane.

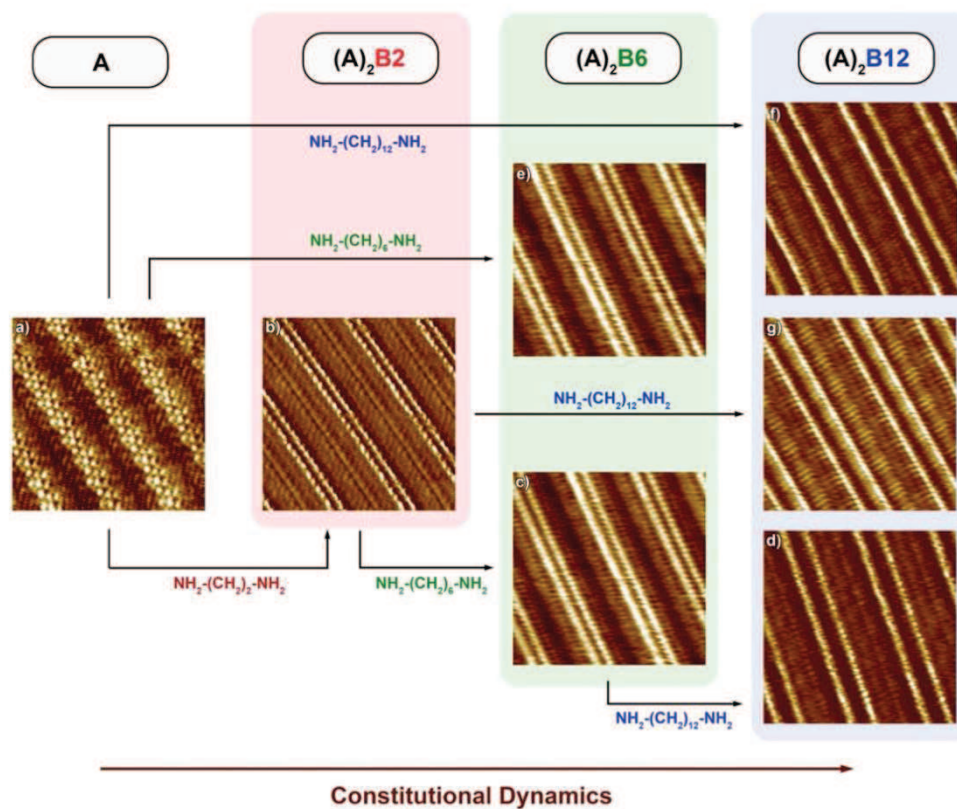


Figure 19. Images STM représentant le processus de bis-transimination in situ. La réaction d'échange d'imines a été effectuée directement sur le graphite (HOPG) et mène à la formation des produits les plus longs. Le processus inverse (c'est-à-dire l'obtention de molécules plus courtes adsorbées sur la surface) nécessite un large excès de réactifs et un temps réactionnel plus long. Les résultats présentés dans cette image démontrent la possibilité d'utiliser la chimie constitutionnelle dynamique sur une surface de graphite. Monocouches de A) 4-hexadecyloxybenzaldéhyde, A<sub>2</sub>B<sub>2</sub>) bis-imine de l'aldéhyde formée avec l'éthylènediamine, A<sub>2</sub>B<sub>6</sub>) bis-imine formée avec le 1,6-diaminohexane et A<sub>2</sub>B<sub>12</sub>) bis-imine formée avec le 1,12-diaminododécane

Pour inverser la réaction, un grand excès de la plus courte diamine (100 équivalents) et un temps de réaction long (10 heures) sont nécessaires. Comme dans le cas de la formation de la couche, les réactions d'échange ont été vérifiées par RMN. En plus d'une augmentation significative de la vitesse, la surface induit une amplification de la quantité d'espèces bis-imines avec le plus grand nombre de groupements méthylènes. Tous ensemble, l'implantation pionnière de CCD basée sur des imines à l'interface solide-liquide révèle une amplification de la conversion et une accélération de la formation et de l'échange d'imines sans précédent dues à la surface de graphite.

Le chapitre 6 contient les conclusions générales de ce travail et résume les conclusions de chaque chapitre.

Le chapitre 7 présente la partie expérimentale, les détails des différentes expériences, les protocoles de synthèse ainsi que les procédures de caractérisation des produits synthétisés.

# 1. MOLECULAR DYNAMICS

*“Every art and every inquiry, and similarly every action and pursuit, is thought to aim at some good; and for this reason the good has rightly been declared to be that at which all things aim.”*<sup>[1]</sup>

The Universe, from the beginning until now, combines simple parts to form more complicated ones, from atoms to molecules, from molecules to proteins, from proteins to cells, from cells to apes, from apes to human thinking about the chain of events that lead to creation of Man and their thoughts.<sup>[2]</sup> The higher complexity is therefore considered to be either the good at which all things aim, or the pursuit aiming at the good.<sup>[1]</sup> In either case, the generation of higher degrees of complexity is natural, indispensable and maybe even an inevitable principle of evolution.<sup>[3]</sup> Chemistry itself followed a similar path in the last two centuries,<sup>[4]</sup> growing more and more complex and evolving from molecular chemistry, which deals with the formation and dissociation of covalent bonds, to supramolecular chemistry – “*chemistry beyond the molecule*”.<sup>[5]</sup> By analogy to biological evolution, chemistry has also adopted approaches which render it dynamic,<sup>[6,7]</sup> selective, evolutionary, and finally adaptive.<sup>[8]</sup>

The dynamicity in chemistry proceeds through many levels, from atoms and molecules of several Ångströms to assemblies of millimetric scale, with every increase in dimension leading to a higher level of complexity. Considering the possible relationships between multiple dynamics in a system, there are three ways in which two or more dynamic features can interact: 1) they can be isolated when one has no interaction with the other, 2) they can be concerned when a change in one enhances or diminishes the other one, or 3) they can be *in concerto*, tuned so that one cannot exist without the other one. The intertwined dynamic molecular processes are therefore another mean of generation of higher complexity.<sup>[9–17]</sup>

## 1.1. Types of molecular dynamics

The dynamicity of a molecule can be seen from different perspectives. For example, we can look at the geometry and relative positions of several parts of the molecule which may change in time. We may follow changes in bonding or we can observe an exchange of parts of the molecule. In all cases, we look at a process of one state of the matter changing into another state. Such a process takes a certain initial composition (input), and at a given rate produces an outcome (output) with certain probability. All three parameters, input, rate and output, are valid descriptors of the dynamic process and can serve as ways to classify different types of dynamics. The dynamic processes can be present at the same time or even one may be based on another. Altogether, they contribute to the inherent properties of matter which we observe at the macroscopic level.

In the following chapters, several types of dynamicity will be discussed in detail and it is therefore necessary to introduce them here. Some of the denominations for those types of dynamicity are generally accepted terms (conformational, constitutional) and will be used as such, while others have been used in a variety of contexts in the literature (motional, reaction) and will be defined only for the purpose of this thesis. As discussed already, some types of dynamicity inherently comprise other types. For example, it is impossible to perform oscillating reaction without breaking

and forming any bonds. Therefore the dynamics classification as such is hardly universal and reflects a somewhat subjective point of view.

### 1.1.1. Covalent constitutional dynamics

Constitution is the description of a molecule based on covalent bonds between atoms comprising the molecule. Therefore any change in constitution requiring at least one covalent bond to break and one to form is considered covalent constitutional dynamics. Among the most common processes qualified as constitutional dynamics are tautomerism, sigmatropic rearrangements, electrocyclic reactions or any exchanges of a part of the molecule for a different part, like in the imine exchange reaction.

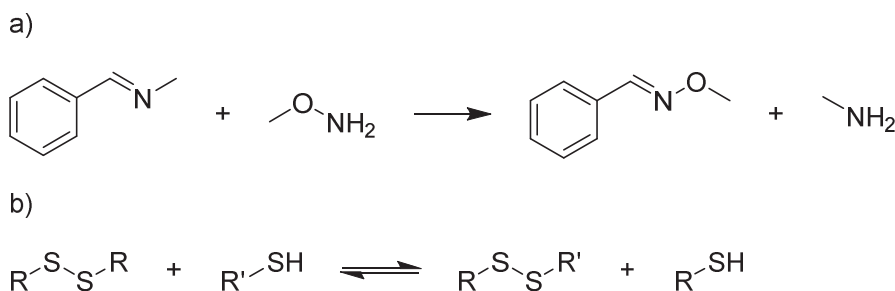


Figure 1.1-1 Covalent constitutional dynamics: a) reaction of an imine with methoxyamine to give an oxime and a free amine, b) reversible constitutional exchange of disulfides reacting with thiols.

General constitutional dynamics, taking into account also non-covalent bonds, is a key feature which enables the construction of dynamic combinatorial libraries (DCL), where a large pool of compatible components forms various possible combinations in one mixture. The construction of DCLs has attracted much attention recently<sup>[6,18–27]</sup> as this approach provides a fast and efficient way to readily generate and test large libraries of potentially active pharmaceutical molecules and circumvent the need for tedious and elaborate separate syntheses of thousands of chemical species and their expensive testing and purification. In order to form a DCL, many different components are mixed in one pot to form all possible combinations. The target (typically an enzyme, protein, active site, recognition pattern etc.) is then exposed to this dynamic mixture and its response (inhibition, activation, binding) is monitored. In fact, the effective species does not need to be physically present in the original dynamic mixture because the target of interest can favour the assembly of the effective molecule (“the lock assembles its key”<sup>[6,24]</sup>).

Covalent constitutional dynamics is change in structure of the molecule which requires covalent bond breaking and reforming.

### 1.1.2. Configurational dynamics

Configurational dynamics is closely related to the constitutional dynamics also requiring for a covalent bond to break and reform, but the product of the reaction has the same constitution as before the reaction differing only in the stereochemistry around an atom or a bond. The aspect of bond breaking/reformation is important in order to distinguish between similar processes. For example, the racemization of trisubstituted amines occurs through nitrogen inversion, while racemization of bromotriarylmethane occurs through the dissociation of the C-Br bond (formation of relatively stable carbocation and bromide) and C-Br bond reformation (Figure 1.1-2). The trisubstituted amine racemization is not considered configurational dynamics but the latter is. Similarly the *cis/trans* isomerism requires the dissociation of one of the bonds of the double bond to allow free rotation but atoms of the molecule have not exchanged, and therefore *cis/trans* isomerism is another example of configurational dynamics. The energetic barrier is not considered, thus the rate of the process is irrelevant.

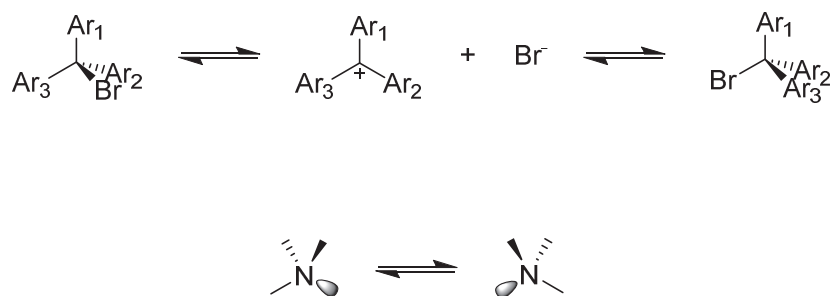


Figure 1.1-2 Isomerization of bromotriarylmethane is an example of constitutional dynamics since the C-Br bond must dissociate and reform for the inversion process to take place. On the other hand, a trisubstituted amine isomerises through nitrogen inversion mechanism and is therefore an example of motional dynamics (*vide infra*).

Configurational dynamics is a change in stereochemistry of an atom or a bond comprising for one bond breaking/reformation.

### 1.1.3. Motional dynamics

At the molecular level, motional dynamics describe a process of displacement of one molecule or its part with respect to another linked to it, wherein the linkage is broken and reformed in different positions. The nature of the linkage can range from covalent, to coordination, to hydrogen bonds and van der Waals interactions. One molecule or a part of it is considered as an internal inertial system, along or around is the second one moving. An example of motional dynamics in chemistry is the isomerization of trisubstituted amines (*vide supra*) or non-directional displacement of  $\eta^6$ -ruthenium in complexes with polycyclic aromatic compounds like anthracene or corannulene.<sup>[28]</sup> In biology, this motional dynamics is behind the epitomical molecule kinesin, which walks directionally along the microtubule in a cell (Figure 1.1-3).<sup>[29–37]</sup>

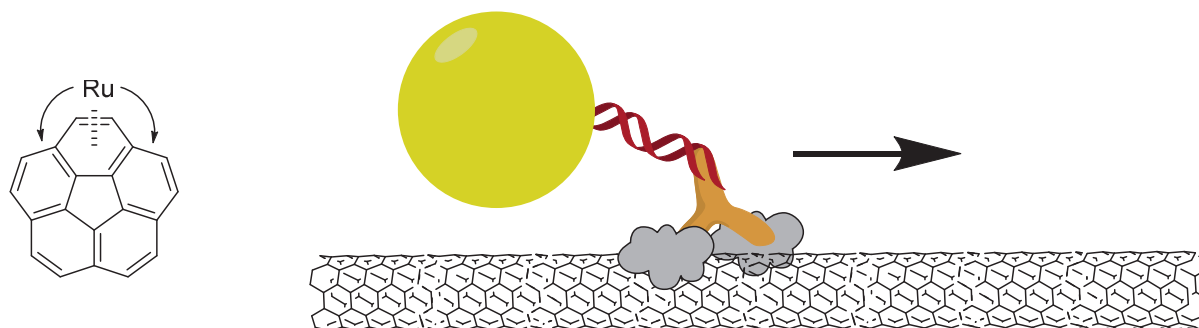


Figure 1.1-3 A fluxional ruthenium complex with corannulene is constantly moving by ruthenium displacement between the aromatic rings (left). Kinesin (right), the epitomical cellular walker, is transporting a cargo from the centre of the cell towards the surface along a microtubule track.

Motional dynamics is a process of displacement of only one molecule or its part with respect to another which can be described by a simple displacement vector.

### 1.1.4. Reaction dynamics

A chemical reaction is a basic process of transformation of matter, where reactants are consumed to give products at a certain rate under given conditions. The rate is investigated by reactions kinetics, monitoring the concentration of species over time to evaluate basic parameters: the order of the reaction, the rate constants and the activation parameters. On the other hand, the reaction dynamics do not concern the rate as the concept pertains to the ability of a reaction to give different products from the same starting material or mixture of starting materials as a function of applied conditions.



However, reaction dynamics and reaction kinetics may overlap in certain cases. For example, dynamic kinetic resolution<sup>[38]</sup> defines a concept following which a reaction gives different products due to very different kinetic parameters of two concurring reactions. One of the most famous applications of dynamic kinetic resolution is the hydrolysis of esters by lipase (known also in asymmetric version for enantiomer selection from racemic mixtures).

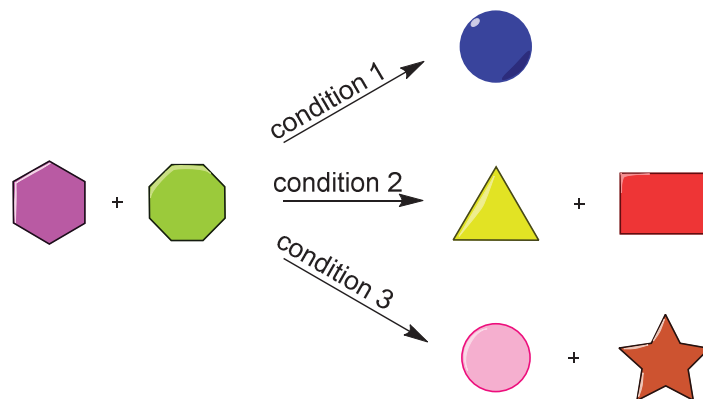


Figure 1.1-4 Schematic representation of reaction dynamics: reagents under different conditions form different products or product mixtures. Different conditions 1-3 can also hold for very different reaction time in case of dynamic kinetic resolution reactions.

Reaction dynamics is condition-modulated variability of the output of a reaction starting from the same reagent or mixture of reagents.

### 1.1.5. Other types of molecular dynamicity

#### Conformational dynamics

Conformation describes the relative position of different parts of the molecule at a certain moment. A change in conformation can be the result of a rotation around a single bond or elongation of the bond due to the thermal vibration. All molecules at temperatures above 0 K undergo conformational changes (vibrational only for diatomic molecules). There is, in principle, an infinite number of different conformations. Each conformation has a given energy and in equilibrium those conformations are distributed according to the Boltzmann distribution. The rate of interconversion between given conformations is determined by temperature and the energy barrier (energy of the transition state, deeply studied in case of cyclohexane<sup>[39–42]</sup>). The energy barrier strongly depends on the nature of the bond, its substituents and steric hindrance thus covering range from 3 kcal mol<sup>-1</sup> for the rotation of a methyl group in the molecule of ethane<sup>[43]</sup> up to *ca.* 40 kcal mol<sup>-1</sup> in case of 1,1'-binaphthyl-2,2'-diols (BINOL)<sup>[44]</sup> or hindered amines,<sup>[45]</sup> a value which makes the rotation practically impossible and leads to two separable conformational isomers – atropisomers (Figure 1.1-5).

Unlike motional dynamics, conformational exchange does not involve any bond dissociation and re-formation and cannot be described by a simple displacement vector. For example, in the case of cyclohexane inversion, half of the substituents move from an equatorial to axial position, but the second half is performing exactly the opposite displacement. Similarly, the racemization of BINOL derivatives implies a change in the relative position of the naphthalene rings, but the hydroxyl groups are displaced in the opposite direction and therefore it does not qualify as motional dynamics. Moreover, both of these examples of dynamics proceeds without any bond dissociation.



Figure 1.1-5 Cyclohexane and its derivatives (left) were thoroughly studied for their conformational dynamicity. Axially chiral binaphthalene derivatives like BINOL (right) are frequently used in enantioselective synthesis.

Conformational dynamics is such a process by which relative positions of the parts of a molecule change without breaking any bond.

### Oscillating chemical reactions

Oscillating chemical reactions repeat periodically without any addition of energy, fuel or external stimulus. There are only a few known reactions of this type: the Belousov-Zhabotinsky reaction, the Briggs-Rauscher reaction, the Bray-Liebhafsky reaction and the iodine clock reaction. They all are very similar, and rely on the periodically changing concentration of halogens (bromine, iodine) at different redox states. A typical setup requires iodate, hydrogen peroxide, malonic acid and a strong mineral acid, with starch being used to magnify the visual effect. In the case of the iodine clock reaction, the iodate is reduced by hydrogen peroxide to iodine (coloured) which is then oxidised by hydrogen peroxide back to iodate. Thus, hydrogen peroxide acts as both an oxidising and a reducing agent. Moreover, the difference in relative rates of the two reactions enables observation of periodic colour changes.<sup>[46–49]</sup>

### Brownian motion

At temperatures above 0 K all atoms and molecules are in constant movement called Brownian motion. While a single isolated molecule would move constantly straight, the Brownian motion is chaotic as a result of frequent atomic or molecular collisions. Therefore the Brownian motion is linked to the characteristic of bulk. In general use, the term “Brownian” is used to denote processes which happen spontaneously, randomly and do not require any activation energy.<sup>[50,51]</sup>

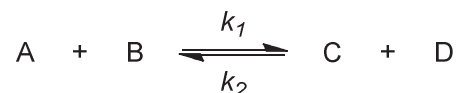
## 1.2. Reversible chemical reactions

Reversibility represents a unique feature in chemistry. It may be looked at as a way to go back one step and, if needed, to grant the possibility of repairing an error made. For example, the replication of the genetic information from one cell to a whole human body necessitates billions of billions of nucleobase to nucleobase “copy/paste” steps, with even a single error becoming potentially fatal. Even the most reliable copying mechanism cannot ensure an error-free copy of such a large amount of information, which means that this information would not propagate to next generations unless a repair mechanism was present.<sup>[52–55]</sup> On the other hand, the reversibility also presents an opportunity of diversification and adaptation as certain distribution of products can redistribute upon the application of an external stimulus.<sup>[7,23,56]</sup>

A reversible chemical reaction is one which leads to an equilibrium mixture of products and which can go in either direction upon a change in conditions, as stated by the Le Chatelier’s principle.<sup>[57,58]</sup> The chemical reversibility was described for the first time by Berthollet in 1803 who noticed that in salt lakes calcium carbonate can react with sodium chloride to give calcium chloride and sodium carbonate, an opposite outcome to the known reaction at that time.<sup>[59]</sup> He also correctly pointed out that the conditions determine which direction the reaction proceeds: “*Les circonstances qui peuvent favoriser l’efflorescence sont un mélange convenable de muriate de soude et de*

carbonate de chaux et une humidité soutenue à une température élevée;... C'est par ces circonstances, que j'ai observées sur les bords du lac Natron, que j'ai cru pouvoir expliquer la formation continue d'une immense quantité de carbonate de soude.<sup>[59]†</sup>

Under given conditions, a reaction gives a certain ratio of reactants and products which is called equilibrium constant  $K$  and for a reaction

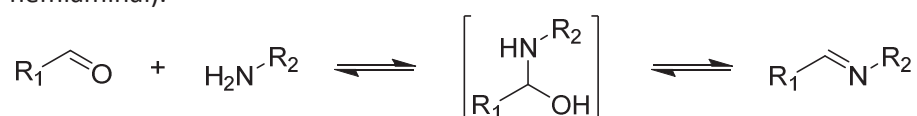


with  $k_1$  being the rate of forward and  $k_2$  the rate of backward reaction, it is defined as<sup>[60]</sup>

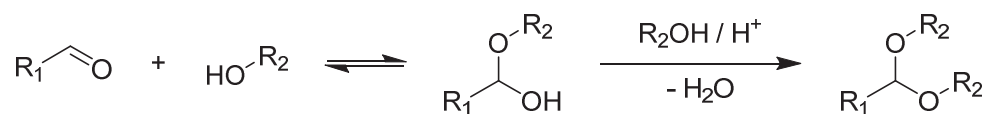
$$K = \frac{[C][D]}{[A][B]} = \frac{k_1}{k_2}$$

Among the most studied reversible chemical reactions are:

- **Imine formation and exchange** – a reaction between a carbonyl compound and an amine to form an imine. The reaction proceeds through a hemiaminal intermediate which can or cannot be observed in the reaction mixture. Hemiaminal formation and decomposition are therefore inherently reversible. Imines can also react with amines to perform a fully reversible imine exchange (or transimination), that involves formation of the reversibly formed aminal intermediate (of similar properties to hemiaminal).<sup>[61–66]</sup>



- **Hemiacetal (acetal) formation and exchange** – addition of a hydroxyl group to a carbonyl to form a hemiacetal (or hydrate in case of reaction with water). The second step, the formation of the acetal, has the equilibrium strongly shifted towards the starting materials and requires the removal of water under acidic catalysis to effectively produce the acetal. The reverse reaction, hydrolysis, usually occurs rapidly in slightly acidic aqueous media. Both acetals and hemiacetals can react with alcohols to perform a transacetalization, reversible exchange reaction analogous to transimination.<sup>[67–69]</sup>



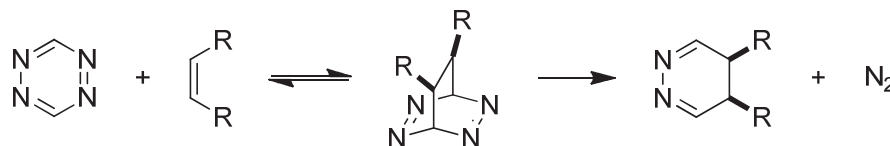
- **Metathesis** – two alkenes react to form a new pair of alkenes with exchanged substituents attached to the double bond, which proceeds through a double [2+2] electrocyclic reaction catalysed by Grubbs catalyst. In principle, the reaction is reversible but in practice, the elimination of ethylene gas is required to drive the reaction one way.<sup>[70]</sup>



- **Reversible electrocyclic reactions and rearrangements** – the most famous reversible electrocyclic reaction is the Diels-Alder reaction, a [4+2] cycloaddition of a diene to an alkene (dienophile).<sup>[71]</sup> Retro-Diels-Alder reactions usually take place when very

† „The conditions which favour precipitation are a convenient mixture of sodium chloride and calcium carbonate and enhanced humidity at higher temperatures;... It is due to these conditions that I was able to explain the continuous formation of extensive amounts of sodium carbonate on the shores of the Natron lake.“

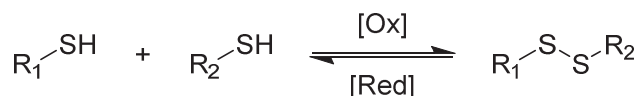
stable small molecules (typically  $N_2$ , making the reaction irreversible) or when large conjugated  $\pi$ -systems are produced.<sup>[72]</sup> The Claisen and Cope rearrangements are among the most famous reversible rearrangements.<sup>[73]</sup>



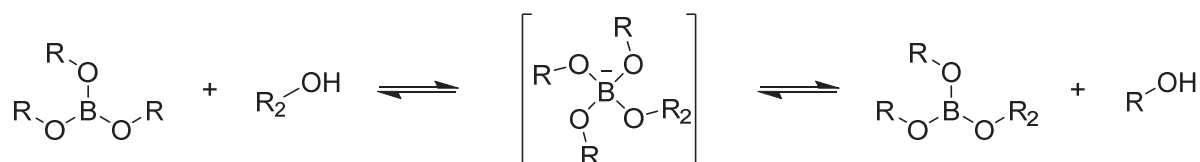
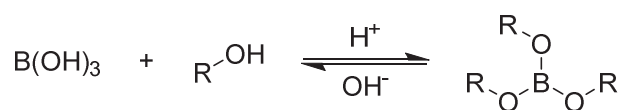
- **Michael/retro-Michael reaction** – the addition of a nucleophile to the double bond of a  $\alpha,\beta$ -unsaturated carbonyl or similar conjugated electron-accepting compounds. The  $\alpha,\beta$ -elimination is called retro-Michael reaction and occurs readily in cases involving good leaving groups, formation of a large conjugated  $\pi$ -systems or in cases of highly acidic protons in the  $\alpha$ -position.<sup>[74–76]</sup> An example of the tandem Michael addition/retro-Michael elimination is the Morita-Baylis-Hillman reaction.<sup>[77–80]</sup>



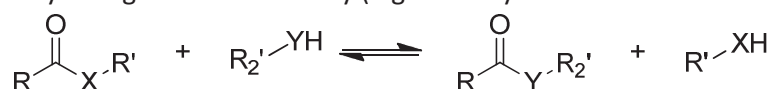
- **Thiol-disulfide redox reaction and disulfide exchange** – a reversible oxidation of two thiols to form a disulfide bond. The disulfide can be readily reduced under mild conditions. The disulfides react with thiols under basic conditions to exchange one of the thiolates bound in the disulfide.<sup>[19,20,22,56,81–84]</sup>



- **Boronic esters** – boronic acids are readily formed from boronic acids and alcohols and easily hydrolysed under basic condition to give boronates. The electron-deficient character of the boron atom also enables boronic trans-esterification reactions to occur under mild conditions.<sup>[85]</sup>



- **Transacylation** – the transfer of the acyl group formed from a carboxylic acid. This transfer may result in retention of the functional group (e.g. transesterification) or may change the functionality (e.g. aminolysis of esters to form amides).<sup>[38,86–96]</sup>



$X, Y = O \text{ or } NH$

- **Coordination bond formation and exchange** – the formation of metal complexes and ligand exchange has been deeply documented in the literature. The possibility of having several oxidation states of the coordinating metal adds another level of complexity to the system.<sup>[15,20,97–106]</sup>

Among the reversible reactions described thus far, the imine formation and exchange are particularly attractive because it amalgamates interesting features:

1. They can be performed in a vast variety of solvents, from water to cyclohexane, with very different polarities, being limited only by the solubility of the reactants.<sup>[107]</sup>
2. They can be modulated by many stimuli, such as pH, solvent polarity and composition,<sup>[107,108]</sup> presence of coordinating metals<sup>[102,109]</sup> or even electric field.<sup>[110]</sup>
3. The reactions proceed under mild conditions, typically at room temperature and within a pH range of 4 - 10, and can be performed in biocompatible media.
4. A large pool of the reagents are commercially available, many are found in nature and have a biological effect.
5. A large variety of protocols exist for the synthesis of amine and aldehyde derivatives.
6. The aldehyde and amine functional groups are not in principle toxic.

### 1.3. General aspects of the imine bond

Imines are characterised by the presence of a carbon - nitrogen double bond (Figure 1.3-1). In the literature, imines are often referred to as Schiff bases, being named after the German-Italian chemist Hugo Schiff who prepared them for the first time,<sup>[111]</sup> and bases due to their weak basic character. However, many misuses and misinterpretations of the term “Schiff base” are common among chemists. The IUPAC Glossary<sup>[112]</sup> defines a Schiff base as an imine subclass of general formula  $R'N=CR_2$ , where  $R' \neq H$ . Other commonly used name is “azomethine”, which originally designated compounds of the general formula  $R'N=CHR$  but is now considered synonymous with the term Schiff base, and the name “anil” - defined by a general structure  $R'N=CR_2$ , where  $R'$  = phenyl or a substituted phenyl group. Imines are also differentiated according to the nature of their parent carbonyl compound: imines derived from aldehydes are called aldimines, imines arising from ketones are referred to as ketimines.

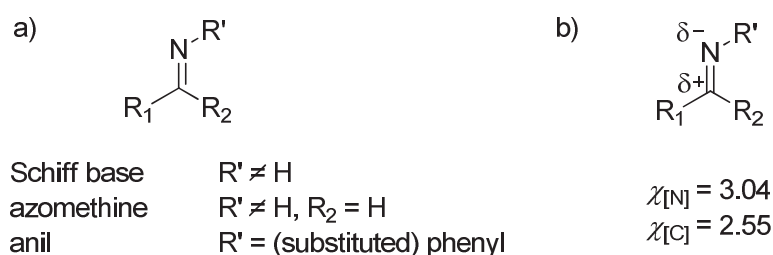


Figure 1.3-1 a) Schematic structure and nomenclature of imines according to IUPAC. b) The electronegativity difference between carbon and nitrogen atoms causes polarization of the double bond to give the partial charges indicated.

Like the carbon - oxygen double bond of a carbonyl, the imine bond is polarised due to the difference in atom electronegativity, which generates a partial negative charge on the nitrogen atom. The polarisation makes the imine susceptible to attack on the electrophilic carbon atom by a variety of nucleophiles, such as water (causing hydrolysis to give the carbonyl compound and amine via the intermediate hemiaminal, older works use the term “carbinolamine”), alcohols (giving hemiaminals

and acetals), thiols (giving thio(hemi-) aminals) or amines to perform an imine exchange reaction (sometimes called transimination, discussed in Chapter 2.3 on page 56) via aminal intermediates.

The electrophilicity of the imine carbon varies with the electronic properties of its substituents and parallels that of carbonyl compounds. The electrophilicity can be quantified by measuring the relative rate of reaction with a given nucleophile.<sup>[113]</sup> As expected, electron-withdrawing substituents, such as nitro group, halogens or carbonyl, increase the reactivity towards nucleophiles while electron-donating groups like the hydroxyl or dimethylamino decrease the rate of reaction. These electronic effects propagate through a conjugated  $\pi$ -system. The electron-withdrawing character of the  $\text{CF}_3$ - group also has a strong effect on the  $\text{sp}^2$  carbon of the carbonyl or imine when attached directly, rendering the double bond extremely polarised. Trifluoromethyl ketones and imines thus show different behaviours than other carbonyl compounds and favour the formation of compounds with an  $\text{sp}^3$  carbon configuration, like hydrates, hemiacetals, acetals, hemiaminals or aminals, depending on the type of nucleophile.<sup>[114,115]</sup>

Aldimines and unsymmetrical ketimines can exist in two configurations along the imine double bond: *Z* (*cis*) and *E* (*trans*), the latter being generally favoured for steric reasons. The configuration can be flipped by UV-irradiation from *E* to *Z*; however the thermal relaxation to the thermodynamically favoured *E* isomer generally proceeds quickly through a lateral nitrogen inversion process.<sup>[116–121]</sup> A kinetically stable *Z* configuration has been observed in the case of hydrazones, acylhydrazones<sup>[10]</sup> and oximes (Figure 1.3-2).<sup>[121–124]</sup>

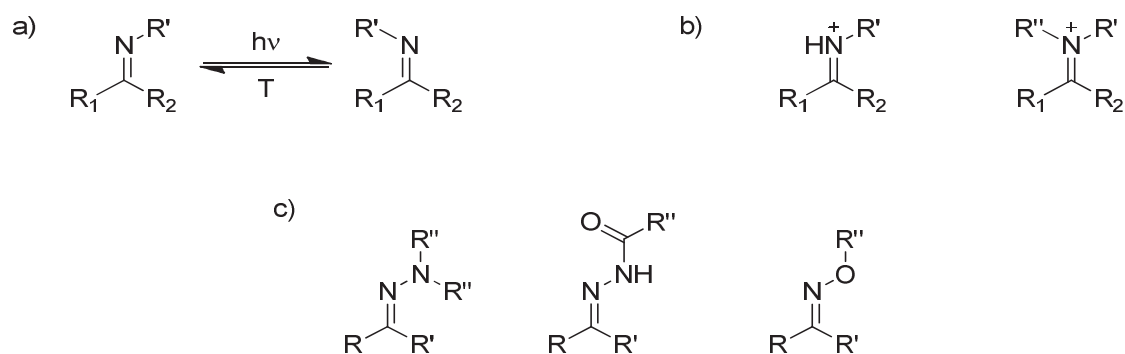


Figure 1.3-2 a) The thermodynamically favoured *E* form of imine can isomerise to the metastable *Z* form by UV irradiation. The transformation back to the *E* form proceeds thermally by nitrogen inversion. b) Imines can be protonated to form the iminium salts; secondary amines also condense with carbonyls to form iminium salts. c) Structural analogues of imines: hydrazones are formed by reaction of a carbonyl compound with hydrazine or its derivative with one  $\text{NH}_2$  group; acylhydrazones are formed from hydrazides; oximes are formed from hydroxylamine or its *O*-alkyl derivatives.

Imines are weakly basic compounds which can be protonated by strong acids, like sulfonic acids.<sup>[125]</sup> Cationic iminium species are also formed by reacting a secondary amine with a carbonyl under acid catalysis and water removal (molecular sieves, azeotropic distillation) or by alkylating imines with strong alkylating agents such as dimethyl sulfate or methyl iodide. The resulting iminium salts are unstable and react readily with any nucleophile, usually water, ultimately leading to hydrolysis of the imine to give the carbonyl compound and protonated amine.

### 1.3.1. Imine formation and imine exchange

#### 1.3.1.1. *Mechanism of imine formation*

Imines are formed by the reaction of a carbonyl compound with an amine and the mechanism has been studied in great detail by Jencks and Leussing.<sup>[61–64,126–130]</sup> During the course of the reaction (Figure 1.3-3), the electrophilic carbon atom of carbonyl group **1** is attacked by the

nucleophilic nitrogen atom of amine **2** followed by a shift of an electron pair from the double bond to the oxygen atom. This zwitterionic intermediate **3a** is highly unstable and can either revert to starting materials or be stabilised by a protonation/deprotonation sequence to give a hemiaminal intermediate **3c**. The stability of the hemiaminal strongly depends on the nature of the substituents and the reaction conditions. As a result, the hemiaminal either goes undetected as in case of aromatic aldimines or represents the major species present in the solution, a situation encountered in the formation of aliphatic ketimines. In the following step, the hydroxyl group of the hemiaminal intermediate **3c** gets protonated turning it into good leaving group **3d**. After elimination of a molecule of water, the positive charge on carbon atom is compensated by the electron pair of the nitrogen atom forming a double bond. The positively charged iminium ion **4a** is stabilised through deprotonation by the medium, giving the final imine compound **4b**.

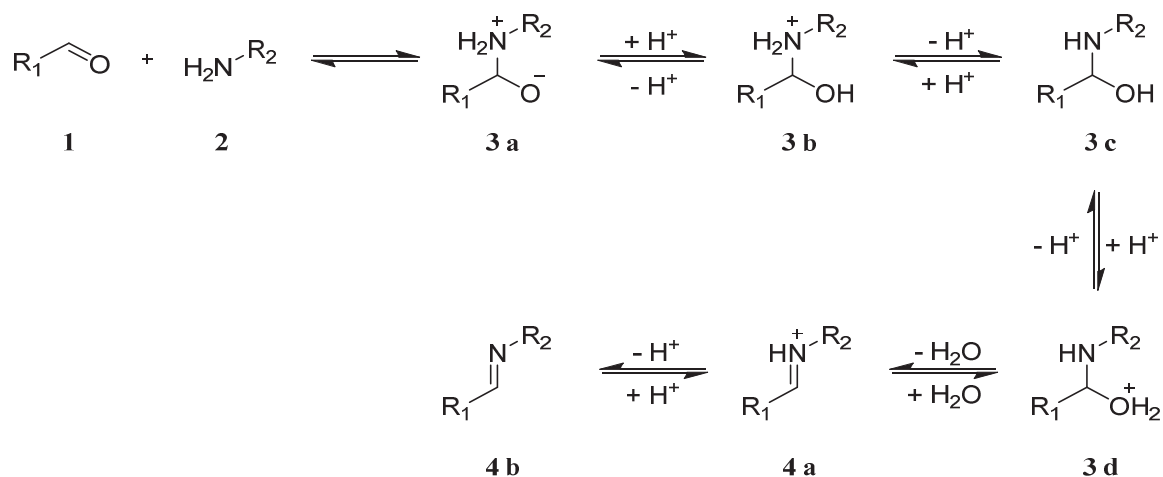


Figure 1.3-3 A plausible mechanism of imine formation. Multiple protonation and deprotonation steps are formally involved, with the protons coming from the solvent, usually protic, or from residual water in the solvent. The aldehyde reacts with the amine to form the hemiaminal (older works use the term “carbinolamine”) which is sometimes observable as an intermediate.

It is important to note several characteristics of the imine formation reaction mechanism:

- 1.) All steps are fully reversible and the equilibrium of the reaction can be shifted in either direction by changing the conditions.<sup>[61]</sup>
- 2.) Water is eliminated in the forward reaction and thus imine formation is disfavoured in aqueous media or in the presence of adventitious water.<sup>[107]</sup>
- 3.) The elimination step leading to the imine is acid-catalysed while the addition step is inhibited by the protonation of the amine. Therefore, pH is a key parameter that affects both the kinetics and the thermodynamics of the reaction.<sup>[61,62,64]</sup>

There are several other reactions which give imine compounds. Among the most interesting transformations is the proline-catalysed C=C/C=N exchange reaction of 5-arylidene barbiturates and imines. The aldehyde residues undergo dynamic exchange to give rise to a new imine and a new 5-arylidene barbiturate (Figure 1.3-4).<sup>[131]</sup>

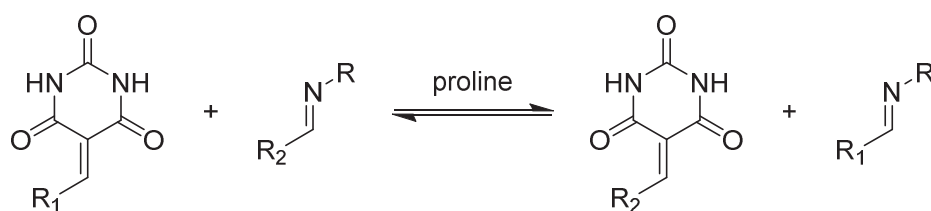


Figure 1.3-4 Reversible aryldene exchange between imines and barbiturates (catalysed by proline).



### 1.3.1.2. Mechanism of imine exchange

The imine exchange reaction, sometimes called transimination, is a general term applied to all reactions in which one of the imine components, aldehyde or amine, is exchanged for a different moiety. There are three possible mechanisms: 1.) imine hydrolysis and reformation, 2.) amine exchange, 3.) imine metathesis. Each of these mechanisms can be used to explain the imine exchange reaction under different conditions.

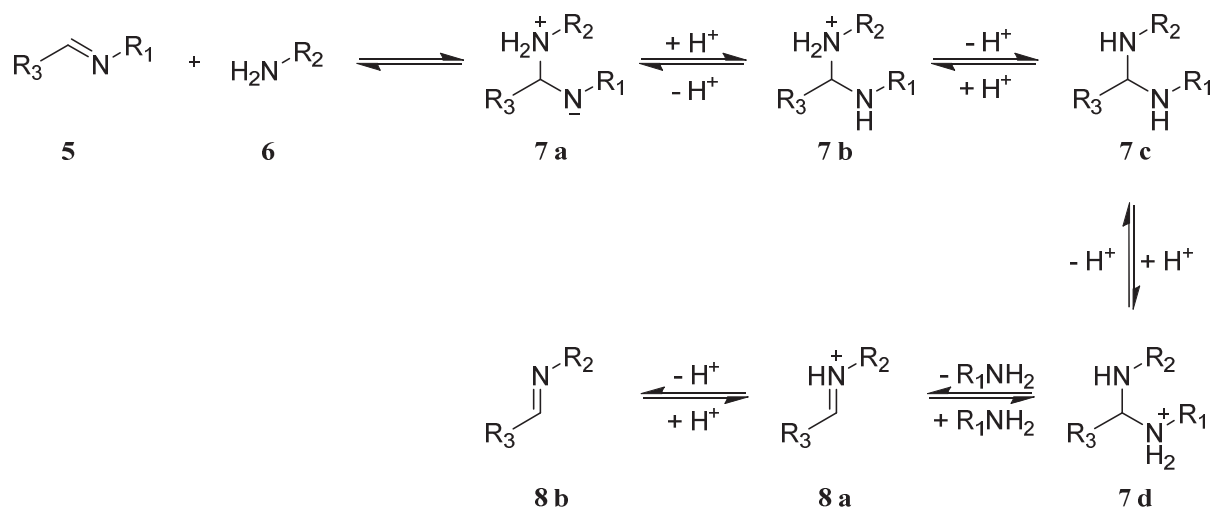


Figure 1.3-5 Elementary steps of the mechanism of the amine exchange reaction. The character of  $R_3$  strongly affects the composition of the reaction mixture. For example, when  $R_3$  is 2-hydroxyphenyl no aminal intermediates are observed in the NMR spectrum. On the other hand, when  $R_3$  is 2-pyridyl, the aminal is usually the dominant species in the solution.

The amine exchange mechanism occurs through a nucleophilic attack of the imine by the unbound amine to form an iminal intermediate, which then releases the original amine moiety to form the new imine (Figure 1.3-5).

The imine hydrolysis mechanism is favoured when the aldehydes are in large excess over the amine, so that all the amines are bound as imines. The reaction is simply the reverse of the imine formation process described above, involving a hemiaminal intermediate. The liberated amine can then react with another aldehyde.

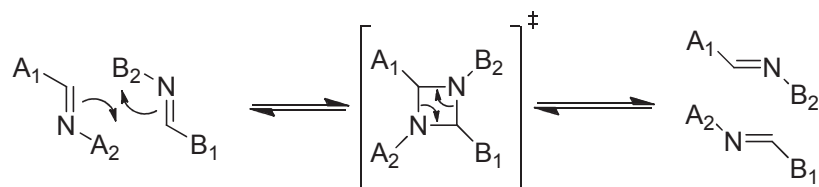


Figure 1.3-6 Proposed mechanism for imine metathesis through the [2+2] cycloaddition of two imines.

The imine metathesis mechanism may apply when only imines are present in solution and in the absence of water or amine. It involves the [2+2] cycloaddition of the two imine bonds forming a 1,3-diazetidinium intermediate, which undergoes retro [2+2] cycloaddition to give the original or a new pair of imines (Figure 1.3-6). However, establishment of this mechanism is difficult since absolutely anhydrous conditions are practically impossible to achieve and residual water in the mixture can be responsible for the occurrence of the reaction. It is noteworthy that all imine exchange mechanisms are, in principle, reversible.



### 1.3.2. Imines in coordination chemistry

The nitrogen atom of the imine bond has a lone pair of electrons which can be employed in formation of coordination bonds with metals or metal cations. As imines are formed by condensation of an amine with a carbonyl compound, a large array of imines can be readily created without the need of tedious syntheses of a large number of well-defined ligands. In this manner, imine ligands formed either by conventional synthesis or *in situ* have indeed been used with various metal ions to build diverse supramolecular architectures,<sup>[98,105,132–140]</sup> molecular containers,<sup>[141–143]</sup> to design many different specific salen-type catalysts,<sup>[144–148]</sup> specific sensors,<sup>[149–151]</sup> luminescent molecules,<sup>[152–154]</sup> and in many other applications.

The coordination bond between the metal ion and the imine nitrogen is in fact formed reversibly, like the imine linkage itself, and the energy of this bond strongly depends on the character of the metal, its oxidation state and the steric hindrance introduced by the imine ligand. Therefore, metal complexes of imines exhibit double dynamics, the covalent imine dynamics and the metal coordination dynamics. This feature has been used in the formation of doubly dynamic combinatorial libraries.<sup>[103,137,142]</sup> A further combination with disulfide linkages has been studied as an example of a triply dynamic systems.<sup>[56]</sup>

The presence of a coordinating cation during the imine formation may affect both kinetics and equilibrium compositions,<sup>[128]</sup> and several divalent metals like lead, cadmium, manganese, magnesium or zinc have been shown to exert a strong effect.<sup>[127]</sup> Typically,  $Zn^{2+}$  catalyses the formation, hydrolysis and exchange of the imine, and also changes the rate determining step under neutral pH by trapping the hemiaminal intermediate.<sup>[155]</sup> Also, the involvement of the nitrogen lone pair in the formation of a dative bond with a metal leads to a stronger polarisation of the imine bond and thus facilitates the imine exchange reaction in the presence of a competitive amine.<sup>[64,101,109]</sup> On the other hand, imines formed from reagents bearing electron-donating groups bind more strongly to the metal.<sup>[109]</sup>

An important issue concerning the imine process in the presence of coordinating cations is to distinguish if, the reaction proceeds in the coordination sphere of the metal, or if the binding occurs after the imine is formed. This difference has already lead to contradictory results in the literature, for example in reporting on  $Cu^{2+}$  ion activity: if the stability of the complex between copper and a reacting amine is low (like in case of ethylamine), McDonnell *et al.* reported copper as a highly active catalyst for imine formation and hydrolysis.<sup>[155]</sup> But if the complex is strong (such as that of amino acids acting as bidentate ligands) the ability of the amine nitrogen for nucleophilic attack on the carbonyl is lowered due to coordination, thus the reaction can only proceed with the non-coordinated substrate and negligible activity of  $Cu^{2+}$  is reported by Hopgood and Leussing.<sup>[127]</sup>

Nucleophiles coordinated to metal cations are still able to react with suitable electrophiles.<sup>[156]</sup> For example, a cobalt(III) complexes bearing five ammonia groups and one  $\alpha$ -ketopropionate are stable under acidic or neutral conditions, but quickly react if a strong base is added leading to deprotonation of one of the ammonia groups and its subsequent reaction with the neighbouring carbonyl of the ketopropionate to give an imine.<sup>[157–159]</sup> Both the amine and carbonyl compounds, as well as the resulting imine, are bound to the metal during the entire course of the reaction, and therefore the process occurs exclusively in the coordination sphere of the metal. In a similar fashion, other transformations have been examined within a coordination sphere, such as the synthesis of long coordinating polyamines,<sup>[157,160,161]</sup> and tandem imine formation-electrophilic alkylations.<sup>[162]</sup> Furthermore, the reactivity of different metal centres have also been investigated.<sup>[163]</sup>

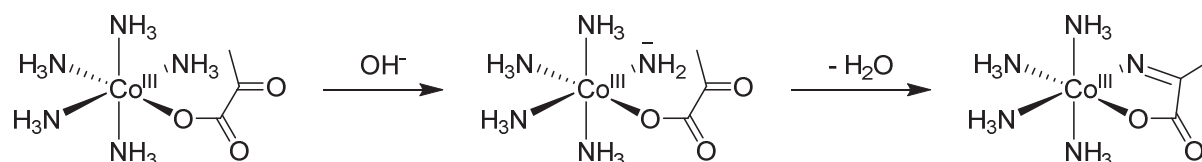


Figure 1.3-7 The formation of imine in the coordination sphere of  $\text{Co}^{3+}$  ammonia complexes. Strong base is needed for deprotonation of one of the ammonia groups and the reaction with ketopropionate to occur.

Polyamines bearing more than one amino group, and imines derived from those amines, can wrap around one coordinating metal, or covalently link several coordination spheres. In the case of ethyleneimine oligomers and their derived imines, polynuclear complexes with controllable distances between metal cations can be formed.<sup>[164–166]</sup> If the polyamines are mixed with aldehydes in a certain ratio, that only some of the amino groups can form imine, a tautomeric equilibrium between imine and aminal is established. Nice example has been demonstrated by Drew *et al.*<sup>[167]</sup> where clever design of a ligand allowed for the construction of a dynamic cavity which can adjust the size to fit a series of different coordinating metals (Figure 1.3-8).

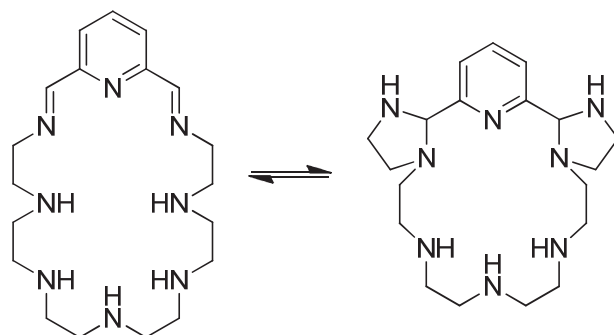


Figure 1.3-8. Ring contraction and expansion to accommodate different sized metal ions in the cavity.<sup>[167]</sup>

In fact, the coordination to a metal can also stabilise and favour the formation of the hemiaminal intermediates when condensation to imines cannot proceed.<sup>[168]</sup> In some specific cases, the condensation of amines with carbonyls can be switched between the imine and the aminal formation and *vice versa*. For example, under pH control, tris(aminomethyl)phosphine was reacted with benzaldehyde derivatives (Figure 1.3-9) and formation of triazaphosphadamantane was observed,<sup>[169]</sup> instead of the expected chelating tris-imine.<sup>[170–172]</sup>

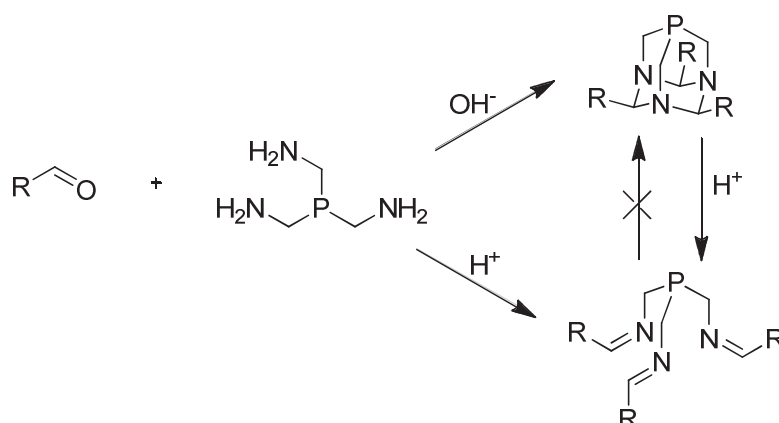


Figure 1.3-9. Formation of either an the imine or the aminal can be, in specific cases, controlled by pH, like in case of the condensation of an aldehyde with tris(aminomethyl)phosphine.<sup>[169]</sup>

The coordination sphere of a metal cation is geometrically organised and the atoms of the participating ligand are forced to occupy defined positions around the metal, which in turn leads to

generation of distinct stereoisomers.<sup>[173]</sup> The preorganization of the coordination sphere has served as a template for the synthesis of various imine-based inherently chiral helical structures.<sup>[174–176]</sup> Due to the dynamic nature of the bonds employed in their formation, those helicates can invert stereoselectively upon a stimulus,<sup>[98,177]</sup> or can undergo long-range structural reorganisation leading to dramatic change in length of the molecule.<sup>[178]</sup>

Imines derived from diamines and salicylaldehyde derivatives are called *salen* ligands.<sup>[125]</sup> They form very stable complexes even with weakly coordinating metals which are supported by deprotonation of the phenolic OH groups, thus leading to charge balancing of the metal cation. These complexes are widely used as catalysts.<sup>[144–146,179–181]</sup> Bis-imines formed from pyridine-2,6-dicarboxaldehydes are called pincer ligands and represent another group of common catalysts (Figure 1.3-10).<sup>[147,148,182–186]</sup>

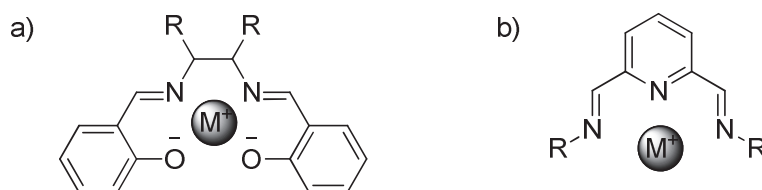


Figure 1.3-10 a) The salen ligand complexes are formed from a metal cation, a diamine and two molecules of salicylaldehyde or its derivatives. The ligand has four coordinating sites, comprising two imine nitrogens and two phenolic oxygens; deprotonation of the phenols balances the positive charge of the cation and thus leads to a stronger binding.

Introduction of a chiral group to the coordination sphere of a metal has been shown to cast enantioselectivity and diastereoselectivity upon the alkylation reactions of substrates bound in its coordination sphere.<sup>[187–189]</sup> Amino acids are widely used as chiral selectors as they are readily commercially available in very high enantiomeric purity. To this extent, amino acids, including the only non-chiral amino acid glycine, have been reacted enantioselectively with aldehydes to give  $\alpha$ -amino- $\beta$ -hydroxycarboxylic acids.<sup>[187–189]</sup> Pyridoxal, a naturally occurring aldehyde, also forms complexes with coordinating metals.<sup>[126,190]</sup>

### 1.3.3. Vitamin B6: biological imine-amine carrier

Amino acids are fundamental building blocks of living organisms. Based on their availability, they are divided into two groups: essential amino acids which cannot be synthesised in the human body, and non-essential ones which are formed metabolically. The metabolic pathway of the synthesis of amino acids involves the enzymatic reductive amination of  $\alpha$ -ketocarboxylic acid (provided by the Krebs cycle<sup>[191]</sup>) by a cofactor pyridoxamine 5'-phosphate, generally called vitamin B6 (Figure 1.3-11).

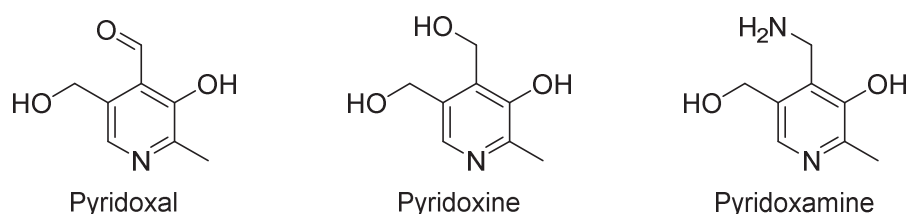


Figure 1.3-11 Vitamin B6 consist of three similar compounds, pyridoxal (aldehyde), pyridoxine (alcohol) and pyridoxamine (amine), which are interconverted in an organism. Active forms of the species are phosphorylated on position 5'.

The scheme of the transamination mechanism is presented in Figure 1.3-12. Initially, pyridoxamine **9** forms an imine **10** with the carbonyl group of the  $\alpha$ -ketocarboxylate. The imine then undergoes two-step pseudo hydride shift: first, by simultaneous action of a base on the benzylic

hydrogen and protonation by acid on the nitrogen atom of the pyridine ring, a quinoidal intermediate **11** is generated.<sup>[192,193]</sup> In the next step, the proton is transferred from protonated base to the  $\alpha$ -carbon of the carboxylate with concomitant deprotonation of the pyridine to restore the aromatic system **12**. However, the carbon-nitrogen double bond is now shifted, and consequently, the  $\alpha$ -ketocarboxylate has been reduced to an amino acid and pyridoxamine is oxidised to an imine. After hydrolysis, the pyridoxal 5'-phosphate (P5P) **13** is liberated. P5P is a naturally occurring aldehyde, which together with pyridoxamine and pyridoxine (Figure 1.3-11) form so called vitamin B6 group.<sup>[194]</sup> P5P serves as a cofactor in the biochemical decomposition (digestion) of amino acids.<sup>[195]</sup>

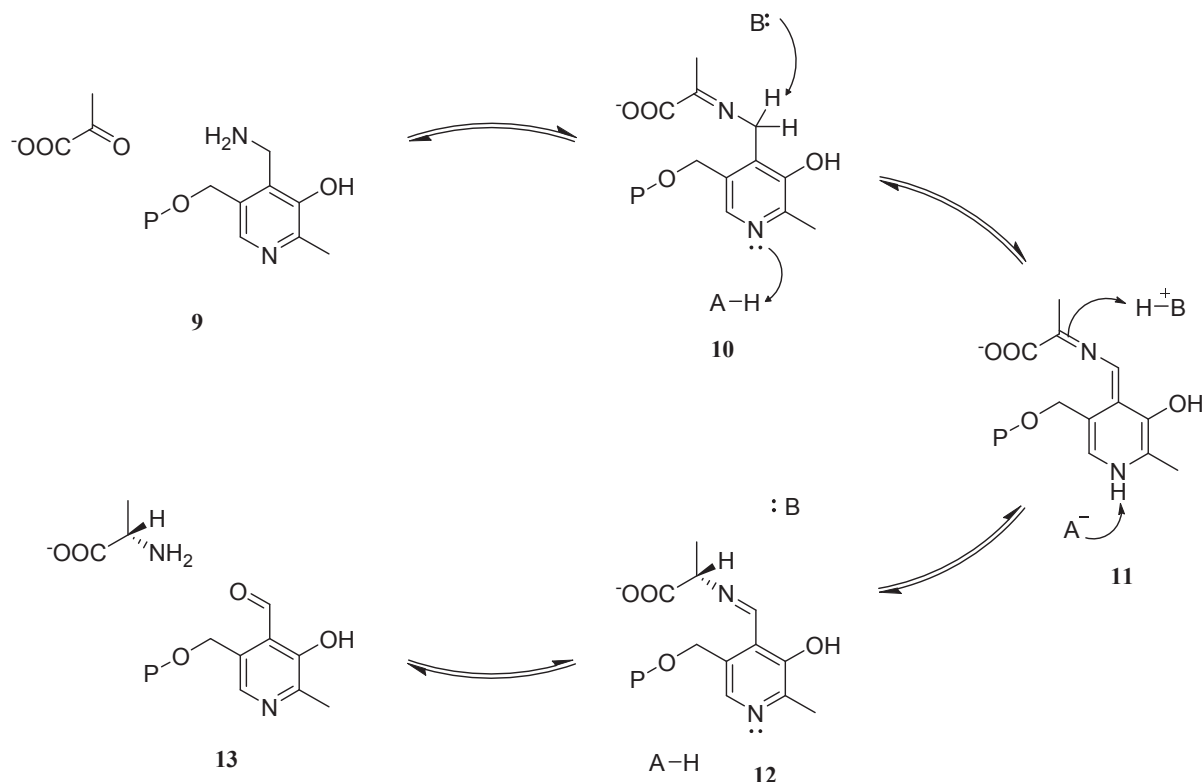


Figure 1.3-12 The mechanism of the synthesis of amino acids by P5P-mediated reductive amination of  $\alpha$ -ketocarboxylate involves formation of the imine, followed by a pseudo hydride shift and imine hydrolysis. The carbon-nitrogen double bond shift during the reaction is facilitated by formation of the conjugated quinoidal structure of the protonated pyridine ring. P in the scheme denotes phosphate,  $PO_3^{2-}$ .

The importance of transamination reactions in the organisms has triggered extensive research efforts in the field of Schiff bases of pyridoxal<sup>[129,196–205]</sup> and their analogues, and several general trends for the imine formation can be extracted. For example:

1. the formation of the imine is enhanced by higher pH<sup>[107,206,207]</sup>
2. branching at the  $\beta$ -position of the carboxylic acid stabilises the imine<sup>[208,209]</sup>
3. the presence of a coordinating metal increases the rate of imine formation and its stability<sup>[126,210,211]</sup>
4. a fluorine-imine gauche effect was demonstrated<sup>[212]</sup>
5. P5P has been used to label specific amino acid residues in enzymes<sup>[213]</sup> or to prepare relatively stable iminium species<sup>[214]</sup>
6. aliphatic diamines form equilibrium mixtures of imine and cyclic amins<sup>[215–217]</sup>

The equilibrium between the cyclic aminal and the open imine form in the case of pyridoxal and aliphatic diamines represents an interesting feature involving the displacement of an aldehyde residue between two nitrogen atoms. It is also type of transformation which can be linked to motional and constitutional dynamics.

## 2. THE IMINE BOND – A VERSATILE CHEMICAL LINKAGE

### 2.1. Concept

Imines are among the most frequently used types of compounds in dynamic covalent, adaptive and supramolecular chemistry due to their ease of formation, reversibility and exchange. Successful construction of a functional dynamic covalent system relies upon three basic features: 1) high conversion of the constituents to products, 2) fast rate of formation of the system and 3) fast response to stimuli applied on the system.<sup>[19,20]</sup> High conversion is necessary for the efficiency of formation of the system, while the rate of formation and exchange are desired for practical reasons, i.e. reduced lag time between mixing the components or a stimulus application, and the time at which the system reaches thermodynamic equilibrium. Such systems are referred to be under thermodynamic control, unlike conventional organic reactions which are controlled kinetically.

The heteromeric linkage of the imine double bond consists of the fusion of an amine and carbonyl. The question which arises from this bond asymmetry is “What are the ideal amines and carbonyls required to yield imines in the shortest amount of time, with maximum conversion and rapid exchange?”

The reactivities of different amine derivatives have been studied, and now the scale of nucleophilicity of amine derivatives forms part of any organic chemistry textbook. Further experiments have been performed by Dr. Manuel Chaur and Sirinan Kulchat<sup>‡</sup> in our group with the following outcome: aldehydes react the fastest with primary amines (giving imines), slightly slower with hydrazines (forming hydrazones), followed by hydrazides (forming acylhydrazones) and finally hydroxylamines (giving oximes). The ease of the exchange reaction decreases with lower rates of formation of those products, i.e. exchange of an amine in imine proceeds under milder conditions than that of an oxime. When all four amine derivatives are mixed together (amine, hydrazine, hydrazide and hydroxylamine) and reacted with an aldehyde, immediate formation of the most stable oxime is observed, perhaps due to faster reaction of a hydroxylamine derivative with an imine compared to reaction with an aldehyde. This observation is in agreement with the result of Jencks *et al.*<sup>[63,130]</sup> stating that the rate determining step of the imine exchange reaction is the proton transfer in the amination intermediate<sup>§</sup>. On the other hand, the reactivities of aldehydes have been explored only partially in terms of the electrophilicities of various carbonyl compound derivatives.<sup>[113]</sup> Similarly to the nucleophilicity of amines, the electrophilicity of aldehydes determines only part of its efficacy and suitability for the imine-based dynamic covalent systems.

This chapter describes the studies of reactivities of different carbonyl compounds and provides experimental characterisation of the roles of various substituents either directly attached to the carbonyl or to different positions on the aromatic ring of various aromatic aldehydes.

<sup>‡</sup> Unpublished results

<sup>§</sup> The mechanism of the imine exchange reaction is discussed in Figure 1.3-5 on page 26.

## 2.2. Structural properties influencing imine formation

The ability of a carbonyl compound to form an imine consists of the combination of two criteria: high conversion even in aqueous media (thermodynamic criterion) and fast rate of formation (kinetic criterion). Simultaneous evaluation of both might render some difficulties and hence it was separated into two studies based on different experimental approaches. The thermodynamic criterion was extracted from competition experiments in which several carbonyl compounds compete for one amine substrate in water/organic solvent mixture, while the kinetic criterion was determined by conventional kinetic experiments in absence of competing species both in pure organic solvent and in water/organic solvent mixture.

For the competition experiments, a library of 19 available aldehydes was separated into 5 subgroups (Figure 2.2-1) with benzaldehyde present in all of them as reference, diluted in mixture of water/DMSO 3:7 (v/v) and reacted with equivalents of *n*-propylamine. The formation of imines was followed by NMR spectroscopy. After addition of one molar equivalent, the spectra were measured repeatedly until no change in the relative integral intensities was observed, indicating that the thermodynamic equilibrium has been reached.

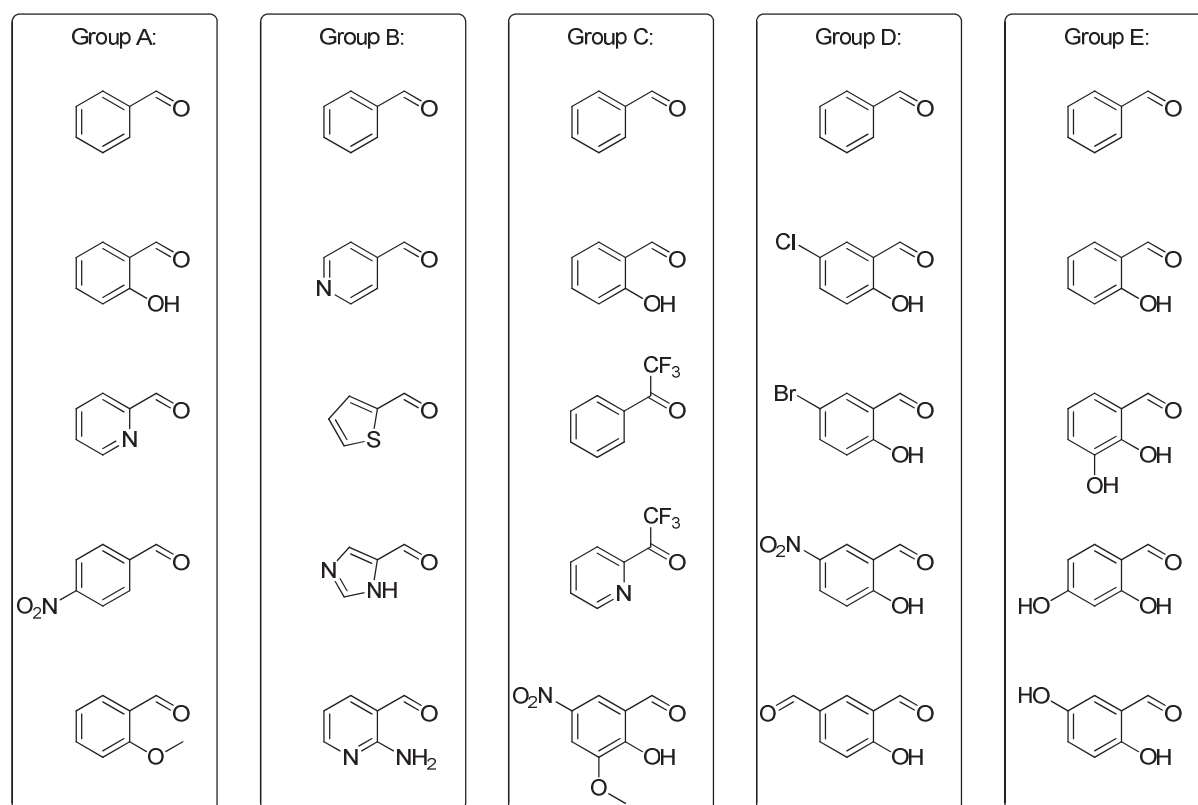


Figure 2.2-1 Scheme of the aldehydes screened for reactivity with *n*-propylamine, divided into five subgroups. The groups A to C involve various heterocyclic aldehydes and trifluoromethylketones, the group D was chosen to explore the role of electron withdrawing substituents in the case of surprisingly reactive salicylaldehyde, and the group E to investigate the role of second hydroxyl-group on the aromatic core.

In the first three subgroups A, B and C, various different aromatic aldehydes and trifluoromethyl ketones bearing either electron-donating (ED) or electron-withdrawing groups (EWG) were investigated. Equimolar mixtures of aldehydes in the group were prepared and then titrated by equivalents of *n*-propylamine. <sup>1</sup>H NMR spectra were recorded 2 hours after mixing the components or after addition of the following aliquot and then again after 24 hours to verify that the equilibrium was reached. Equilibration was reached within 2 hours after addition of up to 3 equivalents of the

amine, but was prolonged to 24 hours after the addition of the fourth equivalent and took 2 days after the final addition of the fifth aliquot. The titration curves are plotted in Figure 2.2-2 through Figure 2.2-6. The total conversion of *n*-propylamine to all imines is provided for clarity.

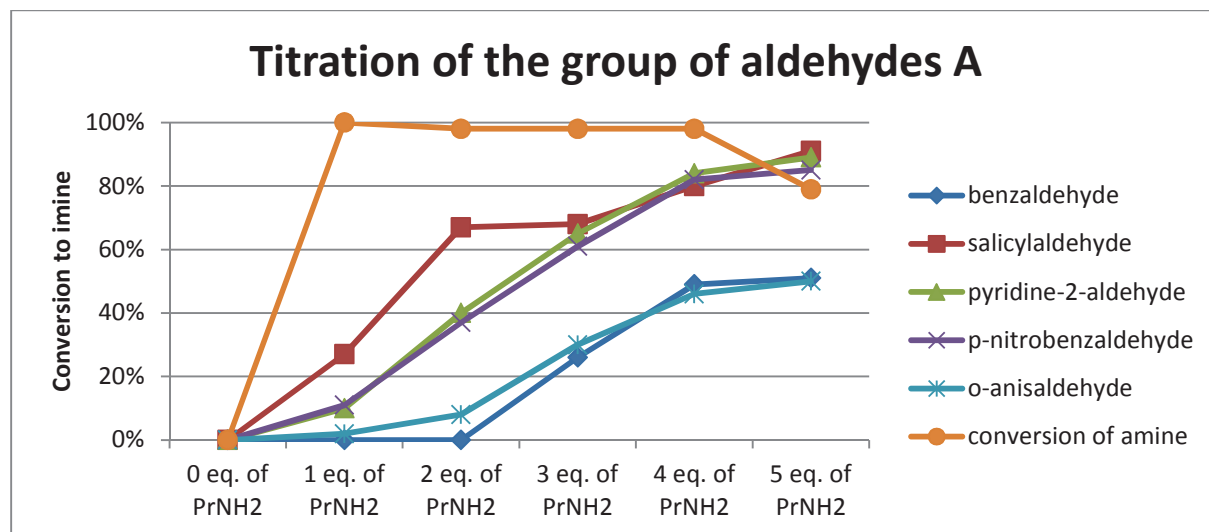


Figure 2.2-2 Titration of the group A of aldehydes by equimolar amounts of *n*-propylamine. Unexpectedly high reactivity of salicylaldehyde was observed even in presence of aldehydes bearing EWG (like *p*-nitrobenzaldehyde) or electron-poor aromatic aldehydes (like pyridine-2-aldehyde).

A surprising trend in reactivity was found: salicylaldehyde (**SALAL**), bearing an ED hydroxyl substituent, was found to be the most reactive aldehyde, more so than aldehydes bearing EWG or electron-poor heterocyclic aldehydes like pyridine-carboxaldehydes, or even very electron-deficient trifluoromethyl ketones. Indeed, the trifluoromethyl ketones under given conditions (water/DMSO 3:7) exist in their hydrated forms which are unreactive towards nucleophilic attack by an amine.

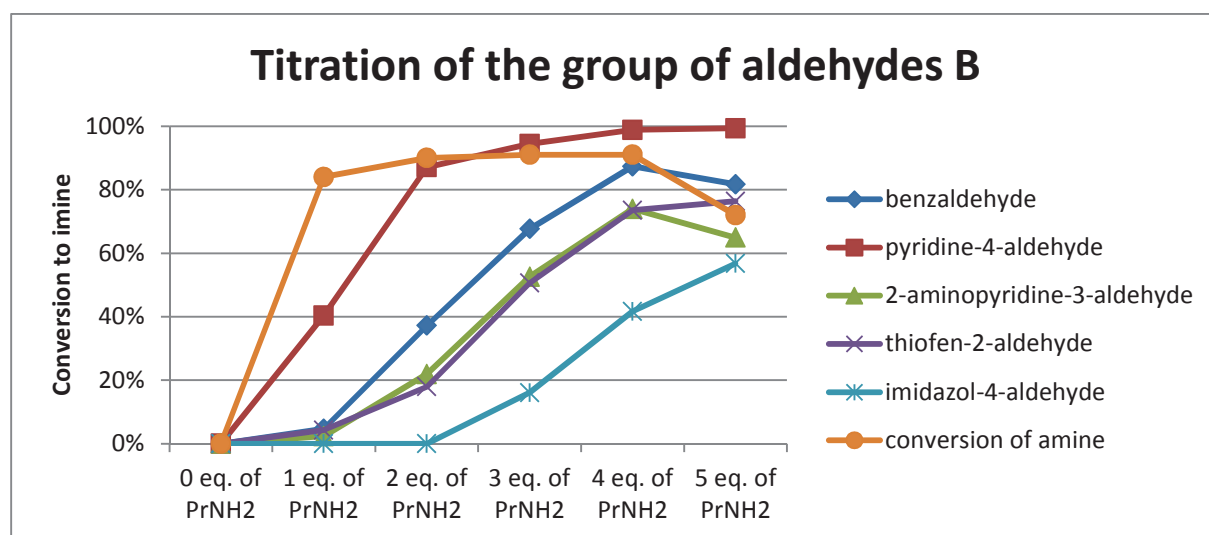


Figure 2.2-3 Group B examines different heterocycles bearing the aldehyde group. Only pyridine-4-aldehyde exceeds the reactivity of benzaldehyde, which was among the least reactive aldehydes in the group A. The 2-aminopyridine-3-carboxaldehyde, capable of formation of the intramolecular hydrogen bond like salicylaldehyde, is also less reactive.

The unexpected reactivity of **SALAL** can be explained by formation of a strong intramolecular hydrogen bond between the hydrogen of the 2-hydroxyl group and the imine nitrogen. This conclusion is supported by comparison of **SALAL** with its methylated derivative, 2-anisaldehyde, which is fairly unreactive under the given conditions, or by comparison with 2-aminopyridine-3-carboxaldehyde, which in spite of the capability of formation of a similar, but weaker, hydrogen bond



is also unreactive (Figure 2.2-3). Introduction of two more substituents, 5-nitro and 3-methoxy, on the **SALAL** core leads to complex behaviour of this derivative which alters the usually high conversion of the first equivalent of *n*-propylamine, maybe due to higher acidity of the medium and partial protonation of the amine (Figure 2.2-4).

The existence of the intramolecular hydrogen bond in salicylimines has been previously reported in the literature in crystal structures<sup>[218–220]</sup> and also suggested in solution<sup>[64,127,128,221]</sup>.

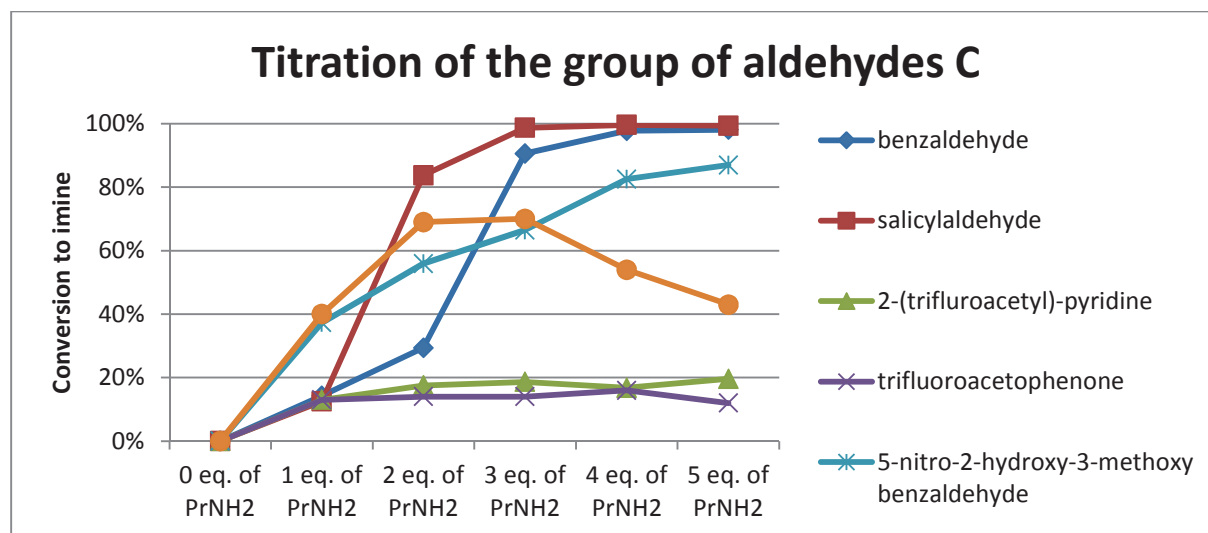


Figure 2.2-4 Group C provides a comparison with trifluoromethyl ketones. The reactivity of these species is lowered by the formation of hydrates in aqueous media, which are less susceptible towards nucleophilic attack by the amine. Salicylaldehyde bearing 5-nitro and 3-methoxy groups exhibit complex behaviour, being superior to salicylaldehyde after introduction of the first equivalent, but falling behind after subsequent additions.

In the group D, the derivatives of **SALAL** bearing EWGs in position 5 (*para* to the aldehyde function) were tested, namely 5-chloro, 5-bromo, 5-nitro and 5-formyl substituted **SALAL**, and compared with non-functionalized benzaldehyde (Figure 2.2-6). Unfortunately, the aldehyde signals were heavily overlapped and unambiguous identification of each aldehyde was difficult, therefore the conversion to imines was based on the aromatic proton signals. Moreover, the situation is further complicated by the fact that 4-hydroxyisophthalaldehyde (“5-formylsalicylaldehyde”) bears two carbonyls, both of which could compete for the amine. Indeed, this double reactivity was confirmed by control experiments: 4-hydroxyisophthalaldehyde was reacted with 1 equivalent of *n*-propylamine in mixture of D<sub>2</sub>O/*d*<sub>6</sub>-DMSO (3:7 v/v) and in *d*-chloroform (Figure 2.2-5). While in chloroform the reaction proceeds only on the carbonyl next to the hydroxyl group, in the mixture of water/DMSO the relative ratio of imines *para* and *ortho* to the OH group is about 1:10 in favour of the latter. Addition of a second equivalent of propylamine leads to formation of the bis-imine. The characterization and identification of different species in the mixture was done by multidimensional proton-carbon correlated NMR.

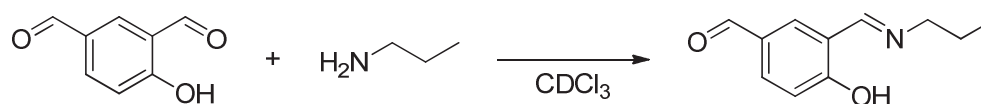


Figure 2.2-5 The reaction of 4-hydroxyisophthalaldehyde in chloroform proceeds clearly on one aldehyde site only. In the mixture of water/DMSO the selectivity by ratio 10:1 still in favour of the OH-bonded imine.

To better understand the actual effect of the EWGs, the kinetics of formation of the *N*-propylimine starting from the corresponding aldehyde was followed by NMR and UV-VIS spectrophotometry (see Section 2.2.2).

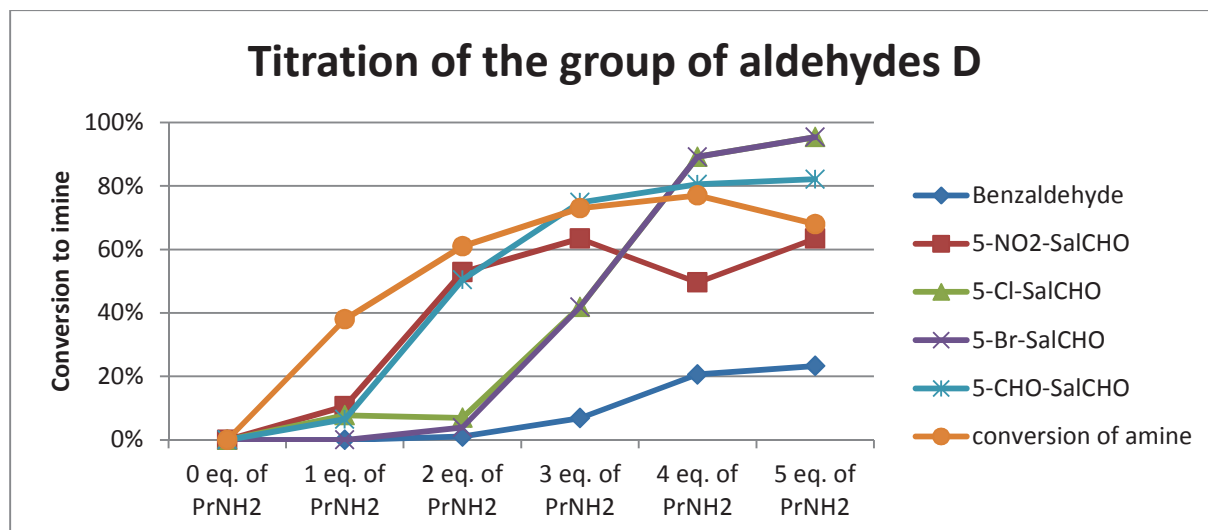


Figure 2.2-6 Group D explores the effect of EWGs on the aromatic ring of salicylaldehyde. The order of reactivity of the derivatives was found to follow the strength of electron-withdrawing properties as described by the Hammett constants. After addition of the fourth equivalent of propylamine the situation is complicated by the double reactivity of 5-formyl derivative.

Group E was explored in order to discern the effect of the second hydroxyl group on the aromatic ring (Figure 2.2-7). It was found that the position of the second hydroxyl only has a small effect. Nevertheless, two different influences on the reactivity of the carbonyl can be distinguished: a) formation of a second intramolecular hydrogen bond in case of 2,3-dihydroxybenzaldehyde increases the strength of the OH...N hydrogen bond leading to higher equilibrium conversion in comparison to **SALAL**; b) the conjugation between two hydroxyl groups in *para* position decreases acidity of phenolic proton and thus weakens the intramolecular hydrogen bond. Surprisingly, an ED hydroxyl at the *para* position conjugated to the aldehyde group does not lead to significant difference in equilibrium conversion. After addition of 1-3 equivalents of *n*-propylamine, 2,3-dihydroxy benzaldehyde is superior to **SALAL** giving nearly an identical conversion as 2,4-dihydroxy derivative, and they are both superior to the 2,5-dihydroxy isomer. After addition of four or five equivalents, the difference in relative conversion is very small or negligible.

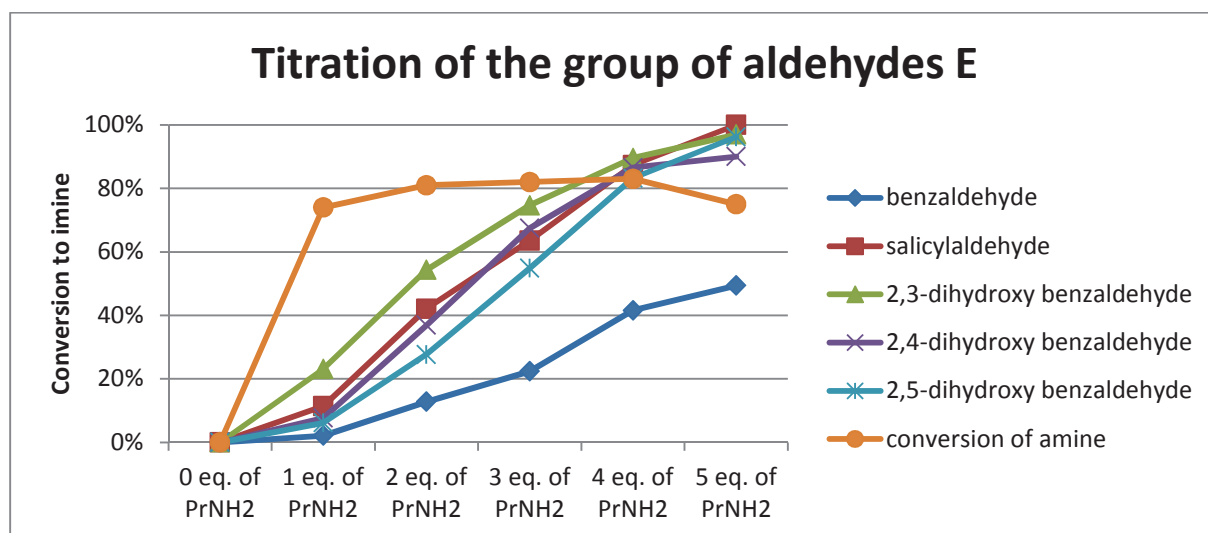


Figure 2.2-7 Group E examines the effect of the second hydroxyl group on the aromatic ring. The major effects are: second intramolecular hydrogen bond in the 2,3-dihydroxy benzaldehyde leading to higher reactivity; effective conjugation in the 2,5-dihydroxy isomer lowering the acidity of the phenolic OH and thus weakening the imine-stabilizing intramolecular hydrogen bond.

The imine formation by condensation of an aldehyde with an amine is accompanied by the elimination of a water molecule. In the reverse reaction, water causes hydrolysis of the previously formed imine back to corresponding aldehyde and amine. Thus the water content in the medium is a crucial parameter in determining the equilibrium conversion of the reaction.<sup>[107]</sup> In principle, the imine formation and the hydrolysis share the same equilibrium constant. Therefore, the choice of approach, i.e. following the formation or hydrolysis of the imine, depends on practical issues like solubility, miscibility and homogeneity. To investigate the stability of the imines of **SALAL** in aqueous solution 20  $\mu\text{L}$  of *N*-propylsalicylaldimine was diluted in a mixture of  $\text{CD}_3\text{CN}$  with  $\text{D}_2\text{O}$  in different ratios, and the equilibrium composition of the mixture was followed by NMR (Figure 2.2-8). Equilibrium was reached within 6 hours for all the samples and the ratio of the imine and the hydrolysed aldehyde was determined by integration of the corresponding signals.

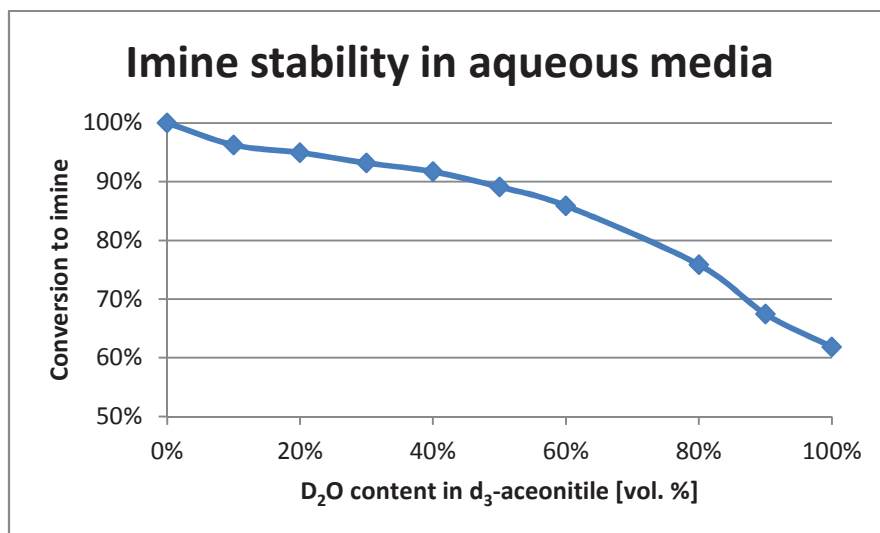


Figure 2.2-8 *N*-propylsalicylaldimine was diluted in media containing different percentage of water in acetonitrile to partially hydrolyse and the equilibrium composition of the mixture was plotted.

As expected, increased water content leads to an increased degree of hydrolysis, but an imine conversion as high as 90 % is still achieved in a solution containing up to 40 % of  $\text{D}_2\text{O}$ . Remarkably high conversion to imine (above 60 %) is observed even in pure  $\text{D}_2\text{O}$ , indicating a strong support provided by the intramolecular hydrogen bond.

The supportive role of the hydroxyl group in imine formation was also investigated in case of carbonyl compounds which normally do not form imines, and rather undergo Michael reactions, like *p*-benzoquinone derivatives (Figure 2.2-9).<sup>[222]</sup> However, the inherent basicity of amines results in deprotonation of the relatively acidic hydroxy groups, as in the case of 2,5-dihydroxybenzoquinone. Here, no condensation of amine with carbonyl compound is achieved, but rather a precipitation of the ammonium salt is observed, as it was proved by NMR and microanalysis of the isolated product. To achieve the condensation of hydroxy-ketones with amines, elevated temperature and acidic media are required.<sup>[223]</sup> These compounds are known and studied for their tautomeric *o*-hydroxy-imine/*o*-amino-ketone equilibria.<sup>[224,225]</sup>

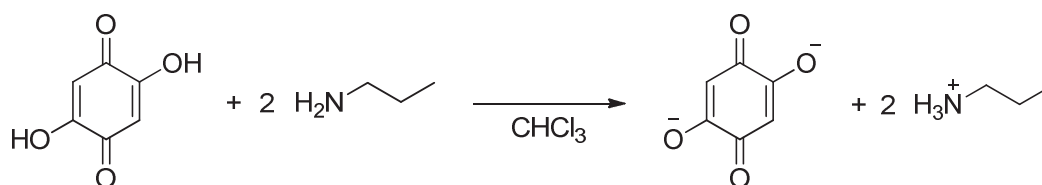


Figure 2.2-9 Basic amines cause deprotonation of relatively acidic dihydroxyquinones.

The possible tautomerism of *o*-hydroxy imines was studied by several groups.<sup>[218–220,225–229]</sup> However, some controversy remains regarding the electronic structure of these compounds. Specifically, it has not been shown whether the proton-displaced structure formed in minor quantities is rather *o*-quinone type or phenoxide-ammonium structure (Figure 2.2-10). The presence of the imine nitrogen atom opens another possibility of examining the actual electronic structure of these compounds through the nitrogen NMR spectra.

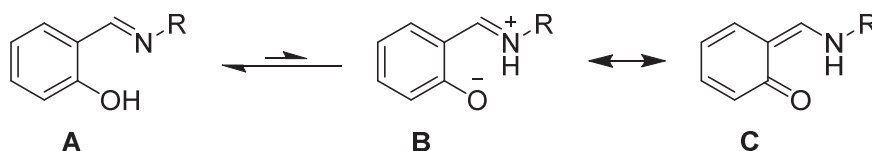


Figure 2.2-10 The possible tautomeric and resonance structures of the salicylaldimines. The dominant species in solution is in the enol form A, however the strong yellow colour resulting from the absorption band around 400 nm in the UV-VIS spectra is attributed to the tautomeric structures B or C.

### 2.2.1. Electronic structure of Schiff bases through nitrogen NMR

There have been numerous NMR studies on the chemical shifts of Schiff bases in  $^1\text{H}$  and  $^{13}\text{C}$  spectra in the literature, summarized in several reviews.<sup>[219,220,225,229]</sup> However, information about the nitrogen ( $^{14}\text{N}$  and  $^{15}\text{N}$ ) NMR of imines is rather scarce,<sup>[192]</sup> probably due to the difficulties in acquiring the spectra.  $^{15}\text{N}$  is a dipolar nucleus giving sharp spectral lines, but the low natural abundance combined with a low gyromagnetic ratio ( $\gamma$ ) makes the acquisition of 1D NMR spectra relatively difficult. On the other hand,  $^{14}\text{N}$  is almost 100 % abundant in nature, but is quadrupolar, giving broad lines in NMR spectra and also has a low gyromagnetic ratio<sup>[230,231]</sup>. Some magnetic properties are summarized in Table 2.2-1.

Nucleus	Natural abundance	Spin	$\gamma/2\pi$ [MHz T <sup>-1</sup> ]
$^1\text{H}$	99.98 %	$\frac{1}{2}$	42.576
$^{14}\text{N}$	99.63%	1	3.077
$^{15}\text{N}$	0.37 %	$\frac{1}{2}$	-4.316

Table 2.2-1 NMR properties of nitrogen nuclei compared with the values for the proton.

The quadrupolar properties of the nucleus are defined by the corresponding Hamiltonian (Equation 1). Quadrupolar energy level splitting and quadrupolar interactions contribute largely to the line broadening<sup>[232]</sup>. An interesting parameter in the Hamiltonian is the parameter  $q$  which defines the gradient of the electric field around the quadrupolar nucleus. For symmetrical electric fields this parameter is close or equal to zero and thus cancels the entire contribution of quadrupolar effects to the complete Hamiltonian. Thus highly symmetrical nitrogen compounds, like quaternary ammonium salts, give sharp  $^{14}\text{N}$  lines. Therefore, examining the line-widths in  $^{14}\text{N}$  NMR spectra can indicate on the local electronic structure around the nitrogen atom.

$$\mathcal{H}_Q = \frac{e^2 q Q}{4I(2I - 1)} [3I_z^2 - I^2 + \eta(I_x^2 - I_y^2)]$$

Equation 1 The Hamiltonian for quadrupolar nucleus, where  $e$  is the electronic charge,  $q$  is the electric field gradient,  $Q$  is nuclear quadrupole momentum,  $I$  is scalar  $I$  which is an operator of the spin of the nucleus and  $\eta$  is the asymmetry parameter.

The aforementioned resonance structures of the salicylaldimine tautomers (Figure 2.2-10) differ largely on the nitrogen atom: while **C** resembles a secondary amine, **B** is a positively charged nitrogen atom and as a consequence, the line width should be dramatically decreased in case of the structure **B** compared to structure **C**. For this purpose, 13 derivatives of imines and related derivatives were prepared and their nitrogen NMR spectra (both  $^{14}\text{N}$  and  $^{15}\text{N}$ ) were compared in neat liquids, solutions in  $\text{CDCl}_3$  and  $\text{TfOH}$  where it is guaranteed that all nitrogens are protonated.

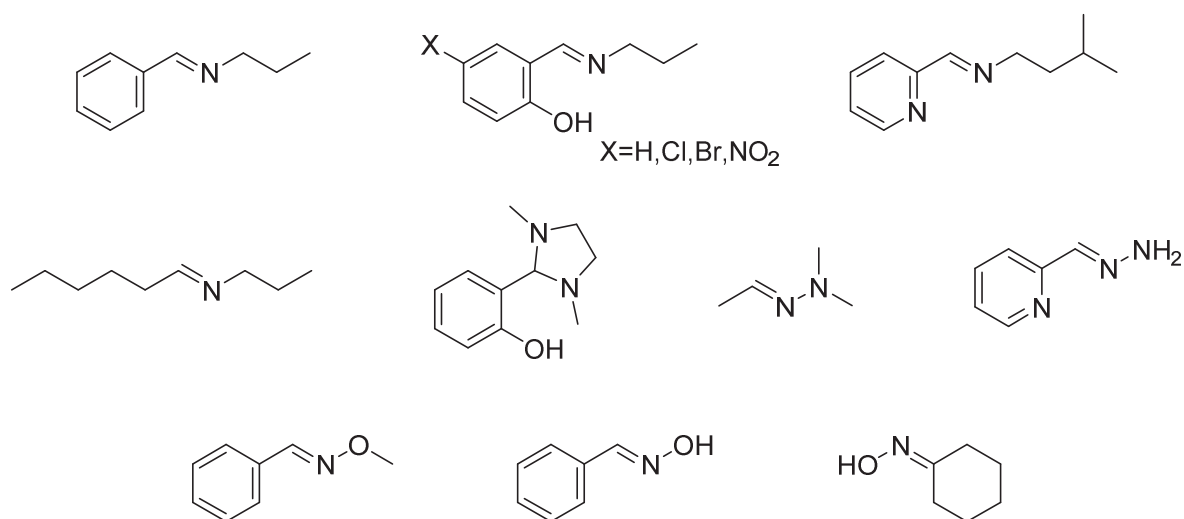


Figure 2.2-11 Series of examined imines and related derivatives by  $^{14}\text{N}$  and  $^{15}\text{N}$  NMR spectroscopy.

The spectra were recorded under three different conditions: a) neat with external  $\text{CD}_3\text{NO}_2$  standard in capillary, b) as a 10 % solution (v/v) in a mixture of  $\text{CDCl}_3/\text{CD}_3\text{NO}_2$  (95:5), c) as a 20 % solution (v/v) in triflic acid with an external  $\text{CD}_3\text{NO}_2$  standard in the capillary. Both the  $^{14}\text{N}$  and the  $^{15}\text{N}$  spectra were recorded with  $\text{d}_3$ -nitromethane serving as the deuterium lock solvent (conditions a) and c) and as a signal reference at  $\delta=0$  ppm. Results are summarized in Table 2.2-2 to Table 2.2-4. The  $^{15}\text{N}$  nucleus gives sharp lines and therefore the line widths, typically around 1.5 Hz, are not reported. The  $^{14}\text{N}$  and  $^{15}\text{N}$  signal shifts strongly correlate.

Structure	$^{14}\text{N}$ shifts [ppm]	$^{15}\text{N}$ shifts [ppm]	$^{14}\text{N}$ line width [Hz]	
			neat	in $\text{CDCl}_3/\text{CD}_3\text{NO}_2$
	-85.66	-81.36	1460	530
	-48.48	-45.06	900	580
	-41.10 -74.31	-35.59 -62.00	1050 1600	620 1200
	-77.32	n.d.	n.d.	820
	-78.46	n.d.	n.d.	870
	-7.78 -128.34	n.d.	n.d.	180 430

Table 2.2-2 Chemical shifts and line widths of  $^{14}\text{N}$  NMR signals in the spectra measured as neat liquids and in  $\text{CDCl}_3$  solutions of studied imine derivatives, n.d. stands for not determined in cases when spectra were not recorded.

By comparing the signal line widths of neat samples with those diluted in chloroform one can estimate the contribution from the viscosity to the line broadening. The line width is decreased by approximately 400 Hz by dilution of the compound in  $\text{CDCl}_3$  in the cases of benzaldehyde imine and pyridine imine, for both the imine and pyridine nitrogen atoms. However in the case of salicylaldehyde imine, this line width is reduced by *ca* 900 Hz, indicating intermolecular interactions to a larger extent than in previous cases. Comparison of the Hammett constants with the line widths of

salicylaldehyde and its derivatives bearing EWGs (5-Cl, 5-Br, 5-NO<sub>2</sub>) exhibit strong nonlinearity, showing that the contribution to the line width does not rise from the acidity of the OH group (see Section 2.2.2 for the effect of EWGs on the rate of formation of the imines). On the other hand, the line widths seem to correlate with the mesomeric effect of the substituent (-M for nitro, neutral for hydrogen, +M for halogens).

Triflic acid was used as a solvent to fully protonate the imine species and to avoid precipitation or side reactions of the resulting iminium salts. The d<sub>3</sub>-nitromethane standard was sealed in capillary and placed into the studied solution (20 % v/v of the compound in TfOH) as a locking and shimming solvent as well as an internal standard referenced at  $\delta=0$  ppm. Results are shown in Table 2.2-3. The line width for benzaldimine and pyridine imine signals is further decreased by approximately 200 Hz when compared to solutions in CDCl<sub>3</sub>, but is slightly increased in the case of salicylaldehyde. This indicates that the effect responsible for line sharpening is much weaker in case of salicyl than in other two cases. Again, the <sup>14</sup>N and <sup>15</sup>N signals strongly correlate. It is noteworthy that protonation of the imine nitrogen leads to observable strong coupling with the azomethine proton of about 18 Hz (details in the Experimental part).

Structure	<sup>14</sup> N shift [ppm]	<sup>15</sup> N shift [ppm]	<sup>14</sup> N line width [Hz]
	-197.97	-196.84	600
	-199.21	-197.68	390
	-165.70 -188.97	-165.81 -187.14	450 650

Table 2.2-3 Nitrogen NMR data of studied imine derivatives in TfOH solutions. The spectrum of pyridine imine shows partial decomposition of the compound and elimination of protonated propylamine (signal at -349 ppm LW 160 Hz).

To complete the overview on the nitrogen NMR parameters of imines and their related derivatives, the spectra were recorded for several other compounds, and the results are summarized in Table 2.2-3. In some cases, the corresponding signal could not be observed, either due to chemical shift in close proximity of the nitromethane reference or due to extreme line widths which make the signal indistinguishable from the background, even after long acquisition times.\*\* If both were accessible, the <sup>14</sup>N and <sup>15</sup>N signals correlate like in the previous examples. The imine nitrogen signal for hydrazones and oximes are slightly shifted downfield compared to imines, but its line width varies largely with the nature of the chemical environment, being extremely large in case of oximes (Table 2.2-4). For example, the N,N-dimethylhydrazone of acetaldehyde gives two appreciably different nitrogen signals: the imine one at -30 ppm with a line width of 600 Hz and the amine one at -279 ppm and a line width of 780 Hz, which are in perfect agreement with observed imine and free amine signals; but the imine signal of the pyridine-2-carboxylhydrazone at -34 ppm has a line width of 1200 Hz, while other nitrogen signals are in good agreement both in chemical shift and line width with related compounds. The *O*-methylbenzoxime was the only oxime compound which gave observable <sup>14</sup>N signal with a line width of 1570 Hz.

\*\* The spectral measurements over the range of 800 ppm, typically required for nitrogen NMR, often bring problems in phase and baseline corrections over the whole range. More details can be found in 7.Experimental part.

Structure	<sup>14</sup> N shifts [ppm]	<sup>15</sup> N shifts [ppm]	<sup>14</sup> N line width [Hz]	
			neat	in CDCl <sub>3</sub> /CD <sub>3</sub> NO <sub>2</sub>
	-29.85 -280.01	-30.13 -279.15	600 780	n.d.
	4.91	Not observed	1570	n.d.
	Not observed	-51.24	Not observed	n.d.
	Not observed	-39.47	Not observed	Not observed
	Not observed	-22.12	Not observed	n.d.
	Not observed	-333.80	Not observed	n.d.
	-34.02 -71.65 -263.70	n.d.	n.d.	1200 1130 820

Table 2.2-4 Overview of the related imine derivatives and their nitrogen NMR parameters, n.d. stands for not determined in cases when spectra were not recorded, Not observed relates to spectra which were recorded, but corresponding signals were not observed in the spectra.

From the data acquired for the <sup>14</sup>N and <sup>15</sup>N NMR signal chemical shifts, line widths, substituent variation and the effect of solvents and protonation, two conclusions can be made: a) the imine signals shift and its line width do not correlate with Hammett constants but rather with a mesomeric effect (Figure 2.2-12), b) full protonation of the imine nitrogen of salicylaldimine does not lead to line sharpening like in related imine compounds. Based on these observations, one can conclude that the prevalent enol form **A** of the salicylaldimine (Figure 2.2-10) gives upon tautomeric shift a quinoid structure **C**, rather than zwitter-ionic phenoxide **B**.

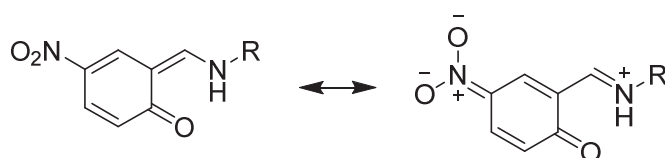


Figure 2.2-12 Suggested explanation of the line width correlation with mesomeric effect. The quinoid structure exists in two resonance forms where one of them puts a partial positive charge on the imine nitrogen. Substituent with +M effect, like halogens, on the other hand significantly broaden the lines by contributing to the secondary-amine character of the nitrogen atom.

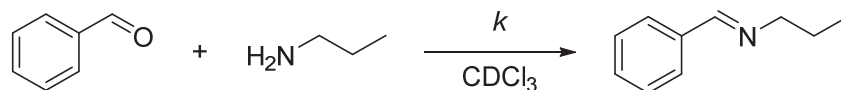
### 2.2.2. Kinetic parameters of imine formation

For any optimal imine-based functional system, high yields and rapid rates of formation are required. Therefore, the rate of the condensation reaction of an aldehyde with an amine forming an imine is, together with overall conversion to the imine, a crucial parameter for the effective and fast construction of imine based systems. The previously identified hits from the aldehyde screening were thus examined also from the kinetic perspective, specifically for the rate of imine formation and imine exchange.

As the kinetic behaviour strongly depends on conditions, perhaps even more so than the equilibrium conversion, it is necessary to establish a link, or a reference point, which can be



compared to related published results. In the case of aromatic imines, the logical choice is benzaldehyde (**BENZAL**), as it is the simplest of aromatic aldehydes. The formation of *N*-propylbenzaldimine was followed by NMR in CDCl<sub>3</sub> (Figure 2.2-13). The integrated signal intensities were processed according to second order kinetics with correction for a non-stoichiometric ratio (Figure 2.2-14).<sup>††</sup>



$$k = (3.26 \pm 0.01) \cdot 10^{-3} \text{ L mol}^{-1} \text{ s}^{-1}$$

Figure 2.2-13 The reference reaction for imine formation: the condensation of benzaldehyde with *n*-propylamine in *d*-chloroform was followed by NMR and the rate constant was evaluated. The conversion under the conditions used herein is quantitative and therefore the inherently reversible reaction follows kinetics of an irreversible reaction.

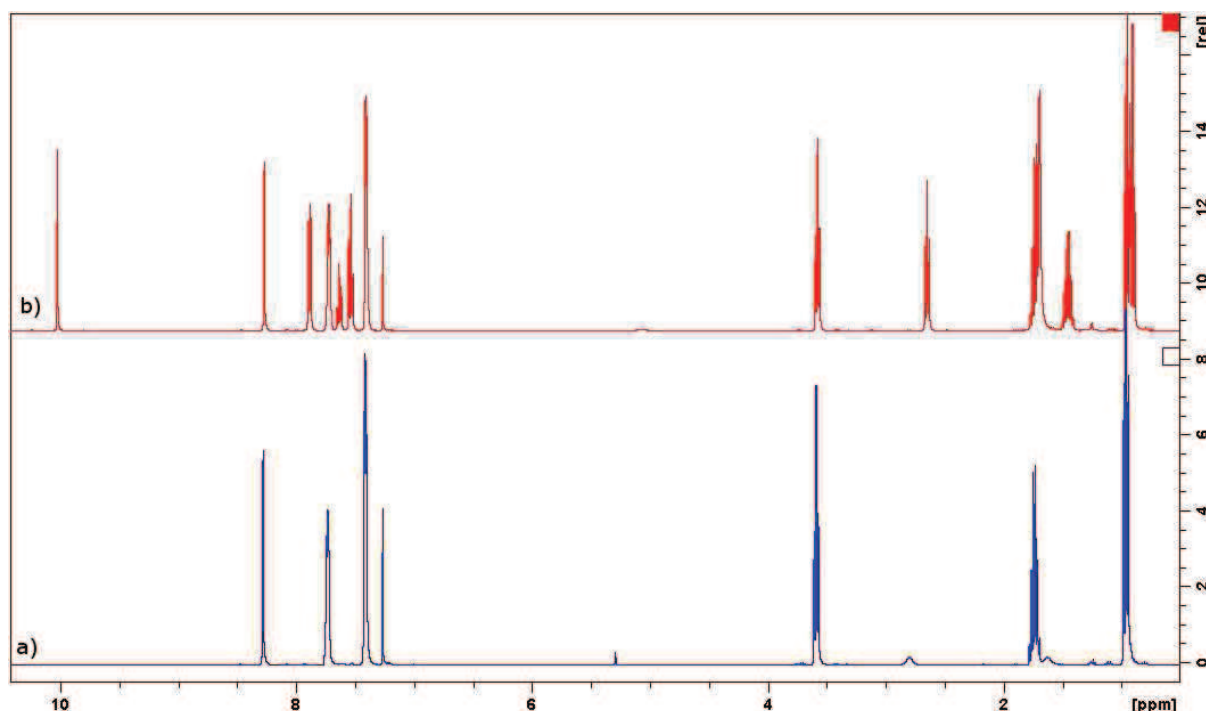


Figure 2.2-14 a) <sup>1</sup>H-NMR spectrum of the *N*-propylimine of **BENZAL** (bottom blue trace): the azomethine  $\text{-N=CH-}$  proton of the imine gives typical signal at around 8.5 ppm, the aromatic CH protons give signals in a wide range of 6 – 9 ppm, depending on the character of the aromatic ring. The signal of the aliphatic  $\text{-N-CH}_2\text{-}$  protons is largely shifted compared to the free amine in solution (approximately by 1 ppm downfield), appearing in the range of 3.5-4.0 ppm. Very fine coupling with the azomethine proton introduces small splitting of the corresponding signal with interaction constant of about 1 Hz, which is a very good identification mark for the imine signals in complicated mixtures. b) The NMR spectrum recorded in the course of the imine condensation reaction (**BENZAL** + *n*-propylamine). The aldehyde peak at 10 ppm is decreasing with time as well as the free amine signal at 2.6 ppm. The peaks corresponding to imine are on the other hand increasing, both for the azomethine (8.25 ppm) and aliphatic (3.6 ppm) part.

Introduction of an EWG on the aromatic core leads to rate acceleration. On the other hand, branching introduced at the  $\alpha$ -position of the amine decreases the rate of the reaction. In the case of the sterically hindered *t*-butylamine, the rate constant of imine formation with *p*-nitrobenzaldehyde

<sup>††</sup> The kinetic models, their mathematic treatment and version for reversible reactions as well as corrections for non-stoichiometric mixing ratio are part of any physical chemistry textbook.<sup>[60]</sup> The data could be fitted both by the function  $[A] = f(t)$ ,  $[A]$  represents the actual concentration of compound A, or the derivative  $(d[A]/dt = f(A))$  form of the kinetic equations. The model and the fitting approach used are always indicated in the corresponding paragraph of the Experimental part.

drops by the factor of about 30 (Figure 2.2-15). The imine formation under the conditions used is quantitative and therefore the irreversible reaction kinetic model was used for fitting.

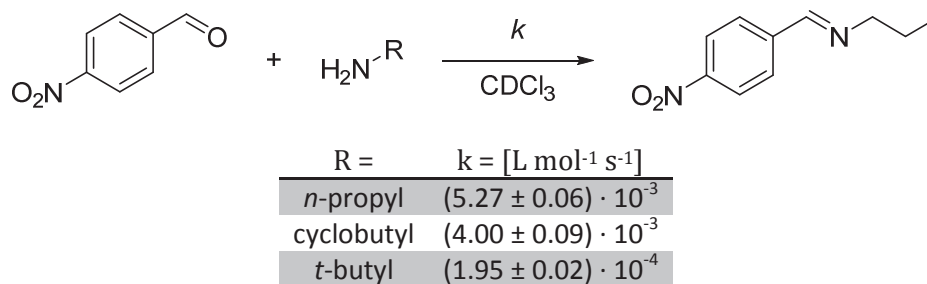


Figure 2.2-15 The rate constants of imine formation from 4-nitrobenzaldehyde and series of amines with increased branching on the  $\alpha$ -carbon of the amine. Steric hindrance of the amino group leads to significant diminishment of the rate constant. The EWG nitro group on the other hand accelerates the rate of formation when compared to plain **BENZAL**.

An unexpected hit from the aldehyde screening was obtained, with **SALAL**, and was further investigated in terms of kinetics. Several substituents were introduced to position 5 on the aromatic ring (i.e. *para* to the OH, *meta* to the carbonyl) and the rate of imine formation was monitored by UV-VIS spectrophotometry, following the intensity of the characteristic absorption band around 400 nm. The optical density of this band was determined by measuring the UV-VIS spectrum at three different defined concentrations. Control experiments in CDCl<sub>3</sub> performed by NMR, indicated the total conversion to imines, and therefore irreversible kinetic model was used for fitting.

Five different substituents were chosen for this study: a single electron-donating 5-hydroxy derivative and four derivatives bearing EWGs, namely 5-chloro, 5-bromo, 5-formyl and 5-nitro (Figure 2.2-16). Similarly to benzaldehyde, the rate of imine formation is increasing with the electron-accepting nature of the substituent. The hydroxyl decreases the rate constant by a factor of about 2, while the chlorine atom increases the rate by about the same factor. A **SALAL** derivative with the 5-formyl substituent<sup>‡‡</sup> possesses two reactive aldehyde groups. As described above (see page 41), these two carbonyls differ dramatically in their reactivities, which depend on the conditions used. In chloroform, only the carbonyl on the position *ortho* to the hydroxyl reacts with amines, and the rate is accelerated by a factor of about 20 compared to the parent **SALAL**. The strongest electron acceptor, the nitro group, causes a rate augmentation by more than two orders of magnitude.

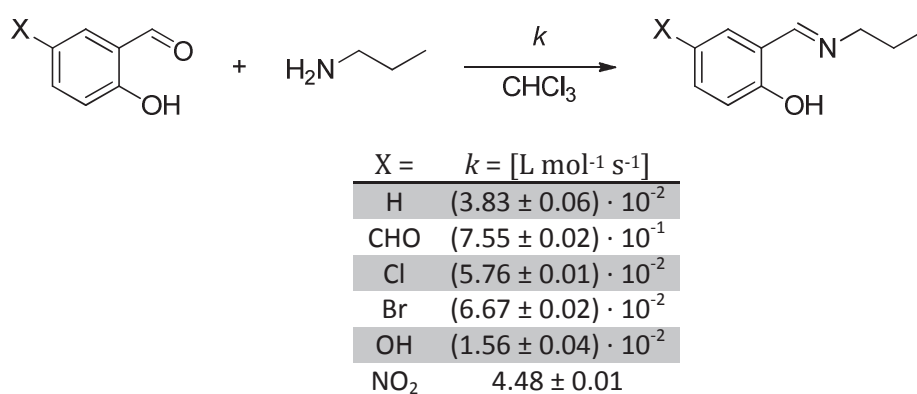
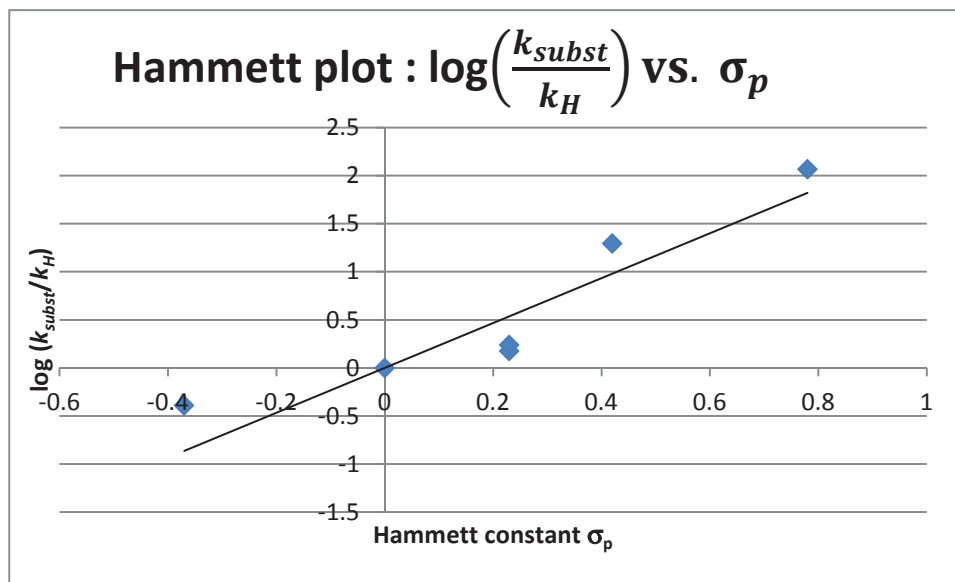


Figure 2.2-16 Rate constants of the imine formation determined for several derivatives of salicylaldehyde in chloroform by UV-VIS spectrometry. EWGs accelerate the rate of formation while ED groups are decelerating it.

From the data collected on the rate of imine formation from **SALAL** bearing substituents in position 5, a more detailed analysis on the role of the OH in the imine formation can be extracted.

<sup>‡‡</sup> Correct name of this compound is 4-hydroxy-*iso*-phthalaldehyde, the nomenclature “5-formyl” is used to reflect the connection with other **SALAL** derivatives studied.

For this purpose, a Hammett plot has been constructed. The logarithm of the rate constant of the reaction with a substituent over the rate constant of the reaction without any substituent was plotted against a set of corresponding Hammett constants, both  $\sigma_p$  and  $\sigma_m$  (Graph 2.2-1).<sup>[233]</sup> A correlation has been found with the  $\sigma_p$  constants, with a slope of 2.33 and the coefficient of determination  $R^2 = 0.9032$ .

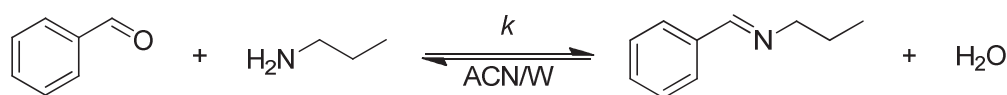


Graph 2.2-1 The Hammett plot of the rate constants of imine formation from the reaction of propylamine with substituted salicylaldehyde derivatives as a function of  $\sigma_p$  constants. Linear regression gives a slope of 2.33 and  $R^2 = 0.9032$ .

The very steep slope suggests building of a negative charge during the reaction (possibly on the phenolic oxygen) and high susceptibility to substituents, probably from the combined effects on the OH group and the carbonyl function. Also, the significantly worse correlation with  $\sigma_m$  constants ( $R^2 = 0.7187$ ) indicates that the effect on the hydroxyl group is more important than the one on the carbonyl group. Consequently, it can be assumed that the rate of the reaction is dominated by the acidity of the OH group and, as a result, the strength of the intramolecular hydrogen bond in the imine formed.

The reactions studied by NMR and UV-VIS in chloroform exhibit total conversion to imines. However in aqueous media, the conversion of an aldehyde to imine is lowered by the occurrence of the reverse reaction, imine hydrolysis, caused by elevated water content in the solution. Accordingly, the kinetics in organic solvent/water mixtures follows the models for reversible reactions taking into account equilibrated amounts of unreacted starting materials. The rate constants for imine formation and the equilibrium constants of these reactions were determined in  $d_3$ -acetonitrile/ $D_2O$  (7:3 v/v) mixture which provides wide range of solubility of both the aldehydes and the amines. The aqueous medium also brings the role of pH into play. To this extent, six aldehydes were treated with 1 eq. of *n*-propylamine in the  $CD_3CN/D_2O$  (7:3 v/v) mixture and the pH was buffered at  $8.73 \pm 0.01$  by 2 M triethanolamine buffer, the imine formation rate constants ( $k$ )<sup>§§</sup> were determined as well as the equilibrium conversion ( $\chi$ ). Results are summarised in Figure 2.2-17.

<sup>§§</sup> Note that the reported rate constants are sum of two subconstants: the rate of the forward reaction and the rate of the backward reaction, tight together by the equilibrium constant, i.e. equilibrium conversion.



Aldehyde	Parameter	Value
benzaldehyde	$\chi = (K)$	70.8 % (2.42)
	$k =$	$(24.29 \pm 0.22) \cdot 10^{-3} \text{ L mol}^{-1} \text{ s}^{-1}$
<i>p</i> -nitrobenzaldehyde	$\chi = (K)$	91.2 % (10.36)
	$k =$	$(27.92 \pm 0.08) \cdot 10^{-3} \text{ L mol}^{-1} \text{ s}^{-1}$
salicylaldehyde	$\chi = (K)$	93.4 % (14.15)
	$k =$	$(18.47 \pm 0.96) \cdot 10^{-2} \text{ L mol}^{-1} \text{ s}^{-1}$
pyridine-2-carboxaldehyde	$\chi = (K)$	84.2 % (5.33)
	$k =$	$(29.22 \pm 0.48) \cdot 10^{-2} \text{ L mol}^{-1} \text{ s}^{-1}$
pyridine-4-carboxaldehyde	$\chi = (K)$	89.0 % (8.09)
	$k =$	$(67.56 \pm 0.51) \cdot 10^{-3} \text{ L mol}^{-1} \text{ s}^{-1}$

Figure 2.2-17 The rate constants of imine formation and equilibrium constants in aqueous media determined for six aldehydes in the mixture of CD<sub>3</sub>CN/D<sub>2</sub>O (7:3 v/v), buffered by triethanolamine (2.0 M) at pH 8.73 (uncorrected for deuterium isotope effect, throughout the measurements).

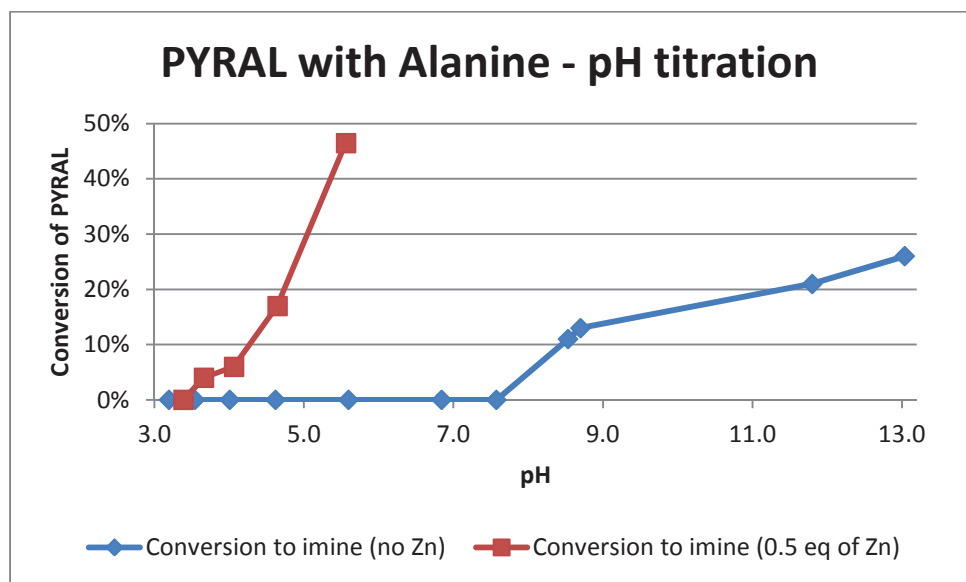
Interestingly the nitro group, responsible for rate acceleration in chloroform, has a negligible effect on the rate constant in ACN/W mixture, but enhances the equilibrium conversion to imine compared to parent **BENZAL** by 20 %. Both hits from the aldehyde screening, pyridine-2-carboxaldehyde (**PYRAL**) and **SALAL**, exhibit higher rate of imine formation by approximately one order of magnitude greater than benzaldehyde, an observation that is similarly found in chloroform. An interesting observation was made with pyridine-4-carboxaldehyde, another reactive aldehyde from the screening experiments, which has an imine formation rate constant approximately four times lower than **PYRAL**, which might be caused by higher degree of hydration of this isomer in aqueous solutions.<sup>[234]</sup>

### 2.2.3. Imines of aminoacids and metal catalysis

Among the naturally occurring compounds bearing an amino group, aminoacids hold a special place as they are the basic building blocks for all proteins and enzyme molecules. The ability of the amino group to undergo condensation with an aldehyde opens a possibility of reversible derivatization of an *N*-terminus of a protein. Several aldehyde derivatives, mostly those with biological relevance, were studied in the literature for their ability to form imines with various amino acids at broad pH ranges and also in presence of metal ions. These imine-forming reactions are particularly important, and play a critical role in the biological transamination process facilitated by vitamin B6.<sup>[64,126,127,129,208]</sup>

**PYRAL** was chosen as a reactive aldehyde to probe the efficiency of imine formation from aminoacids in pure water as a solvent. The corresponding imine formed possesses chelating properties, coordinating to the metal ion by the pyridine-ring nitrogen, the imine nitrogen and by the oxygen atoms of the carboxylate function of the amino acid. This tridentate binding motif fits well in the 2:1 binding stoichiometry with hexacoordinating metal ions, such as zinc(II). In the initial study, a 1:1 mixture of **PYRAL** and alanine was titrated with base, and the difference between the reaction with 0.5 eq. of zinc chloride and those without zinc was plotted as a function of pH (Graph 2.2-2). No conversion to imine was observed without the zinc present until a pH of about 8, and the conversion grows steadily up to about 25 % at pH 13. However, when Zn<sup>2+</sup> is present, the imine formation is observed at pH as low as 3.5 and grows rapidly up to a pH of about 6, achieving approximately a 50 % conversion. Further addition of a base unfortunately leads to large signal broadening and, upon prolonged standing, to formation of a precipitate.

In the next experiment, pyridine-2,6-dialdehyde was reacted with alanine in presence of zinc (Figure 2.2-18). The bis-imine formed from the double condensation with the amino acids form a binding site which is known as a pincer ligand. Again, the reactions with and without zinc were compared. The dialdehyde dissolved in pure water forms an equilibrated mixture of the bis-aldehyde and its mono- and di-hydrate. The signals produced by these species complicate the azomethine region of the NMR spectrum. However, the aliphatic part is well resolved and allows quantification of imine conversion.



Graph 2.2-2 Conversion of **PYRAL** and alanine (both at 20 mM) to the imine as a function of pH in presence or absence of 0.5 eq. of zinc chloride in pure  $D_2O$ . The hexacoordinating zinc ion acts as an active template for the imine formation and thus a higher conversion is reached at much lower pH values. High pH values in the presence of zinc leads to complicated NMR spectra and partial precipitation, therefore these points have been omitted from the graph.

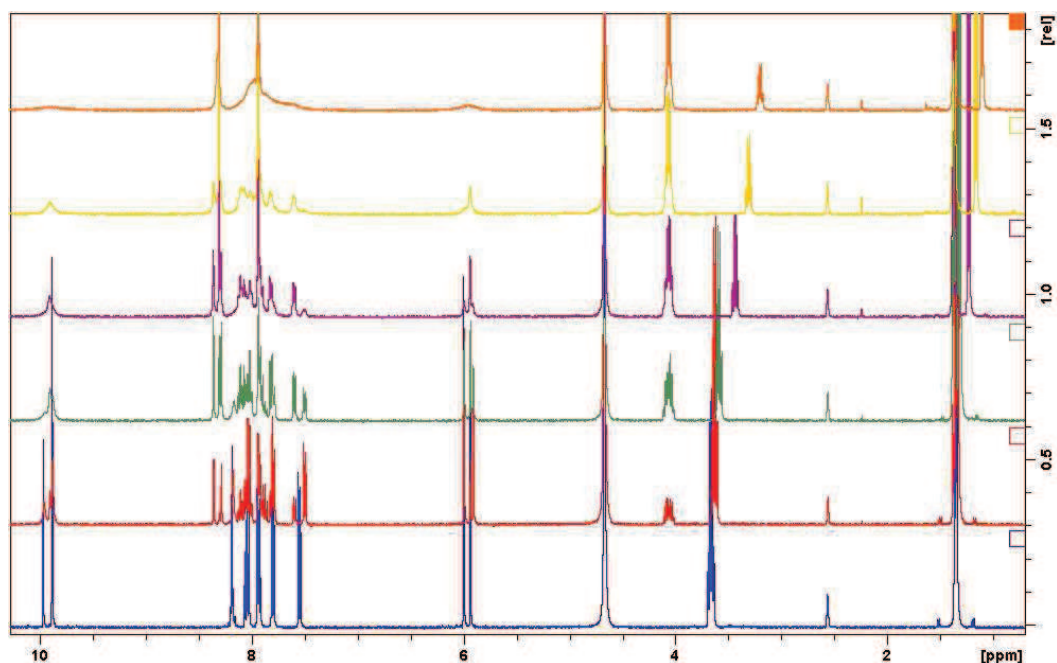
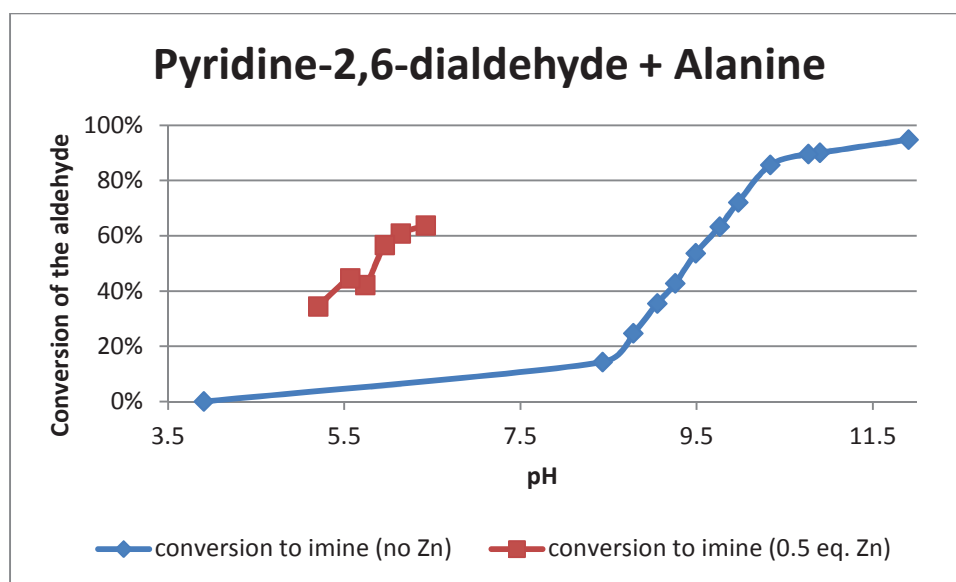


Figure 2.2-18  $^1H$ -NMR spectra of the reaction of 2 eq. of alanine with 1 eq. of pyridine-2,6-dialdehyde at increasing pH. The aldehyde dissolved in  $D_2O$  gives equilibrated mixture of its mono- and di-hydrate (signals at 6 ppm). As a result, the imine part of the spectrum is relatively complicated. On the other hand, the signals of free alanine and its corresponding imine are well separated (3.6 and 4.1 ppm respectively). The free alanine signal shifts upfield with increasing pH as a result of deprotonation of the amino group. The conversion to the imine was calculated from the alanine signals.

In D<sub>2</sub>O, 2 eq. of alanine were mixed with 1 eq. of pyridine-2,6-dialdehyde and the mixture was titrated with stock solution of NaOD in D<sub>2</sub>O (Graph 2.2-3). With increasing pH, the conversion to imines also increases, as expected. The initially formed mono-imine still undergoes dynamic hydration of the unreacted carbonyl function, thus giving a pair of signals in the azomethine region. Also, the signal coming from the alanine part of the imine shows a more complicated splitting pattern than expected from the adjacent methyl group. At pH above 10, significant broadening of the aldehyde and the hydrate peak is observed, indicating a fast equilibration between the two species. At pH as high as 12 the conversion to corresponding bis-imine is almost complete (95 %), and further pH augmentation does not lead to any improvement in imine formation (see Graph 2.2-3).



Graph 2.2-3 Conversion of alanine (2 eq.) to its corresponding imines in the reaction with 1 eq. of pyridine-2,6-dialdehyde in presence of 0.5 eq. of zinc chloride and a comparison with the reaction without zinc. At pH values above 6.5, the spectra are very broad and complicated, therefore these data have been excluded from the graph.

The reaction was reproduced under the same conditions (2 eq. of alanine, 1 eq. of pyridine-2,6-dialdehyde) and 0.5 eq. of zinc chloride was added, the reaction was titrated by stock solution of NaOD like in the previous case. The formation of the imine, most likely coordinated to zinc, is observed even at pH values when only a very little amount of imine is seen in the absence of the metal ion. However, only a narrow range of pH was accessible: similarly to the previous case, dramatic line broadening and ultimately precipitation was observed. Figure 2.2-18 shows the NMR spectra of the titration without the Zn<sup>2+</sup> in solution. Only partial broadening is observed at high pH values. In comparison, Figure 2.2-19 shows the same reaction mixture but with the addition of zinc, and large broadening is observed at pH as low as 7.5. The reason behind the signals disappearing from the spectrum is difficult to interpret. Upon prolonged standing, formation of precipitate is again observed.

Additional experiments were performed to investigate the role of different metal ions, different amino acids and to probe different experimental approaches. However, the formation of uncharacterised precipitate was found to be a rather general problem at elevated pH values. In some cases (Ni<sup>2+</sup>, Co<sup>2+</sup>) DLS experiments revealed formation of microparticles dispersed in the medium. Some of the metals were found to interact with the lateral groups of some amino acids, such as the hydroxyl group in the case of serine, which makes the spectra even more complicated. In general, better results were obtained with larger, more lipophilic amino acids and most importantly, with oligopeptides. However due to the experimental difficulties, this branch of investigation was abandoned.



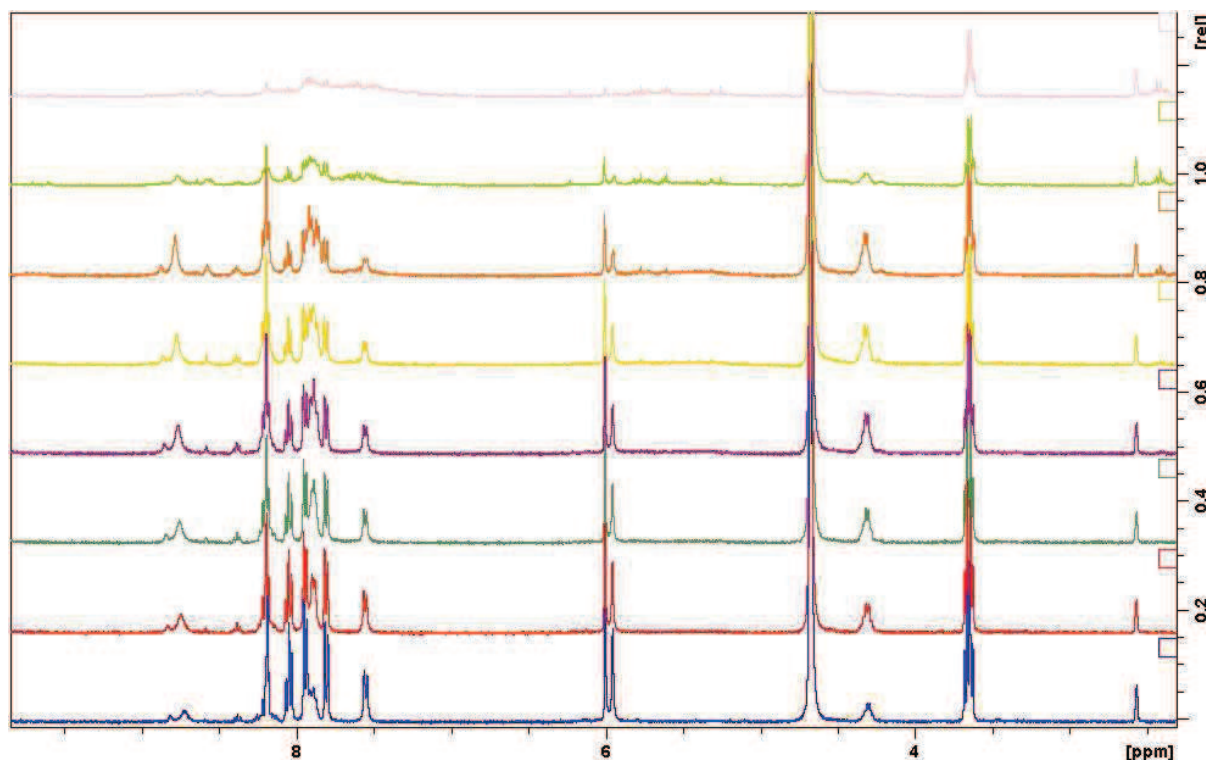
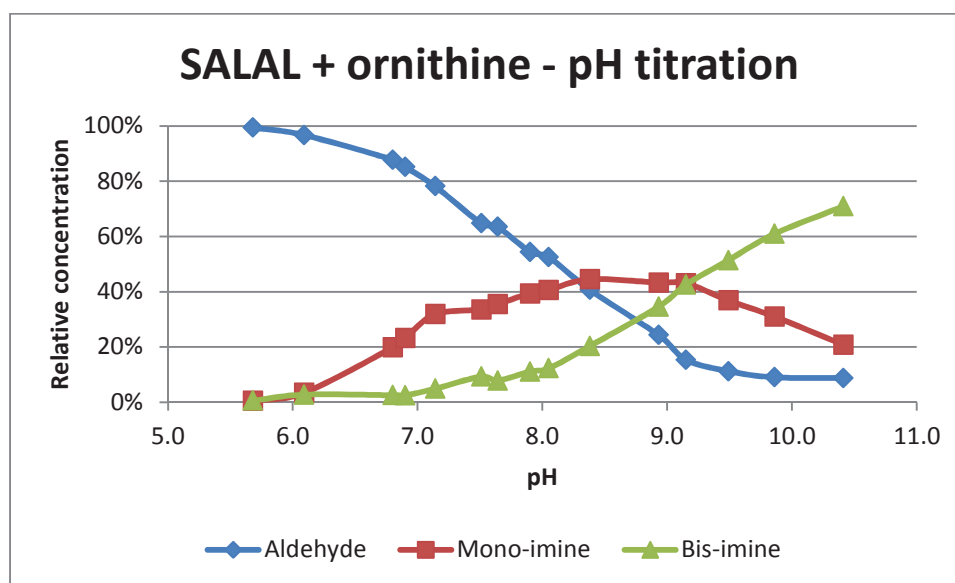


Figure 2.2-19  $^1\text{H-NMR}$  spectra of the reaction of 2 eq. of alanine with 1 eq. of pyridine-2,6-dialdehyde and 0.5 eq. of  $\text{ZnCl}_2$  at increasing pH. Above the pH of 6.5 (upper two traces) the signals get very broad and the spectrum is difficult to interpret.

The aforementioned participation of the lateral function of some aminoacids is particularly interesting in the case of aminoacids bearing a secondary amino group in the molecule, like lysine and ornithine. Both of these amino groups are capable of forming imines, but due to their distance they cannot simultaneously interact with one carbonyl function, i.e. they cannot form an intramolecular aminal. The study was performed with ornithine, which was reacted with **SALAL** in a mixture of acetonitrile-water due to the limited solubility of **SALAL** in pure water (Graph 2.2-4).



Graph 2.2-4 Relative conversion of **SALAL** to the mono- and the bis-imine in the reaction with the amino acid ornithine bearing two amino groups in a mixture of  $\text{CD}_3\text{CN}/\text{D}_2\text{O}$  (7:3 v/v). The mono-imine is a dynamic structure in which the aldehyde residue displaces between the  $\alpha$ - and the  $\delta$ -amino groups as evidenced by 2D NOESY spectra.



The mixture of SALAL with 1 eq. of ornithine was titrated in a  $\text{CD}_3\text{CN}/\text{D}_2\text{O}$  mixture by either NaOD or DBU stock solutions (Figure 2.2-20). The choice of base has no effect on the equilibrium composition of the reaction mixture. First, formation of two mono-imines is observed: the imine formed on the  $\alpha$ -amino group and on the  $\delta$ -amino group of ornithine. These two are present in an equimolar ratio and are dynamically interchanging as evidenced by 2D NMR. An increased pH causes preferential formation of the bis-imine wherein both amino groups react. This leads to the presence of some amounts of free ornithine and unreacted **SALAL** in solution. The reason for the preferential formation of the bis-imine instead of increased mono-imine conversion is unknown. The 2D NMR spectra also show that the mixture undergoes dynamic exchange: the bis-imine is in equilibrium with the mono-imine, which dynamically exchanges the salicylidene residue between the two amino groups, and eventually hydrolyses to give free aldehyde and ornithine. These dynamic processes occur in fully equilibrated samples, i.e. the relative concentration of species is constant, therefore qualifying as a dynamic equilibrium.

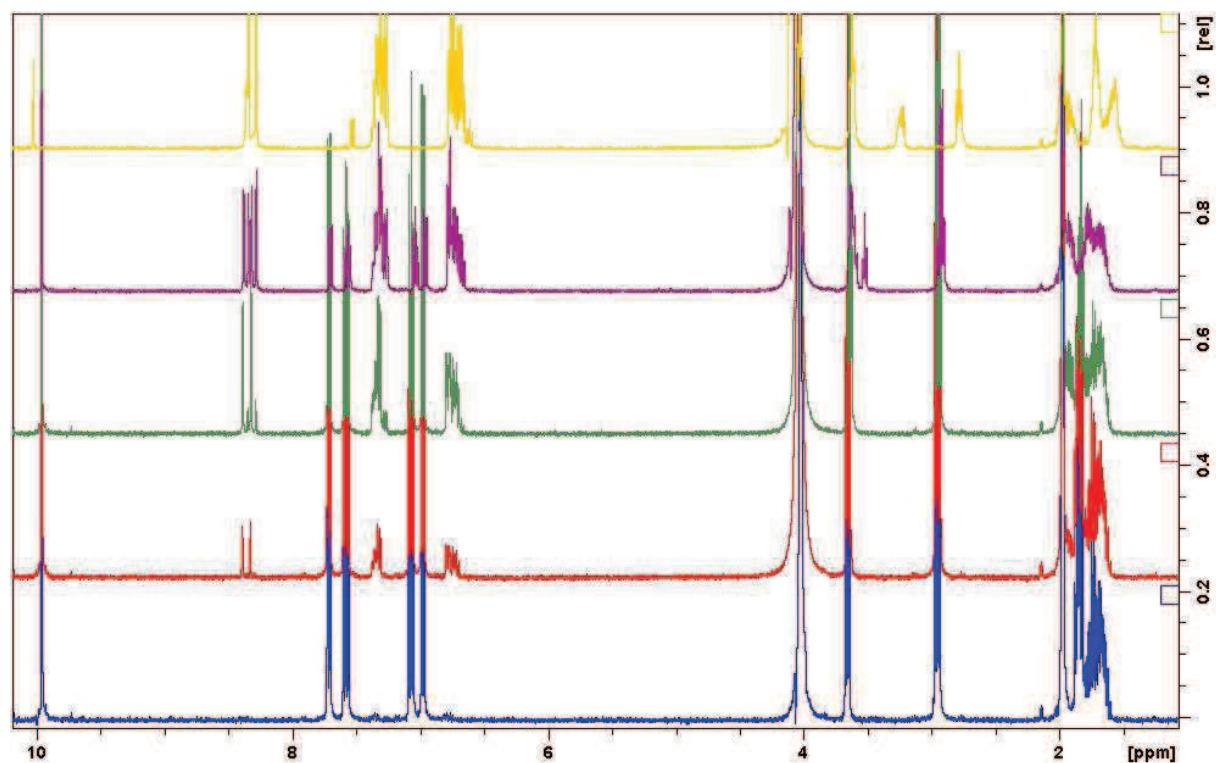
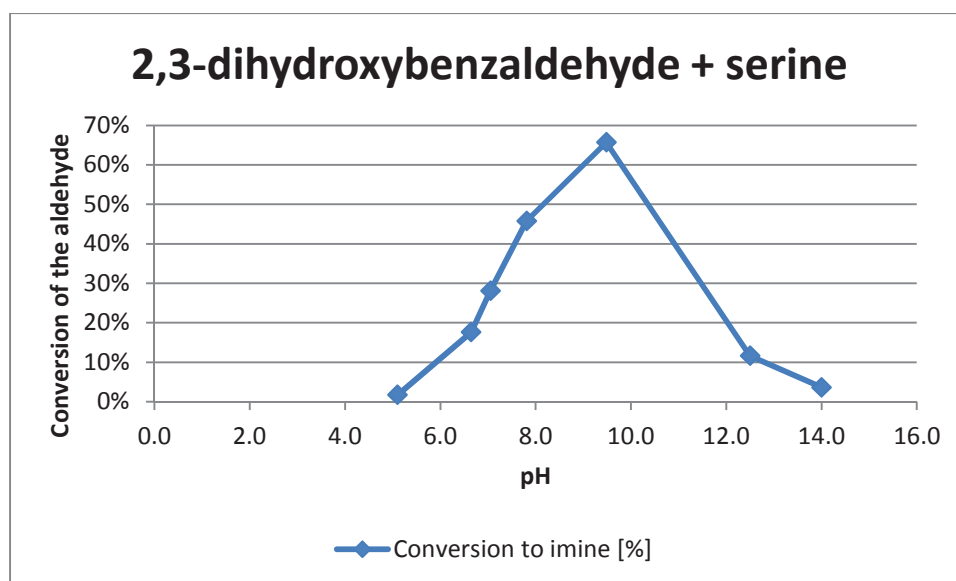


Figure 2.2-20  $^1\text{H}$ -NMR spectra of the reaction of salicylaldehyde with ornithine in a mixture of  $\text{CD}_3\text{CN}/\text{D}_2\text{O}$  (7:3 v/v) at increasing pH. The imine signals emerge as a pair of signals, one belonging to the  $\alpha$ - and the other to the  $\delta$ -amino group. The corresponding  $=\text{N}-\text{CH}-$  and  $=\text{N}-\text{CH}_2-$  signals of imines overlap heavily: the  $\alpha$ -imine has a CH signal overlapped with the water signal, whereas the  $\delta$ -imine  $\text{CH}_2$  overlaps with the CH signal of the free ornithine. Signal identification and assignment has been based on 2D NMR experiments. As the pH increases, the initial formation of mono-imine is observed which is finally overtaken by the formation of the bis-imine.

In order to avoid using a mixture of water and organic solvent, a water soluble aldehyde, 2,3-dihydroxybenzaldehyde, was taken and reacted with serine at different pH. The conversion grows in the range of pH 5 to 10, after which it reaches its peak of about 65 % conversion. Further increase in pH probably leads to deprotonation of one of the phenolic OH groups and consequently, to charge repulsion between the phenoxide and carboxylate anions, ultimately leading to hydrolysis of the imine formed. In Graph 2.2-5, the conversion is plotted as a function of pH while Figure 2.2-21 provides the corresponding NMR traces used for the conversion curve construction.



Graph 2.2-5 Relative conversion to the imine in the case of the 2,3-dihydroxybenzaldehyde reacted with serine in pure  $D_2O$  as function of pH. The dihydroxy derivative of **SALAL** was chosen for solubility reasons. As the pH increases above the typical  $pK_a$  of the phenolic OH, charge repulsion between the carboxylate and the phenoxide leads in the end to enhancement of hydrolysis of the imine.

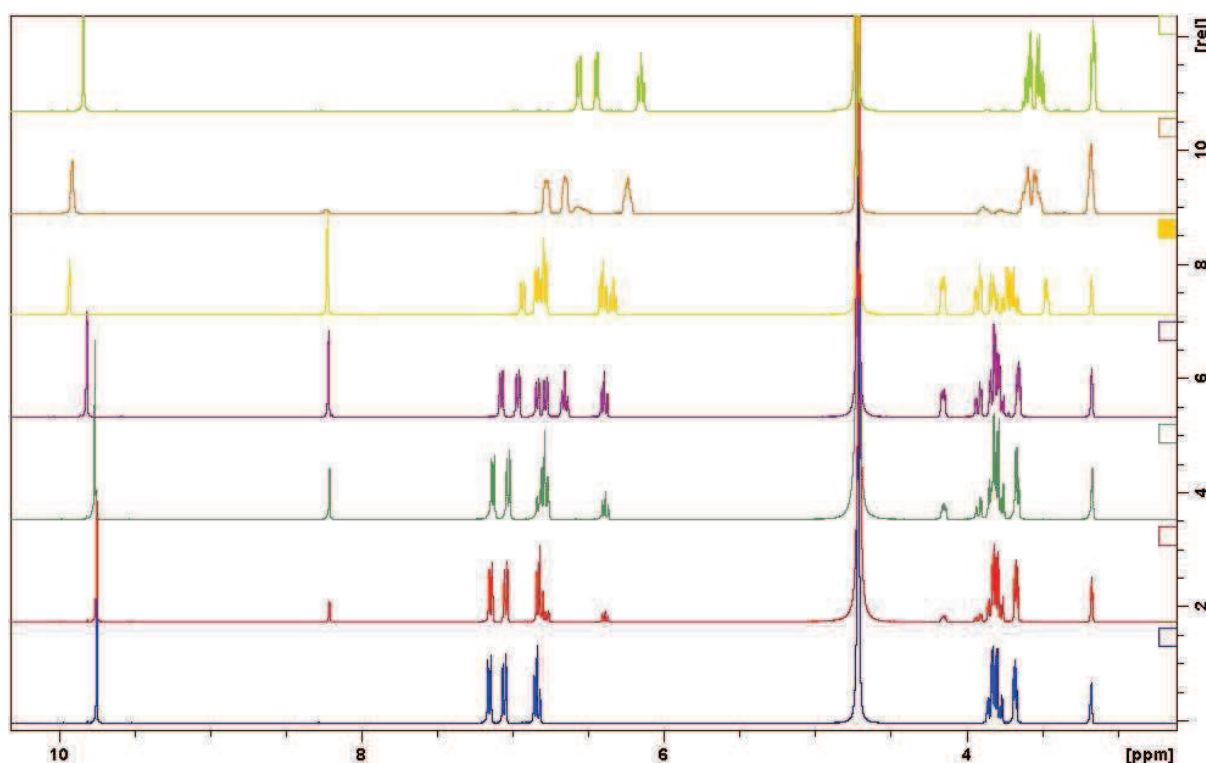


Figure 2.2-21  $^1H$ -NMR spectra of the pH titration of a mixture of 2,3-dihydroxybenzaldehyde with serine. The aldehyde signal decreases with pH while the imine signal increases up to the pH value of about 10 when maximum conversion is reached. Further pH augmentation decreases the imine conversion. The aliphatic signal of serine is shifting upfield upon deprotonation, the aliphatic signal corresponding to the imine formed can be found at 4.1 ppm.

## 2.3. Imine exchange

In constitutionally dynamic systems, a response to a stimulus (in other words “adaptation”) is reflected in the change of the constitution of the system, i.e. in the change of the covalent bonding of its components. The response time to the stimulus is determined by the rate at which the

components can exchange. Therefore, fast component exchange is reflected by fast adaptation. This has two important outcomes: a) the experimental time needed to achieve full equilibration is reduced by fast component exchange and, b) the risk of perturbation of the thermodynamic control over the system by kinetic factors is reduced in quickly responding systems. It is thus feasible to look for reactions and conditions which give the fastest reconstitution of the components.

In the case of the dynamic imine linkage, either of the two components (aldehyde or amine) can exchange in a reversible manner as a response to a change in condition or composition. To this extent, the aldehyde candidates studied previously have been investigated also in terms of the exchange kinetics. The *N*-propyl imines of **SALAL** and **BENZAL** were treated with 1 eq. of *i*-pentylamine in CDCl<sub>3</sub> and the formation of corresponding *N*-*i*-pentyl imines was followed by NMR (Figure 2.3-1 and Figure 2.3-2).



X =	$\chi = (K)$	$k = [s^{-1}]$
H	50 % (1.00)	$(4.38 \pm 0.26) \cdot 10^{-3}$
OH	50 % (1.00)	$(1.26 \pm 0.01) \cdot 10^{-3}$

Figure 2.3-1 Rate constants of the imine exchange reaction in the case of benz- and salicylaldehyde. Exchange between *n*-propyl and *i*-pentyl amine has an equilibrium constant of 1, showing no preference for either of these residues. The rate of exchange for salicylaldehyde is slower, probably due to stabilization of the species by the intramolecular hydrogen bond.

It is noteworthy that the imine exchange reaction follows pseudo-first order kinetics, although the mechanism is inherently bimolecular. This is in agreement with published results of Jencks *et al.*,<sup>[63]</sup> claiming that the rate determining step is the deprotonation of the reversibly formed aminal (a monomolecular process, Figure 1.3-5 on page 33). All other steps, including reversible aminal formation, are kinetically fast. This, on the other hand, does not imply a high concentration of this species in solution, which is only determined by the corresponding equilibrium constant. Therefore, aminal deprotonation can be a rate determining step even though there is very little or no amount of aminal observed.

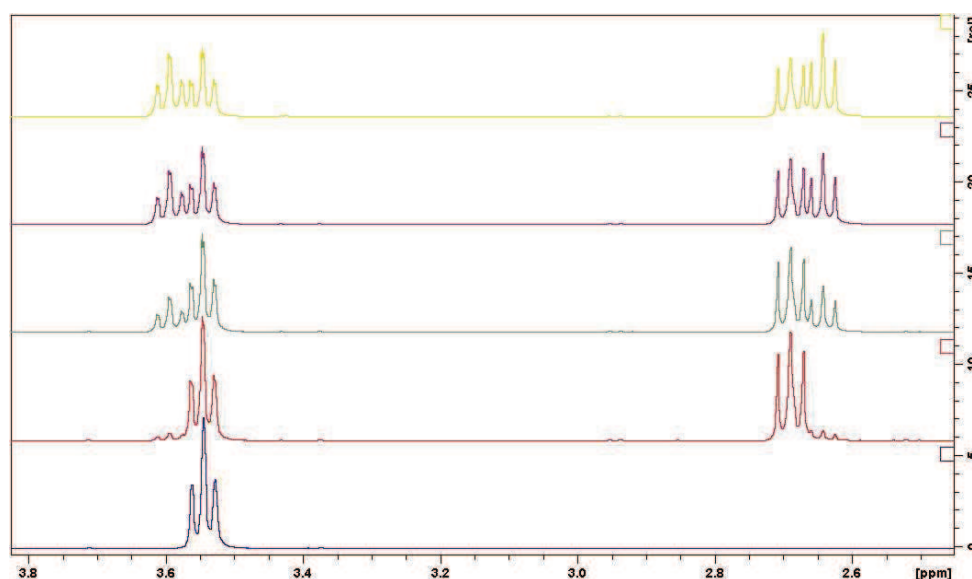


Figure 2.3-2 Representative NMR trace for the imine exchange experiment in CDCl<sub>3</sub> in the reaction of *N*-propyl imine of **SALAL** with *i*-pentylamine. The bottom trace correspond to pure *N*-propyl imine, red trace above is recorded immediately after addition of the *i*-pentylamine, following traces correspond to time stamp 8, 20 and 45 minutes after the addition.

As shown by the exchange rate constants, the intramolecular hydrogen bond present in salicylaldimines acts as stabilizing group not only in the imine formation, but also in the imine exchange. In other words, the rate of exchange is decreased in the case of **SALAL** compared to **BENZAL**. The two amine parts were chosen for their similar behaviour resulting in equimolar amounts of their imines (and consequently also free amines) in the exchange reaction. On the other hand, their signals in the NMR spectra are still well separated and can be fitted by kinetic models. However, when the two exchanging amines are very different, like in the case of *n*-propylamine and aniline, the equilibrium is shifted to one side of the reaction, in this case, in favour of the *N*-propyl imines (Figure 2.3-3). This can be attributed to higher nucleophilicity of *n*-propylamine compared to aniline, even though the imine formed from aniline provides a larger conjugated system. The equilibrium conversion to *N*-phenyl imines does not exceed 10 % and the rate constants for both **SALAL** and **BENZAL** are almost identical in this case.

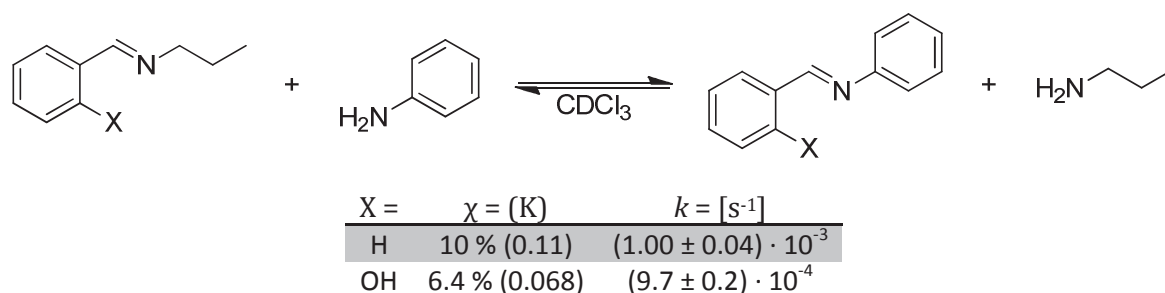


Figure 2.3-3 Exchange rate constants and equilibria in the case of asymmetrical exchange, i.e. one of the exchanging amines has higher affinity towards the imine formation. The contribution of the protective intramolecular hydrogen bond is negligible in this case.

In similar vein to the imine formation reactions, imine exchange was also followed in a  $CD_3CN/D_2O$  (7:3 v/v) mixture. Since there is some unreacted aldehyde in aqueous solutions of studied imine, introduction of the second amine leads to an increased conversion, typically by about 5 %. For practical reasons, this conversion enhancement was neglected in the exchange rate constant calculations.\*\*\*

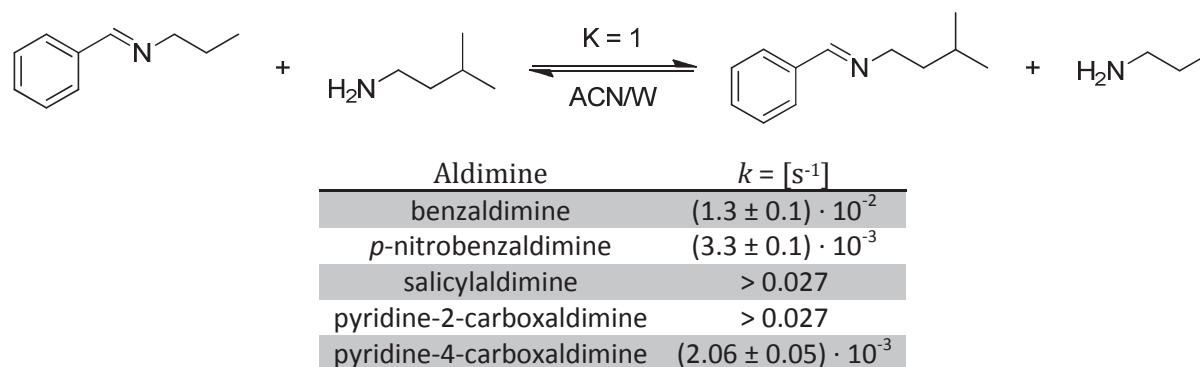


Figure 2.3-4 Rate constants of the imine exchange reaction for several aldimines determined in an acetonitrile/water mixture. Equilibrium constants are equal to 1 in all cases, proving that there is no preference for either of the amine parts. pH was buffered at  $8.73 \pm 0.01$  by 2 M triethanolamine.

A significant difference in the exchange rate constants was found compared to those determined in chloroform (Figure 2.3-4). The protecting effect of the intramolecular hydrogen bonding of salicylaldimines in aqueous media is lost, giving the rate of exchange too fast to be followed by NMR ( $> 0.027 \cdot 10^{-2} s^{-1}$ ), similarly to **PYRAL**. Pyridine-4-aldehyde is again slower in

\*\*\* The simple reversible exchange kinetic model would, in case of accounting for the increased conversion, give a set of four differential equations which cannot be solved analytically. The absence of an analytical solution to these differential equations also prevents the determination of confidence intervals.

exchange than **PYRAL**, like in the case of imine formation. Surprisingly, benzaldimine exchanges faster than its *p*-nitro derivative. The reason for these observations under the given conditions is unknown.

The preceding exchange experiments were performed in excess of the amine part and/or in aqueous media in which some free amine is present in the solution. In fact, this free nucleophile acts as the active species and contributes to the rate of the imine exchange to large extent. A different model must be proposed when the aldehyde is in excess (in which case there is very little or no free amine present) or in the case when two different preformed imines are mixed together.

For this purpose, three imines were synthesized: *N*-propyl imines of **BENZAL** and **SALAL** and *N*-*i*-pentyl imine of **PYRAL**. As shown before, the aldehydes have no preference for either of these two amine residues, giving an equimolar ratio of each when mixed. The imines were distilled from P<sub>2</sub>O<sub>5</sub> to ensure that the compounds were anhydrous and free of residual amines, and sealed under nitrogen. The exchange experiments were performed in d<sub>8</sub>-toluene which was distilled from sodium prior to use and stored under argon. These conditions should ensure the lowest water content possible and thus disfavour the exchange mechanism proceeding through the hydrolysis of the imine and its reformation as well as exchange caused by an excess of nucleophile.

In the first experiment, the exchange between imines of **SALAL** and **PYRAL** was studied. The reaction does not proceed at room temperature, and even after 24 hours there is still no NMR trace of the products of imine exchange. To achieve the exchange, the reaction must be heated up to 70 °C for 1 hour when the peaks of the exchanged products start to emerge (Figure 2.3-5).

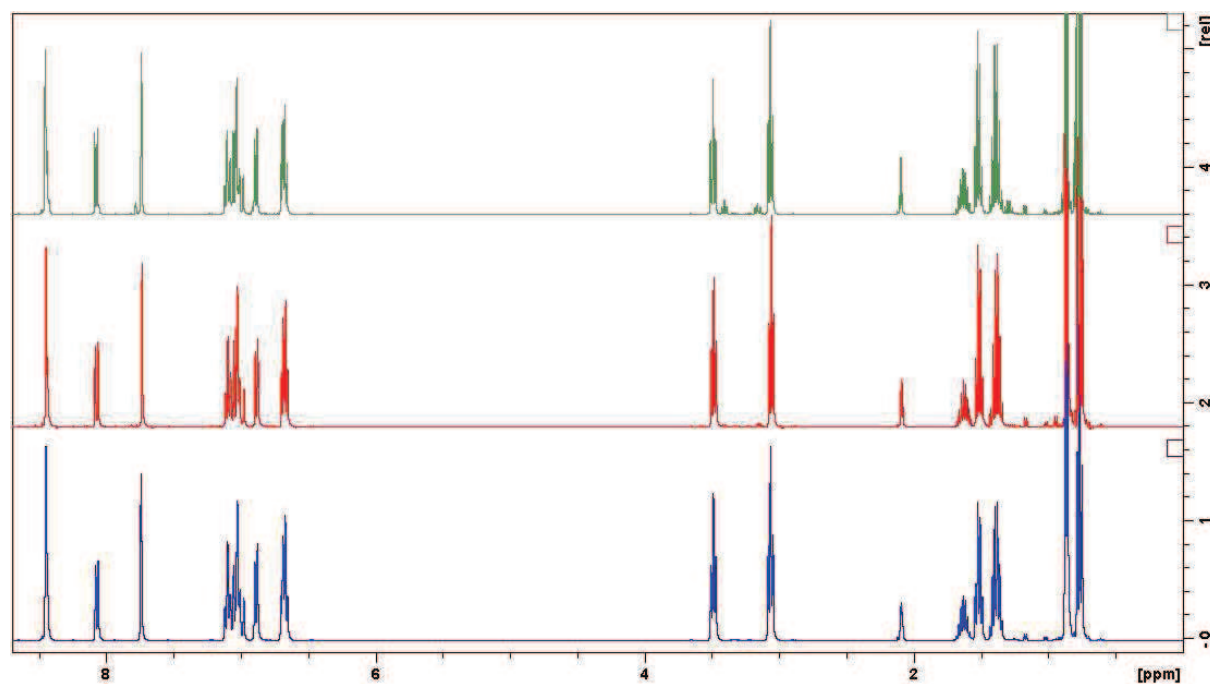


Figure 2.3-5 <sup>1</sup>H-NMR traces of the exchange reaction of imines of **SALAL** and **PYRAL** in d<sub>8</sub>-toluene. There is no observable difference between spectra recorded immediately after mixing and after 24 hours (two lower traces). The imine exchange products start to emerge (two small triplets in between two strong triplets at 3 and 3.5 ppm) after 1 hour heating at 70 °C.

For comparison, the study was repeated with the imine of **BENZAL** instead of **SALAL**. In this case, exchange occurs even at room temperature, giving approximately 10 % conversion after 20 hours. It was thus shown that the relatively acidic phenolic OH (the only source of acidic protons in the reaction mixture) in case of imines of **SALAL** does not catalyse the imine exchange reaction.

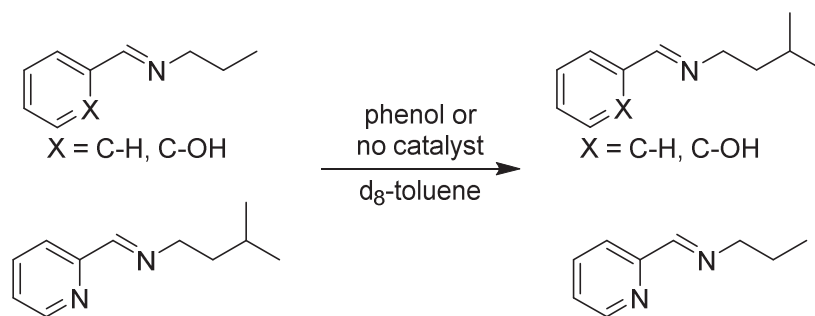
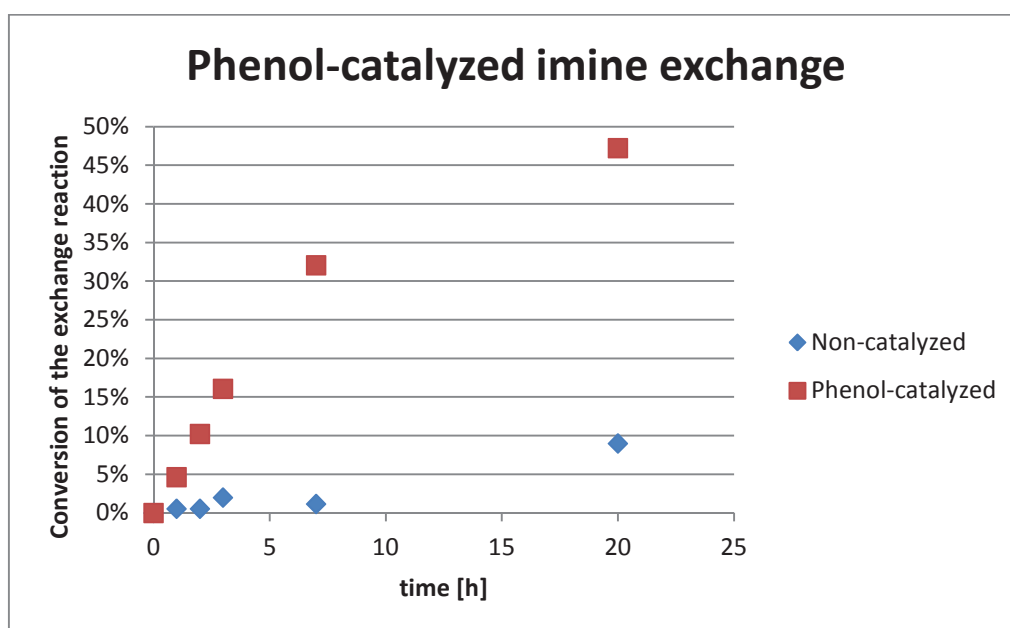


Figure 2.3-6 The effect of the OH-clipped imine was tested in imine exchange reaction.

To show the effect of the phenolic acidity, the exchange reaction of imines of **BENZAL** and **PYRAL** was repeated in presence of 1 eq. of phenol under the same conditions (Figure 2.3-6). Dramatic enhancement of the reaction rate was observed, giving almost equilibrium conversion (47 %) in 20 hours after mixing (Graph 2.3-1 and Figure 2.3-7).



Graph 2.3-1 Phenol catalyses the imine exchange reaction. The relative conversion of catalysed and non-catalysed reaction is shown (1 eq. of phenol was used). The catalysed reaction is almost at equilibrium after 20 hours, while the non-catalysed give only 10 % conversion at the same time.



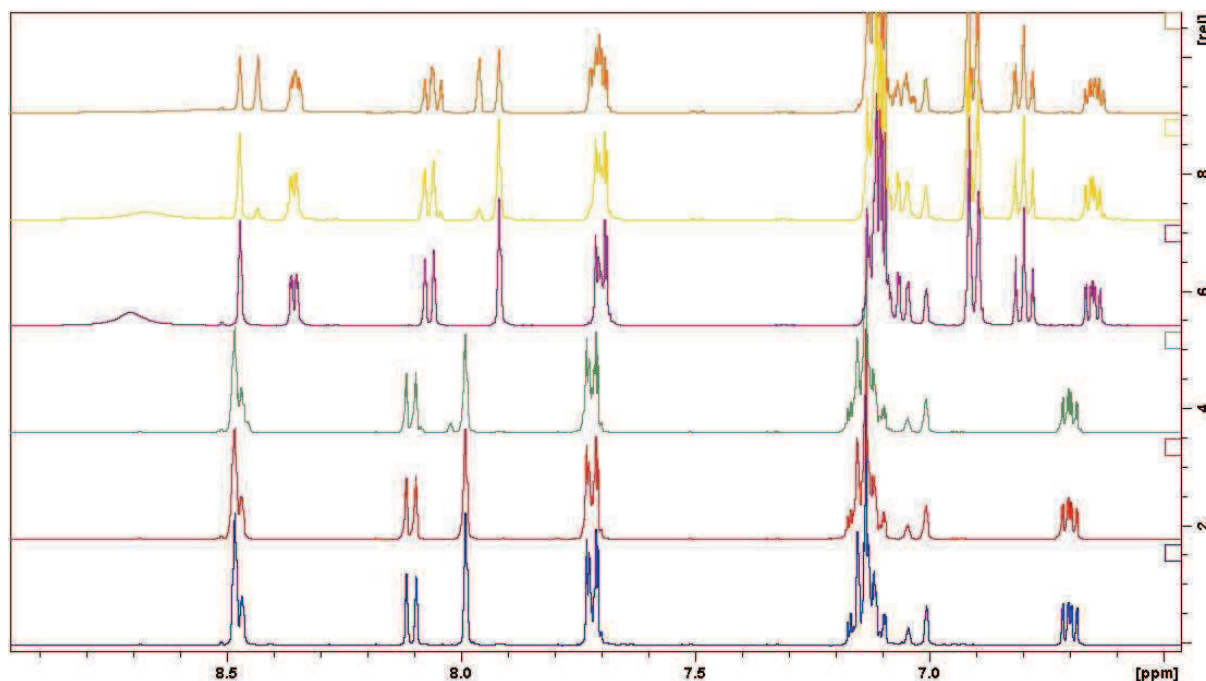


Figure 2.3-7  $^1\text{H-NMR}$  traces of the non-catalysed (lower three) and phenol-catalysed (upper three) imine exchange reaction between imines of **BENZAL** and **PYRAL**. The time stamps for both catalysed and non-catalysed reactions correspond to 0, 1 and 20 hours after mixing. The emergence of the new imine peaks is much faster in the catalysed reaction. The imine peak of the **BENZAL** imines in the non-catalysed reaction is overlapped with one of the pyridine aromatic signals, while the signals of **PYRAL** imines are well resolved (8.0 ppm in the non-catalysed and 7.9 ppm in the catalysed reaction).

## 2.4. Summary of Chapter 2

- An aldehyde screening was performed and the two most reactive aldehydes, salicylaldehyde and pyridine-2-carboxaldehyde, were identified.
- The reactivity of salicylaldehyde has been demonstrated to be the result of the intramolecular hydrogen bond.
- The tautomer of salicylaldimine has been suggested to correspond to the quinoid structure rather than the phenoxide zwitterionic structure.
- The selected aldehyde hits are also superior in terms of kinetics of imine formation.
- The acidity of the phenolic OH was identified to be governing factor in the kinetic activity of salicylaldehyde.
- The selected aldehyde hits are also suitable in terms of exchange kinetics, being superior to other aldehydes in aqueous media.
- The intramolecular hydrogen bond of salicylaldimine was shown to have a protecting effect in non-aqueous media.



## 3. MOLECULAR WALKING VIA DYNAMIC IMINE BOND

### 3.1. Introduction: Molecular walking

Molecular walking is an example of motional dynamics. The walker unit is displaced along the track in a repetitive, step-like mechanism. Nature has developed walking cellular protein motors which consume a fuel to power the displacement of one molecule or part of the molecule with respect to another in a given direction. The fuel provided enables operation against the gradient driving the system towards thermodynamic equilibrium and to actually perform work. Synthetic mimics of this fascinating biological process have been demonstrated, although so far they all operate under thermodynamic control. Artificial molecular walkers operating under kinetic control are still an open challenge.

#### 3.1.1. Biological molecular walkers

The complexity of cellular structure emerging during early cell evolution required a way to reliably organize the interior of the cell, cytosol, and as the cells were growing bigger, also a way to transport diverse cargo from the interior of the cell to the surface as well as in the opposite direction. Early eukaryotes have developed protein molecules which can reversibly bind to the cytoskeleton, and fuelled by ATP, a cellular energy source, they can perform step-like movement along the cytoskeletal track towards one end. If a cargo is attached to this protein, it is dragged by the walking protein to its destination.<sup>[30]</sup> Large numbers of such protein molecules have been discovered and studied until today and they are divided into three major classes: 1.) the kinesin superfamily (KIF) – protein molecules which walks along the microtubule to its plus end (to the surface of the cell),<sup>[29,32]</sup> 2.) dynein – a protein that walks along the microtubule to its minus end (to the cell centre),<sup>[35]</sup> 3.) the myosin superfamily – proteins that walk along actin chains.<sup>[235]</sup>

These cellular motors perform very important tasks throughout the cell's life – starting by separation of chromatin during cell division and organization of cellular structures by moving the organelles to their specified positions, to waste disposal by vesicle transport to the surface and signalling by mRNA transport.<sup>[30]</sup>

To achieve high reliability and performance, the walker system has to fulfil several criteria. The motor protein must remain in contact with its track during the period of making a step, otherwise it would detach from track. Biological motors have typically two binding domains, therefore when one is making a hand-over-hand step, the other keeps the motor protein attached to the microtubule or actin filament.<sup>[99]</sup> Also, the movement must be strictly directional, i.e. when one step is taken towards the plus-end of the microtubule the next step must be in the same direction otherwise all work done during the first step would be lost during the second one. The active site of the walking protein is an ATPase enzyme, which causes conformational changes to the protein backbone leading to destabilization of trailing foot binding to the track and consequently its lifting, overtaking the leading foot and ultimately binding to the track again. Cellular walkers usually form dimeric structures such that the structure of the active ATPase centre before and after the step is

taken is identical, which ensures that the steps can be taken in one direction only for a given protein motor.<sup>[34]</sup>

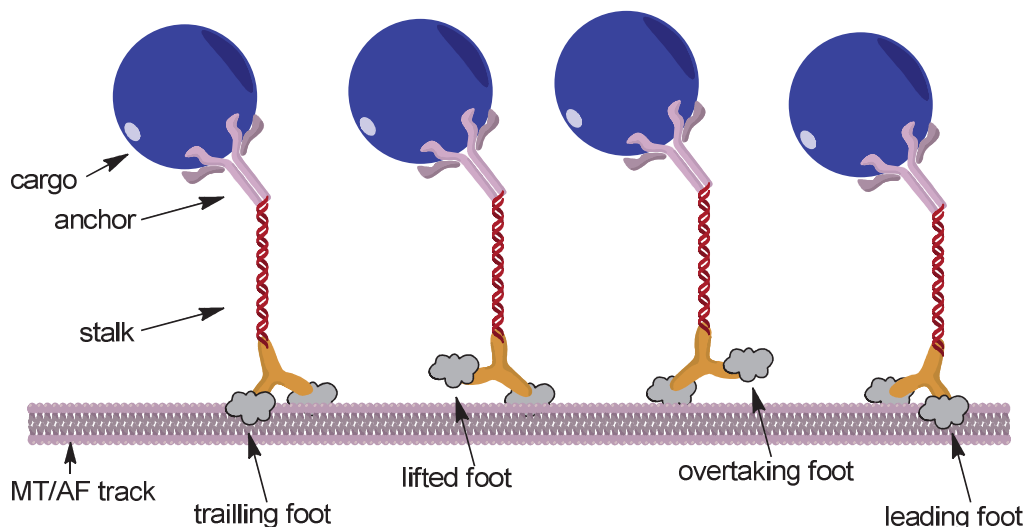


Figure 3.1-1. Schematic description of a biological molecular walker performing a single step.

Important descriptors of the biological walker are the length of the step taken, the speed of walking, and the force applied in pulling a cargo. These values depend on the type of the motor and the size of the cargo. For example, kinesin makes a step of 8.3 nm in one step and can reach a speed of  $0.2\text{--}0.6\ \mu\text{m s}^{-1}$ .<sup>[32,34,99]</sup> Dynein, walking in the opposite direction, can reach a speed of  $5\text{--}10\ \mu\text{m s}^{-1}$  and the step length can vary from 8 nm when carrying a heavy cargo, to 32 nm when no cargo is transported.<sup>[35]</sup> Myosin is capable of moving up to 95 nm in one step event.<sup>[99]</sup> Due to the bipedal structure of the walking motors (dimeric proteins), the length of the cargo displacement is only half as long as the step size, i.e. the distance that the trailing head must overcome to get to leading position. Using optical tweezers, the force applied by the walker on the cargo has been measured to vary from 1.1 pN for dynein up to 8 pN for kinesin.<sup>[35]</sup> Impressive as these steps might be, one has to realize the size of the motors - kinesins are approximately 80-350 kDa proteins with sizes from 50 to 80 nm, dynein being approximately as twice as big.<sup>[29,236]</sup> In other words, the walking proteins perform steps of approximately 10 % of their size.

Many important questions in the field of cellular transporters are still not satisfyingly answered.<sup>[29,30,99]</sup> For example, the cell environment is a relatively concentrated solution of various cellular structures and components, which might be in the way of the walking process. Therefore effective and functional molecular walkers need to avoid or overtake such obstacles, for which Nature apparently found a way although the mechanism is not known. Also, how does the cell manage traffic on its rich highway net of microtubules and filaments? And how does a cargo recognize its predestined motor unit? These and many other questions are now accessible to investigation using innovative emerging techniques like scanning probe microscopies<sup>[237-240]</sup>, fluorescence confocal microscopy<sup>[241-243]</sup>, FRET<sup>[244,245]</sup>, quantum dots<sup>[246-249]</sup> and optical tweezers<sup>[250,251]</sup>.

### 3.1.1.1. Biological tracks & directionality control

The cellular motors work in a unidirectional manner, i.e. they can only walk in one direction along the asymmetric microtubule or filament. Kinesins are walking towards the plus-end of the microtubule (anterograde direction, towards the surface of the cell), while dyneins are moving in the

opposite direction to the minus-end of the microtubule (retrograde direction, towards the cell's nucleus).<sup>[99]</sup> Thus the cargo can be transported in either direction by anchoring to the proper motor unit. In fact, a single cargo can anchor more than one motor, and these motors can even be of different types. As long as one type of motor is inactivated, directional transport of a cargo is observed. Switching the active/inactive unit at the cargo's destination results in backward motion, as was observed in several biological structures.<sup>[252]</sup>

Directional movement of the biological motor proteins requires an inherently bipolar, oriented track, which microtubules are. They are formed from heterodimers of  $\alpha$ - and  $\beta$ -tubulin, where  $\alpha$ -tubulin exposed ends are called minus and  $\beta$ -tubulin end are called plus.<sup>[253]</sup> Elongation (or shrinking) of the microtubules proceeds much faster on the plus end (driven by GTP hydrolysis),<sup>[254]</sup> and, in mammalian cells, the minus ends are often rigidly anchored to other cellular structures. The active site of the motor protein, originally thought to be responsible for directionality of the protein,<sup>[255]</sup> was found to be very conserved throughout the motor protein families,<sup>[256]</sup> and rather than to directionality it contributes to processivity.<sup>[257]</sup> The consensus on the origin of the directionality claims that it is the dimeric form of the walking protein resulting in two feet bound to the track by different strength which prevents the backward steps by the ratchet type mechanism.<sup>[258]</sup> It was further shown, that the directionality of the motor proteins can be biased by ionic strength<sup>[259]</sup> or completely inverted by coupling multiple motor proteins together with respect to individual motor protein.<sup>[260]</sup> A very similar situation is found also in the case of the actin-walking proteins,<sup>[261]</sup> which are inherently capable of walking in either direction along the bipolar, oriented actin filaments. The processivity is again gained by duplication of the walking foot, like in the kinesin family, but the directionality is achieved by different mechanisms.<sup>[262]</sup>

### 3.1.2. Artificial molecular walkers

The fascinating properties of biological walking motors have attracted the attention of chemical research to create simpler, affordable and modular transporters for practical applications. However, several issues emerge when one tries to create non-protein molecular walker. In addition to processivity and directionality required also for biological motors, synthetic molecular walker must have other features which are inherent to biological kinesin-like molecules.<sup>[263]</sup>

- Repeatability – every step taken by the walker should be the same, i.e. consuming the same fuel, performing the same work and overcoming the same distance.
- Progressivity – after performing one step biological walkers have the same structure as before, being ready to make another step. This elegant solution is not guaranteed for artificially designed motors.
- Autonomous functionality – when enough fuel is supplied, the system should keep performing the task until it is finished or until the fuel is depleted, without any intervention.

Several smart and elegant solutions of aforementioned problems have been demonstrated in the literature (Section 3.1.2.3). However, construction of a system of small molecules performing molecular walking and cargo delivery is still a challenge.

#### 3.1.2.1. *Toolbox of molecular machinery*

Molecular walkers are part of a broader family called molecular machines.<sup>[264,265]</sup> Similarly to their macroscopic counterparts, molecular machines are designed to perform work (output) as a response to application of a force or providing fuel (input). The basic phenomena<sup>[266]</sup> as well as state

of the art in this field have been summarized in exhaustive reviews.<sup>[264,265]</sup> From numerous systems in the literature, only a few inspiring examples are presented here for illustration.

The molecules which can undergo a reversible transition between two (or more) chemically distinct states are called molecular switches. The transition from state A to state B can be stimulated for example by light, heat, coordination or electrochemical potential.<sup>[98,267–278]</sup> Different properties of the two states can manifest in various ways – the switch can be an ON/OFF catalyst of a chemical reaction,<sup>[279–281]</sup> the two states can have different electronic structure and conjugation between parts of the molecule<sup>[282]</sup> etc. Finally, the two states can be inherently chiral which can ultimately lead to switchable enantioselective catalysis of Michael addition.<sup>[283]</sup>

Generation of mechanical force from molecular movement represents an attractive concept for nanoscience. The one dimensional motion has been shown using molecules which can change their length as an adaptation to the stimulus, e.g. coordination to metal ion.<sup>[100,178,284]</sup> Extension to two dimensions has been demonstrated for molecular rotors where one part of the molecule is rotating about an axle with respect to another part of the same molecule.<sup>[285,286]</sup> By combination of the two, a unidirectional twister which undergoes simultaneous length change and rotary motion has been prepared.<sup>[287]</sup> Different modes of 3D motion is the case of autonomously operating self-propelled bimetallic nanorods which “swim” in hydrogen peroxide solutions.<sup>[288]</sup> Also, their motion direction can be controlled by acoustic or magnetic fields.<sup>[289]</sup>

Catenanes are mechanically interlocked molecules consisting of two intertwined macrocyclic rings. Similarly, rotaxanes consist of a macrocycle wrapped around a dumbbell-like molecule, so that the stoppers (end-capping groups) prevent the ring from slipping from its central rod-like part. Catenanes bearing both tridentate (like terpyridine) and bidentate (like phenanthroline) ligands in each of their macrocycles can coordinate metal cations by four, five or six dative bonds. As the coordinating demands of copper changes as a function of its oxidation state, the catenane with two Cu(I)-coordinated phenanthrolines in the intersection can be switched by electrochemical oxidation of the copper to Cu(II) to structure with two Cu(II)-coordinated terpyridines in the intersection.<sup>[290,291]</sup> In a similar way, switchable rotaxanes have been introduced, using different oxidation and protonation states.<sup>[292–295]</sup> Recently, a rotaxane bearing several aminoacid residues was used as synthetic peptide synthesizer, a feature which is performed by ribosomes in living cells.<sup>[296]</sup> As the presented examples are powered by external stimulus (fuel), they can, in agreement with the second law of thermodynamics, perform tasks (work).

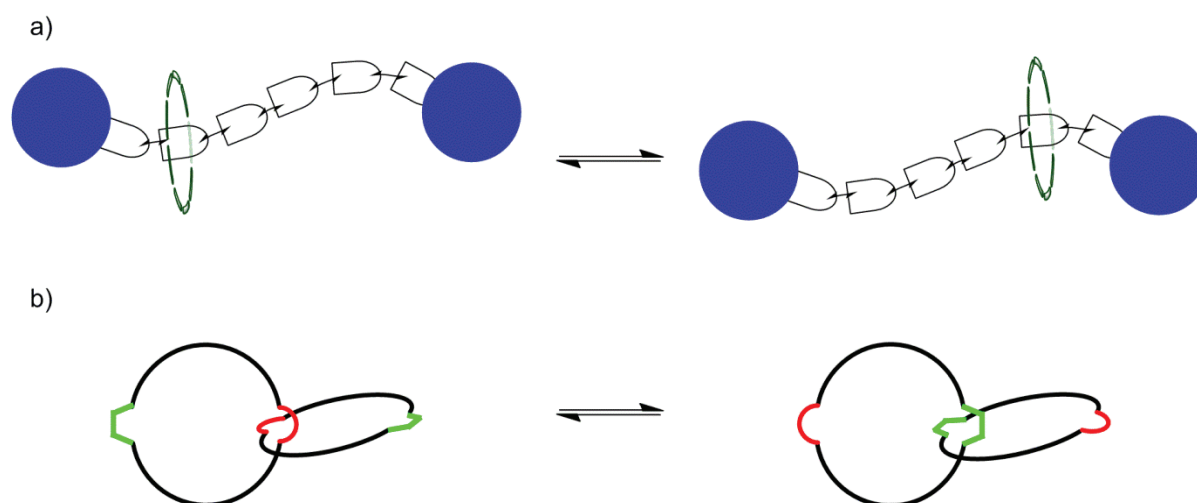


Figure 3.1-2. a) Schematic representation of a switchable rotaxane. Blue circles represent stoppers at the ends of the linear central part, around which a macrocyclic ring is wrapped. b) Schematic drawing of a switchable catenane, two intertwined macrocycles are mechanically interlocked. Two distinct coordinating pockets are indicated in green and red.

From many fascinating machines on the molecular scale, only those which have a resemblance to molecular walking are discussed in following two sections, although many features are common to all molecular machinery. In the following text, the switchable catenanes and rotaxanes are considered shuttles and not walking molecules because the processivity of the displacement from position A to position B, i.e. the fact that the walker doesn't fall off its track, is due to mechanical interlocking of the molecules, unlike the walking motor where the processivity is achieved through bonding (either covalent or noncovalent) of the walker with the track.

### 3.1.2.2. DNA-based molecular walkers

Tremendous progress in the field of DNA synthesis has enabled preparation of complex artificial structures based on long DNA sequences. The formation of a stable, yet reversible duplex of matching DNA sequence provides a unique way to design and control the system. In the first example of a DNA walker,<sup>[297]</sup> single-stranded foot and foothold DNA sequences were linked by a simultaneous formation of the duplex with programmed "anchoring" DNA sequence, in which one part is complementary to the foothold and one to the foot sequence. Also some non-pairing nucleobases are present. Specific sequences for each foot, foothold and anchor provide precise control over the binding of each foot to its designed foothold. After addition of a DNA sequence fully complementary (energy gain by complementarity with previously non-pairing nucleobases)<sup>[298]</sup> to the anchor, the foot is released from its foothold. This released foot can now be anchored to a different foothold by addition of the corresponding anchoring sequence. By crosslinking of two feet, one obtains a molecular DNA biped with feet addressable by specific DNA sequences.

Many fascinating examples have been demonstrated using the complementarity of the DNA sequence and even autonomous modes of operation has been introduced.<sup>[299–301]</sup> A more detailed overview of this rich and swiftly evolving field can be found in the published review.<sup>[263]</sup>

### 3.1.2.3. Small-molecule walkers

All previous examples of smart machines capable of molecular walking share a single drawback: their size (molecular weight) is enormous. The ideal molecular walker is a small molecule requiring a simple track so that these systems can be easily modified to match the particular needs and conditions. Also, controlled synthesis of large sophisticated molecules is generally more costly than for smaller molecules. This motivated research in the field to achieve a system which is capable of performing the molecular walking in an oriented manner using small molecules and easily accessible tracks.

Controlled step-like motion was demonstrated<sup>[302,303]</sup> using a combination of two independent dynamic reversible reactions operating under different conditions: acylhydrazone exchange and disulfide exchange. While hydrazone exchange proceeds under acid catalysis (by either Brønsted or Lewis acid), the disulfide exchange requires basic conditions to generate thiolate anions which then induces the exchange of disulfides. Alternatively the disulfide exchange can be performed using a sequence of reduction and oxidation step – the reduction breaks the disulfide linkage into two thiols which are then linked again by oxidation. By introduction of both hydrazide and disulfide in one molecule one can address each of the feet separately by periodic changes in pH. The mechanism is illustrated in Figure 3.1-3. The track is synthesized with the walker unit already attached by both acylhydrazone and disulfide foot. The track also contains an aldehyde and another disulfide linkage. Under neutral conditions the molecule is stable. By acidification the acylhydrazone group becomes labile and undergoes reversible hydrolysis and recondensation, but the condensation

can proceed with either the original aldehyde group or the other available aldehyde. The connection to the track remains intact due to stability of disulfide linkage under acidic conditions. Next, the pH is increased which leads to “freezing” of the acylhydrazone dynamics, but on the other hand the disulfide linkage becomes labile and undergoes disulfide exchange. Thus second step is performed and the walker unit is displaced along the track.

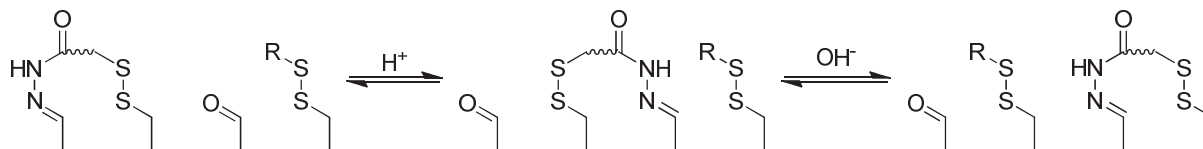


Figure 3.1-3. Schematic representation of acylhydrazone/disulfide diade used for molecular walking.

Each of the steps performed in disulfide-acylhydrazone step-like motion is non-directional, in other words, it has 50% chance to perform a step forward, but has also 50% chance to make a step back. Therefore after several cycles of pH changes the distribution of species attached along the track is statistical and equilibrium is reached. However, the mixture is still dynamic in nature and can be qualified as dynamic equilibrium in which species interconvert but their overall ratio does not change.

Enhancement of directionality was achieved by introduction of a photoisomerizable double bond in the track.<sup>[304]</sup> The sequence of the acylhydrazone-disulfide exchange is inverted in this case (Figure 3.1-4). The track is synthesized with the walker unit attached at one end and with the double bond in the Z configuration. This configuration brings the walker unit in proximity to the second disulfide linkage and therefore under basic conditions the disulfide exchange proceeds. If the double bond is in E configuration the exchange proceeds less effectively. When the walker unit is attached in the central position on the track and then the photoisomerization of the double bond is performed, high strain is introduced into the macrocyclic structure. Following acidic acylhydrazone exchange proceeds unidirectionally (i.e. the original acylhydrazone bond is hydrolysed and new one is formed with the other carbonyl without recondensation with the original carbonyl) to release the strain accumulated in the macrocycle by the photoisomerized double bond. In this manner, the directionality reached up to 95 %.<sup>[304]</sup>

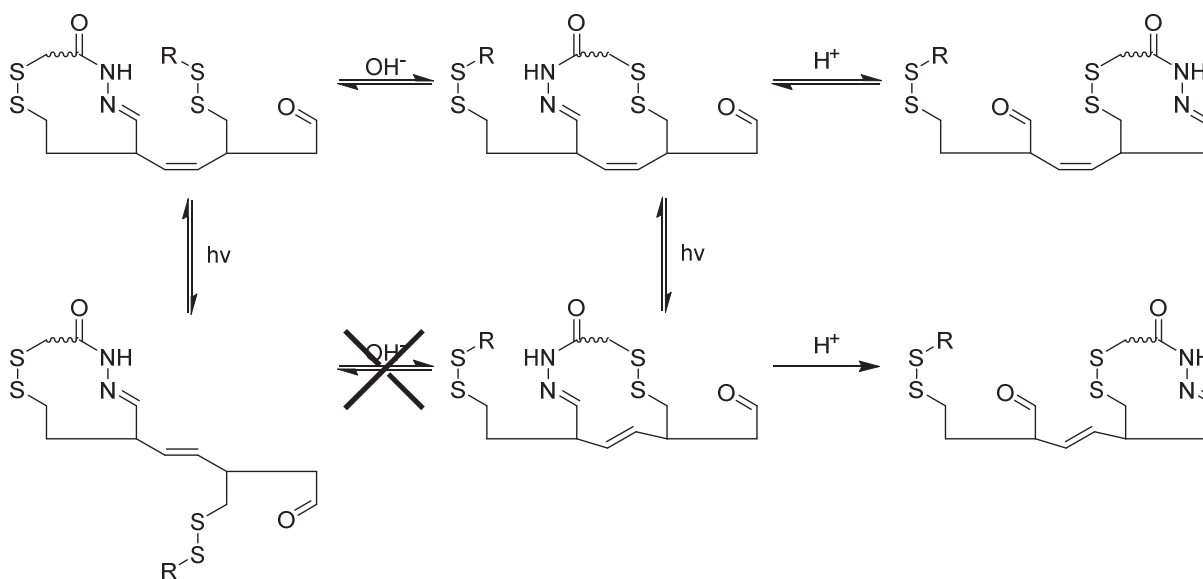


Figure 3.1-4. Photoisomerizable double bond enhances the directionality in ratchet type molecular walking.



Another non-directional walker was demonstrated based on reversible Michael/retro-Michael reaction of a *p*-nitrostyrene derivative and a linear polyamine chain.<sup>[74]</sup> The principle is illustrated in Figure 3.1-5. The trimethyl(2-(4-nitrophenyl)prop-3-en-1-yl)ammonium salt reacts with the terminal nitrogen of the selectively protected polyamine chain. After deprotection (removal of Boc by TFA) the walker unit undergoes Michael addition to a neighbouring amino group on the alkene conjugated with the aromatic ring and the nitro-group forming an intermediary seven-membered ring. This ring breaks through the retro-Michael reaction with 50 % chance to open on each side to allow the walker unit to be either displaced to the next nitrogen atom or to the original one. Placing a fluorescent molecule on one end of the track leads to significant fluorescence decrease over time as the nitrophenyl group serves as a fluorescence quencher.

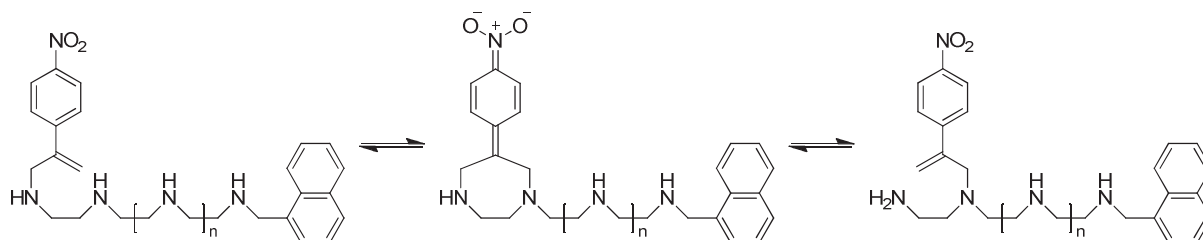


Figure 3.1-5. Small molecule that walks down along a polyamine chain through the reversible Michael addition of the nitrostyrene derivative.

Unidirectionality was introduced also for this type of walker by attachment of two different aromatic groups (phenylpropyl and 1-naphthylmethyl) on the polyamine chain. The walker unit starts at the position next to the phenylpropyl group and slowly walks towards the naphthylmethyl-substituted end.<sup>[305]</sup> However, once the equilibrium is reached, the walker cannot be reverted to the starting position, nor recycled, and hence this type of walker is one-use-only. A similar principle of single unidirectional displacement has been applied to mimic the natural ribosome function by synthesizing oligopeptides with well-defined sequence.<sup>[296]</sup>

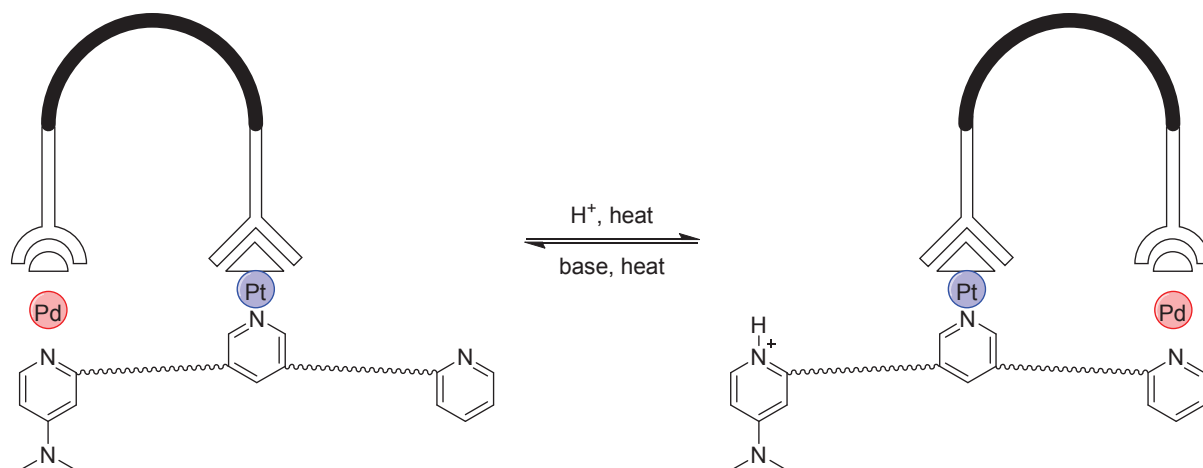


Figure 3.1-6 Reversible directional displacement of the coordinating biped along the track of pyridine ligands. Protonation of the more basic pyridine leads to displacement of the labile palladium foot while more strongly bound platinum foot remains permanently attached to its site.

Finally, a reversible unidirectional walker has been demonstrated, working as a biped with pH controlled heat driven coordinating feet.<sup>[306]</sup> The two feet are based on two different metal ions: palladium as the labile foot and platinum as the fixed one (Figure 3.1-6). The labile palladium foot can exchange between two pyridine coordinating sites, out of which one bears a *p*-dimethylamino group. This substitution leads to an enhanced nucleophilicity, but also to increased basicity. Therefore, under basic conditions the palladium foot occupies the more nucleophilic site, but upon



acidification this site gets protonated and the labile foot shifts to the less basic, non-substituted pyridine ring while the platinum foot remains constantly locked in its position. The complexity of the walker and the track is demonstrated by more than 12 synthetic steps required and by the molecular mass of the system higher than 2 kDa.

### 3.1.3. Concept

The phenomenon of molecular walking, well known in cellular biology and also studied on artificially synthesized systems was brought to the field of the reversible aldehyde-amine condensation. First, non-directional two-site displacement was examined as well as ways to influence and to control the system and the rate at which it operates. Then the system was probed on longer multi-site tracks of various topologies. Also, experimental evidence on the mechanism of observed motional dynamics as well as demonstration of basic steps is provided. The results to this point were published.<sup>[307]</sup> Finally, the directionality control was explored.

## 3.2. Imine bond-based small molecule walkers

Dynamic Covalent Chemistry (DCC)<sup>[6,20–22,26,27,308,309]</sup> rests on the implementation of reversible covalent reactions for the generation of dynamic covalent/combinatorial libraries (DCLs) of constituents from the reversibly connecting components. The reversible imine formation process deserves a particular attention in view of the ubiquity of the amino function in substances of interest in chemistry, biology<sup>[310]</sup> and materials science.<sup>[311]</sup> As it proceeds with the liberation of water, its dynamic character depends on and may be controlled by the presence of water. To further extend its scope in the realm of DCC, the exploration of the imine forming and exchange reactions of a number of aldehydes with typical amines was undertaken (see Chapter 2). The observations show much more than simple molecular reactivity and recognition, uncovering some remarkable features, involving both constitutional and motional covalent processes. An especially attractive processes involving the imines of salicylaldehyde (**SALAL**),<sup>[64,128,209,221,226,312]</sup> is reported adding novel facets to the chemistry of this extensively investigated molecule. They display remarkable formation and exchange features, of much interest for DCC,<sup>[226,312]</sup> for which it might be called an “imine clip” reporting on the internal hydrogen bond established between imine nitrogen and the neighbouring hydroxyl group.

The imines formed by **SALAL** with oligo-amines (such as ethylenediamine, diethylenetriamine, etc...) display particularly interesting intramolecular non-directional motional processes, involving transfer of the salicylidene group between amino groups by reversible covalent bond formation, that bear relation to the synthetic molecular “machines”<sup>[264–266,276,313,314]</sup> and biological motor proteins<sup>[29–32,35–37,99,235]</sup> areas, very actively investigated in recent times. These results were complemented by a comparison with the behaviour of pyridine-2-carboxaldehyde (**PYRAL**)<sup>[199,201,208,315]</sup> and of benzaldehyde (**BENZAL**)<sup>[316,317]</sup> as reference compounds. Imine formation by the related pyridoxal-5-phosphate has been extensively studied in the literature,<sup>[192,205,209,215,217,318]</sup> in view of its importance as biological cofactor (see Section 1.3.3) and the present data may also have implications for the related transamination reactions. Group transfer through making and breaking of covalent bonds has been described for several functional groups, such as acyl or borinyl transfer.<sup>[68,88–91,93,319,320]</sup> The dynamic behaviour of imines is of special interest<sup>[21]</sup> in view of its widespread role in chemistry, biochemistry<sup>[23,24,321–323]</sup> as well as in materials science.

In more general terms, the results reported in this Chapter represent a combination of constitutional and motional dynamic covalent processes (a feature envisaged earlier<sup>[100]</sup>) within the same system, as illustrated schematically in Figure 3.2-1. They lead to the notion of Dynamic Covalent Motions (DCMs), concerning motions that result from reversible covalent bond formation and dissociation within molecules, rather than by changes in non-covalent arrangements within supramolecular architectures. By extension, the processes uncovered also impact on the design of

nanochemical devices of artificial as well as biological significance, whereby simple aldimine systems represent prototypes of entities that may both undergo intramolecular displacement motions and intermolecular exchange of their parts, thus enabling in principle adaptation by structural variation.

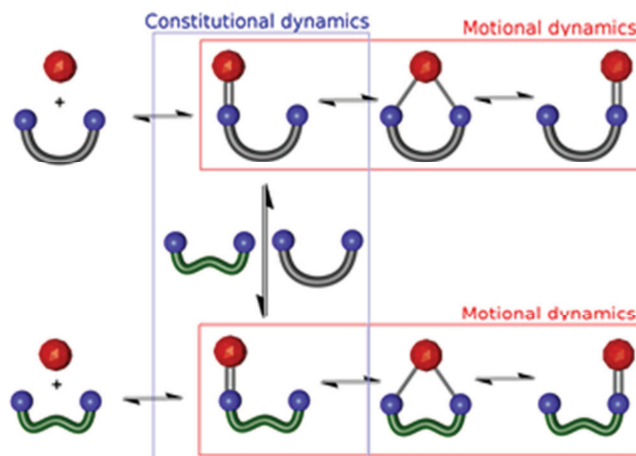


Figure 3.2-1 General scheme of merging motional and constitutional dynamics.

### 3.2.1. Aldehydes with aliphatic $\alpha,\omega$ -diamines

In order to promote high efficiency of formation, high rates of formation and high rates of exchange, a mixed aqueous-organic solvent, aqueous acetonitrile ( $\text{CH}_3\text{CN}/\text{H}_2\text{O}$ , 7/3) was chosen, which in addition to insuring a wide range of solubility also allowed the observation of novel dynamic features. The previously determined kinetic parameters of imine formation and exchange from Chapter 2 relevant to the herewith studied compounds are recapitulated in Table 3.2-1

Aldehyde	$k$ [ $10^{-3} \text{ M}^{-1} \text{ s}^{-1}$ ]	Conversion [%]	Half-life s <sup>[a]</sup>	$R^2$
BENZAL	$61.1 \pm 0.9$	20	818	0.88
SALAL	$71.4 \pm 0.4$	77	700	0.99
PYRAL	$202 \pm 2$	61	248	0.98

<i>N</i> -Propylimine of	$k \cdot K$ [ $\text{M}^{-1} \text{ s}^{-1}$ ]	Conv. to <i>i</i> -pentylimine [%]	Half-life [s] <sup>[a]</sup>	$R^2$
BENZAL	-	50	< 20	-
SALAL	$0.73 \pm 0.02$	50	76	0.97
PYRAL	-	50	< 20	-

Table 3.2-1 Selection of kinetic data from Chapter 2 relevant to the studied phenomena, rates and equilibria for imine formation with *n*-propylamine (top) and for amine exchange of the resulting imine with *i*-pentylamine (bottom). [a] The half-life indicated is calculated from the rate constant and initial concentration of 20 mM for the imine formation and 18.2 mM for the imine exchange. Study was performed in mixture of  $\text{CD}_3\text{CN}/\text{D}_2\text{O}$  7:3 (v/v) with triethanolamine buffer (pH = 8.73) with 20 mM starting concentration of reagents (aldehyde + *n*-propylamine) in 1:1 ratio and followed by NMR. Exchange experiments were performed on samples equilibrated for 3 days adding 1 eq. of *i*-pentylamine (decreasing initial concentration to 18.2 mM) and followed by NMR.

The determined rate of imine exchange is tied with the equilibrium constant of amination, and thus it is concentration dependent (discussed in detail in Section 7.4.1). The criterion of rate concentration dependence is thus applicable to distinguish between the intermolecular and intramolecular mechanism of the process under study.

In fact, transamination can be performed as exchange of either the amine part (discussed above) or the aldehyde part. Thus, addition of 1 eq. of **SALAL** to the equilibrium mixture of **PYRAL** + *n*-propylamine leads to reequilibration of the mixture giving 24 % and 76 % of the *n*-propylimines of

**PYRAL** and **SALAL**, respectively. Similarly, when equilibrated mixtures of **PYRAL** + *i*-pentylamine and **SALAL** + *n*-propylamine are combined in a mixture of acetonitrile/water (7:3, v/v), reequilibration takes place again to give an equimolar mixture of *n*-propyl and *i*-pentylimines of **PYRAL** (45 %) and **SALAL** (55 %, note that this exchange is not proceeding in non-aqueous media as discussed on page 59). Both experiments illustrate the constitutional exchange expected for exchanging aldehyde/amine systems.

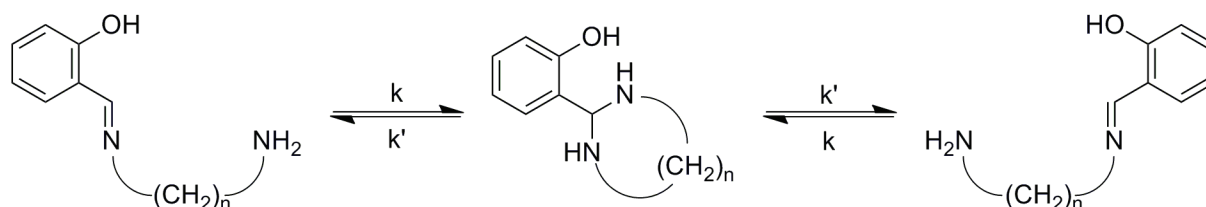


Figure 3.2-2 The intramolecular imine exchange reaction occurs through the cyclic aminal intermediate.

The amine exchange process on imines may occur either by hydrolysis followed by recondensation or by addition of the new amine to the imine double bond to give a gem-diamine/aminal intermediate. It follows that, if the amine groups undergoing exchange are linked, as in  $\alpha,\omega$ -aliphatic diamines, an intriguing situation presents itself, whereby intramolecular self-exchange takes place, with bonding fluctuation on imine-aminal-imine interconversion, via a cyclic aminal that may or may not be present in significant amounts, depending on the relative stability of the two entities under the conditions used (Figure 3.2-2). Such a process thus performs a motional-type displacement of two molecular moieties relative to one another.

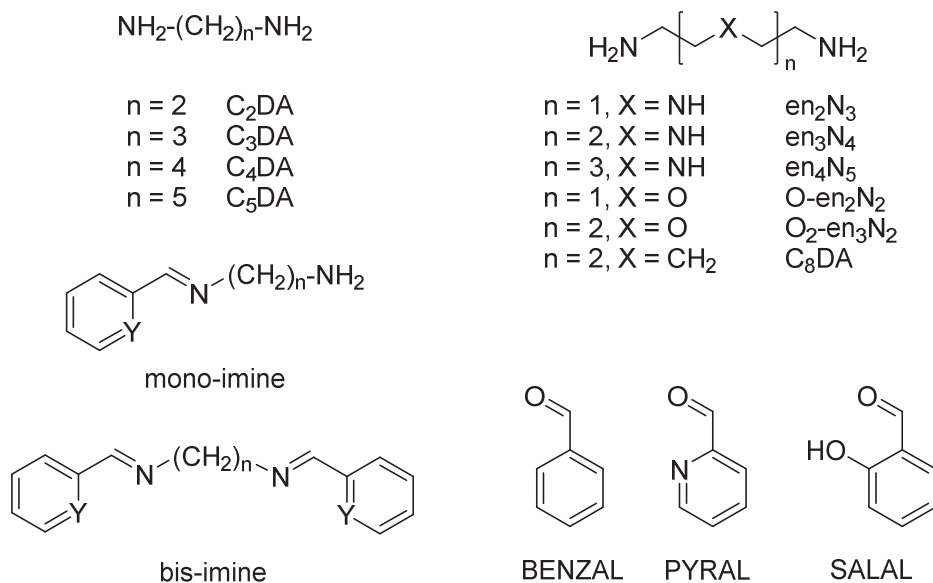


Figure 3.2-3 The amines and aldehydes used throughout the motional study and their condensation products.

Indeed, the reactions of the aldehydes with the simple aliphatic diamines  $\text{H}_2\text{N-(CH}_2\text{)}_n\text{-NH}_2$  (Figure 3.2-3) turned out to follow such a scheme. When **SALAL**, **BENZAL** and **PYRAL** were mixed with a diamine in chloroform, a mixture of mono-imine and bis-imine was obtained and sharp  $^1\text{H-NMR}$  signals were observed, as one would expect<sup>[324,325]</sup> (Figure 3.2-4). However, the situation was very different when the same reactions were run in  $\text{CD}_3\text{CN:D}_2\text{O}$  (7:3 v/v). A 1/1 mixture of **SALAL** and **C<sub>2</sub>DA** displayed very broad  $^1\text{H-NMR}$  signals for the  $\text{CH}_2$  groups and broadened signals for the imine protons, whereas the signals of the aromatic protons were sharp. Signal integration showed that these bands belonged to the mono-imine (about 55 % based on aldehyde). The bis-imine (about 45 % based on aldehyde) was also formed but presented the expected sharp peaks, while the aminal of

**SALAL** is not observed if the imine can be formed, as documented in the literature.<sup>[326]</sup> Moreover, no signal was observed for a  $-\text{CH}(\text{O})(\text{N})$  proton corresponding to the hemiaminal that would form by addition of a water molecule to the imine (expected around 5 – 5.5 ppm). The presence of the very broad peaks at a chemical shift between those expected for  $\text{CH}_2$  protons next to the  $\text{C}=\text{N}$  group and next to an  $\text{NH}_2$  group, was interpreted as indicating the operation of a kinetic process in the mono-imine, whereby the two  $\text{CH}_2$  groups exchange at a rate compatible with the NMR time scale.

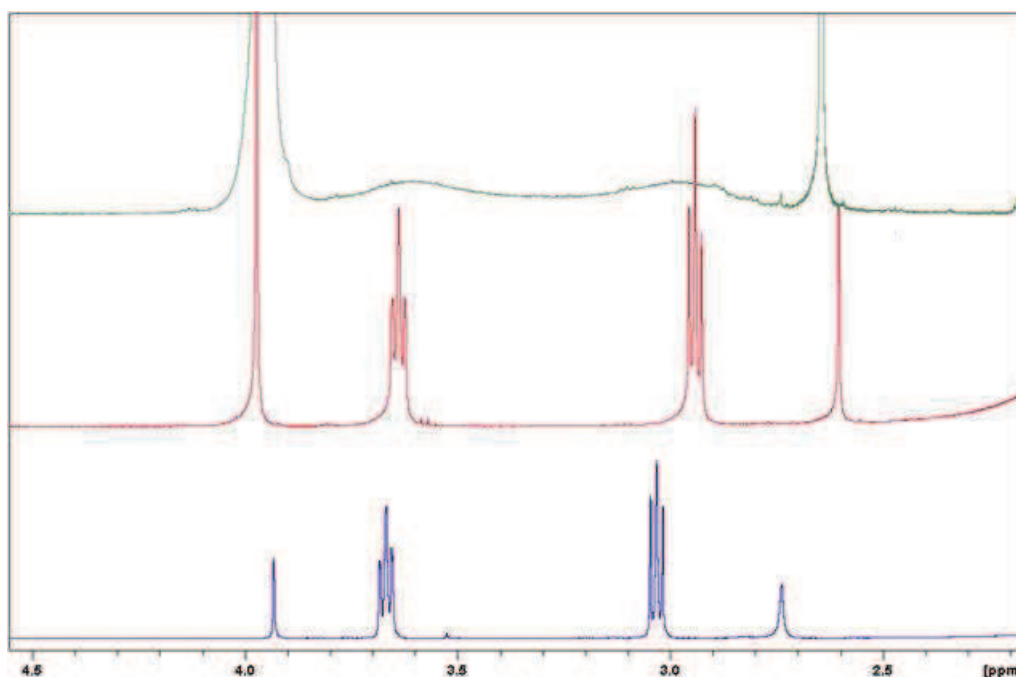


Figure 3.2-4  $^1\text{H}$ -NMR spectra of **SALAL** + **C<sub>2</sub>DA** (in 1:1 ratio) in  $\text{CDCl}_3$  (bottom),  $\text{CD}_3\text{CN}$  (middle) and  $\text{CD}_3\text{CN}/\text{D}_2\text{O}$  (7:3 v/v; top) at 20 mM concentration level. Triplets around 3.65 ppm are  $=\text{N}-\text{CH}_2$ -methylene signal, triplets at 3.05 (bottom) and 2.85 (middle) correspond to the  $-\text{CH}_2-\text{NH}_2$  methylene group. Methylene signals of bis-imine appear at around 4 ppm (overlaps with water signal), free **C<sub>2</sub>DA** is around 2.6-2.7 ppm.

Comparison of half-widths of peaks in deuteriochloroform (1.17 Hz), pure  $\text{d}_3$ -acetonitrile (3.5 Hz) and a mixture of  $\text{CD}_3\text{CN}/\text{D}_2\text{O}$  (7:3 v/v; about 100 Hz) clearly demonstrates the trend. **BENZAL** performs much slower intramolecular exchange than **SALAL**, nevertheless line shape broadening is clearly visible from comparison of spectra taken in *d*-chloroform and a mixture of  $\text{CD}_3\text{CN}/\text{D}_2\text{O}$  (7:3 v/v, pH adjusted to 10.7, see Figure 7.5-1 on page 185).

Variable temperature  $^1\text{H}$ -NMR (VT-NMR) of **SALAL** + **C<sub>2</sub>DA** reaction mixture was performed in  $\text{CD}_3\text{CN}/\text{D}_2\text{O}$  (7:3 v/v) and broadening of the signals of the two  $\text{CH}_2$  groups of the mono-imine with increasing temperature is observed until the coalescence temperature is reached. Above this temperature signals merge into a singlet which gets sharper with further increase of the temperature (maximum around 75 °C, above which the solvent mixture starts to overheat and locking on the solvent signal is not possible). Figure 3.2-6 shows the evolution of VT- $^1\text{H}$ -NMR over the temperature range of 30 °C. The reaction mixture can also be cooled down to approximately 7 °C. Below this temperature phase separation occurs. Phase separation is caused by the solute in the solvent mixture but inhomogeneous-solution behaviour is observed even without any solute (solvent signal splitting) when cooled below 5 °C.

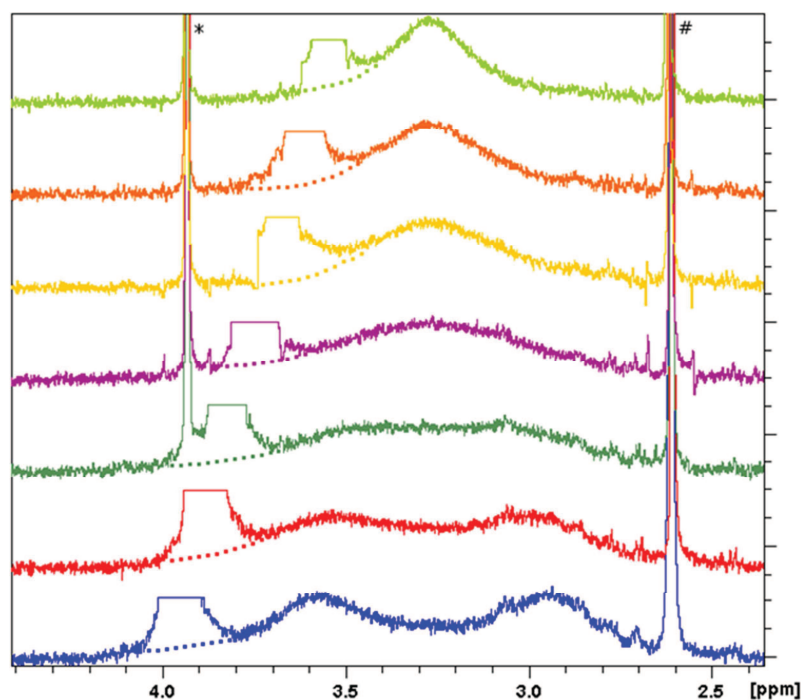


Figure 3.2-5 400 MHz  $^1\text{H}$ -NMR spectra of the methylene region of **SALAL** + **C<sub>2</sub>DA** in  $\text{CD}_3\text{CN}/\text{D}_2\text{O}$  (7:3 v/v), temperatures from bottom to top: 25, 30, 35, 40, 45, 50 and 55 °C, \*peak of bis-imine  $\text{CH}_2$  groups, # peak of unreacted **C<sub>2</sub>DA**, peak of water truncated for clarity.

Variable temperature  $^1\text{H}$ -NMR measurements showed a coalescence of the two broad signals at a temperature of about 37°C (Figure 2). Thus, NMR line shape analysis was performed in the temperature range of 10 - 75 °C (steps of 5 °C) at three different concentrations (4, 20 and 100 mM of both reagents) and three different ratios (2:1, 1:1 and 1:2) of **SALAL** and **C<sub>2</sub>DA**. In all cases, the same coalescence temperature of  $37 \pm 1$  °C was observed, which clearly confirmed that the process is of intramolecular nature, as expected. It is noteworthy that this monomolecular process is observed in NMR samples in equilibrium, which can therefore be qualified as dynamic equilibrium. Furthermore, line shape-fitting analysis (performed using DNMR module in TOPSPIN<sup>®</sup>) gave very consistent rate data suitable for fitting the Eyring equation. This equation is for the purpose of regression transformed into the linear form

$$\ln\left(\frac{r}{T}\right) = \frac{-\Delta H^\ddagger}{R} \cdot \frac{1}{T} + \ln\left(\frac{k_B}{h}\right) + \frac{\Delta S^\ddagger}{R}$$

where  $k_B$  is Boltzman constant,  $h$  is Planck constant,  $R$  is universal gas constant,  $r$  is the rate value,  $T$  is the temperature in K and  $\Delta H^\ddagger$  and  $\Delta S^\ddagger$  are the activation enthalpy and entropy of the reaction, respectively. The linear regression gave the activation enthalpy of  $\Delta H^\ddagger = 9.3 \text{ kcal mole}^{-1}$  and entropy  $\Delta S^\ddagger = -15.8 \text{ cal mol}^{-1} \text{ K}^{-1}$  ( $38.78 \pm 0.47 \text{ kJ mol}^{-1}$  and  $-66.0 \pm 1.5 \text{ J mol}^{-1} \text{ K}^{-1}$  respectively,  $R^2 = 0.9935$ ). The region of NMR spectra with corresponding fitted lines at four temperatures is shown in Figure 3.2-6. The data on rates used for fitting the reaction of **SALAL** + **C<sub>2</sub>DA** in  $\text{CD}_3\text{CN}/\text{D}_2\text{O}$  (7:3 v/v) are given in Table 3.2-2, and the Eyring plot with regression parameters is shown in Figure 3.2-7.

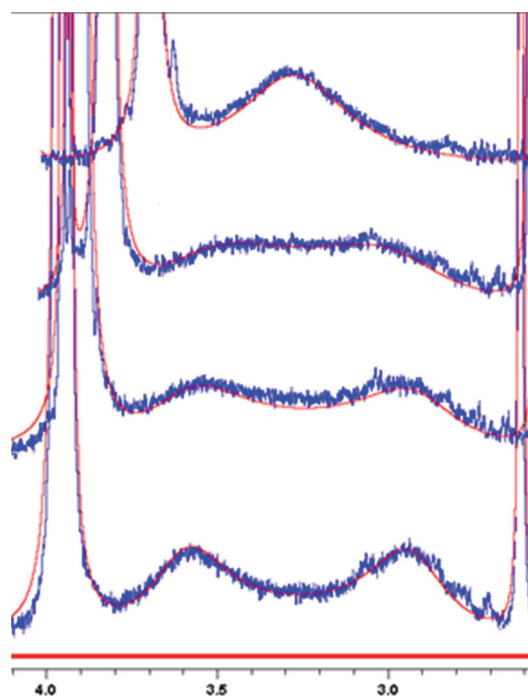


Figure 3.2-6 Example of the line shape fitting analysis of the reaction of **C<sub>2</sub>DA** with **SALAL** in  $\text{CD}_3\text{CN}/\text{D}_2\text{O}$  7:3 (v/v) at pH = 10.7 at temperature 25, 30, 35 and 50 °C. Experimental spectra in blue, calculated fit in red for each temperature. Only sum of the fitted individual signals is shown for clarity.

T [°C]	10	15	20	25	30	35	37	40	45	50	55	60	65	70	75
r [Hz]	171	201	272	365	454	565	671	739	959	1181	1518	2025	2598	3601	4452

Table 3.2-2 Rates of intramolecular exchange reaction of **SALAL** + **C<sub>2</sub>DA** in  $\text{CD}_3\text{CN}/\text{D}_2\text{O}$  (7:3 v/v) in the temperature range 10 – 75 °C determined by the line shape fitting analysis.

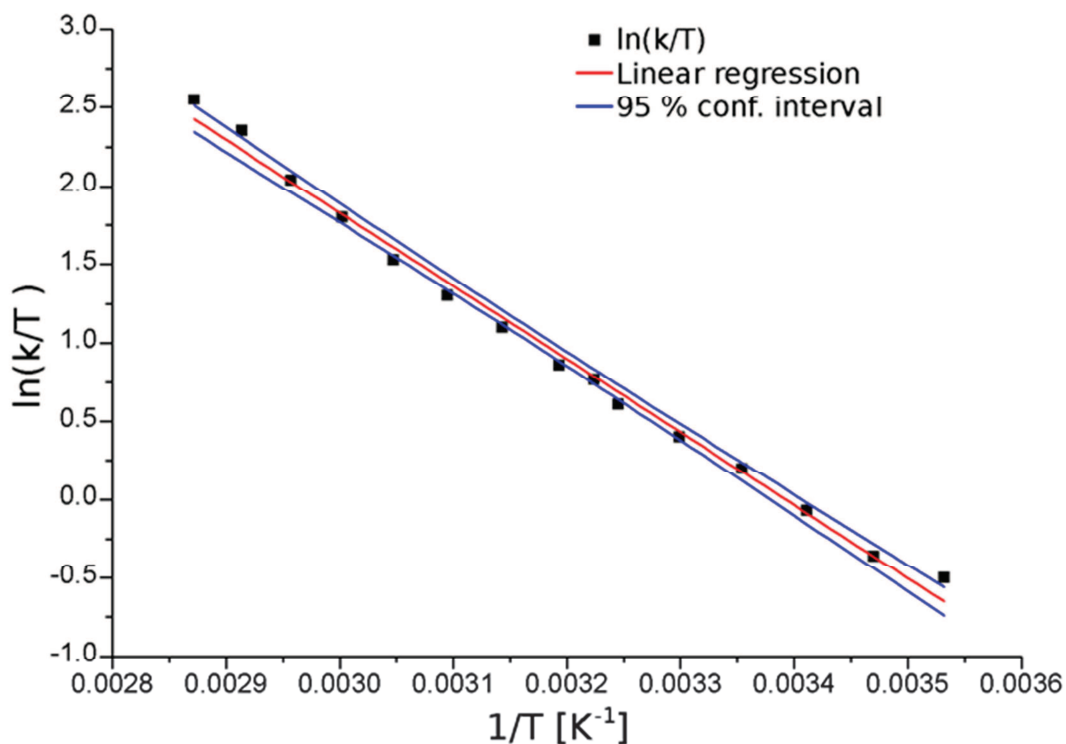


Figure 3.2-7 Eyring plot: rates of the intramolecular exchange reaction of **SALAL** + **C<sub>2</sub>DA** in  $\text{CD}_3\text{CN}/\text{D}_2\text{O}$  (7:3 v/v) in the temperature range 10 – 75 °C fitted by the linear form of the Eyring equation, 95% confidence interval shown,  $R^2 = 0.9935$ .



The rate of exchange was also examined for the effect of pH. The pH of the mixture **SALAL** + **C<sub>2</sub>DA** was varied using DCl or NaOD and again coalescence was determined as an indication of the intramolecular exchange rate. The coalescence temperature of the two methylene signals of the mono-imine was found to be independent of pH in the range 9.3–12.0 (Figure 7.5–8); below pH 9 only very small amounts of the mono-imine were formed (bis-imine and free **C<sub>2</sub>DA** prevail) and for pH above 12 the acetonitrile/water mixture tended to phase separate. For all following results, the pH of the mixture was adjusted to  $10.7 \pm 0.1$  by DCl or NaOD.

In order to investigate the possibility of exchange between more distant terminal amino groups, similar line shape analysis and/or <sup>1</sup>H-NMR EXSY<sup>[327–331]</sup> studies (discussed in Section 3.2.2.4, and in Section 7.5.2 with experimental details) were conducted with the longer aliphatic diamines H<sub>2</sub>N-(CH<sub>2</sub>)<sub>n</sub>-NH<sub>2</sub>, propylenediamine (**C<sub>3</sub>DA**, n=3), putrescine (**C<sub>4</sub>DA**, n=4) and cadaverine (**C<sub>5</sub>DA**, n=5). The independence of the rate of exchange of the two N-CH<sub>2</sub> groups from concentration was taken as a diagnostic of the intramolecular nature of the process. The rates of end-to-end exchange decreased rapidly on chain lengthening, as may be expected (Table 3.2-3), going from 365 Hz for **C<sub>2</sub>DA** down to 10 Hz for n=4 in **C<sub>4</sub>DA**, and to not observable for n=5, as the intermolecular exchange becomes faster than the intramolecular one (discussed in Section 3.2.1.2).

As in the case of the shorter homologue, the activation parameters for **SALAL** + **C<sub>3</sub>DA** can be calculated. The situation in this case is complicated by an important overlap of the mono-imine signals with the water signal, therefore only a few points could be analysed:  $\Delta H^\ddagger = 32.9 \pm 1.8 \text{ J mol}^{-1}$ ,  $\Delta S^\ddagger = -91.6 \pm 5.7 \text{ J mol}^{-1} \text{ K}^{-1}$ ,  $R^2 = 0.9932$ .

H <sub>2</sub> N-(CH <sub>2</sub> ) <sub>n</sub> -NH <sub>2</sub>	n =	2	3	4	5
SALAL	intra	365	187	10	- <sup>[b]</sup>
	inter	- <sup>[a]</sup>	0.22	- <sup>[a]</sup>	0.32
PYRAL	intra	0.17	0.5	1.4	0.60
	aminal opening $r'$	0.44	1	- <sup>[c]</sup>	- <sup>[c]</sup>
	aminal closing $r$	1.35	74	- <sup>[c]</sup>	- <sup>[c]</sup>

Table 3.2-3 Rates of the intramolecular imine exchange of **SALAL** and **PYRAL** were determined by the line-shape fitting analysis and EXSY methods from NMR data. The intramolecular values are given as the rates of the end-to-end displacement, which in case of **PYRAL** were calculated from residence times in the imine and the aminal state from the individual rates stated below. [a] Exchange observed, but broad signal shapes or low intensities prevent quantification. [b] Exchange not observed. [c] No aminal signals are observed in the spectrum therefore the value cannot be calculated.

The intramolecular process was similarly observed with **PYRAL**, but at widely different rates (Table 3.2-3). With **C<sub>2</sub>-DA** and **C<sub>3</sub>-DA**, **PYRAL** forms stable cyclic aminals which predominate over the imines in solution,<sup>[326]</sup> in clear contrast to **SALAL**, where the aminal is not seen. Nevertheless, dynamic equilibrium between the ring and chain forms takes place (Figure 3.2-8) and can be quantified. To make the rates of such exchanges comparable with other end-to-end exchanges, they were calculated according to Figure 3.2-2 from the residence times  $\frac{1}{r}$  and  $\frac{1}{r'}$  of the protons in the two states, as

$$\frac{1}{2\left(\frac{1}{r} + \frac{1}{r'}\right)^{-1}}$$

where  $r$  is rate of ring closing and  $r'$  is rate of ring opening. Since the cyclic intermediate is symmetrical, the chance of opening on each nitrogen site is the same, giving 50 % probability to go back and 50 % probability to perform end-to-end exchange. For **C<sub>4</sub>-DA** and **C<sub>5</sub>-DA**, no aminals are observed and direct determination of the end-to-end displacement rate was possible. Coalescence of the signals of mono-imine and aminal could not be reached and thus 2D EXSY was used to determine the corresponding rates.



Similarly to **PYRAL**, the dynamic equilibria between aminals of **C<sub>2</sub>DA** and **C<sub>3</sub>DA** and their imine forms have been also observed with **BENZAL**, however 2D EXSY did not provide reliable data to calculate the rates of the process due to low overall conversion of the aldehyde. Only rough estimation of the rate of about 15 Hz can be extracted from the line shape data (the aminor signals were not well resolved from the background and thus neglected). The fact that the aminor are formed with other aldehydes supports the existence of cyclic aminor as an intermediate of the intramolecular exchange in the case of **SALAL**, even though it is not detected. The formation of intermediate geminal diamines has been studied in detail for pyridoxal-5-phosphate.<sup>[215,217]</sup>

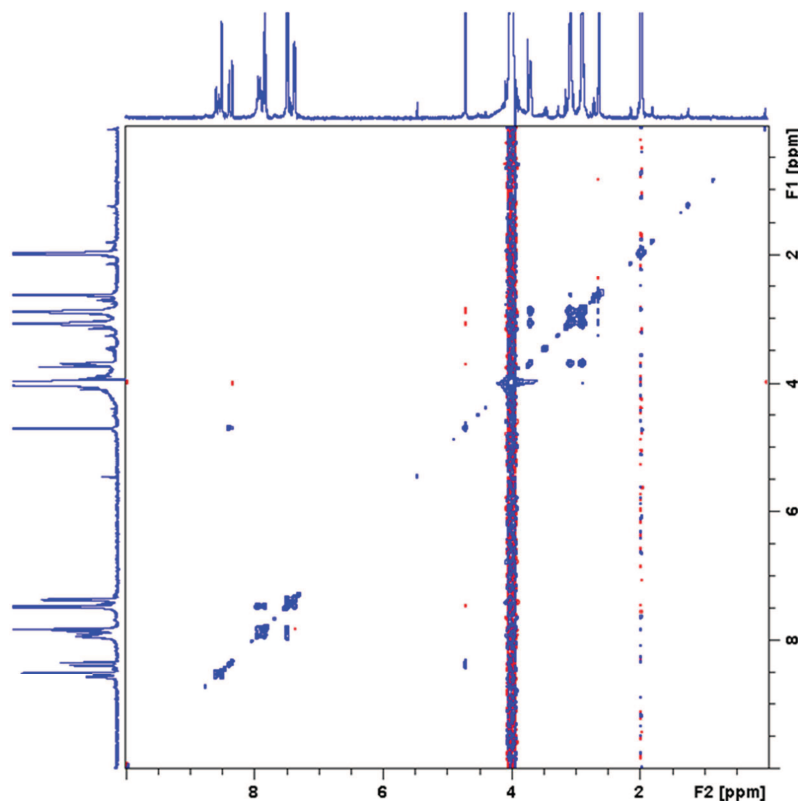


Figure 3.2-8 2D <sup>1</sup>H-NOESY spectrum of **PYRAL** + **C<sub>2</sub>DA** in  $CD_3CN/D_2O$  (7:3 v/v). The imine and the aminor have exchange cross-peaks (cross-peak between the aminor signal at 4.42 ppm and the imine signal at 8.17 ppm as well as the methylene groups in the aliphatic region). The signals of the methylene groups of the aminor correspond to the five-membered ring which can open to give the mono-imine (peaks at 2.92 and 3.17 ppm belonging to the aminor structure are exchanging with the imine peaks at 3.75 ppm and 2.84 ppm).

### 3.2.1.1. Aminor intermediate in the intramolecular imine exchange

The mechanism of intramolecular exchange between the two methylene groups =N-CH<sub>2</sub> and H<sub>2</sub>N-CH<sub>2</sub> in the mono-imine formed from an α,ω-diamine and an aldehyde requires going through a cyclic aminor form as shown in the case of **SALAL** in Figure 3.2-2. Such a process represents an intramolecular molecular motion involving the continuous exchange of the salicylidene group between the two ends of the **C<sub>2</sub>DA** molecule in a binary rhythm of “stepping-in-place” type. **SALAL** strongly prefers the imine state and the presence of an aminor cannot be detected by recording the NMR spectra directly. However, **PYRAL** and **BENZAL** give equilibrium mixtures of cyclic aminor and imine forms which interchange, as can be seen in 2D NOESY spectra (Figure 3.2-8). In addition, the VT-NMR in the range 25 - 75 °C showed signal broadening of the signals which are involved in the exchange process, but coalescence could not be reached (Figure 7.5-9 and Figure 7.5-10). Variation

of concentration doesn't affect the temperature dependent signal shape evolution and thus proves the intramolecular nature.

**SALAL** must follow the same mechanism for intramolecular exchange. Evidence that the intermediary aminal is also formed in the case of **SALAL** was obtained when the reaction rate was slowed down dramatically by changing the solvent system to  $\text{CDCl}_3/\text{CD}_3\text{CN}$  1:1 (v/v) and replacing simple diamines by diethylenetriamine,  $\text{en}_2\text{N}_3$ . Even in this case, the aminal broad signal at 4.42 ppm is only observed after recording 1024 scans. The identity of the signal was confirmed by comparison with the condensation product of **SALAL** with *N,N'*-dimethylethylenediamine, which is unable to form an imine. In the corresponding 2D NOESY spectrum, shown in Figure 3.2-9, a positive cross peak (with respect to the positive diagonal peaks) between the imine proton and the "hidden" proton at 4.42 ppm is observed.

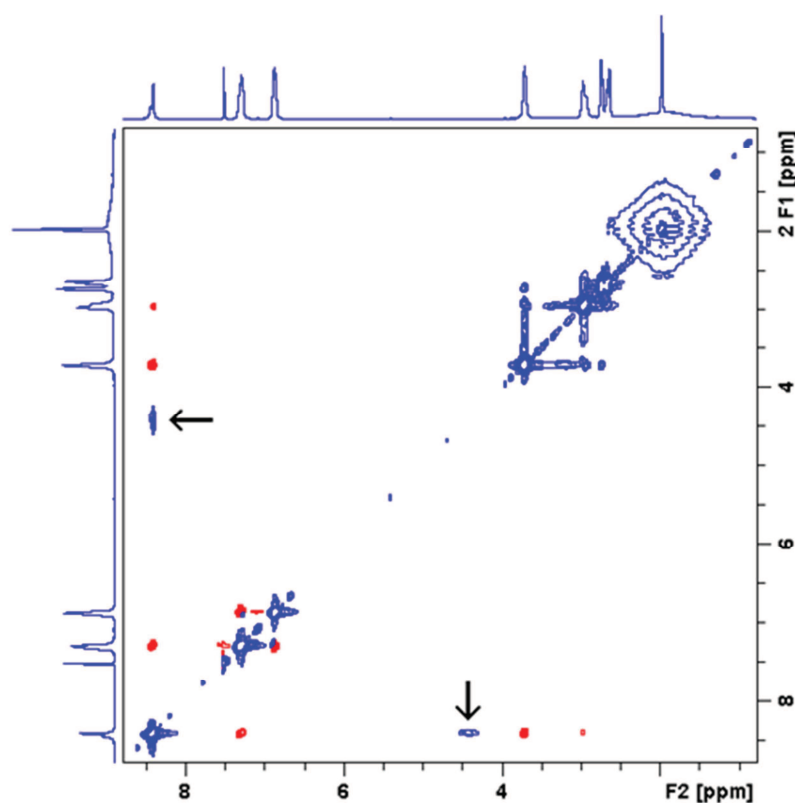


Figure 3.2-9 2D  $^1\text{H}$ -NOESY spectrum of **SALAL** +  $\text{en}_2\text{N}_3$  in  $\text{CDCl}_3/\text{CD}_3\text{CN}$  1:1 (v/v). The exchange cross-peaks between the mono-imine and the aminal form are indicated by arrows. Chemical exchange cross-peaks in the aliphatic region are partially overlapped with NH/OH broad proton signals.

The estimation of the amount of aminal present in the case of **SALAL** is rendered difficult by the fast exchange process in  $\text{CD}_3\text{CN}/\text{D}_2\text{O}$  (7:3 v/v) and the preferential formation of the imine. An approximate amount of the aminal form can be calculated by  $^{13}\text{C}$ -NMR line-shape fitting analysis of the mixture of **SALAL** and **C<sub>2</sub>DA**. Significant broadening of the azomethine carbon signal at 166 ppm is observed. This arises from the fast exchange with the aminal carbon, whose position was approximated to be 90 ppm, by accepting the position of the aminal signal formed from **SALAL** and *N,N'*-dimethylethylenediamine. With the rate of exchange already evaluated from  $^1\text{H}$ -NMR line-shape analysis, the fitted model can be optimized in terms of the percentage of aminal as the only variable, giving an estimation of 3 % of the aminal form and 97 % imine form.

Altogether, the phenomenon of the aldehyde displacement between the nitrogen atoms of diamines is general and leads itself to a variety of interesting extensions (Section 3.2.2).

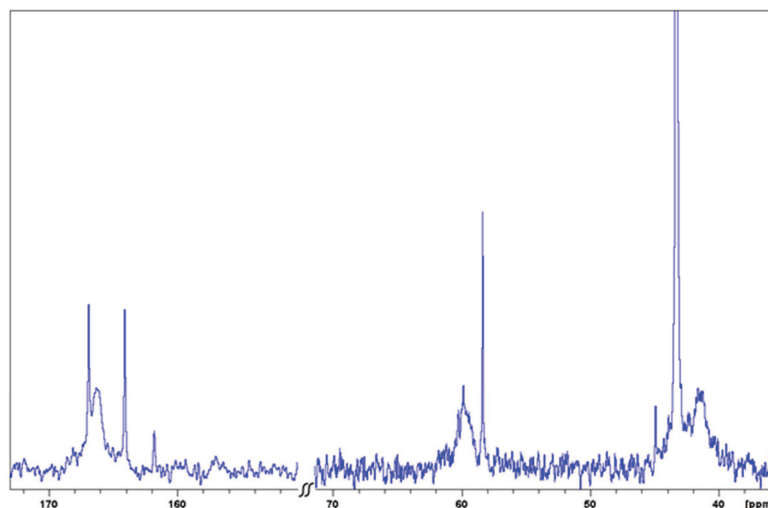


Figure 3.2-10  $^{13}\text{C}$ -NMR spectrum of **SALAL** + **C<sub>2</sub>DA** in  $\text{CD}_3\text{CN}/\text{D}_2\text{O}$  (7:3 v/v). Two broad peaks at 60 ppm and 41 ppm correspond to methylene groups; the broad peak at 166 ppm is the azomethine signal.

### 3.2.1.2. Entangled motional and constitutional dynamics

Intermolecular and intramolecular exchanges are always present at the same time in the reaction mixture resulting from a dynamic equilibrium distribution of the products (unreacted, mono- and bis-imine) of equimolar amounts of **SALAL** and a diamine. Intermolecular constitutional exchange may occur by the reaction of a free diamine, acting as a nucleophile, with mono-imine and replacing its amine part, and thus competing with the intramolecular process. It can be observed by 2D NMR spectra where cross-peaks indicate exchange between free diamine and mono-imine giving the very same imine and free diamine. Indeed, cross-peaks in the 2D  $^1\text{H}$ -NMR NOESY spectrum of **SALAL** with **C<sub>2</sub>DA** and **C<sub>3</sub>DA** in  $\text{CD}_3\text{CN}:\text{D}_2\text{O}$  (7:3 v/v) were indicative of an intermolecular exchange (Figure 3.2-12), but in case of **C<sub>2</sub>DA** the breadth of the corresponding mono-imine signals prevents the quantification of the exchange rate. The intermolecular nature of the process was always confirmed by the concentration dependence of the exchange rate, which was much slower than the intramolecular process (Table 3.2-3) for shorter diamine chains, but became comparable in case of cadaverine. The EXSY data for **SALAL** and **C<sub>3</sub>DA** gave a good fit for first order kinetics, which is in agreement with the mechanism of intermolecular imine exchange, and the intramolecular exchange rate was not determined, in this case being overridden by the intermolecular one.

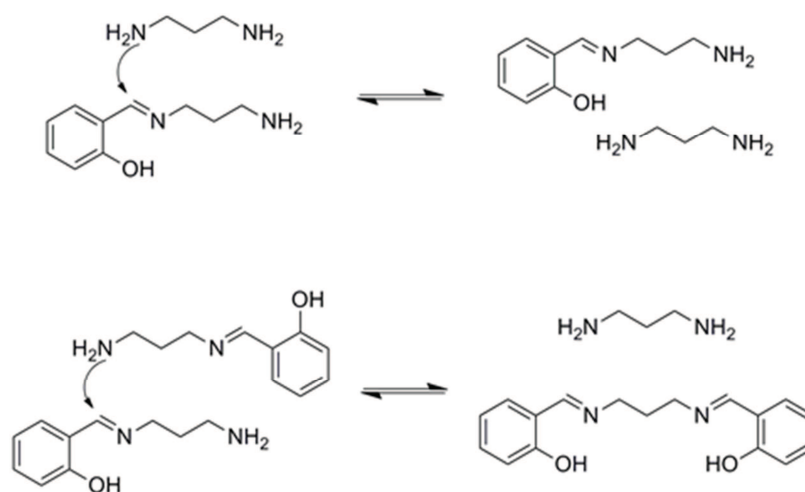


Figure 3.2-11 Intermolecular imine exchange processes revealed by EXSY.

Another exchange reaction is evidenced by the cross-peak between mono- and bis-imine signal demonstrating that bis-imine is also formed by condensation of two mono-imine molecules eliminating free diamine and giving the bis-imine (Figure 3.2-12).

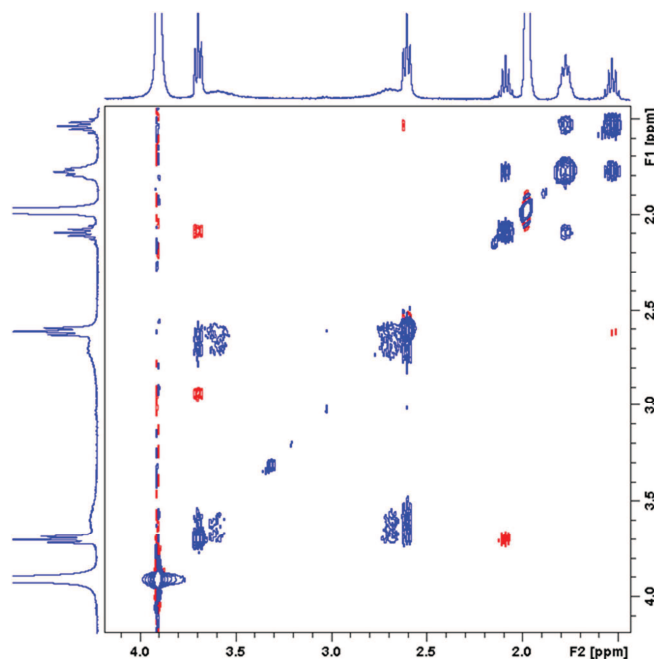


Figure 3.2-12 2D  $^1\text{H}$ -NOESY spectrum of **SALAL** + **C<sub>3</sub>DA** in  $\text{CD}_3\text{CN}/\text{D}_2\text{O}$  (7:3 v/v). The assignment of peaks corresponds to structures in the previous figure; bis-imine: triplet at 3.70 ppm and quintet at 2.1 ppm; mono-imine: two broad signals at 3.60 and 2.70 ppm and multiplet at 1.80 ppm; free **C<sub>3</sub>DA**: triplet at 2.60 ppm and quintet at 1.55 ppm. The cross-peaks indicate two intermolecular exchange processes described in the previous figure and one intramolecular exchange process.

It was shown above that imines formed by **SALAL** with diamines present both intramolecular motion and intermolecular exchange. When only one diamine is present in the solution, the intermolecular exchange results in the same composition of the mixture as before the reaction in a degenerate process. However, when there are two or more different diamines present, the imine can react with either of these amines, thus undergoing constitutional change by transimination. In the simple case where **SALAL** was mixed with 1 equivalent of both **C<sub>2</sub>DA** and **C<sub>3</sub>DA** (each component at 20 mM concentration in  $\text{CD}_3\text{CN}/\text{D}_2\text{O}$  7:3 v/v), the  $^1\text{H}$ -NMR spectrum showed the intramolecular motions in both mono-imines (although the signals of the **C<sub>2</sub>DA** and **C<sub>3</sub>DA** mono-imines are very close and very broad and therefore cannot be separated), while 2D EXSY experiments revealed incorporation of both diamines into the mono-imines with rates of intermolecular exchange similar to those obtained with only one diamine at the same concentration ( $0.45 \pm 0.05$  for **C<sub>2</sub>DA**<sup>+++</sup> and  $0.34 \pm 0.01$  Hz for **C<sub>3</sub>DA**).

In similar fashion, addition of 5-chlorosalicylaldehyde to an equilibrated mixture of 5-hydroxysalicylaldehyde and **C<sub>2</sub>DA** (1 eq. each) gave an  $^1\text{H}$ -NMR spectrum containing the  $\text{CH}=\text{N}$  proton signals of all the mono and bis-imines formed, together with broad signals for the  $\text{CH}_2\text{-CH}_2$  protons, resulting from the superposition of the corresponding signals of each mono-imine (for NMR trace see Figure 7.5-21). These data again indicate the occurrence of equilibration and constitutional dynamics by intermolecular exchange of both the amino and the salicylidene groups.

<sup>+++</sup> Estimation from single cross-peak evaluation, full dataset is not available due to signal width and overlap.

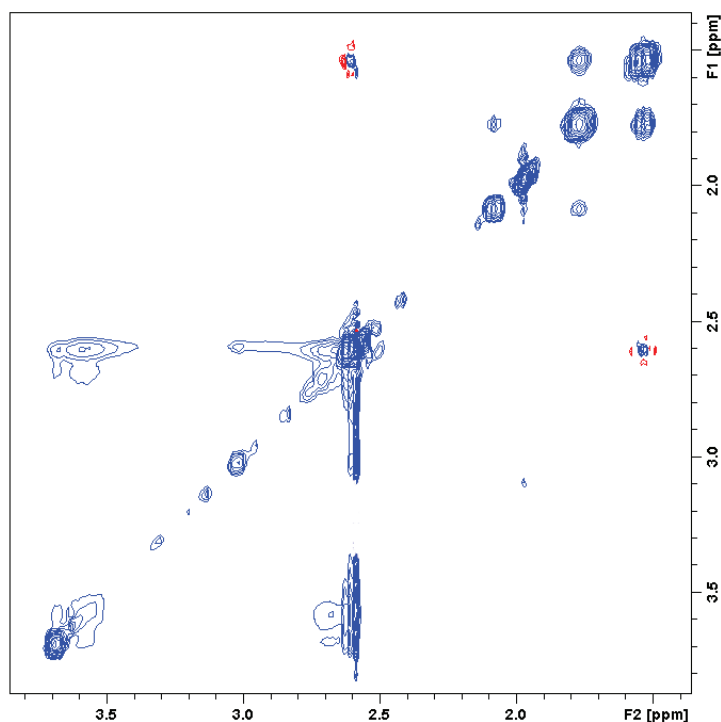


Figure 3.2-13 Aliphatic region of the  $^1\text{H}$ -NOESY NMR spectrum of the mixture of **SALAL** with 1 eq. of **C<sub>2</sub>DA** and 1 eq. of **C<sub>3</sub>DA**. Cross-peaks shown are attributed to intermolecular exchanges. The fast intramolecular ones lead to significant broadening of signals 3.55 and 2.65 ppm and thus low intensity of cross-peaks in 2D spectra.

Taken together, the data above indicate that mono-imines of  $\alpha,\omega$ -diamines undergo both internal and intermolecular exchange of components, thus merging motional and constitutional dynamics. The internal process corresponds to: a) a stepping-in-place when the initial imine is regenerated backward from the intermediate aminal and, b) to taking a single step forward when the salicylidene group goes over to the other nitrogen site (Figure 3.2-2).

It is noteworthy that EXSY analysis provides a unique analysis of complicated dynamic equilibria as shown above, i.e. even in cases when products of a reaction are identical to the starting materials or when the signals are partially overlapped.

### 3.2.1.3. Rate control

The intramolecular group transfer process described on the aldehyde molecules **SALAL** and **PYRAL** consists of taking a step from one nitrogen atom to the adjacent one, and is therefore of a motional type. In scope of potential applications of the system, it is of much interest to be able to modulate the speed at which the steps are taken. There are several ways to achieve such control.

#### a) Introduction of substituents

The aromatic core of **SALAL** allows for a wide range of substitution in up to four positions. Introducing various substituents from electron-withdrawing to electron-donating, both the electrophilicity of the carbonyl (or imine) and the acidity of the OH group are modified (see Section 2.2.2). These two factors markedly influence the rate of the internal motion of **C<sub>2</sub>DA** as can be seen in Figure 3.2-14, showing the signals of the two  $\text{CH}_2$  groups of the mono-imine. The spectrum of the mono-imine of **C<sub>2</sub>DA** with the most electron-donating 4-diethylamino group substituted **SALAL** shows two well separated signals with visible triplet structure of the signals. The less electron-donating 5-

hydroxy group gives two well separated but broad signals, similar to **SALAL** itself. The electron-withdrawing 5-chloro derivative presents only one broad signal for both CH<sub>2</sub> groups with a coalescence temperature around 12 °C. The most electron-withdrawing substituent, 5-nitrosalicylaldehyde, displays only one relatively sharp signal for both CH<sub>2</sub> groups.

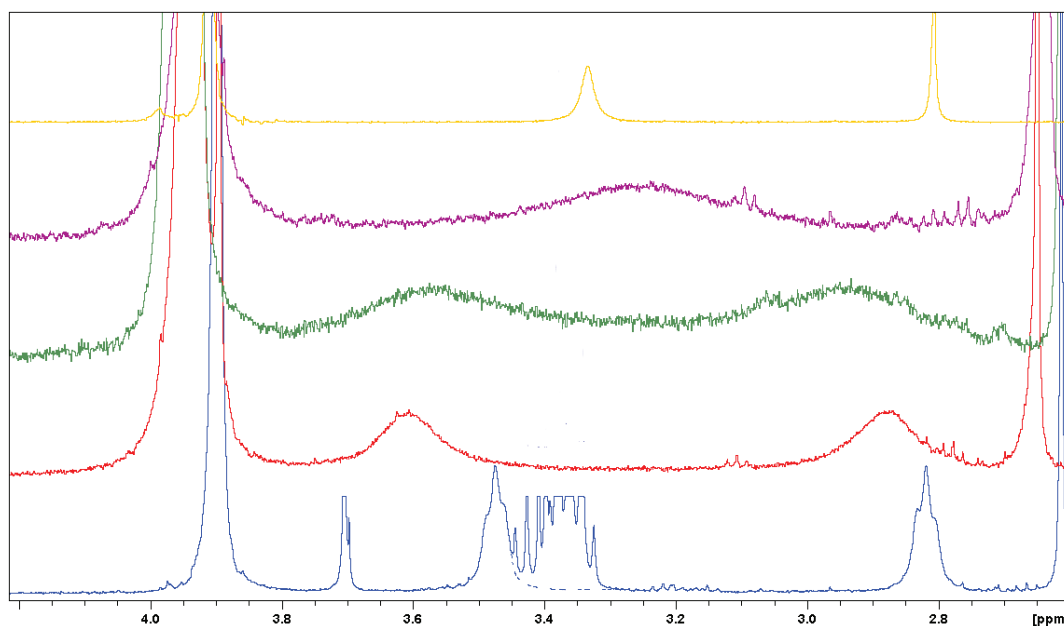


Figure 3.2-14 Methylene region of the <sup>1</sup>H-NMR spectra of imines of **C<sub>2</sub>DA** with **SALAL** bearing various substituents: 4-Et<sub>2</sub>N (blue), 5-OH (red), non-substituted **SALAL** (green), 5-Cl (purple) and 5-NO<sub>2</sub> (yellow), from bottom to top. Signals of the ethyl groups in the bottom trace have been truncated for clarity.

The line-shape fitting analysis provides an access to the intramolecular exchange rates. The range of motion speeds (Table 3.2-4) is remarkably wide: while substitution by a slightly electron-donating 5-hydroxy group lowers the rate to approximately half that of non-substituted **SALAL**, the strong electron-donor 4-diethylamino group drops the rate to as low as 5 % of its original value. A 4-hydroxy substitution has an effect very similar to that of a 5-hydroxy group, although the activation enthalpy is close to that of the 4-diethylamino group, differing mostly in activation entropy (activation parameters listed in Table 3.2-5). Introducing electron-withdrawing groups has an even larger effect: the weakly electron-accepting 5-chlorosalicylaldehyde increases the motion rate three times compared to **SALAL**. In the case of the strongest electron-acceptor, the 5-nitro group, the two methylene signals are already coalesced at temperatures above 5 °C. The initial parameters for the line-shape analysis were thus extracted by comparison of the signal chemical shifts in different solvents for various substituents. The effect of the nitro group shoots the motion rate up into the range of about 17 kHz, a 50 fold increase in speed, thus covering a range of three orders of magnitude.

<b>SALAL</b> derivative	4-Et <sub>2</sub> N	4-OH	5-OH	H	5-Cl	5-NO <sub>2</sub>
Motion rate [Hz]	20	108	148	365	1040	~17 000

Table 3.2-4 Rate of the intramolecular imine exchange at 25 °C was determined by the line-shape fitting analysis. In the case of 5-nitrosalicylaldehyde the rate is only rough estimation because the signals of the CH<sub>2</sub> groups of the ethylene unit are already coalesced at temperatures above 5 °C.

VT-NMR experiments were performed for **C<sub>2</sub>DA** and 5 derivatives (4-diethylamino, 4-hydroxy, 5-hydroxy, 5-chloro and 5-nitro) of **SALAL** and the spectra were evaluated by THE line-shape analysis to obtain the rates of motion as functions of temperature. These rates were then also fitted by the Eyring equation and the activation parameters were calculated (Table 3.2-5). Interestingly, the activation enthalpy varies only moderately changing from electron-donating 5-hydroxy to electron-withdrawing 5-chloro substitution (and maybe even 5-nitro, although the data are only estimative in

this case) but the activation entropy differs greatly. Similar behaviour is also found for substitution in position 4, but further experiments are required to prove the trend.

Aldehyde	$\Delta H^\ddagger$ [kJ mol <sup>-1</sup> ]	$\Delta S^\ddagger$ [J mol <sup>-1</sup> K <sup>-1</sup> ]	R <sup>2</sup>	Mono-imine	Bis-imine
SALAL	38.8 ± 0.5	-66.0 ± 1.5	0.9935	51 %	42 %
4-diethylamino	41.4 ± 1.0	-80.3 ± 3.1	0.9913	63 %	24 %
5-hydroxy	29.0 ± 0.7	-106.9 ± 2.2	0.9910	64 %	34 %
5-chloro	29.3 ± 0.3	-89.1 ± 0.8	0.9985	74 %	22 %
4-hydroxy	44.1 ± 1.2	-57.6 ± 3.9	0.9909	37 %	14 %
5-nitro <sup>[a]</sup>	28	-70	-	62 %	23 %

Table 3.2-5 Activation parameters for the intramolecular C<sub>2</sub>DA motion for various aromatic core substitutions of SALAL and composition of the equilibrium mixture at 20 mM concentration of both reagents in CD<sub>3</sub>CN/D<sub>2</sub>O 7:3 (v/v) at pH 10.7 and 25 °C. Difference between 100 % and sum of mono-imine and bis-imine is the unreacted aldehyde. [a] insufficient data for statistical evaluation of the fitting, provided activation parameters are only rough estimations.

### b) Solvent composition

The rate of the intramolecular exchange in the SALAL-C<sub>2</sub>DA mono-imine is also very dependent on the composition of the solvent. Gradually changing the CD<sub>3</sub>CN:D<sub>2</sub>O solvent composition from 5:5 to 6:4, 7:3, 8:2 and 9:1, the coalescence temperature of the CH<sub>2</sub> <sup>1</sup>H-NMR signals increased from 29 °C to 32, 37, 46 and 80 °C respectively (NMR traces given in Figure 7.5-2 to Figure 7.5-7), corresponding to rates of internal motion at 25 °C from 552, to 442, 365, 226 and 158 Hz, respectively (Table 3.2-6). In pure d<sub>3</sub>-acetonitrile, the methylene signals appear as sharp triplets, and the rate of intramolecular exchange is only 7 Hz at 25 °C. In this case obviously coalescence cannot be reached since it is higher than the boiling point of acetonitrile (82 °C). The exchange rates have been determined by the line-shape analysis over a range of temperatures of about 50 °C and used to calculate the Eyring activation parameters (Section 7.5.1.1). It is thus possible to modulate the rate of the process by changing the nature or the composition of the solvent in a much more delicate way compared to core substitution.

D <sub>2</sub> O percentage	50 %	40 %	30 %	20 %	10 %	0 %
Coalescence temperature [°C]	27	31	37	46	75	n.d.
Rate at 25 °C [Hz]	552	442	365	226	158	7

Table 3.2-6 Intramolecular exchange rates at 25 °C and corresponding signal coalescence temperatures of the mono-imine of SALAL with C<sub>2</sub>DA at different proportions of D<sub>2</sub>O in CD<sub>3</sub>CN; n.d. for not determined in the case of coalescence temperature above the boiling point of the solvent used.

### c) Temperature

Finally, as already shown in the previous examples, temperature variation allows for a very fine and gradual adjustment of the exchange rates.

In total, the speed of the internal group displacement motion may be modulated easily in three different ways: coarse adjustment by introduction of substituents on the SALAL core, more gentle adjustment by changing the solvent composition, and fine tuning by temperature. The effect of other factors that may affect the speed of this process, such as pH, addition of a chemical effector, etc. could be investigated. By a combination of these different effects, one may expect to be able to cover a range of rates even larger than the four orders of magnitude demonstrated in previous examples.

## 3.2.2. Aldehydes with ethyleneimine oligomers

The intramolecular exchange process described above for simple aliphatic  $\alpha,\omega$ -diamine molecules (Figure 3.2-2) becomes particularly attractive when one considers its extension to more



complex polyamine molecules such as linear polyamine chains. The end-to-end transfer of an aldehyde residue on a diamine unit, together with the formation of an intermediate aminal, allows one to envision systems where the aldehyde moiety would effect a back-and-forth, non-directional “walk” along a polyamine chain such as diethylenetriamine ( $\text{en}_2\text{N}_3$ ) and its longer analogues, triethylenetetraamine ( $\text{en}_3\text{N}_4$ ) and tetraethylenepentamine ( $\text{en}_4\text{N}_5$ ), as well as the biogenic amines spermine and spermidine, which contain amino sites separated by two, three or four methylene groups (Figure 3.2-3), thus suggesting an intriguing extension into the area of motional dynamic involving relative displacement of two linked molecules presented in Figure 3.2-15.

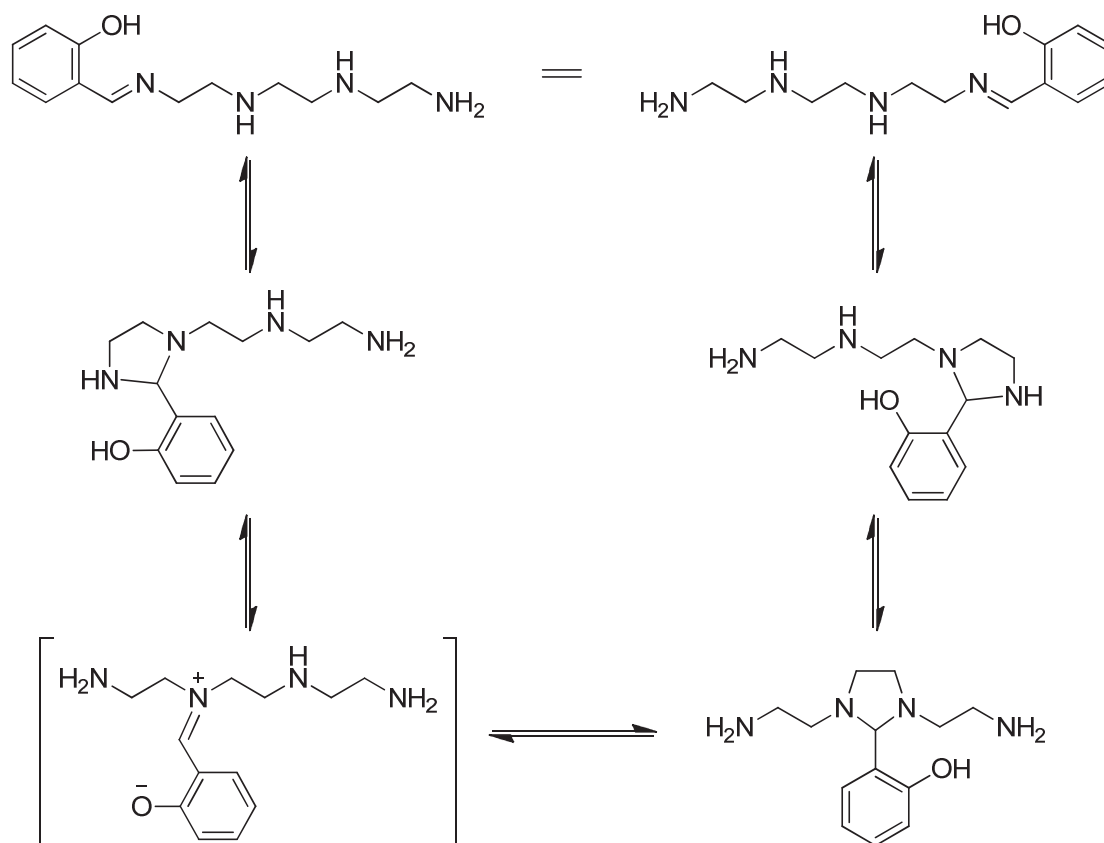


Figure 3.2-15 Proposed mechanism of **SALAL** end-to-end displacement in the reaction with  $\text{en}_3\text{N}_4$ .

When 2D  $^1\text{H-NMR}$  measurements were performed on the reaction of **SALAL** with  $\text{en}_2\text{N}_3$  or  $\text{en}_3\text{N}_4$ , EXSY analysis of the cross-peaks indicated that intramolecular exchange was taking place between the two ends of the polyamine moiety. In the case of  $\text{en}_4\text{N}_5$  it could not be observed, as it is probably so slow that it is hidden under the faster intermolecular exchange, similarly to the case of  $\text{pr}_2\text{N}_3$  which has a longer distance between the nitrogen sites. The data from these EXSY experiments are given in Table 3.2-7. The intermolecular exchange rate for 20 mM and 8 mM solutions of both components in  $\text{CD}_3\text{CN}:\text{D}_2\text{O}$  (7:3 v/v) fits again very well with first order kinetics. The intermolecular exchange, which can occur by intermolecular reaction with an external partner (such as a solvent molecule or an amine group) at the terminal imine or an intermediate iminium state, would correspond to the falling-off in biological motor systems.

Polyamine	$\text{en}_2\text{N}_3$	$\text{en}_3\text{N}_4$	$\text{en}_4\text{N}_5$	$\text{pr}_2\text{N}_3$
Intramolecular rate [Hz]	$0.60 \pm 0.05$	$0.28 \pm 0.03$	Not observed	Not observed
Intermolecular rate [Hz] <sup>[a]</sup>	Not observed	Not observed	$0.40 \pm 0.04$	$0.15 \pm 0.02$

Table 3.2-7 Rates of intra- and intermolecular exchange processes as determined by EXSY analysis of 2D  $^1\text{H-NMR}$  data. [a] Rate of the first order intermolecular exchange given at 20 mM concentration of both reagents.

Such processes, where a given molecule moves along another one, are of great interest as nanomechanical molecular devices both in biology and in nanoscience and the design of synthetic systems effecting analogous molecular motions has also attracted much attention (see the Introductory Section 3.1 for specific examples and corresponding references).

The present case would represent a very simple implementation of such behaviour. One may further note that, whereas in the biological systems the attachment of the molecules and the walking process involve formation and rupture of supramolecular interactions, in the present case, the motion is enabled by a dynamic covalent bond forming and breaking. The processivity of the displacement arises from double bonding of the salicylidene residue to the polyamine track in all stages of the walking process.

### 3.2.2.1. Mechanism of walking along the polyamine chain

In fact, the mere existence of intramolecular exchange is not sufficient proof that the aldehyde residue is really moving along the polyamine strand. Indeed, a long chain might adopt a conformation which would allow a direct "jump"-type, end-to-end transfer of the aldehyde unit from one terminal nitrogen to the second terminal free  $\text{NH}_2$ , even though the results obtained with cadaverine, **C<sub>5</sub>DA**, indicate that such a distant jump is not very likely to happen. The strong preference for the imine formation over amination in the case of **SALAL** is here very beneficial, because it makes the spectra much easier to decipher compared to **PYRAL**, which forms multiple amination and mixed imine-aminations, leading to a complex  $^1\text{H-NMR}$  spectrum, which is very difficult to unravel and impossible to quantify. However, when *N*-propylsalicylaldehyde is treated with *N,N'*-dimethylethylenediamine in  $\text{CDCl}_3$  the amination is obtained with  $K = 1.4$ , indicating that **SALAL** is capable of amination formation as well.

To investigate whether the aldehyde moiety is indeed "walking" along the polyamine track molecule, the oxa-analogue of **en<sub>3</sub>N<sub>4</sub>**, where the two internal nitrogen atoms are replaced by oxygens, **O<sub>2</sub>-en<sub>3</sub>N<sub>2</sub>**, was studied. The absence of the secondary amines on the track prevents formation of amination and iminium states and, indeed, prevents intramolecular exchange as the observed process was found to be concentration dependent, indicating intermolecular exchange, with first order kinetics. The exchange rate values were  $0.30 \pm 0.02$  Hz and  $0.17 \pm 0.02$  Hz for 20 mM and 8 mM solutions, respectively. Similarly, 1,8-diaminooctane (**C<sub>8</sub>DA**) as **en<sub>3</sub>N<sub>4</sub>** analogue having methylene groups instead of secondary nitrogens also exhibit only intermolecular exchange at  $0.12 \pm 0.02$  Hz for 20 mM and  $0.04 \pm 0.01$  Hz for 8 mM solutions.

In similar fashion, diethylenetriamine analogues were investigated. The results with **C<sub>5</sub>DA** gave a good fit with first order kinetics (Table 3.2-3) and thus showed the exchange to be intermolecular. The **en<sub>2</sub>N<sub>3</sub>** on the other hand performs an intramolecular exchange (Table 3.2-7) at  $0.60 \pm 0.05$  Hz under given conditions. The oxa-analogue **O-en<sub>2</sub>N<sub>3</sub>** was studied by EXSY. Surprisingly, an intramolecular exchange was observed with rates of  $0.22 \pm 0.02$  Hz and  $0.18 \pm 0.01$  Hz at 20 and 8 mM respectively. The unexpected behaviour can be explained by the known *gauche effect* of the oxygen atoms in hydrocarbon chains.<sup>[332]</sup>

To further support the "walking" mechanism, the derivative of **en<sub>3</sub>N<sub>4</sub>** with two **SALAL** moieties attached as imines and a third one forming a central amination (bis-imine-amination), **Sal<sub>3</sub>-en<sub>3</sub>N<sub>4</sub>**, was synthesized and treated with methoxyamine, expecting that it would first react with the imine double bond and thus release one of the terminal  $\text{NH}_2$  groups. As **SALAL** prefers to form a terminal imine, the group of the central amination should thereafter move from the central position towards the end of the **en<sub>3</sub>N<sub>4</sub>** molecule, through a lateral amination to the terminal nitrogen site, to give a bis-imine

(Figure 3.2-16). To prove the reasoning of this hypothesis, relative reactivities of aldehyde, imine and aminal towards nucleophilic attack by methoxyamine was examined in separate experiments.

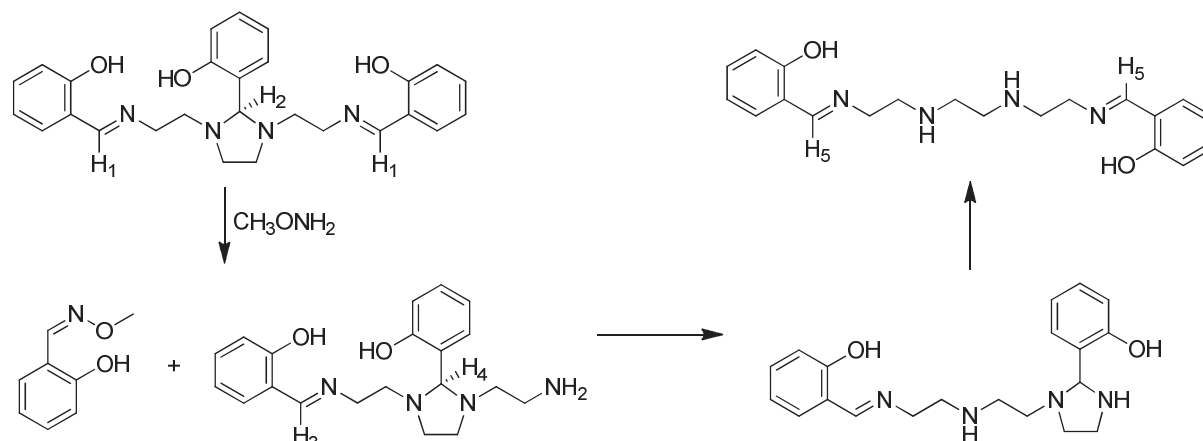


Figure 3.2-16 Mechanistic scheme and proton signal assignment for the reaction of methoxyamine with the bis-imine-aminal **Sal<sub>3</sub>en<sub>3</sub>N<sub>4</sub>**, corresponding to the kinetic experiments in Figure 3.2-17.

**SALAL** and its imine were individually treated with methoxyamine and the rate constant of the reaction was determined. Methoxyamine gives upon condensation with a carbonyl derivative a very stable oxime, whose formation is under given conditions irreversible. On the other hand the basicity (and related nucleophilicity) of methoxyamine is much lower compared to amines changing the rate determining step of the reaction and consequently the order of the exchange reaction to second order kinetics. In chloroform, **SALAL** and its propylimine react with methoxyamine with almost the same second order rate constant ( $8.6 \cdot 10^{-5}$  and  $8.4 \cdot 10^{-5} \text{ L mol}^{-1} \text{ s}^{-1}$  respectively), but in CD<sub>3</sub>CN/D<sub>2</sub>O (7:3 v/v) the imine is reacting much faster than the aldehyde ( $6.4 \cdot 10^{-4}$  for **SALAL** and  $1.2 \cdot 10^{-2} \text{ L mol}^{-1} \text{ s}^{-1}$  for its *N*-propylimine). The reaction of *N*-propylimine with 1 eq. of *N,N'*-dimethylethylenediamine to form the aminal proceeds only slowly in CDCl<sub>3</sub>, but after 20 hours the equilibrium mixture contains about 60 % of the aminal and 40 % of the imine.

When equimolar solution of **SALAL**, its propylimine and its aminal (*N*-propylsalicylaldimine and *N,N'*-dimethyl-2-(2-hydroxyphenyl)-imidazolidine) was treated with 3 eq. of methoxyamine (as a free base) both in CDCl<sub>3</sub> and in CD<sub>3</sub>CN/D<sub>2</sub>O (7:3 v/v, pH uncontrolled). A rapid decrease of the aldehyde peak was observed followed by slight decrease of the imine peak intensity. When the aldehyde had reacted completely, in CDCl<sub>3</sub> the imine continues to diminish while the amount of the aminal is constant. In a mixture of CD<sub>3</sub>CN/D<sub>2</sub>O 7:3 v/v, consumption of the aminal is approximately as fast as that of the imine.

From these results it can be concluded that the reaction rates with methoxyamine are in the order aminal  $\lll$  aldehyde  $<$  imine. The re-equilibration between imine and aldehyde is taking place due to the amine liberated by the formation of the oxime both in chloroform and CD<sub>3</sub>CN/D<sub>2</sub>O. The re-equilibration between imine and aminal becomes kinetically relevant only in CD<sub>3</sub>CN/D<sub>2</sub>O, while it is not observed in chloroform. It is thus reasoned that the walking model compound **Sal<sub>3</sub>en<sub>3</sub>N<sub>4</sub>** in chloroform reacts with methoxyamine only at the imine double bond.

Reacting **Sal<sub>3</sub>en<sub>3</sub>N<sub>4</sub>** with one equivalent of methoxyamine (free base) in CDCl<sub>3</sub> at 25 °C gave gradually rise to the signals of a mono-imine-aminal. A steady state concentration was reached and no further increase in concentration was observed as this mono-imine-aminal subsequently transformed into the  $\alpha,\omega$ -bis-imine of **en<sub>3</sub>N<sub>4</sub>**. In the NMR spectra, concomitant disappearance of the bis-imine-aminal signals and appearance of the bis-imine and oxime signals is observed both in azomethine region (Figure 3.2-17) and in the aliphatic part (Figure 7.5-30 on page 201). The corresponding kinetic profile is shown in Figure 3.2-18.

Because the reaction was run in  $\text{CDCl}_3$ <sup>†††</sup> with no free **SALAL** present, an intermolecular mechanism can be excluded, thus confirming the linear displacement process (see Figure 3.2-16). Further evidence in favour of the motion of the **SALAL** moiety along the **en<sub>3</sub>N<sub>4</sub>** chain is provided by the reported observation that **N<sup>1</sup>,N<sup>4</sup>,N<sup>4</sup>-tris((*o*-hydroxyphenyl)methyl) triethylenetetraamine** is formed as a minor product in the borohydride reduction of **Sal<sub>3</sub>en<sub>3</sub>N<sub>4</sub>**.<sup>[165]</sup> The presence of a terminal amine bearing two aldehyde residues may be explained as resulting from the shift of the aldehyde residue of the central aminal over to the terminal nitrogen site through an intermediate iminium state.

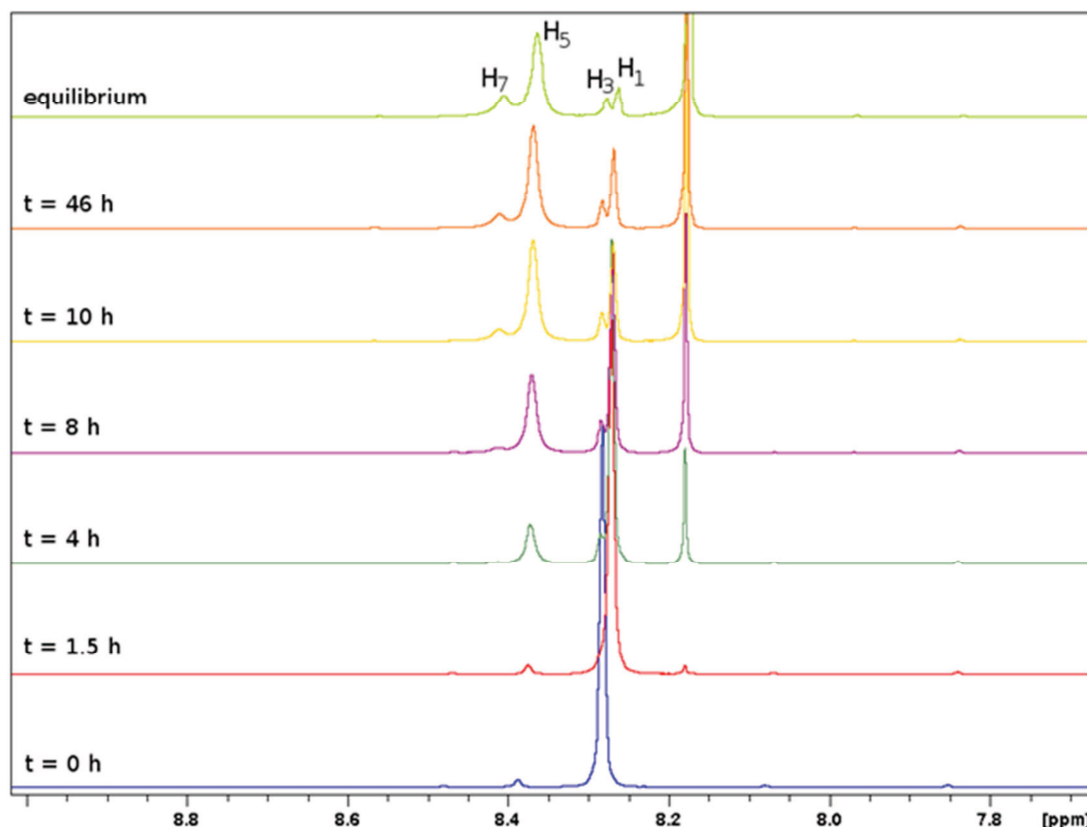


Figure 3.2-17 Detail of the imine and oxime region of the 400 MHz  $^1\text{H-NMR}$  spectra of the reaction of 1 eq. of methoxyamine with **Sal<sub>3</sub>en<sub>3</sub>N<sub>4</sub>** in chloroform. For the signal identification see the previous figure. Concomitant appearance of the oxime and bis-imine peak is observed, while the bis-imine-aminal peak is disappearing. Detail on the aliphatic part of the spectrum is provided in Experimental part. Signal H7, not described in Figure 3.2-16, belongs to the mono-imine of **en<sub>3</sub>N<sub>4</sub>** which is formed by double reaction of **Sal<sub>3</sub>en<sub>3</sub>N<sub>4</sub>** with methoxyamine.

The existence of an iminium species as an intermediate cannot be confirmed by NMR experiments due to its short half-life under the conditions used. However, one might be able to trap it by the participation of a neighbouring nucleophilic group. To this end, sodium 2-formylbenzoate was reacted with one equivalent of **en<sub>2</sub>N<sub>3</sub>** in  $\text{CD}_3\text{CN}/\text{D}_2\text{O}$  7:3 (v/v) and compared to the reaction with propylamine and **C<sub>2</sub>DA** (pH adjusted to 10.7 by DCI). While propylamine and **C<sub>2</sub>DA** give only imine, a new peak appeared at 5.12 ppm in the reaction with **en<sub>2</sub>N<sub>3</sub>** (Figure 3.2-19). By extensive multidimensional NMR characterization (Figure 7.5-12 to Figure 7.5-17 on page 191), it was assigned to the O-CH-N proton of the amino-lactone generated by the internal addition of the carboxylate to the iminium,<sup>[333]</sup> expected to form as a transient species in the displacement process. This observation points to the possibility of trapping the iminium species occurring as intermediates along a polyamine chain, and to observe each consecutive step in the displacement process.

<sup>†††</sup> As control experiment, the same reaction was performed in  $\text{d}_6\text{-DMSO}$  and  $\text{d}_3\text{-acetonitrile}$ , in both cases the situation was similar, however, the best signal separation was achieved in chloroform.

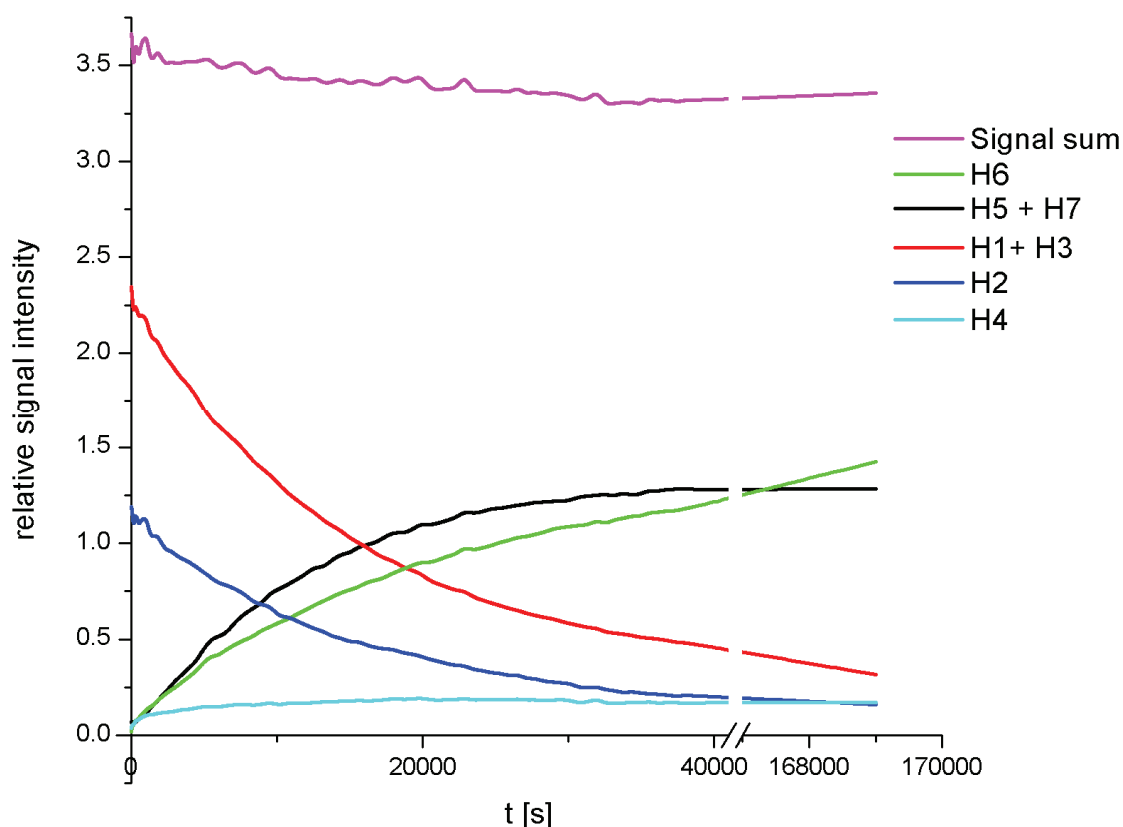


Figure 3.2-18 Signal evolution during the kinetic experiment of **Sal3en3N4** treated with 1 eq. of methoxyamine, the process and the signal assignment given in Figure 3.2-16. Signal H7, not described in Figure 3.2-16, belongs to the mono-imine of **en3N4** which is formed by double reaction of **Sal3en3N4** with methoxyamine. "Signal sum" represent the sum of signals of aminals, imines and oxime and shows that all azomethine (and related) protons are conserved throughout the measurement.

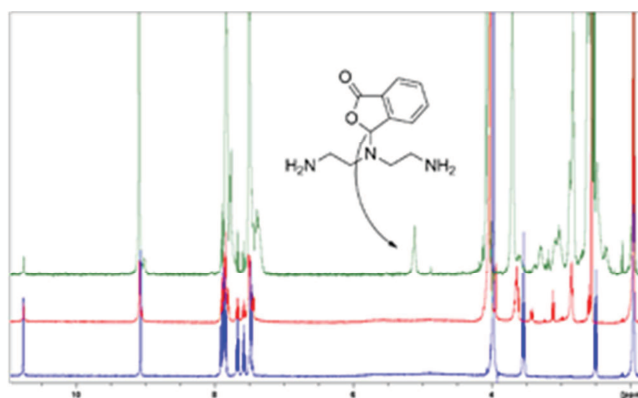


Figure 3.2-19 Comparison of the  $^1\text{H-NMR}$  spectra of sodium 2-formylbenzoate reacted with propylamine (blue), **C2DA** (red) and **en2N3** (green). The signal of the O-CH-N proton of the aminolactone formed is indicated. Full NMR characterization with all signal assignment is given in Experimental part.

### 3.2.2.2. Aldehydes with cyclic ethyleneimine oligomers

The non-directional displacement along the polyamine chain shares the topology with the linear polyamine used, being one-dimensional and length-limited. However, by connecting the two ends of the polyamine chain, cyclic topology of the amine is obtained and thus an infinite motion in a circle can be envisaged. Taking into account the limitation of the two-carbon distance between the

nitrogen atoms (Table 3.2-7), there are several cyclic polyamines available: 1,4,7-triazacyclononane (**tacn**), 1,4,7,10-tetraazacyclododecane (**cyclen**) and 1,4,7,10,13,16-hexaazacyclooctadecane (**hexacyclen**).

The cyclic polyamines bear only secondary nitrogen atoms and thus cannot form imines like the linear polyamines discussed above. Thus upon condensation with aldehydes they are transformed to the corresponding aminals by linking two adjacent nitrogens into a five-membered ring. As shown above (Section 3.2.2.1), the aminal can dissociate one of its N-C-N bonds to form the transient iminium which is highly reactive and immediately reacts with an amine in proximity to form again an aminal. As both amine and the aminal derived from it are symmetric the probability for breaking either of the aminal C-N bonds is equal. Similarly, the intermediary iminium can be attacked by the amine which just dissociated to close the ring between the same pair of nitrogens, or it can react with the nitrogen in the opposite direction and thus displace the aminal by one ethyleneimine monomer. Therefore, the cyclic motion is degenerate and non-directional.

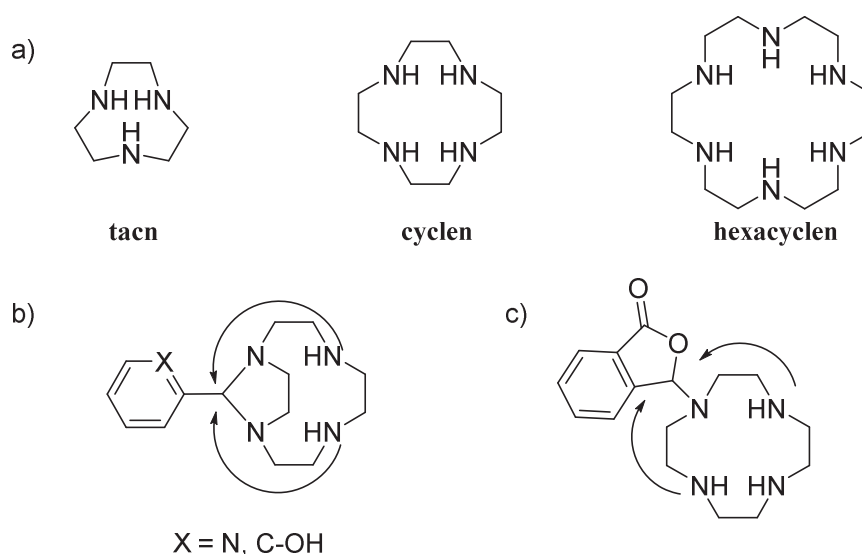


Figure 3.2-20 a) Cyclic polyamines used for intramolecular circular displacement study. b) Non-directional aminal displacement of **SALAL** and **PYRAL**. c) Non-directional displacement of **CAXAL**, capable of aminal-lactone interconversion.

The simplest cyclic polyamine capable of intramolecular aminal displacement is **tacn**. While two nitrogen atoms are involved in aminal formation, the third one can induce the intramolecular motion. To this extent, when **tacn** was mixed with **SALAL**, **PYRAL** or **CAXAL** (1:1 ratio, 20 mM) in  $d_6$ -DMSO, formation of the aminal was clearly observed. It is noteworthy that aminal signals derived from cyclic polyamines are largely downfield shifted compared to linear polyamines (as also reported in literature<sup>[334]</sup>). However the only chemical exchange signals recorded by 2D NMR correspond to the conformational dynamics of the five-membered ring and no displacement is observed. If 1 eq. of trifluoroacetic acid (TFA) was added to the samples, the lines of the signals of the aliphatic methylene groups of the aminal broadened significantly and the exchange signals were visible in the 2D spectra for all aldehydes. In the case of **CAXAL** (added as sodium salt), the aminal CH signal splits into three different signals upon addition of and an acid: the most downfield shifted peak at 6.70 ppm was attributed to **CAXAL** which hydrolysed from the **tacn** and closed the hydroxy-lactone form, the signal at 6.66 ppm corresponds to the amino-lactone closed on one of the **tacn** nitrogens, and finally signal at 6.27 was assigned to the aminal structure. Interestingly, the signal of aminal has a chemical exchange correlation with the amino-lactone peak, proving that these two species coexist in a dynamic equilibrium.

To improve the rate of the intramolecular displacement, more polar solvent can be used. Thus, slow exchange rates in DMSO can be enhanced by employing a mixture of  $d_3$ -acetonitrile/ $D_2O$  (7:3 v/v, hereafter referred as ACN/W). When **SALAL** was mixed with **tacn** in this solvent mixture, formation of the aminal was observed almost instantaneously. The signals of the aliphatic protons appear partly broadened and for unambiguous characterization the water content was lowered to 5%. The signal assignment is shown in Figure 3.2-21a and the multidimensional NMR spectra are given in the Experimental part. The condensation to the aminal leads to formation of two fused rings: one five- and one eight-membered.<sup>[334]</sup> The corresponding  $CH_2$  signals in  $^1H$  NMR spectrum appear as largely overlapped multiplets, but the protons labelled *Hb* (Figure 3.2-21b) are well separated from the other signals, as well as the signal of unreacted **tacn** (sharp singlet). It is noteworthy that the chemical exchange signals between the multiplets observed inherently implies the intramolecular nature of the exchange process, whereas the intermolecular one would appear as exchange cross-peaks with the isolated **tacn** singlet, which were not observed in the 2D NOESY spectrum.

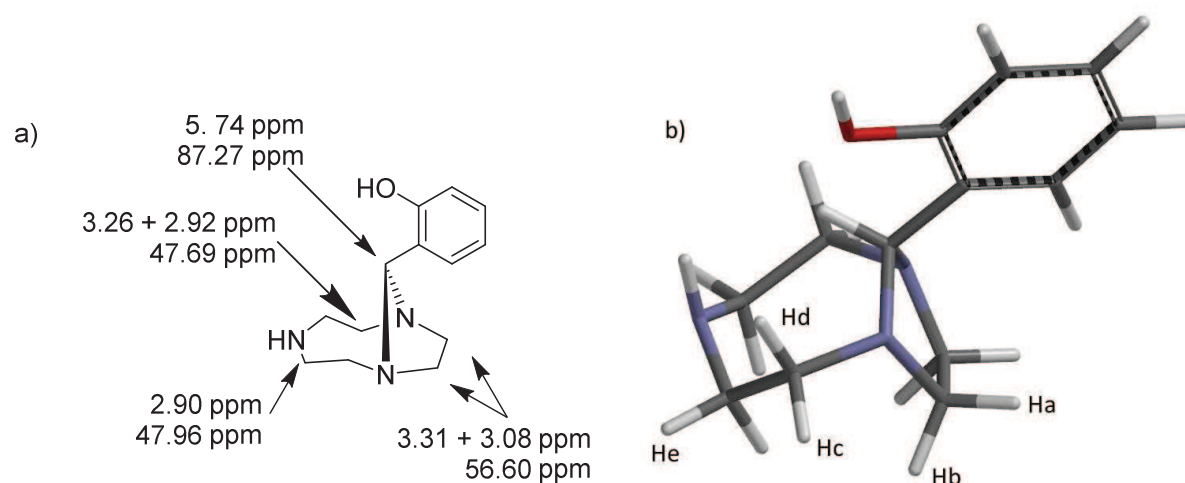
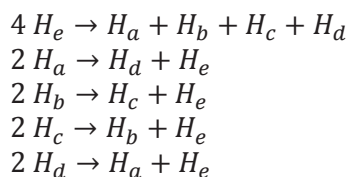


Figure 3.2-21 a) Signal assignment performed by multidimensional NMR. b) MMFF model of the aminal formed from **SALAL** with **tacn**. The conformation of the two fused rings leads to complicated coupling pattern and complex multiplets observed in the spectrum, but the signal of protons *Hb* is well separated at 3.08 ppm.

To understand the chemical exchange cross-peaks, it is necessary to look at the destiny of each hydrogen atom when a single displacement step is made. This exchange pattern can be represented as equations



It is noteworthy that the intermediary iminium is a planar cation which also enables a “ring-flip” of the aminal (antafacial ring re-formation) which transforms protons *Ha* to *Hb* and protons *Hc* to *Hd*. In the 2D NOESY spectrum (Figure 3.2-22), three chemical exchange cross-peaks are observed:

1. Between the signal *Hb* and the overlapped signals of *He+Hc*. This cross-peak is due to the chemical exchange  $Hb \leftrightarrow Hc$  and  $Hb \leftrightarrow He$ , comprising for two proton exchange sharing the same rate.
2. Between *Hb* and the overlapped signals of *Hd+Ha*. This exchange corresponds to the “ring-flip” of the aminal ring.



3. Between the overlapped signals of  $H_e+H_c$  and the overlapped signals of  $H_d+H_a$ . Part of this exchange arises from the “ring-flip”  $H_c \leftrightarrow H_d$  exchange (as in the case 2), and part from the motional displacement  $H_e \leftrightarrow H_a+H_d$  (as in the case 1).

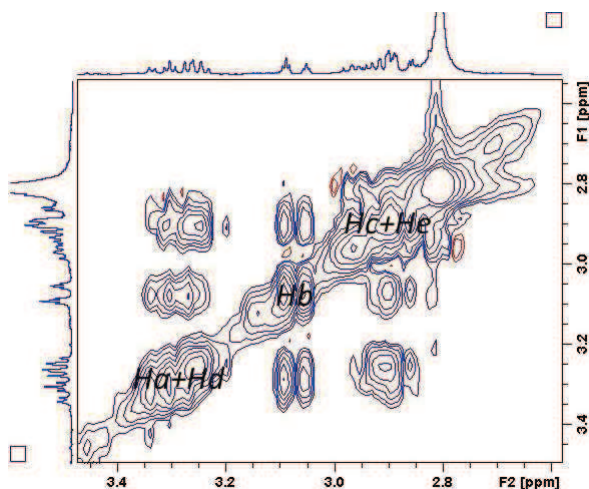
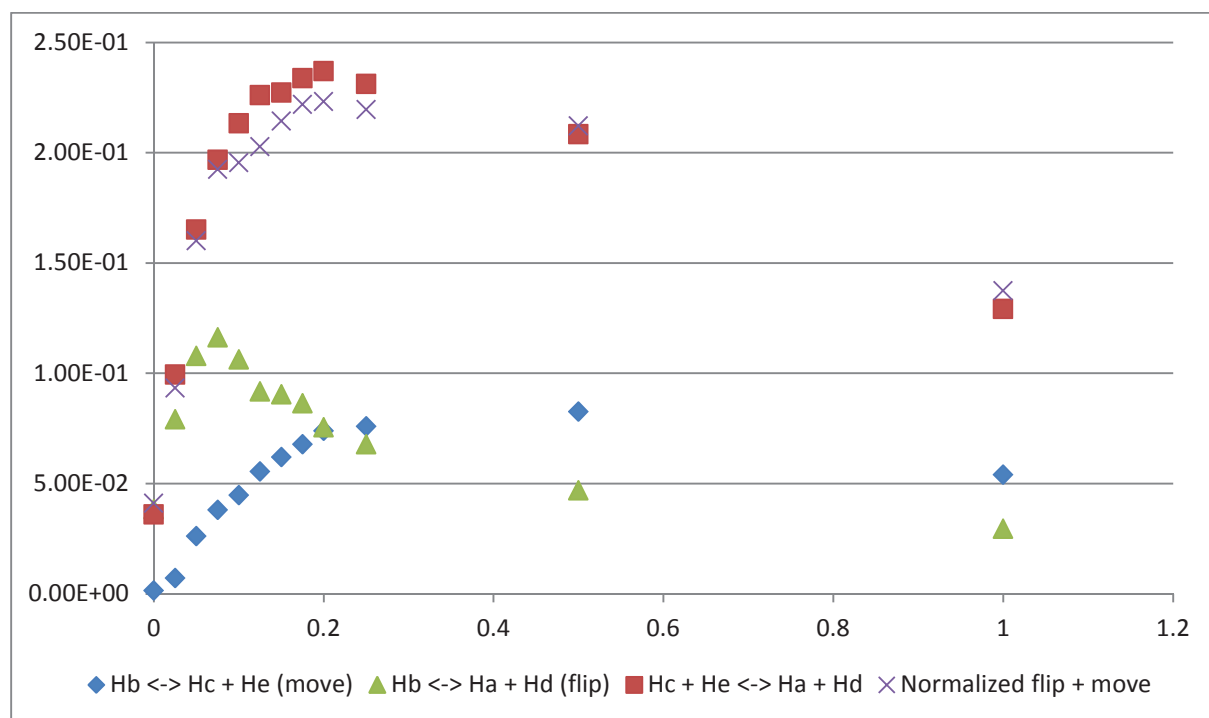


Figure 3.2-22 Zoomed aliphatic part of the 2D NOESY spectrum of the mixture of *SALAL* with *tacn* in an ACN/W solvent mixture. Signal of the proton  $H_e$  overlaps with the signal of  $H_c$ , similar to the overlap between signals  $H_d$  and  $H_a$ . Signals corresponding to the protons  $H_b$  are well separated from others.

From the 2D EXSY experiments the intensity of cross-peaks as a function of the mixing time can be extracted and is shown in Graph 3.2-1. Three different curves were obtained. The exchange assigned to the motional  $H_b \leftrightarrow H_c+H_e$  exchange has the lowest slope of  $0.75 \pm 0.04$  Hz, the ring-flip process has a calculated slope of  $1.8 \pm 0.3$  Hz, and the cross-peak  $H_e+H_c \leftrightarrow H_a+H_d$  of combined displacement and ring-flip has a slope of  $2.50 \pm 0.23$  Hz, which is in a very good agreement with the sum of the two individual rates.



Graph 3.2-1 Cross-peak intensities as a function of the mixing time. Three cross-peaks observed were found to correspond to a single intramolecular exchange process.

Moreover, the calculated sum of the cross-peak integrals  $Hb \leftrightarrow Hc+He$  and  $Hb \leftrightarrow Ha+Hd$  normalized for the number of protons (signal  $He$  comprises for four atoms) fits well with the curve of the cross-peak intensity of the exchange  $He+Hc \leftrightarrow Ha+Hd$ , thus convincingly confirming the results of the 2D EXSY experiments. Unfortunately, the example of **SALAL** reacted with **tacn** in an ACN/W mixture was the only case where the rates of the intramolecular processes could have been obtained.

Both **CAXAL** and **PYRAL** also form aminals with **tacn** efficiently in ACN/W medium, but the resulting aminals are very stable and do not exhibit the intramolecular motion. Acidification of the aqueous samples of aldehydes and cyclic amines leads to extensive hydrolysis of the aminor. The signals of the residual aminor are broad, indicating a fast exchange rate, but due to the low cross-peak intensities in 2D NOESY spectra the quantification has not been performed.

When **cyclen** was examined, very low conversion to aminals (< 5 %) was observed in ACN/W mixtures for all aldehydes. In DMSO, the aminor was formed in acceptable conversion for **SALAL** and **PYRAL** (69 % and 56 % respectively) but no exchange was observed. On the other hand, **CAXAL** did not give any aminor at all. To enhance the intramolecular displacement, the samples were acidified by 1 eq. TFA. Indeed, **SALAL** exhibited enhanced exchange upon addition of the acid, but the signals overlap with residual water signal and therefore prevent integration in the 2D EXSY experiment. **PYRAL** did not provide any exchange signals even upon acidification and addition of more than 1 eq. of TFA leads to extensive hydrolysis. **CAXAL** upon acidification converted partially to its amino-lactone (Figure 3.2-20c) giving a mixture of free aldehyde (7 %), lactone closed on the aldehyde alone (hydroxy-lactone, 36 %) and the amino-lactone on **cyclen** (57 %). Interestingly, the signals in the aliphatic part of the spectrum are broad and largely overlapped, indicating an intramolecular displacement of the lactone in the **cyclen** ring, which was also evidenced by 2D NOESY (Figure 3.2-23). However, the spectra were not suitable for rate evaluation.

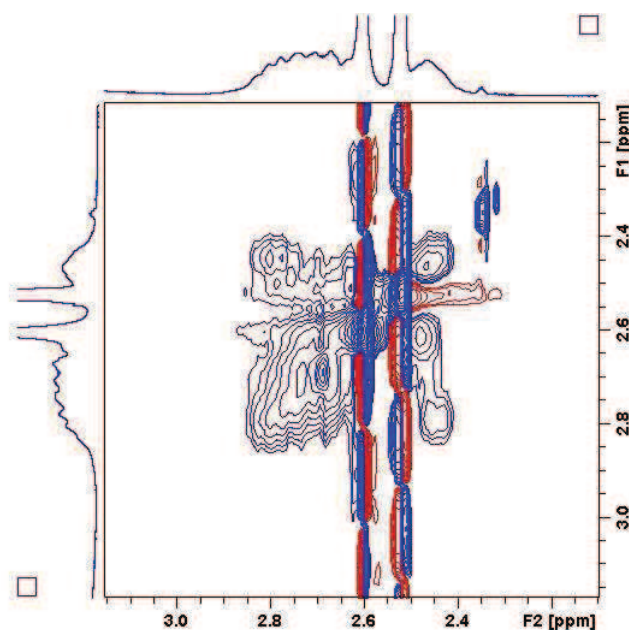


Figure 3.2-23 Magnified aliphatic part of the 2D NOESY spectrum of the mixture of **CAXAL** with **cyclen** acidified by 1 eq. of TFA: the methylene protons appear as non-resolved complex signal, but the exchange cross-peaks observed indicate an intramolecular exchange.

In order to enhance the exchange process without the need for acidification,  $d_4$ -methanol was used as a solvent. When **SALAL** was mixed with **cyclen** in MeOD at (100 mM, both reagents), indeed the formation of the aminor was observed with about 54 % conversion, calculated from the characteristic aldehyde CHO signal at 10.18 ppm and the aminor Ar-CH signal at 5.35 ppm). However

the composition of the mixture strongly depends on the concentration: if the same mixture is prepared at 20 mM, the aminal is still formed in 35 % conversion, but is accompanied by 22 % of the hemiaminal formed by the reaction of the iminium intermediate with  $\text{CD}_3\text{OD}$ , thus giving new signals at 5.63 (Ar-CH) and at 2.65 ppm of the  $\text{CHD}_2$  group ( $\text{CHD}_2\text{OD}$  signal referenced at 3.33 ppm). 2D NOESY spectrum of the mixture at 100 mM indicated that this hemiaminal could be present even at higher concentration, but at less than 1 %, and that this hemiaminal interconverts with the aminal structure (Figure 3.2-24). Importantly, the methylene signals exhibit a very rich pattern of chemical exchange cross-peaks, in which every single peak is exchanging with all others. Such a pattern strongly indicates that intramolecular exchange is indeed taking place, but the corresponding EXSY experiments (at both concentration levels) provided highly erroneous integral intensities of the cross-peaks which were not usable for the rate evaluation.

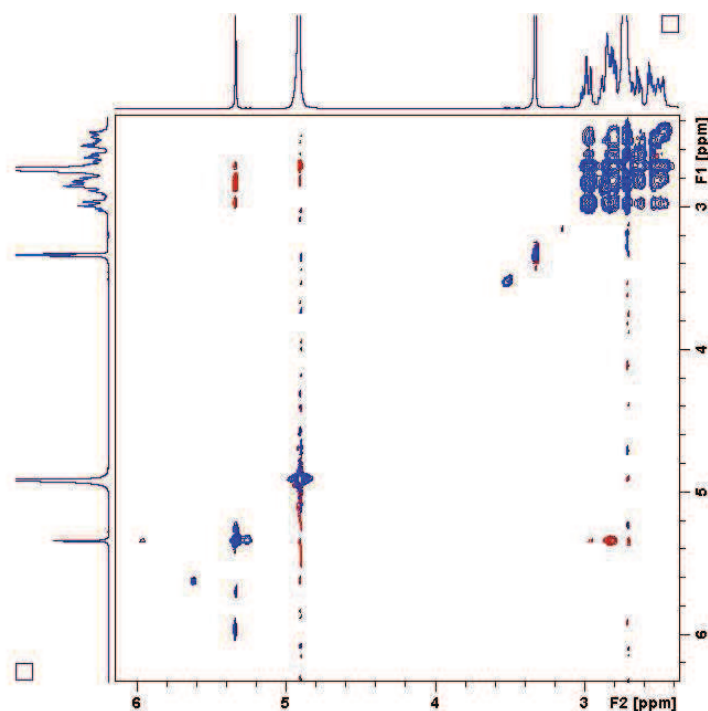


Figure 3.2-24 2D NOESY spectrum of the mixture of **SALAL** and **cyclen** in  $\text{CD}_3\text{OD}$ : the aminal signal at 5.35 ppm has exchange cross-peaks with barely visible broad signals downfield, probably the hemiaminal formed with  $\text{MeOD}$ , and NOE correlation with the aliphatic protons. A complex exchange pattern is observed for the aliphatic signals indicating the intramolecular displacement, although the corresponding EXSY experiments failed.

In the case of **hexacyclen**, formation of multiple aminal species is observed for all aldehydes used. In an acetonitrile-water mixture, only **PYRAL** forms aminals efficiently, but four different aminal signals are observed in the range of 4.8-5.2 ppm and two more around 4.1 ppm. Determination of exchange rates was not performed since it was not possible to attribute the signals to defined structures. In  $d_6$ -DMSO, **SALAL** and **CAXAL** do not form the aminals unless 1 eq. of TFA is added, but in such case, multiple overlapping signals are observed and assignment of the exchange process to defined structures was not possible.

### 3.2.2.3. Branched polyamines

In the case of the branched triamine compound **tren** (tris(2-aminoethyl)amine), EXSY studies enable insight into the behaviour of the reaction mixture it generates with **SALAL** (1:1 ratio, 20 mM) in  $\text{CD}_3\text{CN}:\text{D}_2\text{O}$  (7:3 v/v), where three different imines are observed: mono-imine (59 %), bis-imine (28 %) and tris-imine (10 %) and 3 % of aldehyde remains unreacted. Cross-peaks in the NOESY spectrum

revealed multiple exchange processes involving specific signals. The data from the azomethine signals indicate that the imines are interchanging intermolecularly between themselves rather than reacting with the small amount of available aldehyde (similarly to the case of diamines discussed in 3.2.1.2). In the aliphatic region, the spectrum is more complicated. Nevertheless, the same exchange pattern as described for the azomethine protons can be observed here as well. Furthermore, exchange cross-peaks of =N-CH<sub>2</sub>- protons with H<sub>2</sub>N-CH<sub>2</sub>- protons are clearly visible. Among all the exchange processes, two concentration independent ones, clearly assignable to mono-imine and bis-imine intramolecular interchanges (Figure 3.2-25), could be evaluated with rates of  $3.84 \pm 0.16$  and  $1.13 \pm 0.18$  Hz, respectively.

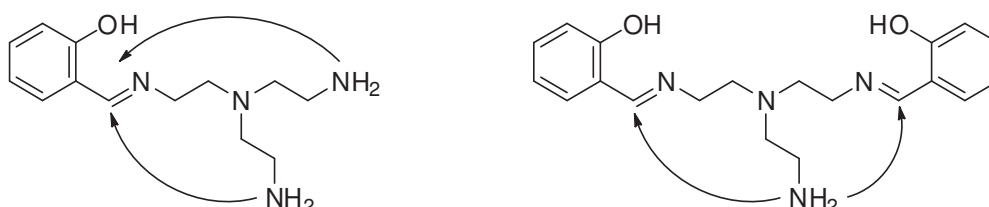


Figure 3.2-25 Intramolecular exchange processes in the mono-imine and the bis-imine of **tren** reacted with **SALAL** observed by NMR with rates obtained by EXSY.

#### 3.2.2.4. EXSY – analysis of exchange rates

2D EXSY<sup>[327–331,335]</sup> represents a unique tool to determine the rates of exchange processes taking place in dynamic equilibrium and in terms of the range of quantifiable rates complements the line-shape analysis. Extension of the spectral range into two dimensions also allows for better separation of concomitant processes in complex mixtures and is to some extent insensitive to partial signal overlap. The procedure of an EXSY experiment is demonstrated on the case of **SALAL** with **tren**, which was presented in the previous Section.

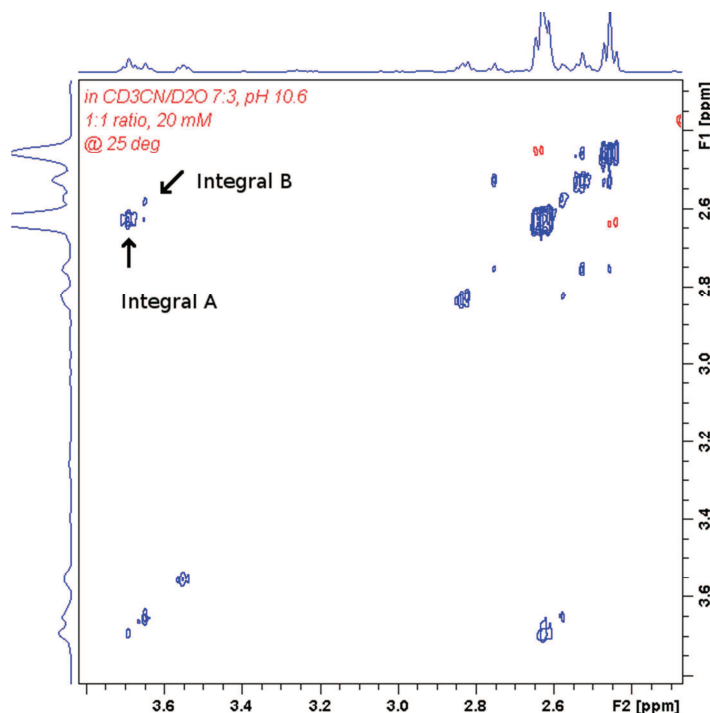


Figure 3.2-26 2D <sup>1</sup>H-NOESY of the mixture of **tren** with **SALAL** in CD<sub>3</sub>CN:D<sub>2</sub>O (7:3 v/v). Cross-peak A indicates the intramolecular exchange present in the mono-imine, cross-peak B is due to the intramolecular exchange of the bis-imine.

The experiment consists of a set of 2D NOESY experiments with different values of the delay in the pulse sequence, called the mixing time ( $t_m$ ). As a sequence *noesyph* was used, the receiver gain was optimized once for the first experiment and kept constant for the sample. A typical set of  $t_m$  values was 0, 0.025, 0.05, 0.075, 0.1, 0.125, 0.15, 0.175, 0.2, 0.25 and 0.5 s, where  $t_m=0$  was used for evaluation of “equilibrium magnetization” (diagonal peak intensity). Baseline correction was performed in both dimensions prior to integration. 2D integration ranges were optimized on the spectrum with  $t_m=0.5$  s and transferred to all others. Integration of the spectra with different mixing times using the same integration ranges provides raw integral data. The procedure is demonstrated on the case of **SALAL** reacted with **tren** (discussed above) where two simultaneously occurring exchange processes are observed and, furthermore, both of them can be quantified from a single data set.

Calculation of exchange rates was performed using the NOESY build-up curve, where the intensity of the cross-peaks is plotted as a function of  $t_m$ . Due to the inherent symmetry of the 2D NOESY spectrum, the average between symmetrical cross-peaks was taken. A typical curve obtained is shown in Figure 3.2-27. The curve grows linearly from  $t_m=0$  until the relaxation becomes important (in the presented case around  $t_m$  of 0.2 s) and this linear part is fitted by linear regression with a forced null x-intercept. The slope of this regression is divided by the “equilibrium magnetization” which is the intensity of diagonal peaks, between which the cross-peak is observed, at  $t_m=0$ . For an exchange between peak A and B, the slope divided by the equilibrium magnetization of peak A gives the rate of exchange  $A \rightarrow B$ ,  $k_1$ , and on the other hand, the same slope divided by the equilibrium magnetization of peak B is the value for the reverse reaction  $B \rightarrow A$ ,  $k_2$ , fulfilling the definition for the equilibrium constant  $K = \frac{c_B}{c_A} = \frac{k_1}{k_2}$ . The rates were verified by the EXSYCalc program<sup>[336]</sup> for  $t_m$  values of 50 ms, 150 ms and 250 ms. EXSYCalc cannot process the entire EXSY experiment and therefore does not provide any statistics on the quality of the data.

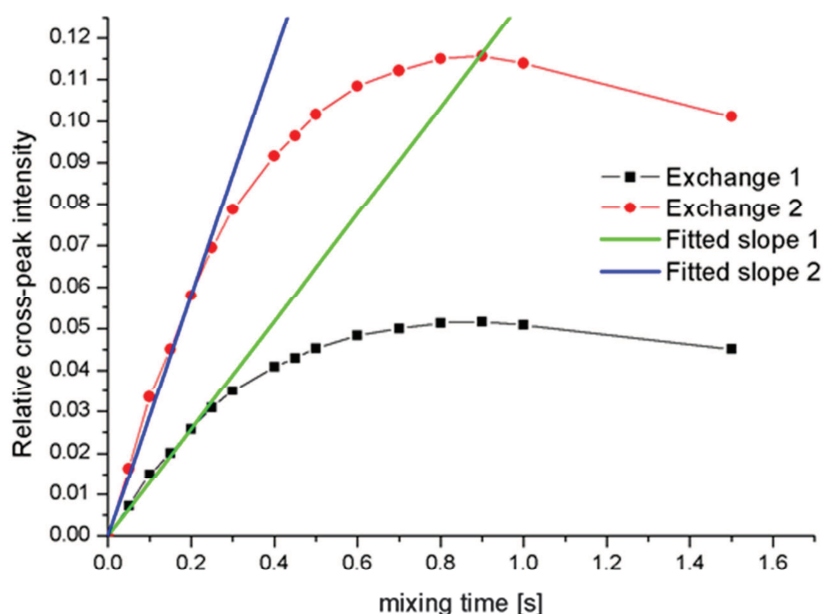


Figure 3.2-27 Typical NOESY build-up curve for a system with two exchanges, here represented on the case of **SALAL** reacted with **tren**. The exchange 1 (black squares) correspond to the intramolecular exchange in the bis-imine of **tren** (cross-peak B in Figure 3.2-26), the exchange 2 (red circles) is due to the intramolecular exchange in the mono-imine of **tren** (cross-peak A in Figure 3.2-26). Both exchange processes can be observed and evaluated simultaneously. An extract from the set of 2D NOESY spectra used for construction of the plot is presented in Experimental part in Figure 7.5-23 to Figure 7.5-25 on page 197, signal assignment is provided in Figure 7.5-26.

For the intramolecular exchange reaction of symmetrical amines where the starting and the end points are the same,  $k_1 = k_2$ . This is very beneficial since peaks of polyamine molecules can overlap heavily in the NMR spectra. With this approach, only one well separated signal is needed to calculate the exchange rate, such as the imine =N-CH<sub>2</sub>-signal, which is strongly shifted downfield compared to the parent amine derivative.

EXSY experiments were recorded for at least two concentration levels, 20 and 8 mM. It was shown that intermolecular imine exchange reactions follow first order kinetics and thus lowering the concentration by a factor of 2.5 should lead to a decrease in the observed rate by a factor of 2.5 as well. This was the criterion used for qualifying the imine exchange as intra- or intermolecular. For all exchange rates, a 95 % confidence interval was calculated. Data with a 95 % confidence interval which was 10 % or less of the rate value were considered good, data with a 95 % confidence interval of 20 % and more were rejected, and data with a 95 % confidence interval between 10 % - 20 % were repeated twice more to make them acceptable (narrowing the confidence interval) or they were rejected (if not reproducible).

### 3.3. Directional walking

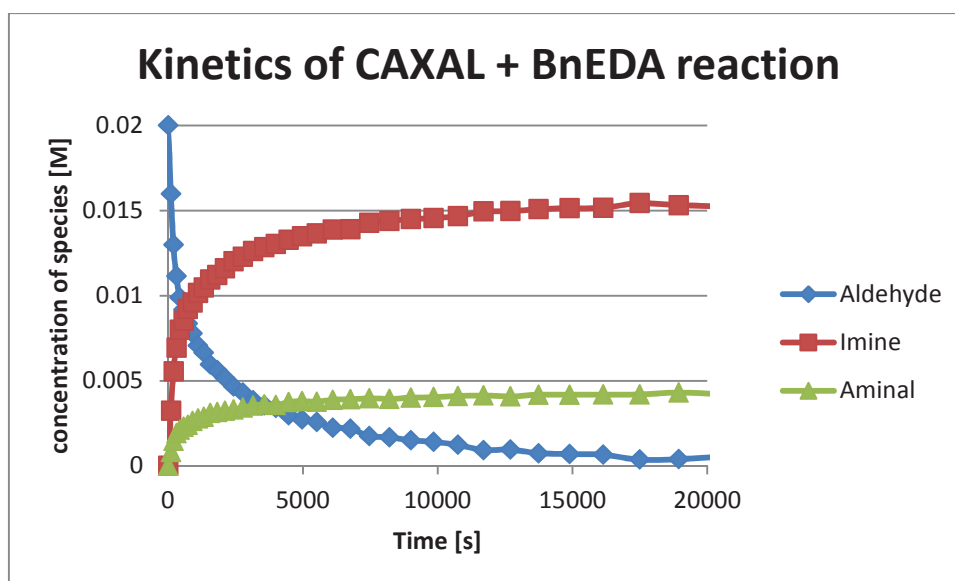
The phenomenon of non-directional walking presented above brings into chemistry the features of random walking, a process of high interest in the field of quantum physics<sup>[337,338]</sup> or biology.<sup>[262]</sup> However, a typical application of this process in chemistry involves some sort of a cargo transport ultimately requiring a directional mode of operation controlled by a stimulus. Also, the walker unit and the track need to remain attached to each other for the entire time of operation, thus fulfilling the condition of processivity. The possibility brought by **CAXAL** to trap the intermediate iminium states by formation of the lactone ring inspired the search for a condition which could provide a directional small-molecule walker controlled by the change in pH.

#### 3.3.1. Lactone formation – trapping of iminium on secondary nitrogens

The displacement of an aldehyde between nitrogen atoms proceeds through repetitive amination ring closure/opening. In the case of primary amines, the ring opening leads to the formation of an imine. However, if the displacement is taking place between secondary amines, the formation of an imine is not possible, but instead an iminium is formed. Due to the positive charge, this intermediate is very unstable and readily reacts with any nucleophile present. In the molecule of **CAXAL**, a nucleophile, the carboxylic group, is inherently present in proximity of the aldehyde function. The reaction of the transient iminium with the carboxylate yields a five-membered lactone ring fused with the benzene core, bearing an amino substituent in position 3. The ester bond in the lactone as well as the formation of the cationic iminium were supposed to act as the pH dependent states which can be addressed by addition of a base or an acid.

In the initial study, *N*-benzylethylenediamine (**BnEDA**) was mixed with the sodium salt of **CAXAL** (in d<sub>6</sub>-DMSO, 20 mM each) and the reaction was followed by NMR (Figure 3.3-1). Concomitant formation of two species, the imine and the amination, was observed reaching the equilibrium in about 4 hours and overall conversion of the aldehyde was about 99 % (Graph 3.3-1). In equilibrium, the imine is present in 77 % and the amination in 21 %, and these products coexist in dynamic equilibrium as evidenced by exchange cross-peaks in the 2D NOESY spectrum (Figure 7.5-44 on page 208).





Graph 3.3-1 The reaction of **CAXAL** with **BnEDA** in  $d_6$ -DMSO followed by NMR: concomitant appearance of the imine and the aminal is observed. In the equilibrium, the mixture contains 77 % of the imine, 21 % of the aminal and about 1 % of the aldehyde remains unreacted.

In the following experiments, the equilibrated DMSO solutions of the mixture of **BnEDA** and the sodium salt of **CAXAL** were titrated by a stock solution of TFA and the  $^1\text{H}$ -NMR spectra were recorded (Figure 3.3-2). After addition of the first equivalent of TFA both the imine and the aminal azomethine signals disappear from the spectrum while the aliphatic region shows two sets of signals of approximately equal intensity. One of the sets appear as a pair of sharp triplets assigned to the hydrolysed **BnEDA**, the other set appears as a broad coalesced signal indicating a fast exchange reaction on the NMR time scale. This indicates that the species undergoes a very fast exchange between imine, aminal, lactone and hydrolysed amine and aldehyde, which was evidenced by the exchange cross-peaks between the broad signal and the two sharp triplets in the 2D NOESY spectrum (Figure 7.5-45 on page 208). The spectra recorded immediately after addition of the acid and one hour after the addition are identical, showing that the equilibrium is established within one minute.

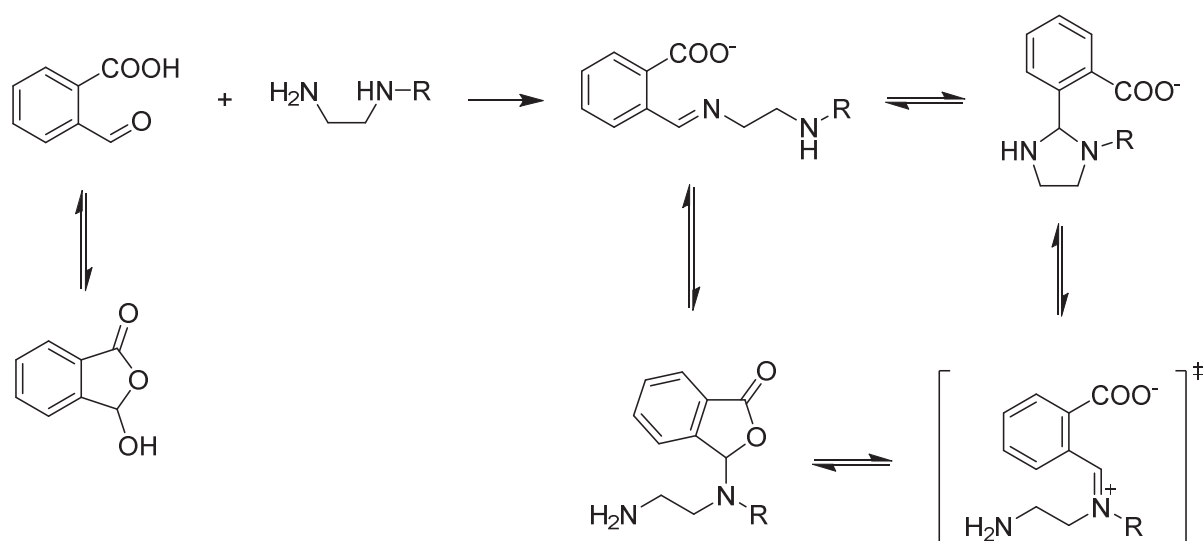


Figure 3.3-1 **CAXAL** and **BnEDA** as model system for directional walking: condensation of the aldehyde with the diamine to give a mixture of imine and aminal which can be converted to the lactone by acidification of the medium.



Addition of the second equivalent of TFA leads to emergence of a new sharp peak at 6.65 ppm assigned to the lactone, formed in 65 % conversion. The aminor and the imine (broad signals) are observable as well in 2 % and 33 % conversion, respectively, and, similarly to the sample before acidification, they are dynamically interconverting as shown by 2D NOESY. The azomethine carbon of the lactone formed bears four different substituents and is therefore chiral. The chirality causes “desymmetrisation” of the benzylic CH<sub>2</sub> protons which are thus diastereotopic and appear in the NMR spectrum as a pair of doublets with a strong coupling of 14.4 Hz. The presence of the lactone peak at 6.65 ppm and the splitting of the benzylic CH<sub>2</sub> signal can serve as a good indication of the formation of the lactone in proximity of the benzylic group.

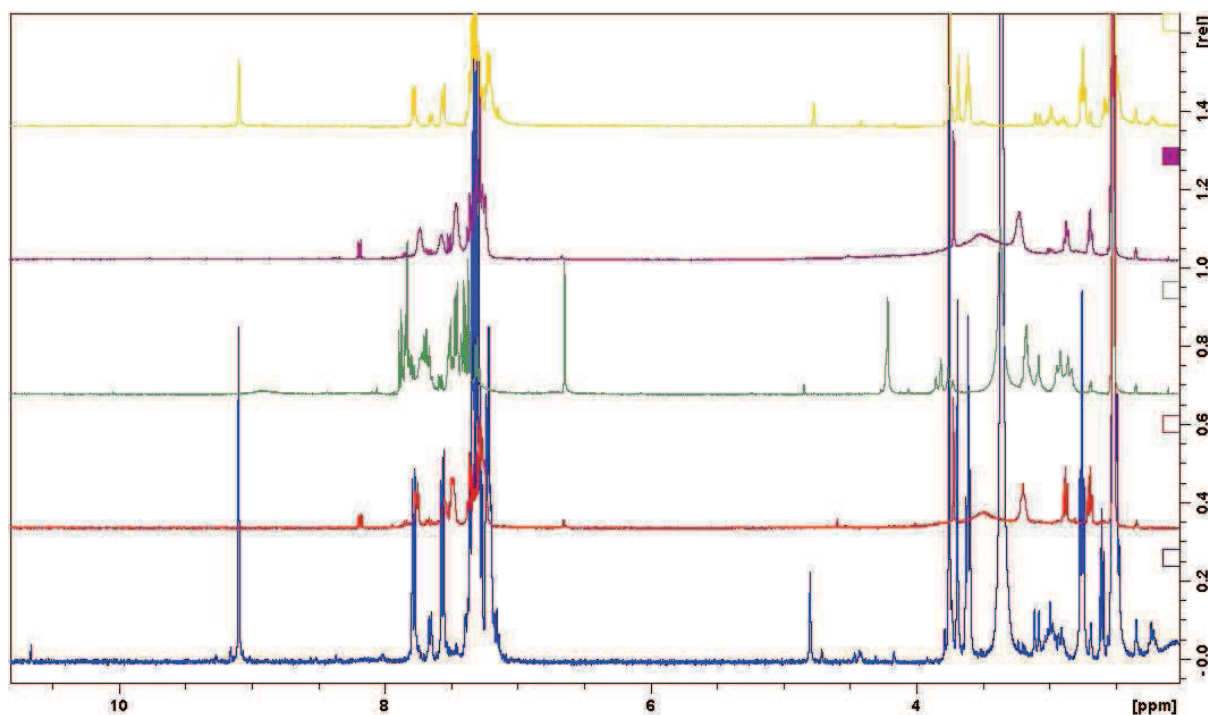


Figure 3.3-2 <sup>1</sup>H-NMR spectra of the mixture of **BnEDA** and sodium salt of **CAXAL**, from bottom to top: equilibrated sample of the condensation reaction (blue); the sample after addition of 1 eq. of TFA (red); the sample after addition of the second equivalent of TFA (green); the sample containing 2 eq. of TFA after addition of 1 eq. of *t*-BuOK (purple); the sample containing 2 eq. of TFA after addition of 3 eq. of *t*-BuOK (yellow).

To examine the reversibility of the lactone formation, the samples after addition of two equivalents of TFA were back titrated with potassium *tert*-butoxide, *t*-BuOK. When the first equivalent of *t*-BuOK was added to the sample with TFA, the spectrum was identical to those after addition of the first equivalent of TFA, showing two sets of signals in the aliphatic region and no azomethine signal. After addition of the second equivalent of the base, however, the spectrum did not change significantly. Addition of the third equivalent of *t*-BuOK was necessary to obtain a spectrum identical to the initial condensation experiment, showing the imine (78 %) and the aminor (22 %) as the only species present in the solution. The NMR traces of the titration by acid and back-titration by base are given in Figure 3.3-2.

The experiments on **BnEDA** reacted with **CAXAL** prove the concept of the directionality control of the displacement of an aldehyde along the polyamine chain (Figure 3.3-3). Under basic conditions there are not enough protons available for the formation of the transient iminium and therefore only imine/aminor equilibrium is established. Addition of the acid allows for aminor ring protonation on either of its nitrogen atoms (nitrogens are called “primary” and “secondary” like in the parent amine although they are tertiary and secondary in the aminor structure). If the protonation occurs on the “secondary” nitrogen the aminor opens to form the imine on the “primary” one, however if the protonation occurs on the “primary” amine the ring opens to provide

an iminium which immediately stabilises by formation of the lactone. The lactone ring closure/opening indeed depends on the acidity of the medium: upon addition of a base the labile ester bond is cleaved and the iminium formed is stabilized by the formation of the aminal, which consequently re-equilibrates with the imine form. From the mechanism-energy point of view the system can therefore be attributed to the Brownian ratchet mechanism.<sup>[263]</sup>

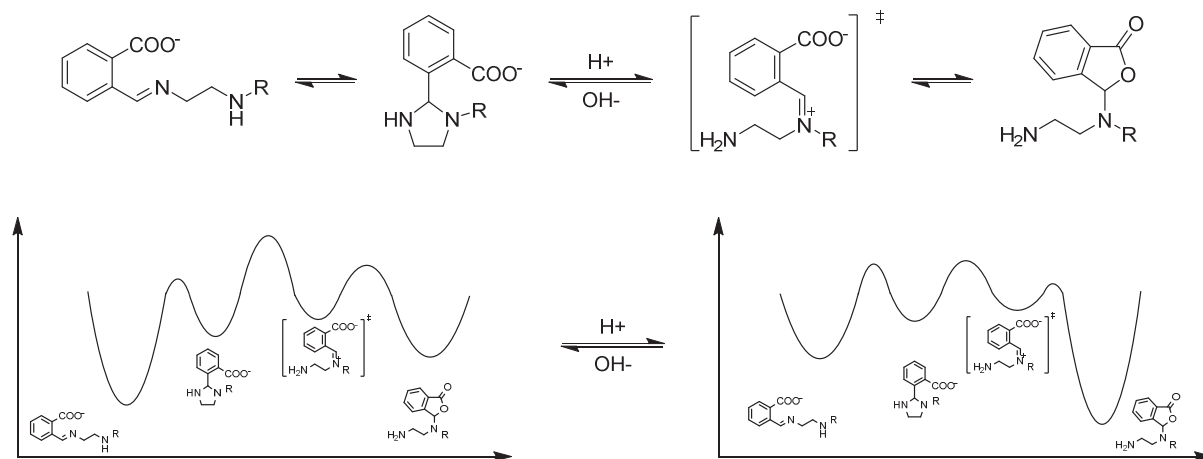


Figure 3.3-3 Representation of the pH dependent displacement of **CAXAL** between the two nitrogen sites of **BnEDA** with a schematic energy diagram: under basic conditions the imine and the aminal coexist in dynamic equilibrium but the formation of the transient iminium is impossible due to the absence of an acid. After acidification, the iminium is formed but is immediately trapped in the form of the lactone. Addition of a base leads to opening of the labile ester bond and consequently to reestablishment of the imine-aminal equilibrium.

The experimental difficulties, notably the extensive hydrolysis after addition of 1 eq. of acid and the imine/aminal inner equilibrium, lead to the search for a **CAXAL** derivative with improved performance in the directional displacement. First, introduction of substituents at the position 4, *para* to the aldehyde function, was examined (Figure 3.3-4a). Two groups with the opposite properties were chosen: a) the strongly electron-withdrawing nitro group which could lead to higher electrophilicity of the aldehyde and thus to increased conversion in the reaction with an amine; b) the strongly electron-donating dimethylamino group which could provide stabilization for the transient iminium thus decreasing the amount of hydrolysed product upon acidification (Figure 3.3-4b). The nitro derivative was synthesised using the published procedure,<sup>[339]</sup> the dimethylamino derivative is described in the Experimental part.

The presence of the nitro substituent indeed increases the electrophilicity of the aldehyde, but it in turn also changes its character: the electron deficient carbonyl function reacted with amines providing only  $sp^3$  hybridised products like aminals, hemiaminals or hydrates and no imine signal was observed in the NMR spectra. On the other hand, the electron-donating properties of the dimethylamino group make the aldehyde very unreactive and only very low conversion to either of the products of the condensation with amines is observed.

In the non-directional displacement studies, **SALAL** exhibited very convenient properties: it produced almost uniquely the imine even when reacted with diamines which can form aminals, and it also gave a very high conversion even in aqueous media. Therefore, another derivative, 2-formyl-3-hydroxycarboxylic acid (Figure 3.3-4c), was envisaged and synthesized using the published protocol.<sup>[340]</sup> The presence of the hydroxyl group *ortho* to the aldehyde resembles the structure of **SALAL**, while the carboxylic function in the other *ortho* position is similar to the structure of **CAXAL**. Moreover, the hydroxyl is conjugated with the aldehyde and can thus contribute to the stabilization of the iminium in a similar way as envisaged before for the dimethylamino derivative (Figure 3.3-4d). Indeed, this derivative is capable of formation of both the imine and the lactone, which can be interconverted by the action of acid or base, and the results are discussed in the Section 3.3.3.

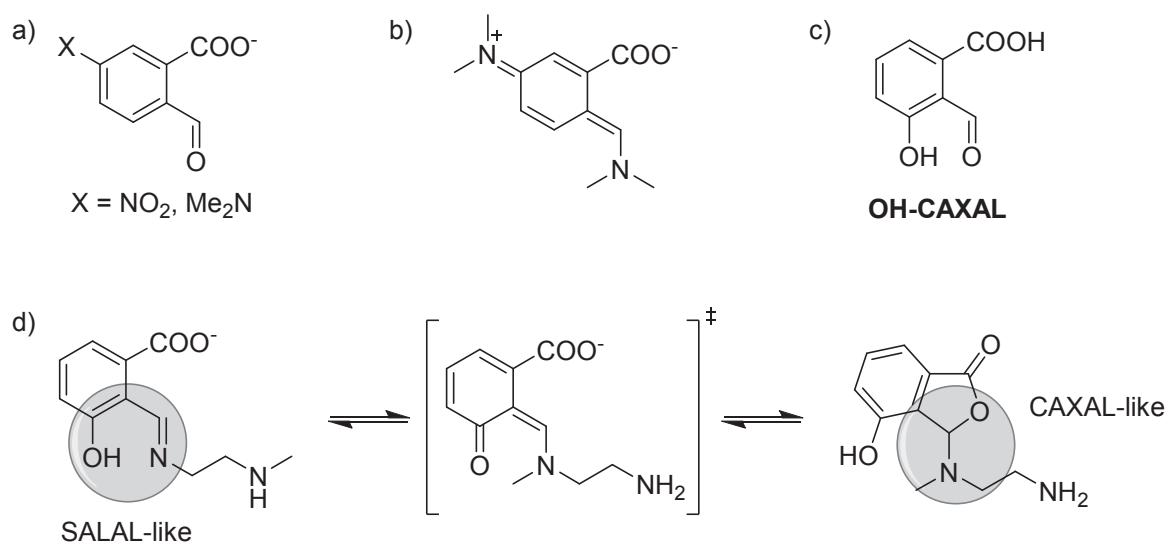


Figure 3.3-4 Structure variations of **CAXAL**: a) EWG or ED substitution in the position *para* to the aldehyde strongly influences its reactivity and properties, but nitro and dimethylamino groups did not lead to improved performance of the parent **CAXAL**, b) possible stabilization of the transient iminium by a push-pull conjugated system, c) 2-formyl-3-hydroxycarboxylic acid comprising for the structural properties of both **SALAL** and **CAXAL**, d) the participation of the hydroxyl group in the stabilization of the imine on a primary nitrogen, stabilization of transient iminium by conjugation with the aldehyde, and lactone formation by the reaction with the carboxylate function in the position *ortho*.

### 3.3.2. Desymmetrisation of the walking track

The non-directional displacement discussed in the Section 3.2 was demonstrated on symmetrical polyamine chains where the two termini of the linear track are indistinguishable from each other. For the introduction of directionality of the motion, however, the two termini must be different to some extent in order to provide two distinct states for the walker unit to reside in. Also, for practical reasons, the track should be rather easily accessible in variety of lengths starting from readily available commercial compounds. It was therefore necessary to explore some possibilities of desymmetrisation of the polyethyleneimine oligomers.

First, the case of **BnEDA** explored before was extended to derivatives containing a longer polyamine chain. These derivatives are readily available by reductive amination of **BENZAL** by commercially available ethyleneimine oligomers like **en<sub>2</sub>N<sub>3</sub>** or **en<sub>3</sub>N<sub>4</sub>** (Figure 3.3-5a). When these polyamines are mixed with the sodium salt of **CAXAL**, the formation of the imine is observed in the NMR spectrum, accompanied by the formation of amins. Also, the mixed imine-aminal species, formed by the reaction of one polyamine with two molecules of **CAXAL**, were observed. Acidification was performed by step-wise addition of equivalents of TFA. For efficient formation of the lactone, one equivalent of TFA per amino group was necessary, i.e. three for the track derived from **en<sub>2</sub>N<sub>3</sub>** and four equivalents of the one from **en<sub>3</sub>N<sub>4</sub>**. Under such conditions, one equivalent of the acid serves to neutralize the carboxylate group of **CAXAL**, which can thus close the lactone ring, and the others protonate all the nitrogen atoms except the one where the lactone resides. However, 2D NOESY experiments revealed that the lactone ring does not form on the *N*-benzyl amino site, but rather on one of the nitrogens in the middle of the track. This is probably due to charge repulsion of the protonated amines (Figure 3.3-5b).

The following design involved the reductive amination of **SALAL** instead of **BENZAL** with the same amines **en<sub>2</sub>N<sub>3</sub>** and **en<sub>3</sub>N<sub>4</sub>**. The presence of the hydroxyl group in proximity could lead to formation of the hemiaminal, benzooxazine, on the *N*-benzyl side of the chain (Figure 3.3-5c). However, no formation of such species was observed by NMR under various conditions investigated.

The charge repulsion of protonated amines can be circumvented by employing amines with significantly lower basicity, such as anilines. Therefore, the ethyleneimine oligomers were derivatized by a series of substituted phenyl groups on one of the termini (Figure 3.3-5d). The basicity of the aniline nitrogen was thus further reduced by the presence of EWG on the aromatic core. Unfortunately, the aniline nitrogen of such derivatives is very unreactive and the only species which were formed in the reaction with **CAXAL** were the imine and amins on the nitrogens of the aliphatic amine chain. Under several conditions investigated, no reaction of the aniline nitrogen was observed.

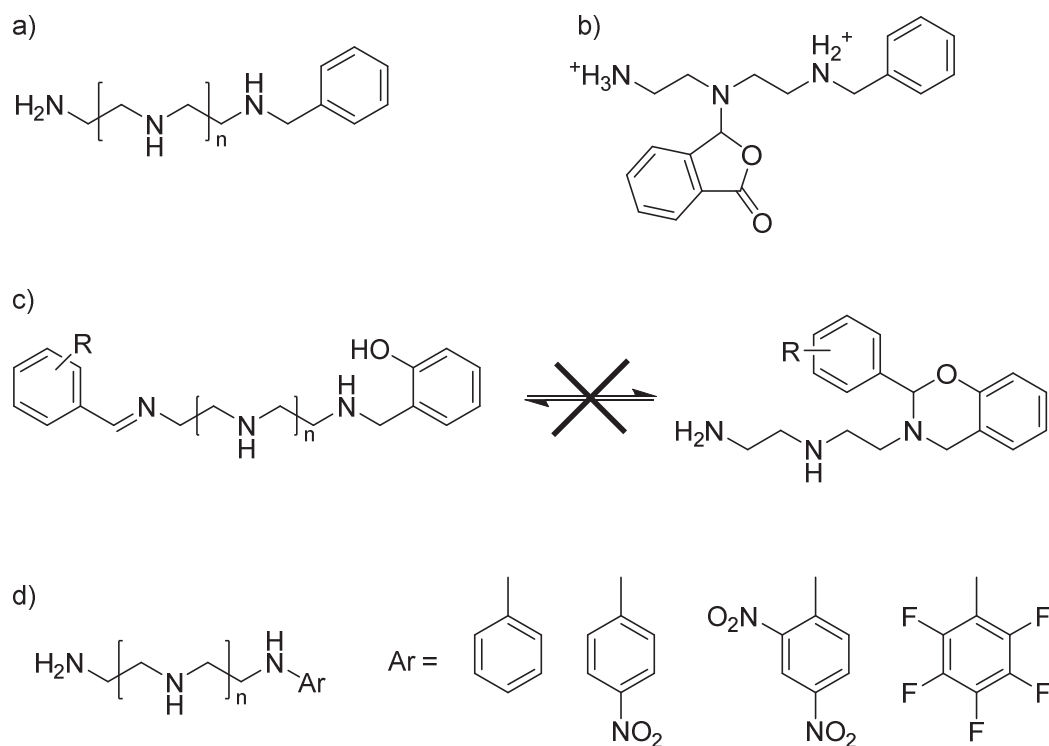


Figure 3.3-5 *N*-alkylated ethyleneimine oligomers as walking tracks: a) tracks prepared by reductive amination of **BENZAL** by commercial polyamines, b) repulsion between positive charges of the protonated track leads to the lactone formation on the nitrogen in the middle of the track, c) tracks prepared by reductive amination of **SALAL** do not form the envisaged benzooxazine structure, d) functionalized anilines possess a nitrogen of lower basicity than aliphatic amines, but such a nitrogen is not reacting with **CAXAL**.

Previous experiments have shown that the lactone ring closure cannot be driven by total protonation of the polyamine chain since such cases lead to preferential charge separation and the lactone resides in the middle of the track. This observation led to the design of tracks bearing a more nucleophilic nitrogen which would not be capable of imine formation, but can still serve as the site for the lactone ring formation. As the first system of such a design, a polyamine chain substituted by *N,N*-dimethyl hydrazine on one side was proposed (Figure 3.3-6a). The synthesis of these derivatives was first attempted by simple alkylation reactions of the *N,N*-dimethyl hydrazine with polyamine bearing a short alkyl chain terminated by a good leaving group, such as bromo or *O*-Ts, on one of the termini of the amine chain. These reactions however do not yield the desired compounds due to the preferential reaction of the *N,N*-substituted nitrogen over the primary one (Figure 3.3-6b), as it was also reported in the literature.<sup>[341]</sup> These reactions thus provide quaternary hydrazinium salts which, unlike in the literature examples, did not show any reversibility of the alkylation.

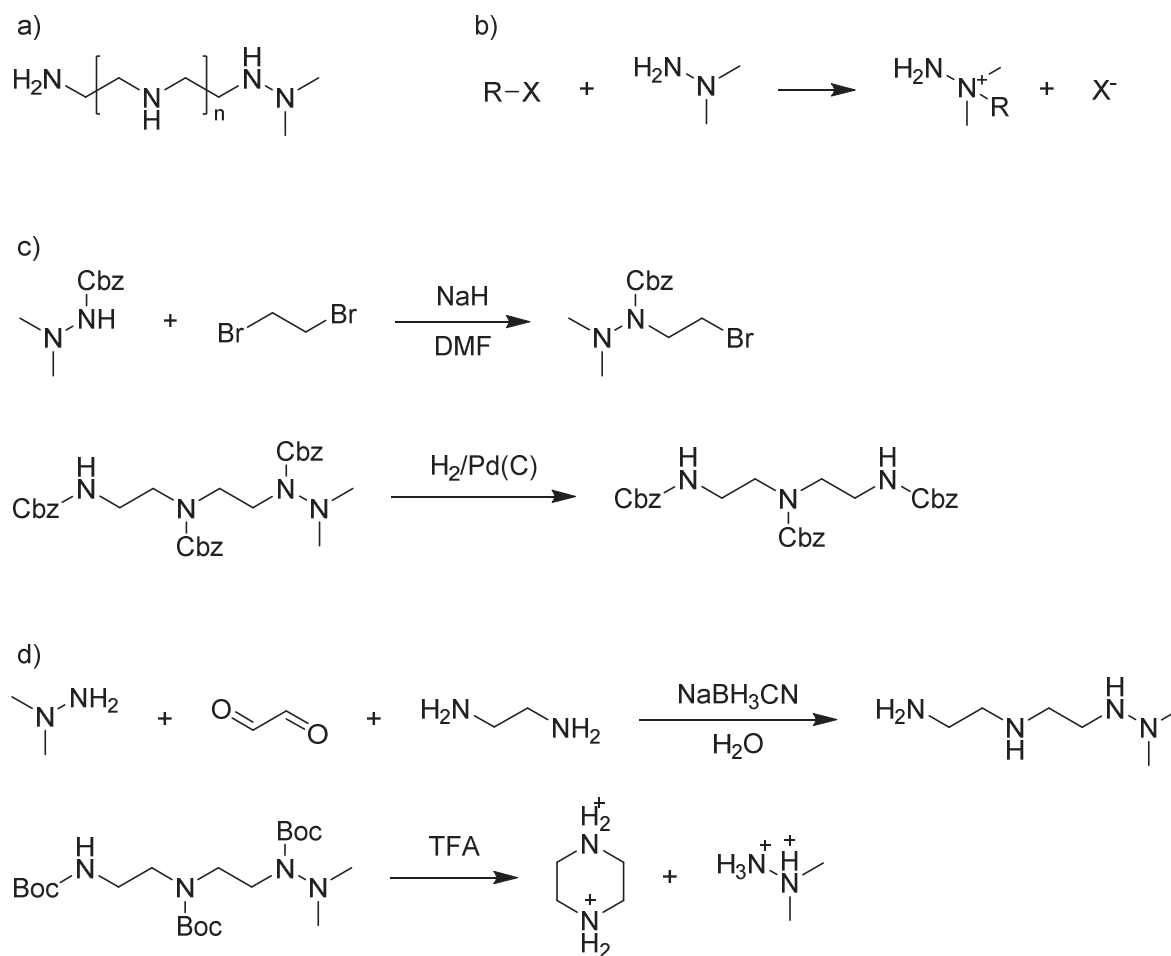


Figure 3.3-6 a) Hydrazine based walking tracks, b) alkylation of *N,N*-dimethyl hydrazine proceeds only on the tertiary nitrogen yielding quaternary hydrazinium salts, c) synthetic procedure for the *N'*-bromoethyl-*N,N*-dimethyl hydrazine, the deprotection of the Cbz groups requires harder conditions than the reductive cleavage of the *N-N* bond, d) double non-symmetric reductive amination of glyoxal by dimethyl hydrazine and aliphatic polyamine yields the desired product, but deprotection of the Boc group, necessary for purification, leads to decomposition of the compound.

The next synthetic approach started from *N'*-Cbz-*N,N*-dimethyl hydrazine which can be deprotonated by the action of a strong base, such as sodium hydride, and reacted with dibromoethane to give a bromoethyl substituted hydrazine, suitable for the reaction with linear polyamines (the procedure for preparation of polyprotected polyamines with one primary amino group unprotected is available in the literature,<sup>[342]</sup> and an improved approach is discussed in Chapter 4). It is noteworthy that this alkylation proceeds only with Cbz protected amines. The alkylation products were fully protected by Cbz and purified by column chromatography. However, the deprotection of the Cbz groups by hydrogenation on palladium requires conditions under which the cleavage of the *N-N* bond is easier than the Cbz deprotection and therefore the products isolated do not contain the desired hydrazine unit (Figure 3.3-6d). Other known procedures for Cbz deprotection, such as HBr/AcOH and BBr<sub>3</sub>, lead to total decomposition of the product.

Another approach involved a double non-symmetric reductive amination of glyoxal which was reacted with both dimethyl hydrazine and the polyamine. First, glyoxal was mixed with the polyamine in water, where the imine linkage formed is readily reversible, and then dimethyl hydrazine was added. The mixture of all imines formed was reduced by sodium cyanoborohydride. The reaction produced a complex mixture of products and was therefore completely derivatized with Boc and purified by column chromatography which provided the desired product. The same procedure was repeated with glyoxal mono-dimethylhydrazone, which became commercially available during the experimentation, with similar results. Unfortunately, the deprotection step

(TFA/CHCl<sub>3</sub>) failed again: the excess of acid necessary for full Boc cleavage also causes full protonation of the polyamine, including a double protonation of the hydrazine unit. This twice charged species acts as a very good leaving group and thus the only products isolated after deprotection was the *N,N*-dimethyl hydrazine and piperazine, formed by the intramolecular nucleophilic substitution of the twice charge hydrazinium by the primary amine.

Many other approaches were investigated involving derivatives of 2-(dimethylhydrazino)-acetaldehyde, 2-(dimethylhydrazino)ethanol or glyoxal mono-benzhydrazone, as well as other protecting groups, such as Fmoc, Alloc or benzyl, or even a combination of different protecting groups. None of these attempts provided the desired product and therefore the hydrazine design was abandoned.

Another highly nucleophilic amine derivative with lower basicity than the aliphatic amines is the hydroxylamine. While hydroxylamine derivatives with primary NH<sub>2</sub> group react with aldehydes to give very stable oximes, an *N*-substituted hydroxylamine derivative cannot condense to oxime, but it can still serve as the site for the lactone formation. First, a procedure analogous to that with dimethyl hydrazine and glyoxal was investigated. To this end, *O*-benzylhydroxylamine was added to the pre-equilibrated mixture of glyoxal and aliphatic polyamine and consequently reduced by sodium cyanoborohydride under acidic conditions (Figure 3.3-7). However, benzyloxyamine under these conditions does not provide the desired product and forms rather the bis-oxime, even when mixed in highly non-stoichiometric ratios. Another approach, analogous to that of hydrazine presented in Figure 3.3-6c was studied with the benzyloxyamine derivative, but similarly to the previous case, the N-O bond cleaves easily under the hydrogenation conditions. None of the procedures examined for the hydrazine design worked for the hydroxylamine derivative either.

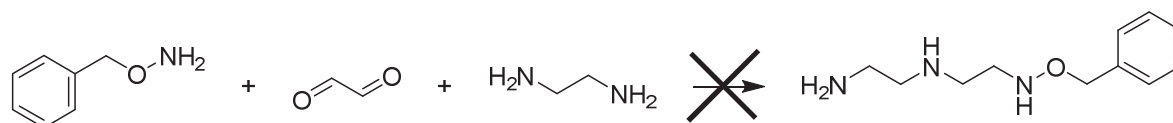


Figure 3.3-7 The double non-symmetric reductive amination involving benzyloxyamine does not yield the desired product and rather the formation of the bis-oxime of glyoxal is observed.

Finally, a different design was proposed: instead of the two-carbon distance between the lactone site and the rest of the ethyleneimine chain, a propylene spacer was chosen (Figure 3.3-8). To this end, a polyamine was dissolved in water and the pH was adjusted to about 7. The mixture was cooled to 0 °C and acrolein was added. Acrolein displays a double reactivity: the carbonyl can react with amino groups to provide imines or amins, and the conjugated double bond acts as a good Michael acceptor. Moreover, while the condensation of the carbonyl function is a reversible and highly dynamic reaction under the conditions used, the Michael addition is irreversible. Furthermore, the low temperature applied during the reaction also favours the Michael reaction of the sterically least hindered nucleophiles, such as primary amines in the present case. Following addition of the benzyloxyamine leads to the formation of the very stable oxime bond. Finally, the reduction of the oxime provides the desired product. Indeed, this procedure provides the desired product, although only in mixture with other isomers and the products of a multiple reaction. Repeated purification on the reverse phase column is therefore necessary, lowering the final yield to only 13 %. However, the benzyloxyamine terminated polyamine chains proved to be suitable tracks for directional walking and the results are discussed in the following Section.



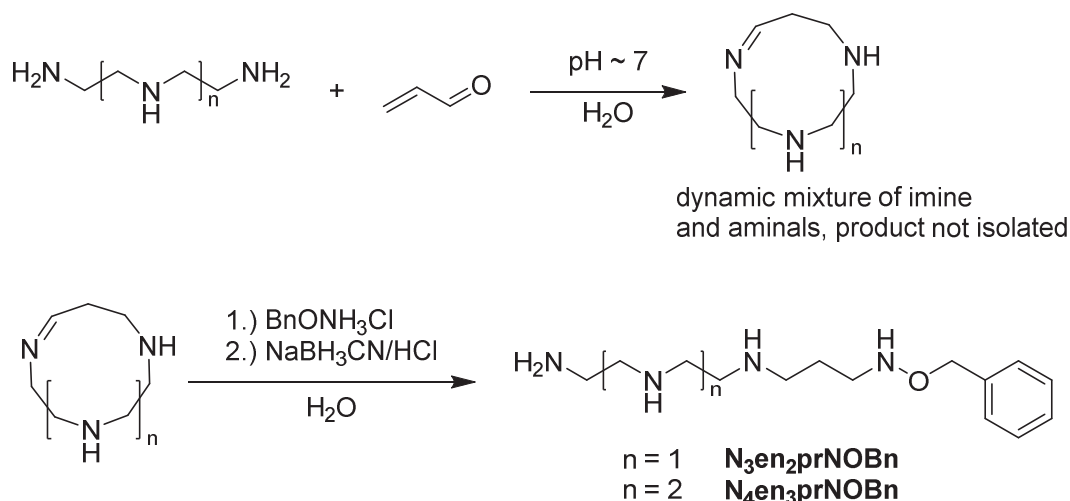


Figure 3.3-8 Synthetic approach for the preparation of benzyloxyamine terminated tracks with  $C_3$  spacer: Michael addition of a polyamine on acrolein is irreversible under the conditions applied, while the condensation of the carbonyl with amines is reversible. Consequent reaction with benzyloxyamine provides stable oximes which after reduction yield the desired track molecules.

### 3.3.3. Directional small-molecule walking

In the previous Sections, the suitable constituents of the directional walking systems were elaborated: 2-formyl-3-hydroxybenzoic acid (**OH-CAXAL**) and benzyloxyamine terminated ethyleneimine oligomers (**N<sub>3</sub>en<sub>2</sub>prNOBn** and **N<sub>4</sub>en<sub>3</sub>prNOBn**). The concept of directionality relies on the ability of formation of imine or lactone controlled by pH, as discussed several times above.

In the search for the optimal conditions, first an ACN/W mixture, used for the non-directional walking experiments, was investigated. To this extent, when **OH-CAXAL** (acid form) was mixed with the **N<sub>3</sub>en<sub>2</sub>prNOBn** (free base form) in CD<sub>3</sub>CN/D<sub>2</sub>O (7:3 v/v), formation of the lactone on the hydroxylamine nitrogen was observed, but addition of either an acid or a base leads to significant hydrolysis and dissociation of **OH-CAXAL** from the track. Notably, the formation of the lactone was observed even in pure D<sub>2</sub>O, however the pH adjustment leads to even more extensive hydrolysis than in an ACN/W mixture. As a result, a mixture of d<sub>6</sub>-DMSO containing 1 % D<sub>2</sub>O was chosen as the solvent and used throughout the following experiments.

Another issue to investigate comes with the choice of the base and the acid used for pH adjustment. The solvent mixture used implies solubility restrictions especially for the base. For this purpose, stock solutions of four different bases were prepared: potassium *tert*-butoxide (*t*-BuOK), sodium methoxide (MeONa), 1,8-diazabicyclo[5.4.0]undec-7-ene (DBU) and triethylamine (Et<sub>3</sub>N). The alkoxide solutions can be prepared as concentrated as about 100 mM, while DBU and Et<sub>3</sub>N are fully miscible with DMSO and 2 M solutions were prepared. For the acids used, 2 M stock solutions of acetic acid (AcOH), TFA and methanesulfonic acid (MeSO<sub>3</sub>H) were prepared and used in the study.

First, equimolar mixtures of **OH-CAXAL** and **N<sub>3</sub>en<sub>2</sub>prNOBn** (20 mM) were prepared and left to equilibrate for 3 days. These solutions contain the lactone structure closed on the hydroxylamine nitrogen in about 90 % conversion, and approximately 10 % of the aldehyde and the polyamine remain unreacted. The imine and aminal structures may also be present but in very low amounts which prevents reliable quantification. Similarly to the case of **BnEDA**, the lactone ring closure comprises for the formation of a chiral carbon atom which in turn leads to splitting of the benzylic protons into a pair of doublets (Figure 3.3-9). Full NMR characterization is provided in the Experimental part. Moreover, the NMR sample was submitted to the MS analysis which confirmed the structure (calc. 414.227, found 415.233 [M+H]).



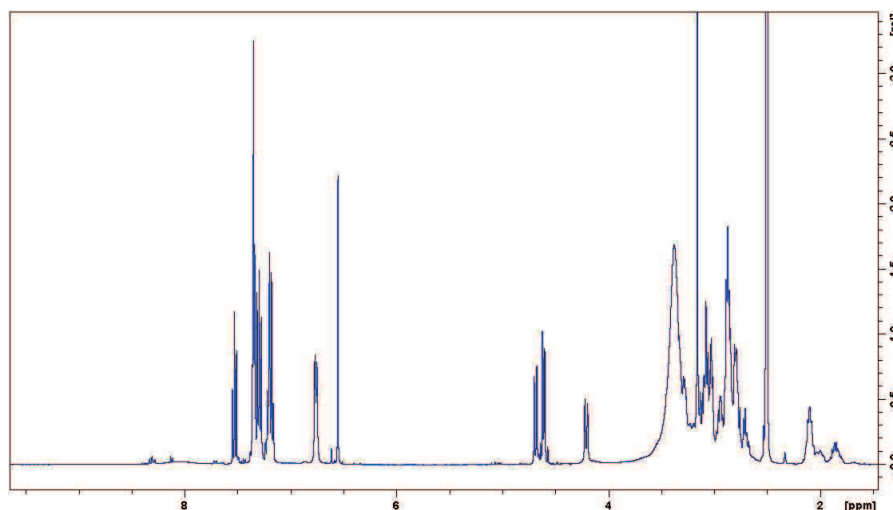


Figure 3.3-9  $^1\text{H-NMR}$  spectrum of **OH-CAXAL** (acid form) mixed with **N<sub>3</sub>en<sub>2</sub>prNOBn** without any pH adjustment. The lactone C-H proton appears as sharp singlet at 6.55 ppm, but its chirality causes splitting of the benzylic protons into a pair of doublets at 4.69 and 4.20 ppm with a coupling of 9.7 Hz. The signals around 2 ppm correspond to the middle methylene group of the propylene spacer in the molecule of **N<sub>3</sub>en<sub>2</sub>prNOBn**. It is evident that apart from the lactone (2.1 ppm) and the unreacted **N<sub>3</sub>en<sub>2</sub>prNOBn** (1.85 ppm) there is a third very broad methylene signal. 2D NOESY spectra suggests that there is indeed some amount of amina (not clear with which nitrogen atoms) and some imine, although the intensity of the corresponding signals in  $^1\text{H-NMR}$  spectrum does not allow for quantification.

These solutions were thereafter titrated by a stock solution of a base. When aliquots of  $\text{Et}_3\text{N}$  were added, no change in the NMR spectra was observed even after addition of up to 10 equivalents. On the other hand, addition of either of the alkoxide bases leads to emergence of a new peak at around 8.46 ppm, which could resemble the imine peak. However, the intensity of this peak depends on the experimental approach: if small amounts of the base are added one after another, the intensity of the peak correlates with the expected intensity of the imine formed, but when 2 equivalents of the alkoxide are added in one portion, the intensity is largely diminished and new broad peak arises around 9.13 ppm. Moreover, HSQC experiment didn't provide a correlation with any carbon signal. Furthermore, this peak was observed also in the sample containing only the **OH-CAXAL** deprotonated by the alkoxide base, and was therefore assigned to a side-reaction of the aldehyde alone. It's noteworthy that the formation of this side-product is not reversible and addition of an acid does not decrease its intensity. Finally, the DBU was investigated as a base. In this case, clear and fast conversion of the lactone to the imine was observed by NMR (Figure 3.3-10) by addition of a total of 3 eq. of DBU. It is noteworthy that the reaction reaches equilibrium within less than five minutes after the base addition, and the final solution contains the imine in about 90 % conversion while the other 10 % is in the form of amina. As evidenced by 2D NOESY, these two species interconvert, which results also in significant broadening of the signals in the  $^1\text{H-NMR}$  spectrum.

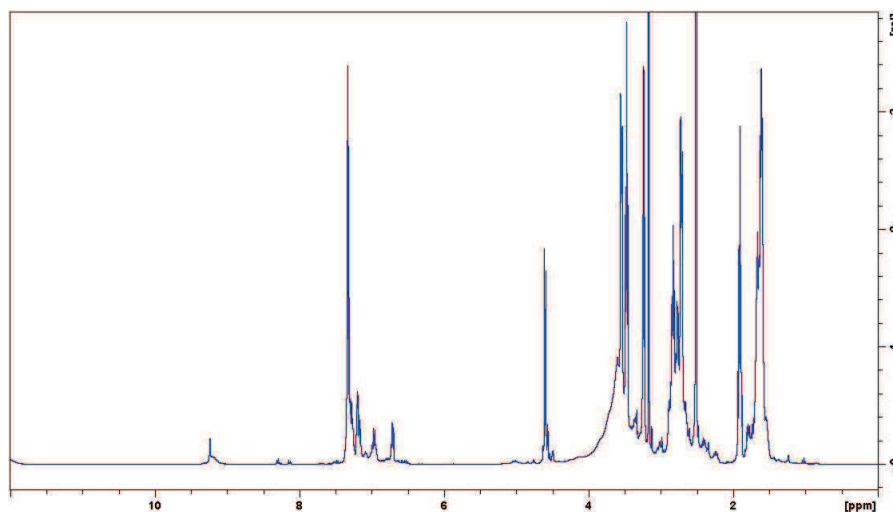


Figure 3.3-10  $^1\text{H-NMR}$  spectrum of the mixture of **OH-CAXAL** and  **$\text{N}_3\text{en}_2\text{prNOBn}$**  after addition of 3 eq. of DBU. The lactone sharp singlet at 6.55 ppm has disappeared completely, as well as the pair of doublets of the benzylic protons. Instead, broad imine signal at 9.15 ppm and sharp singlet of benzylic protons at 4.60 ppm appeared. The broad imine signal is accompanied by a small, but sharp singlet. This signal could belong to the imine structure which has also an aminor on the adjacent nitrogen (two aldehyde molecules reacting with one track), and which therefore cannot exchange between imine and aminor. Also, 2D NOESY indicated chemical exchange between the imine peak and the aminor peak, both appearing as broad signals at 9.15 and 4.75 ppm. HSQC and HMBC experiments confirmed the structure.

Next, the effect of the different  $\text{pK}_a$  of the acids chosen was studied. The sample previously titrated with DBU (3 eq.) was first back-titrated by AcOH, but no change in the NMR spectrum was observed up to the addition of 10 eq. of the acid. On the other hand, addition of  $\text{MeSO}_3\text{H}$  leads to dramatic changes in the spectrum, reverting most of the species back to the lactone form, but relatively high hydrolysis is observed as well. If the sample is allowed to equilibrate for a few days, the hydrolysed **OH-CAXAL** reacts again with the  **$\text{N}_3\text{en}_2\text{prNOBn}$**  track providing the desired lactone, however such a reaction is intermolecular and the walking concept fails in fulfilling the need for processivity. Finally, the addition of TFA leads to quantitative conversion of the imine to the lactone without extended hydrolysis. The Figure 3.3-11 shows the titration of the mixture of **OH-CAXAL** and  **$\text{N}_3\text{en}_2\text{prNOBn}$**  by first DBU, and then TFA. It is noteworthy that this base-acid cycle can be repeated three times until the excessive generation of the DBU-TFA salt start to perturb the NMR experiment.

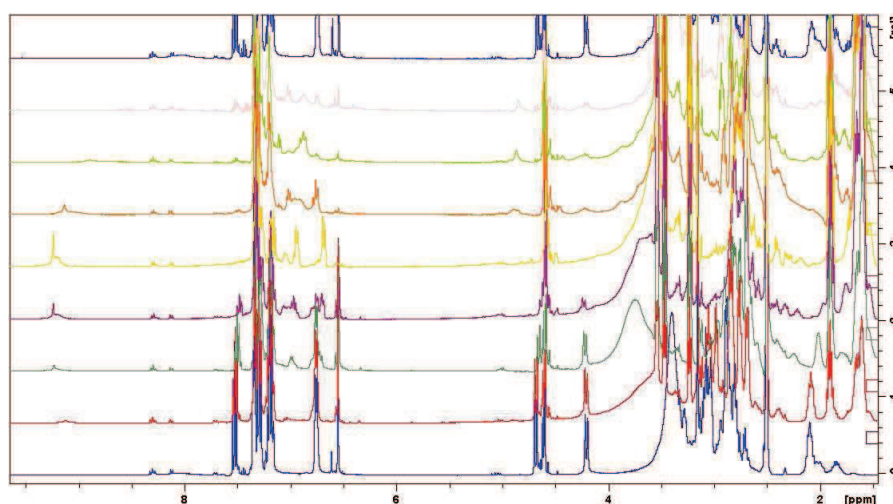


Figure 3.3-11 Titration of the mixture of **OH-CAXAL** and  **$\text{N}_3\text{en}_2\text{prNOBn}$**  by first DBU (0, 0.8, 1.6, 2.4 and 3.2 equivalents of DBU from bottom blue to yellow traces respectively) and then by TFA (0, 0.8, 1.6, 2.4 and 3.2 equivalents of TFA from orange to top blue trace, respectively).

In conclusion, the experiments shown above prove the concept of the directional walking of an aldehyde along the polyamine chain using the imine and the lactone structures to trap the aldehyde at one of the extremities of the polyamine track. Further experiments will be performed to demonstrate the walking on various track lengths, to obtain the conditions under which only one molecule of aldehyde reacts with the polyamine track, and to show the ability of the system to transport cargo over a distance.

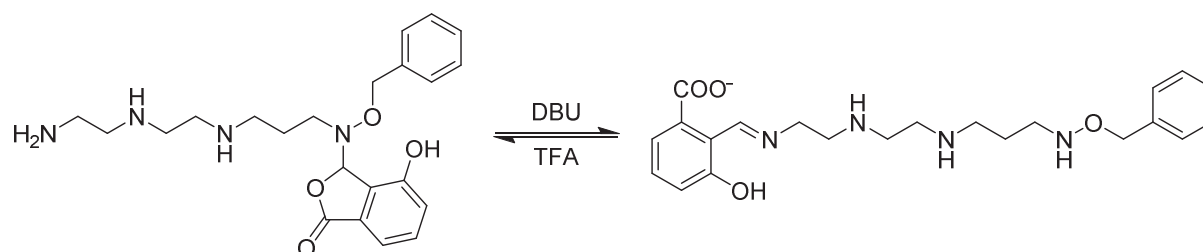


Figure 3.3-12 Scheme of the reaction of a small molecule (**OH-CAXAL**) walking along the polyamine chain (**N<sub>3</sub>en<sub>2</sub>prNOBn**).

### 3.4. Summary of Chapter 3

- A simple degenerate intramolecular displacement of aldehyde residues between the nitrogen atoms of small aliphatic diamines has been demonstrated.
- The rate of the displacement was shown to be finely controllable over a wide range by the action of temperature, the solvent composition and the substituent introduced on the aromatic core of the aldehyde.
- The intramolecular exchange process is accompanied by the intermolecular one, thus merging constitutional and motional dynamics within one system.
- The motion has been extended to linear polyamines thus introducing a non-directional small-molecule walker which displaces along the track via reversibly formed intermediary species of different valency.
- The motion was also shown for branched and circular polyamines which introduce different topologies of the displacement process.
- The directionality control over the walking process has been introduced by desymmetrisation of the track and by pH-dependent trapping of the aldehyde residue at the extremities of the polyamine chain.

## 4. DYNAMIC REACTION SELECTIVITY

### 4.1. Introduction

Dynamic combinatorial libraries (DCLs)<sup>[6,12,20,22,24,26,56,82,104,108,226,323,343]</sup> are formed by reversibly linked components giving an equilibrium mixture of products under thermodynamic control. The reversibility of the linkage allows constitutional exchange by the means of constitutional dynamic chemistry (CDC) providing all possible combinations of constituents without the need for tedious synthesis and purification of large number of compounds. By application of a stimulus, the DCL undergoes constitutional adaptation where some species are amplified while others are depleted.<sup>[344,345]</sup> These features have proven the attractiveness of DCLs for material science,<sup>[11,80,84,310,346–353]</sup> for the synthesis of nanoarchitectures,<sup>[15,16,141,143,354–359]</sup> receptors<sup>[360]</sup> and sensors<sup>[361]</sup> as well as in research for biologically active compounds.<sup>[21,23–25,321,322,362–365]</sup> In fact, only the “virtual presence”<sup>[6]</sup> of all combinations is required as the amplified species can be formed upon the application of the stimulus – in the terms of the “lock and key” principle, the lock assembles its key. Deconvolution of the DCL, which consists of systematic removal of single components and verification of functionality of the reduced library, provides a way to identify of the species of interest.

Imines are particularly interesting for DCL construction due to their ease of formation and exchange, usually under mild conditions. The imine bond is a heteromeric linkage formed by condensation of an amine and a carbonyl compound. It is also satisfactorily orthogonal<sup>[11,12,366–370]</sup> to many other reversible bonds and its dynamic nature can be “frozen” by reduction or other transformations.<sup>[371]</sup> Simplification of the complex mixture of species in the library is achieved through adaptive sorting,<sup>[38,105,372–375]</sup> for example in the course of crystallisation,<sup>[103,376,377]</sup> oxidation,<sup>[378]</sup> distillation<sup>[379,380]</sup> or coordination.<sup>[98,137,381–392]</sup>

This chapter initially concerns a theoretical approach for representation and comparison of DCLs, which is used thereafter for quantification of the efficiency of selection during self-sorting processes. Also, it identifies key differences in supramolecular dynamics<sup>[393]</sup> between self-sorting upon applying an exogenous selector and self-sorting by increasing the complexity of the library,<sup>[366,394,395]</sup> resulting in “*simplicity*” of a DCL. The self-sorting, or selection, driven by the complexity is demonstrated for aldehyde-amine libraries in the cases of 2+2 and 3+3 mixtures as well as for multivalent polyamines. Finally, the concept is applied in the synthesis of polyamine derivatives, in which aldehydes serve as dynamic selective protective groups. The preparative scale synthesis was elaborated in collaboration with Dr. Anne Meister and the experiments done by Dr. Meister are indicated in the text.

### 4.2. Representation of dynamic reaction networks

In reaction dynamics, the outcome of the reaction network is determined by the conditions used. In other words, the outcome of the reaction (product or ratio of products) is dependent on the presence or absence of a driving force for formation of particular product. It has been demonstrated in the literature that DCLs can be sorted for example by, for example, distillation,<sup>[379,380]</sup>

crystallization<sup>[103,376,377]</sup> or oxidation.<sup>[378]</sup> Any sorting process can be represented as a selection process by the means of linear algebra in the form of a selection matrix.

The representation of selection can be explained through the example of distillation sorting of an imine library. The library is formed from  $m$  derivatives of aldehydes (which can be algebraically represented as vector  $\mathbf{X}$ ) and the same number of amine derivatives (vector  $\mathbf{Y}$ ). If the aldehydes are distributed as columns and amines as rows, a square matrix  $\mathbf{XY}$  of possible products  $x_i y_j$  is obtained (Table 4.2-1). In the ideal case, every possible combination in this matrix has the same mole fraction (population). When a selector is applied, such as distillation, redistribution of the product populations takes place, giving ideally only a number  $m$  of products, while all other species are depleted (in the case of a total selection). If the aldehydes  $\mathbf{X}$  and amines  $\mathbf{Y}$  are initially sorted on the basis of boiling points, the matrix obtained after the selector is applied is an identity matrix, or it can be transformed to a diagonal identity matrix by swapping its rows/columns (Table 4.2-1).

	$X_1$	$X_2$	...	$X_z$		$X_1$	$X_2$	...	$X_z$
$Y_1$	$1/m$	$1/m$	...	$1/m$	selector	$1$	$0$	...	$0$
$Y_2$	$1/m$	$1/m$	...	$1/m$		$0$	$1$	...	$0$
...	...	...	...	...		...	...	$1$	...
$Y_z$	$1/m$	$1/m$	...	$1/m$		$0$	$0$	...	$1$

Table 4.2-1 A hypothetical selection experiment: matrix  $\mathbf{XY}$  of initial populations ( $\mathbf{I}$ ) is transformed into the matrix of final products ( $\mathbf{F}$ ) by the action of a selector. The selector is such that it enhances the formation of  $x_i y_i$  adducts and disfavors formation of  $x_i y_j$  adducts. Typical example of such a selector is the distillation driven self-sorting of dynamic libraries.

The selection process can be generalized. In an  $n$ -component reaction,<sup>§§§</sup> each component is represented by a vector  $\overrightarrow{\mathbf{R}}_n$  of  $m$  reagents  $\mathbf{X}$ . By mixing the components in equimolar ratio we create a tensor  $\mathbf{T}_{R_1 \rightarrow n, m}$  of order  $n$ , normalized such that  $\sum_{R_1 \rightarrow n, m} \mathbf{T}_{R_1 \rightarrow n, m} = \mathbf{m}$ . By the action of a selector, this tensor changes values of its elements (redistribution of reaction products) to give an identity tensor (in case of total selection) or tensor which can be transformed to identity tensor by swapping the vectors, i.e. a tensor in which diagonal elements  $\mathbf{T}_{i_1=i_2=\dots=i_n} = 1$  and off-diagonal elements  $\mathbf{T}_{i_j \neq i_k} = 0$ . It is important to point out:

1. If the selector is not part of the tensor (like the distillation or oxidation process) reduction of the size (eliminating one reagent) of the tensor does not in principle affect the selection.
2. The size  $x$  of the vectors  $\overrightarrow{\mathbf{R}}_n$  can be in principle different giving a rectangular instead of a square tensor.
3. The selector might apply only on some of the  $\overrightarrow{\mathbf{R}}_n$  vectors, e.g. metal cation can change imine distribution without touching distribution of disulfides while pH changes the disulfide distribution without redistributing imine populations.
4. The aforementioned algebraic description of the selection phenomenon can also be interpreted using graph theory, where each component vector would be represented as a column of compounds and each of its elements would have a connection to all compounds in neighbouring column. The thickness of the connection would represent the relative population in the mixture. This representation makes the agonistic-antagonistic relationships more obvious, but on the other hand quantification and deconvolution is less evident.

§§§ Typically  $n=2$ , like in the case of aldehyde-amine libraries, but examples of up to  $n=4$  are demonstrated in the literature.<sup>[56]</sup>

An important process is so-called “deconvolution” of a dynamic library. Deconvolution simply relates to removal of a given component from the mixture, e.g. removing one aldehyde and one amine and repeating the distillation. Thus to fully deconvolute the imine library, it is necessary to perform the distillation experiments on the libraries  $m \times m$ ,  $(m-1) \times (m-1)$ ,... to  $1 \times 1$ , giving in total  $m$  independent experiments. It is noteworthy that for the general case of  $n$ -dimensional tensor this value is always  $m$ , regardless the dimensionality  $n$ . Also, it is possible to remove just one of the reacting partners, e.g. an aldehyde, and keep its amine counterpart in the distillation mixture. Such an experiment would be represented by a rectangular instead of a square matrix. In the following Sections, only the simplest case of a square 2D matrix is discussed for clarity. However, the extensions to the general case of a rectangular  $n$ -dimensional tensor can be envisaged.

#### 4.2.1. Quantification of selection for a two-component libraries

Using the same example of the distillation sorted imine library, a system for quantification of the selection in two-component libraries can be proposed. The imines are formed by the general scheme  $A+B = C$ . Taking, for example, three aldehydes A and three amines B a  $3 \times 3$  matrix of imines is created. This matrix before the distillation represents the initial composition of the library, and is therefore called  $I$ , and its elements  $i_{ij}$  represent the molar fraction (population) of each imine. After the distillation, we get a new matrix representing the molar fractions of obtained imines, called the final matrix  $F$ . The selection process can now be seen also as a matrix called the selector matrix  $S$ , defined by the formula

$$F = I + S$$

The selector matrix  $S$  can be used to quantify the selection. As seen in the schematic representation in Table 4.2-1, the elements of the diagonal have increased (by  $(m-1)/m$ ) and the off-diagonal elements have decreased (by  $-1/m$ ). In practise, the elements  $s_{ij}$  of the selection matrix  $S$  are obtained as the difference in mole fraction (population) of the products before and after the selector is applied. In principle, due to the mass conservation law, the sum of the elements of the selector matrix is 0. However, in practice all chemical processes lead to some loss (residue after distillation, incomplete reactions etc.), and therefore the sum of the elements  $s_{ij}$  of matrix  $S$  is a small negative number. Now, the selection index  $\sigma$  can be defined as follows

$$\sigma = \frac{\sum_{i,j} |s_{i,j}|}{2}$$

where the factor of 2 allows for the fact that each decrease in population of a given product is compensated by an increase of a different one. If the species in rows and columns are sorted such that after selection the positive (amplified) species are on the diagonal, then the positive elements (amplified species) are on diagonal, then the negative elements (depleted species) are off-diagonal, and the selection index is simply the sum of elements on the diagonal.

It is important to consider the possible values of  $\sigma$  by examining the limiting cases. In the case of a selector which doesn't change the population of the species, the elements of the selector matrix  $s_{ij}$  are all equal to zero and thus also the value of the selection index  $\sigma$  is zero. In the case of an ideal selection, i.e. initial  $3 \times 3$  matrix consists of equal amounts of all species and after selection only three products are obtained (Table 4.2-2), the selection index is equal 2 (or in general  $m-1$ ). In another case, where only three products form in the initial population but redistribute upon action of a selector to give three different products, the value of the selection index is 3 (or  $m$  for the general case).



	X <sub>1</sub>	X <sub>2</sub>	X <sub>3</sub>
Y <sub>1</sub>	1/3	1/3	1/3
Y <sub>2</sub>	1/3	1/3	1/3
Y <sub>3</sub>	1/3	1/3	1/3

selector		
2/3	-1/3	-1/3
-1/3	2/3	-1/3
-1/3	-1/3	2/3

+

	X <sub>1</sub>	X <sub>2</sub>	X <sub>3</sub>
Y <sub>1</sub>	1	0	0
Y <sub>2</sub>	0	1	0
Y <sub>3</sub>	0	0	1

Table 4.2-2 A schematic representation of an ideal selector and its corresponding selector matrix. An equally populated mixture of all possible products is transformed to only three selected species.

It is obvious that value of the selection index is a function of the size of the initial matrix, for a 2x2 matrix it takes values from 0 to 2, for a 4x4 it can be up to 4. To generalize the selection descriptor, the selection index can be transformed into a percentage value called the selection strength  $\varepsilon$  as follows: for  $x$  number of derivatives A or B, the values of the selection index  $\sigma$  from 0 to  $(m-1)$  define a range from 0 to 100 %, and values from  $(m-1)$  to  $m$  define the range from 100 to 200 % (Figure 4.2-1). Thus an ideal selector has strength of 100 %, a selector which inverts the populations has strength of 200 %, and a selector which does not influence the system has strength of 0 %. All other cases fall in between those values.

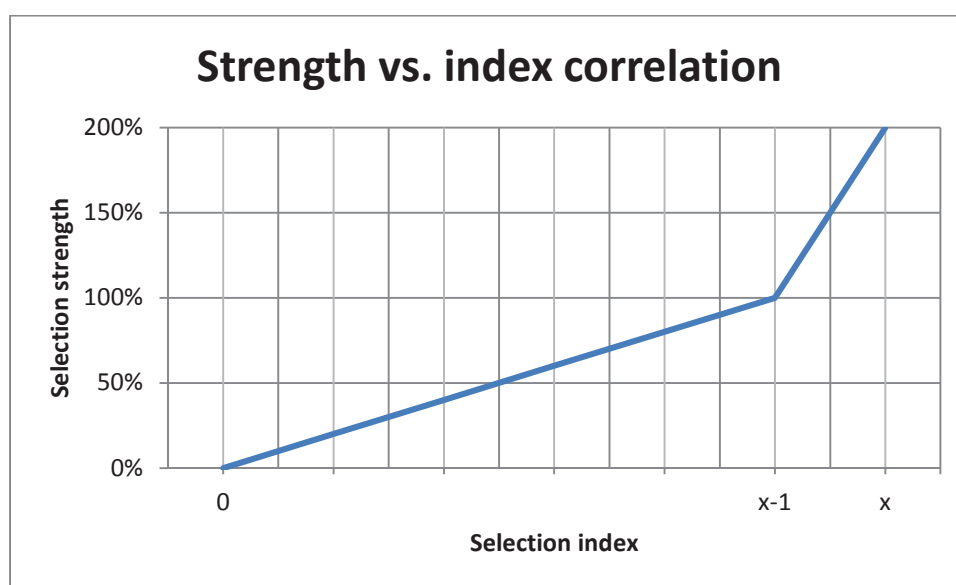


Figure 4.2-1 Graphical representation of the dependence of the selection strength on the selection index.

As for all descriptors, a single value does not completely describe the system but serves only for quick comparisons. The mathematical construction above enables single-value comparison of different selection systems.

#### 4.2.2. Simplexity: selection in dynamic reaction networks

Considering dynamic reaction selectivity, which will be discussed below, the selection is driven by the complexity of the reaction mixture. In other words, the selection for a given product is a result of an increased number of species in the mixture. In such a case, the selector is inherent to the selection matrix, i.e. the feature of selectivity is encoded in the components. This property will be said to define the *simplexity*. If one or more components of the library are removed, the selection can be strongly perturbed or even completely lost. Therefore, to perform the deconvolution of such a system, all combinations of reagents must be experimentally explored requiring for  $(2^m - 1)^n$  experiments. Clearly, the number of experiments rises exponentially as the system gets more complex and even just for a 3+3 library 49 experiments are required.

Quantification of the selection in the case of simplexity is complicated by the fact that the selector is inherently present in the matrix and the matrix of initial populations  $\mathbf{I}$  (as in the abovementioned case) is not available. In such case, the *deconvolution* of the full constitutional



matrix is required. In practice it means that all combinations of reactants A are mixed with all combinations of reactants B. In the case of an imine library, it means that every single aldehyde and every single amine, as well as all combinations of two or more aldehydes or amines, are not added to the library and the equilibrium composition of the resulting mixture is determined.

The result of the deconvolution enables for construction of the selection matrix  $S$ . Its elements  $s_{i,j}$  are defined as

$$s_{i,j} = (f_{i,j} - \overline{\mu_{i,j}})(1 - std_{i,j})$$

where  $s_{i,j}$  is the element of the selection matrix,  $f_{i,j}$  is the population of the product in the full matrix (i.e. that where all constituents are present),  $\overline{\mu_{i,j}}$  is the mean of the population of this product in all the deconvolution experiments where this product can be formed (i.e. both its constituents are present) and  $std_{i,j}$  is the standard deviation of the population of a given product through the deconvolution experiments. The term  $(f_{i,j} - \overline{\mu_{i,j}})$  defines the result of a selection process, as discussed above, and its value falls in between -1 and 1. The term  $(1 - std_{i,j})$  reflects the variation of the population of a given product through the deconvolution and warrants a closer look. In a hypothetical case, a product  $x_i y_j$  is formed in 100 % conversion when all the constituents of the library are present. But through the deconvolution experiments, its conversion is constantly 0 %. It seems logical that the selection for its 100 % formation requires large effort. Conversely, if its conversion varies greatly between 0 and 100 % through the deconvolution, it seems that the change to 100 % conversion would be easier. Therefore, for a constant conversion through the deconvolution experiment, the  $std_{i,j}$  will be close to 0 and the whole term close to 1. For a fluctuating conversion it will be close to 0.5, thus reducing the contribution to the selection caused by this product. In other words, this term describes how great is the propensity to form a given product. With the selection matrix in hand, it is possible to calculate the selection index and thereafter the selection strength, analogously to the case of an external selector described above. It is noteworthy that due to the  $(1 - std_{i,j})$  term the sum of the elements of the selector matrix no longer needs to be zero. Also, due to this term, the selection strength in the simplicity selection should be lower than in the selection driven by an external force.

## 4.3. Constitutional selection in aldehyde-amine libraries

### 4.3.1. Selection in the 2+2 aldehyde-amine libraries

Aldehydes react with amines to provide a series of products. The type of the resulting molecule is determined by the structure of the parent compounds. It is thus possible to form imines, as in the case of salicylaldehyde (**SALAL**) with primary amines (Section 2.2), amins in the case of pyridine-2-carboxaldehyde (**PYRAL**) with short  $\alpha,\omega$ -diamines (Section 3.2), or to generate amino-lactones derived from 2-carboxybenzaldehyde (**CAXAL**) reacted with secondary amines (Section 3.3) as illustrated in Figure 4.3-1. Due to the reversibility of the formation, these products can dynamically interconvert in the mixture adapting to a change in conditions.

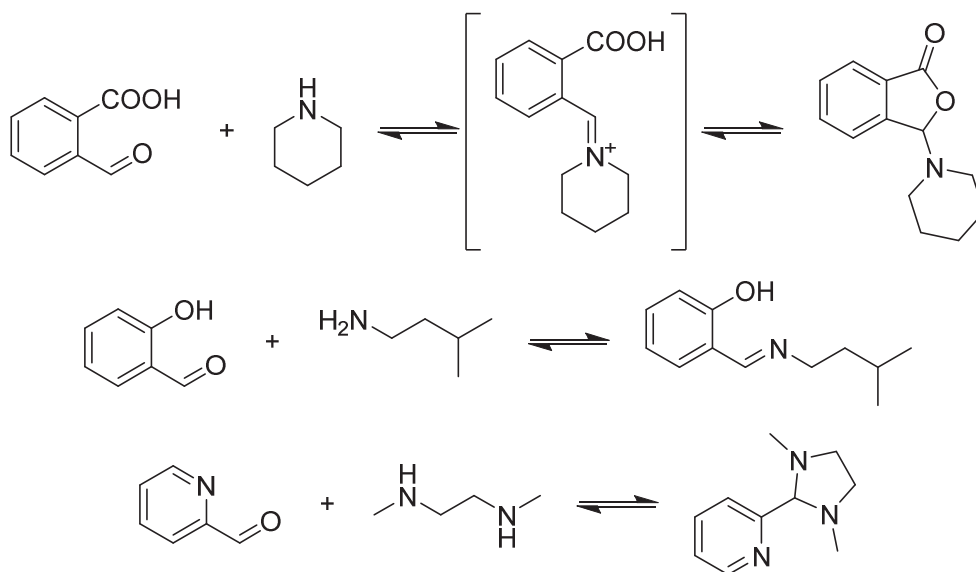


Figure 4.3-1 The reactions of with corresponding amines forming the expected products: amino-lactone of **CAXAL**, imine of **SALAL** and amination of **PYRAL**.

Initially, simple condensation experiments of **SALAL** and **CAXAL** were performed in  $d_6$ -DMSO containing 1 % of  $D_2O$ . The addition of  $D_2O$  ensured a relatively constant amount of water in the reaction mixtures during the condensation reaction, and this solvent mixture was used throughout the NMR experiments. First, **SALAL** was reacted with *i*-pentylamine (**IPA**) and the formation of the imine was followed by  $^1H$ -NMR spectroscopy. The reaction proceeds quickly, establishing equilibrium in a few minutes, and giving the imine as the only product observed in the reaction mixture. In similar fashion, **CAXAL** was mixed with piperidine (**PIP**) and the NMR spectra were recorded. The formation of the amino-lactone was observed immediately after mixing, equilibrium being reached within one hour with the amino-lactone as the only species present in the solution. Spectra of both products are given in Figure 4.3-2. It is noteworthy that **CAXAL** in solution exists as a dynamic mixture of two structures: carboxyaldehyde and hydroxy-lactone (discussed in Section 3.3.1). The characteristic signal of the lactone C-H proton occurs at a very similar chemical shift for the hydroxy- and amino-substituted derivatives, and therefore in all cases involving **CAXAL**, a 2D NOESY spectrum was recorded to establish the NOE interactions with the amine part of the molecule.

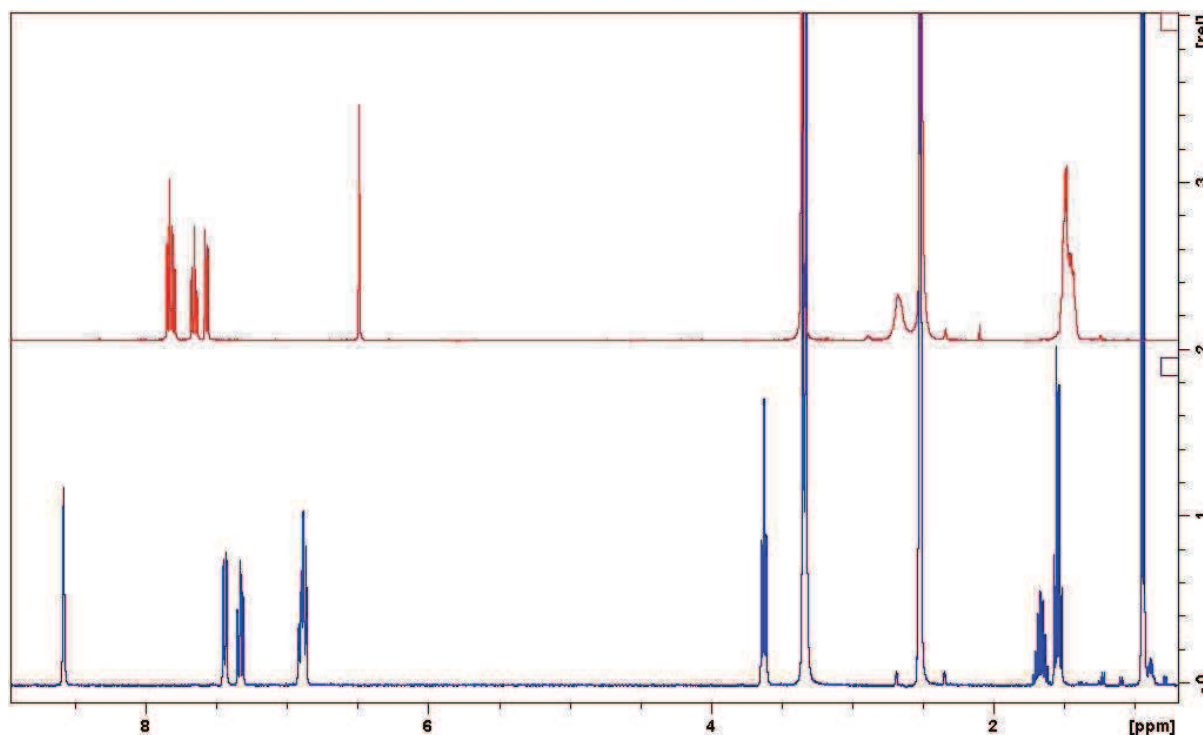


Figure 4.3-2 The imine formed from **SALAL** and **IPA** (bottom blue trace) and the lactone derived from **CAXAL** and **PIP** (top red trace) are formed as the only products when the reagents are mixed in  $d_6$ -DMSO + 1 %  $D_2O$ . The reactions reach equilibrium in less than 1 hour.

The **SALAL+IPA** and **CAXAL+PIP** pairs form the expected products and can be called “matching” pairs. The outcome of the reactions of the unmatching pairs, i.e. **CAXAL+IPA** and **SALAL+PIP** was also examined but in both cases complicated behaviour was observed. When **CAXAL** was mixed with 1 eq. of **IPA**, equilibrium was reached almost instantaneously. The aliphatic signals of **IPA** shifted downfield (by up to 0.5 ppm) and the aromatic protons appeared as a clear sharp pair of doublets and a pair of triplets assigned to a single species. However the azomethine CH proton appeared as a broad signal at 6.9 ppm. The HSQC spectrum did not show any cross-peak of this signal with any carbon peak and also the correlation for the N-CH<sub>2</sub> protons was missing. An extended acquisition of the <sup>13</sup>C spectrum revealed two broad signals at 46 and 144 ppm, assigned to the N-CH<sub>2</sub> and the azomethine carbons, respectively. The shift of the azomethine carbon signal lies in between the imine (typically around 155 ppm) and the aminal or lactone signal ranges (around 85-95 ppm). The NOESY spectrum also indicated chemical exchange between the azomethine signal and the residual water signal, probably resulting from the overlap with the hemiaminal OH proton. From these results it can be concluded that the product formed undergoes rapid interconversion between imine, lactone and hemiaminal.

When **SALAL** was mixed with **PIP**, approximately 30 % of the aminal formed from 2 amine molecules and 1 aldehyde was observed immediately. The composition of the mixture remained constant for 2 days. However, upon prolonged standing new set of peaks became apparent, notably sharp singlets at 7.95 and 5.65 ppm, as well as set of multiplets heavily overlapped with the residual water signal, accompanied by a strong colour change from bright yellow to deep red. These signals could be due to a Mannich type of reaction of **SALAL** leading to the condensation of two aldehyde molecules.

In subsequent experiments, the propensity towards the formation of the expected product was tested in presence of competing amine of a different type, i.e. each aldehyde was reacted with equimolar mixture of the two amines. **SALAL** showed a very high preference for imine formation reacting solely with **IPA** and leaving **PIP** unreacted in the solution. However, the conversion of the

aldehyde in this case was not complete and approximately 10 % of the aldehyde remained unreacted although the aldehyde CHO signal was broad.

In contrast, **CAXAL** under the same reaction conditions provided two products: the lactone on the **PIP** ring was formed in about 39 % yield and the imine derived from **IPA** was present in about 61 % yield. Furthermore, the imine of **IPA** exhibited broad signals in the  $^1\text{H-NMR}$  spectrum, indicating an underlying dynamic process fast on the NMR time scale, a similar process to the case of **CAXAL** reacted only with **IPA**. This was also supported by VT-NMR measurements: by increasing the temperature from 25 to 45 or 65 °C the imine N=CH- signal at 8.52 ppm became sharper and shifted upfield towards the very broad signal around 6.5 ppm. The spectra are given in Figure 4.3-3.

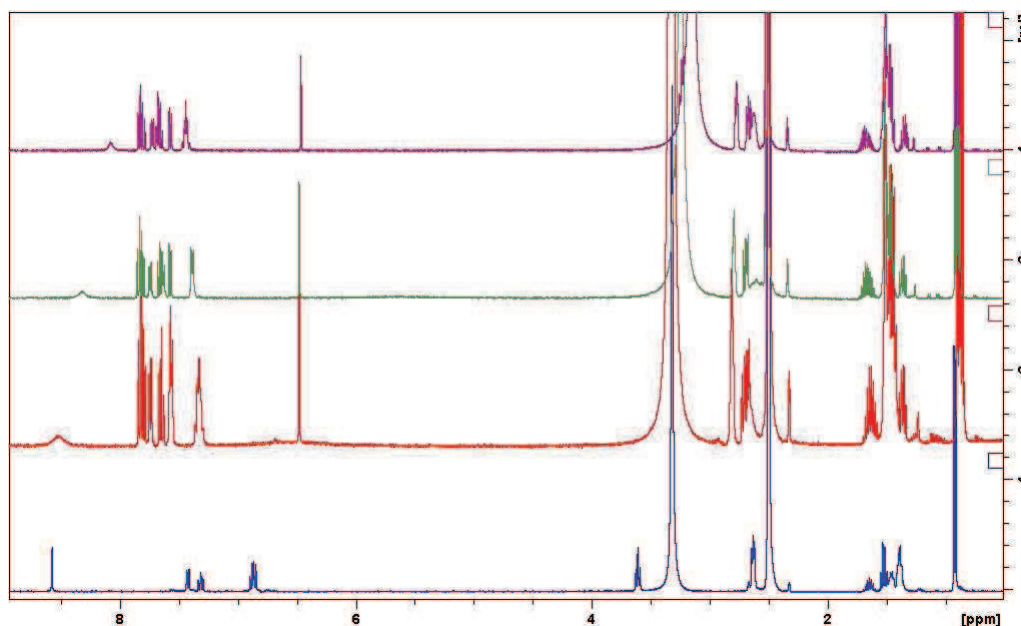


Figure 4.3-3 The spectrum of **SALAL** with 1 eq. of **IPA** and **PIP** (bottom blue trace) shows only the imine present in the reaction mixture and **PIP** stays untouched in the solution. **CAXAL** reacted with the two amines gives two products: the lactone formation derived from **PIP** is evidenced by the sharp singlet at 6.5 ppm and the imine of **IPA** has a signal at 8.5 ppm. The imine undergoes fast intramolecular imine-lactone exchange leading to peak broadening. Increased temperature leads to signal sharpening - spectra recorded at 25 (red), 45 (green) and 65 °C (purple, top trace).

Next, experiments involving two aldehydes competing for one amine were performed. When **SALAL** and **CAXAL** were mixed with **IPA** (1 eq. each), formation of the products of both aldehydes was observed. However, after a prolonged reaction time, the imine formed from **SALAL** began to dominate and at equilibrium, established after 48 hours, the imine of **SALAL** was present in 77 % conversion and the product from **CAXAL** (dynamic imine-lactone) in 23 % conversion. When **PIP** was reacted with the aldehyde mixture, the fast reaction of **CAXAL** led to rapid formation of the corresponding lactone and after three hours the reaction reached and equilibrium where only this product was present, leaving **SALAL** unreacted in the solution.

Finally, the full 2+2 aldehyde-amine experiment was performed. Thus, **SALAL** and **CAXAL** were mixed with **IPA** and **PIP** (20 mM each) and the formation of the products was followed by  $^1\text{H-NMR}$  spectroscopy. Equilibrium was reached in about 5 hours and the final mixture contains only two products: the imine of **SALAL** + **IPA** and the lactone of **CAXAL** + **PIP** (Figure 4.3-4). By comparison with the previous experiments which showed that both aldehydes were capable of reaction with both amines and *vice versa*, only the “matching” products were formed from the four possible combinations.

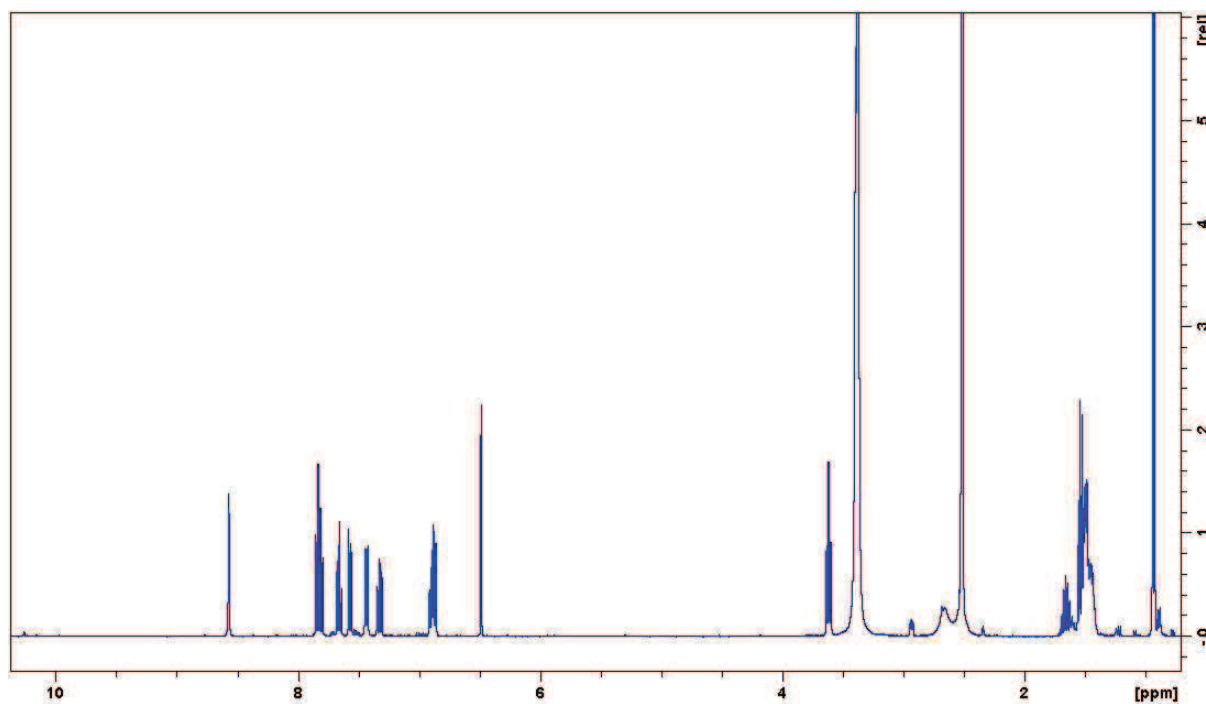


Figure 4.3-4  $^1\text{H}$ -NMR spectrum of the dynamic library composed of **SALAL** and **CAXAL** treated with **IPA** and **PIP** (20 mM each). While **SALAL** provides only its imine with **IPA** (azomethine singlet at 8.55 ppm, =N-CH<sub>2</sub>-triplet at 3.6 ppm), **CAXAL** gives only the lactone with **PIP** (lactone singlet at 6.5 ppm, N-CH<sub>2</sub> signals at 2.6 ppm).

Taking another aldehyde, **PYRAL**, into play gives the opportunity of formation of aminal species, different to the lactone and imine. Indeed, **PYRAL** efficiently formed both five- and six-membered-ring aminals with *N,N'*-dimethyl-1,2-diaminoethane (**Me<sub>2</sub>EDA**) or *N,N'*-dimethyl-1,3-diaminopropane (**Me<sub>2</sub>PDA**), reaching quantitative conversion when mixed with either of the two diamines. When the aldehyde was reacted with an equimolar mixture of **Me<sub>2</sub>EDA** and **Me<sub>2</sub>PDA**, the preferential formation of the five-membered ring was observed (77 % conversion to the aminal of **Me<sub>2</sub>EDA**). Notably, both **SALAL** and **CAXAL** reacted with these diamines as well in high conversion (about 90 % for **SALAL** and quantitative for **CAXAL**), giving similar aminal structures. Conversely, **PYRAL** provided its corresponding imine quantitatively when reacted with **IPA**, but gives complicated mixture of products when mixed with **PIP**, with an overall conversion of the aldehyde of about 40 % (mixture of aminal, hemiaminal and hydrate).

Proceeding to the mixed aldehydes, the combination of **PYRAL** and **SALAL** was examined first. The propensity of **PYRAL** to form the aminal (both with **Me<sub>2</sub>EDA** and **Me<sub>2</sub>PDA**) was assessed in the presence of the imine-forming primary amine **IPA**. To this end, **PYRAL** was mixed with **IPA** and one of the diamines (20 mM each) and the NMR spectra were followed in time. The spectra taken shortly after mixing showed the presence of the imine as the major product of the reaction. However, the mixture continued to evolve over time, to finally reach equilibrium after 3 days. In the equilibrated solutions, the aminal was the dominant species in case of both diamines, giving 79 % of the six-membered and 82 % of the five-membered derivative. It is noteworthy that the high preference for formation of the five-membered aminal in the separate experiment (77:23 in favour of the aminal of **Me<sub>2</sub>EDA** over **Me<sub>2</sub>PDA**) is translated in only negligible 3 % enhancement of the aminal-over-imine selectivity in the competition experiment with **IPA**.

Interestingly, when **SALAL** was exposed to the same amine reagents, i.e. equimolar mixture of **IPA** with one of the diamines, the imine was formed first, as in the reaction with **PYRAL**, but the reaction evolved over three days to finally reach an equilibrium containing mostly the aminal (60 ± 2 % for both diamines). These experiments show that both **PYRAL** and **SALAL** have a high propensity to form aminals, regardless of whether the size of the ring is five- or six-membered. For comparison, the

two aldehydes were allowed to compete for one amine. Thus when an equimolar mixture of **SALAL** and **PYRAL** was mixed with 1 eq. of **IPA**, the conversion to corresponding imines was 68 % and 29 % for **SALAL** and **PYRAL** respectively. Similarly, when these aldehydes were reacted with **Me<sub>2</sub>PDA**, the conversion to aminals reached 31 % and 63 % for **SALAL** and **PYRAL** respectively.

The full 2+2 selection was then examined for the case of **SALAL** mixed with **PYRAL**. An equimolar mixture of the two aldehydes was mixed with 1 eq. of equimolar mixture of **IPA** and **Me<sub>2</sub>EDA**, or **IPA** and **Me<sub>2</sub>PDA**. In both cases the results were similar: rapid high conversion of **SALAL** to its products was observed and the ratio between aminal and imine changed slightly in favour of the imine as the reaction approached equilibrium. In contrast, **PYRAL** remained largely unreacted over the first few hours. As the reaction evolved, the aminal of **PYRAL** was formed in larger quantities while the concentration of corresponding imine stayed relatively constant. Equilibrium was reached within 24 hours and the final composition for **Me<sub>2</sub>PDA** amounted to 74 % imine of **SALAL** and 26 % of the aminal and exactly the opposite ratio for the imine and the aminal of **PYRAL**, respectively (Figure 4.3-5). In the case of **Me<sub>2</sub>EDA**, the relative concentrations of the imine-aminal species reached the ratio of 80:20 and followed the same trend as in the case of **Me<sub>2</sub>PDA**.

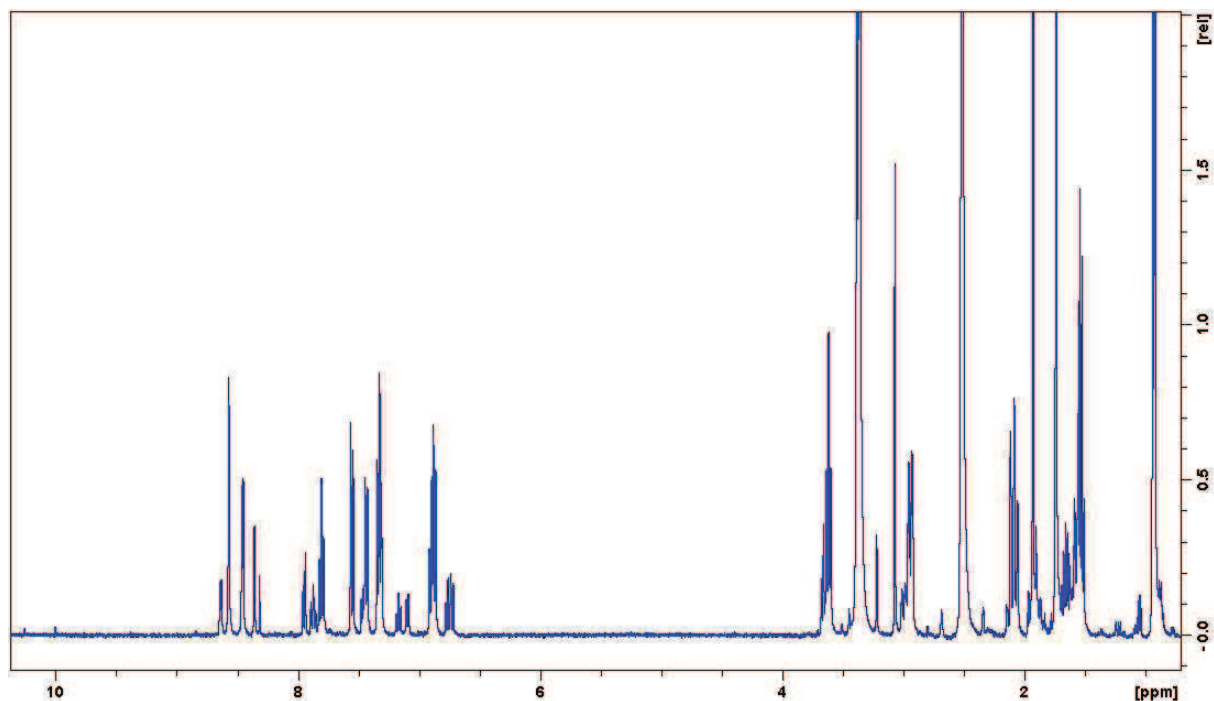


Figure 4.3-5 <sup>1</sup>H-NMR spectrum of the 2+2 library consisting of **SALAL**, **PYRAL**, **IPA** and **Me<sub>2</sub>PDA**. Only trace amounts of unreacted aldehydes are observed (below 1 %). The preferred products (imine of **SALAL** and aminal of **PYRAL**) are formed in 76 % conversion while the non-preferred ones are present in 24 %.

Finally, the combination of **PYRAL** and **CAXAL** with their matching amines was investigated. As indicated above, **CAXAL** reacted with both aminal-forming diamines in quantitative conversion, while **PYRAL** with **PIP** gave a complicated mixture of products in overall 40 % conversion. When **PYRAL** was mixed with 1 equivalent of each **PIP** and **Me<sub>2</sub>PDA**, the corresponding aminal formed with a high selectivity of about 88 % and 12 % was converted to the aminal formed by the reaction with two molecules of **PIP**. However, when **CAXAL** was exposed to the same amine mixture, a spectrum with two sets of signals was obtained. The first set of sharp peaks was assigned to the lactone formed on **PIP**, but the second set consisted of very broad, largely overlapping signals. The 2D NOESY spectrum indicated chemical exchange of the signals in the aliphatic part of the spectrum which was assigned to the dynamic equilibrium between the aminal of **Me<sub>2</sub>PDA** and the lactone formed on one of its nitrogen atoms. The shape of the signals allowed only a rough estimation of the relative concentrations of the products, indicating that 10 % of **CAXAL** had reacted with **PIP** and about 90 %



with **Me<sub>2</sub>PDA**. The combination of two aldehydes with one amine counterpart was also examined: **PIP** reacted with the two aldehyde to form solely the lactone of **CAXAL**, leaving **PYRAL** completely unreacted in solution, while **Me<sub>2</sub>PDA** gave a mixture of the two aminals in 44 % and 55 % conversion for **PYRAL** and **CAXAL** respectively.

As previously, the 2+2 aldehyde-amine selection experiment was performed for **PYRAL**, **CAXAL**, **Me<sub>2</sub>PDA** and **PIP**. When all four reagents were mixed, an immediate reaction of **CAXAL** and **PIP** was seen, giving both the lactone of **PIP** and the aminal with **Me<sub>2</sub>PDA**. As the reaction proceeded, the ratio increased in favour of the lactone due to the slower formation of the aminal of **PYRAL**, reaching equilibrium after 3 days. The equilibrated mixture was composed of 97 % the aminal of **PYRAL** and only 3 % of the aldehyde remained unreacted, while **CAXAL** formed the lactone in 94 % conversion and the aminal in only 6 %. Notably, replacement of the diamine by **Me<sub>2</sub>EDA** led to almost identical results within  $\pm 2$  % difference in relative conversions (Figure 4.3-6).

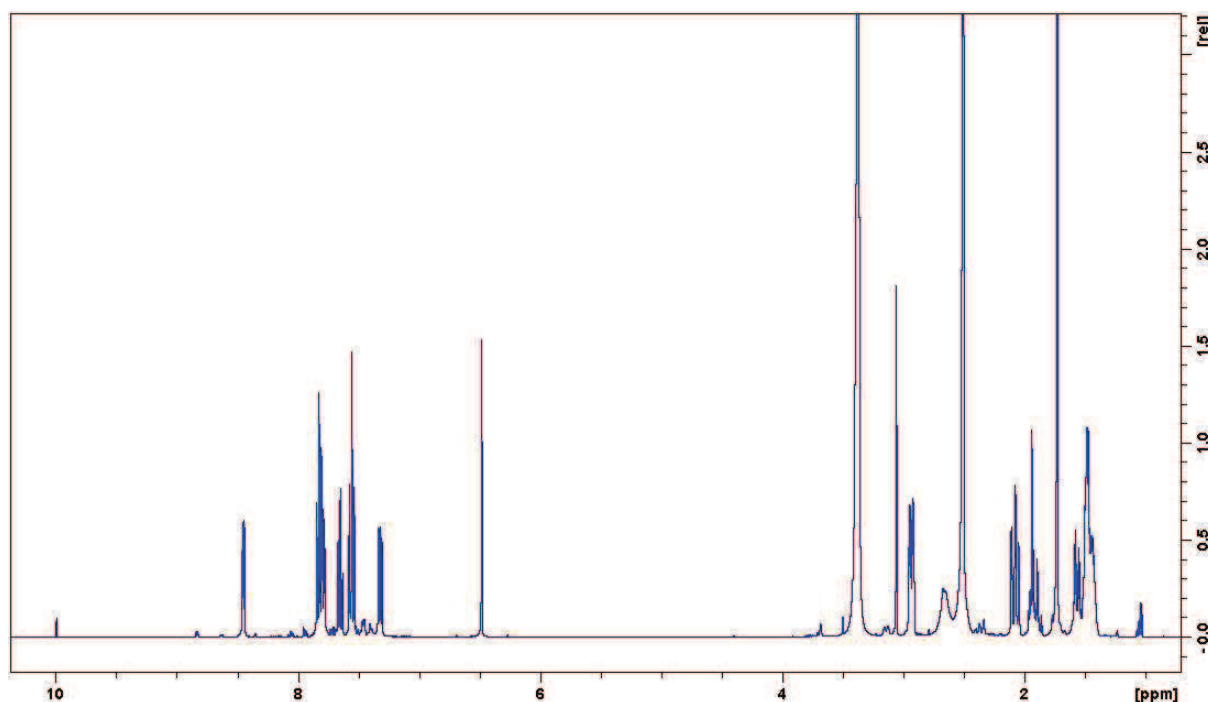


Figure 4.3-6 <sup>1</sup>H-NMR spectrum of the mixture of **PYRAL** and **CAXAL** reacted with **Me<sub>2</sub>PDA** and **PIP**. The quantification was based on the azomethine signals. The lactone of **CAXAL** appears as sharp singlet at 6.5 ppm, while the minor aminal product gives a small broad signal around 3.7 ppm. Similarly, the aminal of **PYRAL** shows a sharp singlet at 3 ppm and the unreacted aldehyde is observed as small peak at 10 ppm.

It is noteworthy that **PYRAL** can be replaced in the experiments by **BENZAL** with similar results. However, due to the lower reactivity of **BENZAL**, significant amounts of unreacted aldehyde were observed in the NMR spectra.

The selection in 2+2 libraries discussed above represents a new type of self-sorting process. Unlike the selection driven by an external force (distillation, oxidation), the simplification of a given library results from the complexity of its composition. The equilibration proceeds due to a network of interconnected reactions leading to an amplified formation of the selected species and depletion of the non-preferred ones. The phenomenon of simplicity shows that complexity has properties which simplicity lacks. Specifically, a non-selective species reacting with several compounds is forced to be selective towards a given product when a different selective species is present and completely monopolises one of the components.



### 4.3.1.1. Quantification of simplicity selection

The complexity-driven selection described above can be quantified using the model introduced in the Section 4.2. The procedure of quantification is described in detail on the case of **SALAL** and **CAXAL** reacted with **IPA** and **PIP**, and the quantification results for the other selection experiments are also provided. In the full 2+2 experiment, only two species were observed: the imine of **SALAL** and the lactone of **CAXAL**. The final matrix is thus an identity matrix:

	SALAL	CAXAL
IPA	1	0
PIP	0	1

In the separate experiments, both of these products were also formed quantitatively:

	SALAL	CAXAL
IPA	1	0
PIP	0	1

	CAXAL
PIP	1

Also the “not-matching” pairs were examined:

	SALAL	CAXAL
PIP	0.30	1

	CAXAL
IPA	1

When the two amines were reacted with only one of the aldehydes, a distribution of products and in the case of **SALAL** incomplete reaction was observed by NMR:

	SALAL	CAXAL
IPA	0.9	0
PIP	0	1

	CAXAL
IPA	0.61
PIP	0.39

Similarly, when the two aldehydes were treated with only one of the amines, a distribution of products in the case of **SALAL** was observed by NMR:

	SALAL	CAXAL
IPA	0.77	0.23
PIP	0	1

	SALAL	CAXAL
PIP	0	1

From the conversion values through the deconvolution the mean and its standard deviation can be calculated for each product:

$$x[\text{SALAL} + \text{IPA}] \in \{1, 0.9, 0.77\}, \bar{\mu} = 0.89, \text{std} = 0.12$$

$$x[\text{SALAL} + \text{PIP}] \in \{0.3, 0, 0\}, \bar{\mu} = 0.1, \text{std} = 0.17$$

$$x[\text{CAXAL} + \text{IPA}] \in \{1, 0.61, 0.23\}, \bar{\mu} = 0.61, \text{std} = 0.39$$

$$x[\text{CAXAL} + \text{PIP}] \in \{1, 0.39, 1\}, \bar{\mu} = 0.80, \text{std} = 0.35$$

From these values, the selector matrix can be constructed:

$$\begin{bmatrix} (1 - 0.89)(1 - 0.12) & (0 - 0.61)(1 - 0.39) \\ (0 - 0.1)(1 - 0.17) & (1 - 0.8)(1 - 0.35) \end{bmatrix} = \begin{bmatrix} 0.1 & -0.37 \\ -0.08 & 0.13 \end{bmatrix}$$

The sum of absolute values of the selector matrix gives a selector index of 0.34, which can be expressed as the selection strength of 34 %. Using the same approach, selection strength of the

**SALAL** and **PYRAL** with **IPA** and **Me<sub>2</sub>PDA** system was calculated as 24 % (the same value for **Me<sub>2</sub>EDA**), and for the mixture **PYRAL** and **CAXAL** with **Me<sub>2</sub>PDA** and **PIP** the selection strength is 48 %.

#### 4.3.1.2. Kinetics in simplicity experiments

The most important feature of simplicity experiments is the fact that they are governed by thermodynamics and therefore relate to the equilibrium composition of the mixture. However, the relative ratio of species formed immediately upon mixing the components can be very different from the final equilibrium, as mentioned in several cases above. Also, the equilibration of the mixture proceeds through a network of interconnected reactions, each with a given rate constant, and the equilibrium is thus established when the sum of all reaction rates is zero. Kinetics is therefore inherently involved in the simplicity experiments. One example can be briefly illustrated on the library consisting of **SALAL**, **CAXAL**, **IPA** and **PIP**.

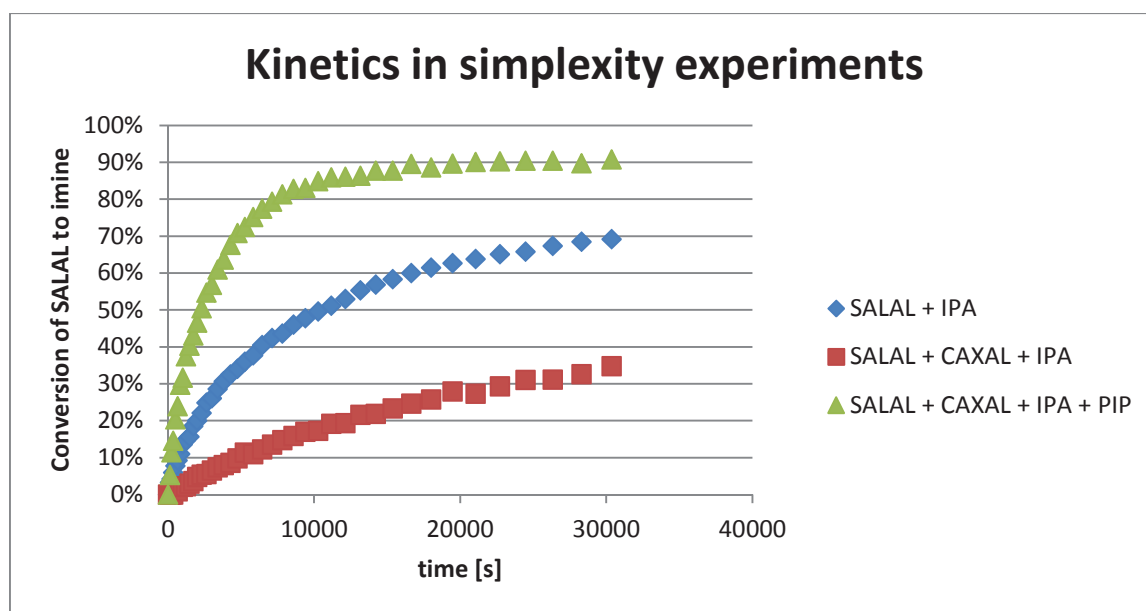
To demonstrate the role of the reaction network, the condensation of **SALAL** with **IPA** was followed with increasing complexity of the mixture. Initially, only these two reagents were mixed in  $d_6$ -DMSO with 1 % of  $D_2O$  and the conversion to the imine was observed. To eliminate the effect of pH on the kinetics, a triethanolamine buffer (800 mM, apparent pH = 9.20 – 9.40) was used throughout the following experiments. The signals arising from the buffer protons as well as residual water signal appear in the 2-5 ppm region of the spectrum, whereas the aldehyde and imine peaks are at 10 or 8 ppm respectively, and their integration is therefore not perturbed. The condensation experiment was performed at 20 mM of both reagents, and the data provided a value for the second order rate constant of  $0.02 \text{ M}^{-1} \text{ s}^{-1}$  with overall conversion to the imine of about 90 % (note that in the reaction without a buffer the conversion was quantitative).

In the following experiment, **CAXAL** was first mixed with **SALAL** and then 1 eq. **IPA** was added. Again, the conversion to the imine of **SALAL** was followed (Graph 4.3-1).<sup>\*\*\*\*</sup> The rate of the reaction of **SALAL** was significantly lower in this case and at equilibrium there was only 77 % conversion. This observation shows that the competition of two aldehydes for one amine affects both the equilibrium (conversion) and the kinetics (rate of formation).<sup>++++</sup>

Finally, a mixture of the two aldehydes was mixed with both **IPA** and **PIP** (20 mM each), so that each aldehyde had its “matching” partner, and the conversion of **SALAL** to its imine was again followed by NMR spectroscopy. Interestingly, very fast imine formation was observed in this case, the rate being higher even when compared to the initial **SALAL+IPA** experiment (Graph 4.3-1). This observation might reflect the possibility of catalysis of the aldehyde condensation reactions by secondary amines (formation of iminium species), as known in the literature.<sup>[396,397]</sup> Again, it demonstrates that the complexity of a reaction mixture can strongly influence not only the equilibrium composition, but also the kinetic properties.

<sup>\*\*\*\*</sup> As mentioned before, **CAXAL** gives under these conditions a dynamic mixture of imine and lactone and the integrals are not suitable for kinetic analysis.

<sup>++++</sup> The equilibrium constant and the rate constant are, of course, still the same. It is the apparent equilibrium and kinetics resulting from the presence of new species that lead to different observations.



Graph 4.3-1 Relative percentage of the imine formed by the reaction of **SALAL** + **IPA** plotted as a function of time. The rate is significantly lower when **CAXAL** is added to the mixture as a result of competition of two aldehydes for one amine. Interestingly, when also **PIP** is also added, the rate is higher than the previous two rates, indicating a catalysis due to **PIP**.

#### 4.3.2. Extended complexity in 3x3 aldehyde-amine library

In the previous Section, the process of selection and amplification in dynamic libraries caused by an increased complexity of its components, called simplicity, was demonstrated on three examples of 2+2 aldehyde-amine mixtures. In fact, three different aldehydes as well as three different amines were used for the experiments, which ultimately leads to the idea of increasing the complexity even further, by creating a 3+3 aldehyde-amine library composed of the components used in previous studies. To this end, a mixture of **SALAL**, **PYRAL** and **CAXAL** was mixed with a mixture of **IPA**, **Me<sub>2</sub>PDA** and **PIP** (20 mM each), so that each component could react with its preferred counterpart, and the NMR spectra were recorded (Figure 4.3-7). It is noteworthy that the equilibration in this case takes up to about a week, but it can be speeded up by heating the mixture at 60 °C overnight. The equilibrated samples contained the imine of **SALAL** and **IPA** in 88 % conversion and the aminal of **SALAL** and **Me<sub>2</sub>PDA** in 12 %. The ratio for the imine and the aminal of **PYRAL** was exactly the opposite as that for **SALAL**. **CAXAL** provided only its lactone with **PIP**.

The library was also prepared in several concentrations: 4, 10, 20, 60 and 100 mM of the components. It has been demonstrated in the literature that the target concentration of species can play a role in the selection process.<sup>[345]</sup> However, the equilibrium composition of the library at the concentrations indicated above was constant, showing that this is not the case, at least not in the concentration range investigated.

The library was also assessed for the effect of pH. For this, the pre-equilibrated library was titrated with up to 4 equivalents of acid (MeSO<sub>3</sub>H) or up to 2 eq. of base (*t*-BuOK). After addition of 1 eq. of base almost complete hydrolysis of the aminals of both **SALAL** and **PYRAL** was observed while the imines underwent only 26 % hydrolysis. After addition of the second equivalent of MeSO<sub>3</sub>H, the imine hydrolyses reached 60 % and **CAXAL**-derivative hydrolysis was detectable. Continued titration by acid led to complete hydrolysis of imines and extensive hydrolysis of the **CAXAL**-derivative, finally giving after the addition of total of 4 equivalents only the hydrolysed products. It can be therefore concluded that the most labile structure under acidic conditions is the aminal, followed by the imine, with the lactone being the most stable. In contrast, upon titration by base, disappearance of the lactone was observed. Interestingly, this lactone depletion was not accompanied by the emergence of the aldehyde peak of **CAXAL**, but rather of a new imine of **CAXAL** with **IPA** and liberation of **SALAL**

was observed. This example is another demonstration of the reaction network interconnecting the species within the dynamic library.

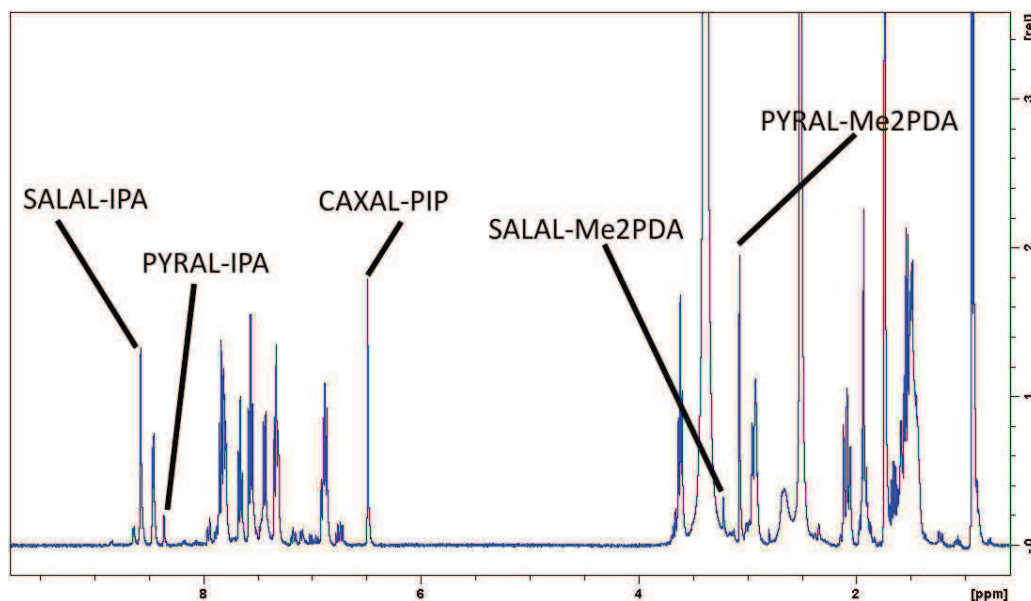


Figure 4.3-7  $^1\text{H-NMR}$  spectrum of the 3+3 aldehyde-amine library with assignment of the peaks. Three major species are formed: imine of **SALAL**, aminoral of **PYRAL**, and lactone of **CAXAL**, the latter being the only product of this aldehyde.

Full deconvolution of this 3+3 dynamic library was performed, i.e. all possible combinations of aldehydes were treated with all possible combinations of amines, in total involving 39 experiments, some of which have been described in Section 4.3.1. From the relative conversions to given products the selector matrix could be calculating, providing a selection index of 0.77 and a selection strength of 38 %. The full set of matrices is provided in the Experimental part.

### 4.3.3. Multivalency and simplicity

Selection in dynamic aldehyde-amine libraries described in Section 4.3.1 and 4.3.2 is due to the preference of a given aldehyde for its matching amine derivative, namely **SALAL** reacts with primary amines, **CAXAL** with secondary and **PYRAL** with 1,2- or 1,3- secondary diamines. The establishment of equilibrium proceeds through an intermolecular reaction with a different amine molecule. This brings an interesting question of the aldehyde selectivity for the same functional groups within one polyamine molecule. The intermolecular exchange would here be replaced by an intramolecular one, thus giving a sequence of aldehydes defined by the structure of the polyamine used. In other words, multivalency of a polyamine molecule could serve as the organization principle.<sup>[398]</sup>

Five polyamine derivatives were chosen to investigate multivalency sorting: *N*-benzyl-ethylenediamine (**BnEDA**), diethylenetriamine (**en<sub>2</sub>N<sub>3</sub>**), triethylenetetraamine (**en<sub>3</sub>N<sub>4</sub>**), spermidine (**SPE**) and *N*-(3-aminopropyl)-ethylenediamine (**PEA**, Figure 4.3-8). The only commercially unavailable product, **PEA**, was synthesized by Michael addition of acrylonitrile to ethylenediamine, subsequent reduction by  $\text{H}_2/\text{RaNi}$ , and purification by vacuum distillation. The same three aldehyde derivatives as discussed in previous cases were also used for this study.

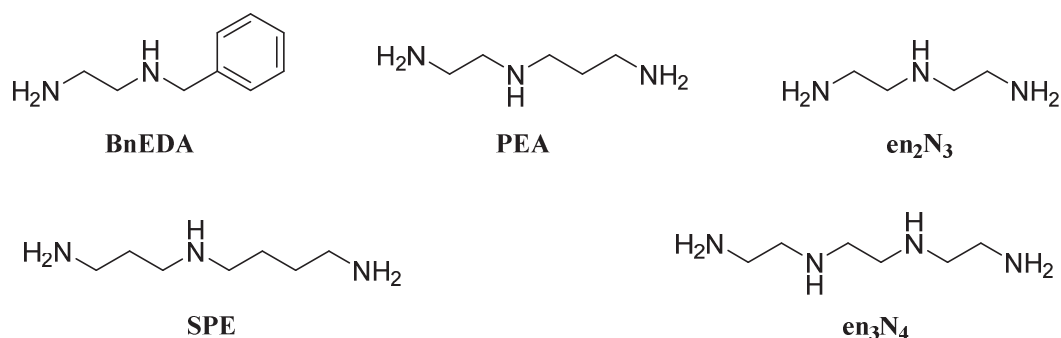


Figure 4.3-8 Polyamine derivatives used in the study of dynamic aldehyde-multivalent polyamine libraries.

First, the case of **BnEDA** was examined. This diamine has one primary and one secondary nitrogen, and the latter was shown before to act as a site for the lactone ring formation (Section 3.3.1). Initially, the aldehydes **CAXAL** and **SALAL** were reacted separately with the diamine. In both cases broad NMR spectra were recorded, indicating fast exchange between species, and in the case of **CAXAL** the azomethine peak disappeared completely from the spectrum. Next, a mixture of the aldehydes (20 mM each) was treated with **BnEDA** (1 eq.) and allowed to equilibrate at 60 °C overnight. The dominant product formed (about 70 %) was the expected imine-lactone: the imine of **SALAL** formed on the primary nitrogen and the lactone of **CAXAL** closed on the secondary nitrogen (Figure 4.3-9). However, **CAXAL** also provided its imine (15 %) and about 17 % remained unreacted (equilibrium between aldehyde and hydroxy-lactone). The formation of the imine by **CAXAL** also resulted in larger amounts of unreacted **SALAL** (30 %) as it cannot react with secondary amines. Note that some amins were formed as well, but the complicated overlap of signals in the important region prevented quantification.

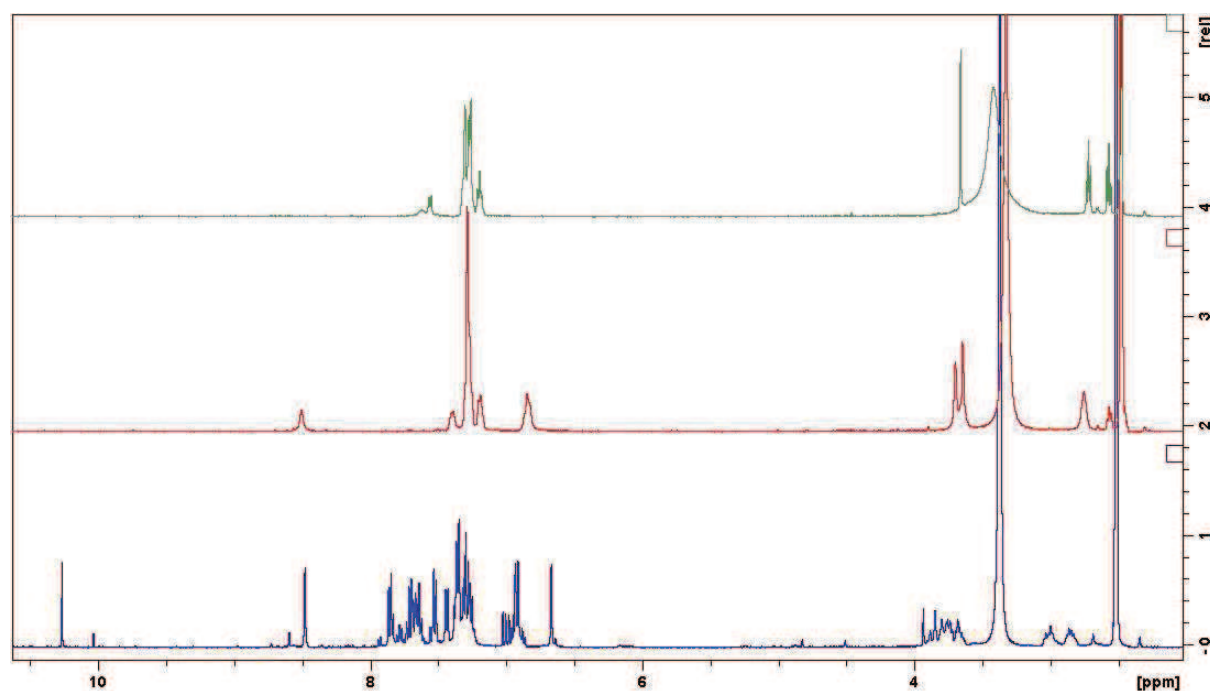


Figure 4.3-9 <sup>1</sup>H-NMR spectrum of the mixture of **SALAL**, **CAXAL** and **BnEDA** showing that the dominant species in the solution is the imine-lactone (in about 70 %), but other species are formed as well (bottom blue trace). **BnEDA** was reacted also individually with each aldehyde and the spectra are given for comparison (**SALAL** - red middle trace, **CAXAL** - green top trace).

Next, the imine formation of **SALAL** on the primary nitrogens at the extremities of the polyamines **en<sub>2</sub>N<sub>3</sub>**, **en<sub>3</sub>N<sub>4</sub>**, **SPE** and **PEA** was studied. Each of the polyamines was reacted with 2 equivalents of **SALAL** and the NMR spectra were monitored (Figure 4.3-10), reaching equilibrium in

all cases within 30 minutes. Very broad signals over the whole spectral region were observed in the case of **en<sub>2</sub>N<sub>3</sub>** and **PEA**, indicating a fast exchange. **SPE** under the same conditions gave two different imine signals, each a relatively sharp singlet at around 8.5 ppm. When **SPE** or **PEA** was reacted with only one equivalent of the aldehyde, two relatively broad and largely overlapped signals were observed. These signals were deconvoluted by line-shape fitting showing about a 1:1 ratio of two signals and indicating no preference for the imine formation on either of the two sides. However, a much more complicated mixture was observed in the case of **en<sub>3</sub>N<sub>4</sub>**. The NMR spectrum revealed four different imine signals (three sharp and one broad) and three aminal peaks. Thus, in this case, all possible combinations of imine-aminal structures (aminal on the central two nitrogen atoms) were formed in an essentially statistical fashion.

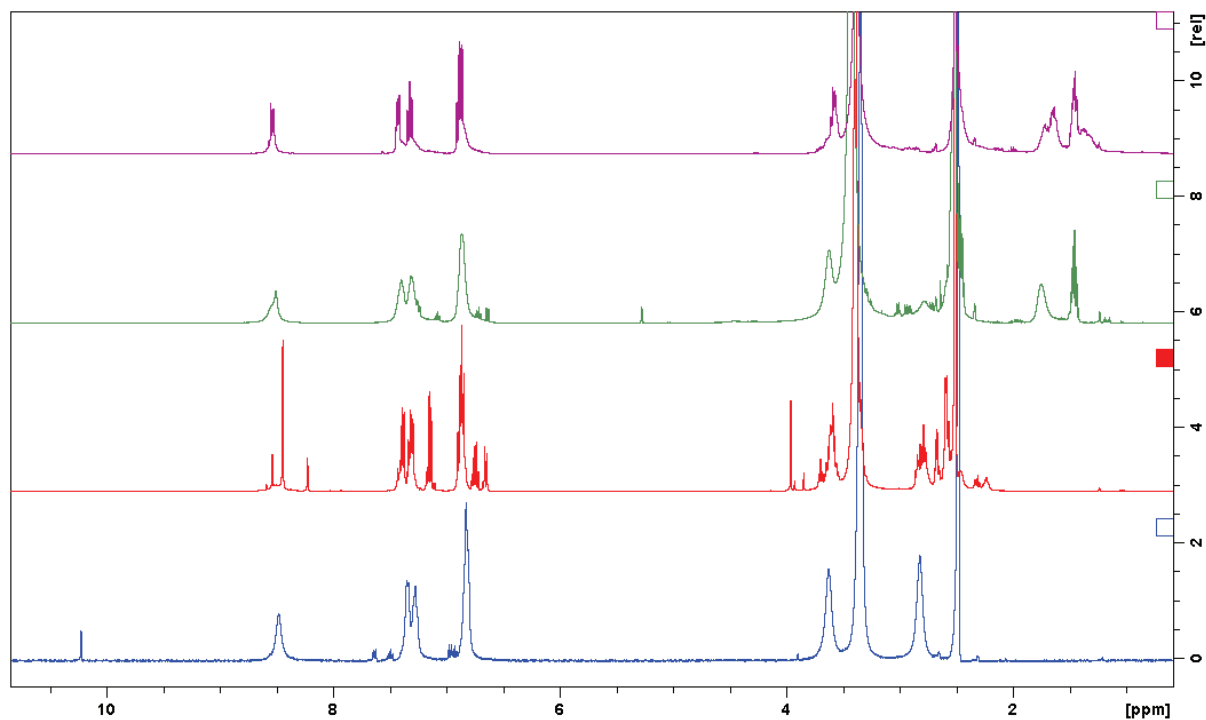


Figure 4.3-10 Spectra of 2 equivalents of **SALAL** reacted with 1 equivalent of (from bottom to top): **en<sub>2</sub>N<sub>3</sub>**, **en<sub>3</sub>N<sub>4</sub>**, **PEA** and **SPE**. Dynamic equilibrium resulted in broad signals in the case of **en<sub>2</sub>N<sub>3</sub>** and **PEA**. The aldehyde peak in the case of **en<sub>2</sub>N<sub>3</sub>** is due to imprecise stoichiometry. A complicated mixture of products was observed in the case of **en<sub>3</sub>N<sub>4</sub>** and the spectrum indicates the coexistence of multiple imines as well as multiple aminals. The spectrum of **SPE** shows two relatively sharp imine peaks corresponding to two different imines at the extremities of the polyamine chain.

In the following experiment, **SPE** or **PEA** was treated with both **SALAL** and **PYRAL** (1 eq. each). While **PEA** is capable of formation of either five- or six-membered-ring aminals, **SPE** can form only the six-membered one. By design, **SALAL** should form an imine and **PYRAL** should provide an aminal. However, when the NMR spectra were recorded, a statistical distribution of all possible products was observed. Specifically, in the case of **PEA**, both aldehydes gave a mixture of imines and aminals formed on both sides of the polyamine. Moreover, considerable amounts of unreacted aldehydes were also observed in the spectrum. In the case of **SPE**, the situation is slightly simplified by the fact that seven-membered aminal ring cannot be formed, however at least four imine and two aminal signals were observed and confirmed by 2D NOESY.

Finally, when **en<sub>3</sub>N<sub>4</sub>** was mixed with 2 eq. of **SALAL** and 1 eq. of **PYRAL**, the formation of the imine on the terminal primary amines was observed accompanied by aminal formation between the central two nitrogen atoms in an overall conversion of about 60 % (Figure 4.3-11b). Of course formation of other species was observed as well, notably imines of **PYRAL** (28 %) and the aminal of **SALAL** (12 %), together with significant amounts of unreacted aldehyde (27 % of **SALAL** and 13 % of **PYRAL**).



Several other aldehyde-polyamine combinations were examined, especially those comprising **CAXAL** for the lactone formation. However in all such cases very complex mixtures were observed by NMR, and notably, in combinations involving **CAXAL**, a large amount of the other aldehyde remained unreacted. Altogether, these results for multivalent polyamines indicate that a stronger selection is required to observe formation of only the desired species.

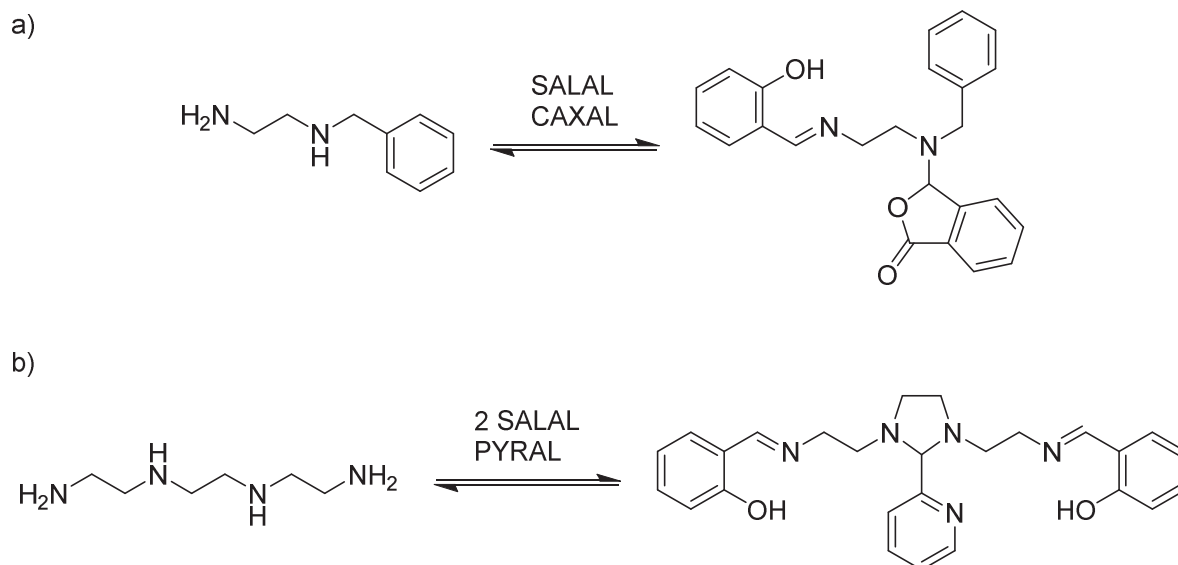


Figure 4.3-11 Selection by multivalent polyamines: a) **BnEDA** reacted with imine-forming **SALAL** and lactone-forming **CAXAL** gave the desired product in about 70 % conversion. b) Formation of imines at extremities of **en<sub>3</sub>N<sub>4</sub>** was accompanied by the formation of a ring of **PYRAL** with the central pair of nitrogen atoms.

## 4.4. Applications – dynamic selective protection

The chemical synthesis of complicated molecules, like natural products, often involves the need for selective reactivity of a chosen functional group in presence of very similar functions. Selective and specific addressing of a given chemical function in complex molecules is enabled by the use of protecting groups.<sup>[399–402]</sup> However, introduction and removal of a protecting group necessitates two more synthetic steps accompanied by a purification procedure. It has therefore been of much interest recently to develop “protecting-group-free” methodology for natural product synthesis.<sup>[403,404]</sup>

Dynamic protecting groups could represent an opportunity intermediate between these two approaches: they can be formed directly in the reaction mixture under thermodynamic control thus protecting the selected function, yet their dynamic nature provides reversibility for easy trans-reaction and thus deprotection without the need for isolation and purification. Moreover, there are several types of dynamic linkages which have been shown to be orthogonal to each other,<sup>[11,12,366–370]</sup> thus providing a pool of reagents for different functional groups,<sup>[405–407]</sup> analogously to the classical protecting groups in organic synthesis.<sup>[399]</sup> Note that dynamic bonds have been also used for dynamic kinetic resolution.<sup>[378,408]</sup>

Imines and related structures have been used as protecting groups in the synthesis of various derivatized amines. Typically, the protection of an amine in the form of an imine allows for generation of a carbanion by the action of a strong base and consecutive selective C-alkylation.<sup>[409–419]</sup> Selective alkylation of the hydroxyl group over the amino group has been demonstrated,<sup>[420–422]</sup> as well as amine protection under oxidative dihydroxylation of a C=C double bond,<sup>[423]</sup> or protection of the aldehyde function against the action of an organometallic compounds.<sup>[424]</sup> As protecting aldehydes, salicylaldehyde<sup>[425–429]</sup> and formaldehyde<sup>[334,430–435]</sup> have been used for selective imine or



aminal formation respectively, thus complementing the formamidine protecting group.<sup>[436–442]</sup> As for deprotection, the typical acidic hydrolysis setup<sup>[409–419]</sup> can be replaced by the transimination reaction by application of hydrazides<sup>[443]</sup> or hydroxylamine derivatives.<sup>[429,444,445]</sup> Moreover, selectivity in the imine formation has been used to differentiate between primary and secondary amines in the same molecule of substrate,<sup>[429,446]</sup> and the preferential formation of a hydrazone over an imine has been applied in the diazotation reaction.<sup>[447]</sup>

The selectivity of different aldehydes for formation of a given product, which was discussed previous Sections, was therefore applied as a dynamic protection in acylation reactions of polyamines. For the proof of principle, *N*-methyl-1,3-diaminopropane (**MePDA**) was used as the amine substrate in this study. Detailed synthetic procedures as well as full characterization are given in the Experimental part.

#### 4.4.1. Selective mono-acylation of diamines

The NMR measurements described above demonstrated the strong preference of **SALAL** for imine formation. Given a substrate with which it could form either the imine or the aminal, the imine signals were always observed. This led to an idea of its use as protecting group for primary amines in presence of secondary ones, as also applied in other instances.<sup>[425–429]</sup> With the chosen diamine, the formation of imine leaves the secondary nitrogen available for acylation (Figure 4.4-1). It is noteworthy that imine formation is indeed reversible, whereas the acylation under given conditions is not. Deprotection of primary nitrogen atoms can be achieved by acidic hydrolysis, but some derivatives can be unstable under such conditions. Thus, use of the imine exchange reaction, discussed in several Sections above, was examined. In this, formation of a more robust imine derivative, such as an oxime or acylhydrazone, was used for the deprotection in a quantitative conversion.

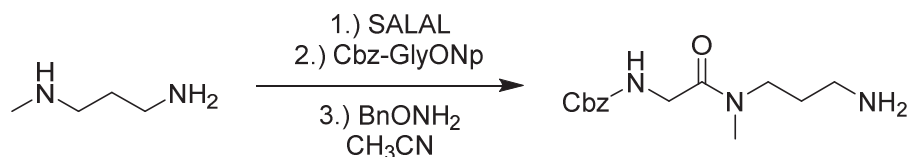


Figure 4.4-1 Selective mono-acylation of *N*-methyl-1,3-diaminopropane by an activated ester of *N*-protected glycine. The selective formation of imine by **SALAL** is used to protect the primary amine in presence of a secondary one.

In acetonitrile, **MePDA** was first mixed with **SALAL** and stirred for 2 hours. Then, *N*-Cbz-glycine *p*-nitrophenyl ester (*N*-Cbz-GlyONp) was added and the mixture was stirred for two hours. Finally, *O*-benzyl hydroxylamine was added and the solution again stirred for 2 hours. The product was obtained by reverse phase chromatography on C18-modified silica using a water/acetonitrile gradient. The *p*-nitrophenol leaving group complicates the separation, therefore after injection of the crude reaction mixture, 0.15 M HCl was also injected, leading to protonation of both the product and *p*-nitrophenoxide. The product was then isolated as the hydrochloride in 82 % yield. As the imine condensation is a reversible reaction, some amount of the diamine remains unreacted in solution. This led to isolation of about 6 % yield of the product of bis-acylation.

The reaction was repeated using different acylating agents, such as acylchlorides or isocyanates, also by using benzhydrazide for the deprotection of **SALAL**. These experiments were performed by Dr. Anne Meister and are listed in Table 4.2-2. The isolated yields of the reaction are in the range of 69 – 86 %.

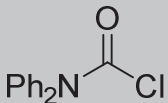
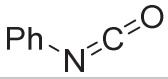
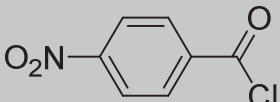
Acylating agent	Solvent	Deprotecting agent	Yield
	CH <sub>3</sub> CN	benzhydrazide	70 %
	CH <sub>3</sub> CN	BnONH <sub>2</sub>	86 %
	CH <sub>3</sub> CN	BnONH <sub>2</sub>	69 %

Table 4.4-1 Isolated yields of selective mono-derivatization of *N*-methyl-1,3-diaminopropane. Experiments performed by Dr. Anne Meister.

In all cases, full NMR characterization was performed to prove the regioselectivity of the acylation step (NOE and HMBC correlations). It is noteworthy that the amides formed exist as a dynamic mixture of two rotamers which interconvert, as proved by 2D NOESY and VT-NMR.

The experiment was reproduced without the use of **SALAL** as protecting group. The product was isolated in 85 % yield, but consisted of a mixture of regioisomers in 2:1 ratio in favour of the product of acylation on the secondary nitrogen. The yield of the bis-acylated product in this case was similar to that in experiment with the protecting group. Importantly, the isolated yields are in all cases significantly higher than the yields of the most generally used procedure of protection of primary amines by trifluoroacetyl,<sup>[342]</sup> which gives yields around 65 % in the first protecting step, whereas the present procedure gives isolated yields above 69 % after three steps, i.e. protection, acylation and deprotection.

The deprotection step is that of forming an oxime of **SALAL**. This oxime is very apolar, unlike to the target product of the reaction, and thus does not complicate the separation. The very low polarity of the oxime formed was observed also for **PYRAL** (discussed below). In contrast, the acylhydrazone formed from benzhydrazide is more polar, and thus the polarity of the deprotection byproduct can be chosen in a way which leads to easier separation. Numerous hydrazides and hydroxylamines are commercially available, so the polarity of the byproduct can be varied over a wide range.

#### 4.4.2. Sequential selective bis-acylation of diamines

The acylation procedure using an imine protecting group presented above provides mono-substituted diamines and the protecting group can be removed under mild conditions giving a more stable imine species. This opens up the possibility of performing a bis-acylation of the diamine in “one pot” fashion without isolation of the mono-derivatized intermediate (Figure 4.4-2).

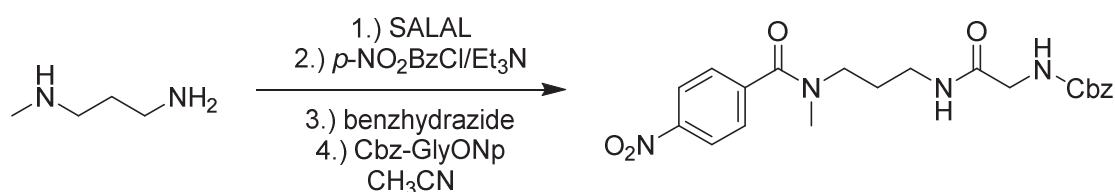


Figure 4.4-2 Selective, sequential, one-pot bis-acylation of *N*-methyl-1,3-diaminopropane by reaction first with *p*-nitrobenzoyl chloride and then with an activated ester of *N*-protected glycine. The formation of the imine of **SALAL** directs the selectivity of the sequence.

To this end, **MePDA** was mixed with **SALAL** in acetonitrile and stirred for two hours at room temperature. Then an equivalent amount of triethylamine was added together with one equivalent

of *p*-nitrobenzoyl chloride and the mixture was stirred continuously for two more hours, after which benzhydrazide (1 eq.) was added for **SALAL** deprotection. After two more hours of stirring *N*-Cbz-GlyONp was added and the mixture was stirred for two more hours. The pure product was obtained by column chromatography giving an overall 78 % yield of the desired product. Also, about 7 % yield of the inverted regioisomer was isolated as well as an 8 % yield of bis-(*N*-Cbz-glycyl)**MePDA**. It is important to point out that the procedure consists of four steps, i.e. protection, first acylation, deprotection and second acylation, performed one-pot, which means an average yield of 94 % per step.

To demonstrate the need of a protecting group, a control experiment similar to the one in previous section was performed. As the first acylating agent, *N*-Cbz-glycine *p*-nitrophenyl ester was used, followed by acetic anhydride in the fourth step. A total yield of 92 % was isolated, consisting of two regioisomers in the same ratio as in the mono-acylation procedure.

The reaction conditions were studied using various combinations of reagents, using either hydroxylamine or hydrazide deprotecting reagents, and also in ethanol as a solvent to demonstrate versatility of the protocol. These experiments were performed by Dr. Meister and showed that the choice of solvent between MeCN or EtOH, as well as type of the deprotecting agent leads to only minor changes in isolated yields (around 2 %). The optimal conditions and the isolated yield of these reactions are listed in Table 4.4-2.

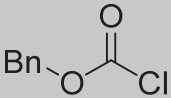
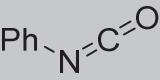
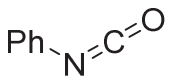
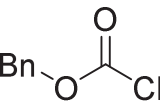
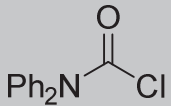
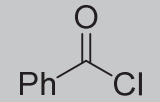
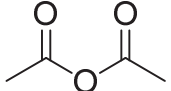
Acylating agent 1	Acylating agent 2	Solvent	Deprotecting agent	Yield
		CH <sub>3</sub> CN	benzhydrazide	60 %
		EtOH	BnONH <sub>2</sub>	82 %
		EtOH	BnONH <sub>2</sub>	60 %
	<i>N</i> -Cbz-GlyONp	CH <sub>3</sub> CN	BnONH <sub>2</sub>	37 %
<i>N</i> -Boc-AlaOSu	<i>N</i> -Boc-PheOSu	EtOH	BnONH <sub>2</sub>	32 %

Table 4.4-2 Isolated yields of sequential selective bis-acylation of *N*-methyl-1,3-diaminopropane. Experiments performed by Dr. Anne Meister. Two other activated esters of aminoacid have been introduced: *N*-Boc-alanine *N'*-hydroxysuccinimide ester (*N*-Boc-AlaOSu) and *N*-Boc-phenylalanine *N'*-hydroxysuccinimide ester (*N*-Boc-PheOSu).

#### 4.4.1. Inverted selectivity of acylations

The protection by **SALAL** as discussed in previous Sections provides diamines acylated on secondary nitrogen. However, products of acylation on the primary nitrogen without derivatization of the secondary one are of interest as well. Moreover, the first two entries in the Table 4.4-2 show an interesting issue: a change in the order of acylating agents leads to a difference in isolated yields of about 20 % (note that change in solvent or deprotecting agent leads only to 2 % change in conversion). Therefore, it can be of interest in some instances to invert the order in which the nitrogen atoms are derivatized.

In this vein, **PYRAL**, which was previously shown to form aminal efficiently, was used as a protecting group instead of **SALAL**. The cyclic aminal formation connects two nitrogen atoms and converts the secondary amine to tertiary (hereafter referred as “secondary”) and the primary one to secondary (“primary”). Subsequent addition of an acylating agent can thus proceed only on the

“primary” nitrogen, giving after deprotection step the inverted regioisomer compared to the protection by **SALAL**.

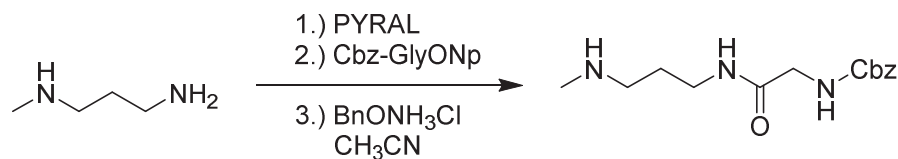


Figure 4.4-3 Inverted selectivity of the mono-acylation of *N*-methyl-1,3-diaminopropane by the activated ester of *N*-protected glycine. The formation of six-membered aminor ring by the reaction with **PYRAL** leads to selective acylation of the “primary” amine in presence of a “secondary” one.

In acetonitrile, **MePDA** was mixed with 1 eq. of **PYRAL** and the solution was stirred for 2 hours. Then, *N*-Cbz-GlyONp was added (1 eq.) as solid. The mixture was stirred at room temperature and after 2 hours *O*-benzyl hydroxylamine hydrochloride and triethylamine (1 eq. each) were added. The reaction was stirred for 2 more hours. The product was obtained by reverse phase chromatography on C18-modified silica. To improve the separation from *p*-nitrophenol, again 0.15 M HCl was injected after the injection of the crude mixture, giving the product as hydrochloride salt in 58 % yield. As shown in previous experiments, **PYRAL** forms aminorals rather efficiently, but is capable of imine formation as well. This leads to a lower selectivity of the acylation, and the product of the acylation of the “secondary” nitrogen is isolated as well (15 %).

In similar fashion to the one-pot bis-acylation using **SALAL** protection, the inverted sequential acylation was also performed using the **PYRAL** protecting group. The procedure was the same as for **SALAL**, as discussed in the previous Section. The product was isolated in 65 % yield, but consisted of both regioisomers in ratio 8:1 in favour of the desired product.

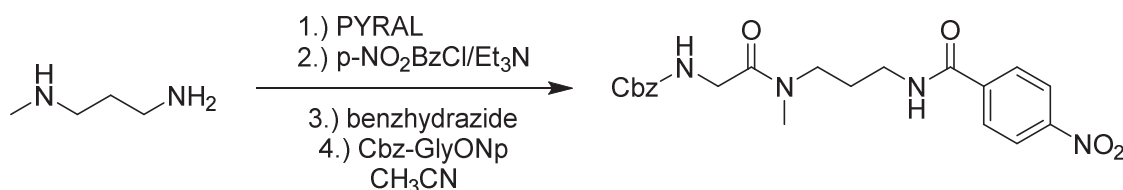


Figure 4.4-4 Inverted sequential bis-acylation – **PYRAL** was used the aminor-forming protecting group driving the selectivity in opposite order to **SALAL**.

Altogether, the experiments shown above show an application of a dynamic aldehyde-amine linkage for syntheses of acylated polyamines. The aldehyde can be chosen in a way that either the primary or the secondary amine centre can be reacted in presence of the other one. Removal of the protecting group was performed by an imine exchange reaction under mild conditions. The demonstrated procedure can be applied for preparation of mono-derivatized diamines or it can even be used to selective sequential bis-acylation in one-pot fashion. The procedure was repeated in different solvents (acetonitrile and ethanol) and using various acylating reagents, proving its versatility of use for the synthesis of diverse polyamine derivatives.

## 4.5. Summary of Chapter 4

- An approach for representation of dynamic combinatorial libraries was proposed. A system of quantification of selection upon self-sorting conditions was envisaged based on the algebraic representation of DCLs.
- The phenomenon of simplicity, i.e. simplicity arising from the complexity of a mixture, was discussed.
- Simplicity was demonstrated on series of 2+2 aldehyde-amine libraries.

- An extended example of simplicity was illustrated on a 3+3 DCL, created by combination of the 2+2 experiments. Specifically, an amplified conversion of the *N*-i-pentylsalicylalimine, *N,N'*-dimethyl-2-(pyrid-2-yl)-hexahydropyrimidine and 3-(piperidin-1-yl)-isobenzofuran-1(3H)-one (imine of **SALAL** and **IPA**, amination of **PYRAL** with **Me<sub>2</sub>PDA** and lactone of **CAXAL** and **PIP**, respectively) was observed as compared to the mixture of reduced complexity of reagents.
- The observed aldehyde selectivity for a formation of a given product of condensation with amines was applied in synthesis of *N*-derivatized polyamines.
- Protection of a primary group in presence of a secondary one was achieved with **SALAL**. Both mono- and bis-derivatization were performed in one-pot fashion.
- Inverted sequential selective derivatization of diamines was demonstrated with **PYRAL**, giving the opposite regioisomers as compared to **SALAL**.
- An imine exchange reaction was used for protecting group removal under mild conditions.

## 5. DYNAMIC IMINE BOND AT THE SOLID-LIQUID INTERFACE

### 5.1. Introduction

In the last decades, supramolecular chemistry<sup>[5,448–450]</sup> elaborated the application of non-covalent interactions to self-assemble chemical entities, with a precision on the molecular scale, to form materials exhibiting programmed chemical and physical properties. However, the labile nature of non-covalent interactions limits the stability of the self-assembled structures, especially in solution, thereby impeding their technological use. In this regard, the possibility of constructing molecular architectures based on more robust, yet reversible, bonds has evolved supramolecular chemistry towards dynamic covalent chemistry (DCC).<sup>[309,451]</sup> The DCC shares key features with supramolecular chemistry; in particular, they both employ reversible bonds enabling the formation of products under thermodynamic control. Both supramolecular chemistry and DCC are modular since they allow for selection and exchange of the components,<sup>[6,20,21,25,26,309,451]</sup> thus representing branches of constitutional dynamic chemistry (CDC).<sup>[8,452]</sup> While early examples of supramolecularly assisted covalent synthesis relied strongly on kinetically controlled reactions for post-assembly covalent modification,<sup>[453,454]</sup> the DCC method takes advantage of the reversible linkage, e.g. disulfide,<sup>[82]</sup> acetal,<sup>[455,456]</sup> ester,<sup>[457]</sup> imine<sup>[27,61,62,65,66,458]</sup> and boronate<sup>[459,460]</sup> bonds, to allow the generation of covalent structures under thermodynamic control. For these reasons DCC has emerged as an efficient and versatile strategy for the design and synthesis of complex molecular systems.

Imines are of particular interest for DCC<sup>[6,20,21,25,26,309,451,458]</sup> since the condensation of an amine with a carbonyl into imine compounds and the imine exchange reactions<sup>[396]</sup> usually take place under mild conditions (discussed in detail in Chapter 2), even in aqueous media, allowing for shifting the equilibrium between imine condensation or hydrolysis. Dynamic exchange involving the C=N bonds in imines is among the most widely used classical dynamic covalent reactions (discussed in Chapters 2, 3 and 4) in fields ranging from biochemistry<sup>[24,322]</sup> to materials science.<sup>[311,461,462]</sup>

On-surface chemistry has recently attracted much attention in nanoscience and molecular electronics, because it represents a novel bottom-up approach for producing defined functional nanostructures through the covalent coupling of precursors rigorously under kinetic control.<sup>[463–468]</sup> Scanning tunnelling microscopy (STM)<sup>[469–471]</sup> is extremely powerful, widely used tool to study ordered molecular architectures at interfaces with sub-nanometre resolution, providing direct insight into the supramolecular world.<sup>[472–482]</sup> Beyond the mere visualization of the two-dimensional (2D) ordering of physisorbed monolayers, recent studies have shown the potential of the STM in a vast area of topics, such as monitoring the molecular dynamics,<sup>[483,484]</sup> molecule manipulation,<sup>[485–490]</sup> or surface chirality.<sup>[491]</sup>

Among self-assembled structures investigated by STM, those comprising boronates<sup>[492,493]</sup> and imines<sup>[494,495]</sup> are particularly attractive. The on-surface synthesis of boroxine<sup>[496]</sup> or imine linkage (both in ultra-high vacuum (UHV)<sup>[497,498]</sup> and at water/gold interface,<sup>[499]</sup>) have been demonstrated, but the reversibility has never been shown on surface.

The project presented in this chapter was done in cooperation with Dr. Artur Ciesielski, Dr. Mohamad El Garah and Sebastien Haar. It reports on sub-molecularly resolved STM of surface-mediated reversible imine formation and exchange processes of aliphatic bis-imines occurring at the solid-liquid interface on highly oriented pyrolytic graphite (HOPG) surface. The results from STM show stark contrast with the results obtained in bulk solution, pointing out the striking role of the HOPG surface on the course of the processes. The STM experiments and adsorption energy calculations were done by Dr. Artur Ciesielski, Dr. Mohamad El Garah and Sebastien Haar.

## 5.2. Dynamic imine bonds on surfaces

### 5.2.1. Design of imine system for the HOPG surface

Molecules are adsorbed on the HOPG surface through relatively strong molecule-graphite van der Waals interactions. Highly ordered 2D structures are obtained due to the molecule-molecule noncovalent interactions. Therefore, to achieve acceptable adsorption to the surface, a benzaldehyde bearing *n*-hexadecyloxy substituent in the *para* position was proposed (experimental details in the Section 7.2.4.1). For the amine part, linear  $\alpha,\omega$ -diamines of different alkyl chain lengths were chosen as they are capable of formation of bis-imines and thus duplicate the long alkyl chain present in the aldehyde moiety (Figure 5.2-1).

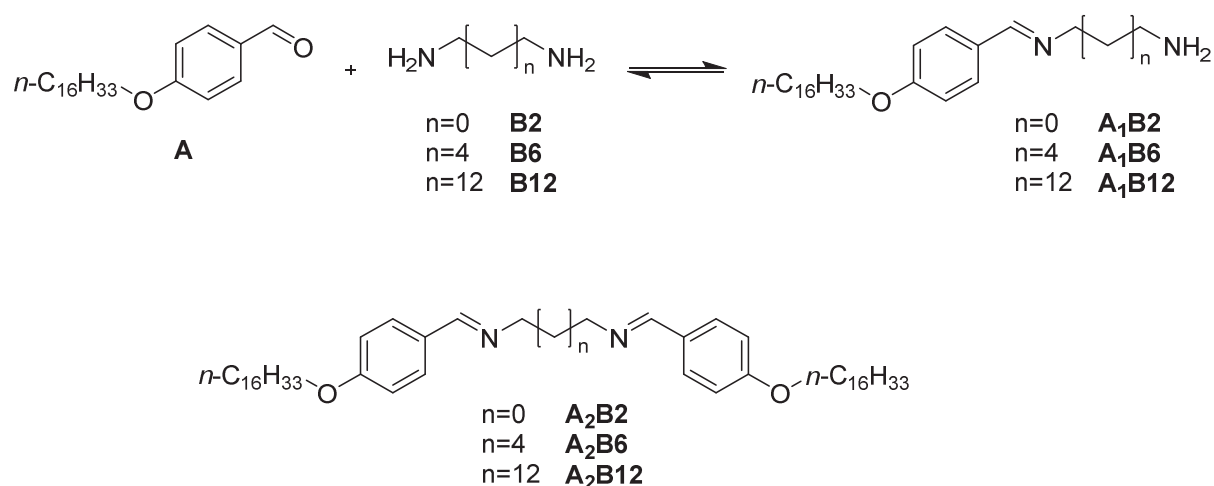


Figure 5.2-1 Compounds employed in the imine formation and exchange on surface studied by STM.

Initially, the self-assembly of the aldehyde **A** alone was investigated. Applying a drop (4  $\mu\text{L}$ ) of a 0.1 mM solution of **A** in 1-phenyloctane on the HOPG surface lead to formation of a crystalline monolayer consisting of a lamellar structure of **A** physisorbed flat on the surface (Figure 5.2-2a). It is noteworthy that the self-assembly of **A** can be described by the formation of trimer-like sub-units (indicated in Figure 5.2-2b), which further expands into lamellar arrays, characterized by an assembly according to an aldehyde-to-aldehyde motif within a given lamella, and tail-to-tail packing between adjacent lamellae. On the other hand, none of the  $\alpha,\omega$ -diamine derivatives (**B2**, **B6** nor **B12**) was found to form ordered structures at the liquid-solid interface, highlighting their highly dynamic nature on the graphite surface on a time scale faster than STM imaging, as determined by their low affinity for HOPG.

The adsorption of the bis-imines formed by condensation of 2 eq. of **A** with 1 eq. of either of the diamines was also tested. The bis-imines **A<sub>2</sub>B2**, **A<sub>2</sub>B6** and **A<sub>2</sub>B12** were synthesized and characterized (Section 7.2.4). Casting a drop (4  $\mu\text{L}$ ) of 0.1 mM solution of these bis-imines in 1-phenyloctane on the HOPG substrate leads to formation of lamellar structures. In the 2D crystals, the long *n*-hexadecyloxy side chains of **A** are clearly visible, and are physisorbed flat on the surface,



whereas the two shorter diamine spacers appear as darker areas on the STM image (Figure 5.2-1c,e,g). Furthermore, linearly aligned bright spots (noticeably visible on the STM images) can be attributed to the phenyl rings of the **A** units. By comparison of the unit cell parameters of all monolayers self-assembled at the HOPG–solution interface (Table 5.2-1) it can be seen that the only difference between those structures is the value of the vector  $a$ . For better comparison, this was divided into two sub-vectors  $c$  and  $d$ , where vector  $d$  comprises the  $n$ -hexadecyloxy side chains and the vector  $c$  is the distance between the phenyl rings. From these values it is clear that the difference between these structures is only defined by the vector  $c$ , i.e. the distance between the phenyl rings and therefore the length of **B** spacer.

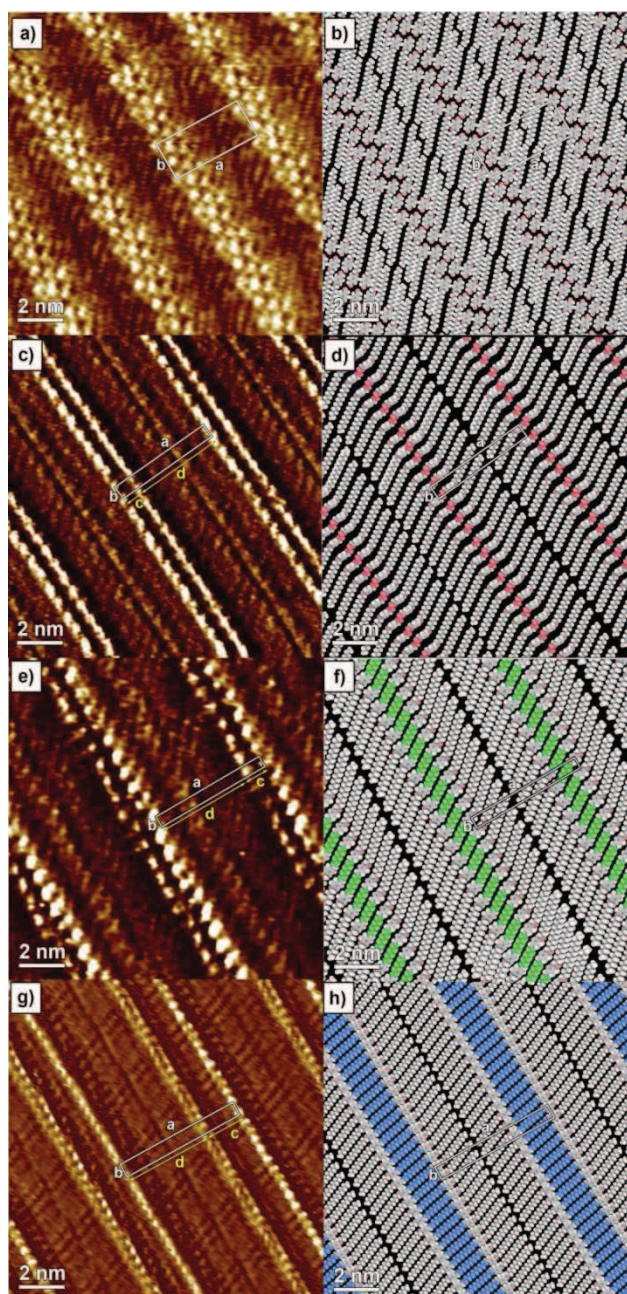


Figure 5.2-2. STM images of self-assembled 2D nanopatterns. Monolayer of molecule a) **A**, c) **A<sub>2</sub>B<sub>2</sub>**, e) **A<sub>2</sub>B<sub>6</sub>** and g) **A<sub>2</sub>B<sub>12</sub>** at the liquid-graphite interface self-assembled from a solution in 1-phenyloctane. Molecular packing motifs of **A**, **A<sub>2</sub>B<sub>2</sub>**, **A<sub>2</sub>B<sub>6</sub>** and **A<sub>2</sub>B<sub>12</sub>** are shown in panels b), d), f) and h), respectively. For clarity, bis-imine spacers, i.e. the aliphatic chains between C=N bonds, have been highlighted using different colours.

Structure	$a$ (nm)	$b$ (nm)	$\alpha$ (°)	$c$ (nm)	$d$ (nm)	$A$ (nm) <sup>2</sup>	$N_{mol}$	$A_{mol}$ (nm) <sup>2</sup>
<b>A</b>	$3.98 \pm 0.31$	$1.71 \pm 0.11$	$92 \pm 2$	NA	NA	$6.80 \pm 0.43$	6	$1.36 \pm 0.43$
<b>A<sub>2</sub>B<sub>2</sub></b>	$4.73 \pm 0.42$	$0.60 \pm 0.06$	$90 \pm 2$	$0.81 \pm 0.01$	$3.92 \pm 0.01$	$2.84 \pm 0.28$	1	$2.84 \pm 0.28$
<b>A<sub>2</sub>B<sub>6</sub></b>	$5.88 \pm 0.54$	$0.60 \pm 0.06$	$90 \pm 2$	$1.94 \pm 0.01$	$3.94 \pm 0.01$	$3.53 \pm 0.35$	1	$3.53 \pm 0.35$
<b>A<sub>2</sub>B<sub>12</sub></b>	$6.51 \pm 0.62$	$0.60 \pm 0.06$	$90 \pm 2$	$2.58 \pm 0.01$	$3.93 \pm 0.01$	$3.91 \pm 0.39$	1	$3.91 \pm 0.39$

Table 5.2-1. Unit cell parameters of **A<sub>2</sub>B<sub>2</sub>**, **A<sub>2</sub>B<sub>6</sub>** and **A<sub>2</sub>B<sub>12</sub>** monolayers. The variation in the diameters of the unit cell is caused only by contribution of the length of the diamine spacer in the bis-imine, here expressed as the sub-vector  $c$ .

In order to determine the enthalpic contribution to the adsorption energies of diamines and bis-imines, several MMFF calculations were performed with the program CHARMM<sup>[500–502]</sup> and the data are presented in Figure 5.2-3. It should be noted that the calculated values are the enthalpy contribution to the free energy of physisorption of an individual molecule, occupying a given surface area. When such adsorption energy is divided by the surface area occupied, the obtained value is, not surprisingly, constant for **A<sub>2</sub>B<sub>2</sub>**, **A<sub>2</sub>B<sub>6</sub>** and **A<sub>2</sub>B<sub>12</sub>** (see Table 5.2-2), which have a comparable molecular conformation.

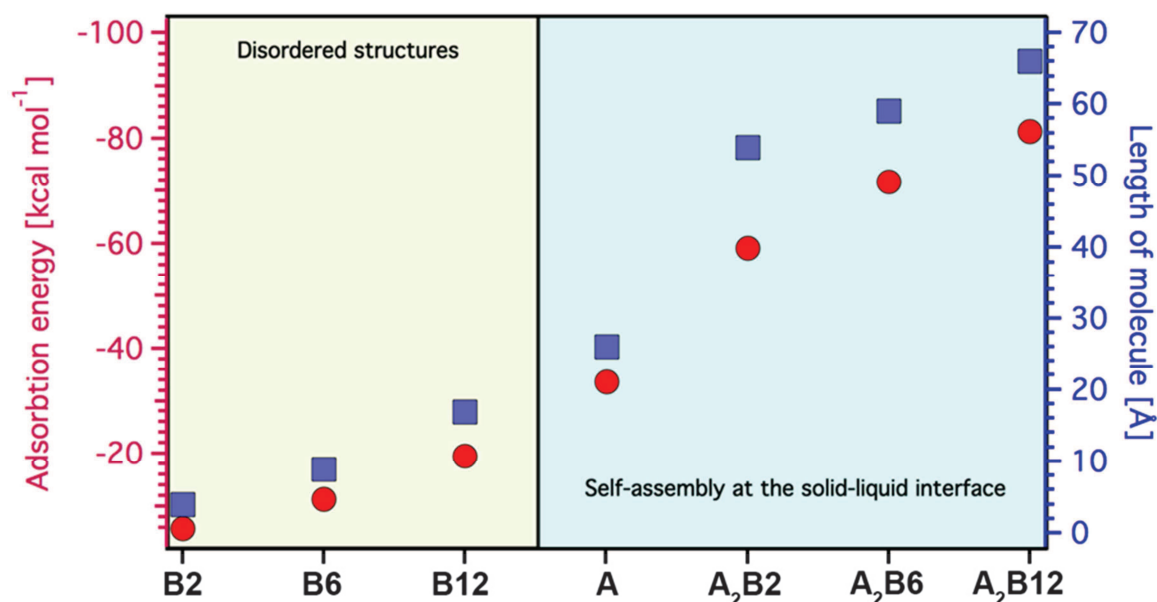


Figure 5.2-3 Comparison of adsorption energies. Adsorption energies of each molecule have been compared with the length of corresponding molecule. Low adsorption energies of diamines **B** prevent formation of order 2D crystalline structures on the HOPG surface.

Molecule	Area [nm <sup>2</sup> ]	dH [kcal mol <sup>-1</sup> ]	dH [eV]	dH/A [kcal mol <sup>-1</sup> / nm <sup>2</sup> ]	dH/A [eV / nm <sup>2</sup> ]
<b>A</b>	$1.36 \pm 0.43$	33.59	1.45	$24.69 \pm 5.92$	$1.06 \pm 0.25$
<b>A<sub>2</sub>B<sub>2</sub></b>	$2.84 \pm 0.28$	59.26	2.56	$20.86 \pm 1.86$	$0.90 \pm 0.08$
<b>A<sub>2</sub>B<sub>6</sub></b>	$3.53 \pm 0.35$	71.76	3.11	$20.32 \pm 1.82$	$0.88 \pm 0.08$
<b>A<sub>2</sub>B<sub>12</sub></b>	$3.91 \pm 0.39$	81.22	3.52	$20.77 \pm 1.88$	$0.90 \pm 0.08$

Table 5.2-2 Enthalpy contributions to the adsorption energy of **A**, **A<sub>2</sub>B<sub>2</sub>**, **A<sub>2</sub>B<sub>6</sub>** and **A<sub>2</sub>B<sub>12</sub>** molecules calculated for single molecules and also presented per nm<sup>2</sup>. Whereas the adsorption energies for single molecules differ largely, the energy gain per surface area is constant.

## 5.2.2. On-surface generation of bis-imines

STM was used to probe the *in situ* synthesis of bis-imines, i.e. synthesis of the bis-imines directly on the HOPG surface by condensation of the aldehyde **A** with diamines **B**. To this end, a 2  $\mu$ L



drop of 0.1 mM solutions (pyridine:1-phenyloctane, 1:99 v/v) of either **B2**, **B6** or **B12** was deposited on top of a monolayer of **A** pre-formed by applying a 4  $\mu\text{L}$  drop of a 0.1 mM solution (aldehyde:diamine ratio 2:1) of **A** in 1-phenyloctane on the HOPG surface. In all three cases, the addition of the diamine resulted in desorption of molecules **A** followed by formation of new type of 2D crystals. By comparison of the unit cell parameters, i.e. length of vectors  $a$  and  $b$ ,  $\alpha$  (angle between the vectors), unit cell area ( $A$ ) and number of molecules in the unit cell ( $N_{mol}$ ) these crystals were found to be identical (Figure 5.2-4) to the monolayers formed by dropcasting a solution of *ex situ* synthesized<sup>\*\*\*\*</sup> bis-imines and presented in Figure 5.2-2.

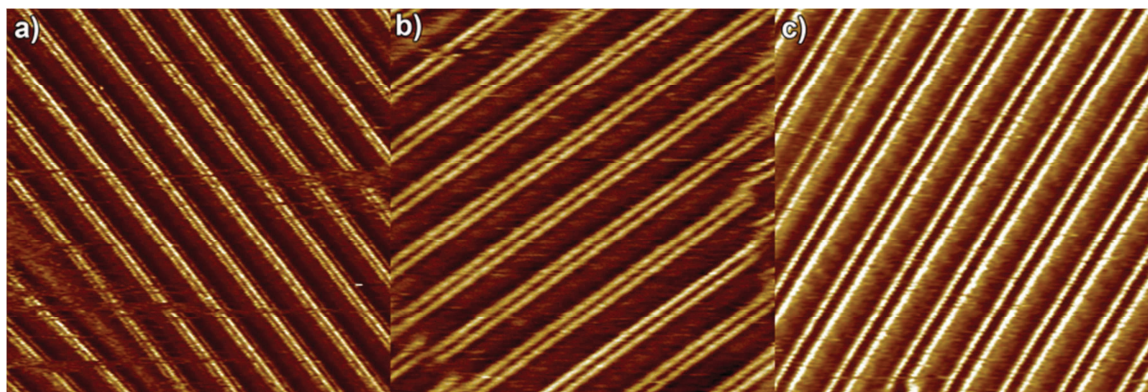


Figure 5.2-4 Comparison of 50 $\times$ 50 nm scale STM images of monolayers formed by the bis-imines **A<sub>2</sub>B<sub>2</sub>** (a), **A<sub>2</sub>B<sub>6</sub>** (b) and **A<sub>2</sub>B<sub>12</sub>** (c).

In most of the cases the size of domains amounts to thousands of  $\text{nm}^2$ . However in approximately 5 % of experiments the **A<sub>2</sub>B<sub>6</sub>** and **A<sub>2</sub>B<sub>12</sub>** bis-imines were found to self-assemble into smaller domains, as displayed in Figure 5.2-5. Only if the single domain sizes exceeded 100 $\times$ 100 nm the crystal was considered good for the imine exchange discussed in Section 5.2.4.

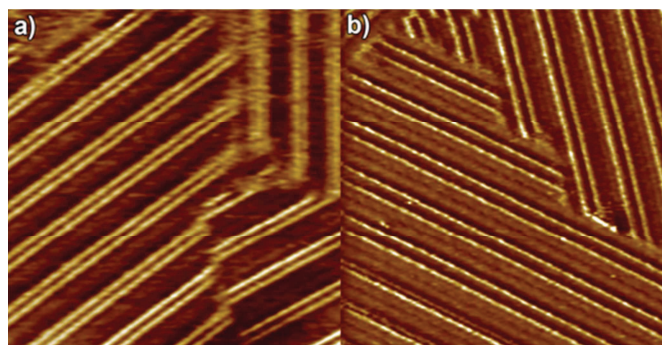


Figure 5.2-5 Comparison of 50 $\times$ 50 nm scale STM images of monolayers formed by bis-imines **A<sub>2</sub>B<sub>6</sub>** (a), **A<sub>2</sub>B<sub>12</sub>** (b), multiple domains are clearly visible.

Interestingly, the condensation reactions occurring at the solid-liquid interface were found to be very fast, fully covering the surface by the bis-imine products in less than 600 seconds after mixing. The timescale of the STM experiments is defined by the scanning rate of STM, which was fixed at 41 s per image. The *in situ* condensation experiments (20 independent experiments) were repeated and the drop was intentionally placed in different positions on the HOPG surface with respect to STM tip. In such a way the average time needed to completely cover the surface can be estimated. This finding was compared to the experiments in bulk solution followed by NMR.

<sup>\*\*\*\*</sup> In the text, *in situ* is used to describe the process performed directly on the HOPG surface, whereas *ex situ* concerns molecules synthesized and characterized by conventional organic synthesis.

### 5.2.3. Kinetics of bis-imine formation in solution

Initially, the condensation of the aldehyde **A** with the diamines **B** was studied by  $^1\text{H-NMR}$  in non-deuterated 1-phenyloctane. However, the solubility of the bis-imines in phenyloctane is rather low (between 1 – 7 mM) which render difficulties in quantification of the signals next to very strong signals coming from the non-deuterated solvent. On the other hand, aldehyde **A** is highly soluble in phenyloctane (up to 0.75 M) and therefore remains in solution during the entire condensation experiment whereas the bis-imines precipitate. To this end, the decrease of the aldehyde concentration could be followed by NMR in the course of the **A** + **B2** condensation in phenyloctane (with  $\text{d}_3$ -nitromethane as external standard in a sealed capillary). If  $\text{d}_8$ -toluene is chosen as a solvent, the solubility of the bis-imines is increased by a large amount and the reaction remains homogeneous even in equilibrium. For the purpose of comparison of the solvents, the **A** + **B2** condensation was performed in both solvents and the rates of aldehyde conversion to imines was followed (Figure 5.2-6).

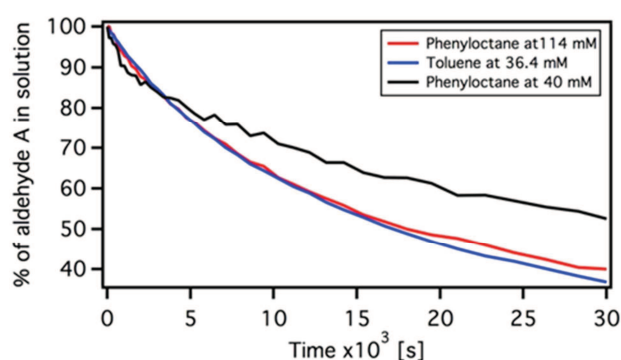


Figure 5.2-6  $^1\text{H-NMR}$  observation of the conversion of the aldehyde **A** to mono- and bis-imines of **B2**. Comparison in toluene and phenyloctane at various concentrations. The curves show the decrease of the  $-\text{CHO}$  aldehyde proton signal (8.53 ppm in phenyloctane and 9.70 ppm in toluene).

In phenyloctane, precipitation of **A<sub>2</sub>B2** was observed when a critical concentration between 3.5 – 7 mM of **A<sub>2</sub>B2** was reached. The kinetic curves (Figure 5.2-7) for the conversion of **A** and formation of the imines **A<sub>1</sub>B2** and **A<sub>2</sub>B2** are consistent with a second order kinetic model up to this point, beyond it, precipitation causes irreversible removal of **A<sub>2</sub>B2** from the reaction mixture.

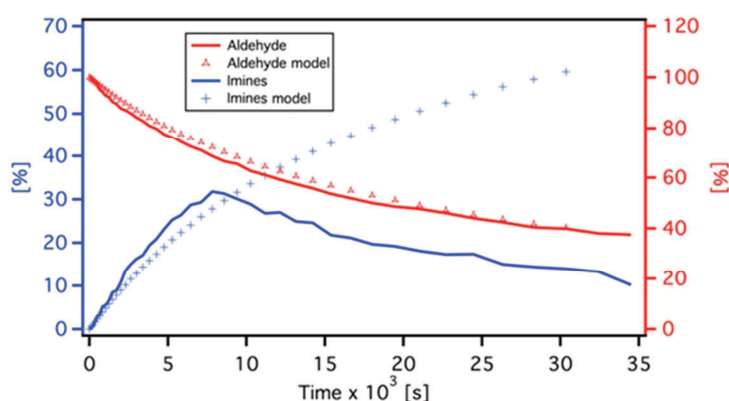


Figure 5.2-7  $^1\text{H-NMR}$  observation of the conversion of aldehyde **A** to mono-imine **A<sub>1</sub>B2** and bis-imine **A<sub>2</sub>B2** in phenyloctane at 114 mM **A** and 57 mM **B2** concentration. The red solid trace is experimental observation of disappearance of the aldehyde  $\text{CHO}$  peak (8.53 ppm), the blue solid trace is the sum of the emerging signals of the mono- and the bis-imine (6.86 and 6.89 ppm, respectively). Both traces are compared with conversions calculated (dotted traces) from the second order kinetic model. The mismatch between observed and calculated imines trace at times longer than  $8 \times 10^3$  s is related to the precipitation of the bis-imine from the solution.

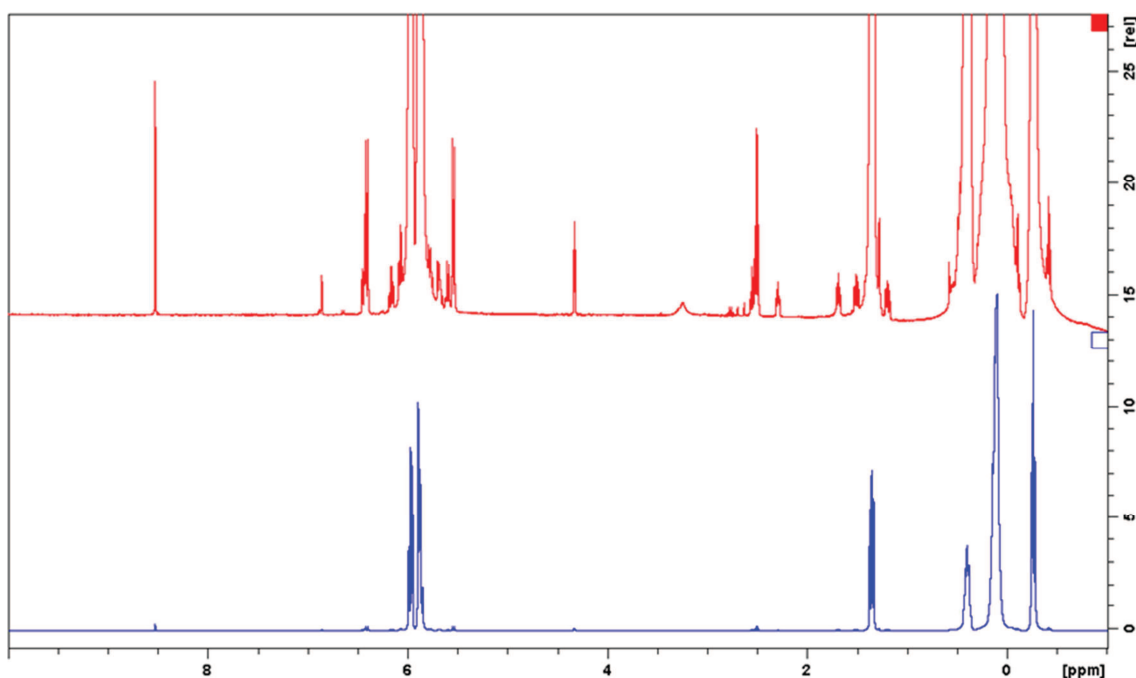


Figure 5.2-8  $^1\text{H-NMR}$  spectra of the reaction **A** + **B2** in phenyloctane (blue trace gives an overview on the full NMR spectrum, red trace is amplified to show the relevant reagent signals: aldehyde peak at 8.53 ppm, mono-imine peak at 6.86 ppm, bis-imine peak at 6.89 ppm, in the aliphatic region the signal at 1.28 ppm corresponds to free **B2**, two triplet at 1.69 and 2.29 ppm correspond to two methylene groups of the mono-imine, and the singlet at 2.70 ppm corresponds to the bis-imine, low in intensity due to precipitation).

It is seen that the kinetics of condensation in toluene and phenyloctane are very similar (slightly slower in phenyloctane). Thus, the rate of the reaction in phenyloctane cannot be higher than in toluene and the data obtained in  $d_8$ -toluene are asymptotic limits for the rates in phenyloctane. Taking into account the poor solubility in 1-phenyloctane, the following kinetic data are therefore derived from  $^1\text{H-NMR}$  experiments in  $d_8$ -toluene.

The condensation reaction of a diamine **B** with the aldehyde **A** to form first the mono-imine and consequently the bis-imine is described by the following general scheme.

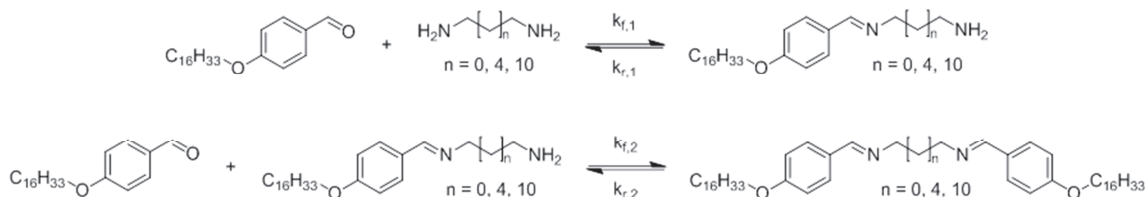


Figure 5.2-9 General scheme for the condensation of aldehyde **A** with a diamine.

As the diamine **B** possesses two functional groups, the actual concentration of amino groups  $[B]$  is twice as high as the diamine concentration. Taking into account the reversibility of the reaction and the fact that the observed rate is the sum of the forward and backward rates  $k_i = k_{f,i} + k_{r,i}$  connected by the equilibrium constant  $K_i = \frac{k_{f,i}}{k_{r,i}}$ , one obtains a set of differential equations:

$$\frac{d[A]}{dt} = -k_1[A - A_{\text{eq}}][B - B_{\text{eq}}] - k_2[A - A_{\text{eq}}][A_1B - A_1B_{\text{eq}}] \quad (\text{E1})$$

$$\frac{d[A_1B]}{dt} = k_1[A - A_{\text{eq}}][B - B_{\text{eq}}] - k_2[A - A_{\text{eq}}][A_1B - A_1B_{\text{eq}}] \quad (\text{E2})$$

$$\frac{d[A_2B]}{dt} = k_2[A - A_{\text{eq}}][A_1B - A_1B_{\text{eq}}] \quad (\text{E3})$$

The initial ( $t=0$ ) and final ( $t=\infty$ ) boundary conditions are the initial  $[A]_0$ ,  $[B]_0$ ,  $[A_1B]_0$  and  $[A_2B]_0$  and the equilibrium  $[A]_{eq}$ ,  $[B]_{eq}$  and  $[A_1B]_{eq}$  concentrations, which are experimentally available by  $^1\text{H-NMR}$ . This set of differential equations can then be solved iteratively in Excel to obtain the second order rate constants. When aldehyde **A** (2 eq., 36.4 mM) is mixed with **B2** diamine (1 eq., 18.2 mM) in toluene, slow formation first of mono-imine and subsequently of bis-imine is observed in the CH=N imine proton region (peak at 8.02 ppm for the mono-imine and at 8.10 ppm for the bis-imine) and in the aliphatic region (peak 2.38 ppm for free ethylenediamine, triplet at 2.89 ppm and 3.48 ppm for mono-imine, and peak 3.99 ppm for bis-imine, for NMR traces see Figure 5.2-11).

The equilibrium is reached after approximately 48 hours and contains 80 % bis-imine, 10 % mono-imine and 10 % unreacted aldehyde. The solutions are homogenous, even at a concentration as high as 180 mM. By plotting the integral intensity of the corresponding signals (aldehyde 9.70 ppm, mono-imine 8.02 ppm and bis-imine 8.10 ppm) the rate constants can be determined by iteratively solving the equations E1-E3. The values obtained for the second order rate constants (as defined in Figure 5.2-9) are  $k_1 = 2.0 \times 10^{-3} \text{ s}^{-1} \text{ M}^{-1}$  and  $k_2 = 2.7 \times 10^{-3} \text{ s}^{-1} \text{ M}^{-1}$  with a very good coefficient of determination  $R^2 = 0.9975$  (experimental and fitted curves in Figure 5.2-10).

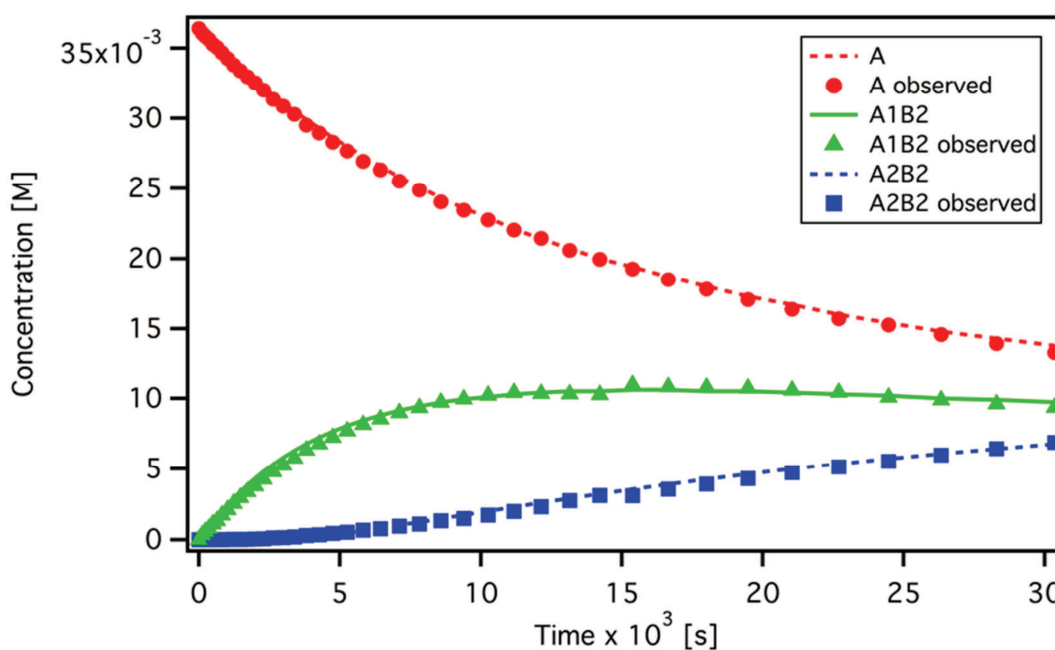


Figure 5.2-10  $^1\text{H-NMR}$  observation of species formation in the reaction of 2 eq. of **A** with 1 eq. of **B2** in  $d_8$ -toluene ( $R^2=0.9975$ ); average of four runs; data based on the integration of the signals of aldehyde 9.70 ppm, mono-imine 8.02 ppm and 8.10 ppm).

With the rate constants in hand, one can estimate the kinetics of the imine formation process in the drop on the HOPG surface in the STM measurement. To fully cover the STM surface ( $1 \text{ cm}^2$ ) a total amount of  $3.5 \times 10^{13}$  of **A<sub>2</sub>B<sub>2</sub>** molecules is needed to be produced by the condensation reactions ( $2.5 \times 10^{13}$  in case of **A<sub>2</sub>B<sub>12</sub>**), based on the area of a unit cell. By mixing 4  $\mu\text{L}$  of 0.1 mM solution of aldehyde **A** with 2  $\mu\text{L}$  of 0.1 mM solution of diamine **B** one gets 6  $\mu\text{L}$  of the solution with the concentration of  $6.67 \times 10^{-5} \text{ M}$  of the aldehyde and  $3.33 \times 10^{-5} \text{ M}$  of the diamine. This means that the required concentration of the bis-imine **A<sub>2</sub>B<sub>2</sub>** in the supernatant solution is  $9.7 \times 10^{-6} \text{ M}$  ( $6.9 \times 10^{-6} \text{ M}$  for **A<sub>2</sub>B<sub>12</sub>**). From the known rate constants and initial concentrations the model given by equations E1-E3 indicates that the reaction time needed to reach this concentration of **A<sub>2</sub>B<sub>2</sub>** is approximately  $1.25 \times 10^7 \text{ s}$ . The fact that full surface coverage is achieved in less than 600 seconds gives rate acceleration by a factor of about  $2 \times 10^4$ .

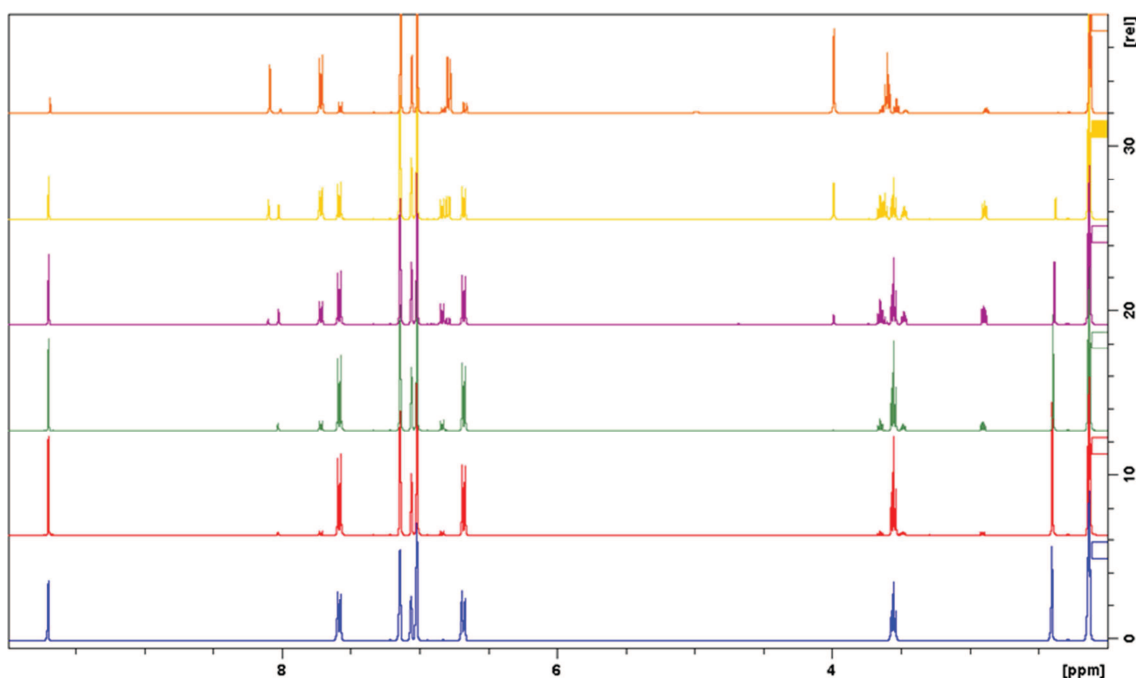


Figure 5.2-11  $^1\text{H-NMR}$  spectra of the reaction of two equivalents of **A** with 1 eq. of **B2** in  $d_8$ -toluene (aldehyde peak at 9.70 ppm, mono-imine peak at 8.02 ppm, bis-imine peak at 8.10 ppm; in the aliphatic region the signal at 2.38 ppm corresponds to the methylene groups of free **B2**, the two triplets at 2.89 and 3.48 ppm correspond to the two methylene groups of the mono-imine, and the singlet at 3.99 ppm corresponds to the bis-imine).

To increase the solubility of the diamines (most importantly **B12**), 1 % of pyridine was added to the 1-phenyloctane solvent. To verify the effect of pyridine, the kinetic experiment for the condensation of the aldehyde **A** with the diamine **B2** was reproduced in  $d_8$ -toluene containing 1 % of pyridine and compared to the experiment without pyridine. The rates of the aldehyde conversion to both mono- and bis-imines are identical (Figure 5.2-12), thus showing that a pyridine content up to 1 % does not affect the kinetics of the processes discussed above.

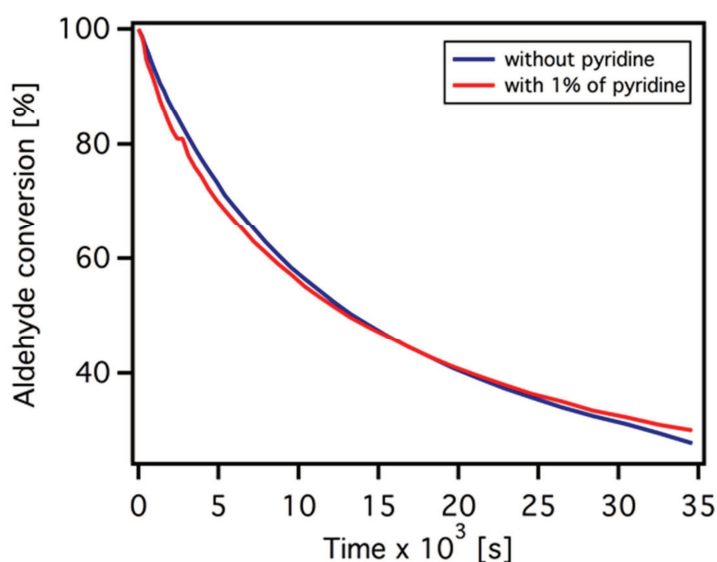


Figure 5.2-12 Conversion of the aldehyde **A** (36.4 mM) to imines in the reaction with **B2** (18.2 mM), comparison of the reaction rates in  $d_8$ -toluene without and with 1 % of pyridine.

The striking acceleration of imine formation of the HOPG surface as compared to bulk solution can be most likely because of two main reasons: (1) at the solid-liquid interface the concentration is at least higher than a saturation regime whereas in solution the concentration is



typically much lower; (2) the pre-ordering of molecules at the surface may facilitate the reaction by lowering the activation barrier. In the present case, the rates and rate constants of the condensation and exchange reactions determined by  $^1\text{H-NMR}$  revealed that the acceleration is in the range of four orders of magnitude. Furthermore, the kinetic experiments in phenyloctane, if available, might indicate even higher acceleration at solid-liquid interface, where molecules have to proceed through desorption-reaction-readsorption sequence.

#### 5.2.4. Surface assisted transimination

In order to fully explore the reversible nature of  $\text{C}=\text{N}$  bonds, and to gain insight into the bis-transimination processes of  $\text{A}_2\text{B}$  molecules, successive *in situ* imine-formation/bis-imine-exchange cycles were performed. As shown before, upon *in situ* addition of 0.5 eq of **B2** on top of a pre-existing monolayer of **A** (Figure 5.2-13a), the  $\text{A}_2\text{B}_2$  motif was obtained (Figure 5.2-13b). Upon subsequent addition of **B6** (0.5 eq) solution, the  $\text{A}_2\text{B}_2$  monolayer was transformed into an  $\text{A}_2\text{B}_6$  structure (Figure 5.2-13c). Finally, the addition of a drop of **B12** (0.5 eq) solution resulted in the formation of an  $\text{A}_2\text{B}_{12}$  2D pattern (Figure 5.2-13d). From the mechanistic point of view, once transimination is taking place on a single molecule embedded in a molecular lamella (typically positioned at the domain boundaries), a structural defect in the supramolecular 2D structure is created. This structural defect can act as seed for the disassembly of adjacent molecules, ultimately leading to the transformation of the entire adlayer.

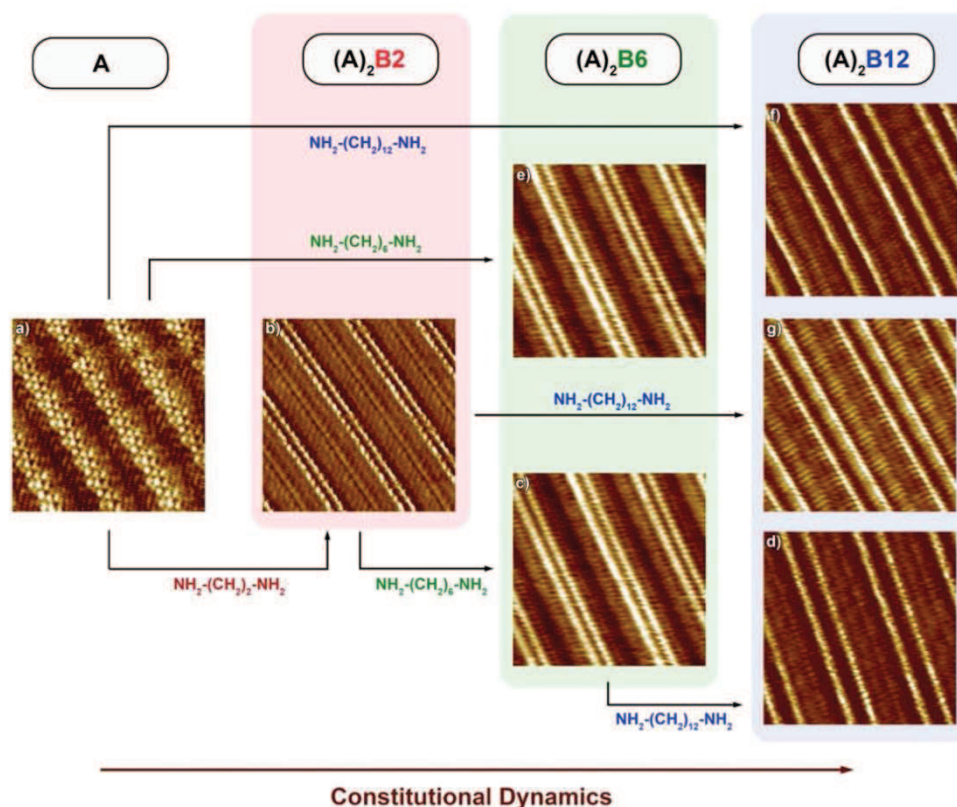


Figure 5.2-13 STM representative images of *in situ* bis-transimination processes. a) monolayer of **A**, b) monolayer of  $\text{A}_2\text{B}_2$ , c) and e) monolayer of  $\text{A}_2\text{B}_6$ , d), f) and g) monolayer of  $\text{A}_2\text{B}_{12}$ . Tunneling parameters:  $I_t = 10 - 15$  pA,  $V_t = 400 - 600$  mV. The size of the STM images (a-g) amounts to  $18 \times 18$  nm. Diamines are colour coded: **B2** red, **B6** green, **B12** blue.

While in the case of **A** + **B** condensations the addition of diamine was always followed by a desorption/adsorption process (lasting ca. 10 min), bis-transimination reactions ( $\text{A}_2\text{B}_2$  to  $\text{A}_2\text{B}_6$  and  $\text{A}_2\text{B}_6$  to  $\text{A}_2\text{B}_{12}$ ) were found to be much faster. Interestingly, the rate of the bis-transimination processes and the formation of the new monolayer structures depends on the length of  $\alpha,\omega$ -diamine,

e.g. **A<sub>2</sub>B<sub>2</sub>** monolayers transform into **A<sub>2</sub>B<sub>6</sub>** after  $3.0 \pm 0.3$  min of desorption/re-adsorption process, whereas **A<sub>2</sub>B<sub>12</sub>** monolayers are formed after  $1.0 \pm 0.1$  min after addition of **B<sub>12</sub>** solution on top of the **A<sub>2</sub>B<sub>6</sub>** structure.

Furthermore, it is important to note that although the number of components in the supernatant solution during the consecutive bis-transiminations increases, only one type of supramolecular pattern is formed at the solid-liquid interface. This surface selection for only one type of bis-imine to be adsorbed can be explained by the different free energies of physisorption of bis-imines with altered **B** units.

The physisorption is an exothermic reaction ruled by the free energy minimization. The minimization of the enthalpy is achieved by maximum packing density at surfaces, which can be equally obtained by formation of tight 2D assemblies of either short (**A<sub>2</sub>B<sub>2</sub>**) or long molecules (**A<sub>2</sub>B<sub>12</sub>**), as calculated in Table 5.2-2. Conversely, because of translational entropy reasons the adsorption of longer versus shorter molecules at the interface is favoured, since upon immobilization at the interface the molecules lose translational entropy *per particle*. Thus, there is higher entropy cost for the adsorption of smaller than for larger/longer molecules as more of small molecules are required for covering the same surface area.

For longer chains the entropic contribution per unit mass to the overall free energy increases due to the reduced configurational space of the molecule at the interface.<sup>[503]</sup> Therefore the preferential physisorption of the molecules comprising the longer bridge, i.e. **A<sub>2</sub>B<sub>12</sub>**, with respect to the shorter **A<sub>2</sub>B<sub>2</sub>** and **A<sub>2</sub>B<sub>6</sub>** at the solution-graphite interface may be considered an entropy driven selective adsorption.

To complete the exchange reaction network, bis-transimination of **A<sub>2</sub>B<sub>2</sub>** with **B<sub>12</sub>** resulted in the formation of **A<sub>2</sub>B<sub>12</sub>** monolayers. It was thus shown that all bis-imine exchange reactions proceed to provide a bis-imine which has higher affinity to the HOPG surface (Figure 5.2-14).

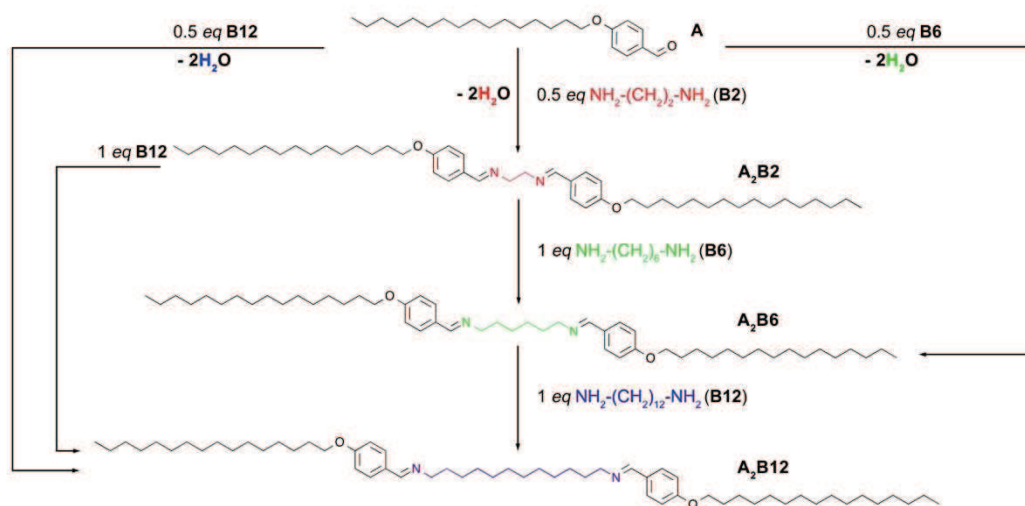


Figure 5.2-14. Condensation of **A** with  $\alpha,\omega$ -diamines, and schematic representation of diamine exchange on the bis-imines investigated at the solid-liquid interface. Diamines are colour coded: **B<sub>2</sub>** red, **B<sub>6</sub>** green, **B<sub>12</sub>** blue.

### Real-time bis-transimination

In order to cast light onto dynamic process of *in situ* bis-transimination, several consecutive images have been recorded after addition of 1 eq. of **B<sub>12</sub>** on top of a pre-existing monolayer of **A<sub>2</sub>B<sub>2</sub>**,

and are shown in Figure 5.2-15. Upon addition of **B12** solution it was possible to visualise step-wise bis-transimination by STM. The Figure 5.2-15a shows the image taken immediately after depositing a drop of **B12**. Obviously the reaction cannot be observed at the single molecule level. During the continuous scan (Figure 5.2-15b-f) over the same sample area, the area of **A<sub>2</sub>B2** domain (indicated in red) decrease, indicating the progress of bis-transimination reaction, and formation of **A<sub>2</sub>B12** domains (in purple).

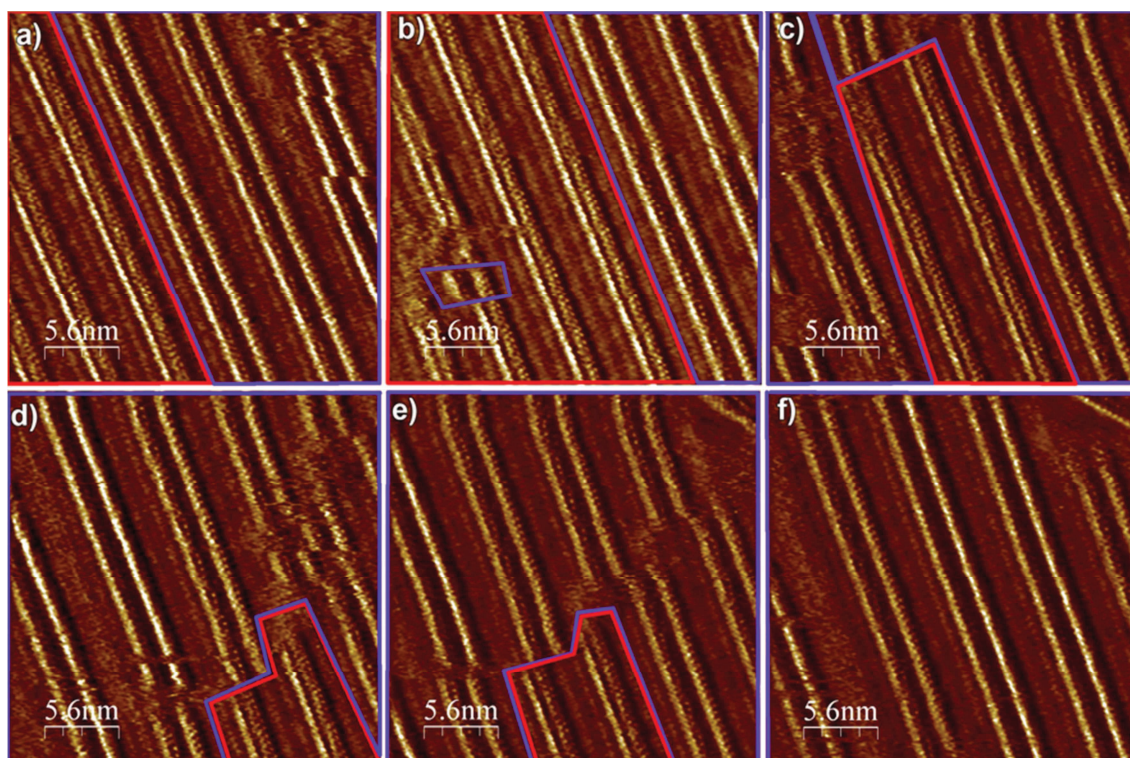


Figure 5.2-15 Series of consecutive STM images showing the exchange reaction at the solid-liquid interface from the **A<sub>2</sub>B2** structure (in red) to **A<sub>2</sub>B12** (in purple). Tunnelling parameters  $I_t = 15 \text{ pA}$ ,  $V_t = 550 \text{ mV}$ . The size of the STM images (a-f) is to  $28 \times 28 \text{ nm}$ .

### 5.2.5. Kinetics and equilibria of transimination by NMR

The bis-transimination, i.e. the **A<sub>2</sub>B2** + **B6** exchange reaction, was investigated in toluene and followed by <sup>1</sup>H-NMR at 600 MHz. The higher field led to partial separation of the **A<sub>1</sub>B6** and **A<sub>2</sub>B6** signals, which can therefore be deconvoluted. To the equilibrated reaction mixtures from the imine formation experiments (Section 5.2.3), 1 eq. of 18.2 mM solution of **B6** in d<sub>8</sub>-toluene was added (reagent ratio **A:B2:B6** = 2:1:1, theoretical concentrations 33.1 : 16.5 : 16.5 mM). The evolution of the <sup>1</sup>H-NMR signals is shown in Figure 5.2-16. Immediate decrease of the signals belonging to **A<sub>2</sub>B2** (both azomethine and aliphatic) is observed with concomitant appearance of the signal of **A<sub>1</sub>B6**. The signal of **B2** is increasing at a slower rate as it is liberated by the double transimination reaction. The signal of **A<sub>2</sub>B6** starts to emerge after a lag time of about 20 minutes. The equilibrium is reached in about 4 hours. Interestingly, the equilibrated mixture contains more of the bis-imine of **B6** than that of **B2**, and conversely more mono-imine of **B2** than **B6**. This can be due to proximity of sterically demanding aldehyde groups in case of the bis-imine **A<sub>2</sub>B2**. For the ease of comparison, the signals in the Figure 5.2-16 were normalized for the number of protons they comprise, in a way that azomethine signal of bis-imines was divided by 2, signal of free **B2** divided by 4 etc., so they are representative for the relative concentration of the species in solution. Signals which are overlapping (like -CH<sub>2</sub>NH<sub>2</sub> signals of **B6** and **A<sub>1</sub>B6** or non-deconvoluted **A<sub>x</sub>B6** azomethine signal) were not normalized and are plotted in respect to secondary ordinate axes.



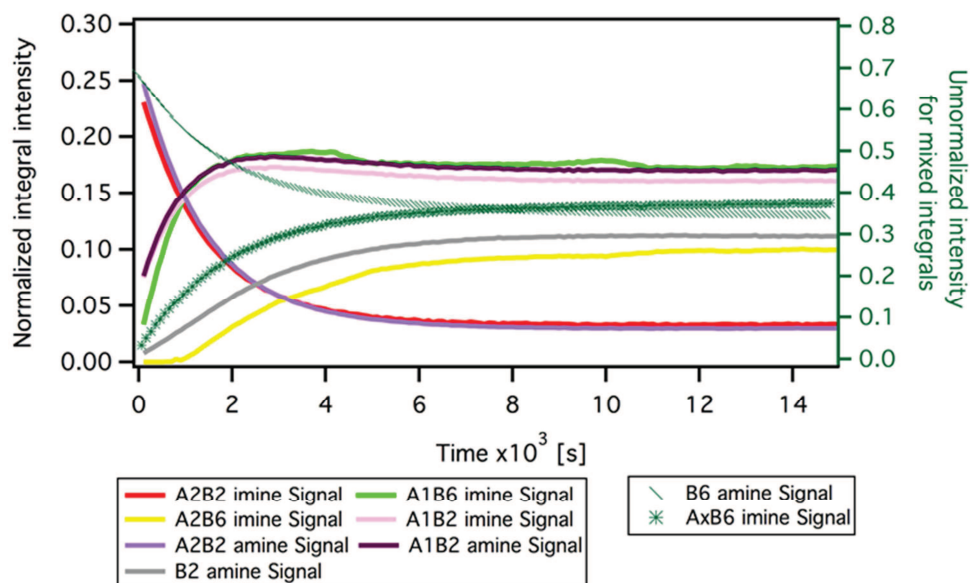


Figure 5.2-16 Signal evolution in the exchange experiments followed by 600 MHz  $^1\text{H-NMR}$ . The NMR signals are normalized for the number of protons, i.e. the signal for  $\text{A}_2\text{B}_x$  is divided by two that for  $\text{B}_2$  divided by 4 etc., so that they correspond to the relative concentrations in solution. Mixed signals ( $\text{B}_6$  amine and  $\text{A}_x\text{B}_6$  imine signals), due to the overlap of the signals from several species, cannot be normalized and are plotted with respect to the right ordinate axis.

The re-equilibration of the reaction mixtures proceeds through several reactions

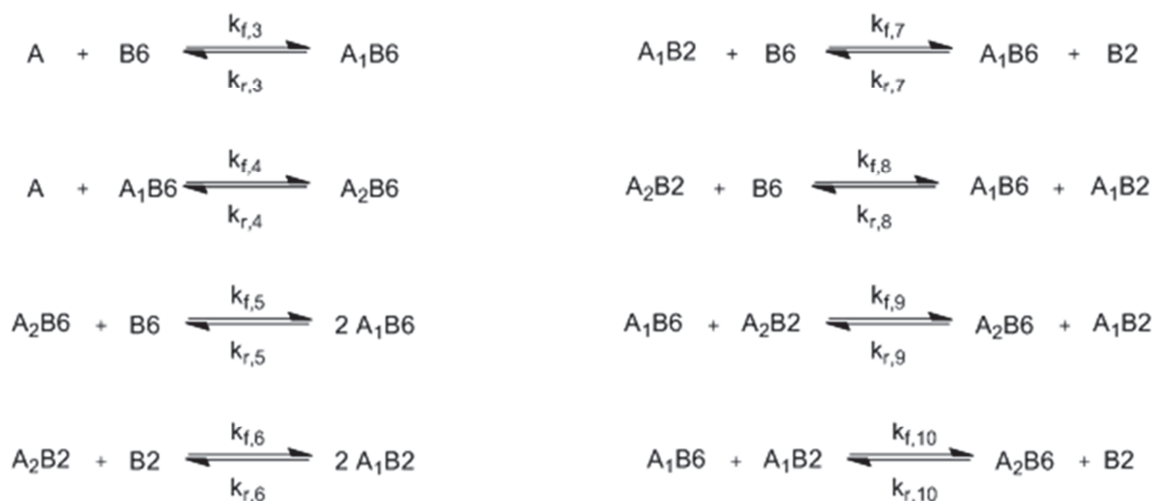


Figure 5.2-17 General scheme for imine exchange processes in the  $\text{A}_2\text{B}_2 + \text{B}_6$  reaction. Due to incomplete conversion, about 10 % of  $\text{A}$  is present as free aldehyde in the solution. However, the timescale for condensation reaction was previously shown to be much higher than for the exchange.

As a result of this complex reaction network, it is difficult to establish a kinetic model. To fully cover the  $1 \text{ cm}^2$  of HOPG surface with  $\text{A}_2\text{B}_6$ ,  $2.8 \times 10^{13}$  molecules are needed (calculated from the unit cell area of a single  $\text{A}_2\text{B}_6$  molecule as reported in Table 5.2-1), which corresponds to  $5.6 \times 10^{13}$  of aldehyde residues. The total amount of aldehyde molecules added is  $2.4 \times 10^{14}$  and thus about 23 % of the aldehyde needs to be transformed to  $\text{A}_2\text{B}_6$  to achieve full surface coverage, as observed by STM in less than 3 minutes. As the imine exchange follows first-order kinetics, the time needed to

reach defined conversion is independent of starting concentration.<sup>§§§§</sup> The time needed to achieve this conversion in solution at 16.5 mM concentration of **B6** as followed by NMR is about 1.1 hours, indicating again kinetic enhancement of the reaction on the HOPG surface. The NMR traces of the kinetic run are given in Figure 5.2-18 (azomethine and aromatic region) and Figure 7.7-1 in the Experimental part (aliphatic region).

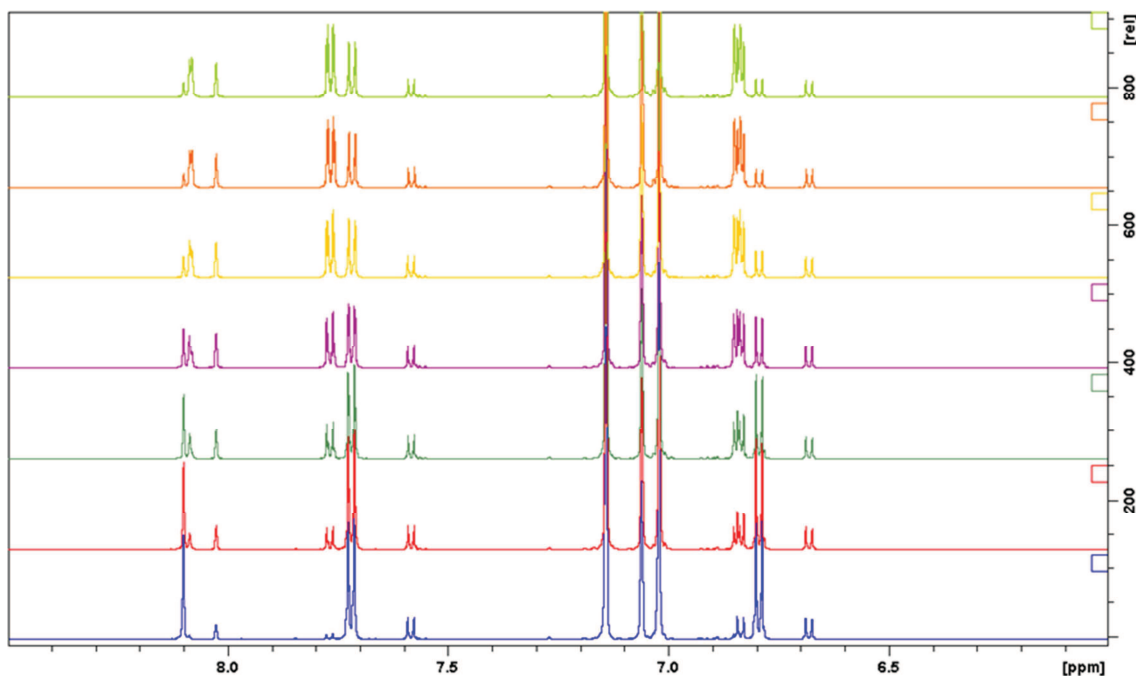


Figure 5.2-18  $^1\text{H-NMR}$  (at 600 MHz, aromatic region) of the signal evolution during the  $\text{A}_2\text{B}_2 + \text{B}_6$  imine exchange reaction (the peaks assignment:  $\text{A}_2\text{B}_2$  8.10 ppm,  $\text{A}_1\text{B}_6$  8.09 ppm,  $\text{A}_2\text{B}_6$  8.08 ppm,  $\text{A}_1\text{B}_2$  8.02 ppm).

### 5.2.6. Reverse in situ bis-transimination

The reversible imine exchange on surface, shown in previous sections, proceeds smoothly when performed in sequence leading to larger/longer molecules. It is however necessary to demonstrate that the HOPG surface does not lead irreversible formation and adsorption of the longest of possible bis-imines. To this extent, a drop of equimolar amounts of **B6** and/or **B2** solutions were applied on top of a pre-existing monolayer of  $\text{A}_2\text{B}_{12}$ , but the diamine exchange was not observed, confirming the significance of the free energy of physisorption in governing the monolayer stabilization. However, by changing the bis-transimination conditions, especially the concentration of the diamine deposited on top of the  $\text{A}_2\text{B}_{12}$  monolayer, the equilibrium of the diamine exchange process can be shifted towards the species incorporating a shorter **B** unit. To this end, 100 eq. of **B6** (2  $\mu\text{l}$  of a 20mM solution in pyridine:1-phenyloctane, 1:99 vol:vol) was applied on top of the  $\text{A}_2\text{B}_{12}$  monolayer (Figure 5.2-19a). After ca. 280 min, the formation of bi-component architectures was observed, as indicated in Figure 5.2-19b, showing the co-existence of  $\text{A}_2\text{B}_{12}$  (blue arrows) and  $\text{A}_2\text{B}_6$  (green arrows) lamellae. While  $\text{A}_2\text{B}_6 + \text{B}_{12}$  bis-transimination process is very rapid (1 min), the  $\text{A}_2\text{B}_{12} + \text{B}_6$  reaction was completed (on the surface) only after ca. 430 min, as evidenced by the disappearance of  $\text{A}_2\text{B}_{12}$  lamellae (over 1  $\mu\text{m}^2$  area, accessible with STM).

<sup>§§§§</sup> The evaluation of time needed for 23 % conversion is analogous to the evaluation of the half-life of first order kinetics reaction, giving  $t_{\text{conversion}} = \frac{-\ln(\text{conversion})}{k}$ .

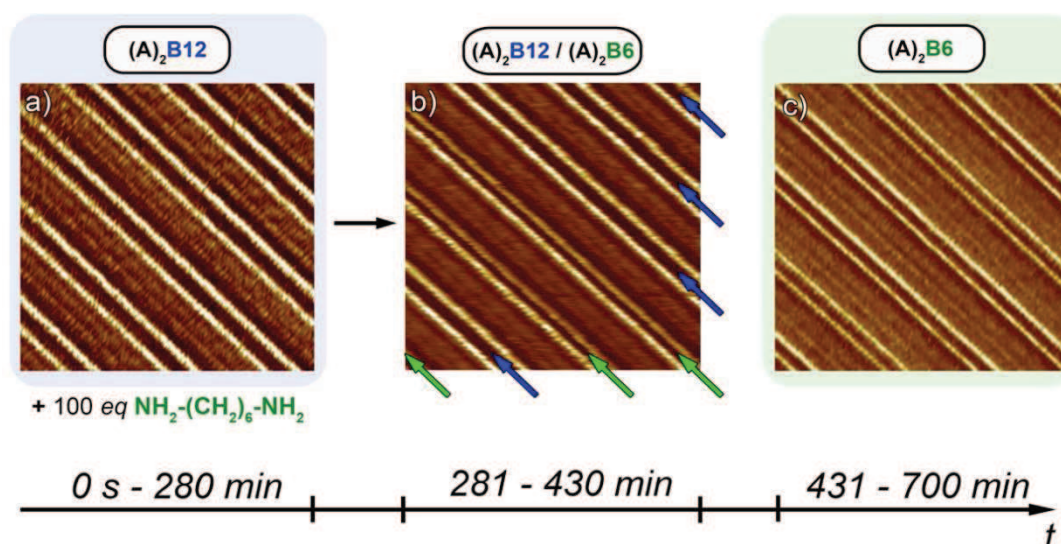


Figure 5.2-19. STM representative images of **A<sub>2</sub>B12** transition into **A<sub>2</sub>B6**. a) **A<sub>2</sub>B12** monolayer, b) co-existing **A<sub>2</sub>B12** and **A<sub>2</sub>B6** domains, c) **A<sub>2</sub>B6** monolayer. The size of the STM images (a-c) amounts to 28 × 28 nm.

It is important to point out, that NMR of the same reaction mixture (2 eq. **A** + 1 eq. **B12** + 100 eq. **B6**) does not contain any bis-imine. Also, even smaller ratios of **B6** added to **A<sub>2</sub>B12** (about 10 eq.) leads to complete transimination of **A<sub>2</sub>B12** into mono-imines and free diamine. This comparison shows the selective amplification of formation of species which have the highest free energy of adsorption (Section 5.2.7).

It is noteworthy that neither **A<sub>2</sub>B12** + **B2** nor **A<sub>2</sub>B6** + **B2** bis-transimination reactions could be accomplished at the solid-liquid interface. Despite exploring very high molar ratios (up to 1000 eq. of diamine **B2**), as well as long reaction times (up to 2 days) by the means of STM, neither the coexistence of different species, nor the diamine exchange could be observed, probably due to evaporation of relatively volatile **B2** before the reaction can take place.

### 5.2.7. On surface selection in dynamic imine library

Dynamic combinatorial libraries are able to undergo constituent amplification in a mixture through component selection in response to a physical stimulus or a chemical effector.<sup>[6,20,21,25,26,309,451,504]</sup> In view of the results above, it was of interest to examine the effect of surface adsorption forces on the set of bis-imines investigated. Experiments were conducted both by STM and NMR to investigate the occurrence of such features on a surface.

Upon deposition of a drop of 0.1 mM equimolar solution of **A<sub>2</sub>B2**, **A<sub>2</sub>B6** and **A<sub>2</sub>B12** only the **A<sub>2</sub>B12** patterns were observed on the HOPG surface, indicating surface induced selection of the library constituent presenting the thermodynamically most stable physisorption. In order to confirm the selective nature of pattern formation, experiment was reproduced 10 times and each time 1 μm<sup>2</sup> surface area (accessible with STM) has been monitored. For each set of experiment, **A<sub>2</sub>B12** patterns were formed within tens of seconds and covered the entire surface of graphite.

The strong selection observed by STM on the HOPG surface was compared to experiments in solution. In d<sub>8</sub>-toluene, the aldehyde **A** (4 eq., 80 mM) was mixed with **B2** (1 eq.) and **B12** (1 eq.) to favour the formation of the corresponding bis-imines **A<sub>2</sub>B2** and **A<sub>2</sub>B12** over the mono-imines (such case is discussed together with kinetics in Section 5.2.5). The mixture was heated at 60 °C overnight to reach the equilibrium. Since precipitation of some bis-imines was observed at room temperature, the NMR spectra were recorded at 50 °C when the solutions were homogenous. In the equilibrated mixture the bis-imines are formed almost quantitatively, approximately 10 % of the aldehyde



remains unreacted which is reflected by approximately 10 % of the  $A_1B_2$  mono-imine formation, while the  $A_1B_{12}$  mono-imine is present in less than 2 %. This can be due to the proximity of sterically demanding aldehyde groups in case of the bis-imine  $A_2B_2$ , in agreement with previous observations (Figure 5.2-16). The bis-imines are formed in the similar amounts, thus indicating that there is no selection for either of the bis-imines formed.

In the next experiment, all three diamines **B2**, **B6** and **B12** (1 eq. and 20 mM each) were reacted in the NMR tube with 6 eq. of aldehyde **A**. Again, the equilibrium was reached by heating at 60 °C overnight and the NMR spectra were recorded at 50 °C to dissolve the precipitate formed in the course of the reaction. In the equilibrated mixture, the bis-imines are formed almost quantitatively, only 8 % of the aldehyde remains unreacted which is reflected by approximately 10 % formation of the  $A_1B_2$  mono-imine while other mono-imines are present only in < 4 % amount (i.e. < 2 % each), again in agreement with previous observations. The bis-imines are formed in the same amounts (with slightly lower amount of  $A_2B_2$ ), thus indicating that there is no selection for either of the bis-imines formed.

Additional STM *in situ* bis-imine selection experiments have been performed to in order explore the potential role of the adsorption energy (which differ for each  $A_2B$  compound), acting as selection/amplification effector. To this end, a 4  $\mu$ L drop containing a mixture of 2 eq. of **A** and three diamines **B2** + **B6** + **B12** (1 eq. and 0.1 mM each) was deposited on top of HOPG surface. Statistical analysis of 10 independent experiments revealed that in majority of experiments patterns of  $A_2B_{12}$  were formed exclusively. However, in 2 out of 10 experiments coexistence of two structures was observed for relatively short period of time (1-3 min) as illustrated in Figure 5.2-20.

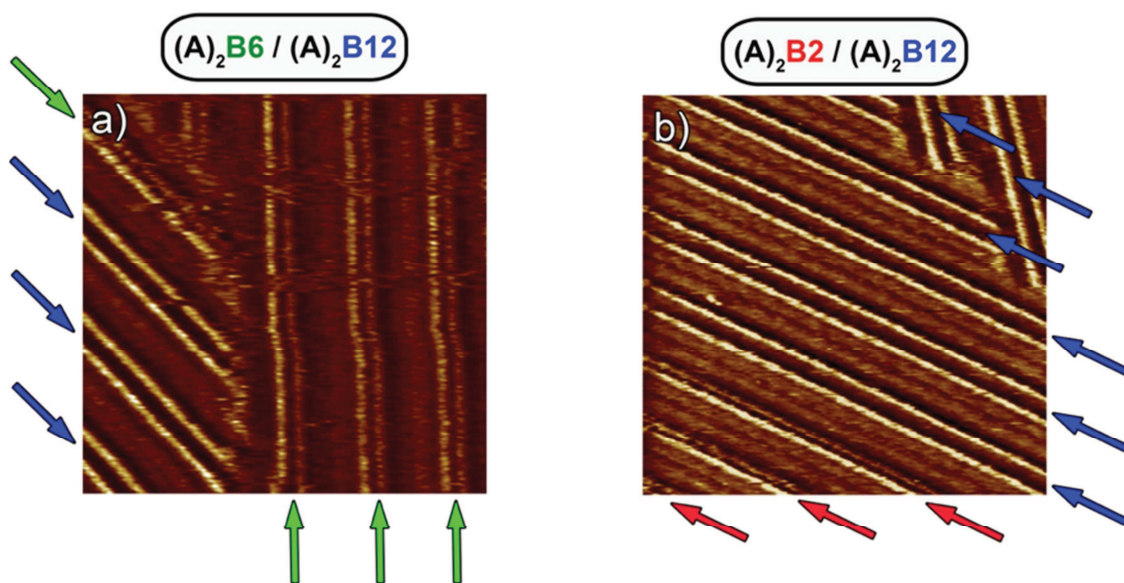


Figure 5.2-20 STM representative images of co-existing  $A_2B$  structures. a) co-existing  $A_2B_6$  and  $A_2B_{12}$  domains, b) co-existing  $A_2B_2$  and  $A_2B_{12}$ . The size of the STM images (a-b) amounts to 30  $\times$  30 nm.

Analysis of the corresponding NMR experiment in toluene, i.e. sample containing 2 eq. of **A** and three diamines **B2** + **B6** + **B12** (1 eq. and 20 mM each), did not provide any reliable insight. Therefore, HPLC analysis of the mixture was performed. To this end, NMR sample (0.5 mL) was reduced by  $Bu_4NBH_4$  (to freeze the imine exchange), acidified by methanolic HCl, evaporated, dissolved in 0.2 mL of methanol and finally injected into the HPLC apparatus (10  $\mu$ L per run). The analysis was repeated five times, run 1 was ignored and the signals from run 2 – 5 were averaged for calculation. The mixture of products after the reduction contained: 24 %  $A_1B_2$ , 32 %  $A_1B_6$ , 33 %

**A<sub>1</sub>B<sub>12</sub>**, 1 % **A<sub>2</sub>B<sub>2</sub>**, 4 % **A<sub>2</sub>B<sub>6</sub>** and 5 % **A<sub>2</sub>B<sub>12</sub>**, as shown in Figure 5.2-21. The eluted fractions were collected and submitted to mass spectrometry which confirmed the identity of the compounds.

From the distribution of species revealed by HPLC, it becomes evident that the formation of **A<sub>2</sub>B<sub>12</sub>** is amplified on the surface, as about 20 % conversion is needed for full surface coverage whereas only 5 % is present in the equilibrated solution.

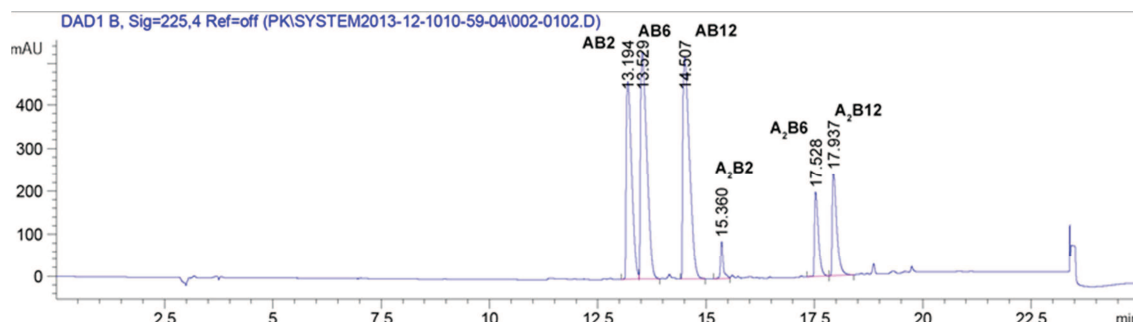


Figure 5.2-21 HPLC chromatogram showing the distribution of species obtained from the reduction of an equilibrated mixture of 2 **A** + **B<sub>2</sub>** + **B<sub>6</sub>** + **B<sub>12</sub>**. The compounds were confirmed by MS spectra of collected fractions.

The marked contrast between the deposition of a dilute solution in phenyloctane on HOPG (revealing **A<sub>2</sub>B<sub>12</sub>** patterns exclusively) and the HPLC analysis (showing statistical distribution) of the same compound mixture indicate that adsorption:

1. drives reaction to completion, as the deposited solution contains mainly mono-imines whereas the surface is covered by bis-imine molecules only
2. leads to an exclusive constituent selection of a specific bis-imine, e.g. **A<sub>2</sub>B<sub>12</sub>**, from the dynamic library of imines present in the solution
3. leads to a specific component amplification, since amount of **A<sub>2</sub>B<sub>12</sub>** in equilibrated solution is not sufficient to fully cover the surface, as observed by STM

The overall process is free-energy driven through the interplay of gain in enthalpy upon molecular physisorption and loss of translational entropy.<sup>[505]</sup> In the present experiments, the free energy of physisorption acts as effector/driving force amplifying a given constituent of a dynamic covalent library. The process is reminiscent of the selective formation of a single entity upon crystallization from a mixture of three equilibrating constituents.<sup>[377]</sup>

The results above taken together stress the crucial role of interactions with the surface as a selection force driving the outcome of covalent chemical reactions, allowing or inhibiting given transformations and thus leading to surface controlled product formation and reaction selectivity, essentially different from the product distribution observed in solution.

### 5.3. Summary of Chapter 5

- Bis-imines of  $\alpha,\omega$ -diamines of different length are packing on the surface in similar lamellar structures which can be differentiated by the distance between the aldehyde residues.
- The condensation reaction of the aldehyde with the diamines can be performed *in situ* on the HOPG surface in 1-phenyloctane.
- The formation of the bis-imines on HOPG is accelerated by four orders of magnitude as compared to bulk solution.
- The imine exchange reaction can be performed and directly followed *in situ* on the HOPG surface.

- The imine exchange on HOPG proceeds readily when longer/larger molecules are formed.
- The kinetics of the imine exchange giving longer/larger molecules is faster than corresponding process in bulk solution.
- The inverted exchange reaction giving shorter/smaller molecules is achievable by large excess of the shorter component(s) to shift the equilibrium.
- Only the bis-imines are selectively adsorbing on the surface from the equilibrium mixture of aldehyde/amine/mono-imine/bis-imine.
- Only the longest/largest bis-imine from complex equilibrium mixture of mono- and bis-imines is adsorbing on the surface.
- The surface amplifies formation of the longest/largest bis-imine which has the highest free energy of adsorption from a complex mixture. The amplified species do not need to be even formed in observable amounts, it is sufficient if they are “virtually present”.
- The surface assisted imine formation and exchange is ruled by the free energy of adsorption.

## 6. CONCLUSIONS & PERSPECTIVES

The manuscript of the thesis presents an amalgamation of several types of dynamics, motional, reactional and constitutional, to introduce new features in various fields of chemistry. It begins with definitions of general terms, explains the concept of reversibility and summarises the most important known reversible reactions, from which the imine formation was chosen for further studies. It also discusses the basic mechanistic questions of imine formation and exchange and gives an overview on applications of the imine chemistry in several fields.

Initial experimentation focused on acquiring the basic knowledge of the imine formation and exchange, notably on identifying the most reactive aldehydes. The reactivity of the selected candidates, salicylaldehyde and pyridine-2-aldehyde, was thoroughly studied by the methods of physical organic chemistry, such as chemical kinetics and electronic structure determination by nitrogen NMR. Moreover, the ambivalent role of the phenolic OH group of salicylaldehyde on its reactivity was observed and experimentally clarified.

The results of these experiments have significant impact in the whole field of constitutional dynamic chemistry based on the utilization of the imine bond as they provide rational and reasoned guideline for the choice of constituents of the dynamic system. Some of the results have been already successfully applied in the group to achieve superior performance in terms of formation and exchange not only for imines, but also for hydrazone, acylhydrazones and oximes. The relatively high stability observed even in aqueous media can lead to interesting discoveries in imine-based covalent dynamics including in biological applications.

Constitutional dynamics of imines was examined in the reaction with polyamines revealing an intertwined motional and constitutional dynamics occurring through the intramolecular imine exchange. The fascinating motional displacement was extensively analysed by available NMR techniques, elucidating the role of derivatization and various conditions on the rate of the motion, and also proving the concomitant intermolecular exchange, thus merging motional and constitutional dynamics in one. The initially observed displacement between two sites was extended to linear polyamines which represents the simplest non-directional small-molecule walking system known. Also, different topologies of the polyamine chain were investigated illustrating the ability of circular or branched motion. Finally, directionality was introduced by pH trapping of different aldehyde-amine condensation products, and it was demonstrated that these products can be converted one into another by the action of base or acid. Finally, a system capable of controllable directional walking was demonstrated which amalgamates the knowledge acquired on different reactivities of aldehyde derivatives. The aldehyde walker unit combines the reactivities of salicylaldehyde and 2-carboxybenzaldehyde, thus profiting from both the imine stabilization by OH "imine-clip" and the iminium trapping by the lactone formation on secondary nitrogen. A hydroxylamine terminated polyamine serves as the track and the control over the system is achieved through addition of a base or an acid.

The directional walking presented here is the first known example of such an artificial system. The search for a directional walker was inspired by the discovery of the biological motors such as kinesin and was pursued by several laboratories around the world. The small-molecule walker developed during the experiments can have a tremendous influence on several fields, ranging

from nanotechnology to chemical biology. With the possibility of controllable oriented displacement, nanoscale cargo transporters can be envisaged. Similarly, active transmembrane transporters are easily accessible using the developed system. Moreover, by creating a macroscopic pH gradient, such a system can be constantly out of equilibrium and thus can perform its task continuously without any intervention. This can also contribute to the development of an artificial cell.

Dynamic combinatorial libraries were studied from a new perspective. A process of “self-sorting” was achieved due to a complexity driven selection for given species, a phenomenon which was called *simplicity*. First, an approach for representation of dynamic combinatorial libraries was proposed, and based on that approach a system for quantification of efficiency of self-sorting processes was suggested. This system was then used to quantify the selection on 2+2 aldehyde-imine libraries which were used for the simplicity demonstration, and the example was even extended to a 3+3 library. The library was shown to adapt to a change in conditions through a network of interconnected reactions, illustrating the dynamic reaction selectivity. The concept was applied in synthesis of *N*-derivatized polyamines using aldehydes as dynamic specific protecting groups. Specifically, salicylaldehyde acts as a protecting group for primary amine via the imine formation while pyridine-2-aldehyde applies for secondary amines due the formation of aminal. Series of mono- and bis-derivatized products were obtained using an imine exchange reaction as a deprotection under mild conditions.

The *simplicity* experiments show interesting and rather unexpected behaviour in chemistry: instead of increased complexity of chemical mixtures with increasing number of reagents, in some cases preferential formation of fewer species is observed. This suggests that an “*order out of chaos*” sorting process can be in some cases the natural, intrinsic or even inevitable principle of organization of matter encoded in the structure of the matter itself. This very general concept was demonstrated to have also very practical applications, such as dynamic selective protecting groups developed here – an approach which can have vast influence in the field of synthetic chemistry and synthesis of complicated molecules such as natural products.

The reversible imine linkage was also studied at the solid-liquid interface by STM. For this purpose, an aldehyde bearing a long alkyl chain was condensed with  $\alpha,\omega$ -diamines of various lengths. The formation and even the reversible imine exchange can be performed directly on the HOPG surface. By comparison with the NMR analysis, the adsorption on the surface was found to largely increase the rate of the reactions. Also, an amplification of the formation of the largest molecules on the surface as compared to bulk solutions was observed and explained in terms of free energy of adsorption.

It is the first shown example of a reversible, dynamic covalent chemistry on a surface. Together with the identification of the governing principles, i.e. enthalpy and entropy of adsorption, construction of sophisticated nanoarchitectures can be envisaged on the surface. The reversibility ensures that errors made in the assembly can be repaired thus paving the way to extremely large uniform structures. The exchange process also enables for easy post-assembly modifications and transformations of the architecture to generate or introduce a function. By combining with irreversible transformations and photolithography, construction of robust and smart materials and systems can be achieved.

In general, the experiments presented here show the path from acquiring very basic knowledge to the development of understanding of the system under study, revealing interesting properties and their application in various fields, thus introducing new features of growing complexity. Finally, these applications demonstrate the general phenomena of motion, selection, amplification and adaptation in chemistry, which represent “*the good at which all things aim.*”<sup>[1]</sup>

## 7. EXPERIMENTAL PART

### 7.1. Instrumentation

NMR spectra were recorded on Bruker Avance 400 (400.14 MHz for  $^1\text{H}$  and 100.62 MHz for  $^{13}\text{C}$ ), Bruker Avance III plus 400 (400.34 MHz for  $^1\text{H}$  and 100.67 MHz for  $^{13}\text{C}$ ), Bruker Avance I 500 (500.13 MHz for  $^1\text{H}$  and 125.61 MHz for  $^{13}\text{C}$ ) and Bruker Avance III 600 (600.13 MHz for  $^1\text{H}$  and 150.90 MHz for  $^{13}\text{C}$ ) NMR spectrometers. Spectra measured in aqueous solutions were referenced on 2,2,3,3-tetradeutero-3-trimethylsilylpropionic acid ( $\delta=0$ ). The other spectra were referenced on residual solvent signal according to Nudelman et al.<sup>[506]</sup>

Deuterated solvents were purchased from Euriso-TOP and used without further purification.

Reagents and solvents were purchased from Sigma-Aldrich, Alfa Aesar, Bachem, ABCR, STREM and Carlo Erba and used without further purification.

pH measurements were done on a Mettler Toledo Seven multimeter with glass electrode calibrated by standard buffer solutions from Sigma-Aldrich (4.01, 7.00 and 10.00). The values were not corrected for the deuterium isotope effect.<sup>[507]</sup>

UV-VIS spectra were recorded on a JASCO V670 dual beam spectrophotometer.

Mass spectra were obtained on Bruker MicroTOF and HRMS on Bruker MicroTOF-Q, both with electrospray ionization. Nominal precision of HRMS analysis is 10 ppm.

Elemental analysis was performed on ThermoFisher Scientific Flash 2000 with absolute precision of 0.3 %.

Melting points were measured on a Büchi Melting Point B-540 apparatus and temperature data are uncorrected.

HPLC analysis was performed on an Agilent 1220 Infinity HPLC instrument equipped with an Agilent Zorbax SB-Aq 5  $\mu\text{m}$ , 4.6x250 mm column, using a water/acetonitrile gradient for elution (flow 1 mL/min, both solvents with 0.01 % TFA, gradient program in the table below). The analysis was repeated 5 times, run 1 was ignored and the signal area was averaged for runs 2-5 for calculation).

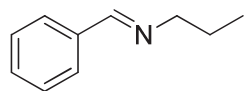
Time	Water	Acetonitrile
0 min	95	5
16 min	5	95
20 min	5	95
20.2 min	95	5
25 min	95	5



## 7.2. Syntheses

### 7.2.1. Imines

#### 7.2.1.1. *N*-propylbenzaldimine

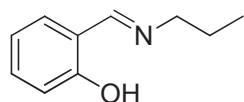


Benzaldehyde (25.0 mL, 246 mmol) was diluted in a mixture of 150 mL of dichloromethane and *n*-propylamine (22.2 mL, 1.1 eq.). The reaction is exothermic. Magnesium sulfate was added to absorb water eliminated during the reaction. The reaction mixture was stirred for 2 hours, then filtered and evaporated on a rotary evaporator to give a viscous liquid. Pure imine was obtained by vacuum distillation (bp 66 °C) from P<sub>2</sub>O<sub>5</sub> at 3.6 mbar, placed over molecular sieves (3 Å) and sealed under nitrogen atmosphere. Yield: 28.2 g (78 %, loss due to the distillation). Analysis consistent with literature.<sup>[508]</sup>

<sup>1</sup>H-NMR (400 MHz, CDCl<sub>3</sub>, 25 °C): δ=8.27 (s, 1 H; N=CH), 7.73 (m, 2 H; Ar-H), 7.41 (m, 2 H; Ar-H), 3.58 (dt, J=1.08, 7.0 Hz, 2 H; CH<sub>2</sub>), 1.73 (m, J=7.2 Hz, 2 H; CH<sub>2</sub>), 0.96 (t, J=7.4 Hz, 3 H; CH<sub>3</sub>)

<sup>13</sup>C-NMR (100 MHz, CDCl<sub>3</sub>, 25 °C): δ=160.72, 136.41, 130.41, 128.54, 128.03, 63.51, 24.08, 11.85

#### 7.2.1.2. *N*-propylsalicyaldimine

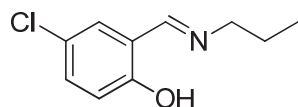


Salicylaldehyde (3.00 mL, 27.7 mmol) was diluted in 50 mL of dichloromethane and *n*-propylamine (2.50 mL, 1.1 eq.) was added. The reaction is exothermic. Magnesium sulfate was added to absorb water eliminated during the reaction. The reaction mixture was stirred for 2 hours, then filtered and evaporated on a rotary evaporator to give a yellow viscous liquid. Pure imine was obtained by vacuum distillation (bp 104 °C) from P<sub>2</sub>O<sub>5</sub> at 4.0 mbar, placed over molecular sieves (3 Å) and sealed under nitrogen atmosphere. Yield: 3.39 g (75 %, loss due to the distillation). Analysis consistent with literature.<sup>[509]</sup>

<sup>1</sup>H-NMR (400 MHz, CDCl<sub>3</sub>, 25 °C): δ=13.66 (br s, 1H; OH), 8.33 (s, 1H; N=CH), 7.30 (dt, J=1.7, 7.8 Hz, 1 H; Ar-H), 7.25 (dd, J=1.8, 7.9 Hz, 1 H; Ar-H), 6.97 (d, J=8.2 Hz, 1H; Ar-H), 6.87 (dt, J=0.7, 7.4 Hz, 1 H; Ar-H), 3.56 (dt, J=0.9, 6.8 Hz, 2 H; CH<sub>2</sub>), 1.73 (m, J=7.2 Hz, 2 H; CH<sub>2</sub>), 0.99 (t, J=7.4 Hz, 3 H; CH<sub>3</sub>)

<sup>13</sup>C-NMR (100 MHz, CDCl<sub>3</sub>, 25 °C): δ=164.49, 161.33, 131.85, 131.03, 118.70, 118.20, 116.82, 61.01, 23.93, 11.53

#### 7.2.1.3. *N*-propyl-5-chlorosalicyaldimine



5-Chlorosalicylaldehyde (3.00 g, 19.2 mmol) was diluted in 50 mL of dichloromethane and *n*-propylamine (1.73 mL, 1.1 eq.) was added. The reaction is exothermic. Magnesium sulfate was added to absorb water eliminated during the reaction. The reaction mixture was stirred for 2 hours, then filtered and evaporated on a rotary evaporator to give a yellow viscous liquid. Crude product was purified by column chromatography on silica (R<sub>f</sub>=0.45) with CHCl<sub>3</sub> as eluent. The final product contained 6 % of the starting aldehyde (evaluated by NMR), repeated chromatography leads

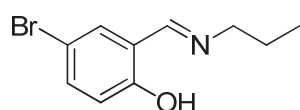
to increased amount of this aldehyde. Yield: 3.56 g (94 %). Analysis was in agreement with literature.<sup>[510]</sup>

<sup>1</sup>H-NMR (400 MHz, CDCl<sub>3</sub>, 25 °C): δ=13.69 (s, 1 H; OH), 8.28 (s, 1 H; N=CH), 7.26 (m, 2 H; Ar-H), 6.92 (d, J=8.7 Hz, 1 H; Ar-H), 3.59 (t, J=6.8 Hz, 2 H; CH<sub>2</sub>), 1.75 (m, J=7.1 Hz, 2 H; CH<sub>2</sub>), 1.01 (t, J=7.4 Hz, 3 H; CH<sub>3</sub>)

<sup>13</sup>C-NMR (100 MHz, CDCl<sub>3</sub>, 25 °C): δ=163.38, 160.05, 131.86, 130.20, 122.88, 119.49, 118.60, 61.21, 23.95, 11.66

MS (ESI): calc. 197.06, found 198.07 [M+H<sup>+</sup>]

#### 7.2.1.4. *N*-propyl-5-bromosalicylaldimine



5-Bromosalicylaldehyde (3.00 g, 14.9 mmol) was diluted in 50 mL of dichloromethane and *n*-propylamine (1.35 mL, 1.1 eq.) was added. The reaction is exothermic. Magnesium sulfate was added to absorb water eliminated during the reaction. The reaction mixture was stirred for 2 hours, then filtered and evaporated on a rotary evaporator to give a yellow viscous liquid. Crude product was purified by column chromatography on silica (*R*<sub>f</sub>=0.49) with CHCl<sub>3</sub> as eluent. The final product contained 3 % of the starting aldehyde (evaluated by NMR), repeated chromatography leads to increased amount of this aldehyde. Yield: 3.50 g (97 %).

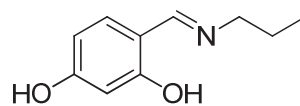
<sup>1</sup>H-NMR (400 MHz, CDCl<sub>3</sub>, 25 °C): δ=13.69 (s, 1 H; OH), 8.24 (s, 1 H; N=CH), 7.36 (m, 2 H; Ar-H), 6.85 (d, J=8.4 Hz, 1 H; Ar-H), 3.56 (t, J=6.8 Hz, 2 H; CH<sub>2</sub>), 1.72 (m, J=7.2 Hz, 2 H; CH<sub>2</sub>), 0.97 (t, J=7.4 Hz, 3 H; CH<sub>3</sub>)

<sup>13</sup>C-NMR (100 MHz, CDCl<sub>3</sub>, 25 °C): δ=163.29, 160.57, 134.68, 133.20, 120.11, 119.09, 109.74, 61.19, 23.94, 11.66

MS (ESI): calc. 241.01, found 242.02 [M+H<sup>+</sup>]

EA: calc.: C 49.61 %, H 5.00 %, N 5.79 %; found: C 48.99 %, H 4.89 %, N 5.64 %

#### 7.2.1.5. *N*-propyl-4-hydroxysalicylaldimine



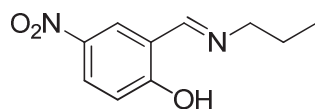
This compound was synthesized by published method.<sup>[511]</sup> 2,4-Dihydroxybenzaldehyde (3.00g, 21.7 mmol) was dissolved in 50 mL of ethanol and *n*-propylamine (1.96 mL, 1.1 eq.) was added. The reaction is exothermic. The reaction mixture was stirred for 2 hours at RT. Solid precipitated out of the solution. It was filtered, washed with diethyl ether and dried under high vacuum. Yield: 2.52 g (65 %). Analysis was consistent with literature.<sup>[511]</sup>

<sup>1</sup>H-NMR (400 MHz, d<sub>6</sub>-DMSO, 25 °C): δ=13.92 (s, 1 H; OH), 9.96 (s, 1 H; OH), 8.32 (s, 1 H; N=CH), 7.15 (d, J=8.5 Hz, 1 H; Ar-H), 6.23 (dd, J=2.2, 8.5 Hz, 1 H; Ar-H), 6.13 (d, J=2.2 Hz, 1 H; Ar-H), 3.45 (t, J=6.7 Hz, 2 H; CH<sub>2</sub>), 1.60 (m, J=7.1 Hz, 2 H; CH<sub>2</sub>), 0.90 (t, J=7.4 Hz, 3 H; CH<sub>3</sub>)

<sup>13</sup>C-NMR (100 MHz, d<sub>6</sub>-DMSO, 25 °C): δ=166.27, 165.00, 162.36, 133.77, 111.50, 107.08, 103.19, 58.55, 24.13, 11.85

MS (ESI): calc. 179.10, found 180.10 [M+H<sup>+</sup>]

### 7.2.1.6. *N*-propyl-5-nitrosalicylalimine



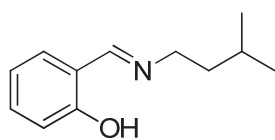
5-Nitrosalicylaldehyde (3.00 g, 18.0 mmol) was diluted in 50 mL of dichloromethane and *n*-propylamine (1.62, 1.1 eq.) was added. The reaction is exothermic. Magnesium sulfate was added to absorb water eliminated during the reaction. The reaction mixture was stirred for 2 hours, then filtered and evaporated on a rotary evaporator to give a deep yellow solid. Crude product was purified by column chromatography on silica ( $R_f=0.19$ ) with  $\text{CHCl}_3$  as eluent. Yield: 3.63 g (97 %). Analysis was in agreement with literature.<sup>[512]</sup>

$^1\text{H-NMR}$  (400 MHz,  $\text{CDCl}_3$ , 25 °C):  $\delta=8.32$  (s, 1 H; N=CH), 8.23 (d,  $J=2.8$  Hz, 1 H; Ar-H), 8.18 (dd,  $J=2.8, 9.3$  Hz, 1 H; Ar-H), 6.93 (d,  $J=9.3$  Hz, 1 H; Ar-H), 3.64 (t,  $J=6.8$  Hz, 2 H;  $\text{CH}_2$ ), 1.79 (m,  $J=7.2$  Hz, 2 H;  $\text{CH}_2$ ), 1.02 (t,  $J=7.4$  Hz, 3 H;  $\text{CH}_3$ )

$^{13}\text{C-NMR}$  (100 MHz,  $\text{CDCl}_3$ , 25 °C):  $\delta=170.89, 163.90, 138.27, 128.53, 128.37, 119.67, 116.14, 58.88, 23.62, 11.44$

MS (ESI): calc. 208.09, found 209.09 [ $\text{M}+\text{H}^+$ ]

### 7.2.1.7. *N*-(3-methylbutyl)salicylalimine

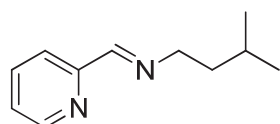


Salicylaldehyde (3.00 mL, 27.7 mmol) was diluted in 50 mL of dichloromethane and *iso*-pentylamine (3.53 mL, 1.1 eq.) was added. The reaction is exothermic. Magnesium sulfate was added to absorb water eliminated during the reaction. The reaction mixture was stirred for 2 hours, then filtered and evaporated on a rotary evaporator to give a yellow viscous liquid. Pure imine was obtained by vacuum distillation (bp 121 °C) from  $\text{P}_2\text{O}_5$  at 4.0 mbar, placed over molecular sieves (3 Å) and sealed under nitrogen atmosphere. Yield: 3.50 g (66 %, loss due to the distillation). Analysis consistent with literature.<sup>[131]</sup>

$^1\text{H-NMR}$  (400 MHz,  $\text{CDCl}_3$ , 25 °C):  $\delta=13.73$  (s, 1 H; OH), 8.37 (s, 1 H; N=CH), 7.33 (t,  $J=7.4$  Hz, 2 H; Ar-H), 7.27 (d,  $J=7.6$  Hz, 1 H; Ar-H), 6.99 (d,  $J=8.3$  Hz, 1 H; Ar-H), 6.90 (t,  $J=7.5$  Hz, 2 H; Ar-H), 3.64 (t,  $J=7.1$  Hz, 2 H;  $\text{CH}_2$ ), 1.75 (m,  $J=6.7$  Hz, 1 H; CH), 1.62 (q,  $J=7.1$  Hz, 2 H;  $\text{CH}_2$ ), 0.99 (d,  $J=6.6$  Hz, 6 H;  $\text{CH}_3$ )

$^{13}\text{C-NMR}$  (100 MHz,  $\text{CDCl}_3$ , 25 °C):  $\delta=164.40, 161.40, 132.02, 131.04, 118.85, 118.38, 117.04, 57.61, 39.84, 25.78, 22.47$

### 7.2.1.8. *N*-(3-methylbutyl)pyridine-2-carboxalimine



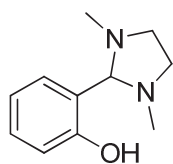
Freshly distilled colourless pyridine-2-carboxaldehyde (5.00 mL, 52.6 mmol) was diluted in 50 mL of dichloromethane and *iso*-pentylamine (6.70 mL, 1.1 eq.) was added. The reaction is exothermic. Magnesium sulfate was added to absorb water eliminated during the reaction. The reaction mixture was stirred for 2 hours, then filtered and evaporated on a rotary evaporator to give a viscous liquid. Pure imine was obtained by vacuum distillation (bp 94 °C) from  $\text{P}_2\text{O}_5$  at 3.6 mbar, placed over molecular sieves (3 Å) and sealed under nitrogen atmosphere. Yield: 5.74 g (62 %). Analysis consistent with literature.<sup>[131]</sup>

$^1\text{H-NMR}$  (400 MHz,  $\text{CDCl}_3$ , 25 °C):  $\delta$ =8.55 (d,  $J$ =4.8 Hz, 1 H; Ar-H), 8.30 (s, 1 H; N=CH), 7.90 (d,  $J$ =7.9 Hz, 1 H; Ar-H), 7.63 (m,  $J$ =1.5, 7.7 Hz, 1 H; Ar-H), 7.20 (m,  $J$ =1.1, 4.9, 7.5 Hz, 1 H; Ar-H), 3.60 (t,  $J$ =7.2 Hz, 2 H;  $\text{CH}_2$ ), 1.60 (m,  $J$ =6.6 Hz, 1 H; CH), 1.53 (q,  $J$ =7.1 Hz, 2 H;  $\text{CH}_2$ ), 0.86 (d,  $J$ =6.5 Hz, 6 H;  $\text{CH}_3$ )

$^{13}\text{C-NMR}$  (100 MHz,  $\text{CDCl}_3$ , 25 °C):  $\delta$ =161.52, 154.65, 149.29, 136.37, 124.44, 121.03, 59.57, 39.65, 25.82, 22.47

## 7.2.2. Compounds for walking

### 7.2.2.1. *N,N'*-dimethyl-2-(2-hydroxyphenyl)-imidazolidine

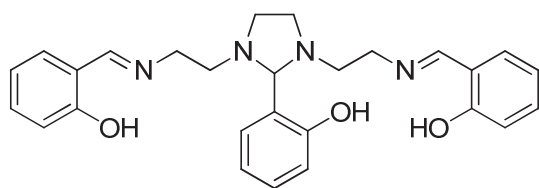


Salicylaldehyde (3.00 mL, 27.7 mmol) was diluted in a mixture of 50 mL of dichloromethane and *N,N'*-dimethylethylenediamine (3.30 mL, 1.1 eq.), the reaction is exothermic. Magnesium sulfate was added to absorb water eliminated during the reaction. The reaction mixture was stirred at RT for 2 hours, then filtered and evaporated on a rotary evaporator to give a yellow viscous liquid (quantitative). Pure product was obtained by vacuum distillation (bp 133-134 °C) from  $\text{P}_2\text{O}_5$  at 5.3 mbar, placed over molecular sieves (3 Å) and sealed under nitrogen atmosphere. Yield: 3.30 g (62 %, loss due to the distillation). Analysis consistent with literature.<sup>[513]</sup>

$^1\text{H-NMR}$  (400 MHz,  $\text{CDCl}_3$ , 25 °C):  $\delta$ =11.47 (br s, 1H; OH), 7.19 (ddd,  $J$ =1.8, 7.4, 8.1 Hz, 1 H; Ar-H), 6.95 (dd,  $J$ =1.7, 7.4 Hz, 1 H; Ar-H), 6.82 (dd,  $J$ =0.9, 8.1 Hz, 1 H; Ar-H), 6.76 (dt,  $J$ =1.2, 7.4 Hz, 1 H; Ar-H), 3.41 (s, 1H; CH), 3.38 (m, 2H;  $\text{CH}_2$ ), 2.54 (m, 2 H;  $\text{CH}_2$ ), 2.26 (s, 6 H;  $\text{CH}_3$ )

$^{13}\text{C-NMR}$  (100 MHz,  $\text{CDCl}_3$ , 25 °C):  $\delta$ =158.16, 130.32, 129.48, 120.16, 117.92, 116.43, 91.47, 51.86, 38.64

### 7.2.2.2. *N,N'*-bis(2-(salicylideneimino)ethyl)-2-(2-hydroxyphenyl)-imidazolidine

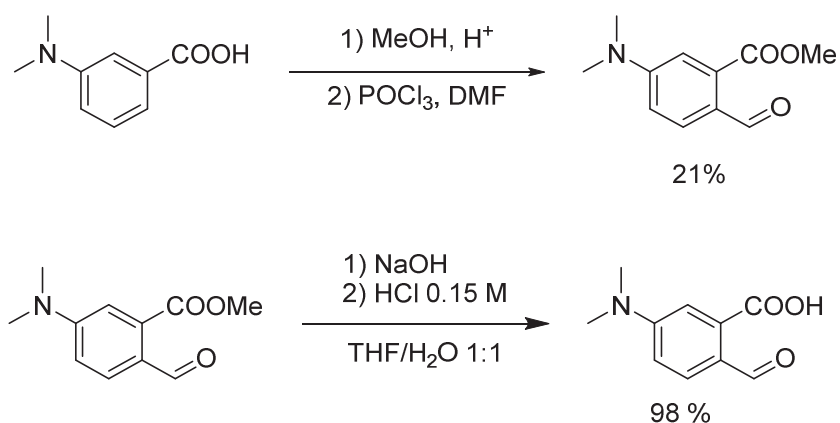


The literature procedure was slightly modified.<sup>[164]</sup> Triethylenetetramine (3.12 g, 21.3 mmol) was diluted in 50 mL of ethanol and salicylaldehyde (7.20 mL, 3.1 eq.) was added giving an exothermic reaction. Magnesium sulfate was added to absorb water eliminated during the reaction. The mixture was refluxed for 3 hours and filtered while still hot. The filtrate was allowed to cool down slowly (fast cooling gives an oil) and precipitation occurred. The precipitate was filtered off, washed with diethyl ether and recrystallized twice from ethanol to remove salicylaldehyde residues. Pure product was sealed under nitrogen atmosphere. Yield: 7.63 g (78 %).

$^1\text{H-NMR}$  (400 MHz,  $\text{CDCl}_3$ , 25 °C):  $\delta$ =13.22 (br s, 2 H; OH), 10.68 (br s, 1H; OH), 8.25 (s, 2H; N=CH), 7.31-7.20 (m, 5 H; Ar-H), 7.00 (dd,  $J$ =1.6, 7.7 Hz, 1 H; Ar-H), 6.93 (d,  $J$ =8.0 Hz, 2 H; Ar-H), 6.86 (dt,  $J$ =0.8, 7.4 Hz, 2 H; Ar-H), 6.82-6.79 (m, 2H; Ar-H), 3.83 (s, 1H; CH), 3.59 (t,  $J$ =6.3 Hz, 4 H;  $\text{CH}_2$ ), 3.43 (m, 2 H;  $\text{CH}_2$ ), 2.97 (dt,  $J$ =6.4, 12.7 Hz, 2 H;  $\text{CH}_2$ ), 2.68 (m, 2 H;  $\text{CH}_2$ ), 2.64 (t,  $J$ =6.6 Hz, 2 H;  $\text{CH}_2$ )

$^{13}\text{C-NMR}$  (100 MHz,  $\text{CDCl}_3$ , 25 °C):  $\delta$ =166.17, 161.18, 158.37, 132.38, 131.50, 131.02, 130.39, 120.95, 118.82, 118.67, 117.11, 117.06, 89.73, 58.60, 52.94, 51.29

## 7.2.2.3. 5-(dimethylamino)-2-formylbenzoic acid



A solution of methyl 3-dimethylaminobenzoate (700 mg, 3.90 mmol) in DMF (20 ml) was cooled in ice bath and  $\text{POCl}_3$  (364 mg) was added dropwise to the mixture. After stirring for 20 min at  $0^\circ\text{C}$ , the mixture was allowed warm up to RT and then heated to  $70^\circ\text{C}$  overnight. After that, the solution was poured into ice and  $\text{NaOH}$  (5 M) was added

until pH = 6. The crude mixture was then extracted with  $\text{Et}_2\text{O}$  and organic layer was washed with  $\text{KHCO}_3$  (15 %) and dried over sodium sulphate. Solvent was removed under reduced pressure and crude product was purified by column chromatography (Petrolether/ $\text{EtOAc}$  3:1) to obtain 169 mg methyl 5-(dimethylamino)-2-formylbenzoate (21%). The published procedure was not successful, but the product analysis was consistent.<sup>[514]</sup>

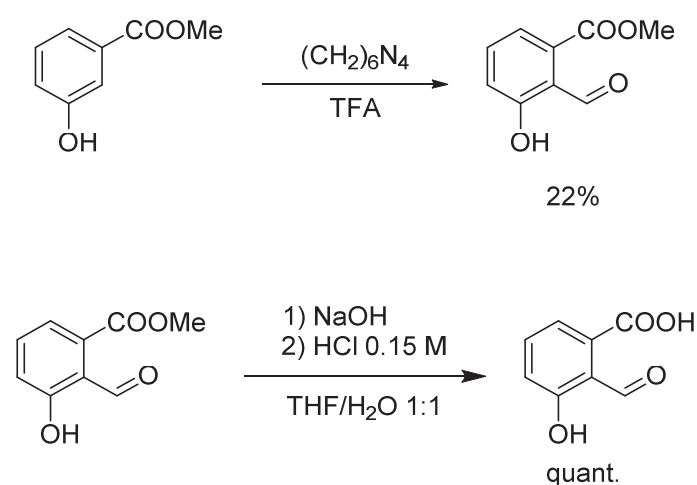
Hydrolysis of the ester was performed by dissolving the ester (169 mg) in 5 mL of THF and addition of 5 mL of 2 M  $\text{NaOH}$  in water. The mixture was refluxed for 3 hours, then acidified by 0.15 M aqueous  $\text{HCl}$  to pH *ca* 4 and injected on reverse phase column. Chromatography was performed using water/acetonitrile gradient (98:2  $\rightarrow$  5:95). Pure product was isolated after evaporation in 98 % yield (155 mg).

$^1\text{H-NMR}$  (400 MHz,  $\text{CDCl}_3$ ,  $25^\circ\text{C}$ ): 9.50 (s, 1H; CHO), 7.87 (d,  $J=2.8$  Hz, 1H; Ar-H), 7.73 (d,  $J=8.8$  Hz, 1H; Ar-H), 6.85 (dd,  $J=2.8, 8.8$  Hz, 1H; Ar-H), 3.23 (s, 6H;  $(\text{CH}_3)_2\text{N}$ )

$^{13}\text{C-NMR}$  (100 MHz,  $\text{CDCl}_3$ ,  $25^\circ\text{C}$ ): 193.01, 166.17, 154.40, 141.90, 133.64, 120.43, 119.00, 112.49, 40.24

MS (ESI): calc. 193.07, found 194.08  $[\text{M}+\text{H}^+]$

## 7.2.2.4. 2-formyl-3-hydroxybenzoic acid



Hexamethylenetetraamine (5.00 mmol, 700 mg) was added to a stirred solution of methyl 3-hydroxybenzoate (5.00 mmol, 760 mg) in TFA (5 mL). The mixture was stirred for 3 h at 75°C. After cooling to RT, solution was diluted with an ice-water mixture (100 mL) and extracted with EtOAc (3x50 mL). Solvent was then removed under reduced pressure and crude product was purified by column chromatography on silica gel (Petrolether/EtOAc 10:1) to obtain 200 mg of methyl 2-formyl-3-hydroxybenzoate (22%).

Hydrolysis of the ester was performed by dissolving the ester (100 mg) in 5 mL of THF and addition of 5 mL of 2 M NaOH in water. The mixture was refluxed for 3 hours, then acidified by 0.15 M aqueous HCl to pH *ca* 1 and injected on reverse phase column. Chromatography was performed using water/acetonitrile gradient (98:2 → 5:95). Pure product was isolated after evaporation in 99 % yield (91 mg).

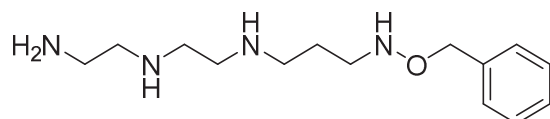
The product was isolated in the hydroxy-lactone form. The equilibrium between the open and close form however depends on the solvent used. The NMR analysis reports for the closed lactone form.

<sup>1</sup>H-NMR (400 MHz, d<sub>6</sub>-DMSO, 25 °C): 10.37 (s, 1H; Ar-OH), 7.88 (br d, J=7.0 Hz, 1H; lactone OH), 7.45 (t, J=7.7 Hz, 1H; Ar-H), 7.24 (d, J=7.4 Hz, 1H; Ar-H), 7.14 (d, J=8.1 Hz, 1H, Ar-H), 6.61 (br d, J=5.6 Hz, 1H; lactone C-H)

<sup>13</sup>C-NMR (100 MHz, d<sub>6</sub>-DMSO, 25 °C): 169.18, 153.94, 133.07, 132.49, 128.93, 121.54, 115.20, 97.62

MS (ESI): calc. 166.03, found 189.02 [M+Na<sup>+</sup>]

EA: calc.: C 57.84 %, H 3.64 %; found: C 57.54 %, H 3.70 %

7.2.2.5. N<sup>1</sup>-(3-(benzyloxyamino)propyl)diethylene triamine

Diethylene triamine (2.00 g, 19.4 mmol) was diluted in distilled water (50 mL) and pH was adjusted to 6.5-7.5 by 1 M HCl. The solution was then cooled to 0 °C in ice bath and acrolein (1.50 mL, 1.04 eq) was added

drop-wise with 20 mL of water. When addition was finished, the solution was kept stirring for 1 hour at temperature below 5 °C. Then, *O*-benzylhydroxylamine hydrochloride (3.10 g, 1.0 eq) was added as a solid, the reaction was removed from ice bath and kept stirring for 1 hour. The the reaction was cooled again to 0 °C in ice bath and sodium cyanoborohydride (1.22 g, 1 eq) was added as solid in small portions to keep the temperature below 5 °C. When the addition was finished, the reaction mixture was slowly acidified by 1 M HCl to pH approximately 1 while keeping the temperature below 5 °C. Then the reaction mixture was concentrated on rotary evaporator, injected on C-18 column and purified by reverse phase chromatography. The initial fractions were collected and evaporated to



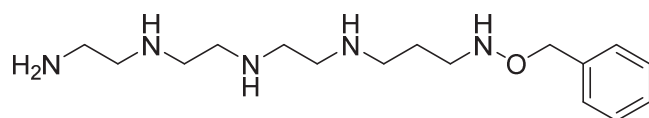
dryness. Then this crude was diluted in 0.2 M NaOH (10 mL) and again injected on reverse phase column. The fraction containing the product (verified by LCMS) was concentrated on rotary evaporator and injected one more time on reverse phase. The third purification provided pure product in 13 % yield (670 mg). The product in the free base form must be stored under argon atmosphere at -20 °C. Nevertheless, degradation was observed over time (3 weeks) requiring for repurification before use. Salts of hydroxylamine derivatives are reported to be more stable than the free bases, however for the use in directional walking a free base form was required. Stock solution in DMSO is stable for about 2 weeks whereas stock solution in water is degrading in a few days. It is noteworthy that different than optimized conditions (temperatures, pH) indicated in the Michael reaction with acrolein lead to extensive aldol polymerization and ultimately null product yield.

$^1\text{H-NMR}$  (400 MHz,  $\text{D}_2\text{O}$ , 25 °C): 7.32 (m, 5H; Ar-H), 4.63 (s, 2H; Ar- $\text{CH}_2$ ), 3.00-2.75 (m, 12H; N- $\text{CH}_2$ ), 1.81 (q,  $J=7.6$  Hz, 2H; C- $\text{CH}_2$ -C)

$^{13}\text{C-NMR}$  (100 MHz,  $\text{D}_2\text{O}$ , 25 °C): 136.55, 129.01, 128.79, 128.59, 75.41, 47.79, 46.74, 45.93, 45.22, 44.12, 38.75, 23.54

HRMS (ESI): calc. 266.211, found 267.216 [ $\text{M}+\text{H}^+$ ]

#### 7.2.2.6. *N*<sup>1</sup>-(3-(benzyloxyamino)propyl)triethylene tetramine



The procedure is analogous the previous one (Section 7.2.2.5). Triethylene tetramine (2.00 g, 13.7 mmol) was diluted in distilled water (50 mL) and pH was adjusted to 6.5-

7.5 by 1 M HCl. The solution was then cooled to 0 °C in ice bath and acrolein (0.91 mL, 1 eq) was added drop-wise with 25 mL of water. When addition was finished, the solution was kept stirring for 1 hour at temperature below 5 °C. Then, *O*-benzylhydroxylamine hydrochloride (2.18 g, 1 eq) was added as a solid, the reaction was removed from ice bath and kept stirring for 1 hour. The the reaction was cooled again to 0 °C in ice bath and sodium cyanoborohydride (1.75 g, 2 eq) was added as solid in small portions to keep the temperature below 5 °C. When the addition was finished, the reaction mixture was slowly acidified by 1 M HCl to pH approximately 1 while keeping the temperature below 5 °C. Then the reaction mixture was concentrated on rotary evaporator, injected on C-18 column and purified by reverse phase chromatography. The initial fractions were collected and evaporated to dryness. Then this crude was diluted in 0.2 M NaOH (10 mL) and again injected on reverse phase column. The fraction containing the product (verified by LCMS) was concentrated on rotary evaporator and injected one more time on reverse phase. The third purification provided pure product in 9 % yield (380 mg). The stability issues are the same as for the shorter analogue as well as the strong conditions dependency.

$^1\text{H-NMR}$  (400 MHz,  $\text{D}_2\text{O}$ , 25 °C): 7.36 (m, 5H; Ar-H), 4.68 (s, 2H; Ar- $\text{CH}_2$ ), 2.90-2.50 (m, 16H; N- $\text{CH}_2$ ), 1.60 (q,  $J=7.7$  Hz, 2H; C- $\text{CH}_2$ -C)

$^{13}\text{C-NMR}$  (100 MHz,  $\text{D}_2\text{O}$ , 25 °C): 136.54, 128.76, 128.73, 128.53, 75.37, 52.00, 51.84, 51.77, 51.35, 48.91, 48.50, 38.95, 22.97

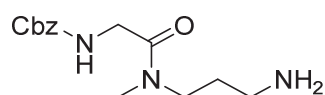
HRMS (ESI): calc. 309.253, found 310.256 [ $\text{M}+\text{H}^+$ ]

#### 7.2.3. Experiments using dynamic protecting groups

The experimental protocols discussed in the manuscript are here reported in detail. For the experiments performed by Dr. Anne Meister the protocols are not provided. It is important to point

out that amide derivatives can exist as two rotamers. This was indeed observed during the NMR analysis, as splitting of the signal in to two sets, and proved by 2D NOESY. The reported analysis therefore comprises for both rotamers. The structures were of course determined by full NMR analysis including HSQC, HMBC, COSY and NOESY spectra, but the corresponding traces are not provided.

### 7.2.3.1. *N*-(Cbz-glycyl)-*N*-methyl-1,3-diaminopropane

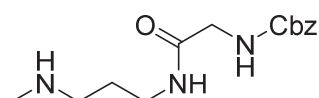


*N*-methyl-1,3-diaminopropane (0.30 g, 3.4 mmol) was diluted in acetonitrile (35 mL) and salicylaldehyde (0.37 mL, 1 eq.) was added. The reaction mixture was stirred at room temperature for 2 hours. Then *N*-Cbz-glycine *p*-nitrophenyl ester (1.14 g, 1 eq.) was added as solid and the mixture was stirred at room temperature. After 2 hours, *O*-benzyl hydroxylamine hydrochloride (0.55 g, 1 eq.) together with triethylamine (0.50 mL, 1 eq.) was added and the mixture was stirred for 2 more hours. Then it was concentrated on rotary evaporator and injected on C18 reverse phase column. After injection of the crude, 10 mL of 0.15 M HCl was injected as well to improve the separation. Pure product was obtained by chromatography using acetonitrile-water gradient (0:100 → 95:5) as hydrochloride salt in 82 % yield (0.88 g). The product of the bis-acylation was isolated in 6 % yield (0.09 g).

<sup>1</sup>H-NMR (400 MHz, CD<sub>3</sub>CN, 25 °C): 7.45-7.30 (m, 5H; benzyl H), 5.11 (s, 2H; Ar-CH<sub>2</sub>), 4.02 + 3.94 (br s, 2H; Gly CH<sub>2</sub>), 3.42 + 3.31 (t, J=6.9 Hz, 2H; N-CH<sub>2</sub>), 2.91 + 2.88 (s, 3H; CH<sub>3</sub>), 2.64 + 2.57 (t, J=6.5 Hz, 2H; CH<sub>2</sub>-NH<sub>2</sub>), 1.66 + 1.59 (q, J=6.6 Hz, 2H; C-CH<sub>2</sub>-C)

<sup>13</sup>C-NMR (100 MHz, CD<sub>3</sub>CN, 25 °C): 168.47, 168.26, 156.57, 156.50, 137.17, 128.45, 127.88, 127.76, 66.06, 45.84, 44.82, 42.36, 42.12, 38.66, 38.51, 33.34, 32.52, 31.15, 30.45

### 7.2.3.2. *N*-(Cbz-glycyl)-*N'*-methyl-1,3-diaminopropane

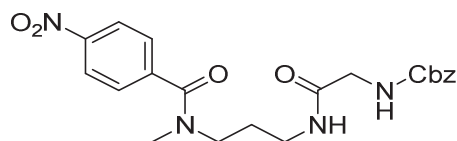


*N*-methyl-1,3-diaminopropane (0.30 g, 3.4 mmol) was diluted in acetonitrile (35 mL) and pyridine-2-carboxaldehyde (0.33 mL, 1 eq.) was added. The reaction mixture was stirred at room temperature for 2 hours. Then *N*-Cbz-glycine *p*-nitrophenyl ester (1.14 g, 1 eq.) was added as solid and the mixture was stirred at room temperature. After 2 hours, *O*-benzylhydroxylamine hydrochloride (0.55 g, 1 eq.) together with triethylamine (0.50 mL, 1 eq.) was added and the mixture was stirred for 2 more hours. Then it was concentrated on rotary evaporator and injected on C18 reverse phase column. After injection of the crude, 10 mL of 0.15 M HCl was injected as well to improve the separation. Pure product was obtained by chromatography using acetonitrile-water gradient (0:100 → 95:5) as hydrochloride salt in 52 % yield (0.56 g). The product of the bis-acylation was isolated in 31 % yield (0.50 g).

<sup>1</sup>H-NMR (400 MHz, CD<sub>3</sub>CN, 25 °C): 7.45-7.30 (m, 5H; benzyl H), 5.11 (s, 2H; Ar-CH<sub>2</sub>), 3.71 (br s, 2H; Gly CH<sub>2</sub>), 3.23 (m, 2H; N-CH<sub>2</sub>), 2.57 (t, J=6.5 Hz, 2H; CH<sub>2</sub>-NH<sub>2</sub>), 2.32 (s, 3H; CH<sub>3</sub>), 1.59 (q, J=6.6 Hz, 2H; C-CH<sub>2</sub>-C)

<sup>13</sup>C-NMR (100 MHz, CD<sub>3</sub>CN, 25 °C): 169.35, 156.76, 137.31, 128.47, 127.94, 127.85, 66.23, 49.26, 44.08, 37.58, 35.35, 28.45

### 7.2.3.3. *N*-(Cbz-glycyl)-*N*-methyl-*N'*-(4-nitrobenzoyl)-1,3-diaminopropane

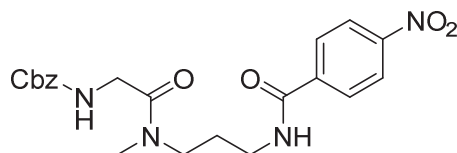


*N*-methyl-1,3-diaminopropane (0.25 g, 2.8 mmol) was diluted in acetonitrile (15 mL) and salicylaldehyde (0.30 mL, 1 eq.) together with triethylamine (0.40 mL, 1 eq.) was added. The reaction mixture was stirred at room temperature for 2 hours. Then *p*-nitrobenzoyl chloride (0.53 g, 1 eq.) was added as solid and the mixture was stirred at room temperature for 2 hours, after which benzhydrazide (0.39 g, 1 eq.) was added and the mixture was stirred for 2 more hours. Then *N*-Cbz-glycine *p*-nitrophenyl ester (0.81 g, 1 eq.) was added as solid and the mixture was again stirred at room temperature for 2 hours. The mixture was then concentrated on rotary evaporator and pure product was obtained by column chromatography on silica using DCM-MeOH gradient elution (99:1 → 90:10), yielding 0.95 g (78 %).

<sup>1</sup>H-NMR (400 MHz, d<sub>6</sub>-DMSO, 25 °C): 8.27 (d, J=8.6 Hz, 2H; Ar-H), 7.89 + 7.72 + 7.45 (t, 1H; NH), 7.66 + 7.59 (d, J=8.3 Hz, 2H; Ar-H), 7.4-7.2 (m, 5H; benzyl H), 5.02 + 5.00 (s, 2H; Ar-CH<sub>2</sub>), 3.58 + 3.44 (d, J=6.0 Hz, 2H; Gly CH<sub>2</sub>), 3.46 + 3.10 (m, 2H; N-CH<sub>2</sub>), 3.13 + 2.90 (m, 2H; N-CH<sub>2</sub>), 2.96 + 2.83 (s, 3H; CH<sub>3</sub>), 1.73 + 1.63 (q, J=6.7 Hz, 2H; C-CH<sub>2</sub>-C)

<sup>13</sup>C-NMR (100 MHz, d<sub>6</sub>-DMSO, 25 °C): 169.40, 169.02, 168.80, 156.90, 148.09, 143.49, 137.48, 128.75, 128.54, 128.21, 128.15, 124.13, 79.62, 65.92, 48.65, 44.95, 44.16, 43.92, 37.29, 36.53, 36.19, 32.57, 28.21, 27.07

### 7.2.3.4. *N*-(Cbz-glycyl)-*N'*-methyl-*N'*-(4-nitrobenzoyl)-1,3-diaminopropane



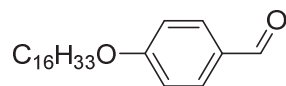
The procedure is analogous to the previous one. *N*-methyl-1,3-diaminopropane (0.30 g, 3.4 mmol) was diluted in acetonitrile (35 mL) and pyridine-2-carboxaldehyde (0.33 mL, 1 eq.) together with triethylamine (0.50 mL, 1 eq.) was added. The reaction mixture was stirred at room temperature for 2 hours. Then *p*-nitrobenzoyl chloride (0.64 g, 1 eq.) was added as solid and the mixture was stirred at room temperature for 2 hours, after which benzhydrazide (0.47 g, 1 eq.) was added and the mixture was stirred for 2 more hours. Then *N*-Cbz-glycine *p*-nitrophenyl ester (1.14 g, 1 eq.) was added as solid and the mixture was again stirred at room temperature for 2 hours. The mixture was then concentrated on rotary evaporator and pure product was obtained by column chromatography on silica using DCM-MeOH gradient elution (99:1 → 90:10), yielding 0.95 g (78 %).

<sup>1</sup>H-NMR (400 MHz, d<sub>6</sub>-DMSO, 25 °C): 8.85 + 8.87 (t, J=5.5 Hz, 1 H; NH), 8.32 (d, J=8.6 Hz, 2H, Ar-H), 8.07 (d, J=8.8 Hz, 2H; Ar-H), 7.4-7.2 (m, 5H; benzyl H), 5.03 (s, 2H; Ar-CH<sub>2</sub>), 3.86 (d, J=5.8 Hz, 2H; Gly CH<sub>2</sub>), 3.36 (m, 2H; N'-CH<sub>2</sub>), 3.27 (m, 2H; N-CH<sub>2</sub>), 2.96 + 2.83 (s, 3H; CH<sub>3</sub>), 1.83 + 1.73 (q, J=7.1 Hz, 2H; (C-CH<sub>2</sub>-C)

<sup>13</sup>C-NMR (100 MHz, d<sub>6</sub>-DMSO, 25 °C): 168.95, 168.62, 165.22, 164.95, 156.95, 149.42, 140.72, 140.68, 137.60, 129.16, 129.08, 128.80, 128.22, 128.12, 124.02, 123.99, 65.80, 46.33, 45.58, 42.58, 42.26, 37.54, 37.48, 34.24, 33.48, 31.17, 28.04, 27.24

## 7.2.4. Compounds for the STM experiments

### 7.2.4.1. *4-Hexadecyloxybenzaldehyde*



In 100 mL of dry DMF, 4-hydroxybenzaldehyde (7.00 g, 57.3 mmol) was diluted and 2.50 g of sodium hydride (as 60 % dispersion in oil, 1.1 eq.) was added. When gas evolution ceased the mixture was allowed to cool back to RT, then 19.25 g of n-hexadecylbromide was added via syringe and reaction was stirred overnight at RT. Then 150 mL of water was added and mixture was extracted 3 x 200 mL of toluene, combined organic extracts were dried over magnesium sulfate and evaporated on rotary evaporator. Pure product was obtained by column chromatography on silica using petrolether / ethyl acetate (99:1 to 70: 30) as eluent. Yield: 5.73 g (29 %).

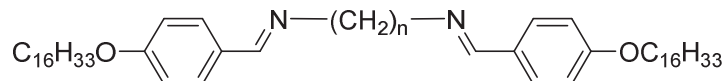
<sup>1</sup>H-NMR (500 MHz, CDCl<sub>3</sub>): 10.12 (s, 1 H), 8.07 (d, J=8.7 Hz, 2 H), 7.23 (d, J=8.7 Hz, 2 H), 4.28 (t, J=6.6 Hz, 2 H), 2.05 (m, 2 H), 1.71 (m, 2 H), 1.50 (m, 24 H), 1.12 (t, J=7.0 Hz, 3 H)

<sup>13</sup>C-NMR (125 MHz, CDCl<sub>3</sub>): 190.84, 164.28, 132.00, 129.72, 114.74, 68.43, 31.95, 29.73, 29.72, 29.72, 29.70, 29.69, 29.68, 29.61, 29.58, 29.40, 29.37, 29.07, 25.98, 22.72, 14.16

EA: calc. C 79.71 %, H 11.05 %; found C 79.41 %, H 10.50 %.

MS: calc. 346.29, found 369.27 [M+Na]

### 7.2.4.2. *N,N'-bis((4-hexadecyloxy)benzylidene)- $\alpha,\omega$ -diamines*



Compounds **A<sub>2</sub>B<sub>2</sub>**, **A<sub>2</sub>B<sub>6</sub>** and **A<sub>2</sub>B<sub>12</sub>** were synthesized according to published protocol.<sup>[515]</sup> Diamine **B** (1.44 mmol) was mixed with two equivalents of 4-hexadecyloxybenzaldehyde (**A**) (1.00 g, 2.89 mmol) in 100 mL of ethanol and refluxed for 2 hours. Reaction mixture was then evaporated to dryness and pure product was obtained by recrystallization of the crude from ethanol.

### 7.2.4.3. *N,N'-bis((4-hexadecyloxy)benzylidene)-1,2-diaminoethane*

Yield: 78 %

<sup>1</sup>H-NMR (400 MHz, CDCl<sub>3</sub>): 8.22 (s, 2H), 7.64 (d, J=8.7 Hz, 4 H), 6.90 (d, J=8.7 Hz, 4 H), 3.99 (t, J=6.6 Hz, 4 H), 3.93 (s, 4H), 1.80 (m, 4 H), 1.46 (m, 4 H), 1.27 (m, 48 H), 0.90 (t, J=6.8 Hz, 6 H)

<sup>13</sup>C-NMR (100 MHz, CDCl<sub>3</sub>): 162.14, 161.17, 129.64, 128.81, 114.40, 68.08, 61.80, 31.98, 29.76, 29.72, 29.66, 29.63, 29.44, 29.21, 29.08, 26.05, 26.00, 22.77, 14.23

EA: calc. C 80.39 %, H 11.24 %, N 3.91 %; found C 80.51 %, H 11.14 %, N 3.84 %

HRMS: calc. 716.622, found 717.627 [M+H]

m.p.: 90 °C

**7.2.4.4. *N,N'*-bis((4-hexadecyloxy)benzylidene)-1,6-diaminohexane**

Yield: 70 %

<sup>1</sup>H-NMR (500 MHz, CDCl<sub>3</sub>): 8.15 (s, 2 H), 7.61 (d, J=8.7 Hz, 4 H), 6.88 (d, J=8.7 Hz, 4 H), 3.95 (t, J=6.6 Hz, 4 H), 3.54 (t, J=6.9 Hz, 4 H), 1.76 (m, 4 H), 1.67 (m, 4 H), 1.23 (m, 56 H), 0.86 (t, J=6.9 Hz, 6 H)

<sup>13</sup>C-NMR (125 MHz, CDCl<sub>3</sub>): 161.08, 160.18, 129.52, 129.06, 114.47, 114.46, 68.09, 61.65, 31.96, 31.00, 29.74, 29.73, 29.71, 29.70, 29.66, 29.63, 29.60, 29.42, 29.40, 29.22, 27.19, 26.04, 22.73, 14.17

EA: calc. C 80.77 %, H 11.47 %, N 3.62 %; found C 80.70 %, H 11.41 %, N 3.56 %.

HRMS: calc. 772.685, found 773.683 [M+H]

m.p.: 87 °C

**7.2.4.5. *N,N'*-bis((4-hexadecyloxy)benzylidene)-1,12-diaminododecane**

Yield: 85 %

<sup>1</sup>H-NMR (400 MHz, CDCl<sub>3</sub>): 8.20 (s, 2H), 7.67 (d, J=7.9 Hz, 4 H), 6.92 (d, J=8.6 Hz, 4 H), 3.99 (t, J=6.6 Hz, 4 H), 3.57 (t, J=7.0 Hz, 4 H), 1.80 (m, 4 H), 1.69 (m, 4 H), 1.46 (m, 4 H), 1.32 (m, 64 H), 0.89 (t, J=6.8 Hz, 6 H)

<sup>13</sup>C-NMR (100 MHz, CDCl<sub>3</sub>): 161.09, 160.09, 129.51, 114.48, 68.11, 61.72, 31.94, 31.06, 29.70, 29.67, 29.60, 29.57, 29.47, 29.40, 29.37, 29.21, 27.37, 26.02, 22.70, 14.13

EA: calc. C 81.25 %, H 11.76 %, N 3.27 %; found C 81.27 %, H 11.73 %, N 3.24 %

HRMS: calc. 856.778, found 857.793 [M+H]

m.p.: 92 °C

**7.3. Example of <sup>14</sup>N-NMR**

Nitrogen NMR spectra were measured on Bruker Avance III plus 400 MHz spectrometer equipped with Prodigy broadband cryoprobe, with the resonance frequencies of 40.566 MHz for <sup>15</sup>N and 28.92 MHz for <sup>14</sup>N. The <sup>15</sup>N-NMR spectra were measured at natural abundance. It is noteworthy that the acquisition of <sup>14</sup>N spectra does not require a cryoprobe. For the <sup>15</sup>N spectra, the pulse sequence consisted of a 30 degree pulse with power-gated decoupling (*zgpg30*), while for the <sup>14</sup>N spectra the decoupling does not lead to any change in the spectrum and therefore is not necessary.

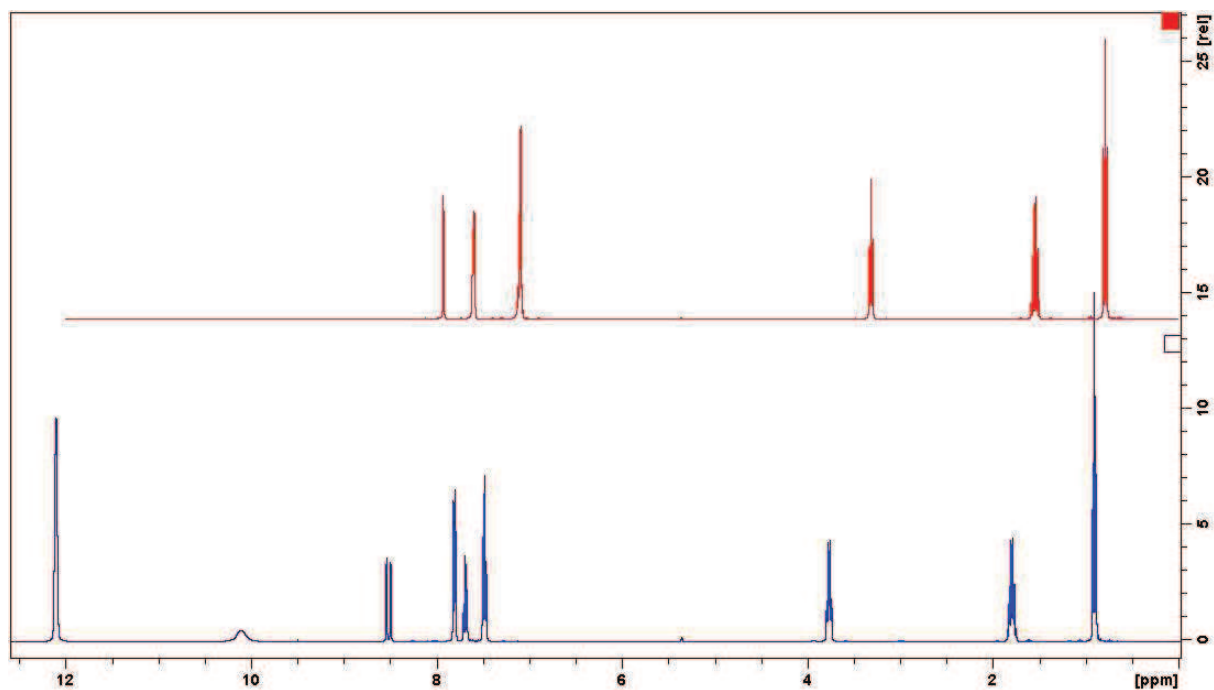


Figure 7.3-1  $^1\text{H}$ -NMR spectra of *N*-propylbenzaldimine: (bottom) neat, (top) as 20 % solution in triflic acid. In triflic acid, the azomethine signal (8.5 ppm) is coupled with the protonated iminium (10.1 ppm) thus showing a coupling of 17.8 Hz, which is in agreement with the range of proton couplings on a *trans*-substituted double bond.

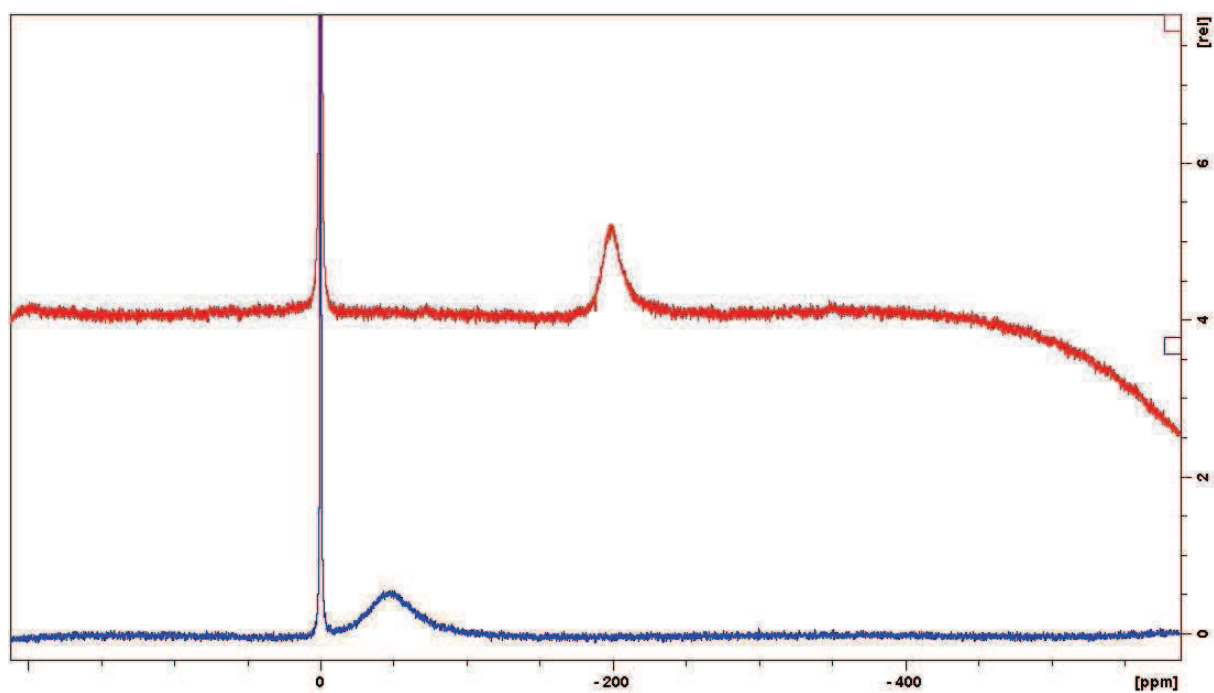


Figure 7.3-2  $^{14}\text{N}$ -NMR spectra of *N*-propylbenzaldimine: (bottom) neat, (top) as 20 % solution in triflic acid. Spectra referenced on  $d_3$ -nitromethane (0 ppm). Significant sharpening of the nitrogen signal as well as upfield shifting is observed.



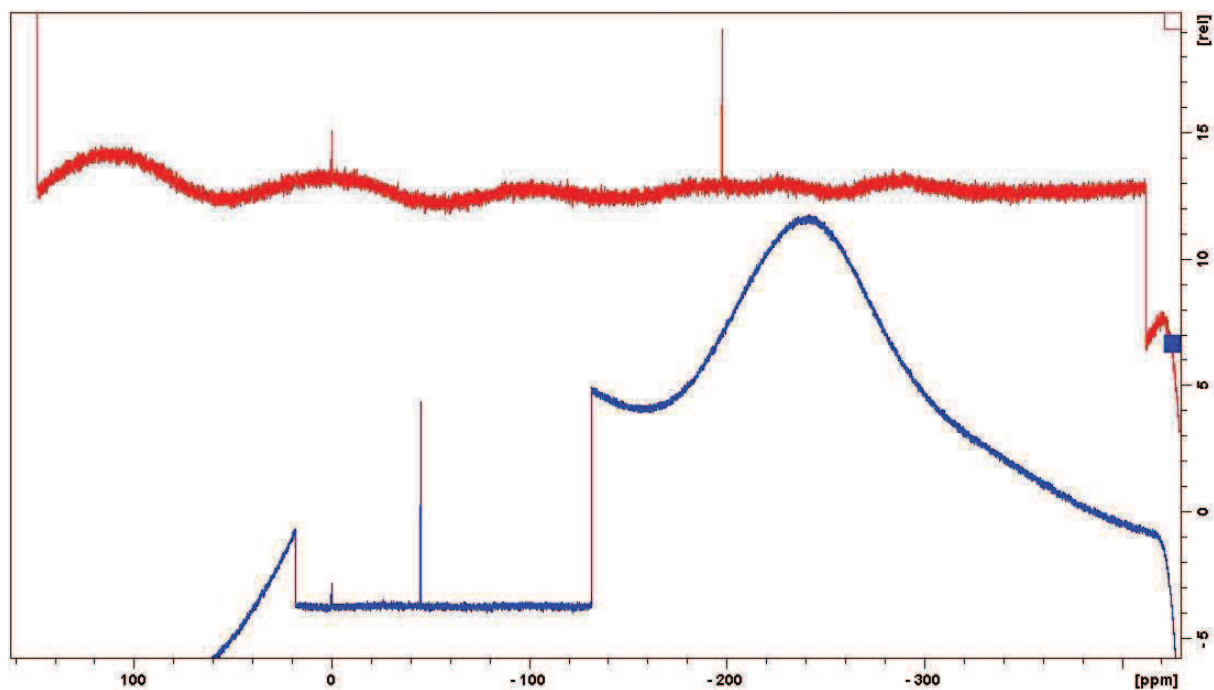


Figure 7.3-3  $^{15}\text{N}$ -NMR spectra of *N*-propylbenzaldimine: (bottom) neat, (top) as 20 % solution in triflic acid. Spectra referenced on  $d_3$ -nitromethane (0 ppm) and measured at natural abundance. Large signal shift upon protonation is observed.  $^{15}\text{N}$ -NMR spectra are acquired on a wide range of ppm and often exhibit a strongly perturbed baseline. Only partial baseline correction on the region of interest was applied in such cases.

## 7.4. Kinetics experiments

### 7.4.1. Mathematic models for kinetic data

Several kinetic measurements were presented in the manuscript. The mathematic treatment was performed according to appropriate kinetic model (first, second, pseudo-first order). These models are part of any physical chemistry textbook.<sup>[60]</sup> The following section summarizes formulas and equations used in the measurements. An explanation of pseudo-first-order kinetics of imine exchange is given in Section 7.4.1.3. In the following Sections,  $[A]$  stand for actual concentration of A,  $A_0$  is the initial concentration,  $A_{eq}$  is the equilibrium concentration and  $A_t$  is a concentration at a given time  $t$ . Both reversible and irreversible models are provided. Please note that for an in principle reversible reaction with quantitative conversion the reversible kinetic model is reduced to the irreversible form. This reduction is only due to mathematic reasons, specifically  $A_{eq} = 0$ , and has no importance for the physical nature of the process under study.

#### 7.4.1.1. *First-order kinetics*

The first-order kinetics expresses the concentration of species by a given equation

$$r = \frac{d[A]}{dt} = -k[A]$$

This equation gives after separation of variables and integration

$$\int_0^t \frac{d[A]}{[A]} = -kdt$$

$$\ln \frac{A_t}{A_0} = -kt$$

In some cases, the differential fitting can be applied

$$\frac{\Delta[A]}{\Delta t} = -k \cdot [A]$$

For reversible first-order rate kinetics, the equation is derived similarly

$$r = \frac{d([A] - A_{eq})}{dt} = -k([A] - A_{eq})$$

Which gives after variable separation and integration a formula

$$\ln \frac{A_t - A_{eq}}{A_0 - A_{eq}} = -kt$$

#### 7.4.1.2. *Second-order kinetics*

The second-order kinetics of a reaction  $A + B \rightarrow C + \dots$  expresses the concentration of species by a given equation

$$r = \frac{d[A]}{dt} = \frac{d[B]}{dt} = -k[A][B]$$

If the stoichiometry of the reaction is given as 1:1 and the reagents are mixed in the same ratio, then the equation can be rewritten as

$$\frac{d[A]}{dt} = -k[A]^2$$

Which after separation of variables and integration gives

$$\int_0^t \frac{d[A]}{[A]^2} = -kdt$$

$$\frac{1}{A_t} - \frac{1}{A_0} = kt$$

Similarly to first order kinetics, the reversibility can be introduced

$$r = \frac{d([A] - A_{eq})}{dt} = \frac{d([B] - B_{eq})}{dt} = -k([A] - A_{eq})([B] - B_{eq})$$

If the stoichiometry of the reaction is given as 1:1 and the reagents are mixed in the same ratio, then the equation can be rewritten and processed as

$$\frac{1}{(A_t - A_{eq})} - \frac{1}{(A_0 - A_{eq})} = kt$$

If the stoichiometry of the reaction is given as 1:1 but the reagents are mixed in different ratio, then the irreversible equation can be expressed as

$$\frac{1}{A_0 - B_0} \ln \frac{A_t B_0}{B_t A_0} = kt$$

In a similar vein, the reversibility can be introduced

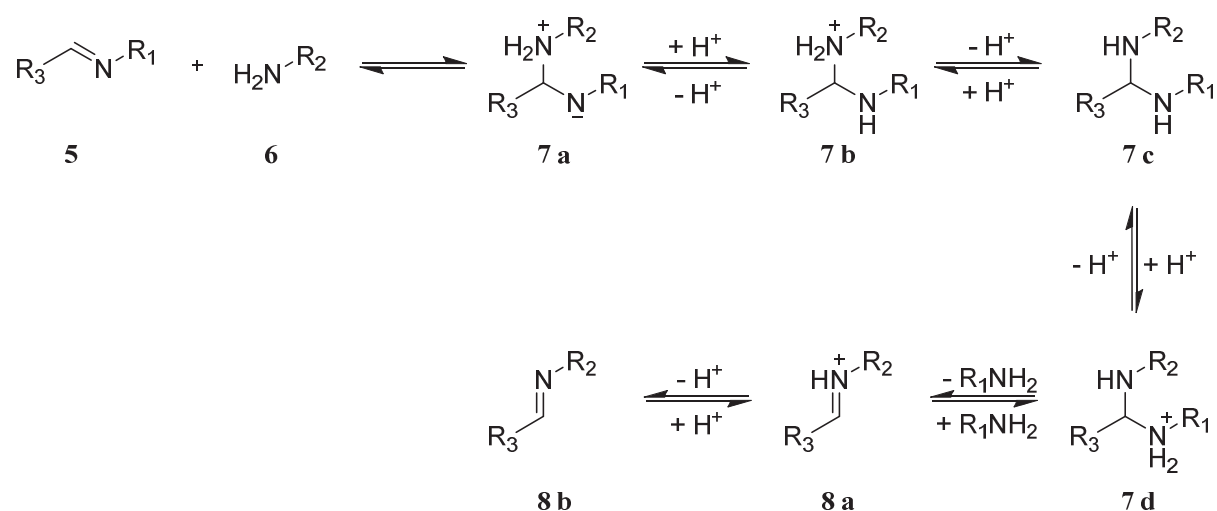
$$\frac{1}{(A_0 - A_{eq}) - (B_0 - B_{eq})} \ln \frac{(A_t - A_{eq})(B_0 - B_{eq})}{(B_t - B_{eq})(A_0 - A_{eq})} = kt$$

Also the differential form can be used

$$\frac{\Delta[A]}{\Delta t} = -k \cdot [A]^2$$

### 7.4.1.3. Imine exchange: pseudo-first-order kinetics

The imine exchange reaction was found to follow the first-order kinetics. However, the process in its nature is bimolecular and the reason for observation of a pseudo-first order behaviour deserves a closer explanation. The mechanism of the imine exchange was discussed in the Section 1.3.1.2 on page 33, for clarity the corresponding Figure is repeated here.



In the literature,<sup>[61,63]</sup> the rate-limiting step was attributed to the deprotonation of the aminal intermediate **7b** or **7d** to give the aminal intermediate **7c**, while all other steps were kinetically fast. The aminal intermediate is formed by the reaction of the imine with an amine and the equilibrium of the reaction is given by the equilibrium constant

$$K = \frac{[7b]}{[5][6]}$$

Since the deprotonation of the structure **7b** is the rate limiting step, the rate of formation of the imine **8b** can now be expressed as

$$r = \frac{d[8b]}{dt} = k[7b]$$

From the definition of the equilibrium constant we can now substitute

$$r = \frac{d[8b]}{dt} = k \cdot K \cdot [5][6]$$

Since amines used in study are very much the same in reactivity, proceeding reaction liberate into the solution an amine which has the same capability to form the aminal, therefore the apparent concentration of **6** is constant (standing for both  $R_1NH_2$  and  $R_2NH_2$ ) and can be denoted as  $Am_0$ . So the term **[6]** can be replaced by the initial  $Am_0$  concentration of **6**, since this is constant in time.

$$r = \frac{d[8b]}{dt} = k \cdot K \cdot [5] \cdot Am_0$$

Accounting the reversibility of the reaction (50 % equilibrium conversion) and definition of reaction rates for **[5]** and **[8b]**, we get

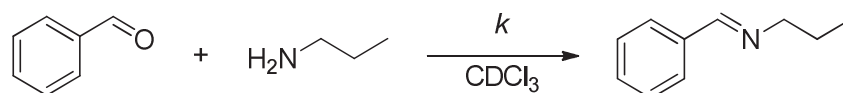
$$\frac{d([5] - 5_{eq})}{([5] - 5_{eq})dt} = k \cdot K \cdot Am_0$$

This formula can be used either in the derivative form or be integrated (analogously to the previous examples). Values of intermediate equilibrium constant  $K$  and rate constant  $k$  cannot be separated by simple experiments.

### 7.4.2. Results of kinetics experiments

The following Sections report on the kinetics of formation and exchange of imines. The experimental data were processed according to the appropriate kinetic equations discussed above. The statistical parameters (the standard deviation  $\sigma$  and the coefficient of determination  $R^2$ ) of the fitting and the rate constants are provided.

#### 7.4.2.1. *N*-propylbenzaldimine formation



In NMR tube, benzaldehyde was mixed with 1 equivalent of propylamine in  $\text{CDCl}_3$ . The spectra were recorded at interval of 177 s. The actual concentration of the aldehyde was 123 mM and of the amine 114 mM. The integration of the peaks of the aldehyde consumed (10.024 ppm) and imine formed (8.270 ppm) was process as second-order reaction kinetics corrected for the non-stoichiometric reagent mixing ratio. Data are plotted in Figure 7.4-1 and the results are given in Table 7.4-1.

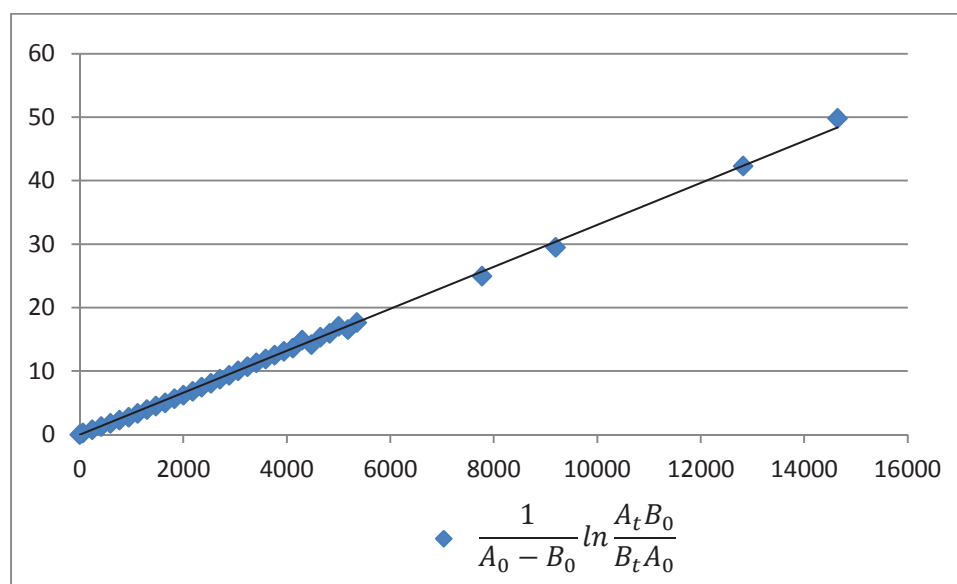
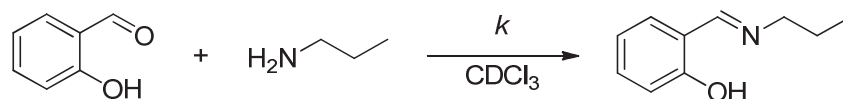


Figure 7.4-1 Plot of the processed NMR integral intensities of the imine formation reaction of benzaldehyde with *n*-propylamine. Data were processed according to second-order reaction kinetics with correction for non-stoichiometric reagent mixing ratio.

$$\begin{aligned} k &= (3.26 \pm 0.01) \cdot 10^{-3} \text{ L mol}^{-1} \text{ s}^{-1} \\ \sigma &= 2.609 \cdot 10^{-5} \text{ L mol}^{-1} \text{ s}^{-1} \\ R^2 &= 0.9981 \end{aligned}$$

Table 7.4-1 Linear regression coefficients and kinetic parameters of imine formation for the reaction of benzaldehyde with *n*-propylamine in  $\text{CDCl}_3$  followed by NMR.

### 7.4.2.2. *N*-propylsalicylaldimine formation



In NMR tube, salicylaldehyde was mixed with 1 equivalent of propylamine in  $\text{CDCl}_3$ . The spectra were recorded at interval of 157 s. The actual concentrations of both the aldehyde and amine were 117 mM. The integration of the peaks of the aldehyde consumed (9.929 ppm) and imine formed (8.358 ppm) was process as second-order reaction. Data are plotted in Figure 7.4-2 and the results are given in Table 7.4-1.

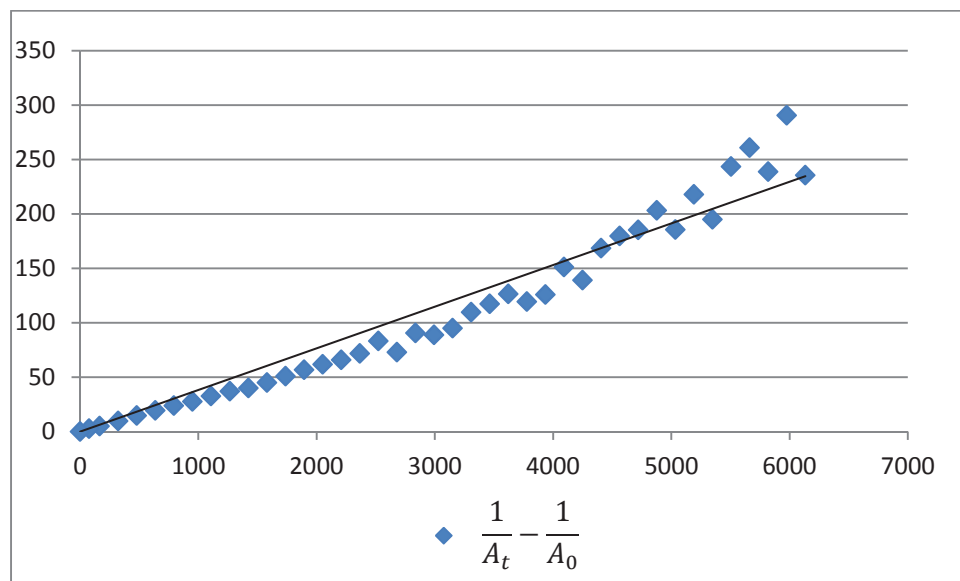


Figure 7.4-2 Plot of the processed NMR integral intensities of the imine formation reaction of salicylaldehyde with *n*-propylamine. Processed according to second-order reaction kinetics.

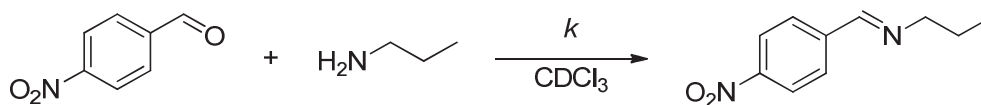
$$k = (3.83 \pm 0.06) \cdot 10^{-2} \text{ L mol}^{-1} \text{ s}^{-1}$$

$$\sigma = 1.681 \cdot 10^{-3} \text{ L mol}^{-1} \text{ s}^{-1}$$

$$R^2 = 0.9570$$

Table 7.4-2 Linear regression coefficients and kinetic parameters of imine formation for the reaction of salicylaldehyde with *n*-propylamine in  $\text{CDCl}_3$  followed by NMR.



7.4.2.3. *N*-propyl-4-nitrobenzaldimine formation

In NMR tube, *p*-nitrobenzaldehyde was mixed with 1 equivalent of propylamine in CDCl<sub>3</sub>. The spectra were recorded at interval of 87 s. The actual concentration of the aldehyde was 119 mM and of the amine 127 mM. The integration of the peaks of the –N-CH<sub>2</sub>– group of the unreacted amine (2.641 ppm) and imine formed (3.635 ppm) was process as second-order reaction kinetics corrected for the non-stoichiometric reagent mixing ratio. Data are plotted in Figure 7.4-3 and the results are given in Table 7.4-3.

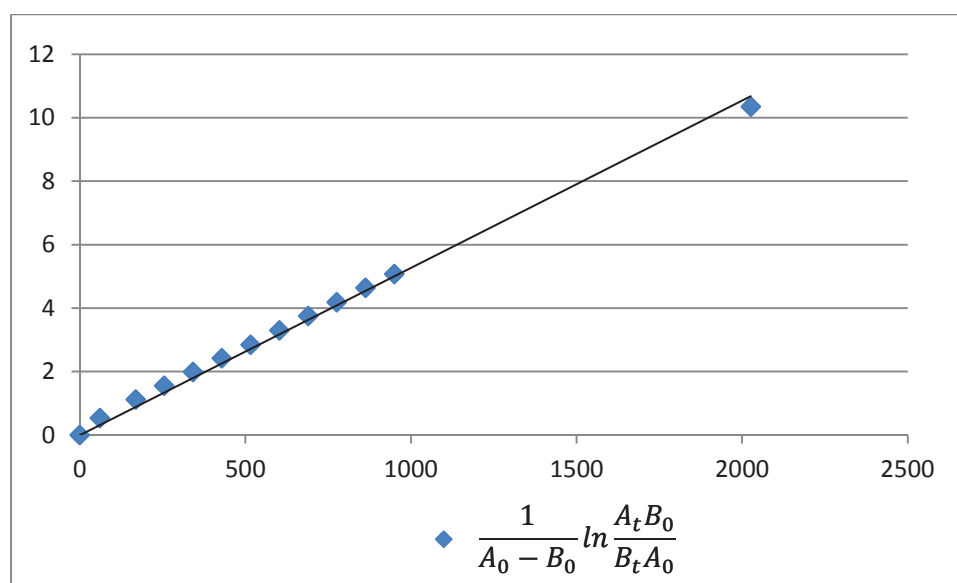
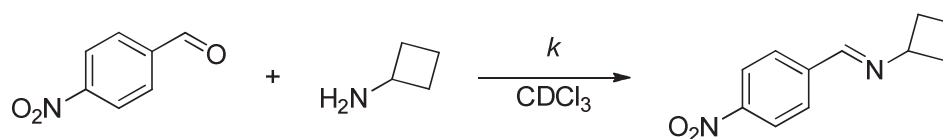


Figure 7.4-3 Plot of the processed NMR integral intensities of the imine formation reaction of *p*-nitrobenzaldehyde with *n*-propylamine, processed according to second-order reaction kinetics with correction for non-stoichiometric reagent mixing ratio.

$$\begin{array}{l}
 k = (5.27 \pm 0.06) \cdot 10^{-3} \text{ L mol}^{-1} \text{ s}^{-1} \\
 \sigma = 1.01 \cdot 10^{-4} \text{ L mol}^{-1} \text{ s}^{-1} \\
 R^2 = 0.9991
 \end{array}$$

Table 7.4-3 Linear regression coefficients and kinetic parameters of imine formation for the reaction of *p*-nitrobenzaldehyde with *n*-propylamine in CDCl<sub>3</sub> followed by NMR.

#### 7.4.2.4. *N*-cyclobutyl-4-nitrobenzalimine formation



In NMR tube, benzaldehyde was mixed with 1 equivalent of cyclobutylamine in  $\text{CDCl}_3$ . The spectra were recorded at interval of 102 s. The actual concentration of the aldehyde was 119 mM and of the amine 123 mM. The integration of the peaks of the  $-\text{N}-\text{CH}_2-$  group of the unreacted amine (3.384 ppm) and imine formed (4.230 ppm) was process as second-order reaction kinetics corrected for the non-stoichiometric reagent mixing ratio. Data are plotted in Figure 7.4-4 and the results are given in Table 7.4-4.

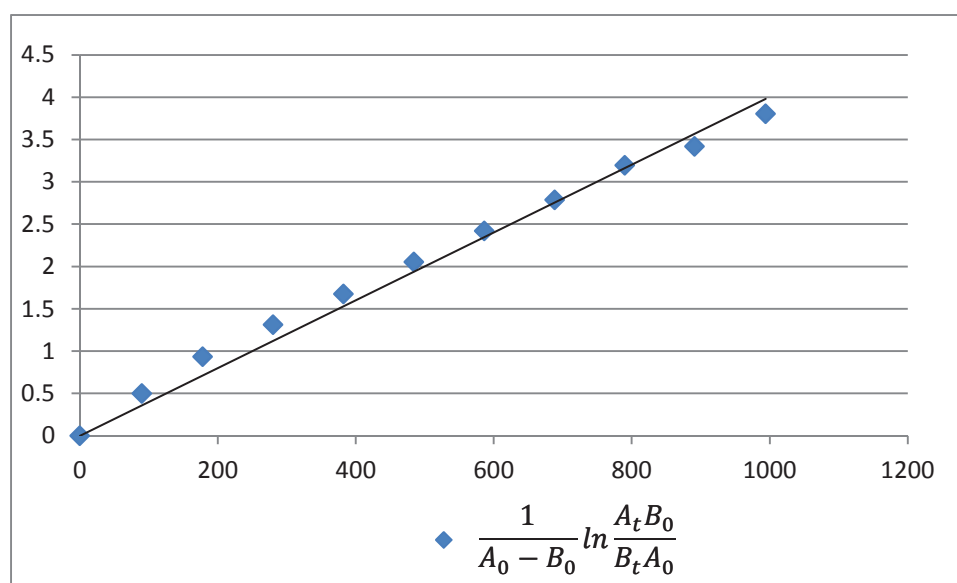


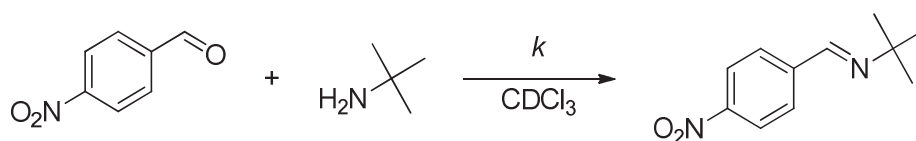
Figure 7.4-4 Plot of the processed NMR integral intensities of the imine formation reaction of *p*-nitrobenzaldehyde with cyclobutylamine, processed according to second-order reaction kinetics with correction for non-stoichiometric reagent mixing ratio.

$$k = (4.00 \pm 0.09) \cdot 10^{-3} \text{ L mol}^{-1} \text{ s}^{-1}$$

$$\sigma = 1.417 \cdot 10^{-4} \text{ L mol}^{-1} \text{ s}^{-1}$$

$$R^2 = 0.9948$$

Table 7.4-4 Linear regression coefficients and kinetic parameters of imine formation for the reaction of *p*-nitrobenzaldehyde with cyclobutylamine in  $\text{CDCl}_3$  followed by NMR.

7.4.2.5. *N-t-butyl-4-nitrobenzaldimine formation*

In NMR tube, benzaldehyde was mixed with 1 equivalent of *t*-butylamine in CDCl<sub>3</sub>. The spectra were recorded at interval of 116 s. The actual concentration of the aldehyde was 119 mM and of the amine 135 mM. The integration of the peaks of the CH<sub>3</sub> groups of the unreacted amine (1.138 ppm) and imine formed (1.300 ppm) was process as second-order reaction kinetics corrected for the non-stoichiometric reagent mixing ratio. Data are plotted in Figure 7.4-5 and the results are given in Table 7.4-5.

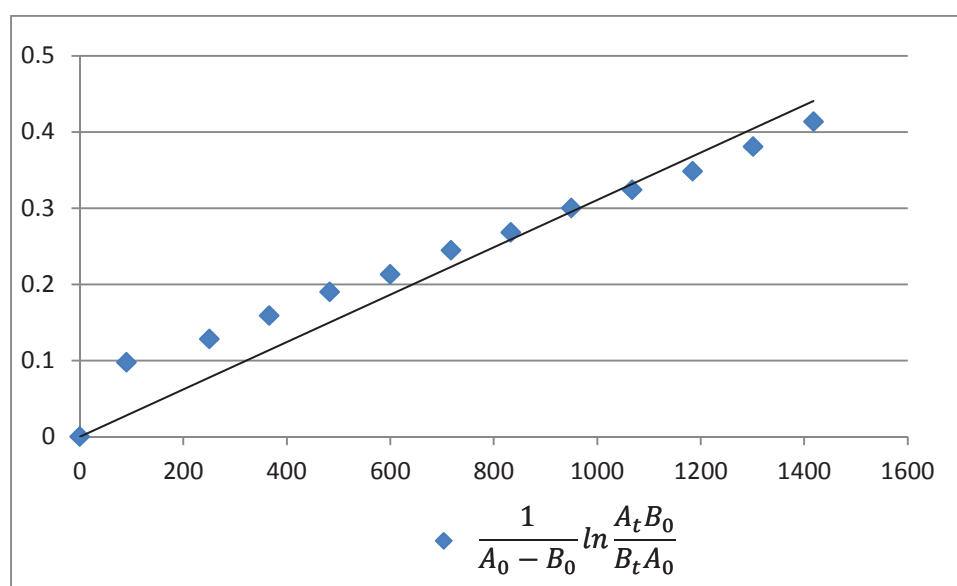


Figure 7.4-5 Plot of the processed NMR integral intensities of the imine formation reaction of *p*-nitrobenzaldehyde with *t*-butylamine, processed according to second-order reaction kinetics with correction for non-stoichiometric reagent mixing ratio.

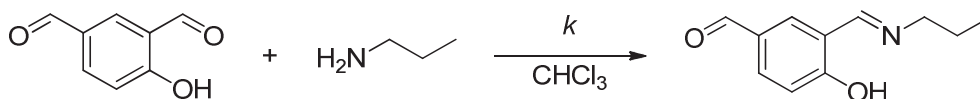
$$k = (3.11 \pm 0.13) \cdot 10^{-4} \text{ L mol}^{-1} \text{ s}^{-1}$$

$$\sigma = 2.232 \cdot 10^{-5} \text{ L mol}^{-1} \text{ s}^{-1}$$

$$R^2 = 0.9773$$

Table 7.4-5 Linear regression coefficients and kinetic parameters of imine formation for the reaction of *p*-nitrobenzaldehyde with *t*-butylamine in CDCl<sub>3</sub> followed by NMR.

#### 7.4.2.6. *N*-propyl-5-formyl-2-hydroxybenzalimine formation



In UV-Vis cuvette, stock solutions of 4-hydroxy-isophthalaldehyde and *n*-propylamine (both in chloroform) were mixed to give equimolar mixture of total volume of 3.000 mL and resulting concentration of both reagents of 0.856 mM. Absorbance at 403 nm was measured at interval of 20 s. The molar absorption coefficient was determined as follows: the NMR spectrum of 112 mM solution of both reagents in CDCl<sub>3</sub> was recorded and showed full conversion of uniquely one aldehyde group to imine while the other aldehyde group remained (identification of the signals of the two aldehyde groups was based on 2D NOESY, HSQC and HMBC spectra). This sample was then diluted to concentrations of 5.0 mM, 1.1 mM and 0.2 mM and the UV-VIS spectra were recorded. The slope of the plot of absorbance as a function of concentration is the molar absorption coefficient, determined to be 2260 L mol<sup>-1</sup> cm<sup>-1</sup>.

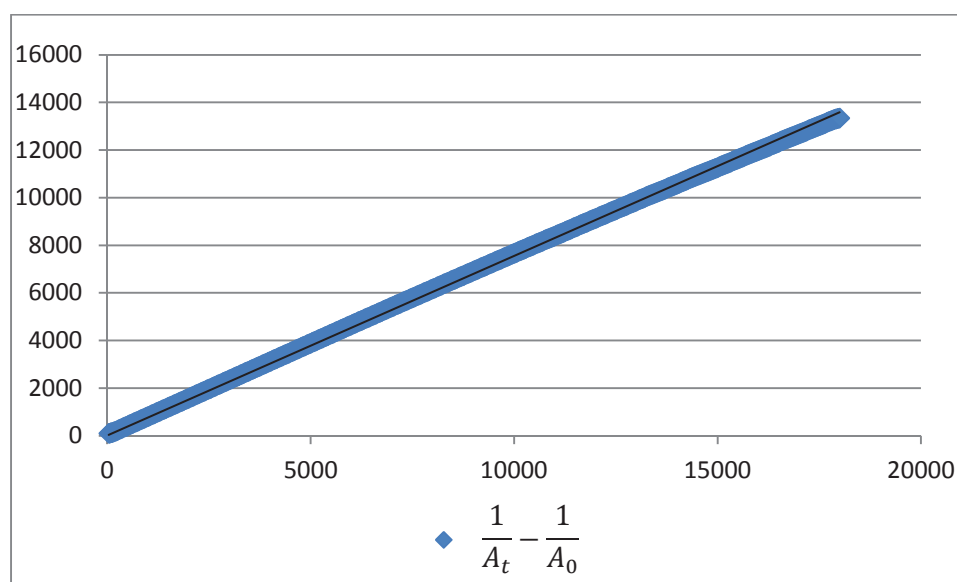


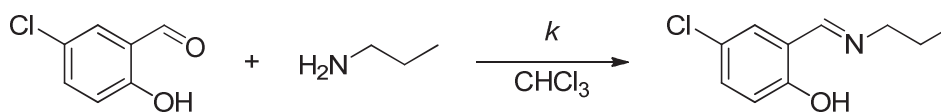
Figure 7.4-6 Plot of the processed UV-Vis absorbance intensities of the imine formation reaction of 4-hydroxy-isophthalaldehyde with propylamine, processed according to second-order reaction kinetics. The reaction shows a total conversion and therefore irreversible kinetic model was used.

The absorbance data were processed according to second-order reaction kinetics and plotted in Figure 7.4-6. Linear regression of the obtained data gave rate constant of  $(7.55 \pm 0.02) \cdot 10^{-2} \text{ L mol}^{-1} \text{ s}^{-1}$ . The regression coefficients are given in Table 7.4-6.

$$\begin{aligned}
 k &= (7.55 \pm 0.02) \cdot 10^{-1} \text{ L mol}^{-1} \text{ s}^{-1} \\
 \sigma &= 6.259 \cdot 10^{-4} \text{ L mol}^{-1} \text{ s}^{-1} \\
 R^2 &= 0.9997
 \end{aligned}$$

Table 7.4-6 Linear regression coefficients and kinetic parameters of imine formation for the reaction of 4-hydroxy-isophthalaldehyde with propylamine in CHCl<sub>3</sub> followed by UV-Vis spectrophotometry.

#### 7.4.2.7. *N*-propyl-5-chloro-2-hydroxybenzaldimine formation



In UV-Vis cuvette, stock solutions of 5-chloro-salicylaldehyde and *n*-propylamine (both in chloroform) were mixed to give equimolar mixture of total volume of 3.000 mL and resulting concentration of both reagents of 3.818 mM. Absorbance at 403 nm was measured at interval of 10 s. Molar absorption coefficient was determined using imine prepared separately (Section 7.2.1.3) as  $\epsilon=190 \text{ L mol}^{-1} \text{ cm}^{-1}$ .

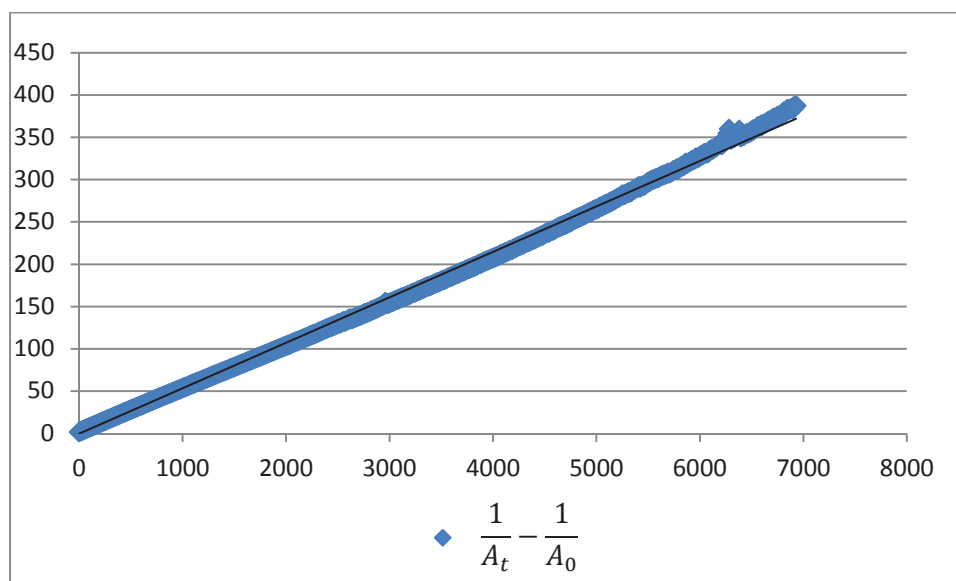


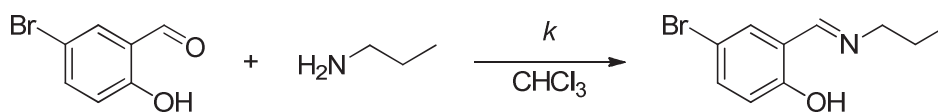
Figure 7.4-7 Plot of the processed UV-Vis absorbance intensities of the imine formation reaction of 5-chloro-salicylaldehyde with propylamine, processed according to second-order reaction kinetics. The reaction shows a total conversion and therefore irreversible kinetic model was used.

The absorbance data were processed according to second-order reaction kinetics and plotted in Figure 7.4-7. Linear regression of the obtained data gave rate constant of  $(5.76 \pm 0.01) \cdot 10^{-2} \text{ L mol}^{-1} \text{ s}^{-1}$ . The regression coefficients are given in Table 7.4-7.

$k =$	$(5.76 \pm 0.01) \cdot 10^{-2} \text{ L mol}^{-1} \text{ s}^{-1}$
$\sigma =$	$2.180 \cdot 10^{-5} \text{ L mol}^{-1} \text{ s}^{-1}$
$R^2 =$	$0.9919$

Table 7.4-7 Linear regression coefficients and kinetic parameters of imine formation for the reaction of 5-chloro-salicylaldehyde with propylamine in  $\text{CHCl}_3$  followed by UV-Vis spectrophotometry.

### 7.4.2.8. *N*-propyl-5-bromo-2-hydroxybenzaldimine formation



In UV-Vis cuvette, stock solutions of 5-bromo-salicylaldehyde and *n*-propylamine (both in chloroform) were mixed to give equimolar mixture of total volume of 3.000 mL and resulting concentration of both reagents of 0.322 mM. Absorbance at 403 nm was measured at interval of 5 s. Molar absorption coefficient was determined using imine prepared separately (Section 7.2.1.4) as  $\epsilon=200 \text{ L mol}^{-1} \text{ cm}^{-1}$ .

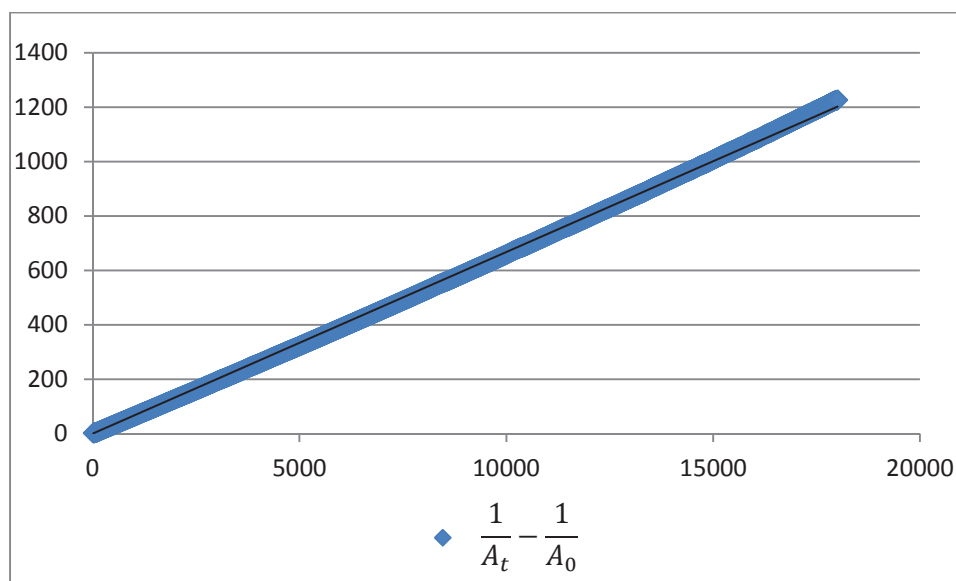


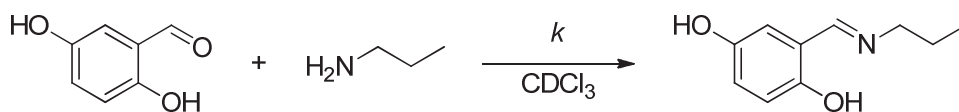
Figure 7.4-8 Plot of the processed UV-Vis absorbance intensities of the imine formation reaction of 5-bromo-salicylaldehyde with propylamine, processed according to second-order reaction kinetics. The reaction shows a total conversion and therefore irreversible kinetic model was used.

The absorbance data were processed according to second-order reaction kinetics and plotted in Figure 7.4-8. Linear regression of the obtained data gave rate constant of  $(6.67 \pm 0.02) \cdot 10^{-2} \text{ L mol}^{-1} \text{ s}^{-1}$ . The regression coefficients are given in Table 7.4-8.

$k =$	$(6.67 \pm 0.02) \cdot 10^{-2} \text{ L mol}^{-1} \text{ s}^{-1}$
$\sigma =$	$3.419 \cdot 10^{-5} \text{ L mol}^{-1} \text{ s}^{-1}$
$R^2 =$	$0.9996$

Table 7.4-8 Linear regression coefficients and kinetic parameters of imine formation for the reaction of 5-bromo-salicylaldehyde with propylamine in CHCl<sub>3</sub> followed by UV-Vis spectrophotometry.



7.4.2.9. *N*-propyl-2,5-dihydroxybenzalimine formation

In NMR tube, stock solutions (in CDCl<sub>3</sub>) of both reagents were diluted in CDCl<sub>3</sub> to give equimolar reaction mixture at concentration of 40 mM in total volume of 0.500 mL. The integral intensities of the signals of aldehyde (9.844 ppm) and imine (8.281 ppm) were followed with increasing interval for 101 minutes (almost equilibrium). Data were processed as second-order reaction kinetics corrected for the non-stoichiometric reagent mixing ratio and are plotted in Figure 7.4-9 and the results are given in Table 7.4-9.

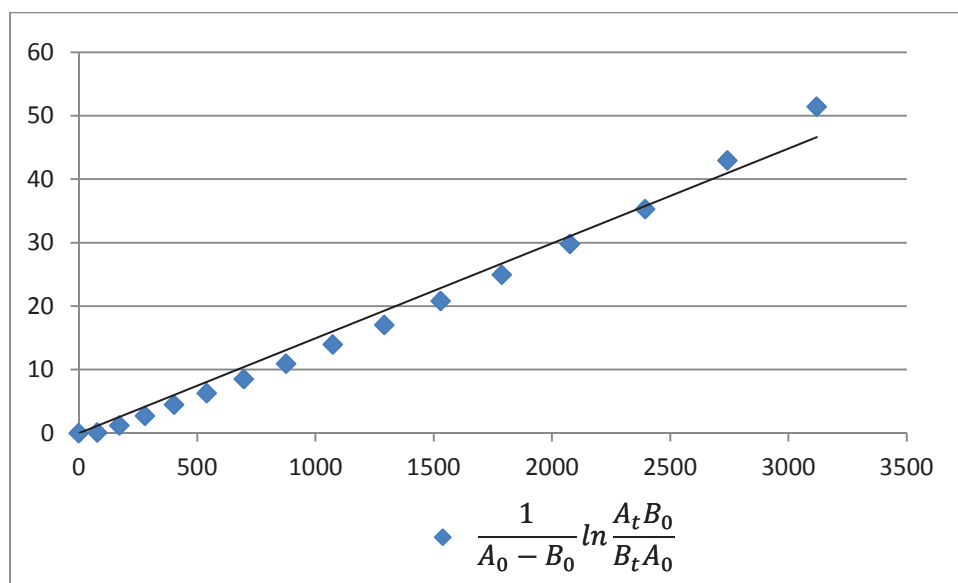


Figure 7.4-9 Plot of the processed NMR integral intensities of the imine formation reaction of 5-bromo-salicylaldehyde with *n*-propylamine, processed according to second-order reaction kinetics with correction for non-stoichiometric reagent mixing ratio.

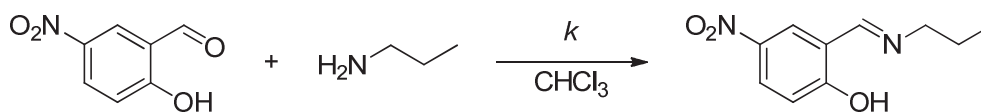
$$k = (1.56 \pm 0.04) \cdot 10^{-2} \text{ L mol}^{-1} \text{ s}^{-1}$$

$$\sigma = 6.71 \cdot 10^{-4} \text{ L mol}^{-1} \text{ s}^{-1}$$

$$R^2 = 0.9870$$

Table 7.4-9 Linear regression coefficients and kinetic parameters of imine formation for the reaction of 5-bromo-salicylaldehyde with *n*-propylamine in CDCl<sub>3</sub> followed by NMR.

### 7.4.2.10. *N*-propyl-5-nitro-2-hydroxybenzaldimine formation



In UV-Vis cuvette, stock solutions of 5-nitro-salicylaldehyde and *n*-propylamine (both in chloroform) were mixed to give equimolar mixture of total volume of 3.000 mL and resulting concentration of both reagents of 0.766 mM. Absorbance at 403 nm was measured at interval of 5 s. Molar absorption coefficient was determined using imine prepared separately (Section 7.2.1.6) as  $\epsilon=4190 \text{ L mol}^{-1} \text{ cm}^{-1}$ .

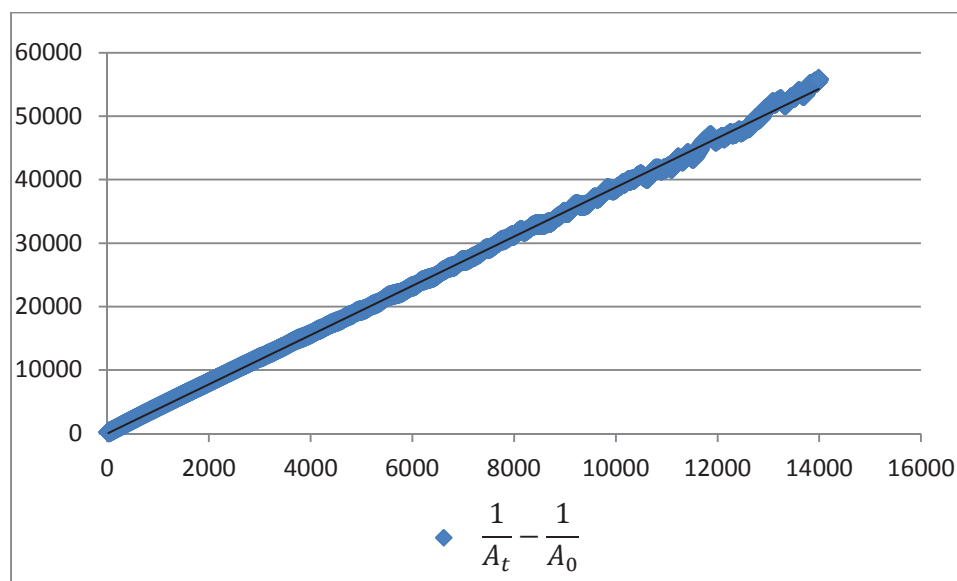


Figure 7.4-10 Plot of the processed UV-Vis absorbance intensities of the imine formation reaction of 5-nitro-salicylaldehyde with propylamine, processed according to second-order reaction kinetics. The reaction shows a total conversion and therefore irreversible kinetic model was used.

The absorbance data were processed according to second-order reaction kinetics and plotted in Figure 7.4-10. Linear regression of the obtained data gave rate constant of  $(3.89 \pm 0.01) \text{ L mol}^{-1} \text{ s}^{-1}$ . The regression coefficients are given in Table 7.4-10.

$$\begin{array}{l}
 k = (3.89 \pm 0.01) \text{ L mol}^{-1} \text{ s}^{-1} \\
 \sigma = 2.430 \cdot 10^{-3} \text{ L mol}^{-1} \text{ s}^{-1} \\
 R^2 = 0.9998
 \end{array}$$

Table 7.4-10 Linear regression coefficients and kinetic parameters of imine formation for the reaction of 5-nitro-salicylaldehyde with propylamine in  $\text{CHCl}_3$  followed by UV-Vis spectrophotometry.

### 7.4.2.11. *N*-propyl-aldimines formation in aqueous media

The imine formation by the reaction of several aldehyde derivatives with *n*-propylamine was studied in aqueous media, specifically a  $d_3$ -acetonitrile/deuterium oxide mixture (7:3, v/v). To this end, 200 mM stock solutions of the reagents were prepared in the solvent mixture. The reagents were mixed in NMR tube in 1:1 ratio and diluted to give the final concentration of 20 mM of both reagents. The NMR spectra were recorded immediately after mixing. The integral intensities of the aldehyde peak and the imine peak were processed according the second-order kinetics. The results of the fitting are provided in Table 7.4-11.

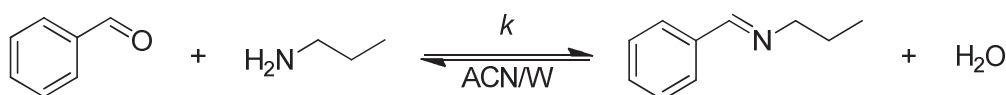


Figure 7.4-11 A general scheme of an imine formation by the condensation of an aldehyde with *n*-propylamine.

Aldehyde	Parameter	Value
benzaldehyde	$\chi = (K)$	70.8 % (2.42)
	$k =$	$(24.29 \pm 0.22) \cdot 10^{-3} \text{ L mol}^{-1} \text{ s}^{-1}$
	$\sigma$	$4.37 \cdot 10^{-4} \text{ L mol}^{-1} \text{ s}^{-1}$
	$R^2 =$	0.9958
<i>p</i> -nitrobenzaldehyde	$\chi = (K)$	91.2 % (10.36)
	$k =$	$(27.92 \pm 0.08) \cdot 10^{-3} \text{ L mol}^{-1} \text{ s}^{-1}$
	$\sigma$	$2.99 \cdot 10^{-4} \text{ L mol}^{-1} \text{ s}^{-1}$
	$R^2 =$	0.9940
salicylaldehyde	$\chi = (K)$	93.4 % (14.15)
	$k =$	$(18.47 \pm 0.96) \cdot 10^{-2} \text{ L mol}^{-1} \text{ s}^{-1}$
	$\sigma$	$4.5 \cdot 10^{-3} \text{ L mol}^{-1} \text{ s}^{-1}$
	$R^2 =$	0.9917
pyridine-2-carboxaldehyde	$\chi = (K)$	84.2 % (5.33)
	$k =$	$(29.22 \pm 0.48) \cdot 10^{-2} \text{ L mol}^{-1} \text{ s}^{-1}$
	$\sigma$	$8.09 \cdot 10^{-3} \text{ L mol}^{-1} \text{ s}^{-1}$
	$R^2 =$	0.9947
pyridine-4-carboxaldehyde	$\chi = (K)$	89.0 % (8.09)
	$k =$	$(67.56 \pm 0.51) \cdot 10^{-3} \text{ L mol}^{-1} \text{ s}^{-1}$
	$\sigma$	$8.51 \cdot 10^{-4} \text{ L mol}^{-1} \text{ s}^{-1}$
	$R^2 =$	0.9984

Table 7.4-11 Summary of the imine formation kinetics for various aldehydes in a mixture of  $CD_3CN/D_2O$  (7:3, v/v). The equilibrium conversion ( $\chi$ ) is also expressed in terms of the equilibrium constant ( $K$ ).

### 7.4.2.12. *N*-propylbenzaldimine exchange with *i*-pentylamine



*N*-propylbenzaldimine was mixed in NMR tube with 1 equivalent of *i*-pentylamine thus giving equimolar reaction mixture at concentration of 564 mM in  $\text{CDCl}_3$ . The reaction was followed by NMR at intervals of 150 s. The integral intensities of  $=\text{N}-\text{CH}_2-$  protons (3.45 – 3.61 ppm) were processed as reversible first-order kinetic reaction with equilibrium constant  $K = 1.00$ . Data are plotted in Figure 7.4-12 and the results are given in Table 7.4-12.

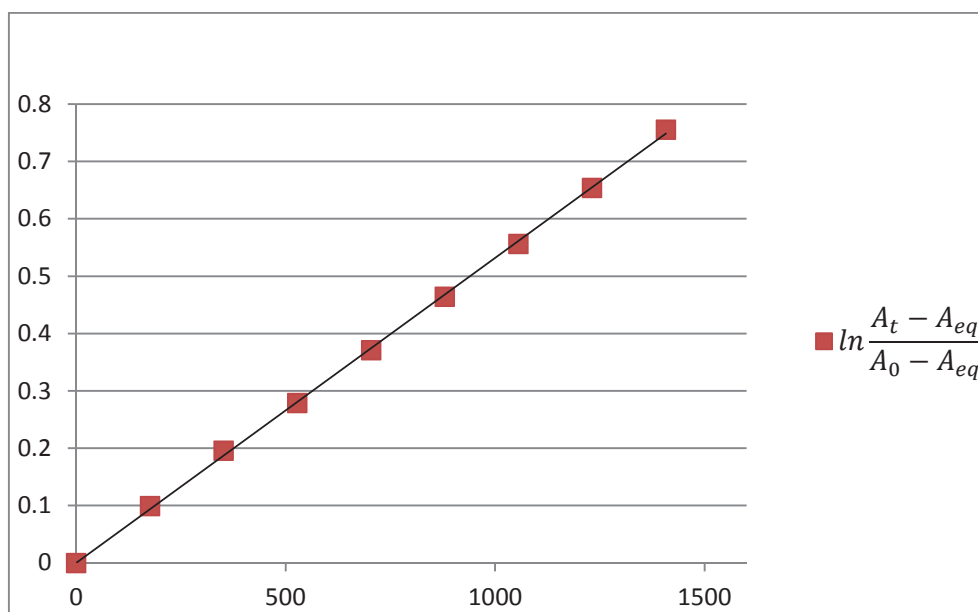
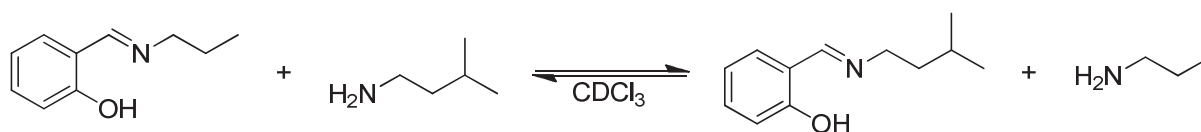


Figure 7.4-12 Plot of the processed integration data of imine exchange reaction for *N*-propylbenzaldimine with *i*-pentylamine in  $\text{CDCl}_3$  followed by NMR. Raw integrals were processed as reversible first-order reaction with equilibrium constant of  $K=1$ .

$\chi = (K)$	50 % (1.00)
$k =$	$(4.38 \pm 0.26) \cdot 10^{-3} \text{ s}^{-1}$
$\sigma =$	$1.16 \cdot 10^{-4} \text{ s}^{-1}$
$R^2 =$	0.9982

Table 7.4-12 Linear regression coefficients and kinetic parameters of imine exchange reaction for *N*-propylbenzaldimine with *i*-pentylamine in  $\text{CDCl}_3$  followed by NMR.

7.4.2.13. *N*-propylsalicylaldimine exchange with *i*-pentylamine

*N*-propylsalicylaldimine was mixed in NMR tube with 1 equivalent of *i*-pentylamine thus giving equimolar reaction mixture at concentration of 152.1 mM in  $\text{CDCl}_3$ . The reaction was followed by NMR at intervals of 157 s. The integral intensities of =N-CH<sub>2</sub>- protons (3.527 – 3.613 ppm) were processed as reversible first-order kinetic reaction with equilibrium constant  $K = 1$ . Data are plotted in Figure 7.4-13 and the results are given in Table 7.4-13.

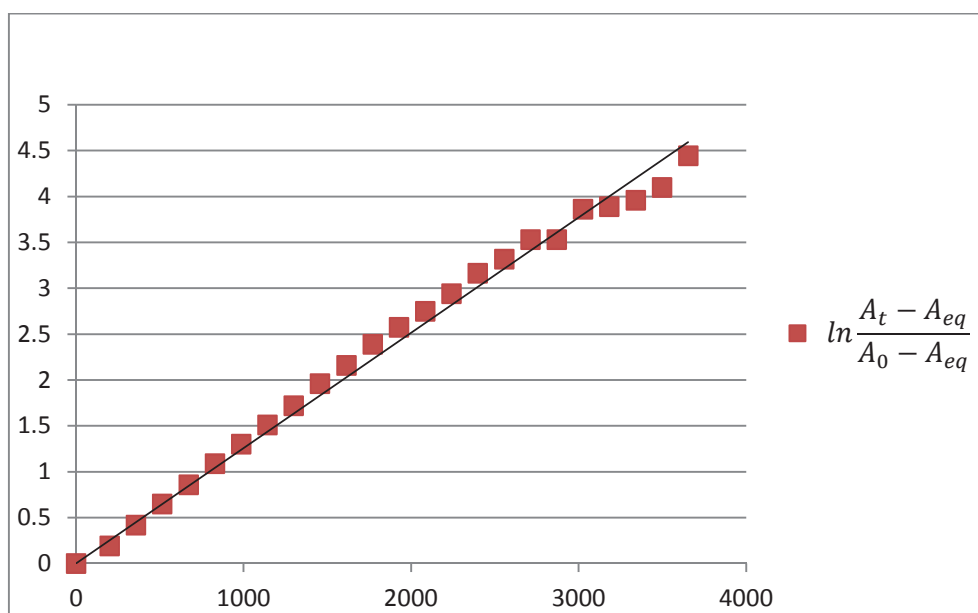


Figure 7.4-13 Plot of the processed integration data of imine exchange reaction for *N*-propylsalicylaldimine with *i*-pentylamine in  $\text{CDCl}_3$  followed by NMR. Raw integrals were processed as reversible first-order reaction with equilibrium constant of  $K = 1$ .

$\chi = (K)$	50 % (1.00)
$k =$	$(1.26 \pm 0.01) \cdot 10^{-3} \text{ s}^{-1}$
$\sigma =$	$2.456 \cdot 10^{-5} \text{ s}^{-1}$
$R^2 =$	0.9924

Table 7.4-13 Linear regression coefficients and kinetic parameters of imine exchange reaction for *N*-propylsalicylaldimine with *i*-pentylamine in  $\text{CDCl}_3$  followed by NMR.

#### 7.4.2.14. *N*-benzylidenaniline exchange with *n*-propylamine



*N*-benzylidenaniline was mixed in NMR tube with 1 equivalent of *n*-propylamine thus giving equimolar reaction mixture at concentration of 264 mM in  $\text{CDCl}_3$ . The reaction was followed by NMR at intervals of 176 s. The integral intensities of  $-\text{CH}=\text{N}-$  protons (8.467 ppm for *N*-benzylidenaniline and 8.280 ppm for *N*-propylbenzaldimine) were processed as reversible first-order kinetic reaction with equilibrium constant  $K = 9.00$ . Data are plotted in Figure 7.4-14 and the results are given in Table 7.4-14.

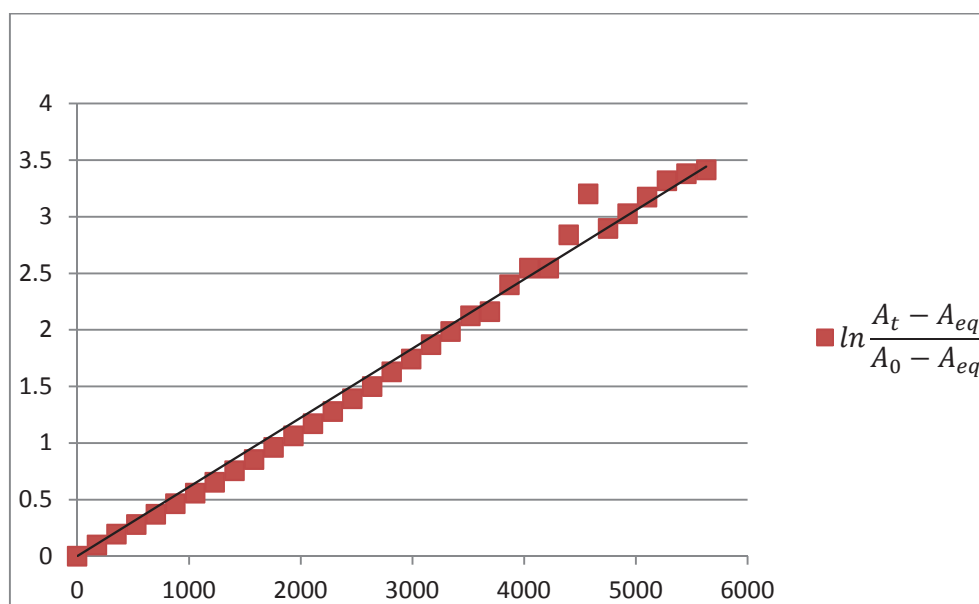


Figure 7.4-14 Plot of the processed integration data of imine exchange reaction for *N*-benzylidenaniline with *n*-propylamine in  $\text{CDCl}_3$  followed by NMR. Raw integrals were processed as reversible first-order reaction with equilibrium constant of  $K=9$ .

$\chi = (K)$	90 % (9.00)
$k =$	$(5.62 \pm 0.04) \cdot 10^{-4} \text{ s}^{-1}$
$\sigma =$	$7.85 \cdot 10^{-6} \text{ s}^{-1}$
$R^2 =$	0.9980

Table 7.4-14 Linear regression coefficients and kinetic parameters of imine exchange reaction for *N*-benzylidenaniline with *n*-propylamine in  $\text{CDCl}_3$  followed by NMR.



7.4.2.15. *N*-propylbenzaldimine exchange with aniline

*N*-propylbenzaldimine was mixed in NMR tube with 1 equivalent of aniline thus giving equimolar reaction mixture at concentration of 564 mM in  $\text{CDCl}_3$ . The reaction was followed by NMR at intervals of 177 s. The integral intensities of  $-\text{CH}=\text{N}-$  protons (8.492 ppm for *N*-benzylideneaniline and 8.308 ppm for *N*-propylbenzaldimine) were processed as reversible first-order kinetic reaction with equilibrium constant  $K = 0.11$ . Data are plotted in Figure 7.4-15 and the results are given in Table 7.4-15.

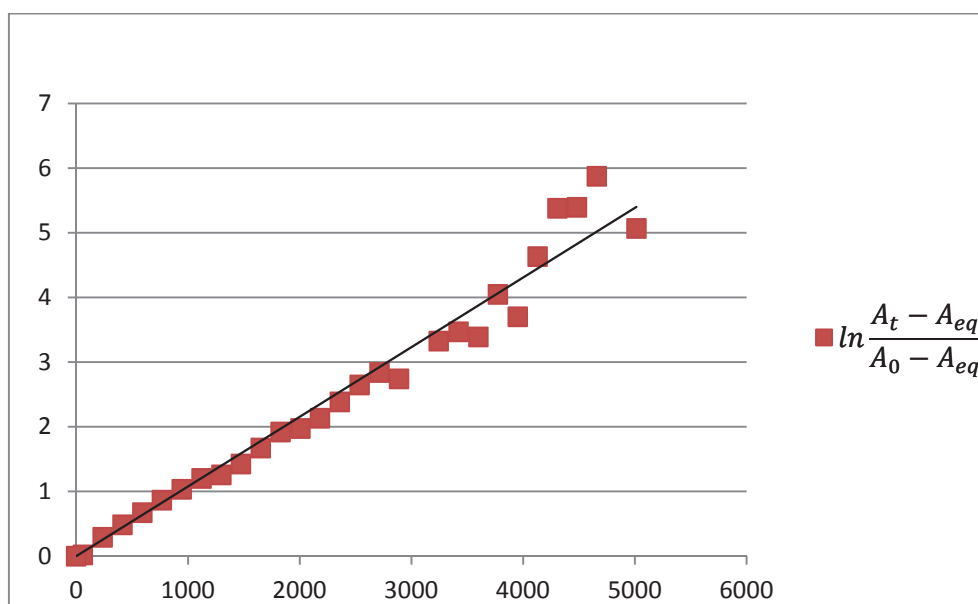


Figure 7.4-15 Plot of the processed integration data of imine exchange reaction for *N*-propylbenzaldimine with aniline in  $\text{CDCl}_3$  followed by NMR. Raw integrals were processed as reversible first-order reaction with equilibrium constant of  $K=0.11$ .

$\chi = (K)$	10 % (0.11)
$k =$	$(1.002 \pm 0.042) \cdot 10^{-3} \text{ s}^{-1}$
$\sigma =$	$2.035 \cdot 10^{-5} \text{ s}^{-1}$
$R^2 =$	0.9916

Table 7.4-15 Linear regression coefficients and kinetic parameters of imine exchange reaction for *N*-propylbenzaldimine with aniline in  $\text{CDCl}_3$  followed by NMR.

### 7.4.2.16. *N*-propylsalicylaldimine exchange with *i*-pentylamine



*N*-propylsalicylaldehyde was mixed in NMR tube with 1 equivalent of aniline thus giving equimolar reaction mixture at concentration of 572 mM in  $\text{CDCl}_3$ . The reaction was followed by NMR at intervals of 157 s. The integral intensities of  $=\text{N-CH}_2-$  protons (2.722 ppm) were processed as reversible first-order kinetic reaction with equilibrium constant  $K = 0.068$ . Data are plotted in Figure 7.4-16 and the results are given in Table 7.4-16.

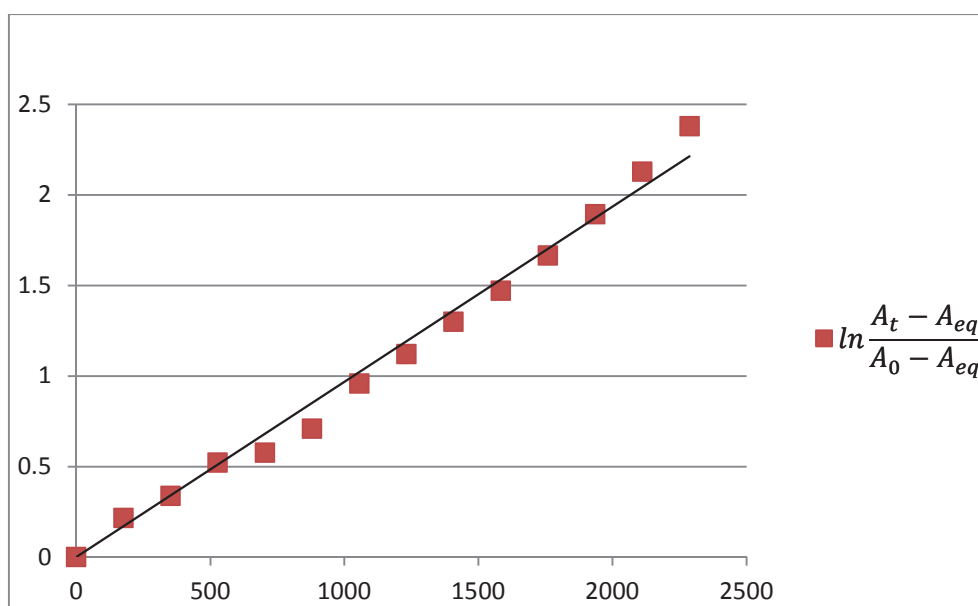


Figure 7.4-16 Plot of the processed integration data of imine exchange reaction for *N*-propylsalicylaldehyde with aniline in  $\text{CDCl}_3$  followed by NMR. Raw integrals were processed as reversible first-order reaction with equilibrium constant of  $K=0.068$ .

$\chi = (K)$	6.4 % (0.068)
$k =$	$(9.68 \pm 0.18) \cdot 10^{-4} \text{ s}^{-1}$
$\sigma =$	$3.20 \cdot 10^{-5} \text{ s}^{-1}$
$R^2 =$	0.9897

Table 7.4-16 Linear regression coefficients and kinetic parameters of imine exchange reaction for *N*-propylsalicylaldehyde with aniline in  $\text{CDCl}_3$  followed by NMR.

7.4.2.17. *N*-benzylidenaniline exchange with *t*-butylamine

*N*-benzylidenaniline was mixed in NMR tube with 1 equivalent of *t*-butylamine thus giving equimolar reaction mixture at concentration of 264 mM in  $\text{CDCl}_3$ . The reaction was followed by NMR at intervals of 241 s. The integral intensities of  $-\text{CH}=\text{N}-$  protons (8.498 ppm for *N*-benzylidenaniline and 8.316 ppm for *N*-*t*-butylbenzaldimine) were processed as reversible first-order kinetic reaction with equilibrium constant  $K = 2.00$ . Data are plotted in Figure 7.4-17 and the results are given in Table 7.4-17.

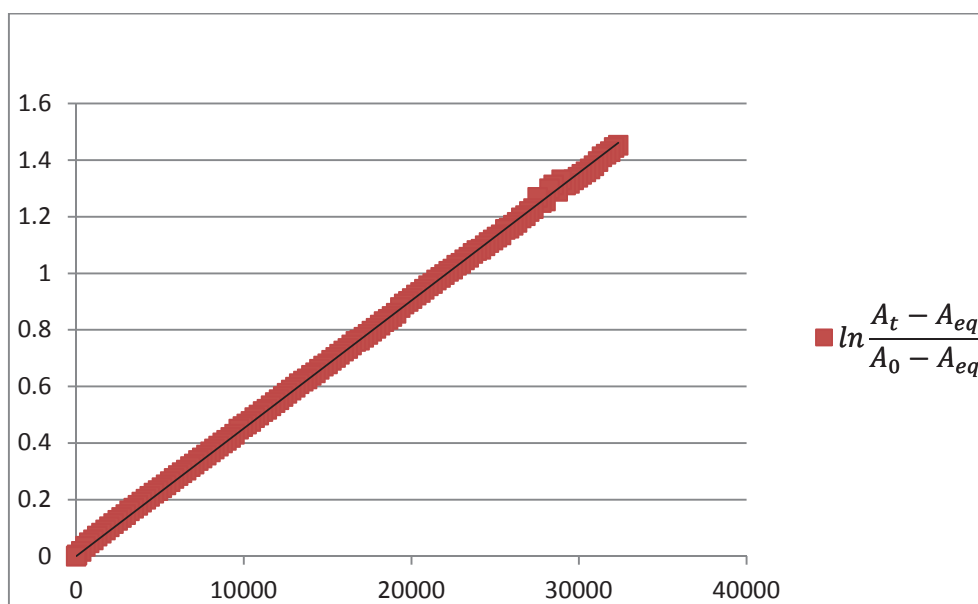


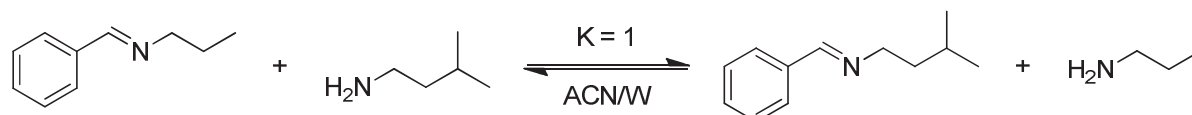
Figure 7.4-17 Plot of the processed integration data of imine exchange reaction for *N*-benzylidenaniline with *t*-butylamine in  $\text{CDCl}_3$  followed by NMR. Raw integrals were processed as reversible first-order reaction with equilibrium constant of  $K=2$ .

$\chi = (K)$	66 % (2.0)
$k =$	$(4.52 \pm 0.01) \cdot 10^{-5} \text{ s}^{-1}$
$\sigma =$	$8.36 \cdot 10^{-8} \text{ s}^{-1}$
$R^2 =$	0.9998

Table 7.4-17 Linear regression coefficients and kinetic parameters of imine exchange reaction for *N*-benzylidenaniline with *t*-butylamine in  $\text{CDCl}_3$  followed by NMR.

### 7.4.2.18. *N*-propyl-aldimines exchange in aqueous media

The imine exchange reaction of several imines derived from various aldehydes was studied in aqueous media, specifically a  $d_3$ -acetonitrile/deuterium oxide mixture (7:3, v/v). To this end, the equilibrated samples from the imine condensation experiments (Section 7.4.2.11) at 20 mM concentration of the starting reagents were mixed with 50  $\mu$ L of a 200 mM stock solution of *i*-pentylamine, thus lowering the concentration level to 18.2 mM. The NMR spectra were recorded immediately after mixing. The integral intensities of the two imine signals (both in the azomethine region and the aliphatic region) were processed according the pseudo-first-order kinetics as discussed in Section 7.4.1.3. The results of the fitting are provided in Table 7.4-18.



Aldimine	Parameter	Value
benzalimine	$k =$	$(12.83 \pm 0.96) \cdot 10^{-3} \text{ s}^{-1}$
	$\sigma$	$6.88 \cdot 10^{-4} \text{ s}^{-1}$
	$R^2 =$	0.9946
<i>p</i> -nitrobenzalimine	$k =$	$(3.32 \pm 0.08) \cdot 10^{-3} \text{ s}^{-1}$
	$\sigma$	$1.16 \cdot 10^{-4} \text{ s}^{-1}$
	$R^2 =$	0.9933
salicylalimine	$k =$	$> 0.027 \text{ s}^{-1}$
	$\sigma$	N/A
	$R^2 =$	N/A
pyridine-2-carboxalimine	$k =$	$> 0.027 \text{ s}^{-1}$
	$\sigma$	N/A
	$R^2 =$	N/A
pyridine-4-carboxalimine	$k =$	$(2.06 \pm 0.05) \cdot 10^{-3} \text{ s}^{-1}$
	$\sigma$	$6.61 \cdot 10^{-5} \text{ s}^{-1}$
	$R^2 =$	0.9937

Table 7.4-18 Summary of the imine exchange experiment in a mixture of  $CD_3CN/D_2O$  (7:3, v/v). The exchange reactions of imines of salicylaldehyde and pyridine-2-aldehyde proceed too rapidly to be followed by NMR and the equilibrium is reached within 60 seconds, which is the time needed to acquire the NMR spectrum. The rate is thus higher  $0.027 \text{ s}^{-1}$ . The ratio between *N*-propyl and *N*-*i*-pentyl imine is 1:1 in all reaction mixture. The overall conversion of the aldehyde to imines is increased when a second amine is added, but for the kinetic evaluation this conversion enhancement (about 5 %) was neglected, as it the kinetic models accounting for the conversion increase are very difficult.

## 7.5. NMR experiments of imine-based molecular motion

The process of intramolecular displacement discussed in Chapter 3 was thoroughly studied by NMR. From the large number of spectra acquired (>10 000 in this project), those which are considered particularly important to prove the concept or structure are provided below. Caption under each spectrum explains the composition of the sample and the important features.

### 7.5.1. NMR experiments of linear imine motion

In the following Figures, the intramolecular displacement is shown on several examples. The Figures also show the importance of the conditions used, which explains why this process was not described before, even though the compounds were studied in many instances. In each caption the Larmor frequency of the spectrometer is indicated, as the line-shape and eventually coalescence of signals is a function of the chemical shift in Hz, therefore it depends on the strength of the magnetic field.

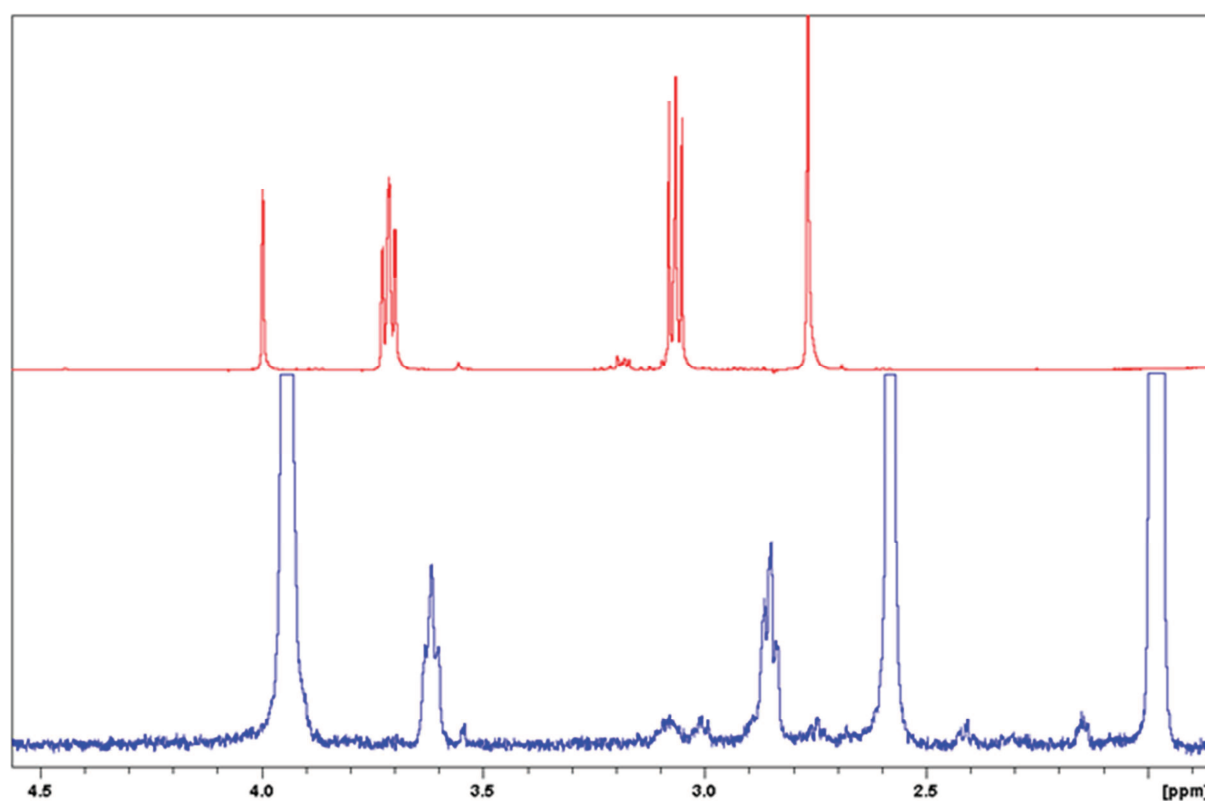


Figure 7.5-1  $^1\text{H}$ -NMR spectra of **BENZAL** + **C<sub>2</sub>-DA** in  $\text{CDCl}_3$  (top) and  $\text{CD}_3\text{CN}/\text{D}_2\text{O}$  (bottom). Triplets around 3.65 ppm is =N-CH<sub>2</sub>- methylene signal, triplets at 3.05 (top) and 2.85 (bottom) correspond to the -CH<sub>3</sub>-NH<sub>2</sub> methylene group. Methylene signals of the bis-imine appear around 4.1 ppm (overlaps with water signal), free **C<sub>2</sub>-DA** is around 2.6-2.7 ppm. Small broadening of the methylene signals indicates acceleration of the intramolecular displacement to some extent, but still relatively insignificant.

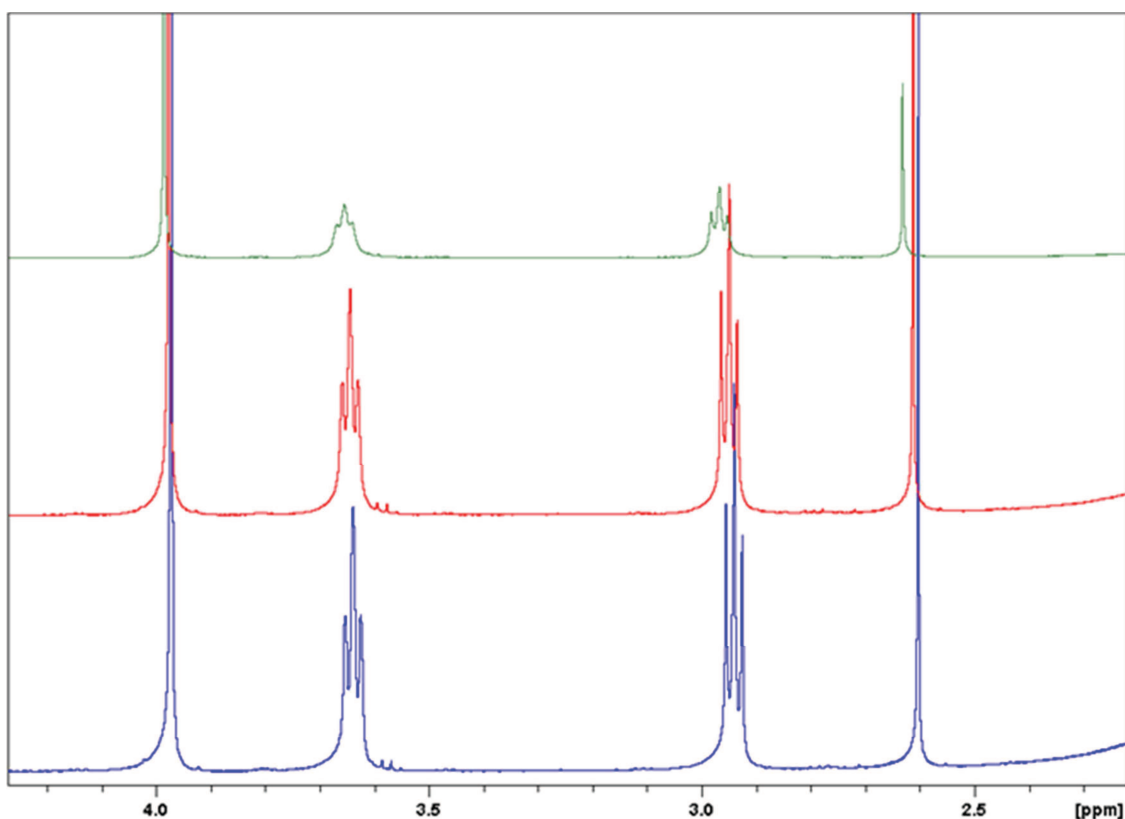


Figure 7.5-2 400 MHz  $^1\text{H}$ -NMR spectra of the methylene region of **SALAL** + **C<sub>2</sub>-DA** in pure  $\text{CD}_3\text{CN}$ , temperatures from bottom to top: 25, 35 and 55 °C. Signal of the methylene groups of the bis-imine is a singlet at 4.0 ppm, the =N-CH<sub>2</sub>-methylene group is a triplet at 3.65 ppm, the -CH<sub>2</sub>-NH<sub>2</sub> methylene group is a triplet at 2.95 ppm, free **C<sub>2</sub>-DA** is a singlet at 2.6 ppm. Sharp triplets are broadening with increased temperature, indicating accelerated intramolecular exchange.

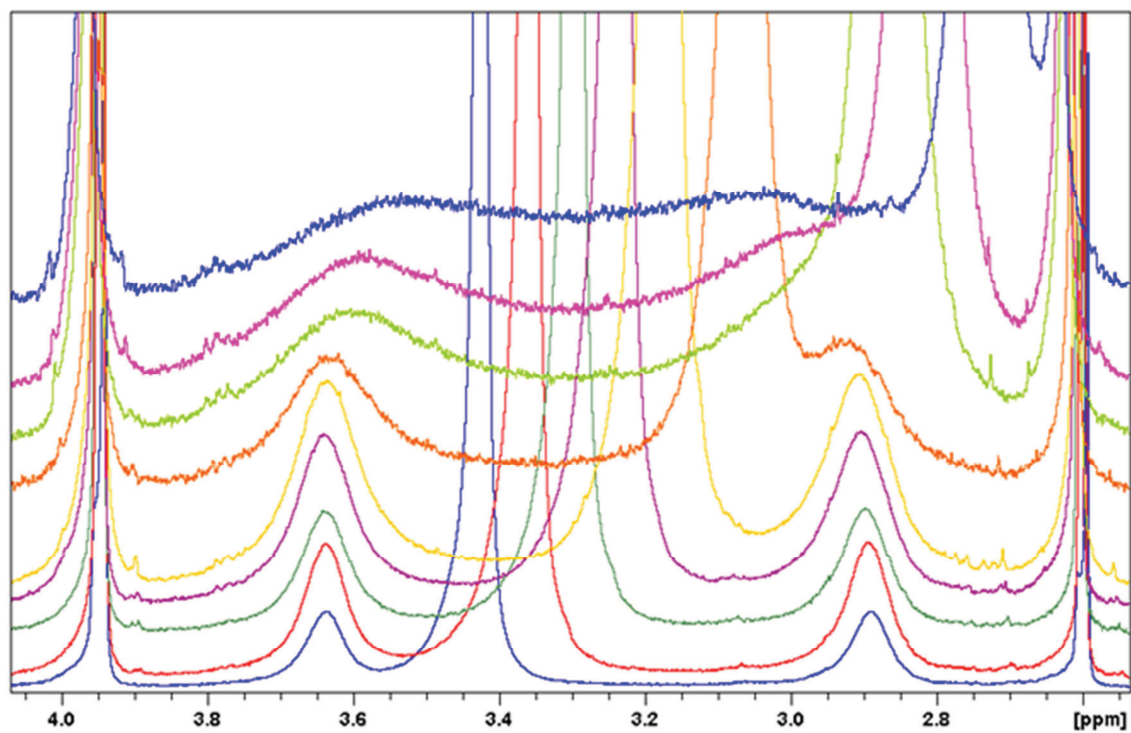


Figure 7.5-3 400 MHz  $^1\text{H}$ -NMR spectra of the methylene region of **SALAL** + **C<sub>2</sub>-DA** in  $\text{CD}_3\text{CN}/\text{D}_2\text{O}$  (9:1 v/v), temperatures from bottom to top: 5, 10, 15, 20, 25, 35, 55, 60 and 70 °C. The triplets already lost the coupling pattern at 5 °C, but full coalescence could not be reached (deuterium lock lost).

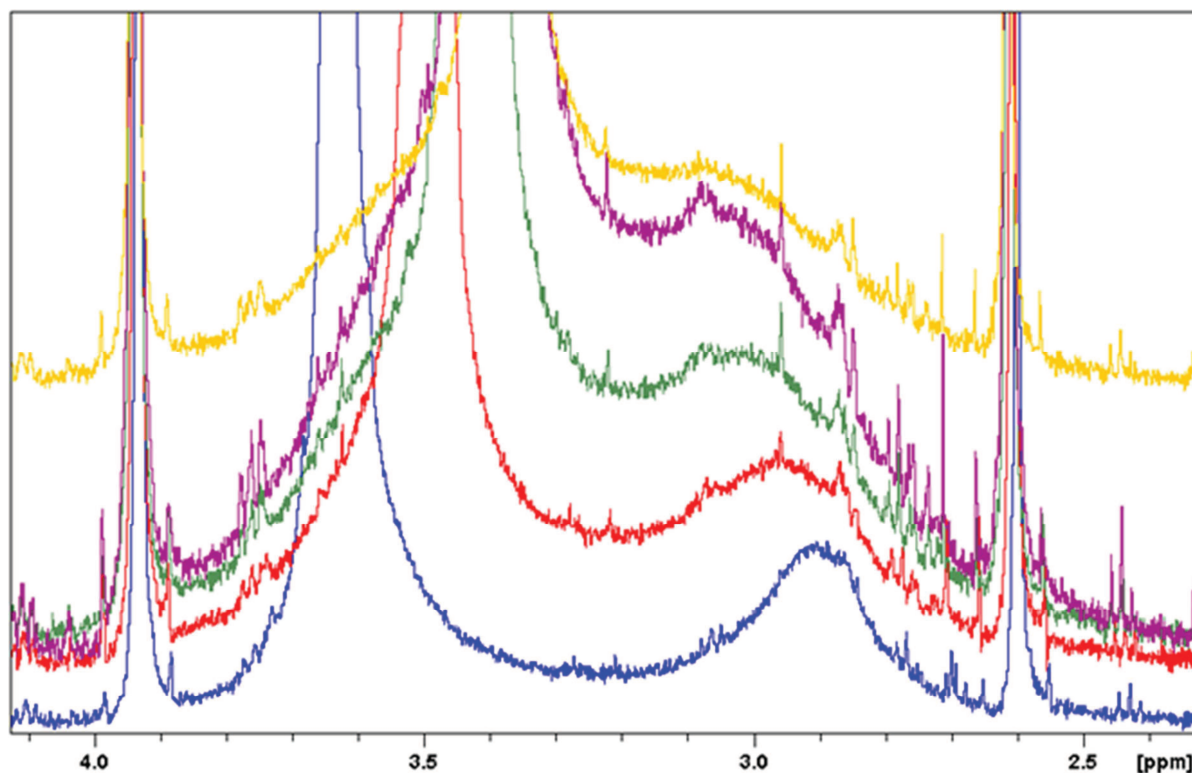


Figure 7.5-4 400 MHz <sup>1</sup>H-NMR spectra of the methylene region of SALAL + C<sub>2</sub>-DA in CD<sub>3</sub>CN/D<sub>2</sub>O (8:2 v/v), temperatures from bottom to top: 25, 35, 40, 42 and 44 °C. The coalescence of the methylene signals was reached at around 44 °C.

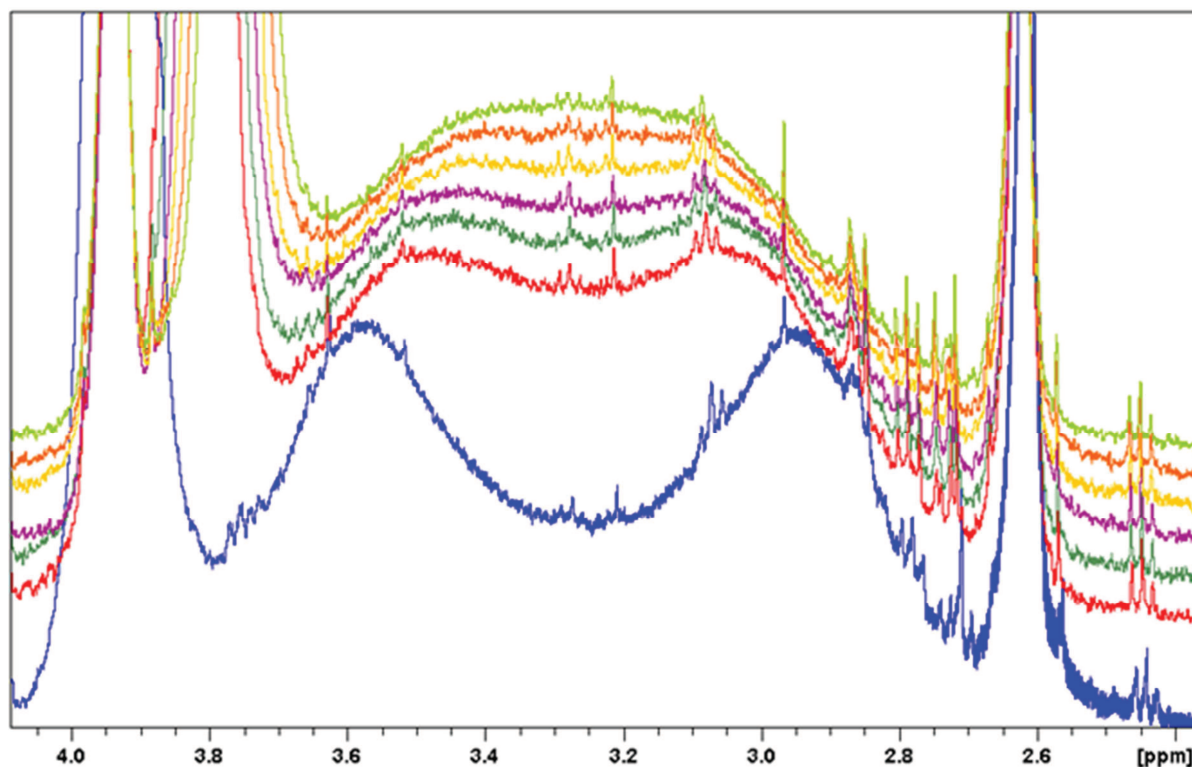


Figure 7.5-5 400 MHz <sup>1</sup>H-NMR spectra of the methylene region of SALAL + C<sub>2</sub>-DA in CD<sub>3</sub>CN/D<sub>2</sub>O (7:3 v/v), temperatures from bottom to top: 25, 34, 35, 36, 37, 38 and 39 °C. The coalescence of the methylene signals was reached at 38 ± 1 °C.



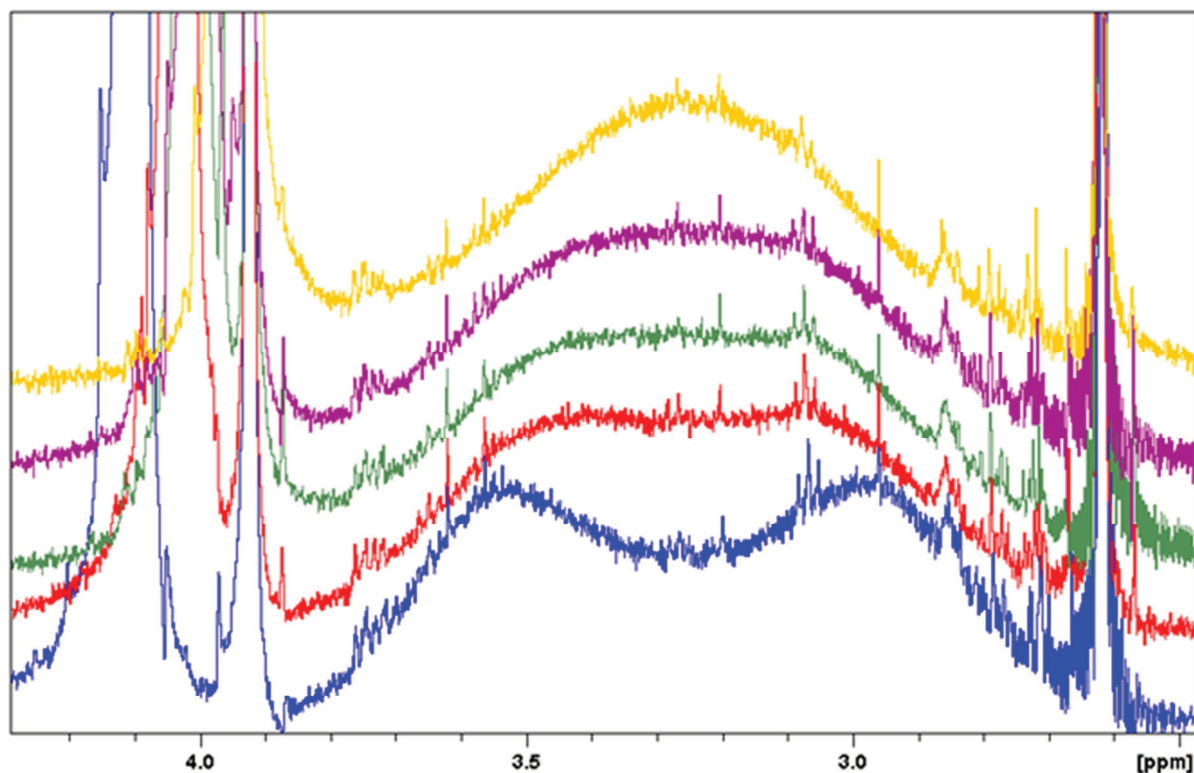


Figure 7.5-6 400 MHz <sup>1</sup>H-NMR spectra of the methylene region of SALAL + C<sub>2</sub>-DA in CD<sub>3</sub>CN/D<sub>2</sub>O (6:4 v/v), temperatures from bottom to top: 25, 30, 31, 32 and 35 °C. The coalescence of the methylene signals was reached at 31 ± 1 °C.

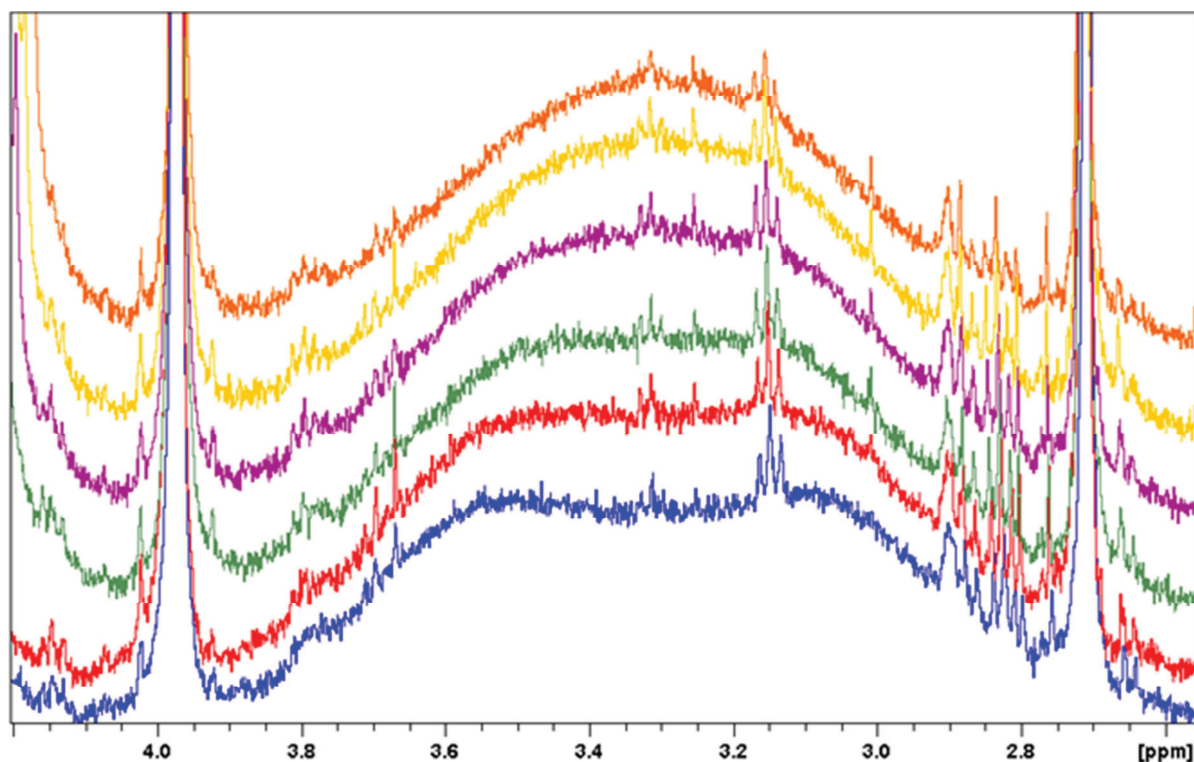


Figure 7.5-7 400 MHz <sup>1</sup>H-NMR spectra of the methylene region of SALAL + C<sub>2</sub>-DA in CD<sub>3</sub>CN/D<sub>2</sub>O (5:5 v/v), temperatures from bottom to top: 25, 26, 27, 28, 29 and 30 °C. The coalescence of the methylene signals is already almost reached at room temperature, being 27 ± 1 °C.

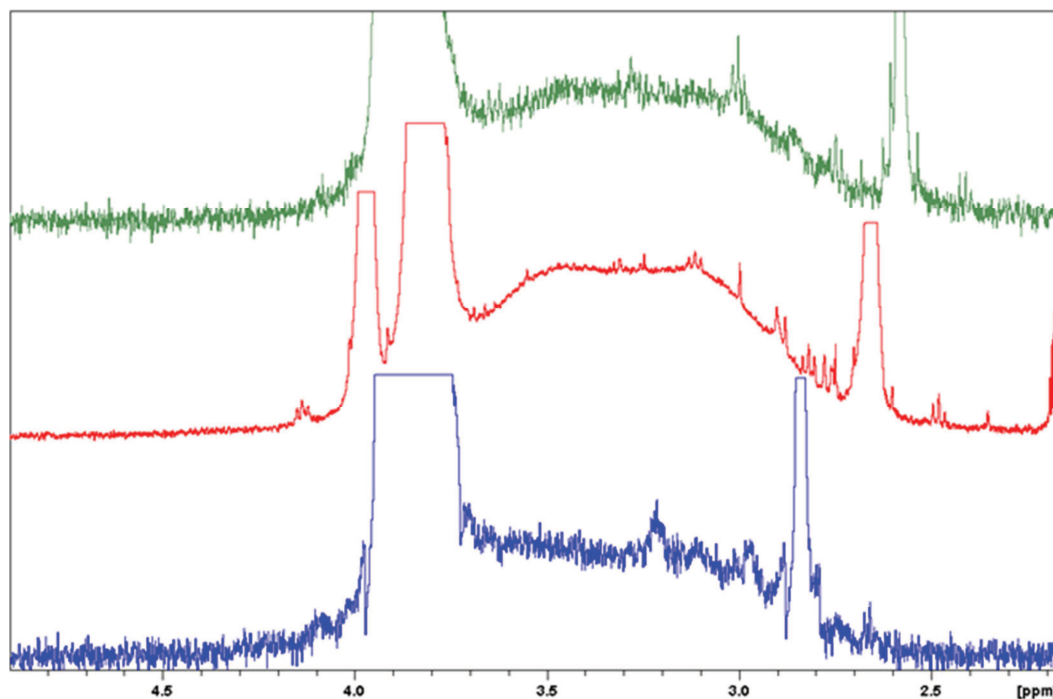


Figure 7.5-8 400 MHz  $^1\text{H}$ -NMR spectra of the methylene region of **SALAL** + **C<sub>2</sub>-DA** in  $\text{CD}_3\text{CN}/\text{D}_2\text{O}$  (7:3 v/v) at 36 °C, pH from bottom to top 9.29 (acidified by DCl in  $\text{D}_2\text{O}$ ), 10.63 (unchanged), and 11.83 (alkalized by KOD in  $\text{D}_2\text{O}$ ). Peaks truncated for clarity. This experiment shows that the coalescence temperature does not depend on pH in range of pH 9.3-11.8.

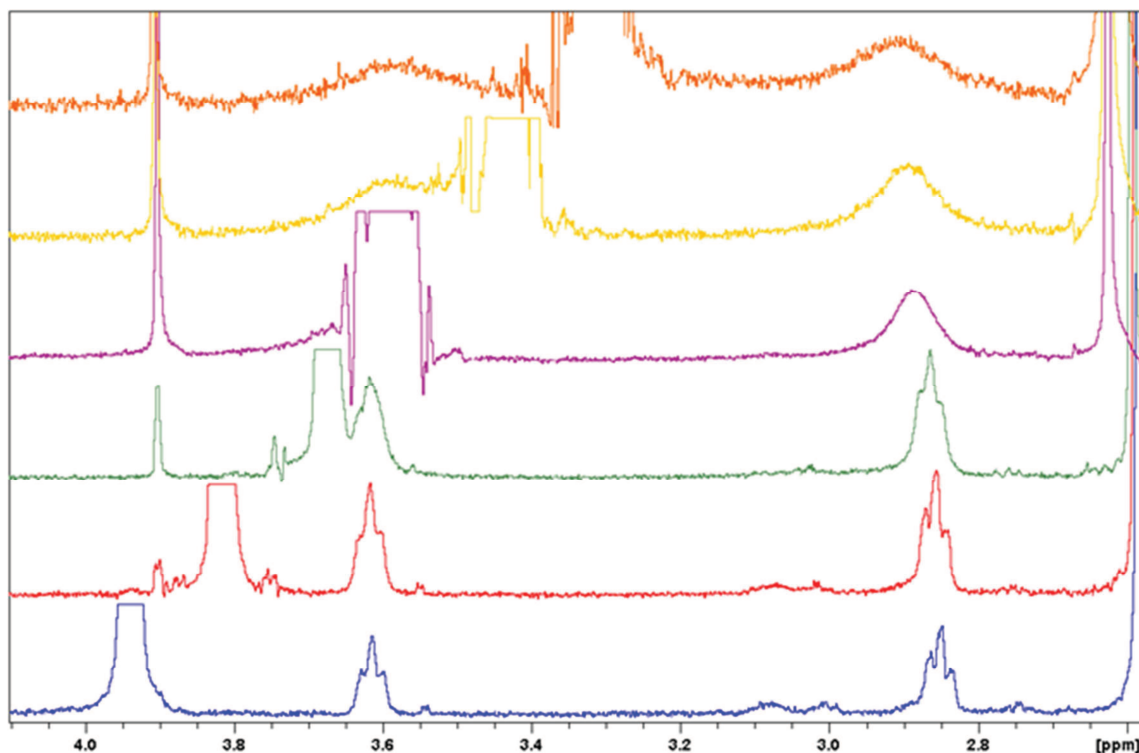


Figure 7.5-9 400 MHz  $^1\text{H}$ -NMR spectra of the methylene region of **BENZAL** + **C<sub>2</sub>-DA** in  $\text{CD}_3\text{CN}/\text{D}_2\text{O}$  (7:3 v/v), temperatures from bottom to top 25, 35, 45, 55, 65 and 75 °C. The two methylene groups of the mono-imine give triplets at 3.62 ppm ( $\text{CH}_2$  group next to imine nitrogen) and 2.85 ppm ( $\text{CH}_2$  group next to amine nitrogen). A small amount of aminoral is present as well, as can be seen in the region 3.0 – 3.1 ppm where weak signals of multiplets of the aminoral can be found. The water signal is gradually shifting from 3.93 ppm at 25 °C to 3.27 ppm at 75 °C. The signal of the two methylene groups of the bis-imine at 3.91 ppm is hidden behind the water peak at 25 °C and is revealed as the temperature increases. The signal of unreacted **C<sub>2</sub>-DA** appears at 2.65 ppm.

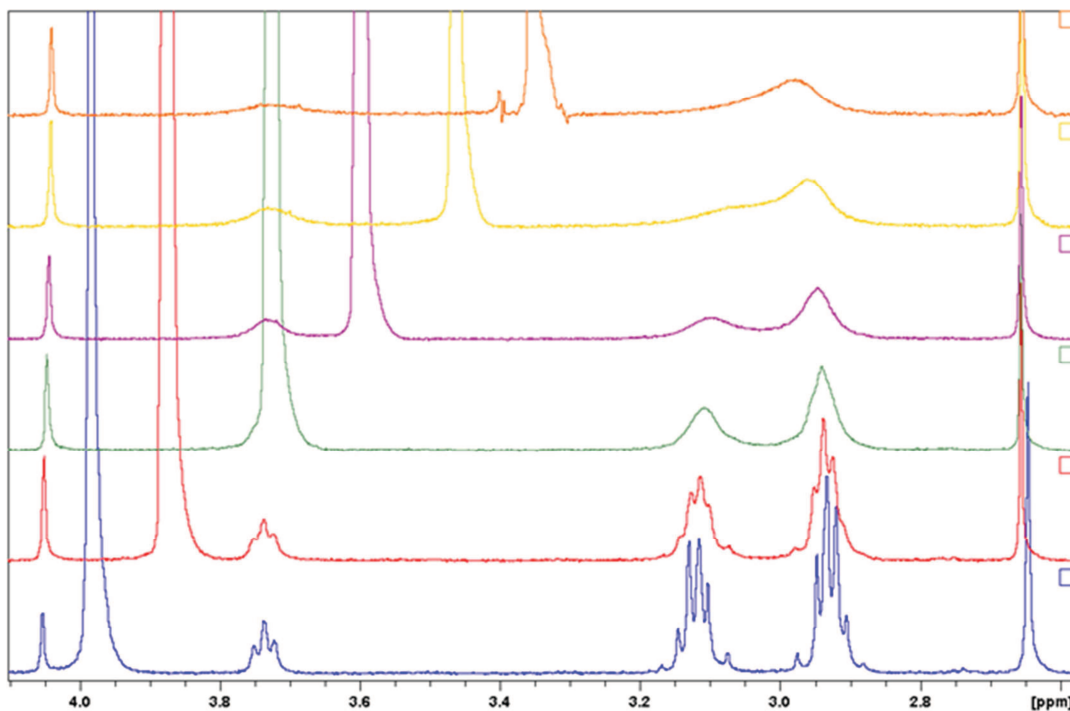


Figure 7.5-10 400 MHz  $^1\text{H}$ -NMR spectra of the methylene region of **PYRAL** + **C<sub>2</sub>-DA** in  $\text{CD}_3\text{CN}/\text{D}_2\text{O}$  (7:3 v/v), temperatures from bottom to top 25, 35, 45, 55, 65 and 75 °C. The signal of the methylene group next to the imine nitrogen in the mono-imine is at 3.74 ppm while the signal of the methylene group next to the amine overlaps with the aminor signals at 2.93 and 3.13 ppm. The aminor is the dominant product of this reaction. The water signal is gradually shifting from 3.98 ppm at 25 °C to 3.33 ppm at 75 °C. The signal of the two methylene groups of the bis-imine is found at 4.05 ppm. The signal of unreacted **C<sub>2</sub>-DA** appears at 2.65 ppm.

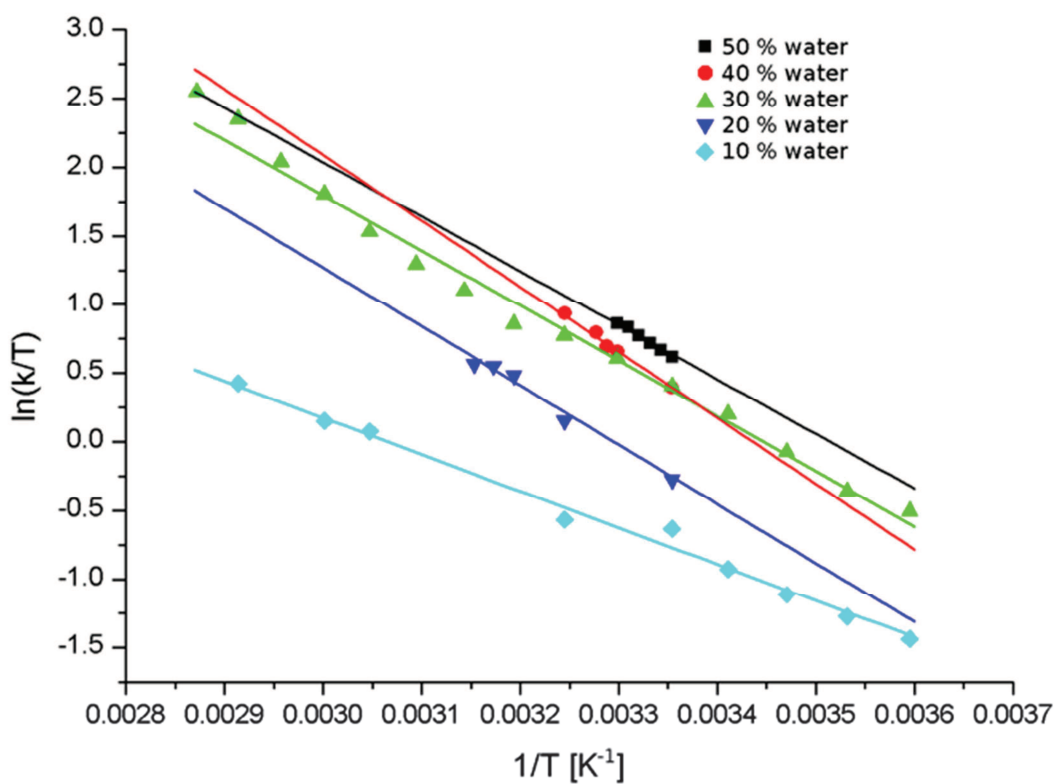


Figure 7.5-11 Graph of Eyring equation fits for different proportions of  $\text{D}_2\text{O}$  in  $\text{CD}_3\text{CN}$ .

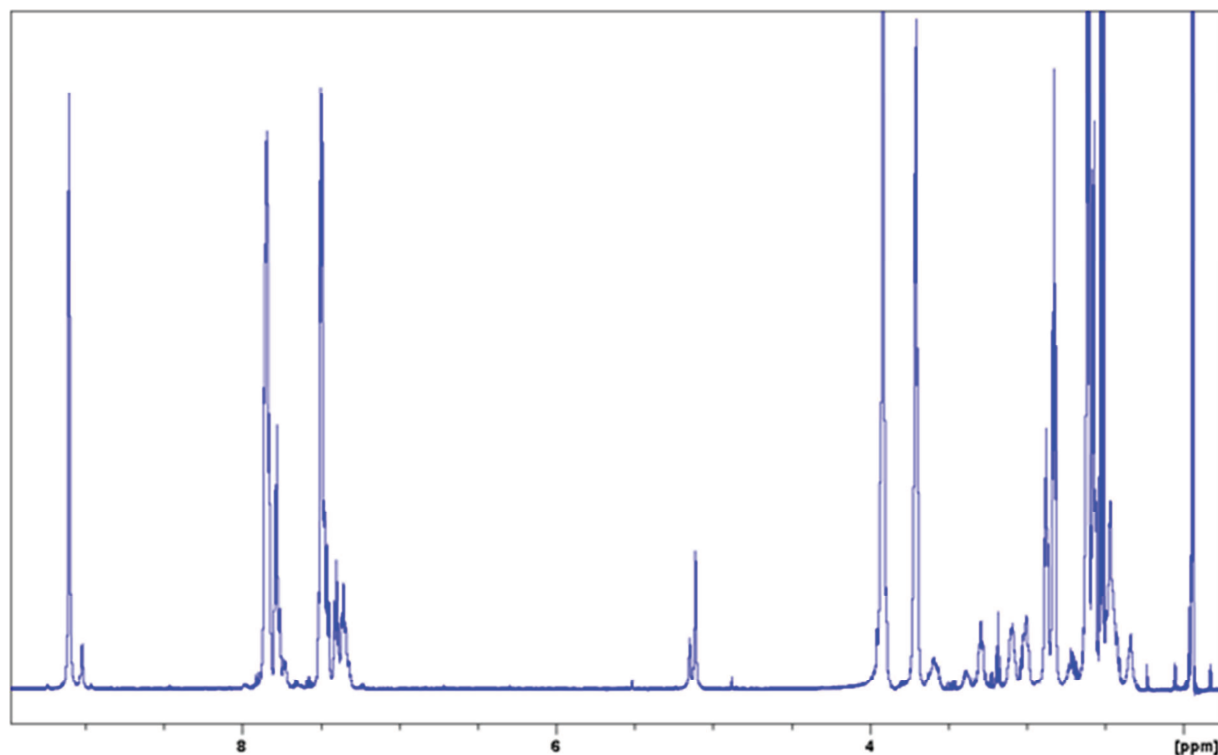


Figure 7.5-12 600 MHz  $^1\text{H}$ -NMR spectrum of sodium 2-formylbenzoate with  $\text{en}_2\text{N}_3$  in  $\text{CD}_3\text{CN}/\text{D}_2\text{O}$  7:3 (v/v) at 100 mM concentration of both at 25 °C. The two peaks at 5.1 ppm correspond to the O-CH-N proton of the central aminolactone; signal assignment in Figure 7.5-17.

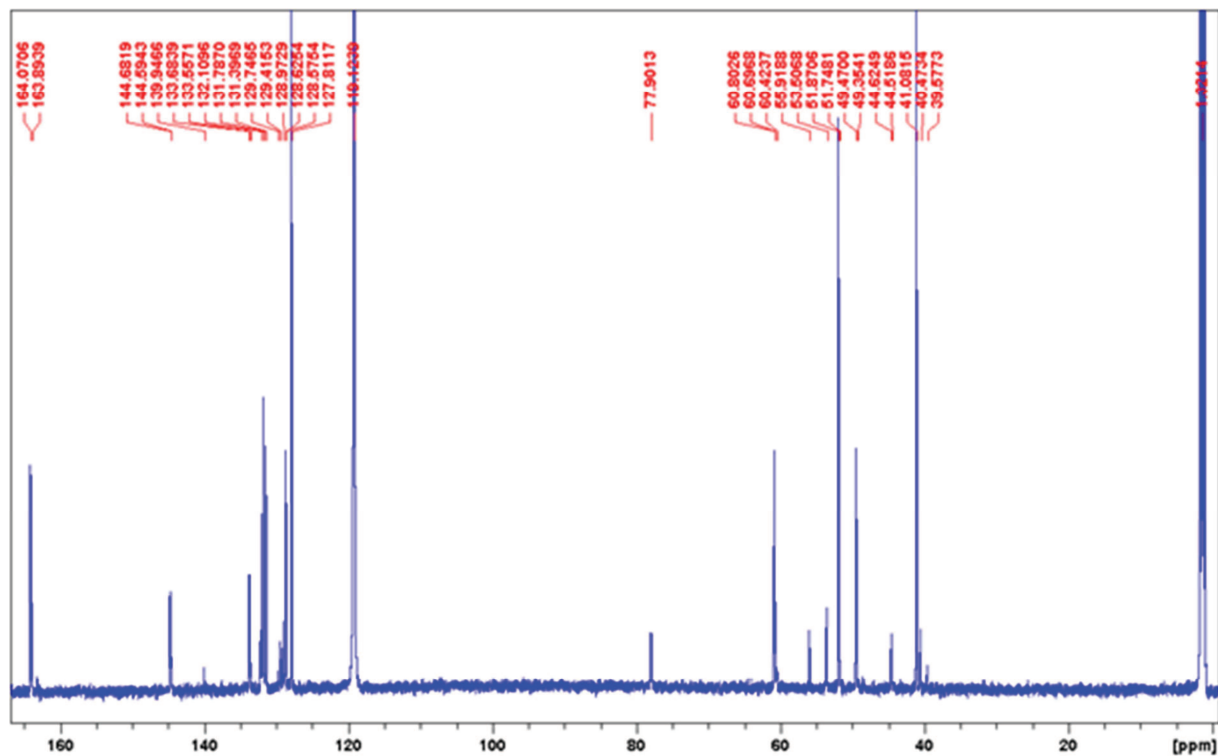


Figure 7.5-13 150.9 MHz  $^{13}\text{C}$ -NMR spectrum of sodium 2-formylbenzoate with  $\text{en}_2\text{N}_3$  in  $\text{CD}_3\text{CN}/\text{D}_2\text{O}$  7:3 (v/v) at 100 mM concentration of both at 25 °C.

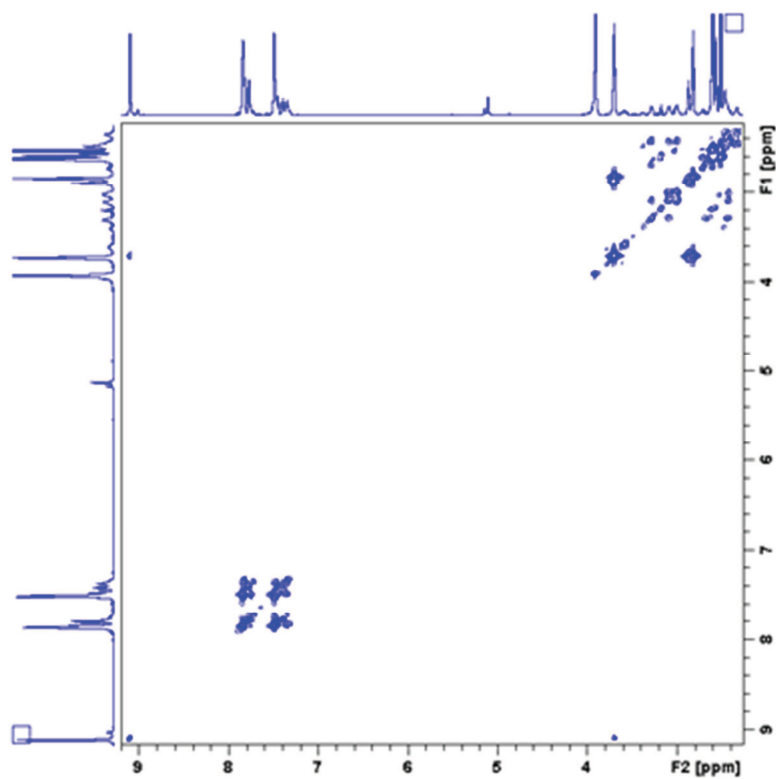


Figure 7.5-14 2D  $^1\text{H}$ -COSY NMR spectrum of sodium 2-formylbenzoate with  $\text{en}_2\text{N}_3$  in  $\text{CD}_3\text{CN}/\text{D}_2\text{O}$  7:3 (v/v) at 100 mM concentration of both at 25 °C.

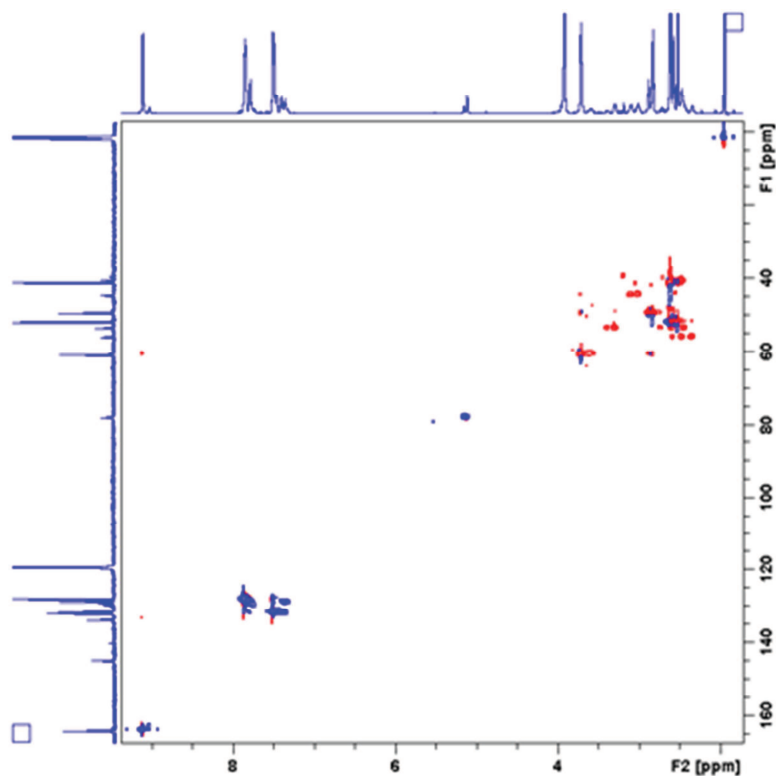


Figure 7.5-15 2D  $^1\text{H}$ - $^{13}\text{C}$  HSQC NMR spectrum of sodium 2-formylbenzoate with  $\text{en}_2\text{N}_3$  in  $\text{CD}_3\text{CN}/\text{D}_2\text{O}$  7:3 (v/v) at 100 mM concentration of both at 25 °C.

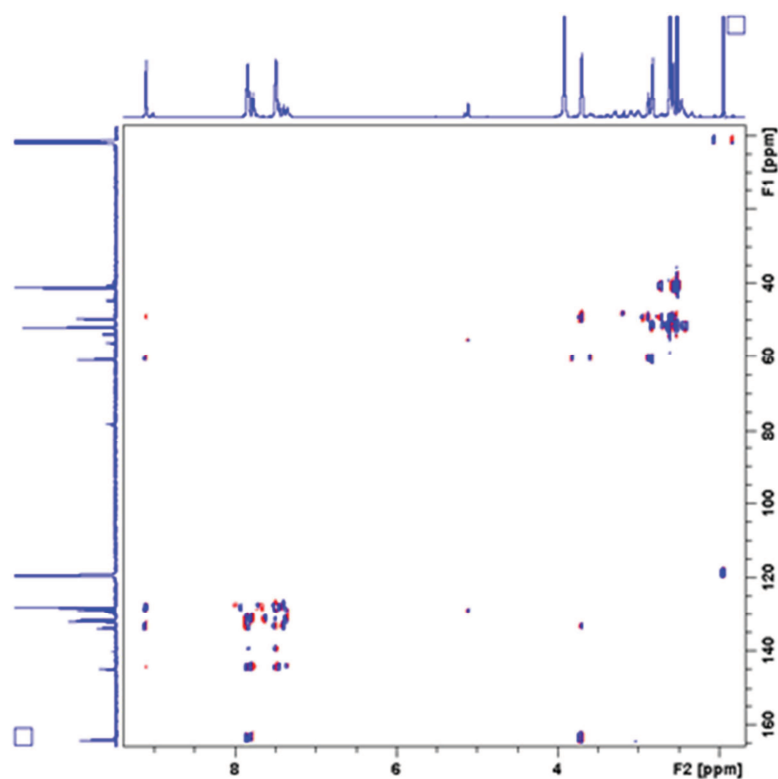


Figure 7.5-16 2D  $^1\text{H}$ - $^{13}\text{C}$  HMBC NMR spectrum of sodium 2-formylbenzoate with  $\text{en}_2\text{N}_3$  in  $\text{CD}_3\text{CN}/\text{D}_2\text{O}$  7:3 (v/v) at 100 mM concentration of both at 25 °C.

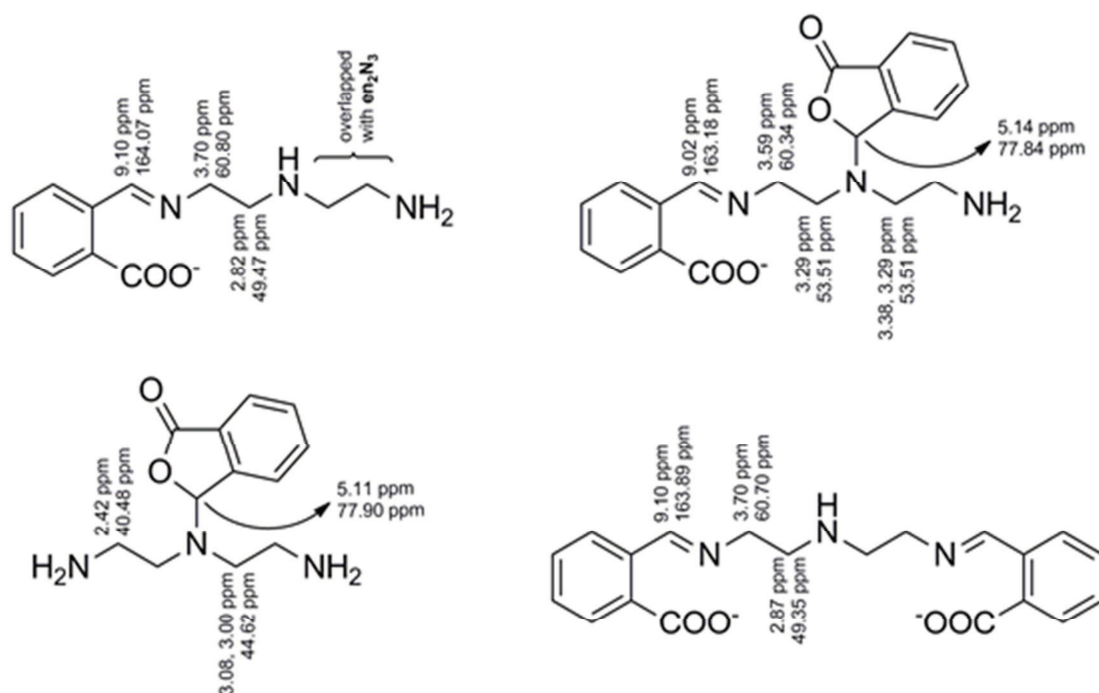


Figure 7.5-17 Structure representation and peak assignment for spectra from Figure 7.5-12 to Figure 7.5-16.

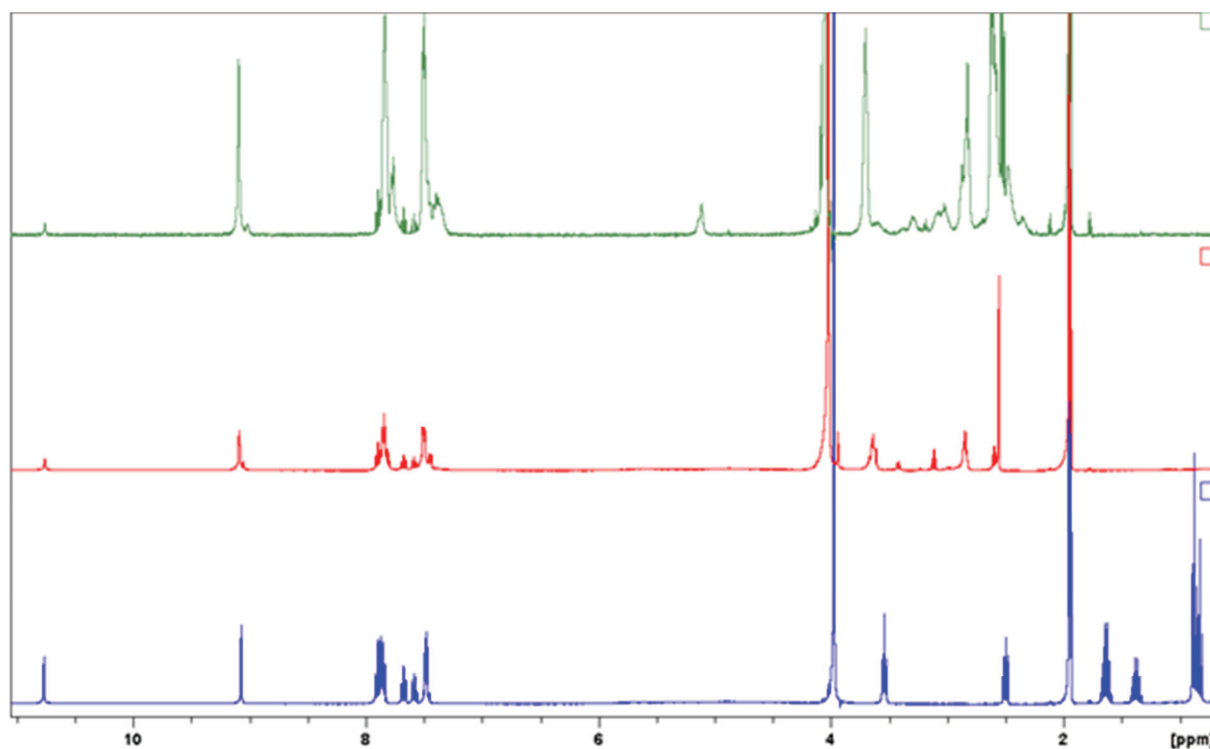


Figure 7.5-18 Comparison of 1D 400 MHz  $^1\text{H}$ -NMR spectra of sodium 2-formylbenzoate reacted with propylamine (blue),  $\text{C}_2\text{-DA}$  (red) and  $\text{en}_2\text{N}_3$  (green) in  $\text{CD}_3\text{CN}/\text{D}_2\text{O}$  7:3 (v/v) at 20 mM concentration of both reagents at 25 °C. pH maintained at  $11.1 \pm 0.1$ . The lactone peak at 5.1 ppm appears only in the case when secondary nitrogen is present. Also, this comparison disproves the aminor structure, as the aminor could be equally formed with  $\text{C}_2\text{-DA}$  and  $\text{en}_2\text{N}_3$ , but only in case of  $\text{en}_2\text{N}_3$  the corresponding signal is observed.

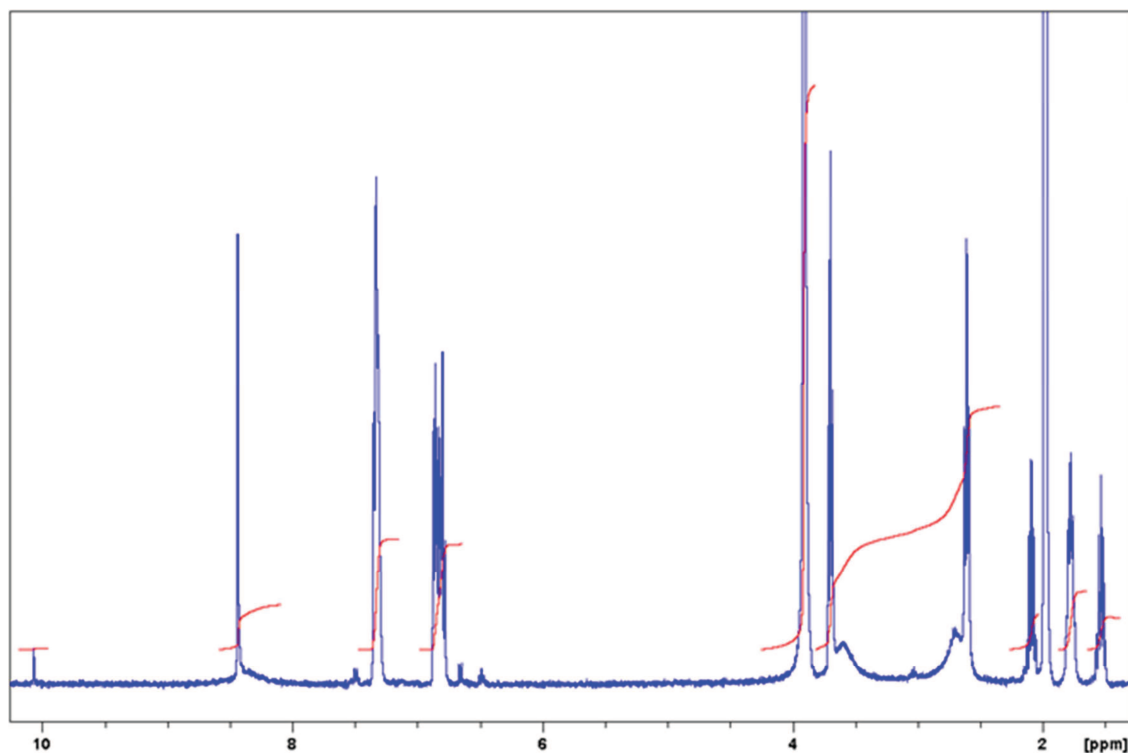


Figure 7.5-19  $^1\text{H}$ -NMR spectrum of a 20 mM equimolar mixture of  $\text{SALAL} + \text{C}_3\text{-DA}$  in  $\text{CD}_3\text{CN}/\text{D}_2\text{O}$  (7:3 v/v). The mixture contains unreacted aldehyde (10.10 ppm), unreacted  $\text{C}_3\text{-DA}$  (2.64 ppm triplet, 1.57 ppm quintet), mono-imine (8.38, 3.64 and 2.73 ppm, broad singlets, 1.81 ppm multiplet), and bis-imine (8.47 ppm singlet, 3.73 ppm triplet and 2.12 ppm quintet).



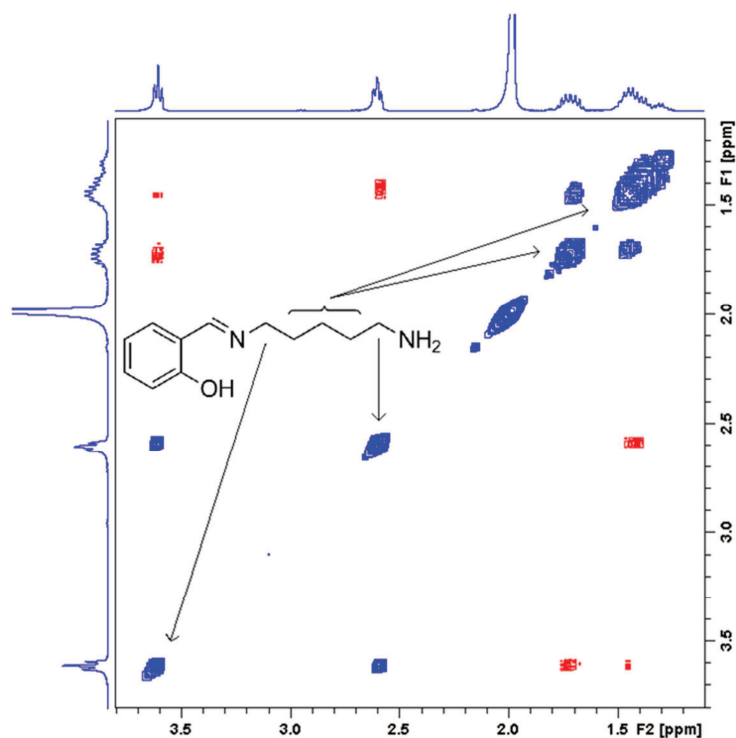


Figure 7.5-20 2D  $^1\text{H}$ -NOESY spectrum of **SALAL** + **C<sub>5</sub>-DA** in  $\text{CD}_3\text{CN}/\text{D}_2\text{O}$  7:3 (v/v). The signal of the methylene group next to imine nitrogen is at 3.61 ppm while the methylene group next to amine nitrogen overlaps with free **C<sub>5</sub>-DA** at 2.60 ppm. The positive cross-peaks correspond to intermolecular exchange of free diamine with mono-imine. It is noteworthy that the intramolecular exchange is probably taking place as well, but it is covered by the faster intermolecular one.

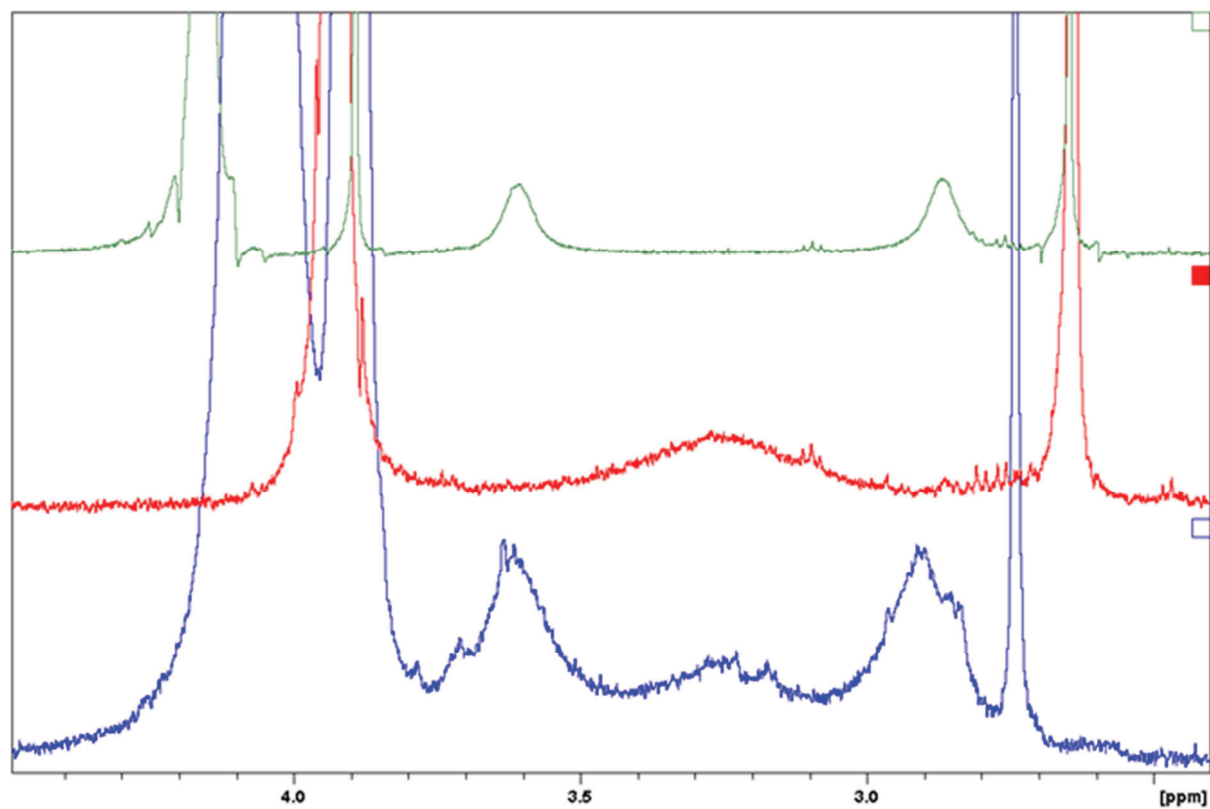


Figure 7.5-21  $^1\text{H}$ -NMR spectra of **C<sub>2</sub>-DA** with 5-hydroxy-**SALAL** (green), 5-chloro-**SALAL** (red) and 5-chloro-**SALAL** added to the equilibrated mixture of **C<sub>2</sub>-DA** with 5-hydroxy-**SALAL** (blue). Evident reequilibration takes place and signals of both mono-imines are observed simultaneously (two broad signals at 3.6 and 2.9 ppm for hydroxy derivative, and broad signal at 3.25 ppm for chloro derivative). Sample suffered heavy precipitation of resulting bis-imines.

### 7.5.1.1. Activation parameters as function of water content

D <sub>2</sub> O content	50 %	40 %	30 %	20 %	10 %	0 %
$\Delta H^\ddagger$ [kJ mol <sup>-1</sup> ]	37.8±1.4	41.3±2.5	38.8 ± 0.5	36.9±3.0	22.5±0.5	16.1±4.8
$\Delta S^\ddagger$ [J mol <sup>-1</sup> K <sup>-1</sup> ]	-65±5	-55±8	-66.0 ± 1.5	-76±10	-129±2	-175±15

Table 7.5-1 Activation enthalpy ( $\Delta H^\ddagger$ ) and entropy ( $\Delta S^\ddagger$ ) of the intramolecular imine exchange of SALAL + C<sub>2</sub>-DA determined in a mixture of CD<sub>3</sub>CN/D<sub>2</sub>O at different percentage of water. The corresponding spectra are presented in Figure 7.5-2 to Figure 7.5-7.

### 7.5.2. Example of EXSY experiment

2D EXSY experiments were used throughout the Chapter 3 to quantify rates of chemical exchange in dynamic equilibria studied. EXSY is a unique tool for the rate analysis, especially in its 2D form, because: a) signals are separated into two dimensions thus reaching better resolution, b) unlike signal line-shape (and the subsequent fitting) the EXSY does not depend on the strength of the magnetic field, c) unlike for line-shape fitting analysis, for EXSY is sufficient to have one well separated signal from other and, d) complex exchange processes can be evaluated simultaneously in one experiment.

The 2D EXSY experiment consists of series of 2D NOESY experiments with different values of one delay in the pulse sequence called mixing time ( $t_m$ ). Only plain noesyph pulse sequence is suitable for EXSY as all its other variants are using gradients and/or the mixing cannot be set as 0, which is necessary for the determination of the so-called equilibrium magnetization (intensity of the diagonal peaks). The receiver gain was optimized once for the first experiment and kept constant for the sample. Typical set of  $t_m$  values was 0, 0.010, 0.025, 0.05, 0.075, 0.1, 0.125, 0.15, 0.175, 0.2, 0.25 and 0.5 s. The 2D integration ranges were optimized on the spectrum at around  $t_m=0.5$  s and transferred to all others. Integration of all spectra with the same integration ranges gave a matrix of integral intensities for the given set of mixing times.

Calculation of exchange rates was performed using the NOESY build-up curve, where the intensity of the cross-peaks is plotted as a function of  $t_m$ . Due to the inherent symmetry of NOESY spectra, the cross-peak intensity was averaged over the diagonal. A typical curve obtained is shown in Figure 7.5-22. The curve grows linearly from  $t_m=0$  until the relaxation becomes important (usually around  $t_m=0.2$  s) and this linear part is fitted by linear regression with forced intercept  $y_{x=0}=0$ . The slope of this regression is also function of the receiver gain. To remove this effect, the slope is divided by the "equilibrium magnetization" which is the intensity of diagonal peaks between which the cross-peak is observed at  $t_m=0$ . Therefore, the slope divided by the equilibrium magnetization of peak A gives the rate of exchange  $A \rightarrow B$ ,  $k_1$ , and on the other hand, the same slope divided by the equilibrium magnetization of peak B is the value for the reverse reaction  $B \rightarrow A$ ,  $k_2$ , fulfilling the definition for the equilibrium constant  $K=c[B]/c[A]=k_1/k_2$ . The rates were verified by EXSYCalc program. For the intramolecular exchange reaction of symmetrical diamines where starting and end points are the same,  $k_1 = k_2$ . This is very beneficial since peaks can overlap heavily in the NMR spectra. With this approach, only one well separated signal is needed to calculate the exchange rate.

EXSY experiments were recorded at two concentration levels, 20 and 8 mM. It was shown that intermolecular imine exchange reactions follow first order kinetic and thus lowering the concentration by factor of 2.5 should lead to decrease in the observed rate by 2.5 as well. This was the criterion used for qualifying the imine exchange as intra- or intermolecular. For all exchange rates, 95 % confidence interval was calculated. Data with 95 % confidence interval which was 10 % or less of the rate value were considered good, data with 95 % confidence interval being 20 % and more were rejected, data with 95 % confidence interval between 10 % - 20 % were repeated twice more to make them acceptable (narrowing the confidential interval) or to be rejected (if not reproducible).

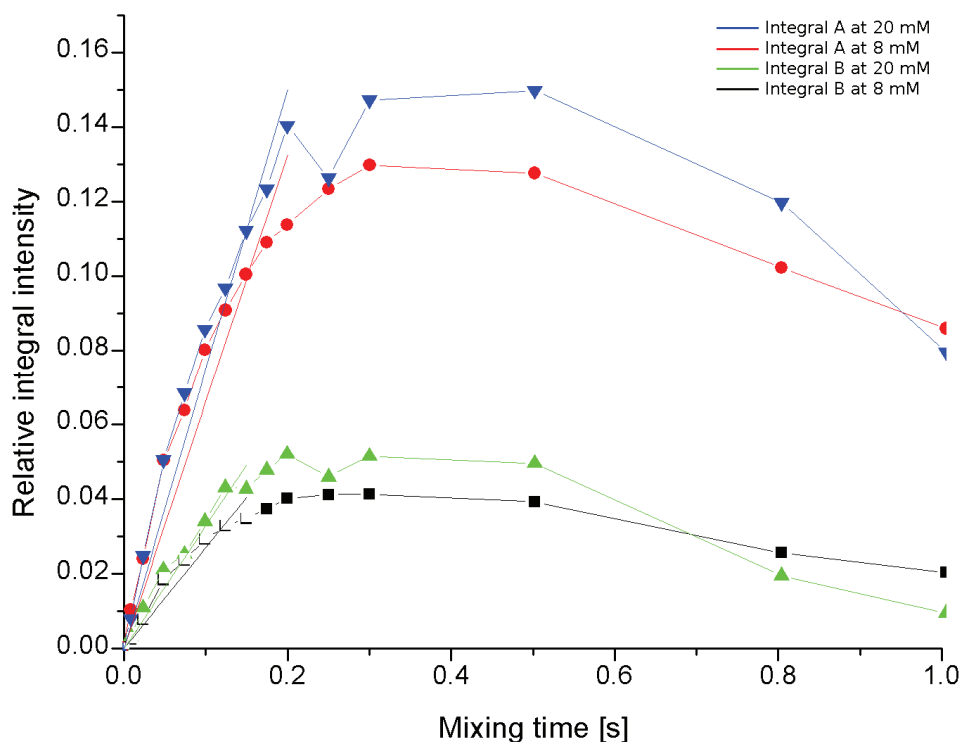


Figure 7.5-22 Typical NOESY build-up curves for the mixture of **SALAL** with **tren** in  $CD_3CN/D_2O$  (7:3 v/v). Two intramolecular exchanges are observed, one in mono-imine and one in bis-imine. The slope is identical for the two concentrations proving the intramolecular character of the process.

An example of a 2D EXSY experiment is shown on reaction of **SALAL** with **tren**. Due to the presence of bis- and tris-imine, exchange pattern is very rich. The 2D NOESY spectra at three mixing time values are given in Figure 7.5-23 to Figure 7.5-25 and Figure 7.5-27. Integration regions are not shown for clarity. A comparison of the obtained rates by NOESY build-up approach and by EXSYCalc program at two different concentrations is given in Table 7.5-2.

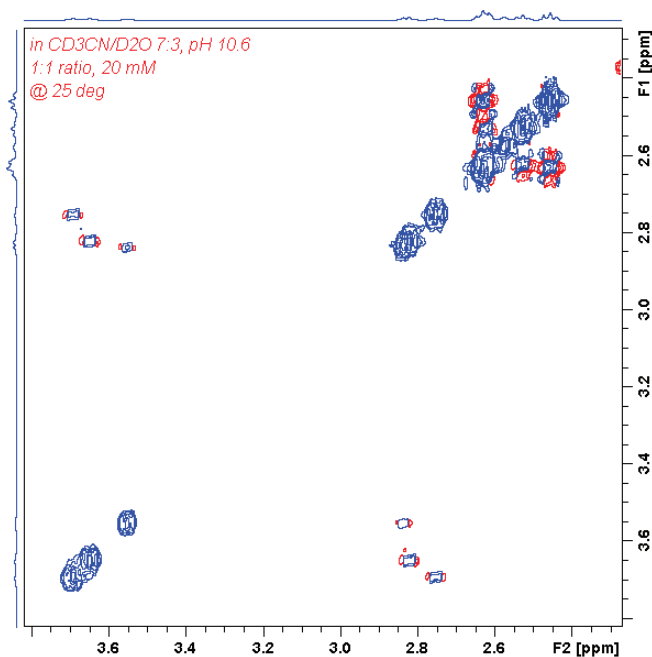


Figure 7.5-23 2D  $^1H$ -NOESY NMR spectrum of **SALAL** with **tren** at 20 mM concentration both in  $CD_3CN/D_2O$  7:3 (v/v). NOESY mixing time = 0 s. The observed cross-peaks are COSY correlations as the NOESY sequence with mixing time = 0 s is essentially identical to the COSY sequence.

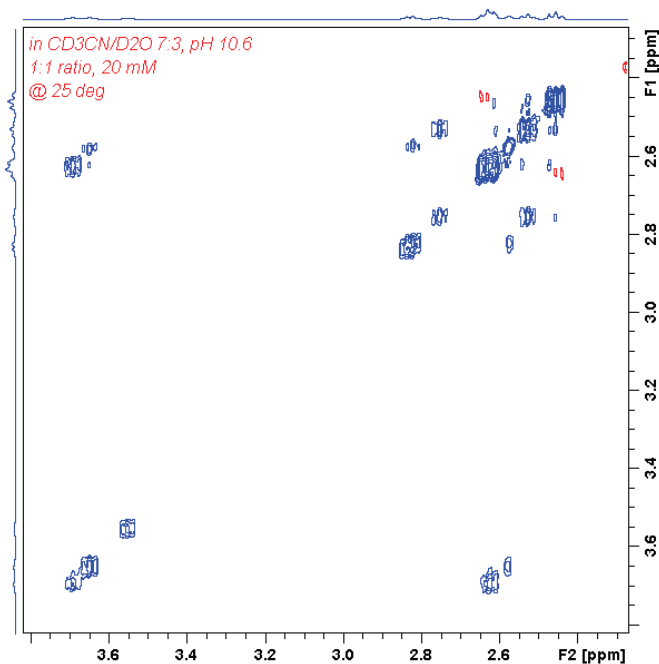


Figure 7.5-24 2D  $^1\text{H}$ -NOESY NMR spectrum of **SALAL** with **tren** at 20 mM concentration both in  $\text{CD}_3\text{CN}/\text{D}_2\text{O}$  7:3 (v/v) at pH = 10.7. NOESY mixing time = 0.500 s.

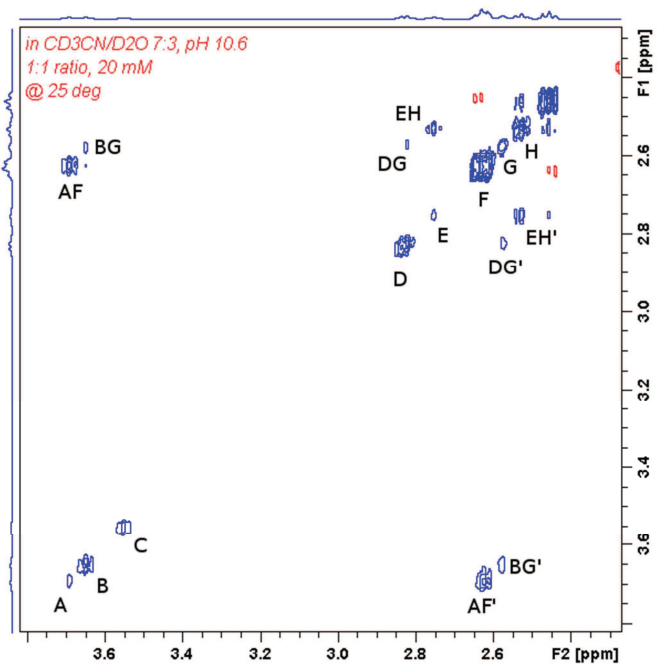


Figure 7.5-25 2D  $^1\text{H}$ -NOESY NMR spectrum of **SALAL** with **tren** at 20 mM concentration both in  $\text{CD}_3\text{CN}/\text{D}_2\text{O}$  7:3 (v/v) at pH = 10.7. NOESY mixing time = 0.800 s. Peaks labelled in this spectrum are assigned to the structures in Figure 7.5-26. Since 2D-NOESY spectra are diagonally symmetrical, average between equivalent peaks was taken into the calculation, i.e. intensity of cross-peak AF + intensity of cross-peak AF' was divided by 2. Signals around 3.6 ppm are well separated and suitable for EXSY calculation.

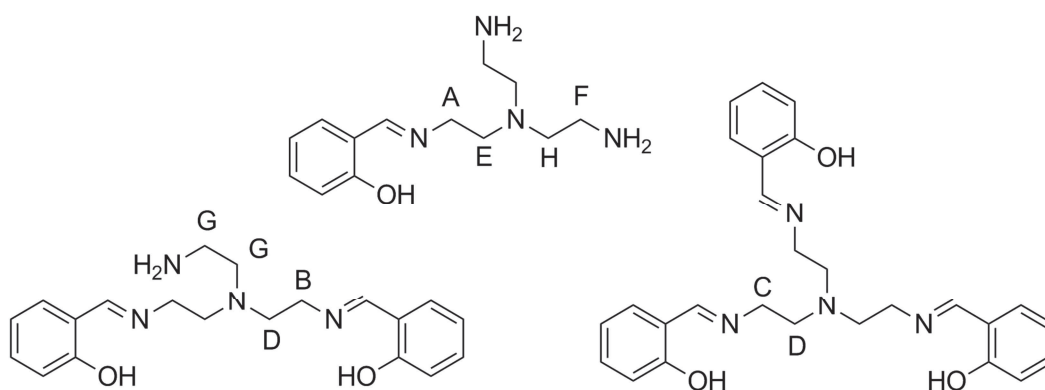


Figure 7.5-26 Structures for peaks assignment in Figure 7.5-25. Signals D and G are superposition of two signals, which is confirmed by other NMR techniques.

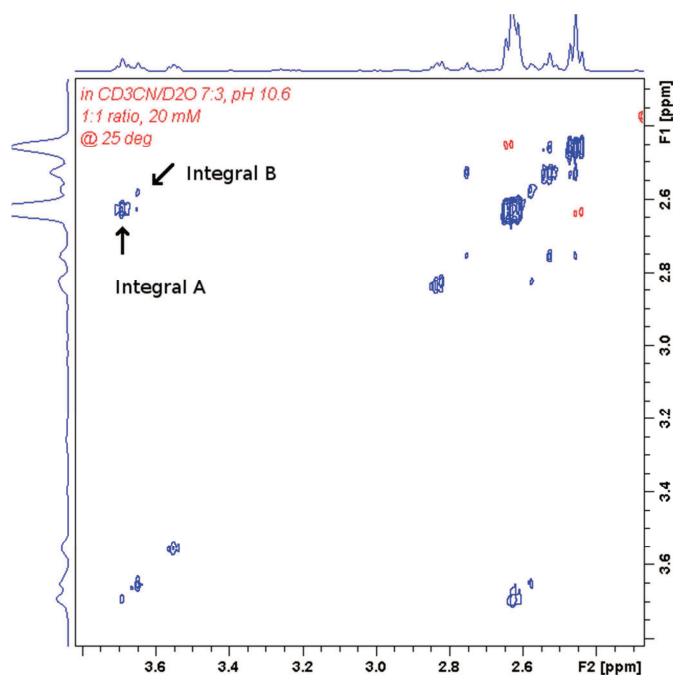


Figure 7.5-27 2D  $^1\text{H}$ -NOESY NMR spectrum of *SALAL* with *tren* at 20 mM concentration both in  $\text{CD}_3\text{CN}/\text{D}_2\text{O}$  7:3 (v/v) at  $\text{pH} = 10.7$ . NOESY mixing time = 1.000 s. Arrows indicate signals which were chosen to plot their relative intensities in Figure 7.5-22.

	Rate at 20 mM by NOESY build-up	Rate at 8 mM by NOESY build-up	Rate at 20 mM by EXSYCalc	Rate at 8 mM by EXSYCalc
Integral A	3.68	4.00	4.00	4.00
Integral B	1.06	1.20	1.25	1.25

Table 7.5-2 Comparison of obtained rates at two different concentrations and EXSYCalc values calculated at mixing time = 0.125 s (in the linear growth region).

### 7.5.3. Kinetic experiments of walking

To prove the ability of *SALAL* to perform a single step, the bis-imine-aminal **Sal<sub>3</sub>en<sub>3</sub>N<sub>4</sub>** was treated by methoxyamine (free base) in  $\text{CDCl}_3$  (control experiments in  $\text{d}_6$ -DMSO and  $\text{CD}_3\text{CN}$ ), as discussed above. Following Figures show the NMR traces recorded after addition of the methoxyamine.

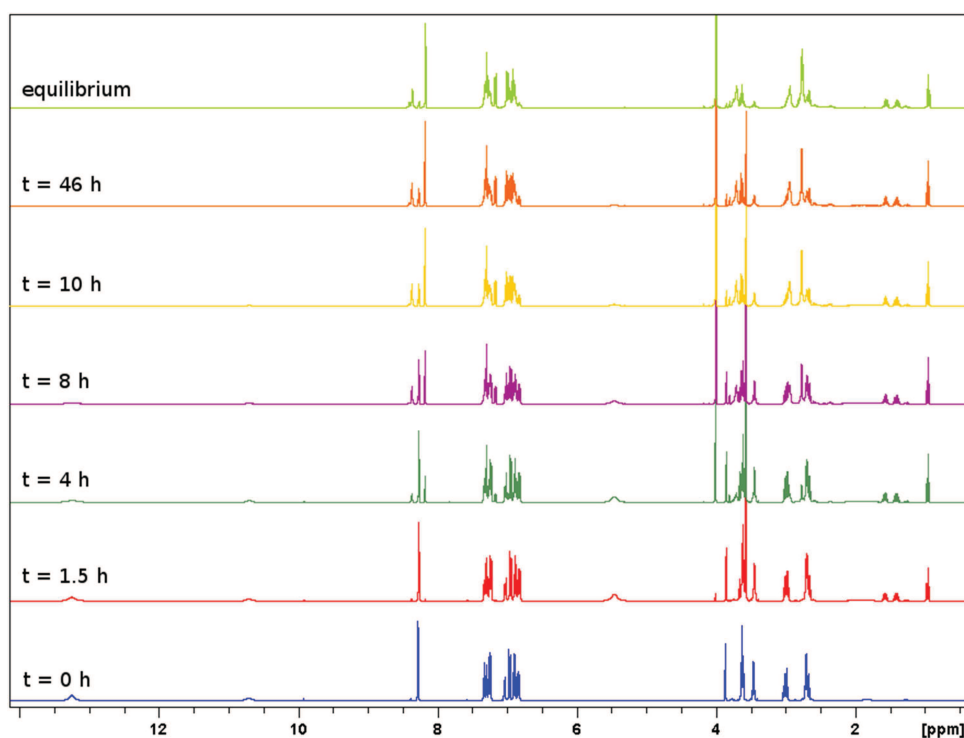


Figure 7.5-28 Overview of the time evolution of the 400 MHz  $^1\text{H}$ -NMR spectra of **Salzen<sub>3</sub>N<sub>4</sub>** treated with 1 eq. of methoxyamine in deuteriochloroform. Time stamps indicated.

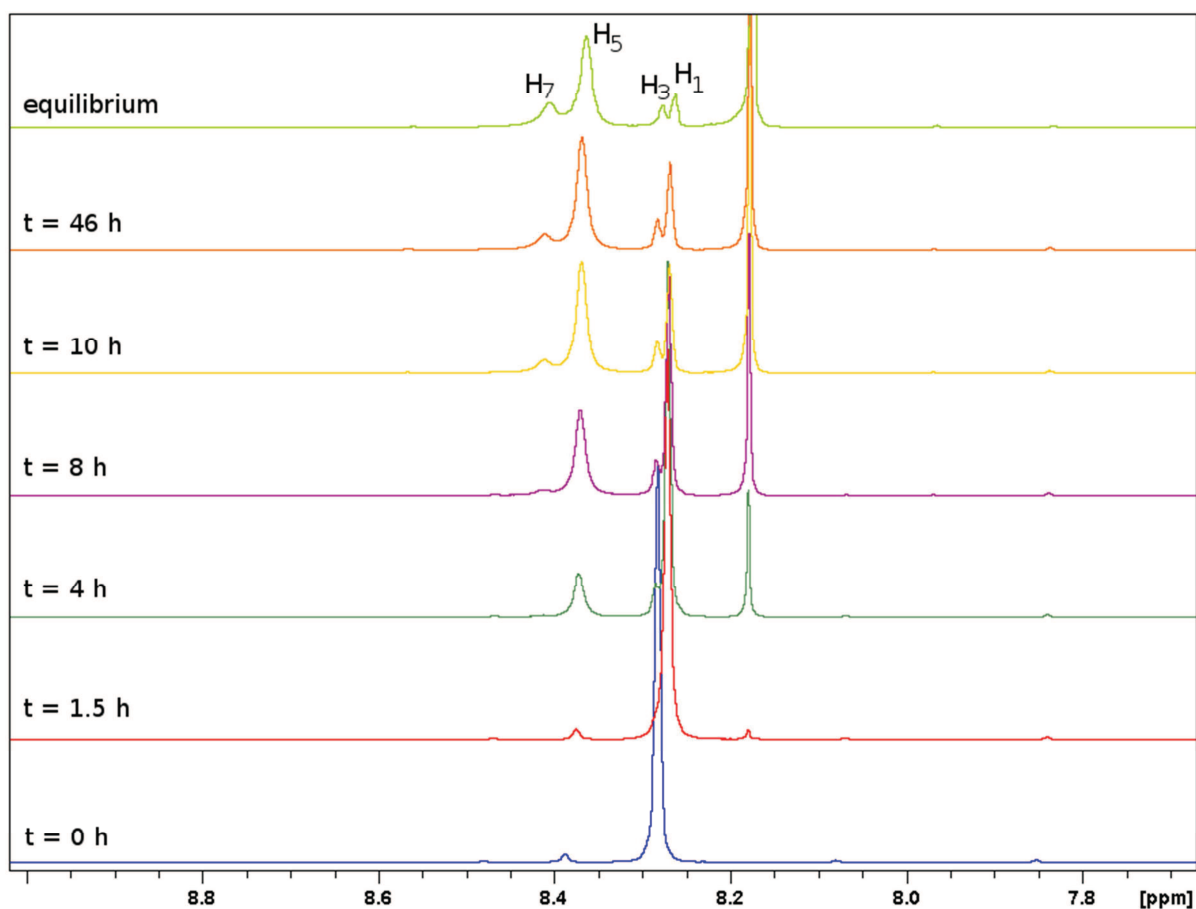


Figure 7.5-29 Detail of the imine and oxime region of the 400 MHz  $^1\text{H}$ -NMR spectra. The initial imine signal of **Salzen<sub>3</sub>N<sub>4</sub>** is decreasing over time, while the oxime signal at 8.19 ppm is increasing. Also, signals of intermediary species are observed. For the signal identification see Figure 7.5-31.

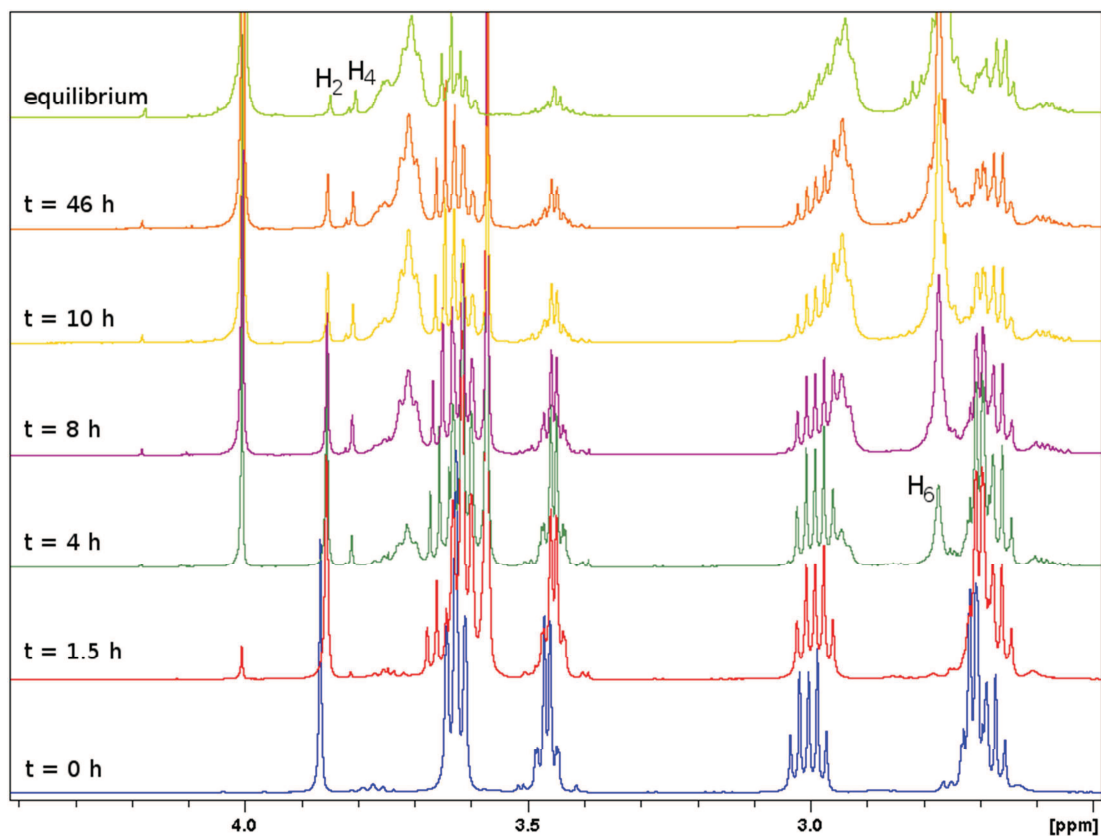


Figure 7.5-30 Detail of the aliphatic region of the 400 MHz  $^1\text{H}$ -NMR spectra. The initial amination signal of **Sal<sub>3</sub>en<sub>3</sub>N<sub>4</sub>** at 3.88 ppm is decreasing over time. Concomitantly, the singlet of the central methylene groups of the final bis-imine is increasing at 3.55 ppm. For the signal identification see Figure 7.5-31.

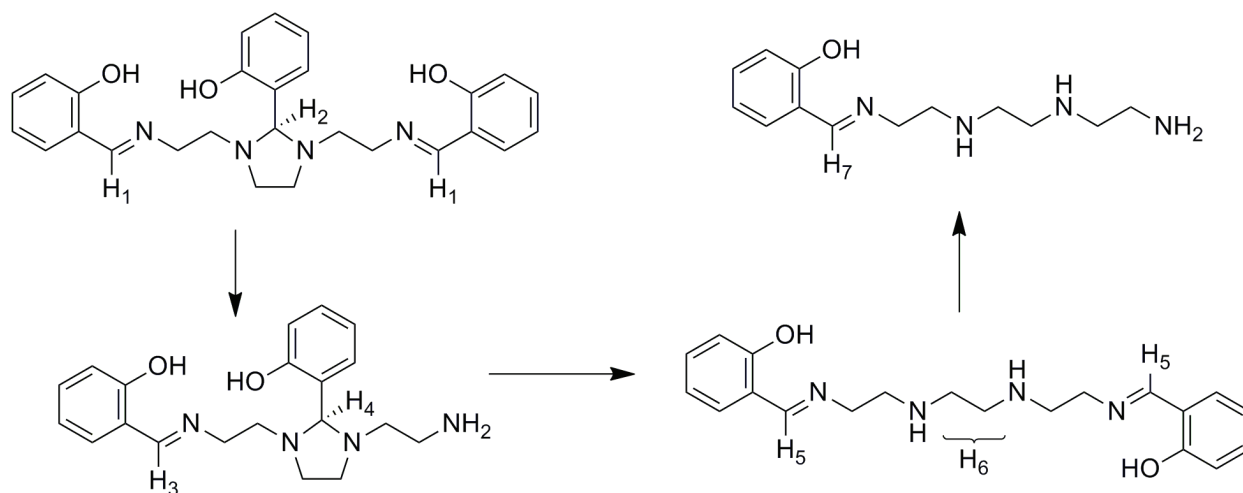


Figure 7.5-31 Mechanistic scheme and proton signal assignment for the reaction of methoxyamine with the bis-imine-amine **Sal<sub>3</sub>en<sub>3</sub>N<sub>4</sub>**, corresponding to the kinetic experiments in the previous Figures.

As control experiment, the same reaction was performed in  $\text{d}_6$ -DMSO and  $\text{d}_3$ -acetonitrile and in both cases the situation was similar, however the best signal separation was achieved in chloroform.



## 7.5.4. NMR experiments of circular motion

### 7.5.4.1. Triazacyclononane

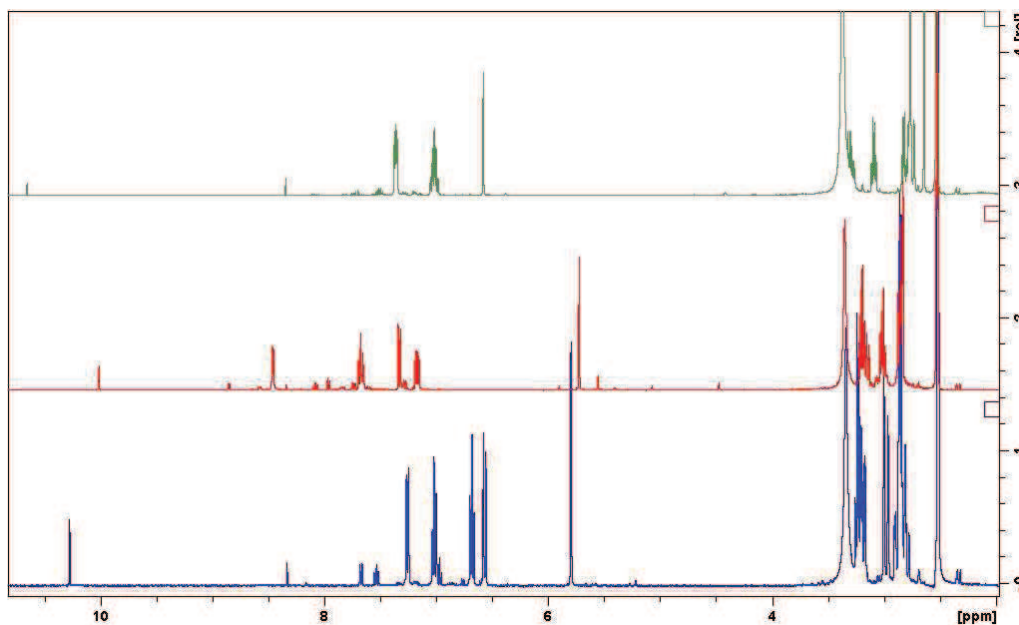


Figure 7.5-32  $^1\text{H-NMR}$  spectra of *tacn* mixed with *SALAL* (blue), *PYRAL* (red) and *CAXAL* (green) in  $d_6\text{-DMSO}$ . In all case the aminal is formed relatively efficiently, but the structures are very stable and no intramolecular exchange is observed, which is also indicated by sharp lines in the aliphatic region. The aminal signals are largely shifted upfield compared to linear polyamines studied before (consistent with the literature<sup>[334]</sup>).

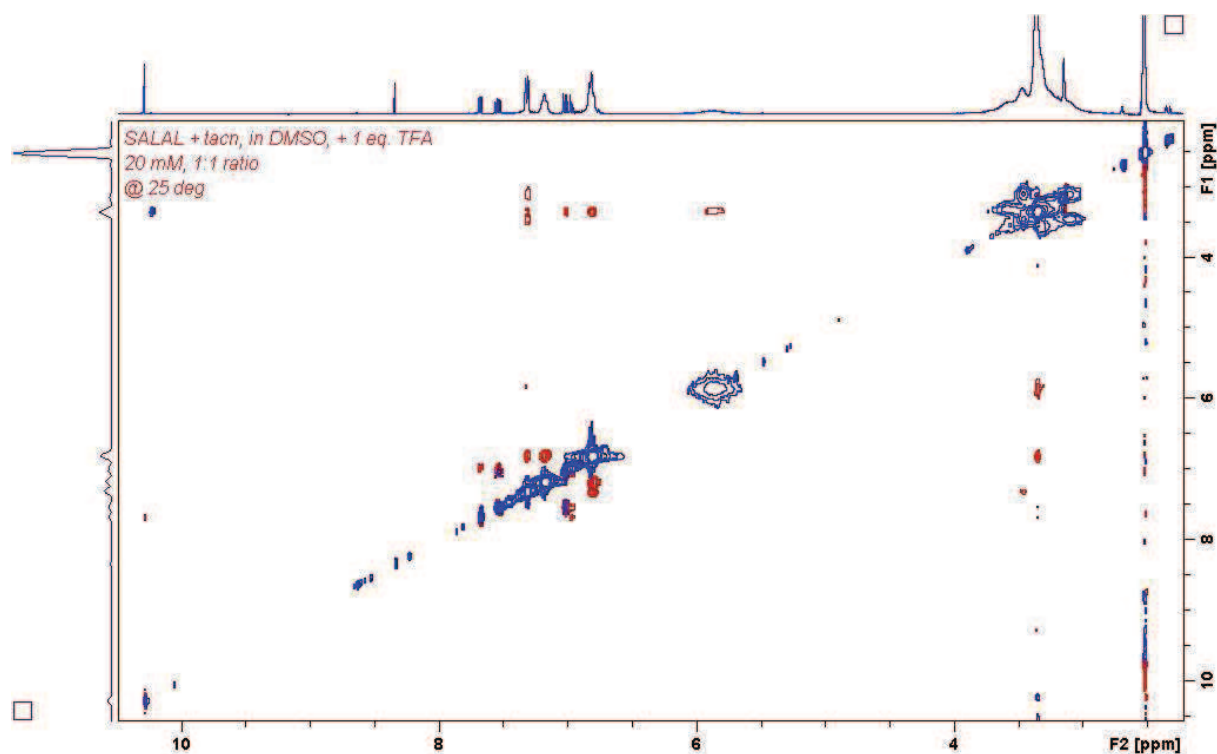


Figure 7.5-33 2D  $^1\text{H-NOESY}$  spectrum of the mixture of *SALAL* with *tacn* in  $d_6\text{-DMSO}$  after addition of 1 eq. of TFA. The signals in the aliphatic part of the spectrum are very broad and overlap, yet they do show chemical exchange cross-peaks. However, the shape and the overlap of the signals prevent the rate determination by EXSY.

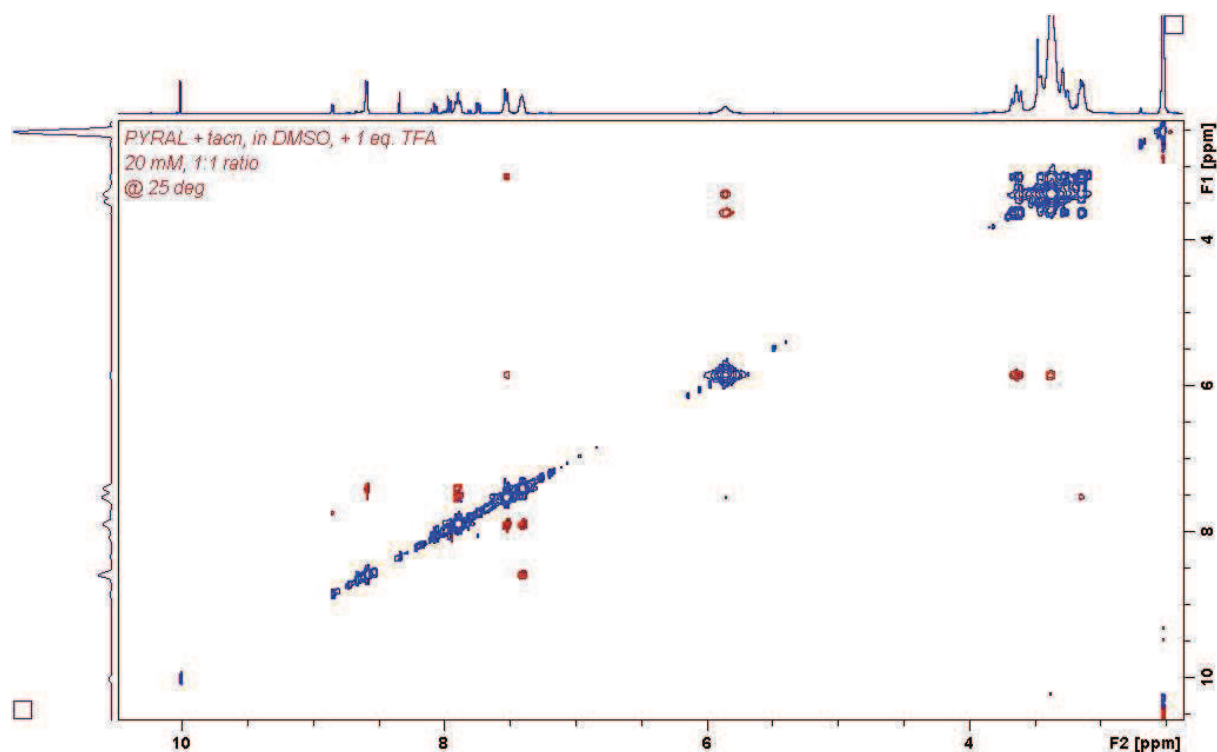


Figure 7.5-34 2D  $^1\text{H}$ -NOESY spectrum of the mixture of **PYRAL** with **tacn** in  $d_6$ -DMSO after addition of 1 eq. of TFA. The signals in the aliphatic part of the spectrum are broadened and they do show chemical exchange cross-peaks. However, the shape and the overlap of the signals prevent the rate determination by EXSY

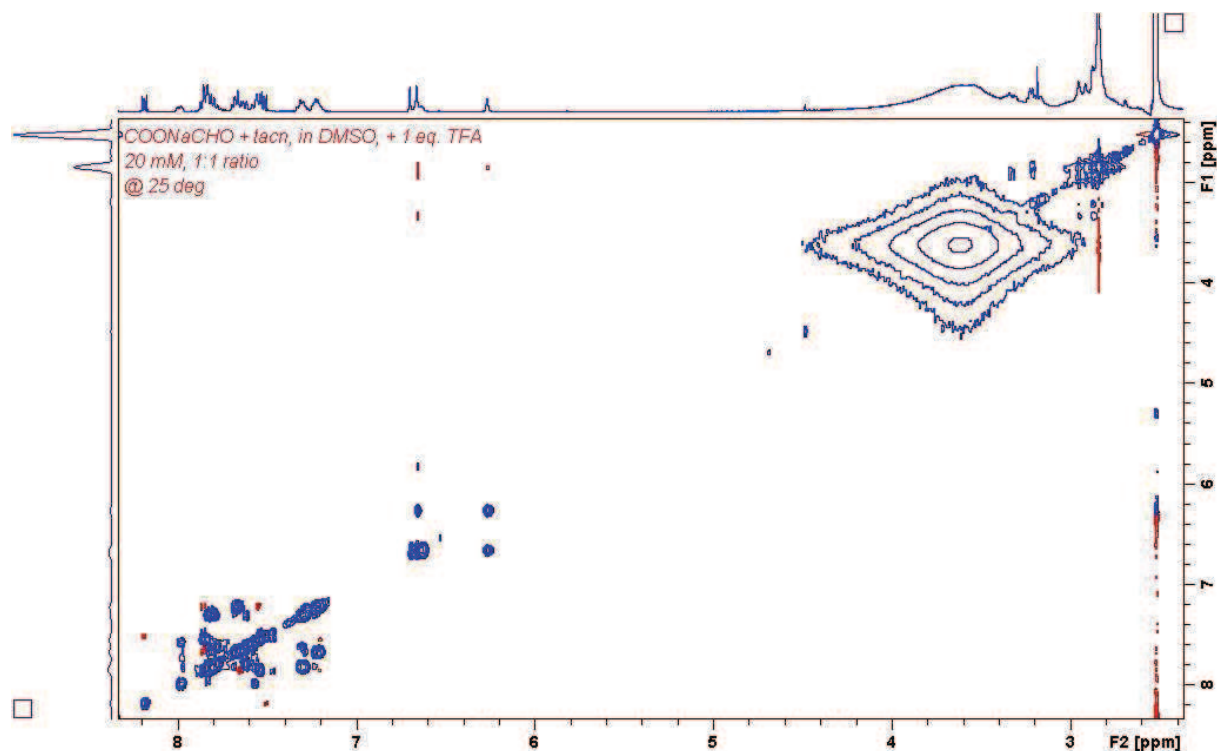


Figure 7.5-35 2D  $^1\text{H}$ -NOESY spectrum of the mixture of **CAXAL** with **tacn** in  $d_6$ -DMSO after addition of 1 eq. of TFA. The signals in the aliphatic part of the spectrum are very broad and overlap with residual water signal, yet they do show chemical exchange cross-peaks. Moreover, the azomethine signals splits into two singlets: one at 6.1 ppm corresponding to the aminor structure, and one at 6.6 ppm corresponding to the lactone structure (the other relatively close signal is the hydroxy-lactone of hydrolysed CAXAL). Furthermore, the aminor and lactone structures do have chemical exchange cross-peaks, indicating a dynamic exchange process between these two forms.

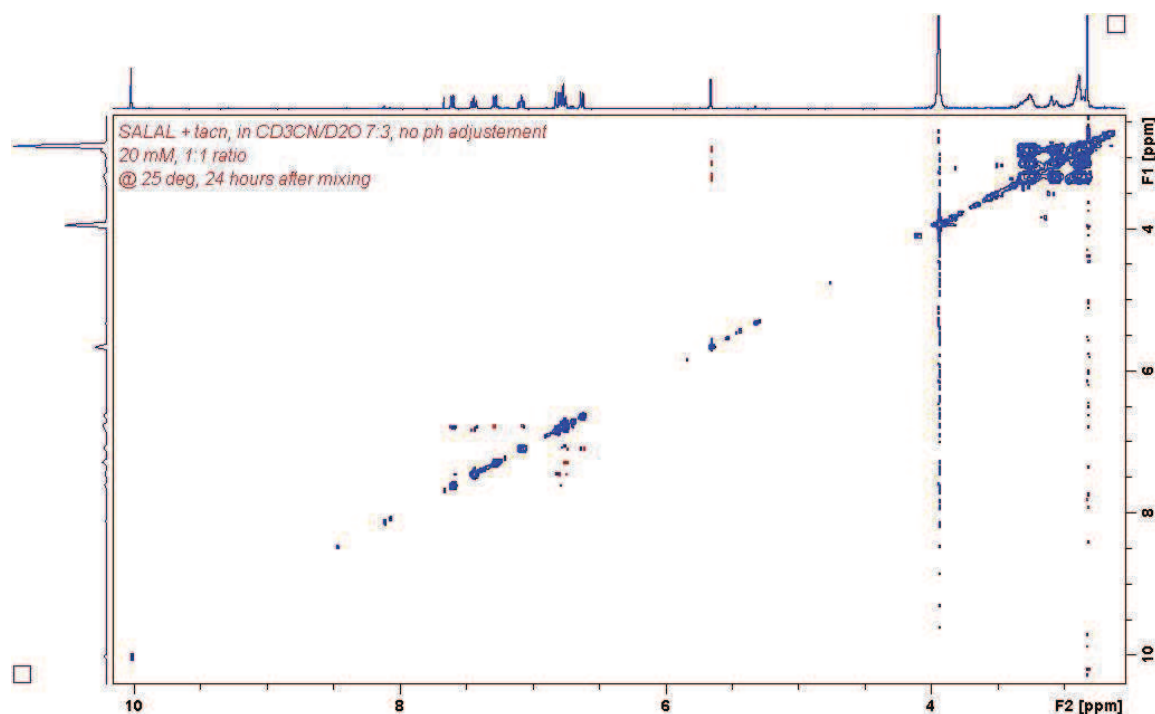


Figure 7.5-36 2D  $^1\text{H}$ -NOESY spectrum of the mixture of **SALAL** with **tacn** in  $\text{CD}_3\text{CN}/\text{D}_2\text{O}$  (7:3). The signals in the aliphatic part of the spectrum are partially broadened, yet they do show chemical exchange cross-peaks. EXSY analysis was performed on the chemical exchange pattern and gave a rate of the intramolecular exchange of 0.75 Hz. Concomitant “ring-flip” process has a rate of 1.8 Hz.

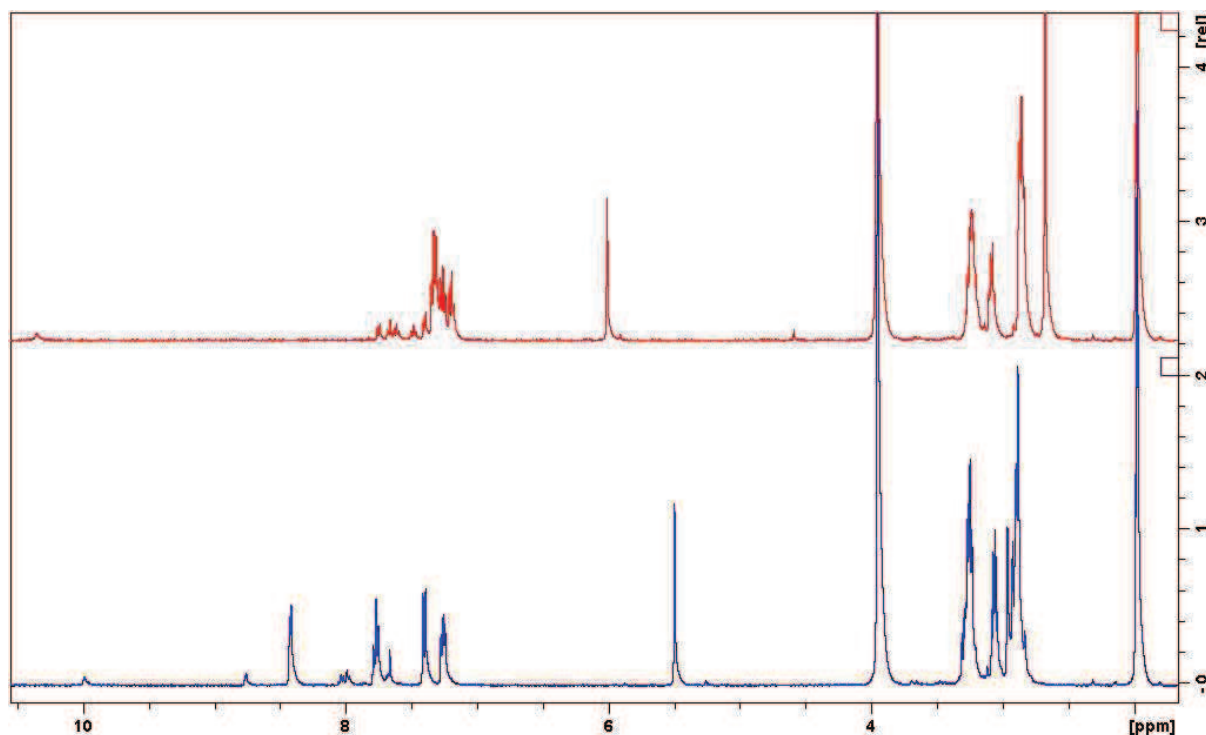


Figure 7.5-37  $^1\text{H}$ -NMR spectra of **tacn** reacted with **PYRAL** (blue) and **CAXAL** (red) in a mixture of  $\text{CD}_3\text{CN}/\text{D}_2\text{O}$  (7:3, v/v). The amins are formed very efficiently, but the structures are very stable, giving sharp line of the aliphatic signals and no exchange cross-peaks in the corresponding 2D NOESY spectra.

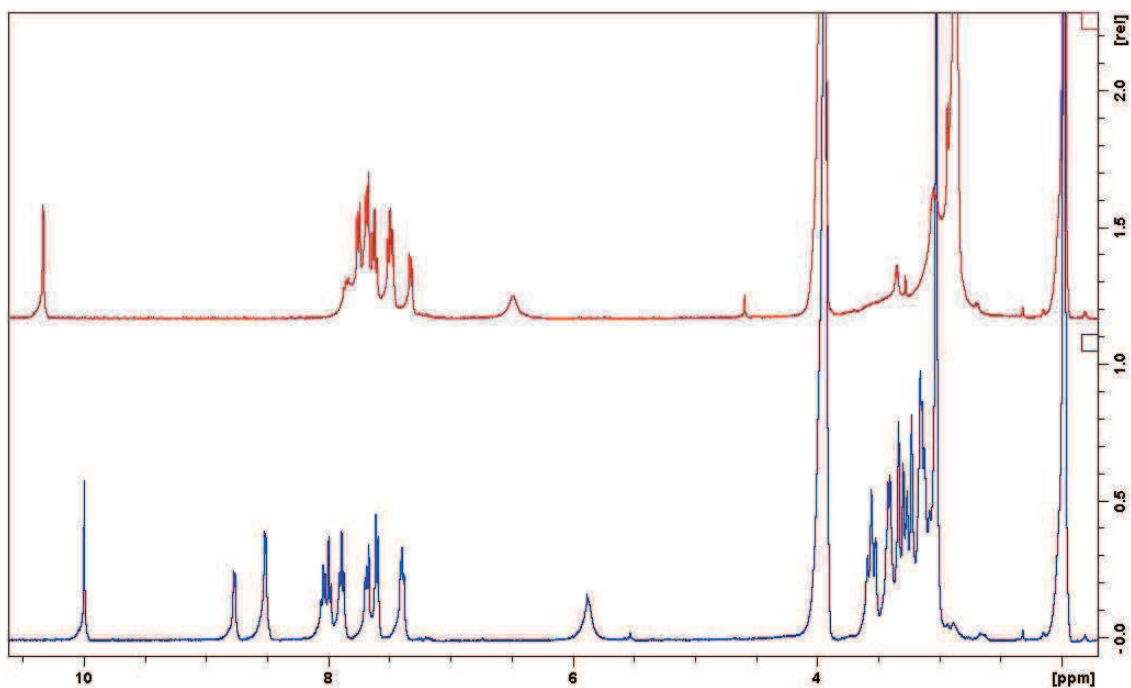


Figure 7.5-38  $^1\text{H-NMR}$  spectra of the same samples as presented in Figure 7.5-37 (**tacn** reacted with **PYRAL** (blue) and **CAXAL** (red)) after acidification by 1 eq. of TFA. Extensive hydrolysis was observed in both cases, the residual aminal signals are broad indicating that the intramolecular exchange is indeed taking place, but no quantification was performed.

#### 7.5.4.2. Cyclen

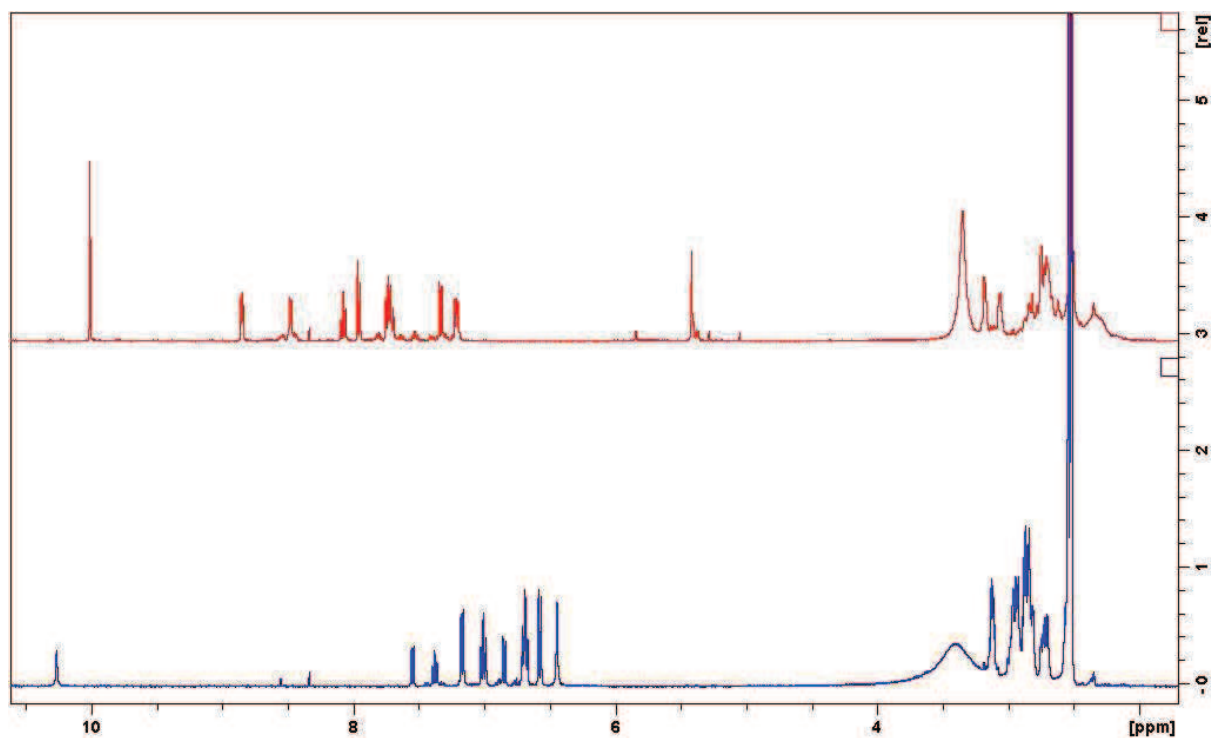


Figure 7.5-39  $^1\text{H-NMR}$  spectra of **cyclen** reacted with **SALAL** (blue) and **PYRAL** (red) in  $d_6\text{-DMSO}$ . The aminal is indeed formed in these two cases (unlike in the case of **CAXAL**, not presented here), but the structures are very stable, giving sharp lines of the aliphatic signals and no chemical exchange cross-peak in the corresponding 2D NOESY spectra.

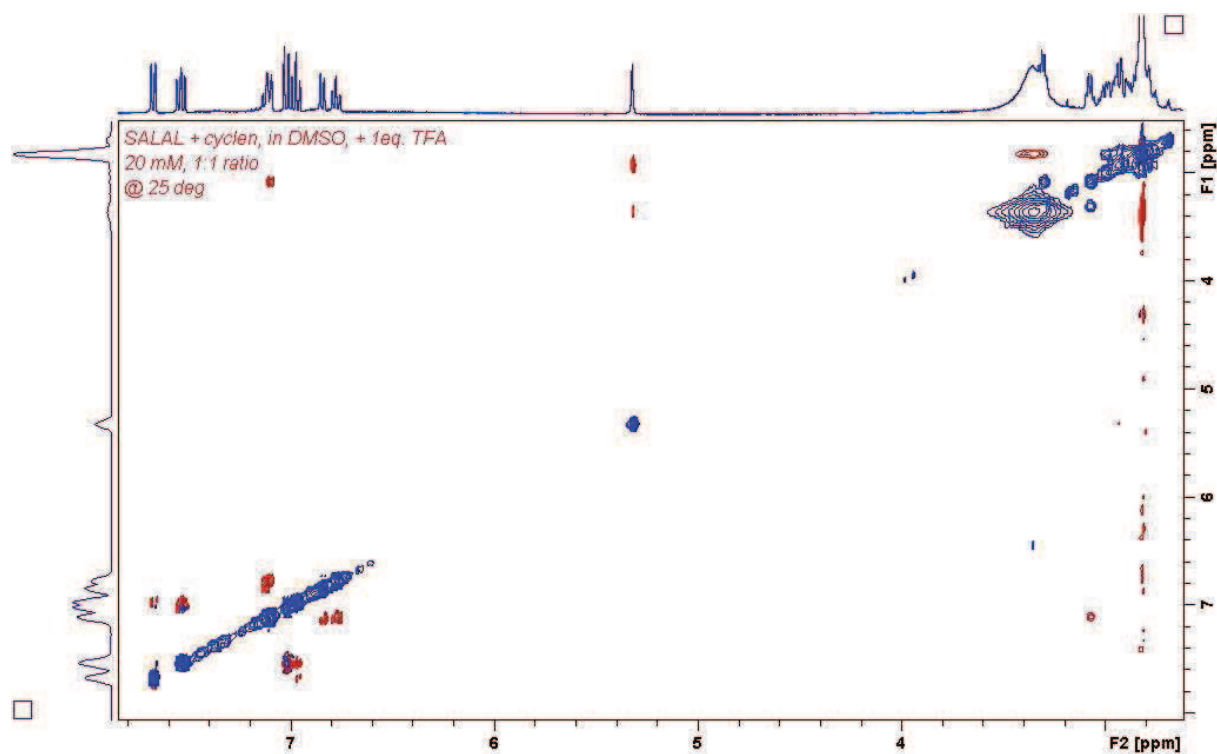


Figure 7.5-40 2D <sup>1</sup>H-NOESY spectrum of **cyclen** reacted with **SALAL** in *d*<sub>6</sub>-DMSO after addition of 1 eq. of TFA. The chemical exchange cross-peaks in the aliphatic region are observed, but they overlap (with each other and with residual water signal) and the 2D integration is heavily flawed by this overlap. No quantification was therefore performed.

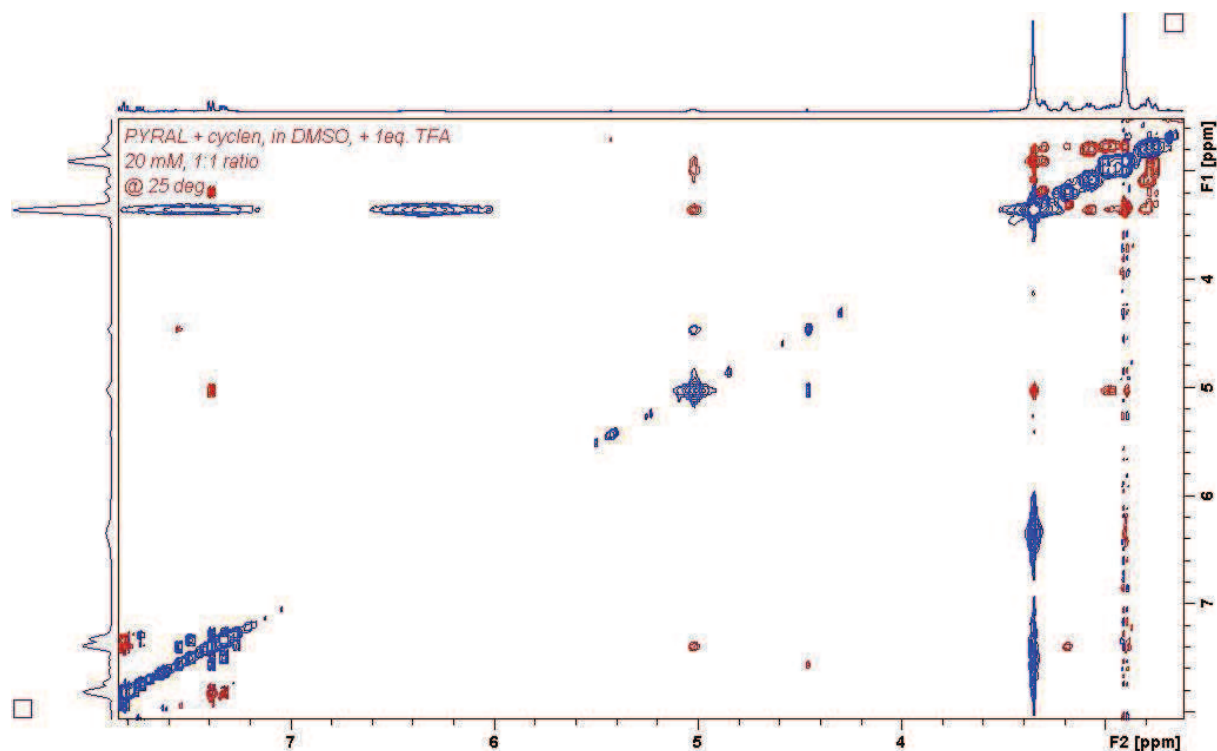


Figure 7.5-41 2D <sup>1</sup>H-NOESY spectrum of **cyclen** reacted with **PYRAL** in *d*<sub>6</sub>-DMSO after addition of 1 eq. of TFA. The aminal structure is stable even after acidification and no exchange peaks are observed. Further acidification by more equivalents of TFA leads to extensive hydrolysis.

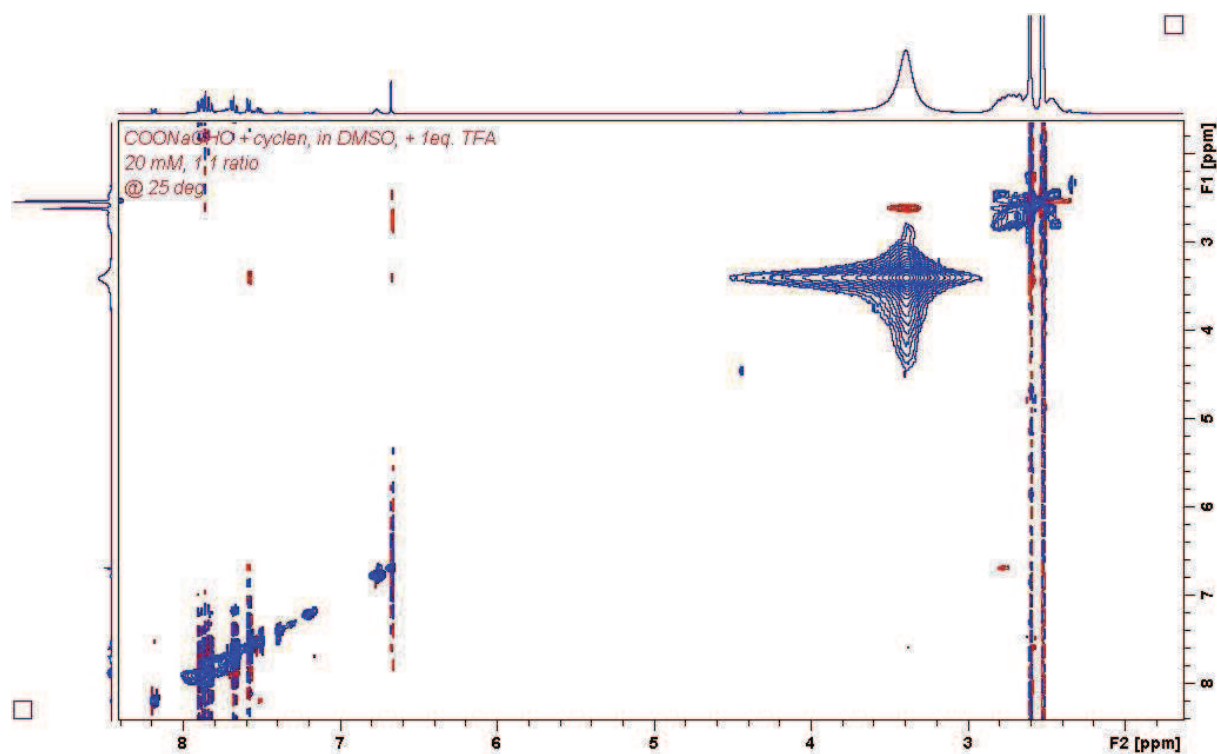


Figure 7.5-42  $^1\text{H}$ -NOESY spectrum of **cyclen** reacted with **CAXAL** in  $d_6$ -DMSO after addition of 1 eq. of TFA. The signals in the aliphatic region are very broad and actually coalesced. Chemical exchange cross-peaks are observable, but cannot be integrated. No quantification of the exchange was performed.

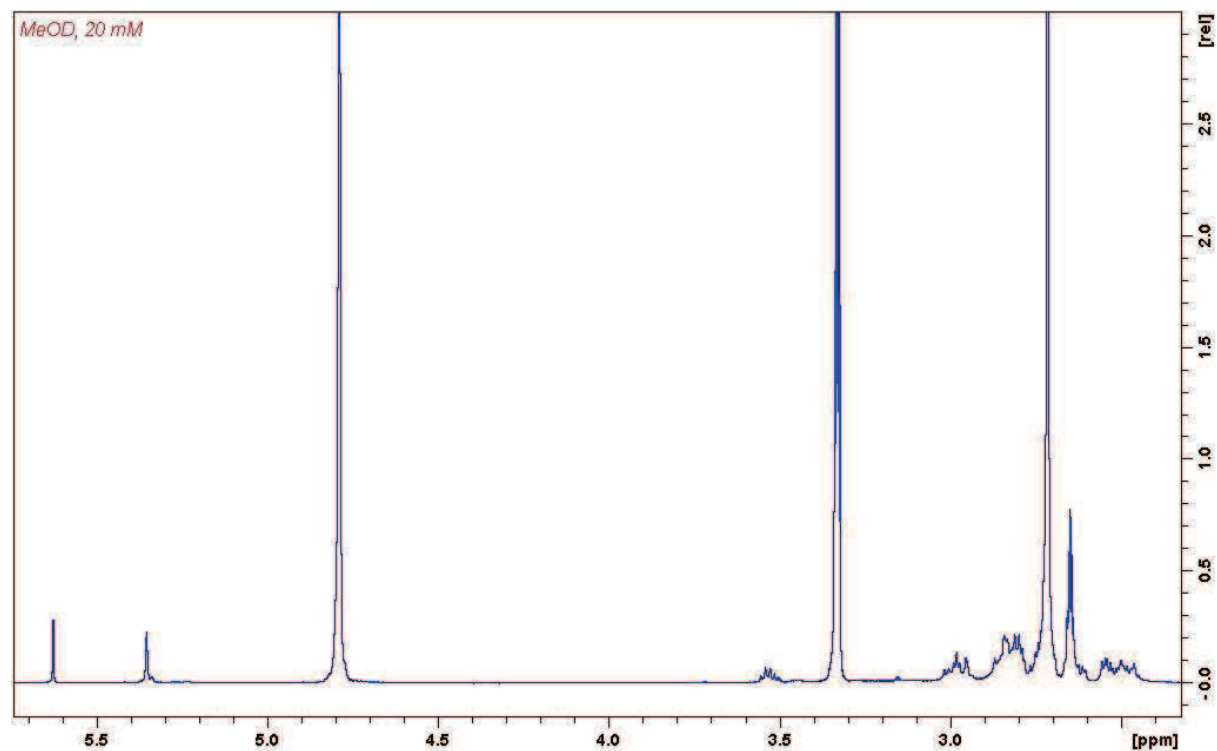


Figure 7.5-43  $^1\text{H}$ -NMR spectrum of **cyclen** reacted with **SALAL** in  $d_4$ -methanol at 20 mM concentration. A hemiaminal formed by the reaction of iminium with the solvent is observed as a singlet at around 5.4 ppm as well as a new  $\text{CHD}_2$  quintet at around 2.6 ppm. The aminal signal is also observed as a singlet at 5.6 ppm. The hemiaminal formation is strongly dependent on concentration – at higher concentration level of reagents this structure is not observed. On the other hand, formation of a bis-aminal (reaction of 2 aldehydes with 1 **cyclen**) becomes important at concentrations as high as 100 mM.



## 7.5.5. NMR spectra for directional walking

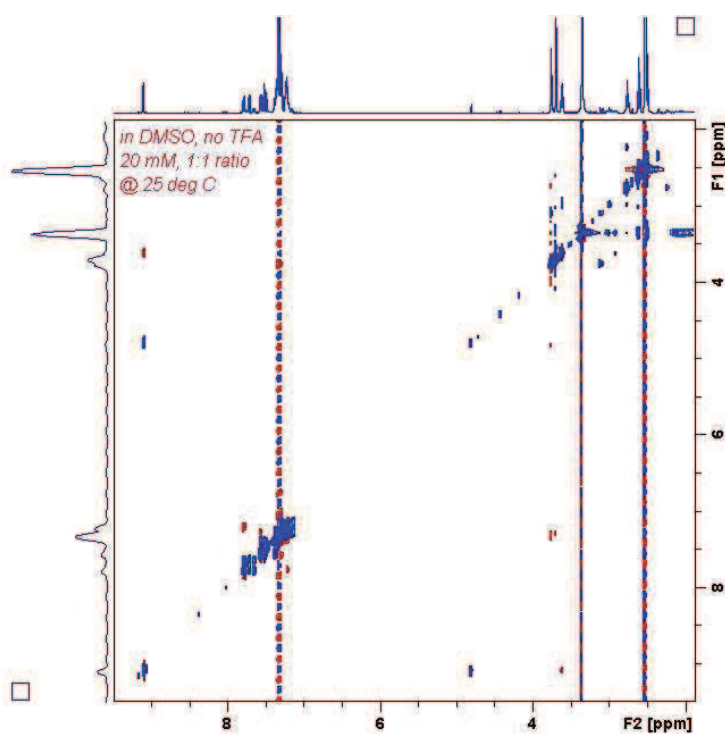


Figure 7.5-44 2D <sup>1</sup>H-NOESY spectrum of the mixture of sodium salt of **CAXAL** with **BnEDA** in *d*<sub>6</sub>-DMSO without any pH adjustment. The imine is the dominant species in the solution, but some aminor is observed as well. Moreover, Chemical exchange between the imine and the aminor is observed by the positive cross-peaks.

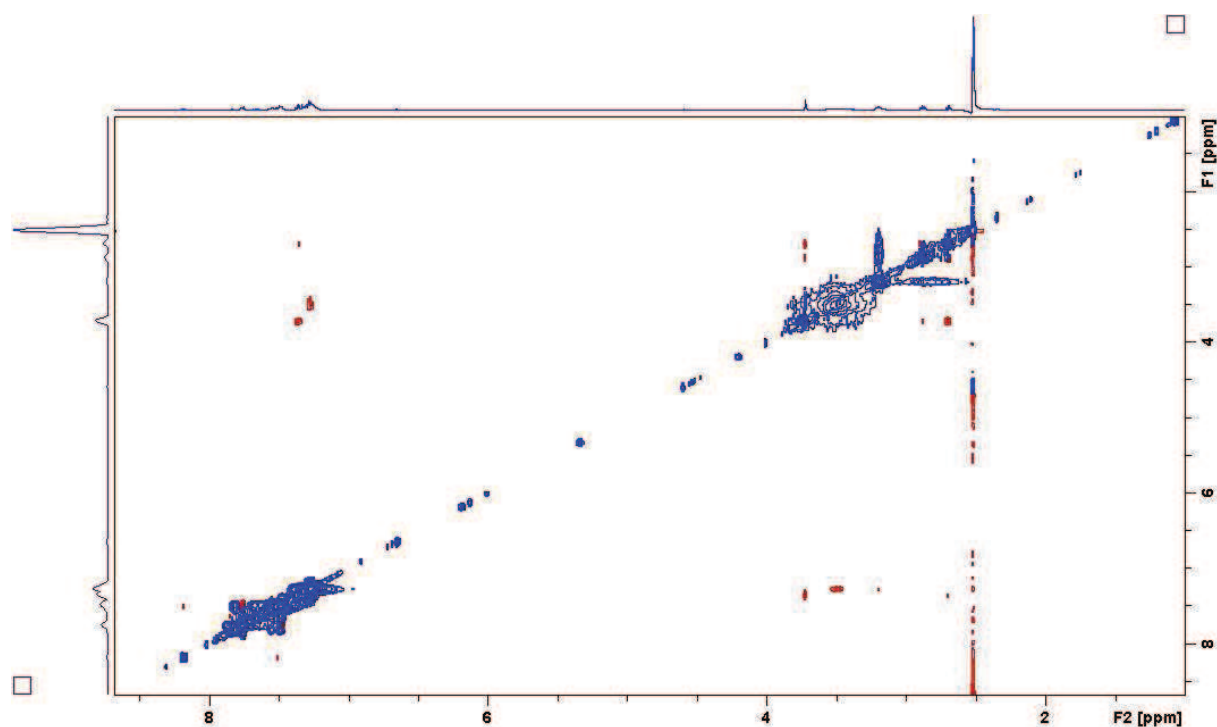


Figure 7.5-45 2D <sup>1</sup>H-NOESY spectrum of the mixture of **BnEDA** with sodium salt of **CAXAL** after addition of 1 eq. of TFA. Very broad signals in the aliphatic part indicate a very fast exchange process between species.



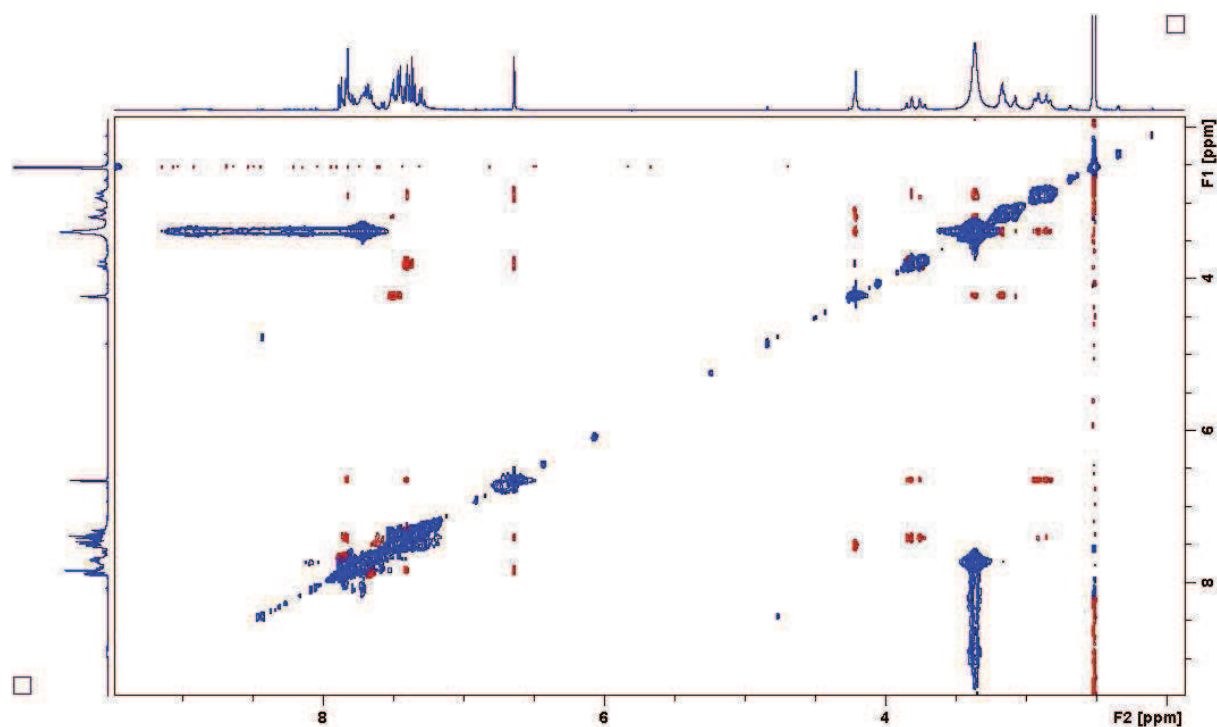


Figure 7.5-46 2D  $^1\text{H}$ -NOESY spectrum of the mixture of **BnEDA** with sodium salt of **CAXAL** after addition of 2 eq. of TFA. The lactone formed appears as a singlet at around 6.6 ppm. The chiral centre on the lactone ring causes splitting of the benzylic  $\text{CH}_2$  protons into a pair of doublets at 3.75 ppm. Some hydrolysis is observed as well, specifically the hydrolysed **BnEDA** appears as a benzylic singlet at 4.2 ppm. NOE interactions of the lactone singlet with the split benzylic signals as well as with the methylene  $\text{CH}_2$  signals prove the structure.

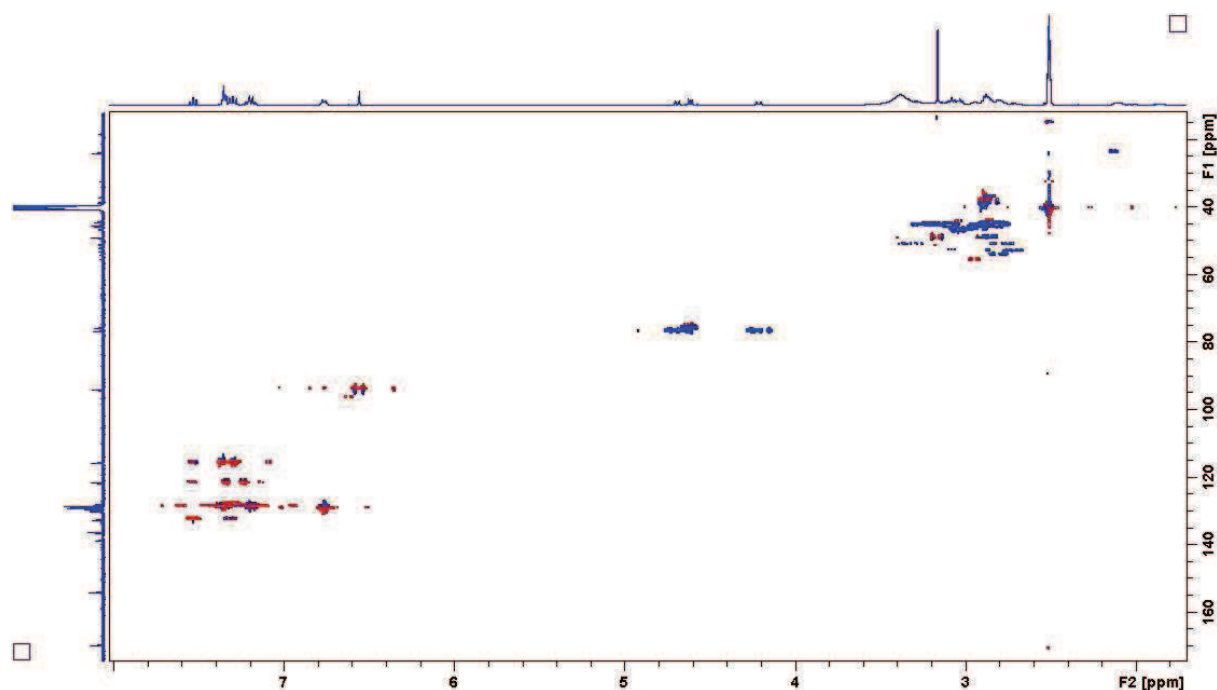


Figure 7.5-47 2D  $^1\text{H}$ - $^{13}\text{C}$  HSQC spectrum of the mixture of **OH-CAXAL** with **N<sub>3</sub>en<sub>2</sub>prNOBn** in  $d_6$ -DMSO without any pH adjustment. (proton spectrum provided in the Section 3.3.3). The chiral centre of the lactone ring causes splitting of the benzylic signals into a pair of doublets at 4.7 and 4.1 ppm. These two signals have HSQC correlation with only carbon signal, proving that they indeed belong to one benzylic  $\text{CH}_2$  group of two diastereotopic protons. Some unreacted **N<sub>3</sub>en<sub>2</sub>prNOBn** is observed as well, appearing as a signal at 4.6 ppm.

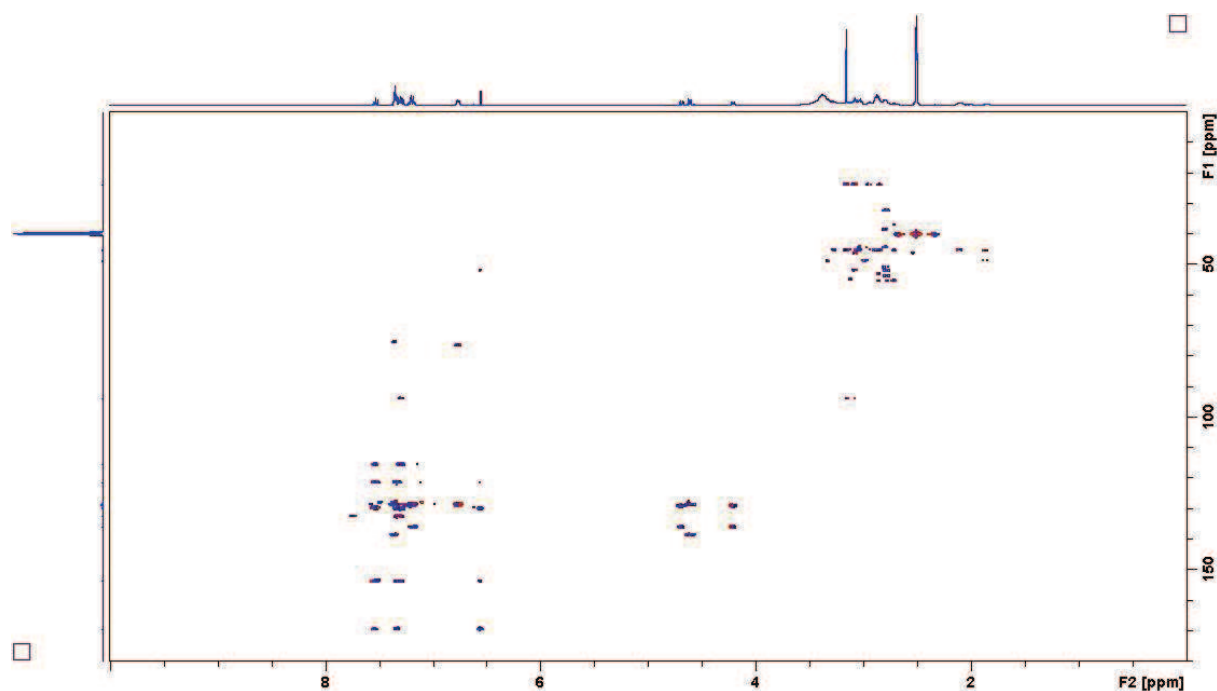


Figure 7.5-48 2D  $^1\text{H}$ - $^{13}\text{C}$  HMBC spectrum of the mixture of **OH-CAXAL** with **N<sub>3</sub>en<sub>2</sub>prNOBn** in  $d_6$ -DMSO without any pH adjustment. The lactone signal at 6.6 ppm has an HMBC correlation with one of the aliphatic  $\text{CH}_2$  signals, proving that the lactone is indeed formed on the terminal hydroxylamine site. It also proves that the structure observed is not an amina, as the amina azomethine proton would have an HMBC correlation with two or three different  $\text{CH}_2$  groups.

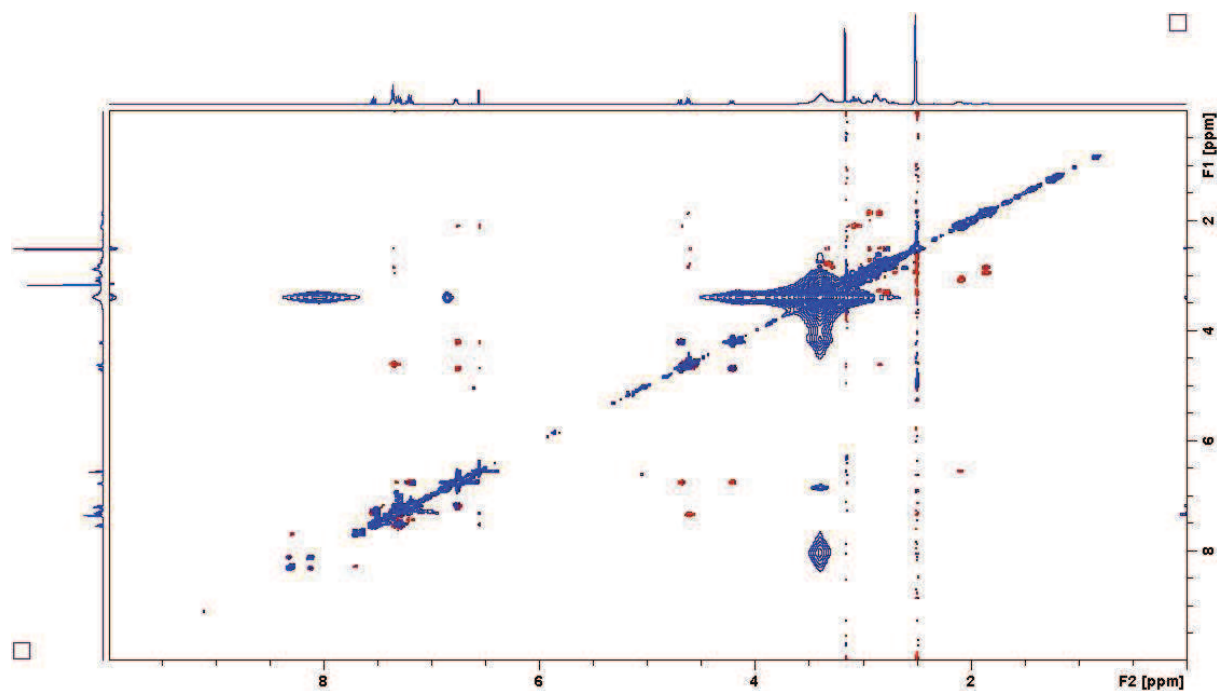


Figure 7.5-49 2D  $^1\text{H}$ -NOESY spectrum of the mixture of **OH-CAXAL** with **N<sub>3</sub>en<sub>2</sub>prNOBn** in  $d_6$ -DMSO without any pH adjustment. The lactone signals at 6.6 ppm has a NOE correlation with the two benzylic doublets and the signal of the middle methylene group of the propylene spacer. The correlation with the terminal methylene signal is visible when the intensity of the spectrum is scaled up, but other correlations are less clear in this case. The observed NOE correlation clearly confirm that the lactone is indeed formed on the terminal hydroxylamine site.

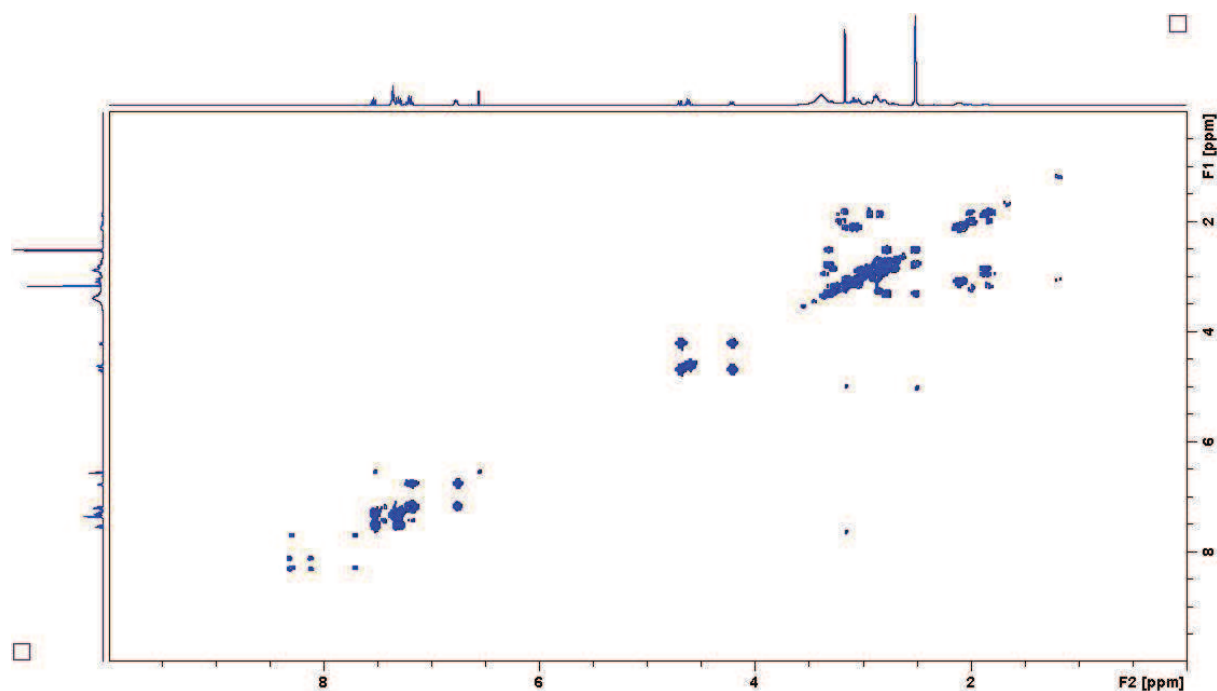


Figure 7.5-50 2D  $^1\text{H}$ -COSY spectrum of the mixture of **OH-CAXAL** with  **$N_3en_2prNOBn$**  in  $d_6$ -DMSO without any pH adjustment. The split benzylic  $\text{CH}_2$  signals have a strong COSY correlation, proving the geminal coupling of a diastereotopic pair of protons.

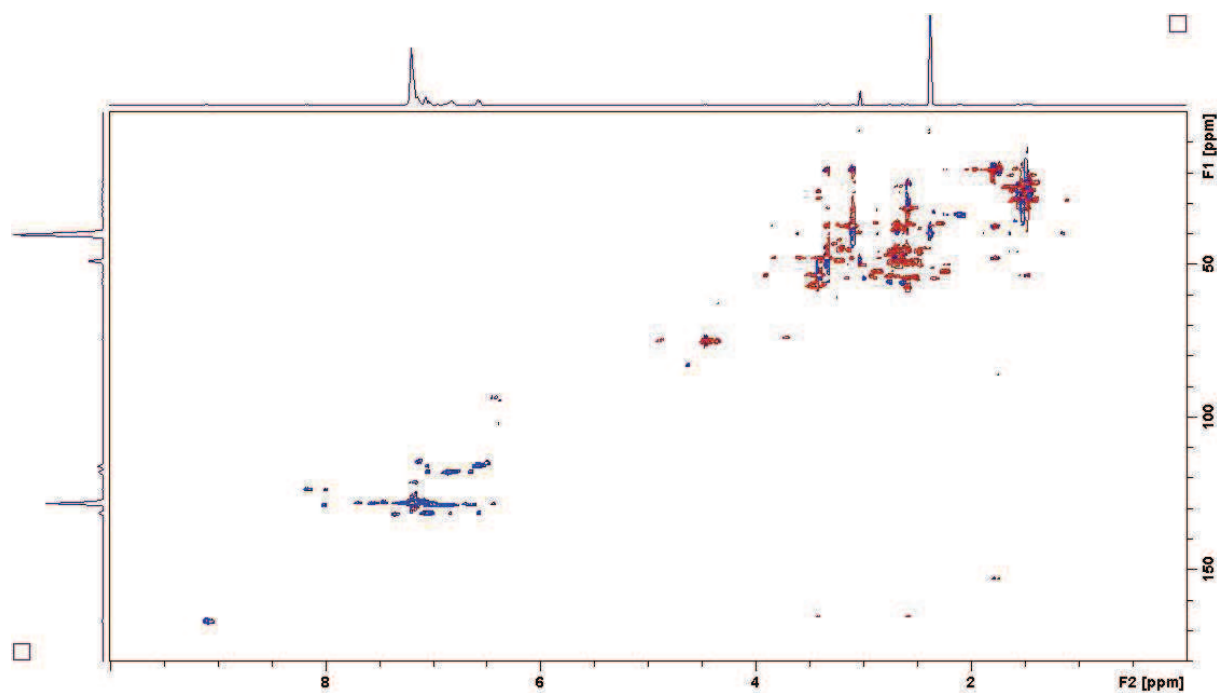


Figure 7.5-51 2D  $^1\text{H}$ - $^{13}\text{C}$  HSQC spectrum of the mixture of **OH-CAXAL** with  **$N_3en_2prNOBn$**  in  $d_6$ -DMSO with DBU. The lactone signal has disappeared from the spectrum, instead an imine signal at 9.1 ppm is observed. This signal has an HSQC correlation with a carbon signal at around 165 ppm, which is the typical region of the imine carbon signals.

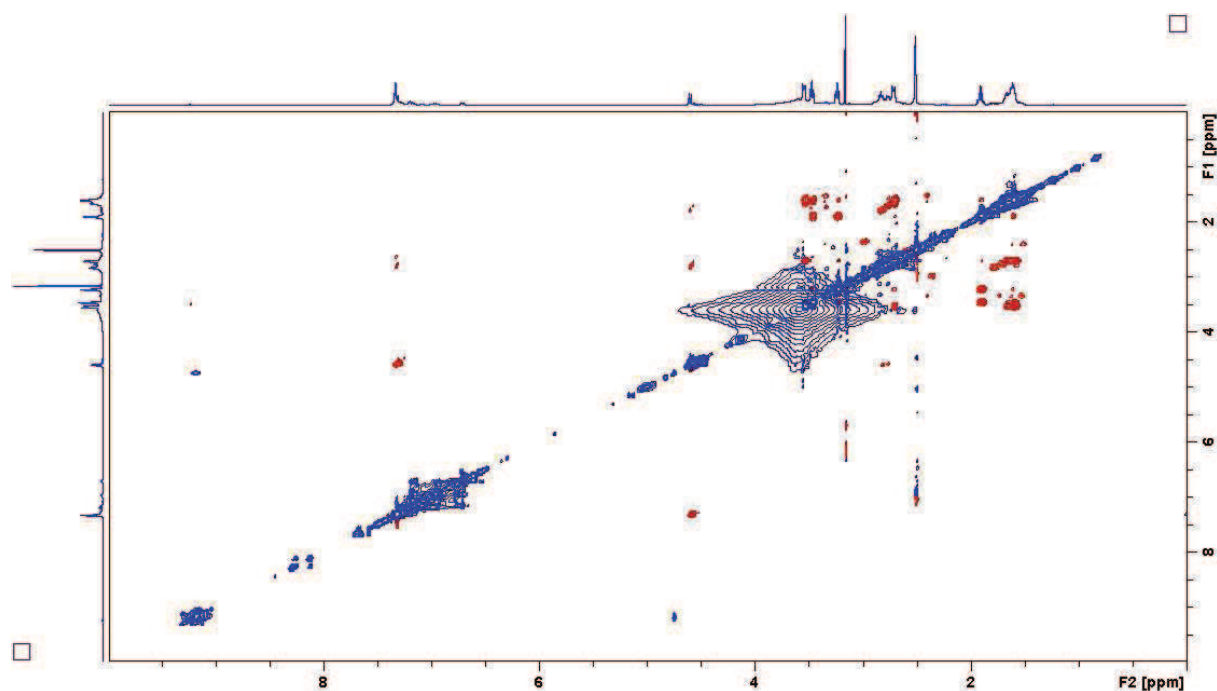


Figure 7.5-52 2D  $^1\text{H}$ -NOESY spectrum of the mixture of **OH-CAXAL** with **N<sub>3</sub>en<sub>2</sub>prNOBn** in *d*<sub>6</sub>-DMSO with DBU. The imine signal at 9.1 ppm has an exchange correlation with a signal at around 4.7 ppm, probably indicating a dynamic exchange with the aminor form. It is noteworthy that the signal at 4.7 ppm is a barely visible broad singlet in 1D  $^1\text{H}$ -NMR spectrum. The NOE interaction of the imine signal with the =N-CH<sub>2</sub> signal is visible when the intensity of the spectrum is scaled up (only small trace in the presented picture), but other correlation are less clear in such case. The strong signals in the aliphatic region are attributed to DBU.

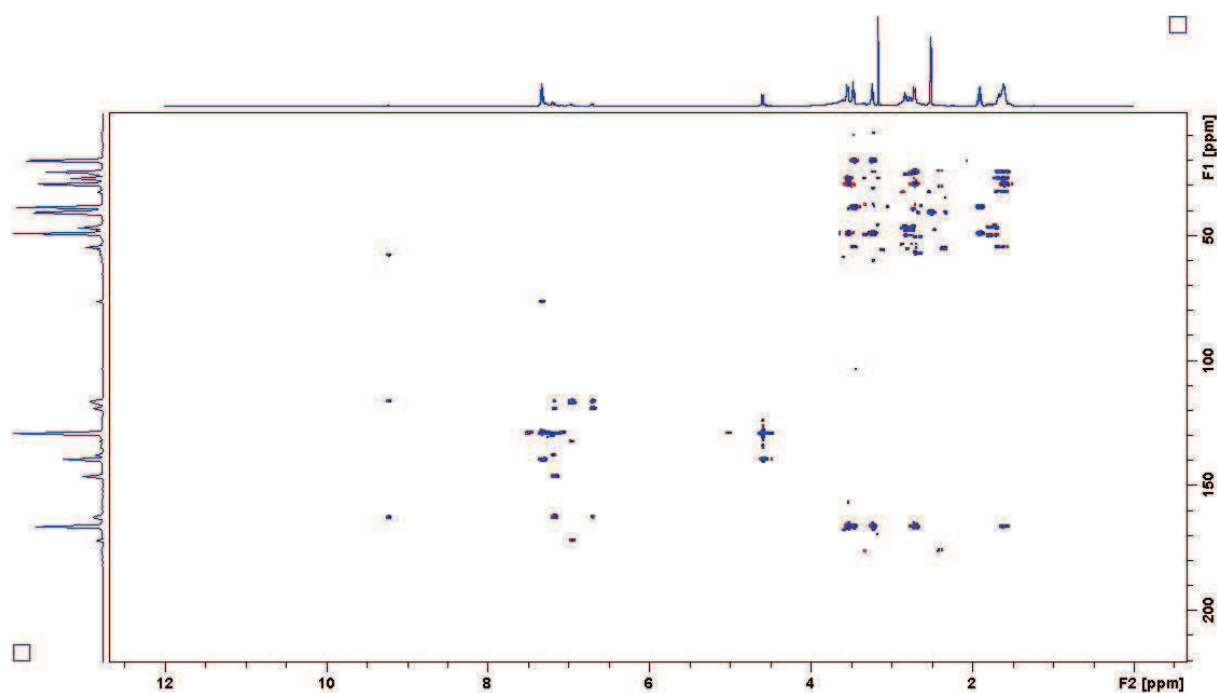


Figure 7.5-53 2D  $^1\text{H}$ - $^{13}\text{C}$  HMBC spectrum of the mixture of **OH-CAXAL** with **N<sub>3</sub>en<sub>2</sub>prNOBn** in *d*<sub>6</sub>-DMSO with DBU. The imine signal at 9.1 ppm has an HMBC correlation with one of the aliphatic signals proving that the imine is indeed formed on the NH<sub>2</sub> terminus of the polyamine chain.

## 7.6. Dynamic reaction selectivity

The Chapter 4 discussed the simplicity selection in 3+3 aldehyde amine library. Since this experiment inherently includes the 2+2 experiments through the deconvolution, the respective selection matrices are provided here. Please note that the molar fraction indicated states for all products formed by the reaction of the two species (if there is more than one). Also, the difference between the sum of each row or column and 100 % is the fraction of unreacted compound.

### 7.6.1. Selection matrices

	SALAL	PYRAL	CAXAL
IPA	0.88	0.12	0
Me2PDA	0.12	0.88	0
PIP	0	0	1

	SALAL	PYRAL	
IPA	0.83	0.17	
Me2PDA	0.17	0.83	
PIP	0	0	

	SALAL		CAXAL
IPA	0.6		0
Me2PDA	0.4		0.59
PIP	0		0.41

		PYRAL	CAXAL
IPA		0.35	0.23
Me2PDA		0.65	0.24
PIP		0	0.53

	SALAL	
IPA	0.5	
Me2PDA	0.5	
PIP	0	

		CAXAL
IPA		0.33
Me2PDA		0.63
PIP		0.04

		PYRAL
IPA		0.22
Me2PDA		0.78
PIP		0

	SALAL	PYRAL	CAXAL
Me2PDA	0.21	0.89	0
PIP	0	0	1

	SALAL	PYRAL	CAXAL
IPA	0.71	0.29	0
PIP	0	0	1

	SALAL	PYRAL	CAXAL
IPA	0.7	0.25	0.07
Me2PDA	0.12	0.52	0.36

	SALAL	PYRAL	CAXAL
PIP	0	0	1

	SALAL	PYRAL	CAXAL
IPA	0.58	0.27	0.15

	SALAL	PYRAL	CAXAL
Me2PDA	0.13	0.7	0.18

	SALAL	PYRAL
IPA	0.75	0.25
Me2PDA	0.25	0.75

	SALAL		CAXAL
IPA	0.81		0.17
Me2PDA	0.19		0.74

		PYRAL	CAXAL
IPA		0.49	0.37
Me2PDA		0.39	0.52

	SALAL	PYRAL	
IPA	0.75	0.25	
PIP	0	0.3	

	SALAL		CAXAL
IPA	1		0
PIP	0		1

		PYRAL	CAXAL
IPA		0.86	0.11
PIP		0	0.89

	SALAL	PYRAL	
Me2PDA	0.9	0.1	
PIP	0	0.34	

	SALAL		CAXAL
Me2PDA	0.75		0.14
PIP	0		0.86

	SALAL		
IPA	0.4		
Me2PDA	0.6		

		CAXAL
IPA		0.27
Me2PDA		0.73

		PYRAL	CAXAL
Me2PDA		0.97	0.06
PIP		0	0.94

	SALAL		
Me2PDA	1		
PIP	0		

			CAXAL
Me2PDA			0.9
PIP			0.1

		PYRAL	
Me2PDA		0.88	
PIP		0.12	

	SALAL		
IPA	0.9		
PIP	0.05		

			CAXAL
IPA			0.61
PIP			0.39

		PYRAL	
IPA		0.74	
PIP		0.18	

	SALAL		CAXAL
PIP	0		1

		PYRAL	CAXAL
PIP		0	1

		PYRAL	
IPA		0.21	
Me2PDA		0.79	

	SALAL	PYRAL	
Me2PDA	0.31	0.63	

	SALAL	PYRAL	
IPA	0.68	0.29	

	SALAL		CAXAL
Me2PDA	0.31		0.69

	SALAL		CAXAL
IPA	0.77		0.23

		PYRAL	CAXAL
Me2PDA		0.44	0.55

		PYRAL	CAXAL
IPA		0.65	0.35

	SALAL		
IPA	1		

	SALAL	PYRAL	
PIP	0	0.4	

			CAXAL
IPA			1

		PYRAL	
IPA		1	

	SALAL		
Me2PDA	0.92		

	SALAL		
PIP	0.3		

			CAXAL
Me2PDA			1

			CAXAL
PIP			1

		PYRAL	
Me2PDA		1	



		PYRAL	
PIP		0.4	

0.123	-0.220	-0.191
-0.232	0.145	-0.337
-0.022	-0.097	0.166

0.732	0.419	0.259
0.461	0.688	0.489
0.023	0.116	0.744

0.169	0.265	0.264
0.318	0.243	0.310
0.078	0.163	0.351

## 7.7. NMR comparison for STM results

The following figures provide detailed NMR data on the imine formation and exchange which were used for a comparison between bulk solution kinetics and kinetics observed by STM on the HOPG surface. The results are discussed in Chapter 5. In the Captions of the following Figures, the molecules are abbreviated in the same fashion as in the text, specifically: 4-(hexadecyloxy)-benzaldehyde **A**, ethylenediamine **B2**, 1,6-diaminohexane **B6** and 1,12-diaminododecane **B12**. The mono-imines formed by the condensation of one molecule of **A** with one amino group of either of the diamines is denoted as **A<sub>1</sub>B<sub>x</sub>**, the bis-imine formed by a double condensation reaction is denoted as **A<sub>2</sub>B<sub>x</sub>**.

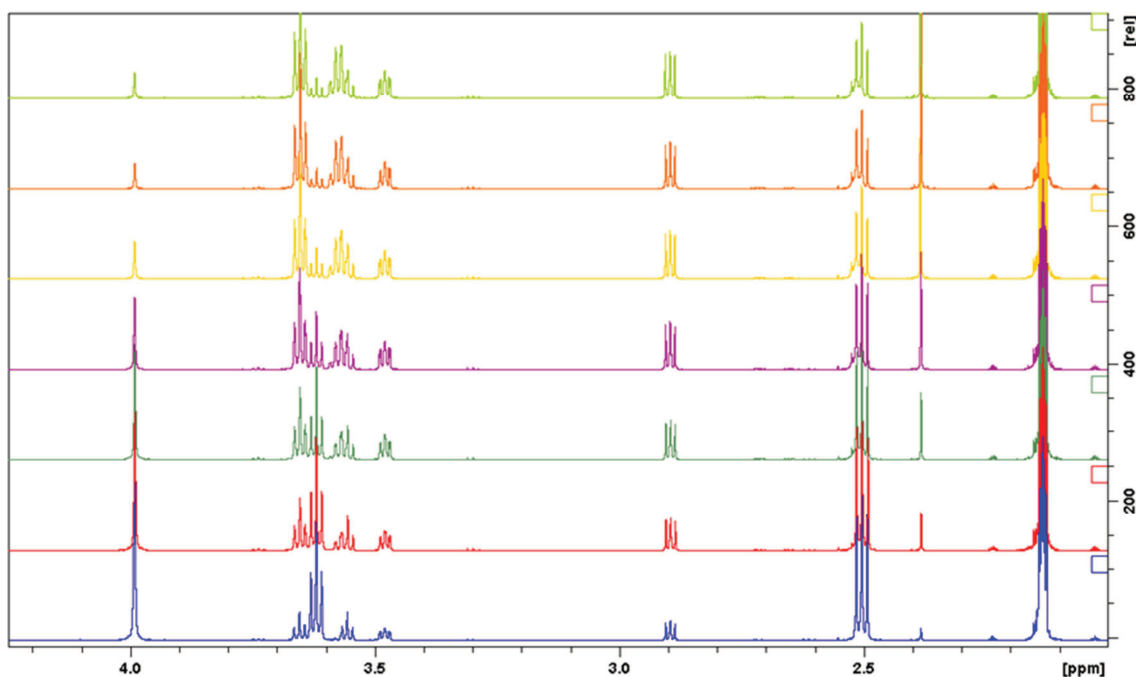


Figure 7.7-1  $^1\text{H-NMR}$  spectrum (at 600 MHz, aliphatic region) of the signal evolution during the  $\text{A}_2\text{B}_2 + \text{B}_6$  imine exchange reaction (the peaks assignment:  $\text{A}_2\text{B}_2$  3.99 ppm,  $\text{A}_1\text{B}_6$  3.55 ppm,  $\text{A}_2\text{B}_6$  3.58 ppm,  $\text{A}_1\text{B}_2$  3.48 and 2.90 ppm,  $\text{B}_2$  2.38 ppm, signal around 2.50 ppm is a mixture of the  $-\text{CH}_2\text{NH}_2$  signals of  $\text{B}_6$  and  $\text{A}_1\text{B}_6$ ).

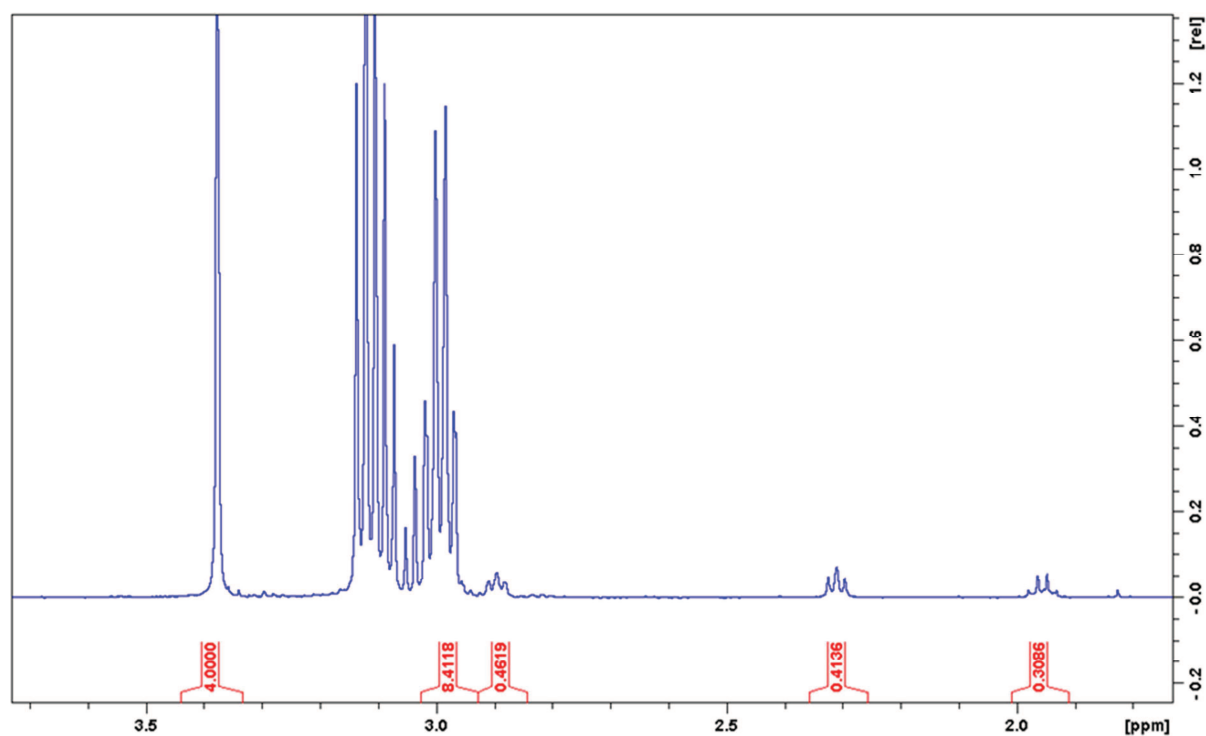


Figure 7.7-2 400 MHz  $^1\text{H}$ -NMR spectrum of the mixture of 4 eq. of aldehyde **A** with **B2** and **B12** diamines (1 eq. each, both 20 mM in  $d_8$ -toluene), aliphatic part. The singlet at 3.4 ppm corresponds to the methylene signals of the **A2B2**, pseudo-quartet at 3.0 ppm contains  $=\text{N-CH}_2$ -signals of both **A1B12** and **A2B12**, triplets at 2.9 and 2.3 ppm correspond to the methylene signals of the **A1B2**, multiplet at 1.95 ppm correspond to the  $-\text{CH}_2\text{-NH}_2$  proton of the **A1B12**.

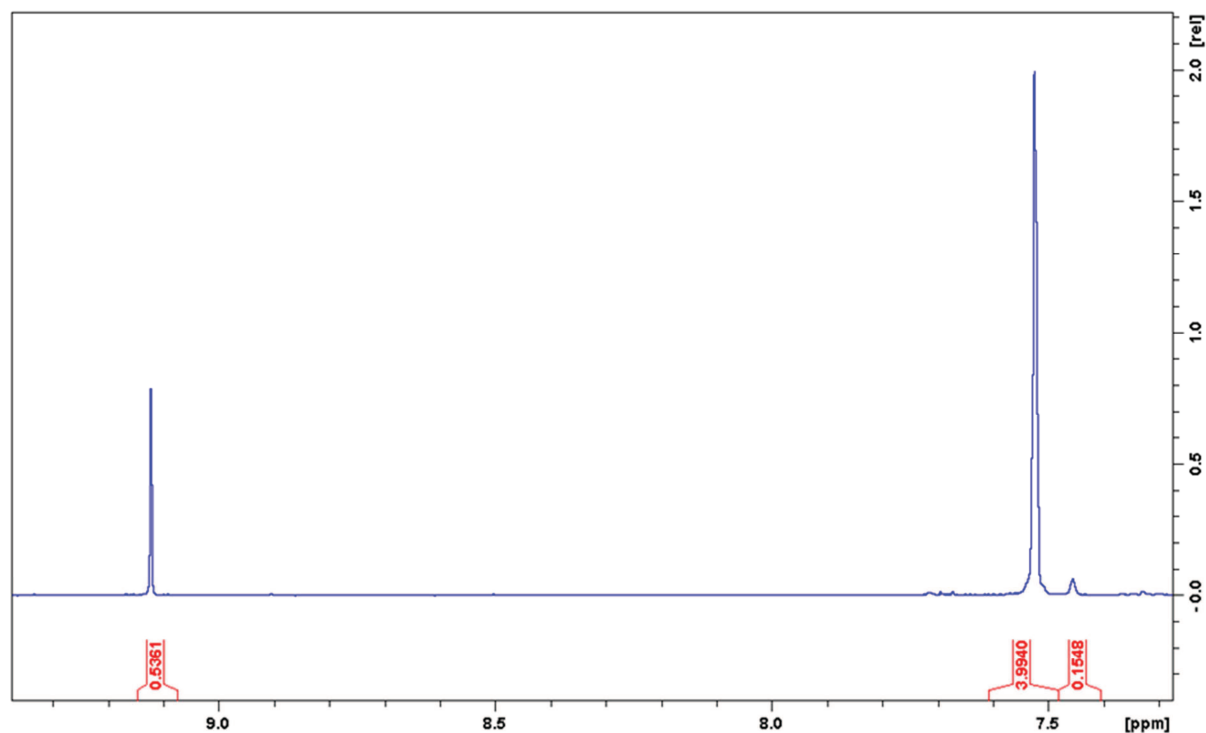


Figure 7.7-3 The aldehyde and imine section of the 400 MHz  $^1\text{H}$ -NMR spectrum of the mixture of 4 eq. of aldehyde **A** with diamines **B2** and **B12** (1 eq. and 20 mM each). Approximately 10 % of the aldehyde remains unreacted (9.12 ppm). The imine signals overlap and only the signal of **A1B2** is separated at 7.45 ppm. Indicated integral values are normalized with respect to the aliphatic part of the spectrum in Figure 7.7-2.

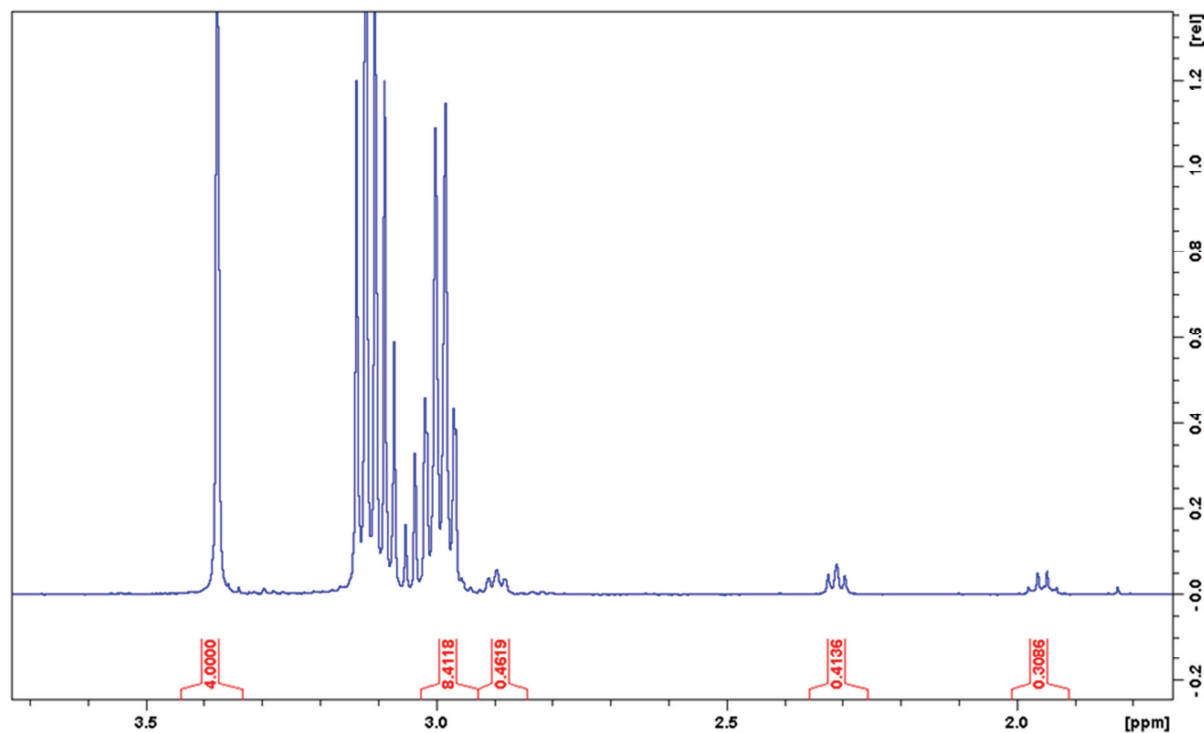


Figure 7.7-4 The aliphatic section of the 400 MHz  $^1\text{H-NMR}$  spectrum of the mixture of 6 eq. of the aldehyde **A** with diamines **B2**, **B6** and **B12** (1 eq. and 20 mM each). The singlet at 3.4 ppm corresponds to the methylene signals of the **A<sub>2</sub>B<sub>2</sub>**, the multiplet at 3.0 ppm contains =N-CH<sub>2</sub>-combined signals of **A<sub>1</sub>B<sub>6</sub>**, **A<sub>2</sub>B<sub>6</sub>**, **A<sub>1</sub>B<sub>12</sub>** and **A<sub>2</sub>B<sub>12</sub>**, triplets at 2.9 and 2.3 ppm correspond to the methylene signals of the **A<sub>1</sub>B<sub>2</sub>**, the multiplet at 1.95 ppm correspond to -CH<sub>2</sub>-NH<sub>2</sub> protons of the **A<sub>1</sub>B<sub>6</sub>** and **A<sub>1</sub>B<sub>12</sub>**.

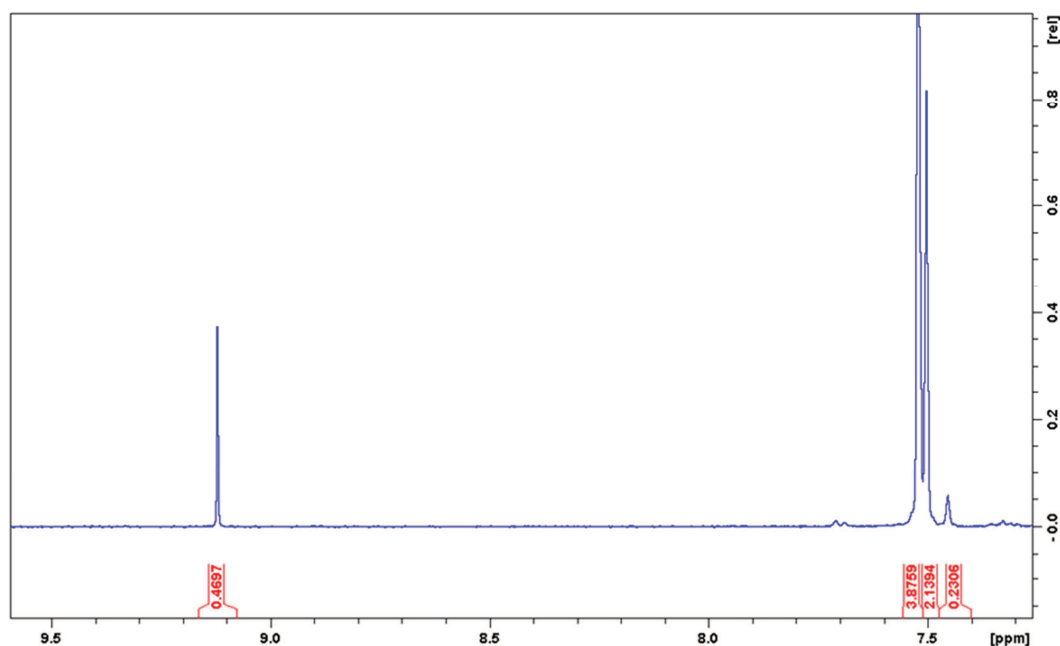


Figure 7.7-5 The aldehyde and imine section of the 400 MHz  $^1\text{H-NMR}$  spectrum of the mixture of 6 eq. of the aldehyde **A** with diamines **B2**, **B6** and **B12** (1 eq. and 20 mM each). Approximately 8 % of the aldehyde (9.12 ppm) remains unreacted. The signals partially overlap: separated single at 7.45 ppm correspond to mono-imine **A<sub>1</sub>B<sub>2</sub>**, the singlet at 7.50 ppm corresponds to **A<sub>2</sub>B<sub>6</sub>**, the singlet at 7.55 ppm contains both **A<sub>2</sub>B<sub>2</sub>** and **A<sub>2</sub>B<sub>12</sub>** signals (corrected integrals obtained by signal deconvolution gives integral intensity of 2.0 for the **A<sub>2</sub>B<sub>6</sub>** at 7.50 ppm and 4.0 for the mixed **A<sub>2</sub>B<sub>2</sub>** and **A<sub>2</sub>B<sub>12</sub>** signal at 7.55 ppm). Indicated integral values are normalized with respect to the aliphatic part of the spectrum in Figure 7.7-4. The ratio of bis-imines **A<sub>2</sub>B<sub>2</sub>** : **A<sub>2</sub>B<sub>6</sub>** : **A<sub>2</sub>B<sub>12</sub>** is 1:1:1.

## BIBLIOGRAPHY

- [1] Aristotle, *Nicomachean Ethics*, Batoche Books, Kitchener, **1999**.
- [2] J.-M. Lehn, *Angew. Chem. Int. Ed.* **2013**, *52*, 2836–2850.
- [3] C. Darwin, *On the Origin of Species*, John Murray, Albermarle Street, London, **1859**.
- [4] J.-M. Lehn, *Proc. Natl. Acad. Sci. U.S.A.* **2002**, *99*, 4763–4768.
- [5] J.-M. Lehn, *Supramolecular Chemistry: Concepts and Perspectives*, VCH, Weinheim, **1995**.
- [6] J.-M. Lehn, *Chem. Eur. J.* **1999**, *5*, 2455–2463.
- [7] N. Giuseppone, J.-L. Schmitt, J.-M. Lehn, *Angew. Chem. Int. Ed.* **2004**, *43*, 4902–4906.
- [8] J.-M. Lehn, *Chem. Soc. Rev.* **2007**, *36*, 151–160.
- [9] M. Pascu, A. Ruggi, R. Scopelliti, K. Severin, *Chem. Commun.* **2012**, *49*, 45–47.
- [10] M. N. Chaur, D. Collado, J.-M. Lehn, *Chem. Eur. J.* **2011**, *17*, 248–258.
- [11] F. Grimm, N. Ulm, F. Gröhn, J. Düring, A. Hirsch, *Chem. Eur. J.* **2011**, *17*, 9478–9488.
- [12] V. Goral, M. I. Nelen, A. V. Eliseev, J.-M. Lehn, *Proc. Natl. Acad. Sci. U.S.A.* **2001**, *98*, 1347–1352.
- [13] B. Icli, E. Solari, B. Kilbas, R. Scopelliti, K. Severin, *Chem. Eur. J.* **2012**, *18*, 14867–14874.
- [14] B. Icli, E. Sheepwash, T. Riis-Johannessen, K. Schenk, Y. Filinchuk, R. Scopelliti, K. Severin, *Chem. Sci.* **2011**, *2*, 1719–1721.
- [15] A. Granzhan, C. Schouwey, T. Riis-Johannessen, R. Scopelliti, K. Severin, *J. Am. Chem. Soc.* **2011**, *133*, 7106–7115.
- [16] A. Granzhan, T. Riis-Johannessen, R. Scopelliti, K. Severin, *Angew. Chem. Int. Ed.* **2010**, *49*, 5515–5518.
- [17] E. Sheepwash, V. Krampl, R. Scopelliti, O. Sereda, A. Neels, K. Severin, *Angew. Chem. Int. Ed.* **2011**, *50*, 3034–3037.
- [18] J.-M. Lehn, *Compt. Rendus Chem.* **2011**, *14*, 348–361.
- [19] J. N. H. Reek, S. Otto, *Dynamic Combinatorial Chemistry*, Wiley-VCH, Weinheim, **2010**.
- [20] P. T. Corbett, J. Leclair, L. Vial, K. R. West, J.-L. Wietor, J. K. M. Sanders, S. Otto, *Chem. Rev.* **2006**, *106*, 3652–3711.
- [21] J. D. Cheeseman, A. D. Corbett, J. L. Gleason, R. J. Kazlauskas, *Chem. Eur. J.* **2005**, *11*, 1708–1716.
- [22] R. A. R. Hunt, S. Otto, *Chem. Commun.* **2011**, *47*, 847–858.
- [23] M. Hochgürtel, J.-M. Lehn, in *Fragment-Based Approaches in Drug Discovery* (Eds.: W. Jahnke, D.A. Erlanson), Wiley-VCH Verlag GmbH & Co. KGaA, **2006**, pp. 341–364.
- [24] O. Ramstrom, J.-M. Lehn, *Nat. Rev. Drug Discov.* **2002**, *1*, 26–36.
- [25] B. L. Miller, Ed., *Dynamic Combinatorial Chemistry in Drug Discovery, Bioorganic Chemistry, and Materials Science*, Wiley, Hoboken, N.J., **2010**.
- [26] S. Ladame, *Org. Biomol. Chem.* **2008**, *6*, 219–226.
- [27] M. E. Belowich, J. F. Stoddart, *Chem. Soc. Rev.* **2012**, *41*, 2003–2024.
- [28] J. S. Siegel, K. K. Baldridge, A. Linden, R. Dorta, *J. Am. Chem. Soc.* **2006**, *128*, 10644–10645.
- [29] N. Hirokawa, *Trends Cell Biol.* **1996**, *6*, 135–141.
- [30] R. D. Vale, *Cell* **2003**, *112*, 467–480.
- [31] M. Schliwa, Ed., *Molecular Motors*, **2004**.
- [32] H. Miki, Y. Okada, N. Hirokawa, *Trends Cell Biol.* **2005**, *15*, 467–476.
- [33] R. Mallik, S. P. Gross, *Current Biology* **2004**, *14*, R971–R982.
- [34] A. Yildiz, M. Tomishige, R. D. Vale, P. R. Selvin, *Science* **2004**, *303*, 676–679.

- [35] R. . Cross, *Current Biology* **2004**, *14*, R355–R356.
- [36] T. Kreis, R. Vale, *Guidebook to the Cytoskeletal and Motor Proteins*, Oxford University Press, Oxford; New York, **1999**.
- [37] P. Dallos, B. Fakler, *Nat. Rev. Mol. Cell Biol.* **2002**, *3*, 104–111.
- [38] P. Vongvilai, O. Ramstrom, *J. Am. Chem. Soc.* **2009**, *131*, 14419–14425.
- [39] E. Juaristi, *Conformational Behavior of Six-Membered Rings*, Wiley VCH, **1995**.
- [40] J. B. Hendrickson, *J. Am. Chem. Soc.* **1961**, *83*, 4537–4547.
- [41] K. Kakhiani, U. Lourderaj, W. Hu, D. Birney, W. L. Hase, *J. Phys. Chem. A* **2009**, *113*, 4570–4580.
- [42] G. Gill, D. M. Pawar, E. A. Noe, *J. Org. Chem.* **2005**, *70*, 10726–10731.
- [43] J. D. Kemp, K. S. Pitzer, *J. Chem. Phys.* **1936**, *4*, 749–750.
- [44] L. Meca, D. Řeha, Z. Havlas, *J. Org. Chem.* **2003**, *68*, 5677–5680.
- [45] S. Davalli, L. Lunazzi, D. Macciantelli, *J. Org. Chem.* **1991**, *56*, 1739–1747.
- [46] B. P. Belousov, *Collection of Abstracts on Radiation Medicine* **1959**, *147*, 145.
- [47] A. Sirimungkala, H.-D. Försterling, V. Dlask, R. J. Field, *J. Phys. Chem. A* **1999**, *103*, 1038–1043.
- [48] A. M. Zhabotinsky, *Biophysics* **1964**, *9*, 306–311.
- [49] W. C. Bray, *J. Am. Chem. Soc.* **1921**, *43*, 1262–1267.
- [50] A. Einstein, A. D. Cowper, R. Fürth, *Investigations on the Theory of the Brownian Movement*, Dover, [New York], **1956**.
- [51] D. Ben-Avraham, S. Havlin, *Diffusion and Reactions in Fractals and Disordered Systems*, Cambridge University Press, Cambridge, **2004**.
- [52] A. J. E. Gordon, D. Satory, J. A. Halliday, C. Herman, *PLoS Genet.* **2013**, *9*, e1003595.
- [53] H. Merrikh, C. Machón, W. H. Grainger, A. D. Grossman, P. Sultanas, *Nature* **2011**, *470*, 554–557.
- [54] A. Paoloni-Giacobino, C. Rossier, M. Papasavvas, S. Antonarakis, *Hum. Genet.* **2001**, *109*, 40–47.
- [55] J. Ninio, *Biochimie* **1991**, *73*, 1517–1523.
- [56] R. J. Sarma, S. Otto, J. R. Nitschke, *Chem. Eur. J.* **2007**, *13*, 9542–9546.
- [57] P. W. Atkins, *The Elements of Physical Chemistry*, W.H. Freeman,, New York :, **c1993**.
- [58] H. L. Le Chatelier, O. Boudouard, *Bull. Soc. Chim. Fr.* **1898**, *19*, 483–488.
- [59] C.-L. Berthollet, *Essai de statique chimique*, Demonville Et Soers, Rue Thionville, Paris, **1803**.
- [60] R. G. Mortimer, *Physical Chemistry*, Harcourt/Academic Press, San Diego, **2000**.
- [61] E. H. Cordes, W. P. Jencks, *J. Am. Chem. Soc.* **1962**, *84*, 832–837.
- [62] E. G. Sander, W. P. Jencks, *J. Am. Chem. Soc.* **1968**, *90*, 6154–6162.
- [63] H. Fischer, F. X. DeCandis, S. D. Ogden, W. P. Jencks, *J. Am. Chem. Soc.* **1980**, *102*, 1340–1347.
- [64] D. L. Leussing, B. E. Leach, *J. Am. Chem. Soc.* **1971**, *93*, 3377–3384.
- [65] S. Patai, Ed., *Carbon-Nitrogen Double Bonds (1970)*, **2010**.
- [66] R. W. Layer, *Chem. Rev.* **1963**, *63*, 489–510.
- [67] H. Hibbert, M. E. Platt, N. M. Carter, *J. Am. Chem. Soc.* **1929**, *51*, 3641–3644.
- [68] D. M. Clode, *Chem. Rev.* **1979**, *79*, 491–513.
- [69] D. Drahoňovský, J.-M. Lehn, *J. Org. Chem.* **2009**, *74*, 8428–8432.
- [70] R. H. Grubbs, *Handbook of Metathesis*, Wiley-VCH, Weinheim, Germany, **2003**.
- [71] P. Reutenauer, E. Buhler, P. J. Boul, S. J. Candau, J.-M. Lehn, *Chem. Eur. J.* **2009**, *15*, 1893–1900.
- [72] R. Göstl, S. Hecht, *Angew. Chem. Int. Ed.* **2014**, n/a–n/a.
- [73] W. v. E. Doering, W. R. Roth, *Tetrahedron* **1963**, *19*, 715–737.
- [74] A. G. Campaña, A. Carlone, K. Chen, D. T. F. Dryden, D. A. Leigh, U. Lewandowska, K. M. Mullen, *Angew. Chem. Int. Ed.* **2012**, *51*, 5480–5483.
- [75] S. Boncel, M. Mączka, K. Z. Walczak, *Tetrahedron* **2010**, *66*, 8450–8457.
- [76] Z.-J. Wu, S.-W. Luo, J.-W. Xie, X.-Y. Xu, D.-M. Fang, G.-L. Zhang, *J. Am. Soc. Mass Spectrom.* **2007**, *18*, 2074–2080.
- [77] Y. Wei, M. Shi, *Chem. Rev.* **2013**, *113*, 6659–6690.

- [78] M. Shi, *The Chemistry of the Morita-Baylis-Hillman Reaction*, Royal Society Of Chemistry, London, **2011**.
- [79] D. Basavaiah, G. Veeraraghavaiah, *Chem. Soc. Rev.* **2012**, *41*, 68–78.
- [80] A. Sanchez-Sanchez, D. A. Fulton, J. A. Pomposo, *Chem. Commun.* **2014**, *50*, 1871–1874.
- [81] E.-K. Bang, G. Gasparini, G. Molinard, A. Roux, N. Sakai, S. Matile, *J. Am. Chem. Soc.* **2013**, *135*, 2088–2091.
- [82] S. P. Black, J. K. M. Sanders, A. R. Stefankiewicz, *Chem. Soc. Rev.* **2014**, *43*, 1861–1872.
- [83] A. Grishina, S. Stanchev, L. Kumprecht, M. Buděšínský, M. Pojarová, M. Dušek, M. Rumlová, I. Křížová, L. Rulíšek, T. Kraus, *Chem. Eur. J.* **2012**, *18*, 12292–12304.
- [84] J. Li, J. M. A. Carnall, M. C. A. Stuart, S. Otto, *Angew. Chem. Int. Ed.* **2011**, *50*, 8384–8386.
- [85] P. M. S. D. Cal, J. B. Vicente, E. Pires, A. V. Coelho, L. F. Veiros, C. Cordeiro, P. M. P. Gois, *J. Am. Chem. Soc.* **2012**, *134*, 10299–10305.
- [86] R. Castangia, M. Austeri, S. L. Flitsch, *Angew. Chem. Int. Ed.* **2012**, *51*, 13016–13018.
- [87] O. P. Chevallier, M. E. Migaud, *Beilstein J. Org. Chem.* **2006**, *2*, 1–6.
- [88] G. E. McCasland, *J. Am. Chem. Soc.* **1951**, *73*, 2295–2297.
- [89] G. Fodor, J. Kiss, *J. Am. Chem. Soc.* **1950**, *72*, 3495–3497.
- [90] E. E. van Tamelen, *J. Am. Chem. Soc.* **1951**, *73*, 5773–5774.
- [91] A. P. Doerschuk, *J. Am. Chem. Soc.* **1952**, *74*, 4202–4203.
- [92] M. Asscher, *J. Org. Chem.* **1976**, *41*, 715–716.
- [93] Y.-H. Ahn, Y.-T. Chang, *Chem. Eur. J.* **2004**, *10*, 3543–3547.
- [94] M. U. Roslund, O. Aitio, J. Wärnå, H. Maaheimo, D. Y. Murzin, R. Leino, *J. Am. Chem. Soc.* **2008**, *130*, 8769–8772.
- [95] F. Xu, B. Simmons, K. Savary, C. Yang, R. A. Reamer, *J. Org. Chem.* **2004**, *69*, 7783–7786.
- [96] A. Kanaya, Y. Takashima, A. Harada, *J. Org. Chem.* **2011**, *76*, 492–499.
- [97] G. Wilkinson, *Comprehensive Coordination Chemistry*, Pergamon, New York, **1989**.
- [98] H. Miyake, H. Tsukube, *Chem. Soc. Rev.* **2012**, *41*, 6977–6991.
- [99] E. L. F. Holzbaur, Y. E. Goldman, *Curr. Opin. Cell Biol.* **2010**, *22*, 4–13.
- [100] M. Barboiu, J.-M. Lehn, *Proc. Natl. Acad. Sci. U.S.A.* **2002**, *99*, 5201–5206.
- [101] W. D. Kerber, D. L. Nelsen, P. S. White, M. R. Gagné, *Dalton Trans.* **2005**, 1948–1951.
- [102] J. R. Nitschke, *Angew. Chem. Int. Ed.* **2004**, *43*, 3073–3075.
- [103] M. Hutin, C. J. Cramer, L. Gagliardi, A. R. M. Shahi, G. Bernardinelli, R. Cerny, J. R. Nitschke, *J. Am. Chem. Soc.* **2007**, *129*, 8774–8780.
- [104] J. R. Nitschke, *Acc. Chem. Res.* **2007**, *40*, 103–112.
- [105] Y.-M. Legrand, A. van der Lee, M. Barboiu, *Inorg. Chem.* **2007**, *46*, 9540–9547.
- [106] M. H. Chisholm, K. Choojun, A. S. Chow, G. Fraenkel, *Angew. Chem. Int. Ed.* **2013**, *52*, 3264–3266.
- [107] C. Godoy-Alcantar, A. K. Yatsimirsky, J.-M. Lehn, *J. Phys. Org. Chem.* **2005**, *18*, 979–985.
- [108] N. Hafezi, J.-M. Lehn, *J. Am. Chem. Soc.* **2012**, *134*, 12861–12868.
- [109] D. Schultz, J. R. Nitschke, *J. Am. Chem. Soc.* **2006**, *128*, 9887–9892.
- [110] A. Herrmann, N. Giuseppone, J.-M. Lehn, *Chem. Eur. J.* **2009**, *15*, 117–124.
- [111] T. T. Tidwell, *Angew. Chem. Int. Ed.* **2008**, *47*, 1016–1020.
- [112] G. P. Moss, P. A. S. Smith, D. Tavernier, *Pure Appl. Chem.* **1995**, *67*, 1307–1375.
- [113] R. Appel, H. Mayr, *J. Am. Chem. Soc.* **2011**, *133*, 8240–8251.
- [114] R. L. Salvador, M. Saucier, *Tetrahedron* **1971**, *27*, 1221–1226.
- [115] S. Sasaki, Y. Kotegawa, H. Tamiaki, *Tetrahedron Lett.* **2006**, *47*, 4849–4852.
- [116] R. M. Moriarty, C.-L. Yeh, K. C. Ramey, P. W. Whitehurst, *J. Am. Chem. Soc.* **1970**, *92*, 6360–6362.
- [117] R. Knorr, J. Ruhdorfer, J. Mehlstäubl, P. Böhrer, D. S. Stephenson, *Chem. Ber.* **1993**, *126*, 747–754.
- [118] J.-M. Lehn, *Chem. Eur. J.* **2006**, *12*, 5910–5915.
- [119] A. T. Cornelia Uncuța, *ARKIVOC* **2003**, *2003*, 29–36.
- [120] R. Glaser, J. Yin, S. Miller, *J. Org. Chem.* **2010**, *75*, 1132–1142.



- [121] F. Blanco, I. Alkorta, J. Elguero, *Croat. Chem. Acta* **2009**, *82*, 173–183.
- [122] S. Nsikabaka, W. Harb, M. F. Ruiz-López, *J. Mol. Struct. THEOCHEM* **2006**, *764*, 161–166.
- [123] D. Y. Curtin, E. J. Grubbs, C. G. McCarty, *J. Am. Chem. Soc.* **1966**, *88*, 2775–2786.
- [124] D. Liotard, A. Dargelos, M. Chaillet, *Theoret. Chim. Acta* **1973**, *31*, 325–333.
- [125] A. A. El-Sherif, M. S. Aljahdali, *J. Coord. Chem.* **2013**, *66*, 3423–3468.
- [126] W. L. Felty, C. G. Ekstrom, D. L. Leussing, *J. Am. Chem. Soc.* **1970**, *92*, 3006–3011.
- [127] D. Hopgood, D. L. Leussing, *J. Am. Chem. Soc.* **1969**, *91*, 3740–3750.
- [128] R. S. McQuate, D. L. Leussing, *J. Am. Chem. Soc.* **1975**, *97*, 5117–5125.
- [129] S. H. Weng, D. L. Leussing, *J. Am. Chem. Soc.* **1983**, *105*, 4082–4090.
- [130] J. L. Hogg, D. A. Jencks, W. P. Jencks, *J. Am. Chem. Soc.* **1977**, *99*, 4772–4778.
- [131] N. Wilhelms, S. Kulchat, J.-M. Lehn, *Helv. Chim. Acta* **2012**, *95*, 2635–2651.
- [132] M. M. J. Smulders, I. A. Riddell, C. Browne, J. R. Nitschke, *Chem. Soc. Rev.* **2013**, *42*, 1728–1754.
- [133] M. D. Wise, A. Ruggi, M. Pascu, R. Scopelliti, K. Severin, *Chem. Sci.* **2013**, *4*, 1658–1662.
- [134] F. Karipcin, G. Baskale-Akdogan, *Russ. J. Coord. Chem.* **2009**, *35*, 588–596.
- [135] K. S. Chichak, S. J. Cantrill, A. R. Pease, S.-H. Chiu, G. W. V. Cave, J. L. Atwood, J. F. Stoddart, *Science* **2004**, *304*, 1308–1312.
- [136] K. S. Chichak, S. J. Cantrill, J. F. Stoddart, *Chem. Commun.* **2005**, 3391–3393.
- [137] J. R. Nitschke, J.-M. Lehn, *Proc. Natl. Acad. Sci. U.S.A.* **2003**, *100*, 11970–11974.
- [138] J. Fan, M. Lal Saha, B. Song, H. Schönherr, M. Schmittel, *J. Am. Chem. Soc.* **2012**, *134*, 150–153.
- [139] M. Schmittel, M. L. Saha, J. Fan, *Org. Lett.* **2011**, *13*, 3916–3919.
- [140] J. Fan, J. W. Bats, M. Schmittel, *Inorg. Chem.* **2009**, *48*, 6338–6340.
- [141] Z. Lin, J. Sun, B. Efremovska, R. Warmuth, *Chem. Eur. J.* **2012**, *18*, 12864–12872.
- [142] T. K. Ronson, S. Zarra, S. P. Black, J. R. Nitschke, *Chem. Commun.* **2013**, *49*, 2476–2490.
- [143] N. M. Rue, J. Sun, R. Warmuth, *Isr. J. Chem.* **2011**, *51*, 743–768.
- [144] P. G. Cozzi, *Chem. Soc. Rev.* **2004**, *33*, 410–421.
- [145] C. J. Whiteoak, G. Salassa, A. W. Kleij, *Chem. Soc. Rev.* **2012**, *41*, 622–631.
- [146] T. Kurahashi, H. Fujii, *J. Am. Chem. Soc.* **2011**, *133*, 8307–8316.
- [147] G. Hamasaka, T. Muto, Y. Uozumi, *Angew. Chem. Int. Ed.* **2011**, *50*, 4876–4878.
- [148] N. E. Borisova, T. G. Gulevich, M. D. Reshetova, V. A. Knizhnikov, *Russ. J. Org. Chem.* **2009**, *45*, 1079–1085.
- [149] K. E. Secor, T. E. Glass, *Org. Lett.* **2004**, *6*, 3727–3730.
- [150] C. Schouwey, R. Scopelliti, K. Severin, *Chem. Eur. J.* **2013**, *19*, 6274–6281.
- [151] S. Nadella, P. M. Selvakumar, E. Suresh, P. S. Subramanian, M. Albrecht, M. Giese, R. Fröhlich, *Chem. Eur. J.* **2012**, *18*, 16784–16792.
- [152] Q. Hou, L. Zhao, H. Zhang, Y. Wang, S. Jiang, *J. Lumin.* **2007**, *126*, 447–451.
- [153] H. Zhang, P. Zhang, K. Ye, Y. Sun, S. Jiang, Y. Wang, W. Pang, *J. Lumin.* **2006**, *117*, 68–74.
- [154] S. Wang, G. Men, L. Zhao, Q. Hou, S. Jiang, *Sensor. Actuator. B Chem.* **2010**, *145*, 826–831.
- [155] C. V. McDonnell, M. S. Michailidis, R. B. Martin, *J. Phys. Chem.* **1970**, *74*, 26–35.
- [156] D. A. Buckingham, J. M. Harrowfield, A. M. Sargeson, *J. Am. Chem. Soc.* **1973**, *95*, 7281–7287.
- [157] B. T. Golding, J. M. Harrowfield, G. B. Robertson, A. M. Sargeson, P. O. Whimp, *J. Am. Chem. Soc.* **1974**, *96*, 3691–3692.
- [158] J. M. Harrowfield, A. M. Sargeson, *J. Am. Chem. Soc.* **1974**, *96*, 2634–2635.
- [159] J. M. Harrowfield, A. M. Sargeson, *J. Am. Chem. Soc.* **1979**, *101*, 1514–1520.
- [160] A. R. Gainsford, R. D. Pizer, A. M. Sargeson, P. O. Whimp, *J. Am. Chem. Soc.* **1981**, *103*, 792–805.
- [161] J. M. Harrowfield, A. M. Sargeson, J. Springborg, M. R. Snow, D. Taylor, *Inorg. Chem.* **1983**, *22*, 186–193.
- [162] P. Comba, N. F. Curtis, G. A. Lawrance, A. M. Sargeson, B. W. Skelton, A. H. White, *Inorg. Chem.* **1986**, *25*, 4260–4267.
- [163] I. P. Evans, G. W. Everett, A. M. Sargeson, *J. Am. Chem. Soc.* **1976**, *98*, 8041–8046.

- [164] T. Isobe, S. Kida, S. Misumi, *Bull. Chem. Soc. Jpn.* **1967**, *40*, 1862–1863.
- [165] L.-W. Yang, S. Liu, E. Wong, S. J. Rettig, C. Orvig, *Inorg. Chem.* **1995**, *34*, 2164–2178.
- [166] J. Chakraborty, S. Thakurta, G. Pilet, R. F. Ziessel, L. J. Charbonnière, S. Mitra, *Eur. J. Inorg. Chem.* **2009**, *2009*, 3993–4000.
- [167] M. G. B. Drew, J. Nelson, S. M. Nelson, *J. Chem. Soc., Dalton Trans.* **1981**, 1678–1684.
- [168] L. You, S. R. Long, V. M. Lynch, E. V. Anslyn, *Chem. Eur. J.* **2011**, *17*, 11017–11023.
- [169] R. Huang, B. J. Frost, *Inorg. Chem.* **2007**, *46*, 10962–10964.
- [170] F. P. Dwyer, N. S. Gill, E. C. Gyarfás, F. Lions, *J. Am. Chem. Soc.* **1957**, *79*, 1269–1273.
- [171] S. Liu, E. Wong, V. Karunaratne, S. J. Rettig, C. Orvig, *Inorg. Chem.* **1993**, *32*, 1756–1765.
- [172] A. Zimmer, I. Müller, G. J. Reiß, A. Caneschi, D. Gatteschi, K. Hegetschweiler, *Eur. J. Inorg. Chem.* **1998**, *1998*, 2079–2086.
- [173] E. C. Constable, *Chem. Soc. Rev.* **2013**, *42*, 1637–1651.
- [174] S. Akine, T. Matsumoto, S. Sairenji, T. Nabeshima, *Supramol. Chem.* **2011**, *23*, 106–112.
- [175] R. Kramer, J. M. Lehn, A. Marquis-Rigault, *Proc. Natl. Acad. Sci. U.S.A.* **1993**, *90*, 5394–5398.
- [176] J. M. Lehn, A. Rigault, J. Siegel, J. Harrowfield, B. Chevrier, D. Moras, *Proc. Natl. Acad. Sci. U.S.A.* **1987**, *84*, 2565–2569.
- [177] M. V. Escárcega-Bobadilla, G. Salassa, M. Martínez Belmonte, E. C. Escudero-Adán, A. W. Kleij, *Chem. Eur. J.* **2012**, *18*, 6805–6810.
- [178] A.-M. Stadler, J. Ramírez, J.-M. Lehn, *Chem. Eur. J.* **2010**, 5369–5378.
- [179] H. M. Möller, M. C. Baier, S. Mecking, E. P. Talsi, K. P. Bryliakov, *Chem. Eur. J.* **2012**, *18*, 848–856.
- [180] V. B. M. Kumar, P. K. Bhattacharya, *Indian J. Chem., Sect. A* **1977**, *15*, 132–134.
- [181] T. Kretz, J. W. Bats, H.-W. Lerner, M. Wagner, *Z. Naturforsch.* **2007**, *62b*, 66–74.
- [182] J. W. Leeland, F. J. White, J. B. Love, *J. Am. Chem. Soc.* **2011**, *133*, 7320–7323.
- [183] A.-M. Stadler, J.-J. Jiang, H.-P. Wang, C. Bailly, *Chem. Commun.* **2013**, *49*, 3784–3786.
- [184] K. Hyodo, M. Kondo, Y. Funahashi, S. Nakamura, *Chem. Eur. J.* **2013**, *19*, 4128–4134.
- [185] J. Ramírez, A.-M. Stadler, N. Kyritsakas, J.-M. Lehn, *Chem. Commun.* **2007**, 237–239.
- [186] B. Gnanaprakasam, E. Balaraman, Y. Ben-David, D. Milstein, *Angew. Chem. Int. Ed.* **2011**, *50*, 12240–12244.
- [187] V. A. Soloshonok, V. P. Kukhar, S. V. Galushko, N. Y. Svistunova, D. V. Avilov, N. A. Kuz'mina, N. I. Raevski, Y. T. Struchkov, A. P. Pysarevsky, Y. N. Belokon, *J. Chem. Soc., Perkin Trans. 1* **1993**, 3143–3155.
- [188] Yu. N. Belokon, A. G. Bulychov, S. V. Vitt, Yu. T. Struchkov, A. S. Batsanov, T. V. Timofeeva, V. A. Tsyryapkin, M. G. Ryzhov, L. A. Lysova, *J. Am. Chem. Soc.* **1985**, *107*, 4252–4259.
- [189] Y. N. Belokon', S. M. Motsishkite, V. I. Maleev, S. A. Orlova, N. S. Ikonnikov, E. B. Shamuratov, A. S. Batsanov, Y. T. Struchkov, *Mendeleev Communications* **1992**, *2*, 89–91.
- [190] I. Correia, J. Costa Pessoa, M. T. Duarte, R. T. Henriques, M. F. M. Piedade, L. F. Veiros, T. Jakusch, T. Kiss, Á. Dörnyei, M. M. C. A. Castro, et al., *Chem. Eur. J.* **2004**, *10*, 2301–2317.
- [191] D. Voet, J. G. Voet, *Biochemistry*, John Wiley & Sons, Hoboken, NJ, **2011**.
- [192] M. Chan-Huot, S. Sharif, P. M. Tolstoy, M. D. Toney, H.-H. Limbach, *Biochemistry* **2010**, *49*, 10818–10830.
- [193] H.-H. Limbach, M. Chan-Huot, S. Sharif, P. M. Tolstoy, I. G. Shenderovich, G. S. Denisov, M. D. Toney, *Biochimica et Biophysica Acta (BBA) - Proteins and Proteomics* **2011**, *1814*, 1426–1437.
- [194] S. L. Ink, L. M. Henderson, *Ann. Rev. Nutr.* **1984**, *4*, 455–470.
- [195] A. C. Eliot, J. F. Kirsch, *Annu. Rev. Biochem.* **2004**, *73*, 383–415.
- [196] E. F. Oliveira, N. M. F. S. A. Cerqueira, P. A. Fernandes, M. J. Ramos, *J. Am. Chem. Soc.* **2011**, *133*, 15496–15505.
- [197] C. S. Rossi, F. Olivo, A. Rabassini, N. Siliprandi, *Arch. Biochem. Biophys.* **1962**, *96*, 650–652.
- [198] D. Heinert, A. E. Martell, *J. Am. Chem. Soc.* **1959**, *81*, 3933–3943.
- [199] K. Nakamoto, A. E. Martell, *J. Am. Chem. Soc.* **1959**, *81*, 5857–5863.
- [200] D. Heinert, A. E. Martell, *J. Am. Chem. Soc.* **1962**, *84*, 3257–3263.
- [201] D. Heinert, A. E. Martell, *J. Am. Chem. Soc.* **1963**, *85*, 183–188.

- [202] C. R. H. Raetz, D. S. Auld, *Biochemistry* **1972**, *11*, 2229–2236.
- [203] H. Hayashi, H. Kagamiyama, *Biochemistry* **1997**, *36*, 13558–13569.
- [204] M. A. Vázquez, G. Echevarría, F. Muñoz, J. Donoso, F. G. Blanco, *J. Chem. Soc., Perkin Trans. 2* **1989**, 1617–1622.
- [205] J. Crugeiras, A. Rios, E. Riveiros, J. P. Richard, *J. Am. Chem. Soc.* **2009**, *131*, 15815–15824.
- [206] M. A. Vázquez, F. Muñoz, J. Donoso, F. García Blanco, *Amino Acids* **1992**, *3*, 81–94.
- [207] D. Heinert, A. E. Martell, *J. Am. Chem. Soc.* **1963**, *85*, 188–193.
- [208] D. E. Metzler, *J. Am. Chem. Soc.* **1957**, *79*, 485–490.
- [209] C. M. Metzler, A. Cahill, D. E. Metzler, *J. Am. Chem. Soc.* **1980**, *102*, 6075–6082.
- [210] D. Heinert, A. E. Martell, *J. Am. Chem. Soc.* **1963**, *85*, 1334–1337.
- [211] V. M. Shanbhag, A. E. Martell, *Inorg. Chem.* **1990**, *29*, 1023–1031.
- [212] C. Sparr, E. Salamanova, W. B. Schweizer, H. M. Senn, R. Gilmour, *Chem. Eur. J.* **2011**, *17*, 8850–8857.
- [213] J. Colanduoni, J. J. Villafranca, *J. Biol. Chem.* **1985**, *260*, 15042–15050.
- [214] E. W. Miles, H. M. Fales, J. B. Gin, *Biochemistry* **1972**, *11*, 4945–4953.
- [215] P. M. Robitaille, R. D. Scott, J. Wang, D. E. Metzler, *J. Am. Chem. Soc.* **1989**, *111*, 3034–3040.
- [216] R. Aigner-Held, R. A. Campbell, G. D. Daves, *Proc. Natl. Acad. Sci. U.S.A.* **1979**, *76*, 6652–6655.
- [217] P. S. Tobias, R. G. Kallen, *J. Am. Chem. Soc.* **1975**, *97*, 6530–6539.
- [218] A. Filarowski, *J. Phys. Org. Chem.* **2005**, *18*, 686–698.
- [219] M. Yıldız, Z. Kılıç, T. Hökelek, *J. Mol. Struct.* **1998**, *441*, 1–10.
- [220] N. Galic, D. Matkovic-Calogovic, Z. Cimerman, *J. Mol. Struct.* **1997**, *406*, 153–158.
- [221] R. M. B. Singh, L. Main, *Aust. J. Chem.* **1983**, *36*, 2327–2332.
- [222] K. Sugita, J. Kumanotani, *Bull. Chem. Soc. Jpn.* **1969**, *42*, 2043–2044.
- [223] G. O. Dudek, S. M. Bloom, *J. Org. Chem.* **1971**, *36*, 235–237.
- [224] G. O. Dudek, *J. Org. Chem.* **1967**, *32*, 2016–2017.
- [225] A. D. Bukhtoyarova, L. V. Ektova, M. M. Shakirov, V. N. Berezhnaya, *Russ. J. Org. Chem.* **2002**, *38*, 851–854.
- [226] A. Star, I. Goldberg, B. Fuchs, *J. Organomet. Chem.* **2001**, *630*, 67–77.
- [227] R. Pichon, G. Le, P. Courtot, *Can. J. Chem.* **1982**, *60*, 8–18.
- [228] P. Courtot, R. Pichon, S. Le, *Tetrahedron Lett.* **1979**, 1591–1594.
- [229] F. Fariña, M. T. Molina, P. Noheda, M. C. Paredes, *Tetrahedron* **1992**, *48*, 8437–8450.
- [230] M. A. Bernstein, K. F. King, X. J. Zhou, *Handbook of MRI Pulse Sequences*, Academic Press, Amsterdam; Boston, **2004**.
- [231] R. C. Weast, M. J. Astle, *Handbook of Chemistry and Physics: A Ready-Reference Book of Chemical and Physical Data*, CRC Press, Boca Raton, Fla, **1982**.
- [232] D. R. Vij, *Handbook of Applied Solid State Spectroscopy*, Springer, New York, **2006**.
- [233] D. H. McDANIEL, H. C. BROWN, *J. Org. Chem.* **1958**, *23*, 420–427.
- [234] K. Abe, H. Endo, M. Hirota, *Bull. Chem. Soc. Jpn.* **1981**, *54*, 466–469.
- [235] R. F. Thompson, G. M. Langford, *Anat. Rec.* **2002**, *268*, 276–289.
- [236] J. A. Spudich, *Science* **2011**, *331*, 1143–1144.
- [237] A. Engel, *Annu. Rev. Biophys. Biophys. Chem.* **1991**, *20*, 79–108.
- [238] H. G. Hansma, L. Pietrasanta, *Curr. Opin. Chem. Biol.* **1998**, *2*, 579–584.
- [239] A. F. Raigoza, J. W. Dugger, L. J. Webb, *ACS Appl. Mater. Interfaces* **2013**, *5*, 9249–9261.
- [240] N. Jalili, K. Laxminarayana, *Mechatronics* **2004**, *14*, 907–945.
- [241] J. B. Pawley, Ed., *Handbook of Biological Confocal Microscopy*, Springer, New York, NY, **2006**.
- [242] P. T. C. So, C. Y. Dong, B. R. Masters, K. M. Berland, *Annu. Rev. Biomed. Eng.* **2000**, *2*, 399–429.
- [243] W. R. Zipfel, R. M. Williams, W. W. Webb, *Nat. Biotech.* **2003**, *21*, 1369–1377.
- [244] B. Prevo, E. J. G. Peterman, *Chem. Soc. Rev.* **2014**, *43*, 1144–1155.
- [245] A. Periasamy, *J. Biomed. Opt.* **2001**, *6*, 287–291.
- [246] A. P. Alivisatos, W. Gu, C. Larabell, *Annu. Rev. Biomed. Eng.* **2005**, *7*, 55–76.
- [247] D. Bera, L. Qian, T.-K. Tseng, P. H. Holloway, *Materials* **2010**, *3*, 2260–2345.

- [248] X. Michalet, F. F. Pinaud, L. A. Bentolila, J. M. Tsay, S. Doose, J. J. Li, G. Sundaresan, A. M. Wu, S. S. Gambhir, S. Weiss, *Science* **2005**, *307*, 538–544.
- [249] E. Petryayeva, W. R. Algar, I. L. Medintz, *Appl. Spectrosc.* **2013**, *67*, 215–252.
- [250] I. Heller, T. P. Hoekstra, G. A. King, E. J. G. Peterman, G. J. L. Wuite, *Chem. Rev.* **2014**, *114*, 3087–3119.
- [251] H. Hess, J. Howard, V. Vogel, *Nano Lett.* **2002**, *2*, 1113–1115.
- [252] C. Iomini, V. Babaev-Khaimov, M. Sassaroli, G. Piperno, *J. Cell. Biol.* **2001**, *153*, 13–24.
- [253] A. Akhmanova, M. O. Steinmetz, *J. Cell. Sci.* **2010**, *123*, 3415–3419.
- [254] R. Heald, E. Nogales, *J. Cell. Sci.* **2002**, *115*, 3–4.
- [255] R. D. Vale, R. A. Milligan, *Science* **2000**, *288*, 88–95.
- [256] R. H. Wade, F. Kozielski, *Nat. Struct. Mol. Biol.* **2000**, *7*, 456–460.
- [257] R. B. Case, D. W. Pierce, N. Hom-Booher, C. L. Hart, R. D. Vale, *Cell* **1997**, *90*, 959–966.
- [258] G. Woehlke, M. Schliwa, *Biochim. Biophys. Acta Mol. Cell. Res.* **2000**, *1496*, 117–127.
- [259] A. Gerson-Gurwitz, C. Thiede, N. Movshovich, V. Fridman, M. Podolskaya, T. Danieli, S. Lakamper, D. R. Klopfenstein, C. F. Schmidt, L. Gheber, *EMBO J.* **2011**, *30*, 4942–4954.
- [260] J. Roostalu, C. Hentrich, P. Bieling, I. A. Telley, E. Schiebel, T. Surrey, *Science* **2011**, *332*, 94–99.
- [261] R. B. Dickinson, L. Caro, D. L. Purich, *Biophys. J.* **2004**, *87*, 2838–2854.
- [262] P. Karagiannis, Y. Ishii, T. Yanagida, *Chem. Rev.* **2014**, *114*, 3318–3334.
- [263] M. von Delius, D. A. Leigh, *Chem. Soc. Rev.* **2011**, *40*, 3656–3676.
- [264] E. R. Kay, D. A. Leigh, F. Zerbetto, *Angew. Chem. Int. Ed.* **2007**, *46*, 72–191.
- [265] V. Balzani, A. Credi, F. M. Raymo, J. F. Stoddart, *Angew. Chem. Int. Ed.* **2000**, *39*, 3348–3391.
- [266] A. Coskun, M. Banaszak, R. D. Astumian, J. F. Stoddart, B. A. Grzybowski, *Chem. Soc. Rev.* **2012**, *41*, 19–30.
- [267] B. L. Feringa, R. A. van Delden, N. Koumura, E. M. Geertsema, *Chem. Rev.* **2000**, *100*, 1789–1816.
- [268] N. Tao, *Nat. Chem.* **2009**, *1*, 108–109.
- [269] J.-P. Sauvage, V. Amendola, Eds., *Molecular Machines and Motors*, Springer, Berlin ; New York, **2001**.
- [270] X. Su, I. Aprahamian, *Chem. Soc. Rev.* **2014**, *43*, 1963–1981.
- [271] R. Göstl, A. Senf, S. Hecht, *Chem. Soc. Rev.* **2014**, *43*, 1982–1996.
- [272] L. Hou, X. Zhang, T. C. Pijper, W. R. Browne, B. L. Feringa, *J. Am. Chem. Soc.* **2014**, *136*, 910–913.
- [273] C. Gao, S. Silvi, X. Ma, H. Tian, A. Credi, M. Venturi, *Chem. Eur. J.* **2012**, *18*, 16911–16921.
- [274] W. Szymański, J. M. Beierle, H. A. V. Kistemaker, W. A. Velema, B. L. Feringa, *Chem. Rev.* **2013**, *113*, 6114–6178.
- [275] H. Nishioka, X. Liang, T. Kato, H. Asanuma, *Angew. Chem. Int. Ed.* **2012**, *51*, 1165–1168.
- [276] S. Saha, J. F. Stoddart, *Chem. Soc. Rev.* **2007**, *36*, 77–92.
- [277] H. Kim, J. Park, K. Noh, C. J. Gardner, S. D. Kong, J. Kim, S. Jin, *Angew. Chem. Int. Ed.* **2011**, *50*, 6771–6775.
- [278] D. Ruiz-Molina, K. Wurst, D. N. Hendrickson, C. Rovira, J. Veciana, *Adv. Funct. Mater.* **2002**, *12*, 347–351.
- [279] M. Schmittel, S. Pramanik, S. De, *Chem. Commun.* **2012**, *48*, 11730–11732.
- [280] M. Schmittel, S. De, S. Pramanik, *Angew. Chem.* **2012**, *124*, 3898–3902.
- [281] M. V. Peters, R. S. Stoll, A. Kühn, S. Hecht, *Angew. Chem. Int. Ed.* **2008**, *47*, 5968–5972.
- [282] S. Castellanos, A. A. Vieira, B. M. Illescas, V. Sacchetti, C. Schubert, J. Moreno, D. M. Guldi, S. Hecht, N. Martín, *Angew. Chem. Int. Ed.* **2013**, *52*, 13985–13990.
- [283] J. Wang, B. L. Feringa, *Science* **2011**, *331*, 1429–1432.
- [284] A.-M. Stadler, N. Kyritsakas, R. Graff, J.-M. Lehn, *Chem. Eur. J.* **2006**, *12*, 4503–4522.
- [285] S. K. Samanta, M. Schmittel, *J. Am. Chem. Soc.* **2013**, *135*, 18794–18797.
- [286] S. K. Samanta, J. W. Bats, M. Schmittel, *Chem. Commun.* **2014**, *50*, 2364–2366.
- [287] S. Yamamoto, H. Iida, E. Yashima, *Angew. Chem. Int. Ed.* **2013**, *52*, 6849–6853.



- [288] Y. Wang, R. M. Hernandez, D. J. Bartlett, J. M. Bingham, T. R. Kline, A. Sen, T. E. Mallouk, *Langmuir* **2006**, *22*, 10451–10456.
- [289] S. Ahmed, W. Wang, L. O. Mair, R. D. Fraleigh, S. Li, L. A. Castro, M. Hoyos, T. J. Huang, T. E. Mallouk, *Langmuir* **2013**, *29*, 16113–16118.
- [290] J.-P. Collin, P. Gaviña, J.-P. Sauvage, *Chem. Commun.* **1996**, 2005–2006.
- [291] D. J. Cárdenas, A. Livoreil, J.-P. Sauvage, *J. Am. Chem. Soc.* **1996**, *118*, 11980–11981.
- [292] N. Armaroli, V. Balzani, J.-P. Collin, P. Gaviña, J.-P. Sauvage, B. Ventura, *J. Am. Chem. Soc.* **1999**, *121*, 4397–4408.
- [293] M.-V. Martínez-Díaz, N. Spencer, J. F. Stoddart, *Angew. Chem. Int. Ed.* **1997**, *36*, 1904–1907.
- [294] H.-P. Jacquot de Rouville, J. Iehl, C. J. Bruns, P. L. McGrier, M. Frasconi, A. A. Sarjeant, J. F. Stoddart, *Org. Lett.* **2012**, *14*, 5188–5191.
- [295] J.-C. Olsen, A. C. Fahrenbach, A. Trabolsi, D. C. Friedman, S. K. Dey, C. M. Gothard, A. K. Shveyd, T. B. Gasa, J. M. Spruell, M. A. Olson, et al., *Org. Biomol. Chem.* **2011**, *9*, 7126–7133.
- [296] B. Lewandowski, G. D. Bo, J. W. Ward, M. Pappmeyer, S. Kuschel, M. J. Aldegunde, P. M. E. Gramlich, D. Heckmann, S. M. Goldup, D. M. D'Souza, et al., *Science* **2013**, *339*, 189–193.
- [297] W. B. Sherman, N. C. Seeman, *Nano Lett.* **2004**, *4*, 1203–1207.
- [298] J. SantaLucia, *Proc. Natl. Acad. Sci. U.S.A.* **1998**, *95*, 1460–1465.
- [299] J. Bath, S. J. Green, A. J. Turberfield, *Angew. Chem. Int. Ed.* **2005**, *44*, 4358–4361.
- [300] Y. Tian, Y. He, Y. Chen, P. Yin, C. Mao, *Angew. Chem. Int. Ed.* **2005**, *44*, 4355–4358.
- [301] P. Yin, H. Yan, X. G. Daniell, A. J. Turberfield, J. H. Reif, *Angew. Chem. Int. Ed.* **2004**, *43*, 4906–4911.
- [302] M. von Delius, E. M. Geertsema, D. A. Leigh, *Nat. Chem.* **2009**, *2*, 96–101.
- [303] M. von Delius, E. M. Geertsema, D. A. Leigh, D.-T. D. Tang, *J. Am. Chem. Soc.* **2010**, *132*, 16134–16145.
- [304] M. J. Barrell, A. G. Campaña, M. von Delius, E. M. Geertsema, D. A. Leigh, *Angew. Chem. Int. Ed.* **2011**, *50*, 285–290.
- [305] A. G. Campaña, D. A. Leigh, U. Lewandowska, *J. Am. Chem. Soc.* **2013**, *135*, 8639–8645.
- [306] J. E. Beves, V. Blanco, B. A. Blight, R. Carrillo, D. M. D'Souza, D. Howgego, D. A. Leigh, A. M. Z. Slawin, M. D. Symes, *J. Am. Chem. Soc.* **2014**, *136*, 2094–2100.
- [307] P. Kovaříček, J.-M. Lehn, *J. Am. Chem. Soc.* **2012**, *134*, 9446–9455.
- [308] F. B. L. Cougnon, N. A. Jenkins, G. D. Pantos, J. K. M. Sanders, *Angew. Chem. Int. Ed.* **2012**, *51*, 1443–1447.
- [309] S. J. Rowan, S. J. Cantrill, G. R. L. Cousins, J. K. M. Sanders, J. F. Stoddart, *Angew. Chem. Int. Ed.* **2002**, *41*, 898–952.
- [310] T. Aida, E. W. Meijer, S. I. Stupp, *Science* **2012**, *335*, 813–817.
- [311] D. Zhao, J. S. Moore, *J. Am. Chem. Soc.* **2002**, *124*, 9996–9997.
- [312] B. Klekota, M. H. Hammond, B. L. Miller, *Tetrahedron Lett.* **1997**, *38*, 8639–8642.
- [313] S. Bonnet, J.-P. Collin, M. Koizumi, P. Mobian, J.-P. Sauvage, *Adv. Mater.* **2006**, *18*, 1239–1250.
- [314] *From Non-Covalent Assemblies to Molecular Machines*, Wiley-VCH, Weinheim, **2011**.
- [315] D. S. Auld, T. C. Bruice, *J. Am. Chem. Soc.* **1967**, *89*, 2083–2089.
- [316] M. M. Sprung, *Chem. Rev.* **1940**, *26*, 297–338.
- [317] V. Saggiomo, U. Luening, *Tetrahedron Lett.* **2009**, *50*, 4663–4665.
- [318] E. E. Snell, W. T. Jenkins, *J. Cell. Comp. Physiol.* **1959**, *54*, 161–177.
- [319] Y.-H. Ahn, Y.-T. Chang, *J. Comb. Chem.* **2004**, *6*, 293–296.
- [320] H. Kessler, G. Zimmermann, H. Fietze, H. Moehrle, *Chem. Ber.* **1978**, *111*, 2605–2614.
- [321] O. Ramström, S. Lohmann, T. Bunyapaiboonsri, J.-M. Lehn, *Chem. Eur. J.* **2004**, *10*, 1711–1715.
- [322] T. Hotchkiss, H. B. Kramer, K. J. Doores, D. P. Gamblin, N. J. Oldham, B. G. Davis, *Chem. Commun.* **2005**, 4264–4266.
- [323] O. Ramstromöm, J.-M. Lehn, in *Comprehensive Medicinal Chemistry II* (Eds.: Editors-in-Chief: John B. Taylor, David J. Triggle), Elsevier, Oxford, **2007**, pp. 959–976.

- [324] K. N. Zelenin, V. V. Alekseyev, I. V. Ukraintsev, I. V. Tselinsky, *Org. Prep. Proced. Int.* **1998**, *30*, 53–61.
- [325] K. N. Zelenin, I. V. Ukraintzev, *Org. Prep. Proced. Int.* **1998**, *30*, 109–114.
- [326] J. M. Locke, R. Griffith, T. D. Bailey, R. L. Crumbie, *Tetrahedron* **2009**, *65*, 10685–10692.
- [327] J. Jeener, B. H. Meier, P. Bachmann, R. R. Ernst, *J. Chem. Phys.* **1979**, *71*, 4546–4553.
- [328] C. L. Perrin, T. J. Dwyer, *Chem. Rev.* **1990**, *90*, 935–967.
- [329] C. L. Perrin, R. E. Engler, *J. Am. Chem. Soc.* **1997**, *119*, 585–591.
- [330] E. W. Abel, T. P. J. Coston, K. G. Orrell, V. Šik, D. Stephenson, *J. Magn. Reson.* **1986**, *70*, 34–53.
- [331] Z. Zolnai, N. Juranić, D. Vikić-Topić, S. Macura, *J. Chem. Inf. Comput. Sci.* **2000**, *40*, 611–621.
- [332] S. Wolfe, *Acc. Chem. Res.* **1972**, *5*, 102–111.
- [333] A. O. Maslat, R. Al-Hamdany, Z. Fataftah, A. J. Mahrath, M. J. Abussaud, *Toxicol. Environ. Chem.* **2003**, *85*, 149–157.
- [334] M. Roger, V. Patinec, M. Bourgeois, R. Tripier, S. Triki, H. Handel, *Tetrahedron* **2012**, *68*, 5637–5643.
- [335] J. Lu, D. Ma, J. Hu, W. Tang, D. Zhu, *J. Chem. Soc., Dalton Trans.* **1998**, 2267–2274.
- [336] J. C. Cobas, M. Martin-Pastor, *EXSYCalc*, Mestrelab Research, **2007**.
- [337] A. M. Childs, D. Gosset, Z. Webb, *Science* **2013**, *339*, 791–794.
- [338] A. Stern, N. H. Lindner, *Science* **2013**, *339*, 1179–1184.
- [339] R. Mirabdolbaghi, T. Dudding, *Org. Lett.* **2012**, *14*, 3748–3751.
- [340] K. Ghosh, R. Karmakar, D. Mal, *Eur. J. Org. Chem.* **2013**, *2013*, 4037–4046.
- [341] T. A. Nigst, J. Ammer, H. Mayr, *Angew. Chem. Int. Ed.* **2012**, *51*, 1353–1356.
- [342] S. Srinivasachari, Y. Liu, G. Zhang, L. Prevette, T. M. Reineke, *J. Am. Chem. Soc.* **2006**, *128*, 8176–8184.
- [343] S. Hamieh, V. Saggiomo, P. Nowak, E. Mattia, R. F. Ludlow, S. Otto, *Angew. Chem. Int. Ed.* **2013**, *52*, 12368–12372.
- [344] N. Giuseppone, J.-M. Lehn, *Chem. Eur. J.* **2006**, *12*, 1715–1722.
- [345] I. Saur, K. Severin, *Chem. Commun.* **2005**, 1471–1473.
- [346] C. Wang, G. Wang, Z. Wang, X. Zhang, *Chem. Eur. J.* **2011**, *17*, 3322–3325.
- [347] D. N. Bunck, W. R. Dichtel, *J. Am. Chem. Soc.* **2013**, *135*, 14952–14955.
- [348] J.-M. Lehn, *Prog. Polym. Sci.* **2005**, *30*, 814–831.
- [349] W. G. Skene, J.-M. Lehn, *PMSE Prepr.* **2004**, *91*, 725–726.
- [350] E. Moulin, G. Cormos, N. Giuseppone, *Chem. Soc. Rev.* **2012**, *41*, 1031–1049.
- [351] T. Ono, S. Fujii, T. Nobori, J.-M. Lehn, *Chem. Commun.* **2007**, 4360–4362.
- [352] T. Ono, S. Fujii, T. Nobori, J.-M. Lehn, *Chem. Commun.* **2007**, 46–48.
- [353] C. B. Minkenberg, F. Li, P. van Rijn, L. Florusse, J. Boekhoven, M. C. A. Stuart, G. J. M. Koper, R. Eelkema, J. H. van Esch, *Angew. Chem. Int. Ed.* **2011**, *50*, 3421–3424.
- [354] Z. Lin, T. J. Emge, R. Warmuth, *Chem. Eur. J.* **2011**, *17*, 9395–9405.
- [355] C. Givélet, J. Sun, D. Xu, T. J. Emge, A. Dhokte, R. Warmuth, *Chem. Commun.* **2011**, *47*, 4511–4513.
- [356] K. Acharyya, S. Mukherjee, P. S. Mukherjee, *J. Am. Chem. Soc.* **2013**, *135*, 554–557.
- [357] K. Acharyya, P. S. Mukherjee, *Chem. Eur. J.* **2014**, *20*, 1646–1657.
- [358] F. B. L. Cougnon, N. Ponnuswamy, N. A. Jenkins, G. D. Pantoş, J. K. M. Sanders, *J. Am. Chem. Soc.* **2012**, *134*, 19129–19135.
- [359] S. J. Rowan, J. F. Stoddart, *Org. Lett.* **1999**, *1*, 1913–1916.
- [360] S. R. Beeren, J. K. M. Sanders, *J. Am. Chem. Soc.* **2011**, *133*, 3804–3807.
- [361] G. J. Mohr, C. Demuth, U. E. Spichiger-Keller, *Anal. Chem.* **1998**, *70*, 3868–3873.
- [362] A. Herrmann, *Chem. Soc. Rev.* **2014**, *43*, 1899–1933.
- [363] S. Duan, W. Yuan, F. Wu, T. Jin, *Angew. Chem. Int. Ed.* **2012**, *51*, 7938–7941.
- [364] B. Buchs (née Levrاند), G. Godin, A. Trachsel, J.-Y. de Saint Laumer, J.-M. Lehn, A. Herrmann, *Eur. J. Org. Chem.* **2011**, *2011*, 681–695.
- [365] G. Godin, B. Levrاند, A. Trachsel, J.-M. Lehn, A. Herrmann, *Chem. Commun.* **2010**, *46*, 3125–3127.

- [366] M. Schmittel, K. Mahata, *Angew. Chem. Int. Ed.* **2008**, *47*, 5284–5286.
- [367] A. Wilson, G. Gasparini, S. Matile, *Chem. Soc. Rev.* **2014**, *43*, 1948–1962.
- [368] C.-H. Wong, S. C. Zimmerman, *Chem. Commun.* **2013**, *49*, 1679–1695.
- [369] M. L. Saha, S. De, S. Pramanik, M. Schmittel, *Chem. Soc. Rev.* **2013**, *42*, 6860–6909.
- [370] A. V. Gromova, J. M. Ciszewski, B. L. Miller, *Chem. Commun.* **2012**, *48*, 2131–2133.
- [371] L. A. Wessjohann, D. G. Rivera, F. León, *Org. Lett.* **2007**, *9*, 4733–4736.
- [372] L. L. Lao, J.-L. Schmitt, J.-M. Lehn, *Chem. Eur. J.* **2010**, *16*, 4903–4910.
- [373] J.-B. Lin, X.-N. Xu, X.-K. Jiang, Z.-T. Li, *J. Org. Chem.* **2008**, *73*, 9403–9410.
- [374] Q. Ji, R. C. Lirag, O. Š. Miljanić, *Chem. Soc. Rev.* **2014**, *43*, 1873–1884.
- [375] M. L. Saha, M. Schmittel, *Org. Biomol. Chem.* **2012**, *10*, 4651–4684.
- [376] C.-F. Chow, S. Fujii, J.-M. Lehn, *Chem. Commun.* **2007**, 4363–4365.
- [377] P. N. W. Baxter, J.-M. Lehn, K. Rissanen, *Chem. Commun.* **1997**, 1323–1324.
- [378] K. Osowska, O. Š. Miljanić, *J. Am. Chem. Soc.* **2011**, *133*, 724–727.
- [379] K. Osowska, O. Š. Miljanić, *Angew. Chem. Int. Ed.* **2011**, *50*, 8345–8349.
- [380] Q. Ji, O. Š. Miljanić, *J. Org. Chem.* **2013**, *78*, 12710–12716.
- [381] S. De, K. Mahata, M. Schmittel, *Chem. Soc. Rev.* **2010**, *39*, 1555–1575.
- [382] K. Mahata, M. L. Saha, M. Schmittel, *J. Am. Chem. Soc.* **2010**, *132*, 15933–15935.
- [383] M. Schmittel, K. Mahata, *Chem. Commun.* **2010**, *46*, 4163–4165.
- [384] K. Mahata, M. Schmittel, *J. Am. Chem. Soc.* **2009**, *131*, 16544–16554.
- [385] M. Schmittel, K. Mahata, *Chem. Commun.* **2008**, 2550–2552.
- [386] M. L. Saha, S. Pramanik, M. Schmittel, *Chem. Commun.* **2012**, *48*, 9459–9461.
- [387] I. Kocsis, D. Dumitrescu, Y.-M. Legrand, A. van der Lee, I. Grosu, M. Barboiu, *Chem. Commun.* **2014**, *50*, 2621–2623.
- [388] V. Niel, V. A. Milway, L. N. Dawe, H. Grove, S. S. Tandon, T. S. M. Abedin, T. L. Kelly, E. C. Spencer, J. A. K. Howard, J. L. Collins, et al., *Inorg. Chem.* **2008**, *47*, 176–189.
- [389] M. L. Saha, K. Mahata, D. Samanta, V. Kalsani, J. Fan, J. W. Bats, M. Schmittel, *Dalton Trans.* **2013**, *42*, 12840–12843.
- [390] M. Schmittel, V. Kalsani, J. W. Bats, *Inorg. Chem.* **2005**, *44*, 4115–4117.
- [391] M. L. Saha, J. W. Bats, M. Schmittel, *Org. Biomol. Chem.* **2013**, *11*, 5592–5595.
- [392] M. L. Saha, M. Schmittel, *J. Am. Chem. Soc.* **2013**, *135*, 17743–17746.
- [393] C. Bohne, *Chem. Soc. Rev.* **2013**, DOI 10.1039/C3CS60352K.
- [394] K. Mahata, M. Schmittel, *Beilstein J. Org. Chem.* **2011**, *7*, 1555–1561.
- [395] S. Neogi, Y. Lorenz, M. Engeser, D. Samanta, M. Schmittel, *Inorg. Chem.* **2013**, *52*, 6975–6984.
- [396] M. Ciaccia, R. Cacciapaglia, P. Mencarelli, L. Mandolini, S. D. Stefano, *Chem. Sci.* **2013**, *4*, 2253–2261.
- [397] S. Bednarz, D. Bogdal, *Int. J. Chem. Kinet.* **2009**, *41*, 589–598.
- [398] C. Fasting, C. A. Schalley, M. Weber, O. Seitz, S. Hecht, B. Kokschi, J. Dervede, C. Graf, E.-W. Knapp, R. Haag, *Angew. Chem. Int. Ed.* **2012**, *51*, 10472–10498.
- [399] P. G. M. Wuts, T. W. Greene, *Greene's Protective Groups in Organic Synthesis*, Wiley-Interscience, Hoboken, N.J, **2007**.
- [400] K. C. Nicolaou, *Classics in Total Synthesis: Targets, Strategies, Methods*, VCH, Weinheim ; New York, **1996**.
- [401] K. C. Nicolaou, S. A. Snyder, *Classics in Total Synthesis II: More Targets, Strategies, Methods*, Wiley-VCH, Weinheim, **2003**.
- [402] K. C. Nicolaou, *Classics in Total Synthesis III: Further Targets, Strategies, Methods*, Wiley-VCH, Weinheim, **2011**.
- [403] P. S. Baran, T. J. Maimone, J. M. Richter, *Nature* **2007**, *446*, 404–408.
- [404] K. C. Nicolaou, *J. Org. Chem.* **2009**, *74*, 951–972.
- [405] Y. Li, X. Liu, *Chem. Commun.* **2014**, *50*, 3155–3158.
- [406] S. Munding, U. Jakob, W. Bannwarth, *Chem. Eur. J.* **2014**, *20*, 1258–1262.
- [407] A. Joosten, Y. Trolez, V. Heitz, J.-P. Sauvage, *Chem. Eur. J.* **2013**, *19*, 12815–12823.
- [408] L. Hu, O. Ramström, *Chem. Commun.* **2014**, *50*, 3792–3794.



- [409] S. Ikegami, T. Hayama, T. Katsuki, M. Yamaguchi, *Tetrahedron Lett.* **1986**, *27*, 3403–3406.
- [410] S. Ikegami, H. Uchiyama, T. Hayama, T. Katsuki, M. Yamaguchi, *Tetrahedron* **1988**, *44*, 5333–5342.
- [411] P. Bey, J. P. Vever, *Tetrahedron Lett.* **1977**, *18*, 1455–1458.
- [412] S. Hanessian, Y. L. Bennani, *Tetrahedron Lett.* **1990**, *31*, 6465–6468.
- [413] B. W. Metcalf, P. Casara, *Tetrahedron Lett.* **1975**, *16*, 3337–3340.
- [414] W. Oppolzer, R. Moretti, S. Thomi, *Tetrahedron Lett.* **1989**, *30*, 6009–6010.
- [415] D. Hoppe, L. Beckmann, *Liebigs Ann. Chem.* **1979**, *1979*, 2066–2075.
- [416] R. Polt, M. A. Peterson, *Tetrahedron Lett.* **1990**, *31*, 4985–4986.
- [417] M. J. O'Donnell, J. M. Boniece, S. E. Earp, *Tetrahedron Lett.* **1978**, *19*, 2641–2644.
- [418] T. Hvidt, W. A. Szarek, D. B. Maclean, *Can. J. Chem.* **1988**, *66*, 779–782.
- [419] J. M. Hornback, B. Murugaverl, *Tetrahedron Lett.* **1989**, *30*, 5853–5856.
- [420] M. Bergmann, L. Zervas, *Ber. dtsch. Chem. Ges. A/B* **1931**, *64*, 975–980.
- [421] L. Szabò, Y. Li, R. Polt, *Tetrahedron Lett.* **1991**, *32*, 585–588.
- [422] M. A. Peterson, R. Polt, *J. Org. Chem.* **1993**, *58*, 4309–4314.
- [423] E. J. Corey, A. Guzman-Perez, M. C. Noe, *J. Am. Chem. Soc.* **1995**, *117*, 10805–10816.
- [424] L. N. Pridgen, L. Snyder, J. Prol, *J. Org. Chem.* **1989**, *54*, 1523–1526.
- [425] J. N. Williams Jr., R. M. Jacobs, *Biochem. Biophys. Res. Commun.* **1966**, *22*, 695–699.
- [426] B. Halpern, A. Hope, *Aust. J. Chem.* **1974**, *27*, 2047–2051.
- [427] A. Abdipranoto, A. Hope, B. Halpern, *Aust. J. Chem.* **1977**, *30*, 2711–2715.
- [428] J. C. Sheehan, V. J. Grenda, *J. Am. Chem. Soc.* **1962**, *84*, 2417–2420.
- [429] A. R. Khomutov, A. S. Shvetsov, J. J. Vepsäläinen, A. M. Kritzyn, *Tetrahedron Lett.* **2001**, *42*, 2887–2889.
- [430] K. Chantrapomma, J. S. McManis, B. Ganem, *Tetrahedron Lett.* **1980**, *21*, 2475–2476.
- [431] J. S. McManis, B. Ganem, *J. Org. Chem.* **1980**, *45*, 2041–2042.
- [432] B. Ganem, *Acc. Chem. Res.* **1982**, *15*, 290–298.
- [433] J. C. Bradley, J. P. Vigneron, J. M. Lehn, *Synthetic Comm.* **1997**, *27*, 2833–2845.
- [434] B. Frydman, S. Bhattacharya, A. Sarkar, K. Drandarov, S. Chesnov, A. Guggisberg, K. Popaj, S. Sergejev, A. Yurdakul, M. Hesse, et al., *J. Med. Chem.* **2004**, *47*, 1051–1059.
- [435] G. R. Orr, D. W. Danz, G. Pontoni, P. C. Prabhakaran, S. J. Gould, J. K. Coward, *J. Am. Chem. Soc.* **1988**, *110*, 5791–5799.
- [436] J. J. Fitt, H. W. Gschwend, *J. Org. Chem.* **1977**, *42*, 2639–2641.
- [437] S. Vincent, S. Mons, L. Lebeau, C. Mioskowski, *Tetrahedron Lett.* **1997**, *38*, 7527–7530.
- [438] A. I. Meyers, *Aldichimica Acta n.d.*, *18*, 59–68.
- [439] S. Vincent, C. Mioskowski, L. Lebeau, *J. Org. Chem.* **1999**, *64*, 991–997.
- [440] S. Vincent, L. Lebeau, C. Mioskowski, *Synth. Commun.* **1999**, *29*, 167–174.
- [441] A. I. Meyers, P. D. Edwards, W. F. Rieker, T. R. Bailey, *J. Am. Chem. Soc.* **1984**, *106*, 3270–3276.
- [442] D. Toste, J. McNulty, I. W. J. Still, *Synth. Commun.* **1994**, *24*, 1617–1624.
- [443] D. R. Mootoo, B. Fraser-Reid, *Tetrahedron Lett.* **1989**, *30*, 2363–2366.
- [444] E. M. Stocking, J. F. Sanz-Cervera, R. M. Williams, *J. Am. Chem. Soc.* **2000**, *122*, 1675–1683.
- [445] K.-J. Fasth, G. Antoni, B. Langström, *J. Chem. Soc., Perkin Trans. 1* **1988**, 3081–3084.
- [446] J. D. Prugh, L. A. Birchenough, M. S. Egbertson, *Synth. Commun.* **1992**, *22*, 2357–2360.
- [447] G. W. J. Fleet, I. Fleming, *J. Chem. Soc. C* **1969**, 1758–1763.
- [448] G. M. Whitesides, J. P. Mathias, C. T. Seto, *Science* **1991**, *254*, 1312–1319.
- [449] L. J. Prins, D. N. Reinhoudt, P. Timmerman, *Angew. Chem. Int. Ed.* **2001**, *40*, 2382–2426.
- [450] F. J. M. Hoeben, P. Jonkheijm, E. W. Meijer, A. P. H. J. Schenning, *Chem. Rev.* **2005**, *105*, 1491–1546.
- [451] Y. Jin, C. Yu, R. J. Denman, W. Zhang, *Chem. Soc. Rev.* **2013**, *42*, 6634–6654.
- [452] J.-M. Lehn, in *Constitutional Dynamic Chemistry* (Ed.: M. Barboiu), Springer Berlin Heidelberg, **2012**, pp. 1–32.
- [453] M. C. T. Fyfe, J. F. Stoddart, *Acc. Chem. Res.* **1997**, *30*, 393–401.

- [454] S. J. Rowan, S. J. Cantrill, J. F. Stoddart, *Org. Lett.* **1999**, *1*, 129–132.
- [455] B. Fuchs, A. Nelson, A. Star, J. F. Stoddart, S. Vidal, *Angew. Chem. Int. Ed.* **2003**, *42*, 4220–4224.
- [456] R. Cacciapaglia, S. Di Stefano, L. Mandolini, *J. Am. Chem. Soc.* **2005**, *127*, 13666–13671.
- [457] G. Kaiser, J. K. M. Sanders, *Chem. Commun.* **2000**, 1763–1764.
- [458] L. Tauk, A. P. Schröder, G. Decher, N. Giuseppone, *Nat. Chem.* **2009**, *1*, 649–656.
- [459] A. P. Côté, A. I. Benin, N. W. Ockwig, M. O’Keeffe, A. J. Matzger, O. M. Yaghi, *Science* **2005**, *310*, 1166–1170.
- [460] A. L. Korich, P. M. Iovine, *Dalton Trans.* **2010**, *39*, 1423–1431.
- [461] M. J. Webber, J. Tongers, C. J. Newcomb, K.-T. Marquardt, J. Bauersachs, D. W. Losordo, S. I. Stupp, *PNAS* **2011**, *108*, 13438–13443.
- [462] N. Giuseppone, *Acc. Chem. Res.* **2012**, *45*, 2178–2188.
- [463] J. V. Barth, *Annu. Rev. Phys. Chem.* **2007**, *58*, 375–407.
- [464] A. Gourdon, *Angew. Chem. Int. Ed.* **2008**, *47*, 6950–6953.
- [465] M. Z. Hossain, J. E. Johns, K. H. Bevan, H. J. Karmel, Y. T. Liang, S. Yoshimoto, K. Mukai, T. Koitaya, J. Yoshinobu, M. Kawai, et al., *Nat. Chem.* **2012**, *4*, 305–309.
- [466] A. Saywell, J. Schwarz, S. Hecht, L. Grill, *Angew. Chem. Int. Ed.* **2012**, *51*, 5096–5100.
- [467] S. Zhang, W.-X. Zhang, Z. Xi, *Angew. Chem. Int. Ed.* **2013**, *52*, 3485–3489.
- [468] M. Di Giovannantonio, M. El Garah, J. Lipton-Duffin, V. Meunier, L. Cardenas, Y. Fagot Revurat, A. Cossaro, A. Verdini, D. F. Perepichka, F. Rosei, et al., *ACS Nano* **2013**, *7*, 8190–8198.
- [469] G. Binnig, H. Rohrer, C. Gerber, E. Weibel, *Phys. Rev. Lett.* **1982**, *49*, 57–61.
- [470] G. Binnig, H. Rohrer, *Angew. Chem. Int. Ed. Engl.* **1987**, *26*, 606–614.
- [471] H. Rohrer, *Proc. Natl. Acad. Sci. U.S.A.* **1987**, *84*, 4666–4666.
- [472] J. P. Rabe, S. Buchholz, *Science* **1991**, *253*, 424–427.
- [473] S. De Feyter, A. Gesquière, M. M. Abdel-Mottaleb, P. C. M. Grim, F. C. De Schryver, C. Meiners, M. Sieffert, S. Valiyaveetil, K. Müllen, *Acc. Chem. Res.* **2000**, *33*, 520–531.
- [474] S. D. Feyter, F. C. D. Schryver, *Chem. Soc. Rev.* **2003**, *32*, 139–150.
- [475] A. M. Jackson, J. W. Myerson, F. Stellacci, *Nat. Mater.* **2004**, *3*, 330–336.
- [476] J. M. MacLeod, O. Ivasenko, D. F. Perepichka, F. Rosei, *Nanotechnology* **2007**, *18*, 424031.
- [477] R. Otero, W. Xu, M. Lukas, R. E. A. Kelly, E. Lægsgaard, I. Stensgaard, J. Kjems, L. N. Kantorovich, F. Besenbacher, *Angew. Chem. Int. Ed.* **2008**, *47*, 9673–9676.
- [478] A. Ciesielski, L. Piot, P. Samorì, A. Jouaiti, M. W. Hosseini, *Adv. Mater.* **2009**, *21*, 1131–1136.
- [479] A. Ciesielski, G. Schaeffer, A. Petitjean, J.-M. Lehn, P. Samorì, *Angew. Chem. Int. Ed.* **2009**, *48*, 2039–2043.
- [480] A. Ciesielski, C.-A. Palma, M. Bonini, P. Samorì, *Adv. Mater.* **2010**, *22*, 3506–3520.
- [481] A. Ciesielski, R. Perone, S. Pieraccini, G. P. Spada, P. Samorì, *Chem. Commun.* **2010**, *46*, 4493–4495.
- [482] M. El Garah, Y. Makoudi, É. Duverger, F. Palmino, A. Rochefort, F. Chérioux, *ACS Nano* **2011**, *5*, 424–428.
- [483] A. Ciesielski, S. Lena, S. Masiero, G. P. Spada, P. Samorì, *Angew. Chem. Int. Ed.* **2010**, *49*, 1963–1966.
- [484] A. Ciesielski, P. Samorì, *Nanoscale* **2011**, *3*, 1397–1410.
- [485] L. Grill, M. Dyer, L. Lafferentz, M. Persson, M. V. Peters, S. Hecht, *Nat. Nano.* **2007**, *2*, 687–691.
- [486] B. Hulsken, R. Van Hameren, J. W. Gerritsen, T. Khoury, P. Thordarson, M. J. Crossley, A. E. Rowan, R. J. M. Nolte, J. A. A. W. Elemans, S. Speller, *Nat. Nano.* **2007**, *2*, 285–289.
- [487] D. F. Perepichka, F. Rosei, *Science* **2009**, *323*, 216–217.
- [488] J. Cai, P. Ruffieux, R. Jaafar, M. Bieri, T. Braun, S. Blankenburg, M. Muoth, A. P. Seitsonen, M. Saleh, X. Feng, et al., *Nature* **2010**, *466*, 470–473.
- [489] J. Mielke, S. Selvanathan, M. Peters, J. Schwarz, S. Hecht, L. Grill, *J. Phys.: Condens. Matter* **2012**, *24*, 394013.

- [490] D. den Boer, M. Li, T. Habets, P. Iavicoli, A. E. Rowan, R. J. M. Nolte, S. Speller, D. B. Amabilino, S. De Feyter, J. A. A. W. Elemans, *Nat. Chem.* **2013**, *5*, 621–627.
- [491] E. Ghijsens, O. Ivasenko, K. Tahara, H. Yamaga, S. Itano, T. Balandina, Y. Tobe, S. De Feyter, *ACS Nano* **2013**, *7*, 8031–8042.
- [492] J. F. Dienstmaier, A. M. Gigler, A. J. Goetz, P. Knochel, T. Bein, A. Lyapin, S. Reichlmaier, W. M. Heckl, M. Lackinger, *ACS Nano* **2011**, *5*, 9737–9745.
- [493] J. F. Dienstmaier, D. D. Medina, M. Dogru, P. Knochel, T. Bein, W. M. Heckl, M. Lackinger, *ACS Nano* **2012**, *6*, 7234–7242.
- [494] F.-Y. Hu, X.-M. Zhang, X.-C. Wang, S. Wang, H.-Q. Wang, W.-B. Duan, Q.-D. Zeng, C. Wang, *ACS Appl. Mater. Interfaces* **2013**, *5*, 1583–1587.
- [495] X.-Y. Wang, T.-F. Jiao, Z.-X. Zhang, T. Chen, M. Liu, L.-J. Wan, D. Wang, *J. Phys. Chem. C* **2013**, *117*, 16392–16396.
- [496] C.-Z. Guan, D. Wang, L.-J. Wan, *Chem. Commun.* **2012**, *48*, 2943–2945.
- [497] S. Weigelt, C. Busse, C. Bombis, M. M. Knudsen, K. V. Gothelf, T. Strunskus, C. Wöll, M. Dahlbom, B. Hammer, E. Lægsgaard, et al., *Angew. Chem. Int. Ed.* **2007**, *46*, 9227–9230.
- [498] S. Weigelt, C. Busse, C. Bombis, M. M. Knudsen, K. V. Gothelf, E. Lægsgaard, F. Besenbacher, T. R. Linderoth, *Angew. Chem. Int. Ed.* **2008**, *47*, 4406–4410.
- [499] R. Tanoue, R. Higuchi, N. Enoki, Y. Miyasato, S. Uemura, N. Kimizuka, A. Z. Stieg, J. K. Gimzewski, M. Kunitake, *ACS Nano* **2011**, *5*, 3923–3929.
- [500] B. R. Brooks, A. D. Mackerell, L. Nilsson, R. J. Petrella, B. Roux, Y. Won, G. Archontis, C. Bartels, S. Boresch, A. Caflisch, et al., *J. Comput. Chem.* **2009**, *30*, 1545–1614.
- [501] B. R. Brooks, R. E. Bruccoleri, B. D. Olafson, D. J. States, S. Swaminathan, M. Karplus, *J. Comput. Chem.* **1983**, *4*, 187–217.
- [502] T. A. Halgren, *J. Comput. Chem.* **1996**, *17*, 490–519.
- [503] P. Samorì, N. Severin, K. Müllen, J. P. Rabe, *Adv. Mater.* **2000**, *12*, 579–582.
- [504] A. M. Belenguer, T. Frišćić, G. M. Day, J. K. M. Sanders, *Chem. Sci.* **2011**, *2*, 696–700.
- [505] M. Bonini, L. Zalewski, T. Breiner, F. Dötz, M. Kastler, V. Schädler, M. Surin, R. Lazzaroni, P. Samorì, *Small* **2009**, *5*, 1521–1526.
- [506] H. E. Gottlieb, V. Kotlyar, A. Nudelman, *J. Org. Chem.* **1997**, *62*, 7512–7515.
- [507] R. Lumry, E. L. Smith, R. R. Glantz, *J. Am. Chem. Soc.* **1951**, *73*, 4330–4340.
- [508] K. a. W. Parry, P. J. Robinson, P. J. Sainsbury, M. J. Waller, *J. Chem. Soc. B* **1970**, 700–703.
- [509] M. A. Torzilli, S. Colquhoun, D. Doucet, R. H. Beer, *Polyhedron* **2002**, *21*, 697–704.
- [510] X. Chen, A. Yamaguchi, M. Namekawa, T. Kamijo, N. Teramae, A. Tong, *Anal. Chim. Acta* **2011**, *696*, 94–100.
- [511] J. S. Rafelt, J. H. Clark, D. J. Macquarrie, C. Boxwell, *J. Chem. Res. (Synopses)* **2000**, *2000*, 564–565.
- [512] Z. Rozwadowski, T. Dziembowska, *Magn. Reson. Chem.* **1999**, *37*, 274–278.
- [513] D. Pijper, P. Saisaha, J. W. de Boer, R. Hoen, C. Smit, A. Meetsma, R. Hage, R. P. van Summeren, P. L. Alsters, B. L. Feringa, et al., *Dalton Trans.* **2010**, *39*, 10375–10381.
- [514] 浩岩崎, 清安井, 充近藤, *Nippon Kagaku Kaishi* **1978**, *1978*, 313–314.
- [515] S. Senapati, B. K. Mishra, G. B. Behera, P. P. Mahendroo, *Bull. Chem. Soc. Jpn.* **1989**, *62*, 321–324.





# MOTIONAL, REACTIONAL AND CONSTITUTIONAL DYNAMICS OF IMINES

## Résumé

Les travaux réalisés lors de cette thèse s'intéressent aux dynamiques de mouvement, de réaction et de constitution des fonctions imines. Les aldéhydes les plus réactives pour cette réaction de condensation ont été identifiées. Un processus d'échange intramoléculaire aléatoire rapide a été observé entre le salicylaldéhyde et l'éthylènediamine dont la vitesse est contrôlée par les substituants, la longueur de la chaîne amine, le solvant et la température. Cette observation conduit à l'élaboration de mouvements de déplacement d'abord non-directionnels puis développés pour devenir directionnels. Une sélectivité dynamique réactionnelle a été introduite sur des mélanges d'aldéhydes et d'amines. Elle a été baptisée simplicité et est utilisée pour de la protection de fonctions. Enfin, la nature dynamique de l'imine a été étudiée à l'interface solide-liquide par microscopie à effet tunnel et montre une accélération et une amplification des produits formés sur la surface.

**Mots-clés** : mouvement moléculaire, bibliothèques combinatoires dynamiques, simplicité, sélection en réseaux réactionnels, effets de surface

## Summary

This thesis reports on the intertwined motional, reactional and constitutional dynamics of imines. It goes from acquiring the basic data about the reaction to applications in various fields of Chemistry. The most reactive aldehydes for the reaction were identified and their reactivities were explained by physical-organic chemistry methods. An intramolecular motion was observed for simple diamines. This observation led to introduction of a non-directional small molecule walking, and eventually to development of a directional walker. A representation of dynamic combinatorial libraries was proposed and then was used for analysis of aldehyde-amine libraries, which exhibit selective amplification of a given species due to the complexity of its composition. This phenomenon was called simplicity. The simplicity example was then used as a concept for dynamic selective protecting groups in acylation of amines. Also, the dynamic imine linkage was also studied on the solid-liquid interface. It was found that the reactions taking place at the graphite surface are largely accelerated and that the formation of the largest molecules is amplified due to the surface.

**Keywords** : molecular walking, dynamic combinatorial libraries, simplicity, selection in reactional networks, surface effect